Mantle composition, age and geotherm beneath the Darby kimberlite field, west central Rae Craton

by

Garrett Alexander Harris

A thesis submitted in partial fulfillment of the requirements for the degree of

Master of Science

Department of Earth and Atmospheric Sciences

University of Alberta

Abstract

The Rae Craton, northern Canada, contains several diamondiferous kimberlite fields that have been a focus of episodic diamond exploration. Relatively little is known about the deep mantle lithosphere underpinning the architecturally complex crust. Previous studies in the region have focused on peridotite mantle xenoliths from Pelly Bay and Repulse Bay-east Rae and Somerset Island-Churchill Province (north Rae), no previous studies have investigated the lithospheric mantle beneath the west central Rae, specifically the Darby kimberlite field.

This study presents bulk and mineral element and isotopic compositional data for peridotite and pyroxenite xenoliths from the Darby kimberlites representing fragments of the west central Rae lithosphere, as well as the first kimberlite eruption age of 542.2 ± 2.6 Ma (2 σ; phlogopite Rb-Sr isochron) for the Darby kimberlite field.

Darby peridotites have low bulk Al_2O_3 contents with highly-depleted olivine (median Mg# = 92.5), more depleted than peridotites from other locations on the Rae Craton such as Somerset Island and east central Rae kimberlites. These values are characteristic of cratonic lithosphere globally. Rhenium-Os T_{RD} model ages are the oldest measured to date from peridotites of the Rae lithosphere, having a mode in the Meso/Neoarchean and ranging to Paleoproterozoic in age (~ 2.3 Ga). One harzburgite xenolith contains a G10D garnet. Concentrate clinopyroxene defines a well constrained mantle geotherm indicating the existence of a ~ 200 km lithosphere thickness at the time of kimberlite eruption, greater than the lithosphere thickness beneath Somerset Island and in good agreement with present-day seismic constraints. Nickel-in-garnet thermometry in grains that do not record temperatures above the mantle adiabat, indicates mantle sampling mainly in the graphite stability field whereas the Al-in-olivine thermometer shows a distinct mantle sampling mode in the diamond stability field.

Abundant pyroxenite and eclogite (low-Cr garnet, $Cr_2O_3 < 1$ wt%) xenoliths found throughout the Darby bodies are also expressed as the dominant garnet type in kimberlite concentrate. Based on thermometry, these rocks range in likely depths of equilibration, from the lower crust into the shallow lithospheric mantle. They give variable Os model ages, with the oldest ages in the Mesoarchean. The abundance of this mafic material reflects derivation from a large mafic body, which may be evident in the layered structure of the Rae Craton mantle root defined by new seismic studies.

Preface

This thesis is an original work by Garrett Harris. Chapters 2 and 3 were combined into a paper and published in the journal of Mineralogy and Petrology, the paper is found in Appendix B; Harris GA, Pearson DG, Liu J, Hardman MF, Snyder DB, Kelsch D (2018) Mantle Composition, Age and Geotherm beneath the Darby Kimberlite field, West Central Rae Craton. Miner Petrol. Data analysis and interpretation in chapter 4 has become a research collaboration project with Fabrizio Nestola at the University of Padova, Padova, Italy.

Acknowledgements

This study was funded through a CERC grant awarded to Dr. D. Graham Pearson and the Diamond Exploration Research Training School (DERTS). Teck is acknowledged for granting access to the Darby property and support with helicopter field costs. Mike Merante provided invaluable assistance in the field. During initial stages of the project Grant Lockhart was involved in useful discussions. Unpublished data were provided by Bluestone Resources Inc., which Dave Kelsch gave permission to report. David Snyder provided a new geophysical image and useful input into interpretation of the lithosphere structure, which was critical for my conclusions.

I would like to thank Graham Pearson for giving me the opportunity to complete this project. To my examiners: Graham Pearson, Thomas Stachel and Bob Luth for reading my thesis and providing feedback. Special thanks to Jingao Liu who pushed me to pursue a Master's degree under Graham Pearson during my time as a Research Assistant. Jingao Liu also provided training regarding Re-Os isotope dilution chemistry and valuable discussions throughout the project. In addition, Sarah Woodland and Mark Labbe provided assistance with Re-Os analysis, including clean lab procedures and training, developing new PGE chemistry, mass spectrometry training and High-Pressure Asher training and maintenance. I thank Andrew Locock for his knowledge and assistance during Electron Microprobe analyses. Yan Luo for her guidance during LA-ICP-MS analysis and assisting with data reduction. Matthew Hardman provided endless support throughout the project and was always available for troubleshooting data reduction problems and interpretation of the eclogitic/pyroxenitic component at Darby. Janina Czas, Stéphane Poitras and Pedro Waterton for useful discussions and guidance with various programs and data reduction spread-sheets. Finally, the ever-growing Arctic Resources Research Group which are too many to list but were always there for support.

To my EAS 100/105 professor Dr. Jack Park at Grant MacEwan University who reinstituted my wonder and passion for geology I had as a kid, he made me realize I wanted to pursue a career as a geologist. Major thanks to my parents, Marcus and Shelly Harris, who encouraged me to attend post-secondary and supported me throughout the duration of my academics.

Table Of Contents

List of Tables

List of Figures

peridotite alteration; pyroxenite (B-4), garnets display granoblastic texture; B-4 in hand sample showing freshest pyroxenite surrounded by kimberlite.

Figure 2.6 Cr-Ca garnet classification plot (Gr tter et al. 2004) of all analyses of Darby xenolith and concentrate garnets with $Cr_2O_3 \geq 1.00$ wt%. Xenolith analyses (orange circles, n = 12) and concentrate analyses (grey circles, n = 51).

Figure 2.7A Box and whisker plot of 100 * Mg# for mantle olivines. Number of samples (n) given for each category. Data from Pearson and Wittig (2008). **B** Ti-Ca plot for all olivine measured. Fields of various rock types taken from of Foley et al. (2013).

Figure 2.8 Olivine Mg# vs. NiO (wt%) for all olivine analyses from Darby kimberlites. Red line is average Mg# of cratonic harzburgitic olivine 92.6 (Pearson and Wittig 2014).

Figure 2.9 All ilmenite macrocryst analyses from Darby kimberlite field displaying ilmenite analyses.

Figure 2.10 Sulfide composition of discrete grains found in peridotites and pyroxenites. Peridotites: M-10-6, M-3-2; Pyroxenites: B-3, B-9, R-2-4.

Figure 2.11 Mg-Fe-Ca garnet ternary diagram for all low-Cr ($Cr_2O_3 < 1$ wt%) xenoliths from Darby ranging from pyrope to almandine and are relatively Ca poor.

Figure 2.12 Histograms of garnet analyses $Cr_2O_3 < 1$ wt% for **A** Xenoliths and **B** concentrate. No Ca-rich xenoliths, 53% (10/19) xenoliths classify as G4. Garnet $Cr_2O_3 < 1$ wt% made up 82% of the garnet concentrate and spans into the G0 unclassified 5%, G4 pyroxenitic/eclogitic is 32%, G3 eclogitic is 63% with some high Ca samples.

Figure 2.13 TiO_2 vs. Na_2O for $Cr_2O_3 < 1$ wt% garnets. Darby garnets are relatively low Na-Ti plotting away from the eclogitic diamond inclusions of after Gurney and Zweistra (1995).

List of Abbreviations

ARL	Arctic Resources Laboratory
BDL	Below Deteection Limit
BSE	Back-scattered electrons
ca.	circa
Cm	Centimeters
D1 & D2	Deformation event 1 & Deformation event 2
F1 & F2	Foliation event 1 & foliation event 2
Ga	Billions of years
HFSE	High Field Strength Elements
HSE	Highly siderophile elements
J/cm	Joules per centimeter
Kg	kilograms
KIMs	Kimberlite Indicator Minerals
km	kilometer
Kv	Kilovolt
LA-ICP-MS	Laser Ablation Inductively Coupled Mass Spectrometry
LILE	Large-Ion Lithophile Elements
LOD	Limit of Detection
Ma	Millions of years
Mg#	Magnesium number
mL/min	Milliliters per minute

mm	millimeter
Na	Nanoamp
nm	nanometer
PAgJ/cm	Prince Albert groupJoules per centimeter
REE	Rare Earth Element
s	seconds
S1 & S2	Planar structure 1 & Planar structure 2
µm	micron
wt%mL/min	Weight percentMilliliters per minute
XRFmm	X-ray fluorescencemillimeter

Chapter 1
Introduction

1.1 Thesis Goals and Objectives

The main goal of this thesis study is to characterize the nature of the lithospheric mantle beneath the western portion of the central Rae Craton by providing the first compositional and geochronological information on mantle xenoliths, xenocrysts, and heavy mineral concentrate recovered from the Darby kimberlite field, Nunavut. The project uses data collected to determine the lithosphere depletion, age and thickness and to examine the variation of these parameters across the Rae Craton. Constraints on the diamond potential below the Darby kimberlite field are discussed as well as gather a greater understanding for diamond potential of the Rae Craton as a whole. To do this, the composition, age and a geotherm for the lithospheric mantle beneath the field has been determined to assess and guide further exploration on the Rae Craton. In addition, a new seismic image of the Rae lithosphere is utilized to speculate on how the xenolith and mineral chemical constraints on the lithosphere beneath the Darby field might be correlated with the larger-scale structure and evolution of the geologically complex Rae Craton and its mantle root.

1.2 Background and Previous Work

Kimberlites bring pieces of the subcontinental lithospheric mantle, as well as diamonds, to the Earth's surface. Diamonds are strongly associated with two distinct parageneses: peridotite or eclogite. Peridotite is the dominant lithology of the mantle and eclogite comprises between ~ 1 % (Schulze 1989) to ~ 5 % (Dawson and Stephens 1975). Despite the disparity in abundance, 33% of diamonds containing inclusions are derived from an eclogitic source, with peridotitic and websteritic parageneses comprising 65% and 2%, respectively (Stachel and Harris 2008). Thus, although eclogite represents a relatively small proportion of the mantle, it appears to have a strong affinity for diamond-forming fluids.

Since the discovery of dimondiferous kimberlites in Canada in 1991, diamond exploration has caused an economic boom in Canada's north. Diamondiferous kimberlites were first discovered on the Slave Craton and this region has since been the heart of Canadian diamonds. Canadian diamonds are some of the best quality diamonds in the world and the ethical/fair diamond trade in Canada has resulted their high demand. To date several mines have operated in Canada, including: Gahcho Kue, Diavik, Ekati, Snap Lake, Jericho, Renard and Victor, all of which operate(d) on the Slave Craton, with the exception of Renard and Victor, which are on the Superior Craton. Other kimberlite fields currently have good mine prospects, e.g., Chidliak on Baffin Island and Fort à la Corne on the Sask Craton. With most of the operating mines already closed or in the end stages of mine life a need for future mines to maintain Canada's diamond economy is clear. Since the bulk of these mines have operated on the Slave Craton, the majority of the exploration and academic research has been conducted in this region. In contrast, despite being second only to the Superior Craton in terms of size, the Rae Craton has experienced relatively little diamond exploration and hence may have significant undiscovered potential.

The Rae Craton contains several kimberlite fields (e.g., Kjarsgaard 2007; Sarkar et al. 2018, submitted) and has been the subject of episodic diamond exploration, with proven diamond-bearing deposits. The Rae Craton is an extensive but complex assemblage of crustal blocks that is as large as the Superior Craton. However, relatively little is known about the deep mantle lithosphere that underpins the architecturally complex crust of this craton. Recent studies of the mantle cargo from kimberlites of the northern and eastern portions of the craton (Irvine et al 2003; Liu et al. 2016; respectively) as well as seismic studies (e.g., Snyder et al. 2015; 2017), have indicated the presence of a thick Archean cratonic root underlying those portions of the craton. The mantle peridotites documented from the kimberlites on Somerset Island are spinel, spinel-garnet and garnet lherzolites, with rare dunites and harzburgites (Mitchell 1987; Kjasgaard and Peterson 1992; Schmidberger and Francis 1999; Irvine et al. 2003), with minor garnet-pyroxenite (Schmidberger and Francis 1999). Irvine et al. (2003) looked at a suite of peridotitic xenoliths (n = 33) from numerous kimberlite bodies on Somerset Island, northern Churchill Province. The Churchill Province, consitists of the Rae and Hearne cratons and are separated by the Snowbird tectonic zone, which either represents a Neoarchaean suture (Jones et al. 2002) or ca. 1.9 Ga suture (Hoffman 1988; Berman et al. 2007). The age of the lithosphere, determined by osmium model ages, T_{RD} on the peridotites, revealed two dominant age peaks: one at ~ 2.0 Ga and the oldest at ~ 2.6 Ga (Irvine et al. 2003). Liu et al. (2016) provided the first insight to the sub-lithospheric mantle beneath the eastern Rae Craton through investigation of a suite of peridotitic xenoliths from two different kimberlite fields; Pelly Bay (n = 18) and Repulse Bay (n = 31). No eclogite was analysed at either of these localities. The Pelly Bay peridotites are mostly highly altered by serpentinization with some having subsequent carbonate infiltration, while Repulse Bay peridotites were almost completely altered by secondary processes such as serpentinization (sub-surficial), silicification/oxidation and carbonation (surficial or subaerial). The age of the lithosphere was determined by osmium model ages and revealed three age peaks: one in the Phanerozoic, one at ~ 1.7 Ga and the oldest at ~ 2.5 Ga. Additional work is required to further understand the complex composition of the lithospheric mantle beneath the Rae Craton over a larger area, especially further west as it approaches the Queen Maud block, the oldest crustal unit in the region (Schultz et al. 2007). These initial studies of Liu et al. (2016) and Irvine et al. (2003) are used to compare xenoliths sampled by the Darby kimberlites located in the west central Rae Craton, which is the focus of this thesis.

1.3 Geological setting

As outlined by Liu et al. (2016), the Rae Craton has undergone circum-craton subduction and collisional accretion through at least seven major (tectonic) events from the Neoarchean to Paleoproterozoic. These events include but are not limited to: (1) the ca. 2.7 to 2.6 Ga amalgamation of the Chesterfield block along the southern margin (Davis et al. 2006); (2) the ca. 2.56 to 2.50 Ga MacQuoid orogeny along the south-eastern margin (Berman 2010; Pehrsson et al. 2013); (3) the ca. 2.5 to 2.3 Ga Arrowsmith orogeny along the western margin (Berman et al. 2005, 2013); (4) the ca. 2.0 to 1.92 Ga Taltson-Thelon orogeny along the western margin (e.g., Hoffman 1988; Hanmer et al. 1992); (5) the ca. 1.92 to 1.90 Ga Snowbird orogeny and the accretion of the Hearne Craton along the southern margin (Berman et al. 2007; Martel et al. 2008); (6) the ca. 1.87 Ga collision of the Meta Incognita-Sugluk-Hall Peninsula block (MISH) in the northeast (e.g., St-Onge et al. 2006a; Berman et al. 2010); and (7) the ca. 1.82 Ga collision with the Superior Craton in the south-southeastern margin during the ca. 1.9 to 1.8 Ga Trans-Hudson orogeny (e.g., Ansdell and Norman 1995; Stern et al. 1995; St-Onge et al. 2006b). Metamorphic and plutonic rocks (e.g., 1.85 to 1.81 Ga Hudson granitic plutons) of the Rae Craton were formed as a result of these orogenic events (Liu et al. 2016). Furthermore, the Kivalliq-Nueltin event (1.77 to 1.70 Ga granitic magmatism, Peterson et al. 2015) shows evidence for crustal reworking and may reflect major basaltic underplating (Peterson et al. 2002, 2015; Petts et al. 2014a).

The Darby Kimberlite field (Figure 1.1), located ~ 200 km southwest of the community of Kugaaruk, Nunavut, provides an opportunity to study the mantle beneath the western portion of the central Rae Craton using mantle xenoliths. The Darby kimberlite field was first discovered via the targeting of magnetic anomalies in 2004, kimberlite being intersected through drilling in 2006 (Counts 2008). Exploration, including drilling, surficial geophysics and sampling continued until 2014 when Teck Cominco decided to withdraw from the project. At that time, Teck Cominco owned 51 % interest, Indicator Minerals 29 % and Hunter Exploration Group had 20 % interest in the Darby Project. To date the Darby kimberlite field contains nine bodies, of which at least eight are kimberlitic with one lamporphere reported. Five of the kimberlites have proven to be diamond-bearing including the 12 hectare ‘Iceberg’ kimberlite (Counts 2008). Although these pipes are considered diamond bearing, low micro-diamond counts and no macro-diamonds recovered resulted in the projects closure (Weir and Farmer 2008) and currently the property is not staked.

The Darby area lies inside a region of continuous permafrost within the Wager plateau (Weir and Farmer 2008). A recent bedrock mapping program was initiated by the Geological Survey of Canada and the Canada-Nunavut Geoscience Office (Sandeman et al. 2001a, b; Sandeman et al. 2005). However, the first geological mapping of the Keewatin area was completed by Heywood (1961) at a scale of 1:506,880 (1 inch to 8 miles). Schau (1982) revisited the area and remapped portions in 1972 and 1973 at a scale of 1:250,000. The regional geological setting and extent of the Darby claim (Weir and Farmer 2008) when it was active in 2007 is shown in Figure 1.2.

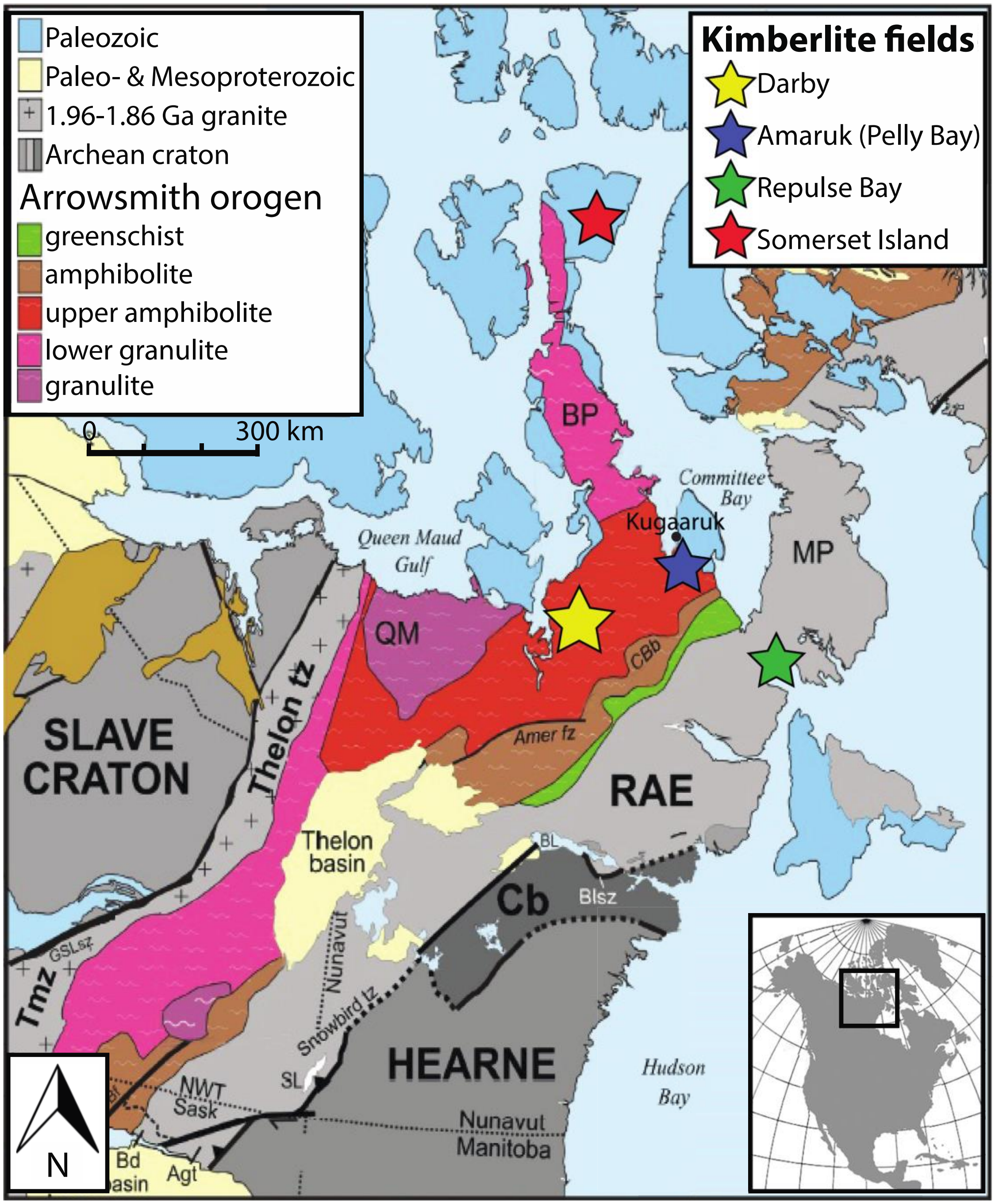

Figure 1.1 Geological setting of the western Churchill Provence (Hearne and Rae Cratons), showing interpreted extent and metamorphic zones of the Arrowsmith orogen on the western flank of the Rae Craton (simplified after Berman et al. 2013). Selected Kimberlite fields shown are Darby (yellow star), Amaruk-Pelly Bay (blue star), Repulse Bay (green star), and Somerset Island (red star).

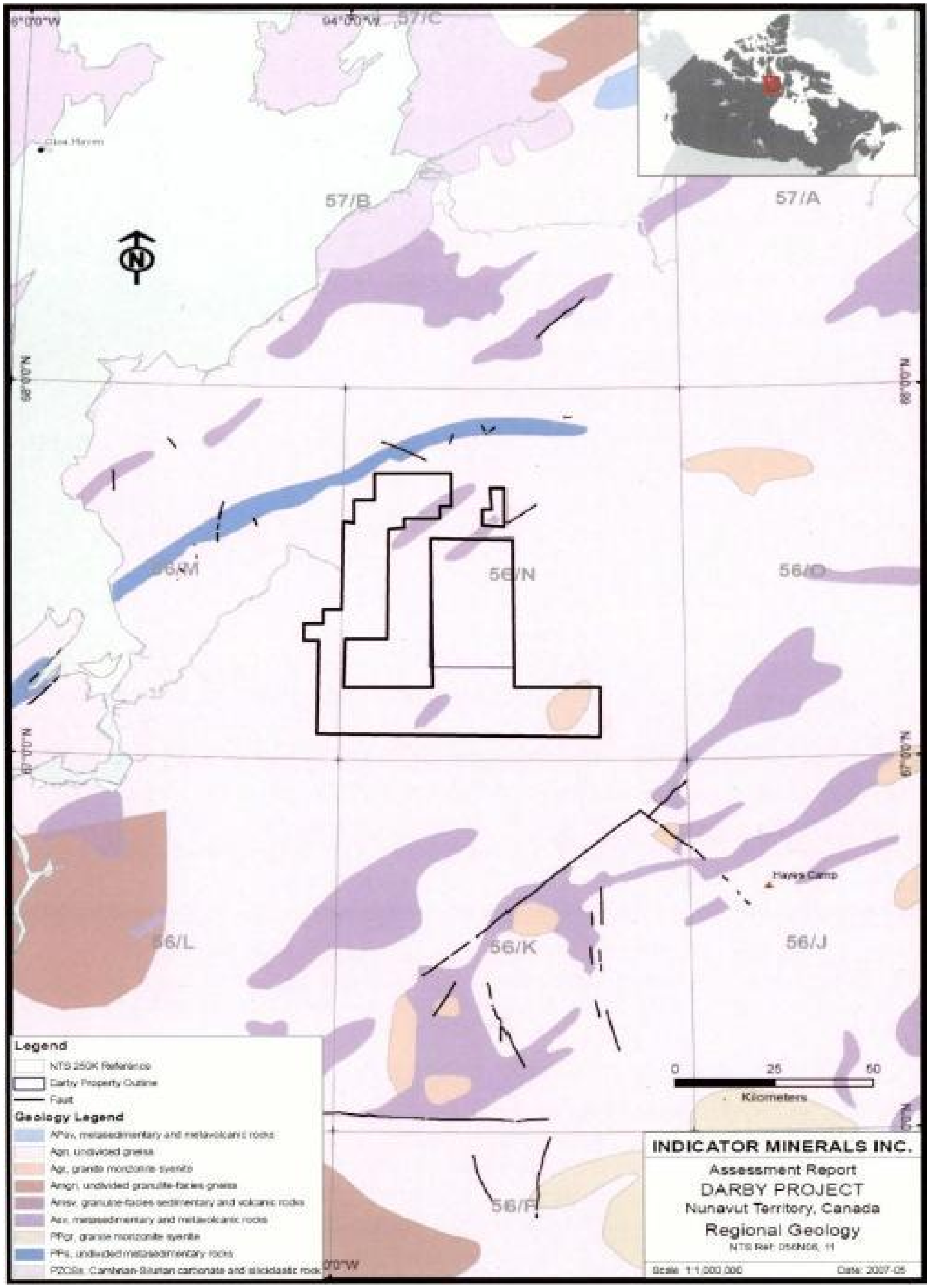

Figure 1.2 The regional geological setting and extent of the Darby claim in 2007. Geology Source: Nunavut Geoscience Sampler DC 2003 – Nunavut Geology Shapefile from Weir and Farmer (2008).

The Rae Craton is generally comprised of Meso- to Neoarchean amphibolite- to granulite-grade granitoid gneisses and komatiite-bearing greenstone belts (Jackson 1966; Frisch 1982; Fraser 1988; MacHattie 2008; Peterson et al. 2010; Wodicka et al. 2011; Pehrsson et al. 2013; LaFlamme et al. 2014; Sanborn-Barrie et al. 2014). The Darby region is covered by extensive Quaternary glacial drift (McMartin 2003) underlain by predominately: (a) Archean granitic gneiss; (b) Archean Prince Albert Group (PAg); (c) Aphebian metadiabase dykes; (d) Neohelikian MacKenzie and/or Franklin diabase dykes; and (e) Archean to Proterozoic granites (Maynes and Doulos 2007). The PAg is the oldest supracrustal unit in the Committee Bay region in the northern Rae (~ 2.7 Ga, MacHattie 2008; Schau, 1982) with well-defined detrital zircons predicting the presence of unrecognized and/or proposed ancient crustal components of ~ 2.7 to 3.7 Ga (MacHattie 2008). It consists of komatiitic flows, dykes and sills interbedded with quartzites, siltstones, shales and iron rich sediments originated from coeval komatiites and underlying basement gneisses of the Brown River Gneiss Complex, demonstrated by structural and metamorphic changes at the contact and a gneissic component within the basal sedimentary rocks of the PAg (Schau 1982). The PAg has undergone multiple deformation and granitic intrusion events during the Late Archean and to a lesser extent in the Early to Middle Proterozoic.

Various Quaternary mapping projects have documented three main phases of ice movement, resolved based upon small scale ice movement features (e.g., Little et al. 2002; McMartin et al. 2003). The oldest movement is a northward movement that is tentatively associated with the last glacial maximum and observed throughout the region (McMartian et al. 2003). The second main ice direction is a northeastward push in the eastern area of the property and a northwestward directed push to the west, with the last main ice direction is north-

northwesterly flow (McMartian et al. 2003). However, minor local ice flow directions, differing from the main flow direction, have been identified throughout the region (McMartian et al. 2003).

Most of the past exploration activity in the area has focused on gold. To the East, the Committee Bay area is underlain by Archean and Proterozoic rocks, which are extensively covered by Quaternary glacial drift (Heywood and Schau 1978). Past gold exploration in the area has been focused on the granite-greenstone terrane of the Archean Prince Albert group (PAg; Heywood 1961). Correlative rocks to the PAg spanning over 2000 km, have been identified as the Murmac Bay group in Saskatchewan (Hartlaub et al. 2001), the Woodburn Lake group north of Baker Lake (host to the Meadowbank deposit; Zaleski et al. 1999) and the Mary River group on Baffin Island (Bethune and Scammell 1997). In the West Laughland Lake Area of the Committee Bay Belt, the regional strikes of the rock units are variable, but most commonly are northerly striking with a significant change in the regional strike of the rock units occurs in the Wolf Lake area (Weir and Farmer 2008). At the Four Hills gold occurrence, complexly refolded iron formations are broadly warped, changing from a northerly regional strike in the western part to a northeasterly regional strike in the eastern part with bedding that dips shallowly unlike the majority of the Committee Bay belt which dips vertically (Weir and Farmer 2008). The change in overall dip and strike in the rock units that occur in the Four Hills area may be the result of deflection of the Committee Bay belt during ductile deformation, either through regional folding or rheological refraction through a tectonothermal front such as the Hudsonian Orogeny (Weir and Farmer 2008). In the Hayes River area, the easterly-striking Walker Lake Shear one forms the dominant structure and its influence is apparent in a number of small shear splays off the main zone (Weir and Farmer 2008). There is a shear splay that is spatially related to the Three

Bluffs gold occurrence, which can be traced along strike from the Three Bluffs to at least the Antler gold occurrence (Weir and Farmer 2008).

To the west of the Darby kimberlite field lies the Queen Maud block (QM; Figure 1.1), for which two tectonic models have been proposed. Hoffman (1987) suggests that an ocean basin that once separated the Slave and Rae which closed by subduction beneath the Rae, followed by a Himalayan-style collision at 1.90 to 2.00 Ga. This suggests the Taltson-Thelon magmatic zone is analogous to the modern-day Himalayas and the Queen Maud block to a deeply eroded Tibetan Plateau (Schultz et al. 2007). However, Chacko et al. (2000) advocate that the Slave and Rae were not separated at 2.00 Ga but were together in the earliest Paleoproterozoic or Archean. Hence, the Taltson-Thelon magmatic zone is comparable to present-day interior mountain belts (e.g., Tian Shan; Schultz et al. 2007). Because, Schultz et al. (2007) showed that there is little evidence for 1.90 to 2.00 Ga metamorphism and tectonic reworking, their data best supports the Chacko et al. (2000) model. Schultz et al. (2007) believe the Queen Maud block is a large crustal block that is the site of an incipient continental rift ~ 2.50 Ga, which then had granitoids produced in early stages of rifting at 2.46 to 2.50 Ga providing the material for a short-lived basin that underwent granulite metamorphism at ~ 2.39 Ga (Schultz et al. 2007). If the plateau model is valid, it would be the result of an earlier orogenic cycle, e.g., the Arrowsmith orogeny (Schultz et al. 2007). This would require a collision between the Slave and Rae at ~ 2.39 Ga or they may have been part of a pre-existing Neoarchean supercontinent (e.g., Aspler and Chiarenzelli, 1998), making the Arrowsmith Orogeny entirely intraplate in nature (Schultz et al. 2007).

The Committee Bay area comprises three distinct Archean-aged subdomains: the Prince Albert group, Northern Migmatite subdomains and the Walker Lake intrusive complex (Skulski et al. 2003; Figure 1.2). The PAg subdomain contains abundant supracrustal rocks of the lower and middle PAg. The lower PAg consists of basalts, komatiites and 2.73 Ga rhyolite, while the middle PAg consists of a sequence of iron formations, psammite, semipelite and < 2.72 Ga quartzite (Skulski et al. 2003). The middle PAg is overlain by a 2.71 Ga dacite, while both the lower and middle PAg were cut by 2.72 Ga syn-volcanic intrusions and post-volcanic intrusions ages 2.61 to 2.59 Ga (Skulski et al. 2003). The Arrowsmith River shear zone separates the PAg and the Northern Migmatite subdomains. The Northern Migmatite subdomain is composed of metasedimentary rocks with lesser mafic and ultramafic rocks from the upper PAg, bracketed to < 2.69 Ga (Skulski et al. 2003). These high-grade metamorphic rocks are cut by variably composed 2.58 Ga plutonic rocks (Skulski et al. 2003). The Walker Lake intrusive complex is in faulted contact with the PAg subdomain proximal to the Walker Lake shear zone but is in intrusive contact with the PAg subdomain elsewhere (Skulski et al. 2003).

The Committee Bay Greenstone Belt is composed of rocks from the PAg which are surrounded in the northwest by the wide, northeasterly-striking, Slave-Chantrey Mylonite Belt and in the south by the narrow, easterly-striking Amer and Wager Bay Shear Zones (Weir and Farmer 2008). Ductile shearing along the Amer and Wager Bay shear zones has been assigned a maximum age of 1.19 Ga and 1.81 Ga, respectively (Henderson and Broome 1990). The Wager Bay shear zone is believed to be a strike-slip fault related to collision of two Archean plates (Parrish 1989). The sinistral reactivation of the easterly-striking structures is believed to post-date emplacement of the Mackenzie dyke swarm at 1.27 Ga (LeCheminant and Heaman 1989) and predate the emplacement of the Franklin dyke swarm at 0.72 Ga (Heaman et al. 1992), which appears to follow a set of pre-existing northwesterly-striking structures in the Committee Bay region.

The two major fault systems in the central portion of the Committee Bay Greenstone Belt that cut PAg rocks are: the northeasterly-striking Kellett Fault and the northwesterly striking Hayes River Fault (Figure 1.2). Several other north-, northwest- and easterly-striking faults occur within the Laughland Lake - Ellice Hills area (Heywood and Schau 1978). Geological and geophysical evidence indicates easterly-striking dextral shearing and northeasterly-striking sinistral shearing components exist and cut or deform rocks of the Committee Bay Greenstone Belt (Weir and Farmer 2008). The northeasterly shears, which are generally parallel to the strike of the rock units, may be part of a conjugate shear set that is related to the easterly-striking Walker Lake and Amer Shear Zones, indicating that the principal component of regional pure shear is oriented north-northwesterly in the Committee Bay Greenstone Belt (Weir and Farmer 2008).

Three phases of ductile deformation are recognized in the rocks of the Committee Bay greenstones (Skulski et al. 2003). The S1 foliation is typically recognized in komatiitic and plutonic rocks, in particular, as a northwest striking fabric parallel to bedding in the komatiites (Skulski et al. 2003). The dominant fabric throughout the Committee Bay region is the northeasterly striking S2 foliation which is axial planar to regional F2 folds (Skulski et al. 2003). This regional foliation is interpreted to represent a composite S2+/-S1 fabric (Skulski et al. 2003). D3 structures include the northeast trending F3 fold and S3 fabrics that overprint D2 fabrics (Skulski et al. 2003). Metamorphic grade increases northeasterly to a metamorphic culmination near Committee Bay (Schau 1982). The southwestern part of the Committee Bay region displays metamorphic grades of upper greenschist to upper amphibolite facies, whereas the metamorphic grade of the northeastern part of the region generally ranges from upper amphibolite to granulite facies (Schau 1982). Both Schau (1982) and Thompson (1998) have discovered evidence for a possible retrograde metamorphic event, superimposed upon the initial regional metamorphism.

To the south, Sandeman et al. (2001 a, b) observed three main deformation phases: development of an extensive bedding parallel foliation, a northeast-southwest directed shortening followed by an upright broad wrapping of D1 and D2 approaching a north-striking axial plane. Granitoid plutonic pluses occurred between 2.64 to 2.58 Ga and 1.85 to 1.83 Ga (Skulski et al. 2002; LeCheminant et al. 1987, LeCheminant and Roddick 1991) with early Proterozoic dyke intrusions followed by Middle Proterozoic granitic stocks and Middle to late Proterozoic mafic dykes.

To the southeast, the Walker Lake intrusive complex contains 2.61 Ga granodiorite to monzogranite that is cut by late- to post-tectonic 1.82 Ma monzogranite (Skulski et al. 2003). The Northern Migmatite subdomain of Skulski et al. (2003) is relatively continuous along strike with the Central subdomain of Sandeman et al. (2005). The northwest corner of the Darby property contains rocks from the northern subdomain, also known as the Northern Barclay Belt and best correlates to Skulski et al.'s PAg subdomain (2003; Sandeman et al. 2005). The rocks in this area of the property are tonalities with metasedimentary and rare metavolcanic supracrustal rocks (Sandeman et al. 2005).

1.4 Samples

Samples were collected at the end of the 2014 summer field season in collaboration with Teck to collect mantle xenoliths from kimberlite float above proven (drilled) kimberlite targets on the Darby property, Nunavut (Figure 1.3). Generally, most of the property is barren tundra with little vegetation other than small shrubs, but is extensively covered with lakes and rivers

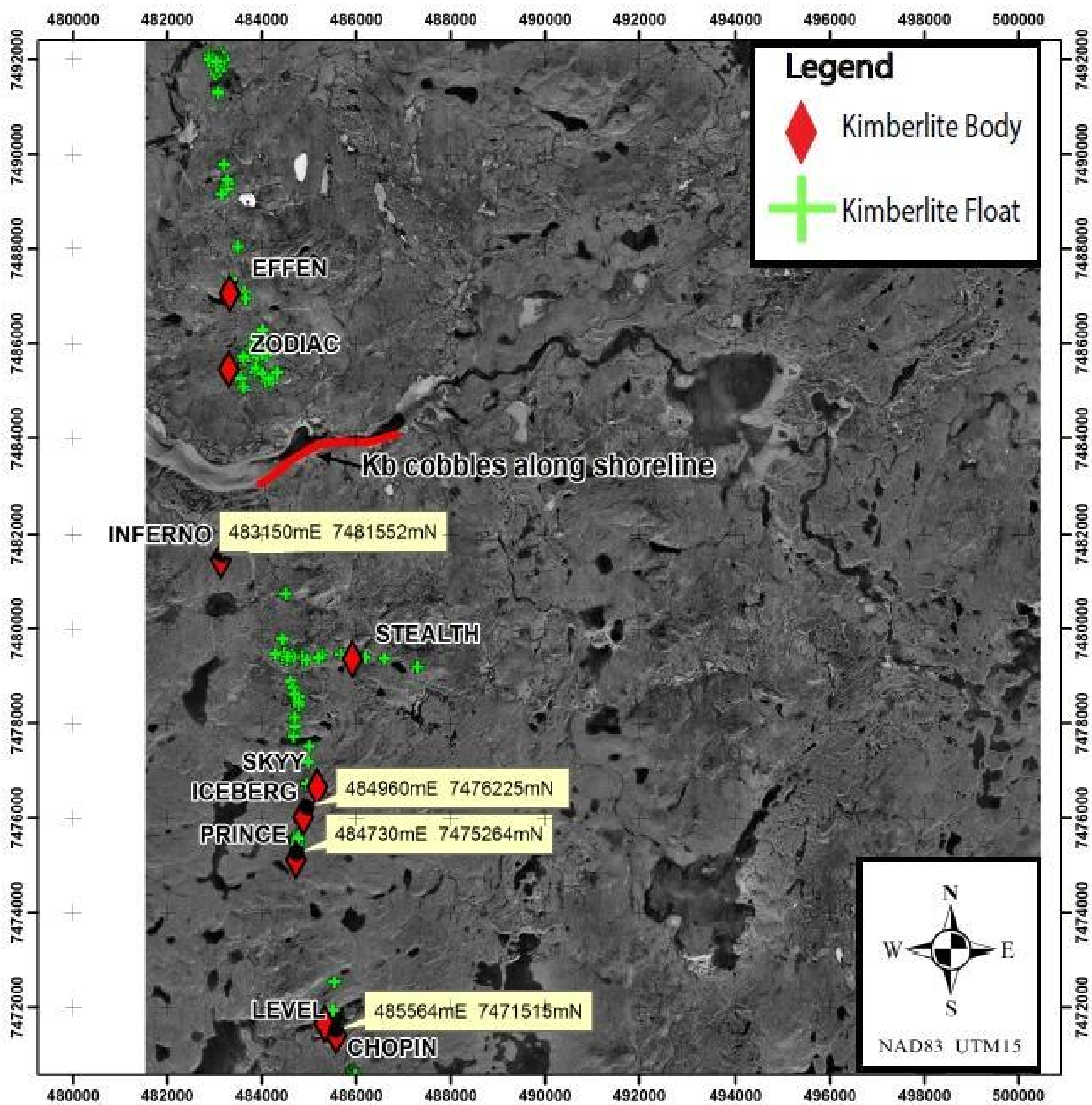

Figure 1.3 Kimberlite bodies proven by drilling (red diamonds) in an ~ N-S trend and float locations (green crosses) across the Darby property.

(Figure 1.4). The Darby kimberlites (GPS locations in Table 1.1; below) occur in a broad north to south trend (Figure 1.3), most likely unrelated to major SW-NE fault systems in the region. Field sampling priorities were Level+Chopin, Prince to Iceberg, and the trend of kimberlite float found between the Sky and Stealth bodies (Figure 1.3), with a day spent sampling each of the three localities above. No sampling occurred north of the river (Effen and Zodiac bodies). Most of the surface kimberlite is highly altered and hence the peridotite xenoliths they contain are generally serpentinized or deeply-weathered. Kimberlite sampled from the northern localities (e.g., Inferno, float trend from Sky to Stealth) is massive coherent kimberlite dominated by olivine and ilmenite macrocrysts plus modal phlogopite. Kimberlite float sampled from the south bodies - Level and Chopin pipes - also consists of massive coherent kimberlite with rare olivine macrocrysts and large abundant ilmenite macrocrysts with no macro-crystalline phlogopite. From the suite collected, a total of 33 mantle xenoliths (14 peridotites and 19 eclogites/pyroxenites) were selected for mineral chemistry and bulk analysis, with rocks identified in the field as "eclogite" at every sampling location.

Table 1.1 Kimberlite pipe locations at Darby.

Kimberlite	UTM_E	UTM_N
Iceberg	484824	7475911
Effen	483323	7487008
Zodiac	483238	7485593
Chopin	485333	7471653
Level	485572	7471406
Inferno	483150	7481552

Prior to sample cutting, minerals were broken off each xenolith via a small needle and tweezers for EPMA analysis. These minerals were then cleaned in de-ionized water and mounted

Figure 1.4 Field pictures taking during Darby kimberlite float sampling and from the helicopter overlooking the Darby kimberlite field.

in epoxy discs. Xenoliths were removed from kimberlite using a combination of either a MK660 saw or Isomet slow speed saw. Small blocks ~ 1 cm x 4 cm x 3 cm were cut from xenoliths to produce thick (100 μm) sections to facilitate analysis of trace elements via laser ablation. All sawn edges were abraded with silicon carbide paper to remove saw marks and possible contamination. Following this all xenoliths and thick section blocks were washed in an ultrasonic bath then placed in new (clean) plastic bags. Once all xenoliths were free from any sort of contamination, some fragments of the freshest eclogite/pyroxenite xenoliths were saved for potential future analyses while the majority of the freshest xenoliths were completely crushed in order to create homogeneous bulk rock powders for whole-rock geochemistry (major elements; trace elements; and highly siderophile elements, HSE including Os, Ir, Pt, Pd and Re).

First a coarse crush for the xenoliths was prepared using small steel hand crushers (High Os-peridotites or Low Os-eclogite/pyroxenite). The crushers were cleaned/washed between xenoliths (e.g., using coarse quartz) to remove potential contamination. The xenolith coarse crush was then powdered using an agate ball mill or by hand in an agate mortar and pestle, from which powders were placed in clean plastic containers. Like the alumina crushers, the agate ball mill/mortar and pestle were cleaned/washed between samples (e.g., using coarse quartz). After the xenoliths were extracted from the kimberlite, a large portion (42 kg) of the remaining kimberlite was sent to Microlithics Laboratories Inc. for the extraction of kimberlite heavy mineral concentrate to allow kimberlite indicator minerals (KIMs) to be examined. This KIM concentrate allowed for a larger database of mantle minerals to be analyzed than is possible from xenolith studies, resulting in a more statistically valid estimation of the mantle lithologies being sampled by the Darby kimberlites. Once the heavy mineral concentrate was received, garnet, olivine, clinopyroxene, and ilmenite were picked and cleaned before being mounted in epoxy discs for analysis. All epoxy discs and thick sections were prepared in-house in the Thin Section Laboratory at the University of Alberta.

1.5 Thesis Layout

The main body of this thesis (Chapter 2 & 3) was combined and submitted as one paper to Mineralogy and Petrology. This paper is currently under review and will be published in the special volume from the 11th International Kimberlite Conference. The fourth Chapter has become a collaboration project and will be published as a separate paper once all required data is gathered in order to have the new mineral officially recognized.

Chapter 2: Major and trace element geochemistry was completed on 31 peridotite and eclogite/pyroxenite xenoliths and utilized EPMA and LA-ICP-MS methodology, respectively.

Chapter 3: Rubidium-Sr, U-Pb and Re-Os Geochronology was applied to phlogopite macrocryts, pyroxenitic rutile and peridotites/eclogites/pyroxenites. These radiogenic isotope systems were used to determine age information for the Darby kimberlites and the lithospheric mantle they erupted through.

Chapter 4: Upon investigation of the rutile bearing pyroxenites, some unique minerals were observed. These minerals, usually associated with lamproites include: jeppeite, freudenbergite, and priderite. In addition, a new mineral ($Na_2Ti_6O_{13}$: Na end-member of jeppeite) was discovered associated with these minerals.

Chapter 2
Major and Trace Element Geochemistry

2.1 Introduction

Samples were petrographically categorized by both hand sample and thick section. The majority of initial observations were completed by hand sample, as under the microscope navigation and identification of minor phases was difficult due to the colors being very dark from overlapping minerals in the thick sections. Therefore, most of the detailed investigatory work in the sections was completed via EPMA which was followed by specific pre-selected analyses by LA-ICP-MS. In addition to this, bulk rock XRF was performed to help characterize the xenoliths prior to geochronology work. All of this work was completed to determine the mantle mineral assemblages and their conditions of equilibration sampled by the Darby kimberlites.

2.2 Analytical methods

2.2.1 Electron Probe Microanalysis: EPMA

Major element analyses of mineral grains were performed by Electron Probe Microanalysis (EPMA), on a CAMECA SX100 or a JEOL8900R at the University of Alberta. All EPMA measurements were completed by via an energy dispersive microanalysis (EDS; qualitative) or a wavelength dispersive microanalysis (WDS; quantitiative), these analyses were conducted with an accelerating voltage of 20 kV, beam current of 20 nA, and a spot size of 2 µm. Precision for major-element EPMA analyses is better than 1 %. Major element analysis for silicates and oxides focused on the 13 oxides SiO_2, TiO_2, Al_2O_3, V_2O_3, Cr_2O_3, MnO, FeO, NiO, MgO, CaO, Na_2O, K_2O, and P_2O_5. Major element analysis for rutile focused on Nb_2O_5, SiO_2, ZrO_2, TiO_2, Al_2O_3, V_2O_3, Cr_2O_3, FeO, MnO, MgO, CaO. All count times and LODs are listed in Table 2.1A&B (below). Multiple spots on larger grains were analysed to assess any heterogeneity within single grains.

2.2.2 Laser Ablation Inductively Coupled Mass Spectrometry: LA-ICP-MS

Trace elements in garnet, clinopyroxene, olivine (Mg# > 91) and rutile (trace and U-Pb isotopes) were analyzed by in-situ laser ablation inductively-coupled plasma mass spectrometry (LA-ICP-MS) at the University of Alberta Arctic Resources Laboratory (ARL) via a Resonetics M-50 193 nm excimer laser-system connected by Nylon tubing to a high-resolution sector-field ICP-MS Thermo Element XR. A total of 24 trace element isotopes (rare earth elements-REE, other high field strength elements-HFSE and large-ion lithophile elements-LILE) were analysed by LA-ICP-MS for garnet, clinopyroxene, and rutile while olivine was analysed for 28 isotope analytes including Al for thermometry calculations. For all analyses, the mass spectrometer was operated in low mass resolution mode ($M/\Delta M$ = ca. 300). Two spots per grain were measured for low-Cr garnets, three spots per grain for peridotitic garnets and single spots for both olivine and clinopyroxene. All silicates were analyzed using a 10 Hz repetition rate with ablation spot size of 130 µm for low-Cr garnet and clinopyroxene, 90 µm for peridotitic garnets, and 193 µm for olivine. Laser energy at the target (fluence) was regulated at ~ 4 J/cm^2. An analysis comprised 30 s of on-peak background gas collection followed by 60 s of ablation. Ablated aerosols were entrained in a He cell gas flow (600 mL/min) and subsequently mixed with N_2 (2 mL/min) and Ar (0.8 mL/min) prior to entering the ICP-MS torch. The ICP-MS was

Table 2.1 Analyzed elements, count times, LODs and standards for acquired major element data, using a CAMECA SX100 or a JEOL JXA-8900R electron probe microanalyzer for **A** silicate and oxides **B** rutile.

A)

Element	**Si**	**Ti**	**Al**	**V**	**Cr**	**Mn**	**Fe**	**Ni**	**Mg**	**Ca**	**Na**
Peak Count Time (s)	30	30	30	30	30	30	30	30	30	30	60
Background Count Time (s)	30	30	30	30	30	30	30	30	30	30	60
Blanket LOD (wt%)	0.016	0.019	0.013	0.026	0.035	0.018	0.014	0.018	0.038	0.014	0.024
Standard	$CaMgSi_2O_6$ diopside Wakefield	TiO_2 Rutile MTI	Frank Smith pyrope garnet	V vanadium Alfa	chromium oxide Alfa	Ni nickel Alfa	$(Mn,Fe)_3Al_2Si_3O_{12}$ spessartine, Navegadora Mine	Ni nickel Alfa	$CaMgSi_2O_6$ diopside Wakefield	$CaMgSi_2O_6$ diopside Wakefield	$NaAlSi_3O_8$ albite VA 131705

Element	**K**	**P**
Peak Count Time (s)	30	30
Background Count Time (s)	30	30
Blanket LOD (wt%)	0.013	0.013
Standard	$KAlSi_3O_8$ sanidine Itrongay	$Ca_5(PO_4)_3F$ apatite, Wilberforce

B)

Element	**Si**	**Ti**	**Al**	**V**	**Cr**	**Mn**	**Fe**	**Mg**	**Ca**	**Nb**	**Zr**
Peak Count Time (s)	30	30	30	50	50	50	50	30	50	50	50
Background Count Time (s)	30	30	30	50	50	50	50	30	50	50	50
Blanket LOD (wt%)	0.008	0.018	0.010	0.013	0.015	0.009	0.009	0.013	0.007	0.019	0.022
Standard	$CaMgSi_2O_6$ diopside Wakefield	TiO_2 Rutile MTI	Frank Smith pyrope garnet	V vanadium Alfa	Cr_2O_3 chromium oxide Alfa	$MnSiO_3$ Rhodonite	Fe_2SiO_4 fayalite Rockport	$CaMgSi_2O_6$ diopside Wakefield	$CaMgSi_2O_6$ diopside Wakefield	Niobium, Nb - ESPI	Zircon $ZrSiO_4$ 639A

operated at 1300 W and a torch depth of 3.6 mm. Argon and helium gas flow, torch position and focusing potentials were optimized in order to achieve optimal signals on Co, La and Th and low oxide production rates (ThO/Th < 0.5 %). Calibration for garnet, clinopyroxene and olivine was performed using NIST SRM 612 in conjunction with internal standardization using isotope ^{43}Ca, while olivine was normalized to ^{29}Si and rutile calibration was performed using Reference Material R10 on ^{48}Ti. All data was reduced offline using Iolite v3 (https://iolite-software.com/). The results of the secondary standards (Figure 2.1, PHN1617-B&C for garnets; Figure 2.2, SC-GB for olivine; Figure 2.3, GP-13 for clinopyroxene; Figure 2.4, R-10 for rutile), agree with the reference values within relative uncertainties of typical 5 to 10 % or better at the 95 % confidence level. As measures of accuracy, 84 % of Ni values in the garnet PHN-B/C agree within 2σ, with several samples plotting above 2σ, which may be attributed to contamination from the >> Ni concentrations of the Darby peridotitic garnets (Figure 2.1). Accuracy and precision for Ni in garnet, over the period encompassing this study is documented in detail by Hardman et al. (2018b, submitted). For olivine SC-GB secondary standard, 80 % of Al and 55 % of V in the olivine agree within 2σ of accepted values (Figure 2.2; Bussweiler et al. 2017). Most elements agreed with the Graham Pearson's unpublished values for GP13 (Figure 2.3), although 2σ were not provided by Graham Pearson's unpublished values, however Ni, Y, Nd, Dy and Gd were all uniformly low compared to their values. For the rutile standard, Nb and Ta were also low with a very large error on V (Figure 2.4, this is attributed to the heterogeneity of this natural rutile standard, which is no longer used as a secondary standard by the ARL.

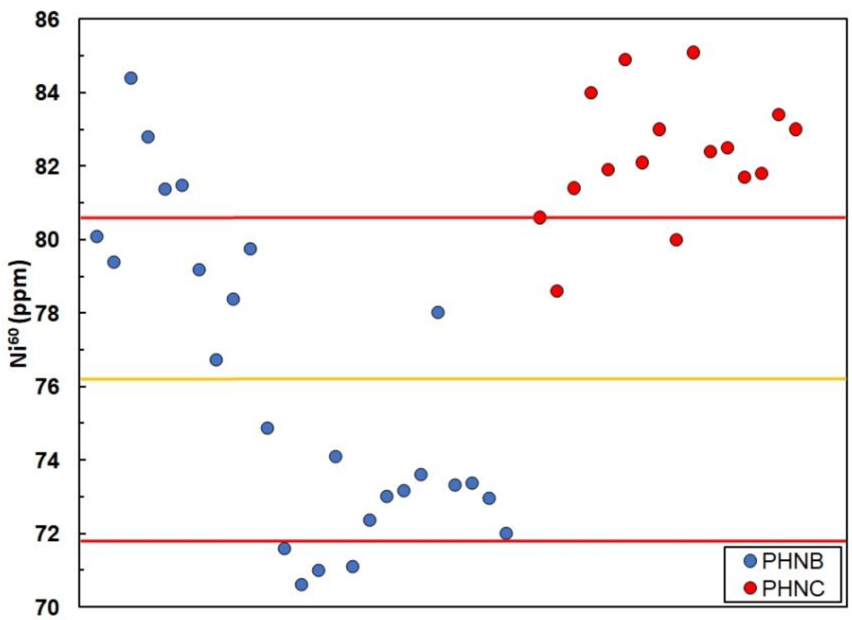

Figure 2.1 Nickel in garnet of secondary standards for PHNB and PHNC over three analytical sessions. Average values and 2σ from Hardman et al. (2018b, submitted).

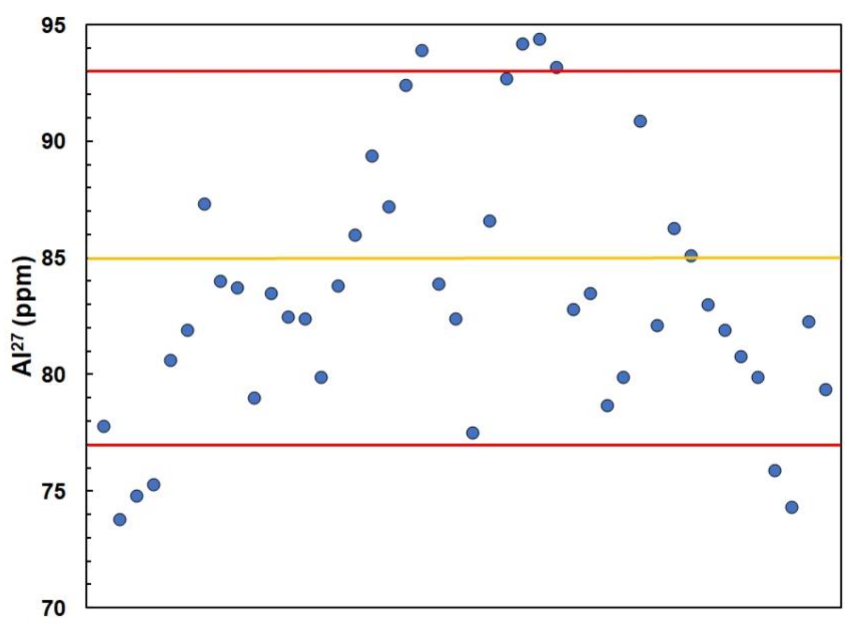

Figure 2.2 Aluminum in olivine of secondary standard for SC-GB over three analytical sessions. Average values and 2σ from Bussweiler et al. (2017).

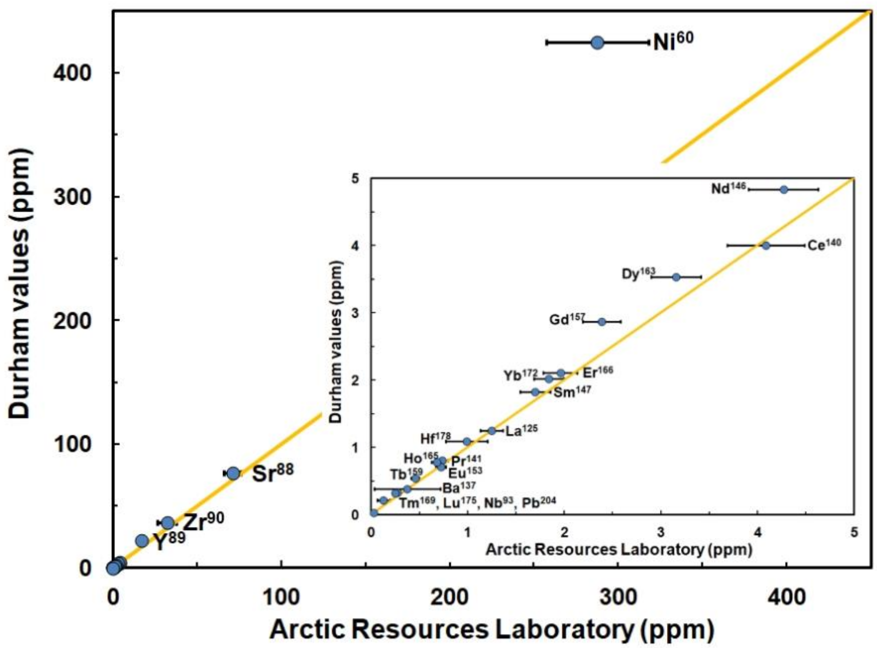

Figure 2.3 Trace elements in clinopyroxene of secondary standard for GP-13 over two analytical sessions. Average values and 2σ from G. Pearson (unpublished).

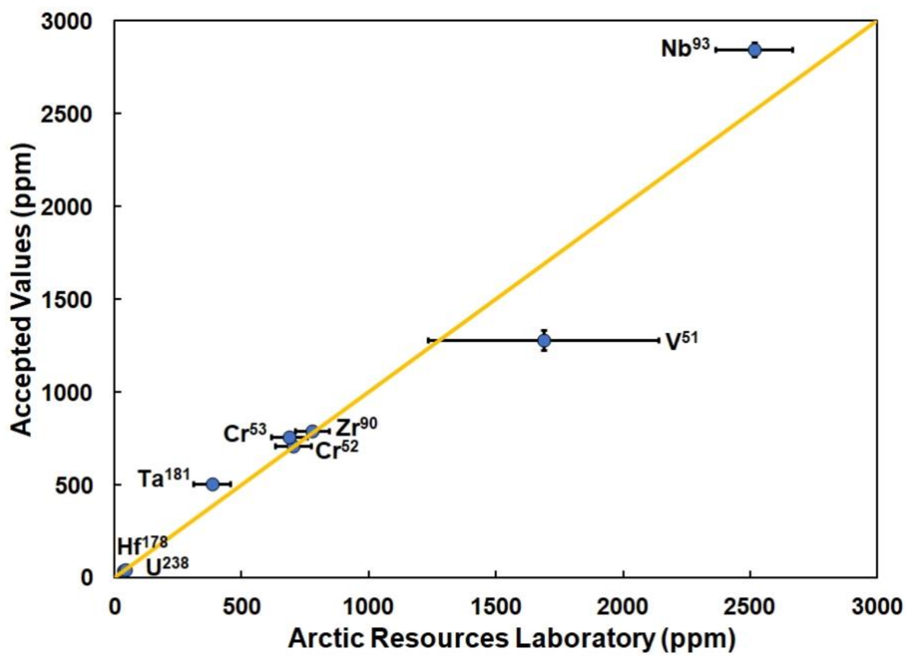

Figure 2.4 Trace elements in rutile of secondary standard for R-10 over two analytical sessions. Average values and 2σ from Luvizotto et al. (2009).

2.2.3 X-ray fluorescence (XRF)

Xenolith rock powders were weighed out for whole-rock major and trace element compositions, ensuring sufficient material was retained for later analysis of highly siderophile elements (HSE including Os, Ir, Pt, Pd and Re). Whole-rock major element and trace compositions were determined through X-ray fluorescence (XRF) on fused glass discs made from rock powders (detailed procedures in Boyd and Mertzman 1987) at Franklin and Marshall College, United States.

2.3 Results

2.3.1 Petrography

Representative photographs of the peridotites and pyroxenites in hand sample and thick section are shown in Figure 2.5. Table 2.2 (below) displays mineralogical, petrographic and other information on xenoliths studied.

Peridotites are generally highly altered, masking their primary mantle textures. The majority of peridotites are dominantly comprised of serpentine with some fresh residual areas of olivine and pyroxene (commonly < 1 mm). Garnets in the peridotites range from 0.1 to 1.0 mm, with minor rare kelyphite rims. Some peridotites show variable levels of infiltration by the host kimberlite.

Eclogites and pyroxenites classified based on IUGS definition (Desmons and Smulikowski 2007) of their clinopyroxene chemistry (below) show equant granular textures. One of these rocks also contains primary plagioclase indicating a crustal origin. Rutile in these rocks is interstitial, forming grains up to 1 mm. Some rutiles have complex reaction rims consisting of perovskite, ilmenite, priderite (KTi_8O_{16}), freudenbergite ($Na_2Ti_8O_{16}$), plus jeppeite ($K_2Ti_6O_{13}$)

Figure 2.5 From top left to bottom right: lherzolite (B-5) displaying olivine, clinopyroxene, amphibole, orthopyroxene and kimberlite infiltration; B-5 in hand sample showing extent of peridotite alteration; pyroxenite (B-4), garnets display granoblastic texture; B-4 in hand sample showing freshest pyroxenite surrounded by kimberlite.

Table 2.2A Petrography of peridotites **B** Petrography of pyroxenites/eclogites.
A)

Sample	**Major Mineral analysis**	**Mg# of olivine**	**Trace Mineral analysis**	**Rock Type- (Xenolith size: cm)**	**Notes**
B-10	amphibole (low total) picotite (chomian spinel) (low total) olivine orthopyroxene diopside perovskite (low total)	91.9	olivine	amphibole lherzolite 10*6*2	-apatite -amphibole is replacing olivine -some spinel inclusions in olvine
B-11	diopside			lherzolite 1*1*0.5	-deeply weathered, few fresh minerals
M-15	garnet olivine	90.7	garnet olivine	garnet dunite 0.5*0.5*0.5	
B-5	picotite (chromian spinel) (low total) diopside augite olivine perovskite (low total) perrierite- (Ce/La) (low total)	92.1	olivine	lherzolite 6cm*8cm*6cm	-euhedural chromite -phlogopite has FeO intergrown along cleavage and some calcite -perovskite is <30um -cpx intergrown with phlogpite with chromite inclusions
B-7	garnet		garnet	garnet dunite 2*4*0.5	
L-5	harzburgitic garnet		garnet	garnet harzbugite 0.5*0.5*0.5	
M-10-4	olivine orthopyroxene	94.3	olivine	lherzolite 1*2*1	-altered although some fresh olivine -calcite
M-10-6	diopside picotite (chomian spinel) (low total) amphibole (low total) olivine perovskite (low total) sulfides	93.1	olivine	amphibole wehrlite 5*4*5	-cpx exsolution into amphibole -(Ni,Fe,Co)S -Barite -very little ilm/spinel

M-21-2/3	amphibole (low total) augite diopside olivine picotite (chomian spinel)	92.8	olivine	amphibole wehrlite 4*3*4	-very homogeneous, difficult to navigate
M-22	diopside olivine	89.1	olivine	lherzolite 1*2*1	
M-22-1	phlogopite olivine pyroxene? sulfides			mantle polymict breccia 2*2*1	-no fresh minerals -sulfides & small olivines -barite & calcite -(Fe, Ni, Cu)S, (Sr, Fe, Ni)S & copper metal -zircon
M-23-1	ilmenite magnetite (low total) titanite (low total) diopside olivine apatite (low total) phlogopite (low total) calcite (low total)	88.6		mantle polymict breccia 3*2*2	-serpentinization but some good olivine
M-24	olivine garnet	92.5	garnet olivine	garnet dunite 1*1*1	-this thick section also has a polymict breccia
M-3-2A/B	phlogopite (low total) calcite (low total) olivine augite ilmenite (low total) chromite magnetite (low total) sulfides	92.7	olivine	phlogopite wehrlite 2*4*3	-cpx intergown with phlogopite -sulfides: (Fe,Ni)S -mostly olivine -monazite -columbite

M-8	olivine			Peridotite 2*3*3	-peridotite was powdered without making thick section or grain mount, no mineral data for this sample
R-2-1/2/3	orthopyroxene diopside augite olivine amphibole (low total) magnetite (low total) picotite (chromian spinel)	92.6	olivine	amphibole lherzolite 3*5*3	-calcite, apatite -picotite exsolution in opx -some magnetite veins/needles between grains

B)

Sample	Major Minerals Analysis	Modal Grt:cpx	Textures	Temperature Krogh (2000)/ crust-mantle	Rock Type- (Xenolith size: cm)	Notes
B-12	garnet			mantle	eclogite/pyroxenite 1*2*0.5	
B-13	diopside augite garnet plagioclase rutile srilankite	60:40		610 crust	garnet plagioclase pyroxenite 8*5*5	
B-3	augite pigeonite garnet ilmenite rutile sulfides	80:20		716 crust	garnet pyroxenite 2*1*1	-barite -chlorapatite $Ca_5(PO_4)_3Cl$ associated with rutile w/ ilm rim
B-4	diopside garnet	60:40	granoblastic	821 mantle	garnet pyroxenite 5*3*6	

B-9	diopside augite garnet rutile sulfides	40:60	granoblastic	775 mantle	pyroxenite 5*5*4	-lots of sulfide inclusions between grain boundaries -perrierite-(Ce/La) -Pb oxide -barite
M-10-5	diopside garnet	70:30	granoblastic	585 crust	garnet pyroxenites 2*1*1	
M-12	garnet			crust	eclogite/pyroxenite 1*0.5*0.5	
M-16	garnet			mantle	eclogite/pyroxenite 1.5*1*0.5	
M-18	garnet			mantle	eclogite/pyroxenite 1*1*0.5	
M-19A	garnet diopside rutile	40:60		850 mantle	garnet pyroxenite 4*4*6	-rutile with jeppeite rim -Ti-rich andradite seen on outer rims of rutile (associated with lamprolites)
M-19B	garnet diopside rutile	30:70		915 mantle	garnet pyroxenite 3*3*4	-perovskite rims on rutile -jeppeite -rutile surrounded by Ti-andradite
M-1	garnet			crust	eclogite/pyroxenite 4*2*0.5	
M-2	garnet diopside rutile ilmenite jeppeite	40:60		738 mantle	garnet pyroxenite 4*2*10	-perovskite
M-2B	diopside garnet rutile perovskite	30:70		1026 mantle	garnet pyroxenite 1*1*0.5	

	priderite jeppeite freudenbergite $Na_2Ti_6O_{13}$ magnetite (very small)					
M-4	garnet			mantle	eclogite/pyroxenite 0.5*0.5*0.5	
M-5	diopside garnet			712 mantle	garnet pyroxenite 2*1*1	
R-1	garnet			mantle	eclogite/pyroxenite 1*1*0.5	
R-2-4	diopside garnet rutile picotite (chromian spinel) (low total) sulfides	60:40		762 mantle	garnet pyroxenite 2*4*6	-lots of sulfides -rutile with perovskite rim -zircon -barite -jeppeite found in rim of ilmenite
R-5	diopside garnet			732 mantle	garnet pyroxenite 0.5*0.5*0.5	

that are most likely the product of an unusual metasomatic melt, of possible lamproitic affinity, producing a complex Na-K-Ti rich metasomatic mineral assemblage (discussed in Chapter 4).

2.3.2 Mineral chemistry - major elements

Following petrographic characterization samples were analysed via EPMA for mineral major element chemistry in individual grains from the xenoliths, mantle xenocrysts and heavy mineral kimberlite concentrate (Table 1 and 2; Appendix A).

2.3.2.1 Peridotite mineral chemistry

Cr-pyrope garnet

Garnets are grouped according to compositional characteristics using the Grütter et al. (2004) classification scheme that discriminates using their Ca-Cr systematics (Figure 2.6). Four of the 14 peridotites contained garnet, one sample containing harzburgitic (G10D) garnet that gives a minimum Cr-saturation pressure of 4.7 GPa using the P_{38} geobarometer (38 mW/m^2 model geothermal gradient; Grütter et al. 2006). The remaining three samples contain lherzolitic (G11) garnets plotting within the G9 CaO-Cr_2O_3 space, including a garnet from a metasomatised dunite (olivine Mg# 90.7). Of the garnets picked from the kimberlite concentrate, 51 grains (18 %) are peridotitic. Of these, 98 % are lherzolitic, in two distinct groups according to the Grütter et al. (2004) subdivisions ("on-craton" 31 % lower Ca/Cr and "off-craton" 67 % higher Ca/Cr). Almost all of the garnets falling in the "on-craton" field have high Ti and classify as G11 excluding one that classifies as G1 Low-Cr megacryst. One garnet classifies as wehrlite (G12).

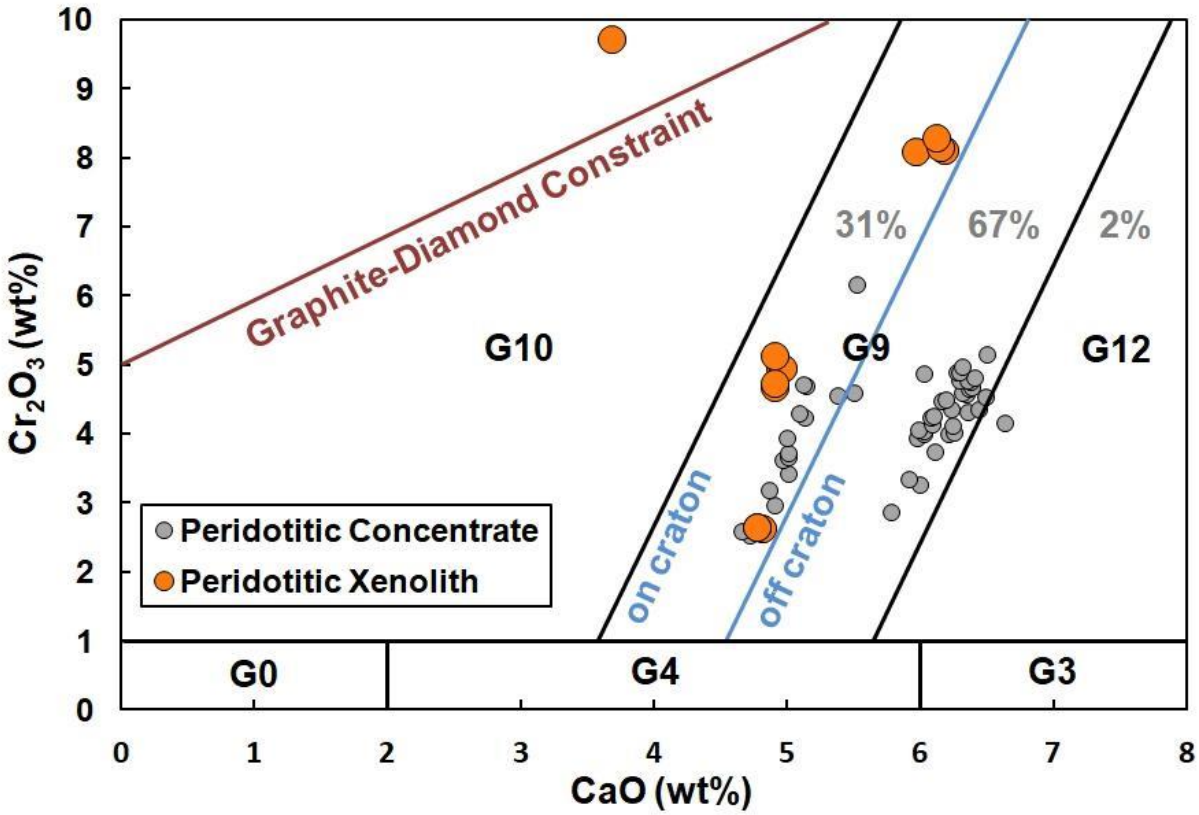

Figure 2.6 Cr-Ca garnet classification plot (Gr tter et al. 2004) of all analyses of Darby xenolith and concentrate garnets with Cr_2O_3 ≥ 1.00 wt%. Xenolith analyses (orange circles, n = 12) and concentrate analyses (grey circles, n = 51).

Olivine

Fresh olivine within the peridotite xenoliths is scarce due to serpentinization and varying levels of carbonation. Olivine compositions were measured from eleven peridotite xenoliths, giving a median Mg# of 92.5, with upper and lower quartiles of 92.8 and 91.3 respectively, very similar to the median for cratonic peridotites worldwide (Pearson and Wittig 2014) and slightly more depleted than peridotites from Somerset Island (north central Rae Craton), and the North Atlantic and Slave Cratons (Figure 2.7A). In addition to the xenoliths, olivine from macrocryst cores sampled in thin section (n = 331) and concentrate (n = 201) were analyzed and those of mantle origin were distinguished based on their high Ni-Mg# relationship (Figure 2.8). The cluster of high Ni-Mg# (0.3 to 0.42 wt% Ni; > 91 % Mg#) concentrate olivines gives a median Mg# of 92.2, overlapping the olivines from the peridotite xenoliths. The general trend of all olivine data is positive, showing a increasing NiO content with a increasing Mg#, differentiating mantle olivines, with higher Mg# from those crystallizing from a kimberlitic melt. Most of the xenoliths are similar to the pristine mantle samples of Foley et al. 2013 (Figure 2.7B), although some samples have increased Ti with one sample enriched in Ca and another enriched in both Ti and Ca. The large scatter observed in Figure 2.7B suggests that the "kimberlitic field" may be larger than suggested by Foley et al. (2013). Although kimberlite Ti-metasomatism appears to be a common feature of the phases sampled (i.e., garnets with high Ni and Ti) by the Darby kimberlites, in a number of samples, the metasomatic agent was lamproite based on other observations, such as the occurrence of jeppeite and priderite - phases only ever observed in lamproites. A small proportion of olivines overlap with the compositions of those from lamproites using the Foley et al. (2013) classification (Figure 2.7B) but the Mediterranean

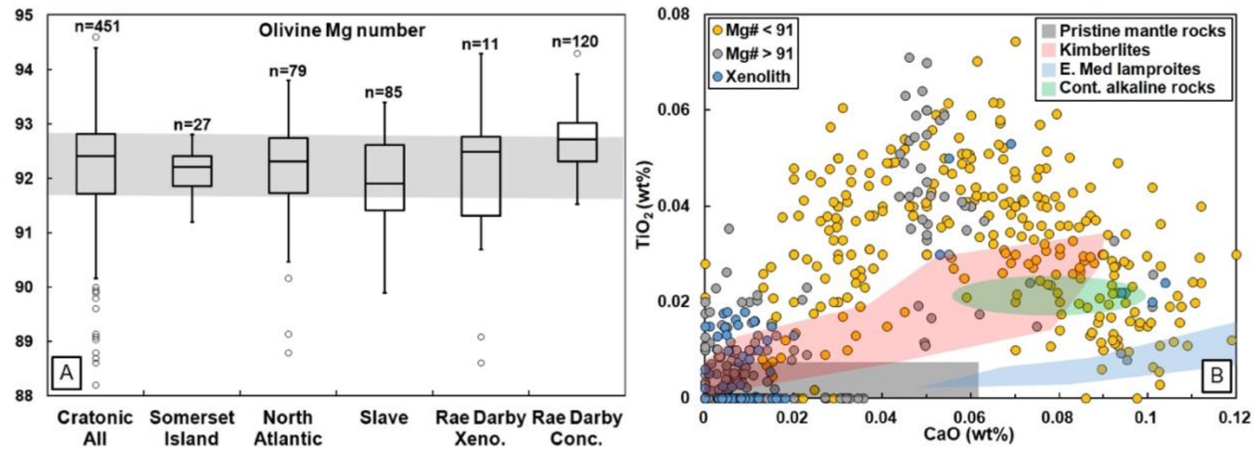

Figure 2.7A Box and whisker plot of 100 * Mg# for mantle olivines. Number of samples (n) given for each category. Data from Pearson and Wittig (2008). **B** Ti-Ca plot for all olivine measured. Fields of various rock types taken from of Foley et al. (2013).

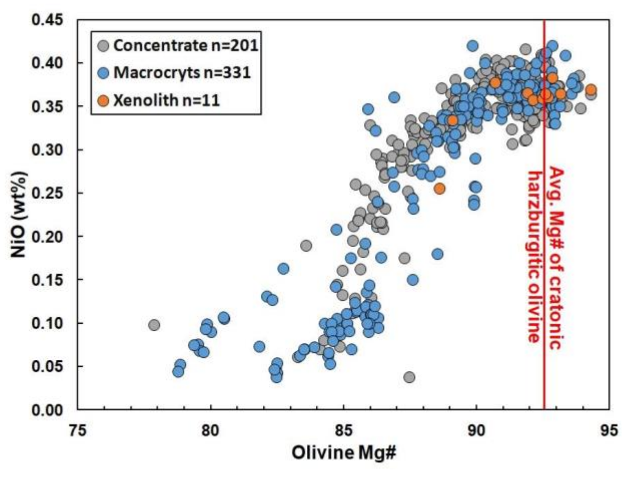

Figure 2.8 Olivine Mg# vs. NiO (wt%) for all olivine analyses from Darby kimberlites. Red line is average Mg# of cratonic harzburgitic olivine 92.6 (Pearson and Wittig 2014).

lamproites analysed to create this field are regarded as chemically distinct from the lamproites intruding cratons (Prelević et al. 2008).

Pyroxenes

Peridotite xenoliths with abundant pyroxenes are scarce, however 10 of the 14 peridiotites studied contain pyroxene. Three samples contain both clinopyroxene and orthopyroxene, with one sample containing only orthopyroxene. The remaining six samples contain only clinopyroxene. Additional clinopyroxene (n = 148) and orthopyroxene (n = 2) were analyzed in concentrate grain mounts. Macrocrystic pyroxenes were rare in the kimberlite with clinopyroxene (n = 9) and orthopyroxene (n = 3). Clinopyroxenes from the peridotite xenoliths are diopsides but did not pass the compositional filters of Grütter (2009) for use in thermobarometry. Likewise, seven clinopyroxene grains derived from mineral concentrate were classified as garnet peridotite-derived using the compositional filters of Grütter (2009). These compositions were used for thermobarometry (below).

Spinel

Five peridotite xenoliths contained spinel, which was identified as picotite or chromium spinel. For any given sample spinel compositions are heterogeneous with various amounts of Cr_2O_3, FeO and MgO. Spinel macrocryst analyses via thick section are picotite spinel (n = 43), Fe-rich spinel (n = 9), magnetite (n = 49) and chromite (n = 3). Concentrate analyses resulted in picotite spinel (n = 5), magnetite (n = 221), titanomagnetite (n = 2) and chromite (n = 2). Most of the magnetite, chromite and titanomagnetite occur as reaction rims on ilmenite or other spinel, although some analyses occur as discrete grains observed along grain boundaires.

Ilmenite and other oxides

Six of the peridotites had other oxides present, among them ilmenite, magnetite, perovskite, titanite, chromite, and perrierite. Two of the samples contained ilmenite and most of the perovskite and perrierite occur as reaction rims on ilmenite or spinel, although some discrete grains were observed along grain boundaries, specifically the samples with other oxides and no ilmenite or spinel. Macrocryst analyses via thick section include: ilmenite (n = 91), with perovskite (n = 25) analyses occurring as complex reaction rims on the ilmenite. Concentrate analyses via grain mount include ilmenite (n = 62) and perovskite (n = 2). All ilmenite macrocryst and concentrate data are shown in Figure 2.9, the solid line denotes kimberlitic ilmenite from non-kimberlitic (Wyatt et al. 2004) with 93 % of 153 grains classifying as kimberlitic.

Amphibole and phlogopite

Four of the peridotites contain amphibole identified by EDS. Four xenoliths contained phologpite identified by EDS, three of which (M-22-1, M-23-1, and one of two xenolith in M-24) based on appearance and composition these rocks were classified as mantle polymict breccias and were not studied in detail.

Sulfides

Sub-micron sulfides were identified by EDS in several samples. However, two peridotite samples contained sulfides large enough for EMPA analyses, all of which were identified as mono-sulfides. Of these they fall to on the Ni+Co rich side of the Fe, S, Ni+Co ternary (Figure

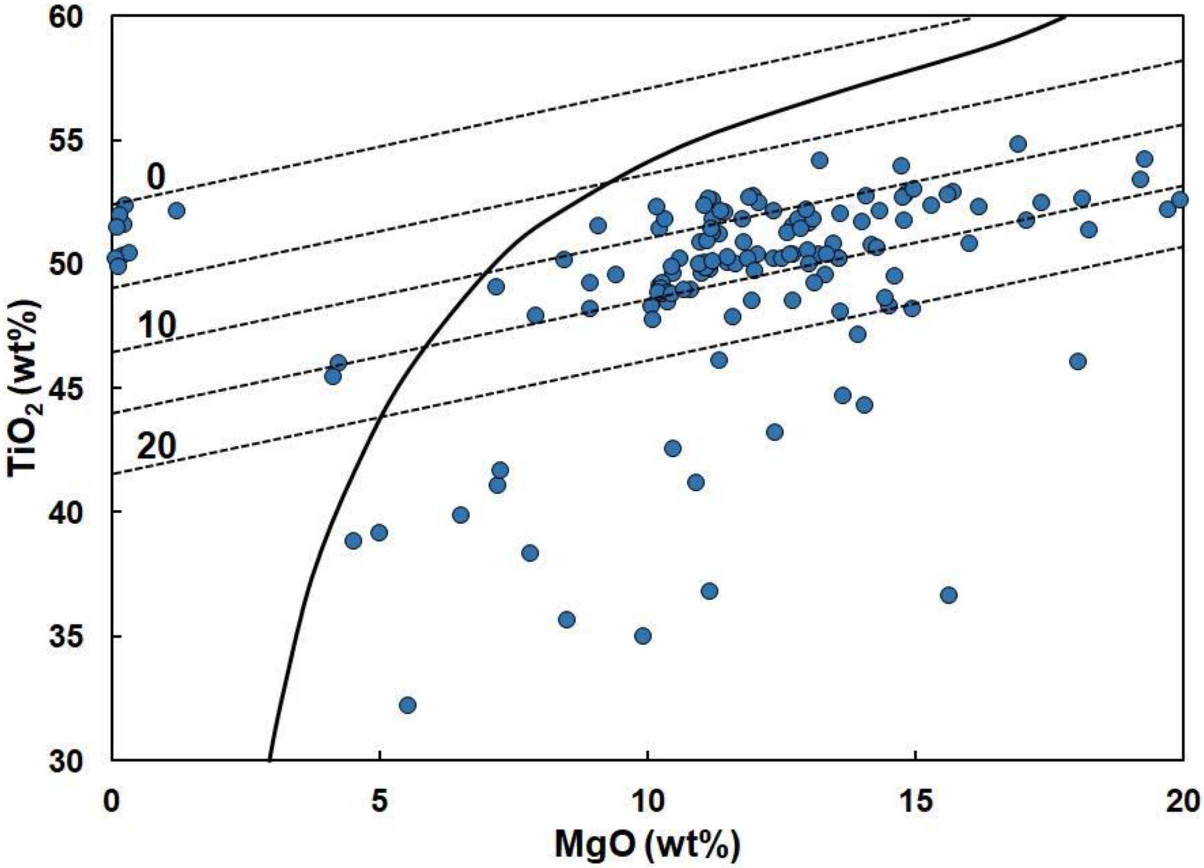

Figure 2.9 All ilmenite macrocryst analyses from Darby kimberlite field displaying ilmenite analyses.

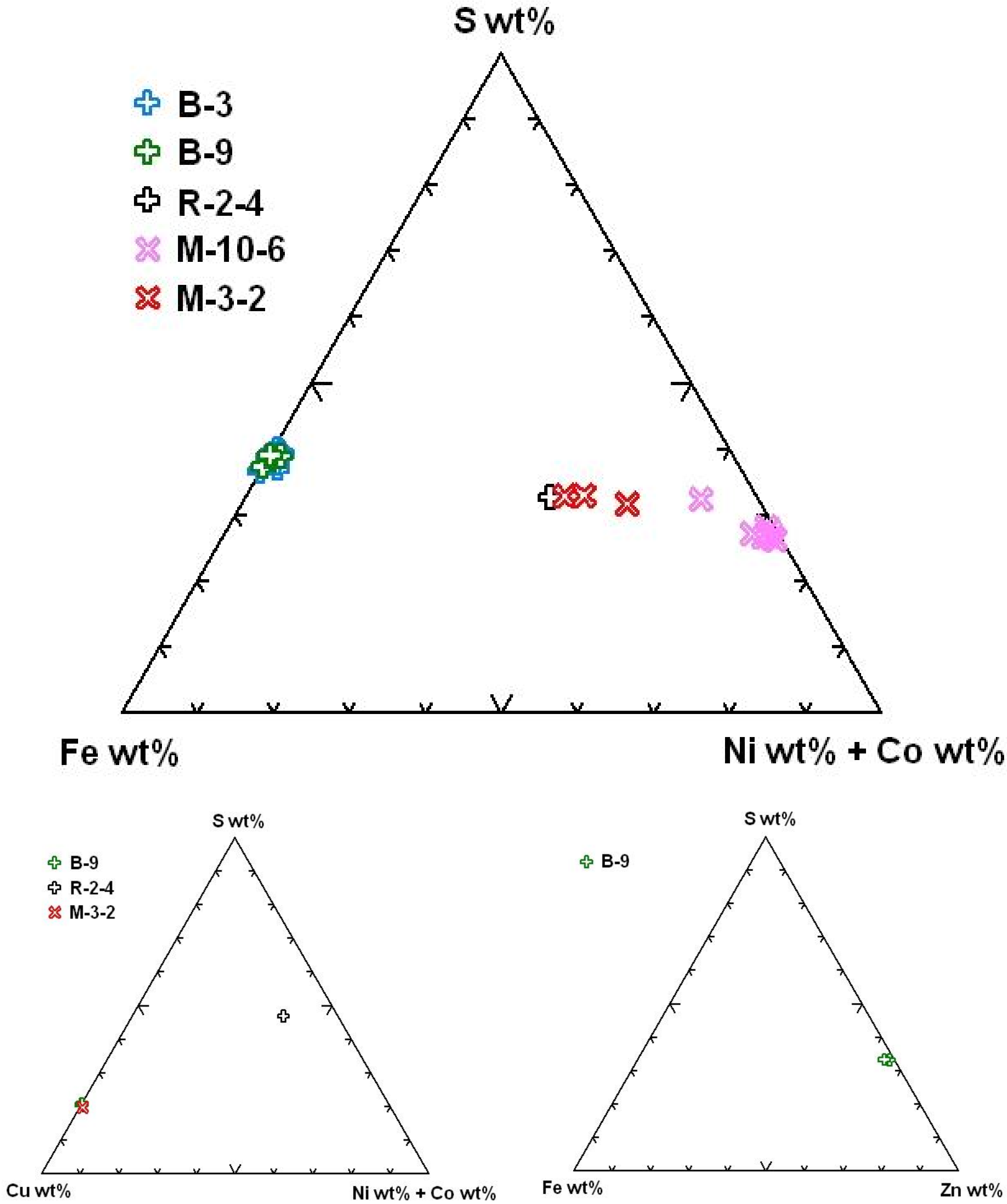

Figure 2.10 Sulfide composition of discrete grains found in peridotites and pyroxenites.

Peridotites: M-10-6, M-3-2; Pyroxenites: B-3, B-9, R-2-4.

2.10), with M-10-6 being rich in Ni+Co and M-3-2 having a slightly larger Fe content. In addition, one of the sulfides in M-3-2 was identified as CuS.

Other

Other notable minerals identified in the peridotites include: three samples with calcite, two with apatite and one with barite. In one peridotite (M-3-2B) monazite and columbite were observed. In addition, apatite macrocrysts are recorded in the kimberlite from the float trend from Sky to Stealth, however xenocrysts in thin section were not studied in great detail thus apatite may be present in the other localities sampled.

2.3.2.2 Pyroxenite mineral chemistry

Low-Cr garnet

Among the xenoliths identified as eclogite in the field, the low-Cr garnets in these lithologies are pyrope-almandine in composition (28 to 65 % pyrope), with less than 30 % grossular component that is slightly more elevated at the more almandine rich end of the array (Figure 2.11). Of these low-Cr xenolith-derived garnets, 53 % are G4 (low-CaO pyroxenite/eclogite; < 6 % CaO), with the remainder being G3 (high-CaO eclogite; Figure 2.12A). This split contrasts with the pyroxenite/eclogite division made on the basis of their pyroxene chemistry suggesting that the Cr-Ca garnet classification for pyroxenites requires refinement or the pyroxene chemistry classification needs refinement.

Of the concentrate-derived garnets (n = 233), 82 % classify as low Cr, with Cr_2O_3 < 1 %. These garnets show a slightly higher ratio of G3 garnets (63 % of concentrate versus 47 % of xenoliths; Figure 2.12B) but nonetheless confirm the high proportion of pyroxenites in the

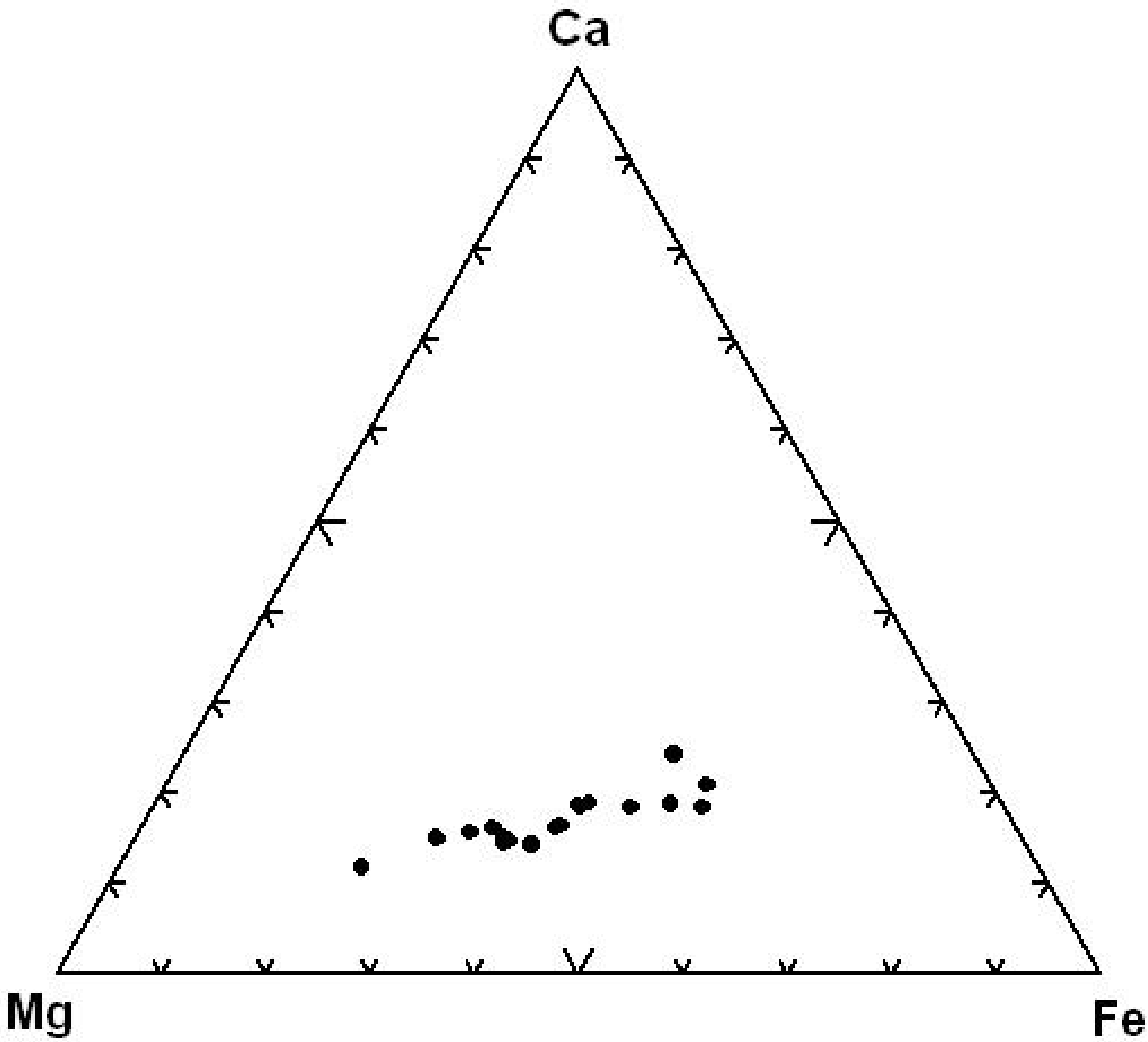

Figure 2.11 Mg-Fe-Ca garnet ternary diagram for all low-Cr (Cr_2O_3 < 1 wt%) xenoliths from Darby ranging from pyrope to almandine and are relatively Ca poor.

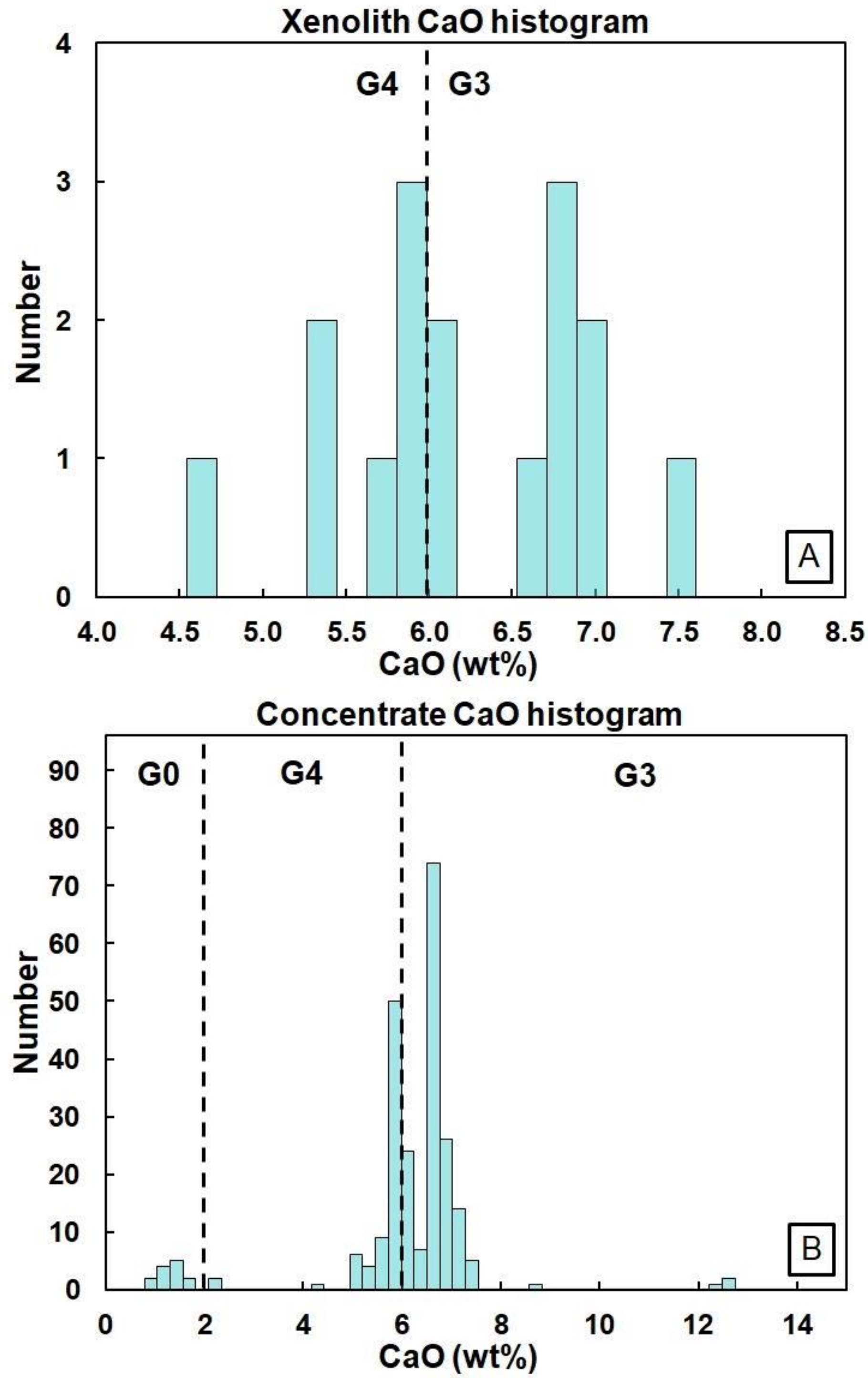

Figure 2.12 Histograms of garnet analyses $Cr_2O_3 < 1$ wt% for **A** Xenoliths and **B** concentrate. No Ca-rich xenoliths, 53% (10/19) xenoliths classify as G4. Garnet $Cr_2O_3 < 1$ wt% made up 82% of the garnet concentrate and spans into the G0 unclassified 5%, G4 pyroxenitic/eclogitic is 32%, G3 eclogitic is 63% with some high Ca samples.

mantle and crust sampled by Darby kimberlites. TiO_2 and Na_2O contents of garnets from the xenoliths and concentrate are uniformly low (< 0.20 and < 0.05 wt% respectively; Figure 2.13) plotting away from the diamond inclusion field of Gurney and Zweistra (1995), and therefore most likely are from shallow depths outside the diamond stability field. However, this Na content in garnet is bulk-rock dependent and these rocks may have come from a protolith with low Na and thus may not be limited to depths outside the diamond stability field.

Traditionally, to classify these low-Cr garnets as having a mantle or crustal origin, the approach of Schulze (2003) has been employed, which utilizes Ca# and Mg# as variables. This approach classified all the Darby low-Cr garnet-bearing xenoliths as being mantle-derived and assigns 82 % of our low-Cr garnet concentrate as mantle-derived. The majority of the pyroxenites are primarily bimineralic with respect to garnet and clinopyroxene (~ 60:40 modal abundance, respectively, ± trace rutile); however, one sample was identified petrographically as a plagioclase-bearing garnet-pyroxenite. This petrographic assessment classified this xenolith as crustal in origin but conflicts with the Schulze (2003) classification. The recent Hardman et al. (2018a) graphical classification scheme reduces the failure rate of crustal garnets by employing log-normalised Pearce element ratios of Ti and Mg/Fe. Using the graphical "crust-mantle" major element discrimination method of Hardman et al. (2018a; Figure 2.14A) on the Darby G3/G4 xenolith and concentrate garnets classifies 47 % of 19 xenoliths and only 23 % of the 233 grains as mantle in origin (Figure 2.14B), indicating that many may have been derived from plagioclase pyroxenite or lower-crustal garnet-bearing lithologies. This interpretation is consistent with the presence of plagioclase in one of the pyroxenites, which is correctly classified as crustal by the Hardman et al. (2018a) scheme. However, the majority of xenoliths fall close to the decision

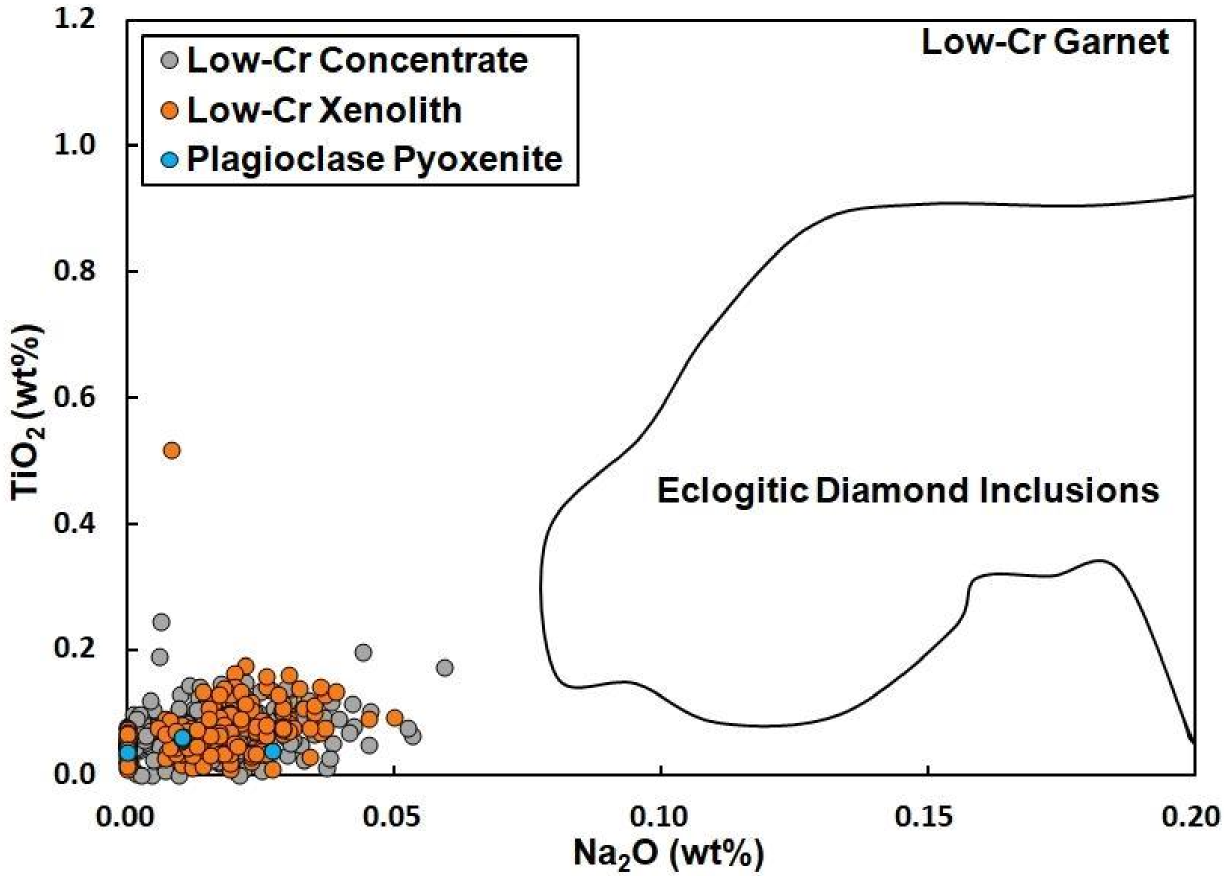

Figure 2.13 TiO_2 vs. Na_2O for Cr_2O_3 < 1 wt% garnets. Darby garnets are relatively low Na-Ti plotting away from the eclogitic diamond inclusions of after Gurney and Zweistra (1995).

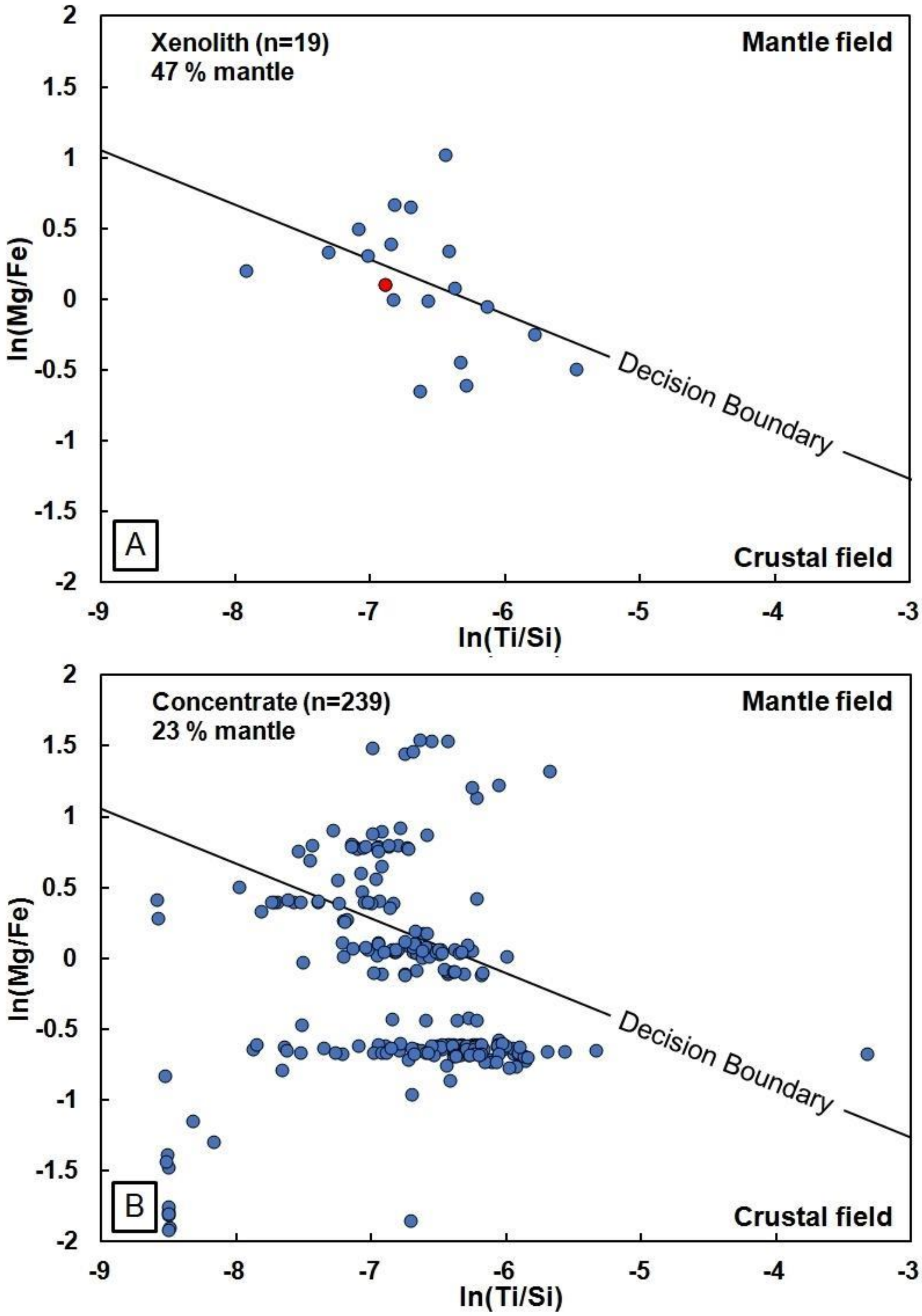

Figure 2.14 Graphical approach for determination of crustal and mantle-derived low-Cr garnets graphical approach modified after Hardman et al. (2018a) for **A** Xenoliths **B** Concentrate. Note: red sample in xenolith plot is plagioclase pyroxenite.

boundary signifying that these samples have a higher probability of misclassification. Therefore, the logistic regression (LR) “crust-mantle” major element discrimination method of Hardman et al. (2018a) was utilized on the Darby G3/G4 concentrate garnets as this scheme further reduces failure rate when compared to the graphical approach. Utilizing this LR approach a larger proportion, 28 % of the 233 grains, classify as mantle in origin (Table 1; Appendix A), indicating that the others have been derived from plagioclase pyroxenite or lower-crustal garnet-bearing lithologies. This interpretation is consistent with the presence of plagioclase in one of the pyroxenites, which is correctly classified as crustal in this LR scheme. However, using an enhanced major and trace element discrimination scheme, Hardman et al. (2018b, submitted) have shown that Eu-anomalies and Sr-concentrations are valuable in classifying mantle garnets and increase classification success rates of low- Cr crust and mantle garnets. The method of Hardman et al. (2018b, submitted) is utilized to classify “crust-mantle” garnets from xenoliths (below).

Pyroxenes

Twelve of the 19 “eclogites” are classified as pyroxenite sensu stricto on the basis of their CaTs versus jadeite (calculated via WinPyrox; Yavux 2013) contents in clinopyroxene, with all samples having low CaTs at < 19 % jadeite (classified as diopside-bearing pyroxenites). Three samples contained clinopyroxene grains of augite composition (B-13, B-9 and B-3) and one sample had pigeonite (B-3). When classified on the basis of Ca-Tschermak’s versus jadeite contents (Figure 2.15), the clinopyroxene in all samples have low jadeite (< 19 %) and low to moderate Ca-Tschermak’s (< 17.5 %). Sample B-3 has grains plotting in the “high-pressure liquidus clinopyroxene” field, while M-2B has grains falling in the Beni Bousera pyroxenites

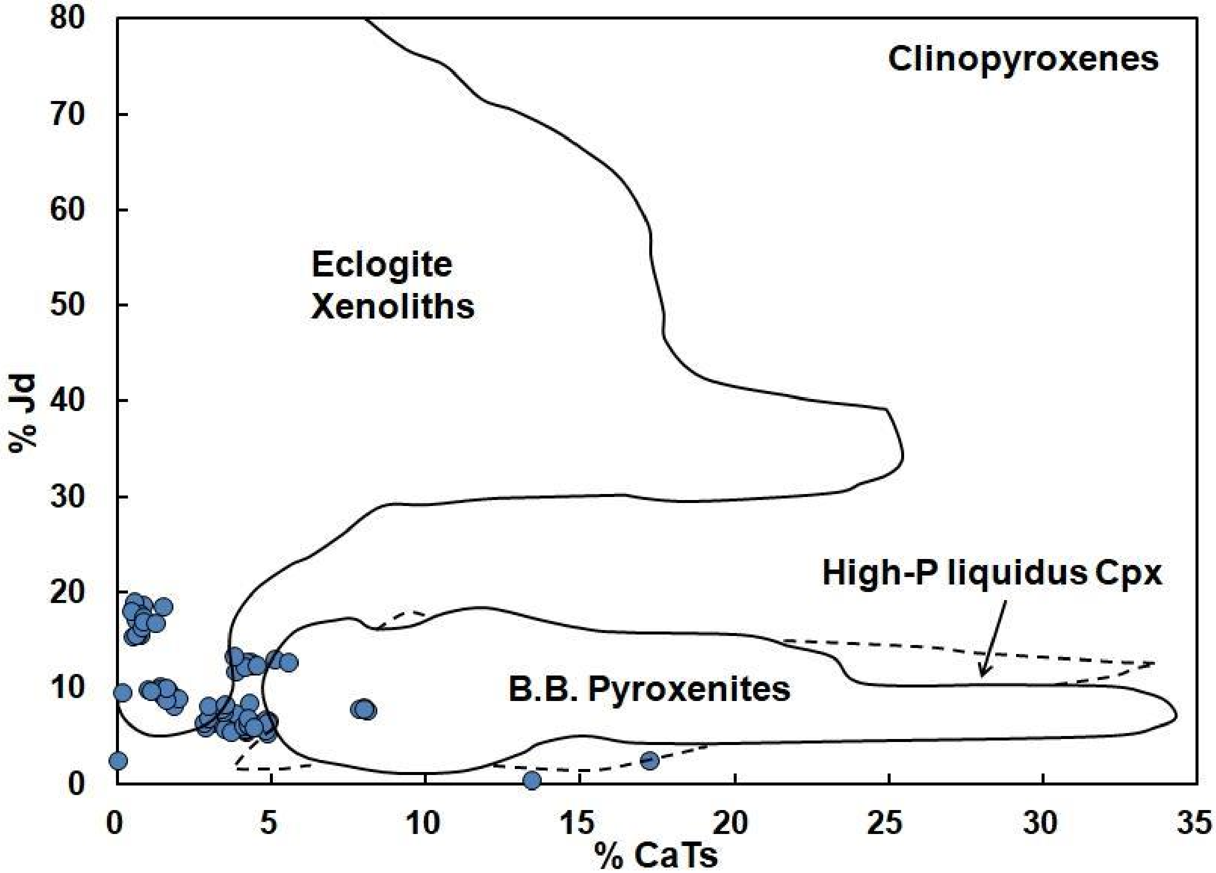

Figure 2.15 Jadeite and Ca-Tschermak's molecular contents of clinopyroxenes from Low-Cr (< 1 wt%) xenoliths compared with Beni Bousera clinopyroxenes (modified after Pearson and Nixon 1996) and high pressure, liquidus clinopyroxenes crystallized experimentally (Thompson 1974; Eggins 1992). Field labeled B.B. Pyroxenites is the range of clinopyroxenes from Beni Bousera (Kornprobst et al. 1990), blue circles are clinopyroxenes from low-Cr garnet xenoliths at Darby.

field. The majority of the data falls between the Beni Bousera eclogite and pyroxenites fields suggesting a new graphical method of differentiating pyroxenites and eclogites needs to be addressed. Thus, based on the low jadeite contents of their clinopyroxenes, all the “eclogites” identified in the field at Darby should be referred to as pyroxenites and will be referred to as such from this point on.

Rutile

Of the 19 pyroxenite xenoliths chosen for study, seven contained rutile. The rutile observed is relatively pure with > 98 wt% TiO_2 and < 0.5 wt% Cr_2O_3. All except two grains from the same sample plot in the mantle+crustal field (0.4 wt% > Cr_2O_3 wt%; Malkovets et al. 2016) showing that this cut off is ineffective in classifying rutile as crustal or mantle, at least for the Darby pyroxenites.

Other oxides

Of the seven pyroxenites that contained rutile, most of the rutile grains have exsolution or reaction rims of ilmenite. However, two samples contained rutile with zircon inclusions. One sample (B-13) contained srilankite-$(Ti,Zr)O_2$ as ~ 5 μm discrete grains on the edge of a rutile.

Sulfides

Sub-micron sulfides were identified by EDS in several samples, with three pyroxenite samples containing grains large enough for EPMA. Two of the samples contained sulfides falling on the Fe-rich side of Fe, S, Ni+Co ternary (Figure 2.10) with one sample containing a sulfide with a compoisiton approaching those of the peridotitic sulfides, i.e., being richer in Ni+Co.

Pyroxenite (B-9) contained several CuS and ZnS crystals, while one of the pyroxenites (R-2-4) contained (Fe, Cu)S and copper metal.

2.3.3 Mineral rare earth element chemistry

Trace element analyses of garnet, diopside, olivine and rutile are shown in Table S3, S4, S5, and S6; Appendix A, respectively. Reported ppm elemental abundances for REE are averaged for multiple spot analyses on the same grain.

Cr-pyrope garnet

Two of the garnet-bearing peridotites display "sinusoidal" garnet REE_N patterns and of the sample set, the harzburgitic (G10) garnet has the most-pronounced "sinusoidal" pattern (Figure 2.16). The other two garnet peridotites have garnets that are light rare earth element (LREE) depleted with La < CI chondrite and are heavy rare earth element enriched (HREE) (~ 10 x CI chondrite). Of the concentrate garnets 63 % (n = 33) show weakly "sinusoidal" patterns. These garnets are dominated by garnets that plot within the "off-craton" portion of the lherzolite (G9) field. The remaining 27 % (n = 14) of the REE_N patterns show the typical $LREE_N$ depleted, $HREE_N$ enriched patterns. These garnets class dominantly as "on-craton" lherzolites (G9; Grütter et al. 2004). However, 4 % (n = 2) had slightly $LREE_N$ enriched patterns at ~ 10 x chondritic and 6 % (n = 3) had slightly $HREE_N$ enriched patterns 10 x chondritic. The Y vs Zr plot (Figure 2.17) shows that the majority of garnets fall along the "Melt Metasomatism" trend dominated by lherzolitic garnets (Stachel and Harris 2008). However, two samples have high Zr and fall right of the "Low-T Phlogopite Metasomatism" trend which is dominated by harzburgitic garnets. The two samples with high Zr are also the samples that show "sinusoidal" REE_N patterns. These

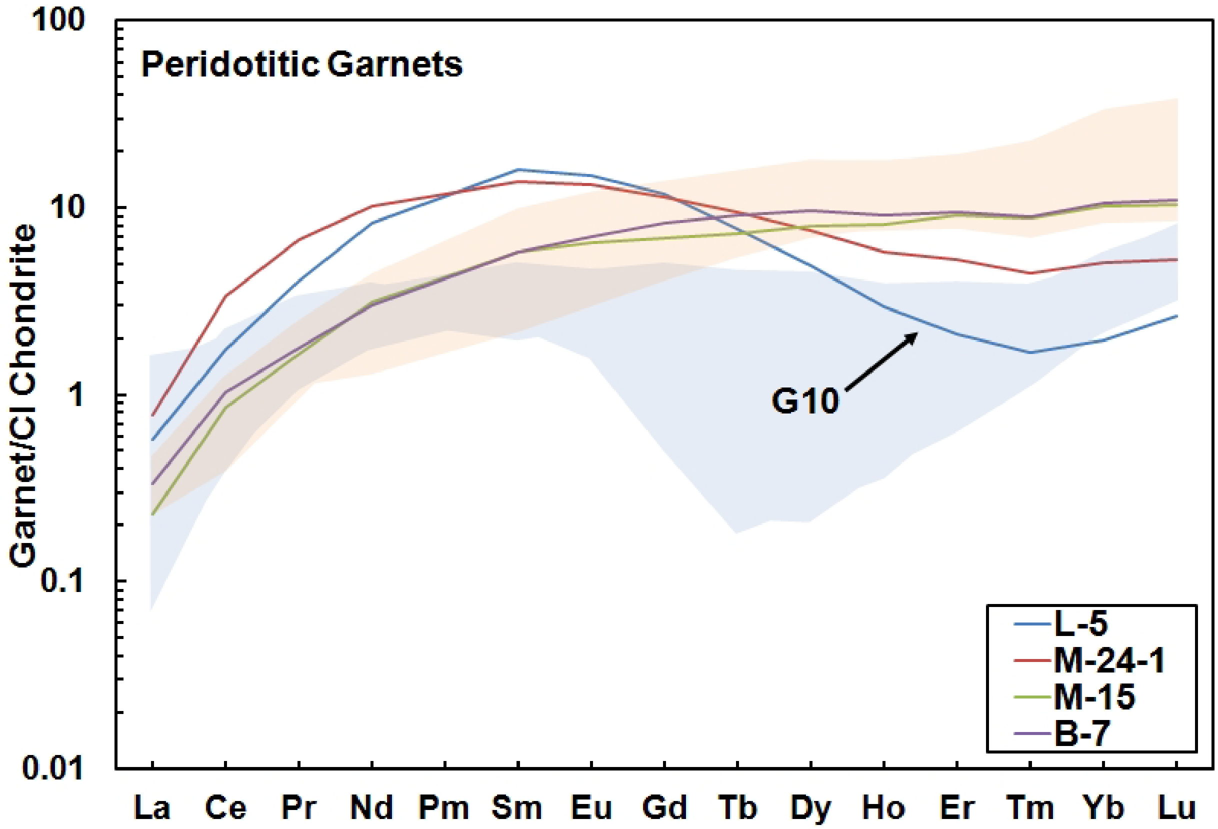

Figure 2.16 REE_N mineral plots for garnet peridotites with Cr_2O_3 > 1 wt%, where lines are for xenoliths and two fields showing patterns observed in concentrate. CI Carbonaceous chondrite normalizing values from McDonough and Sun (1995).

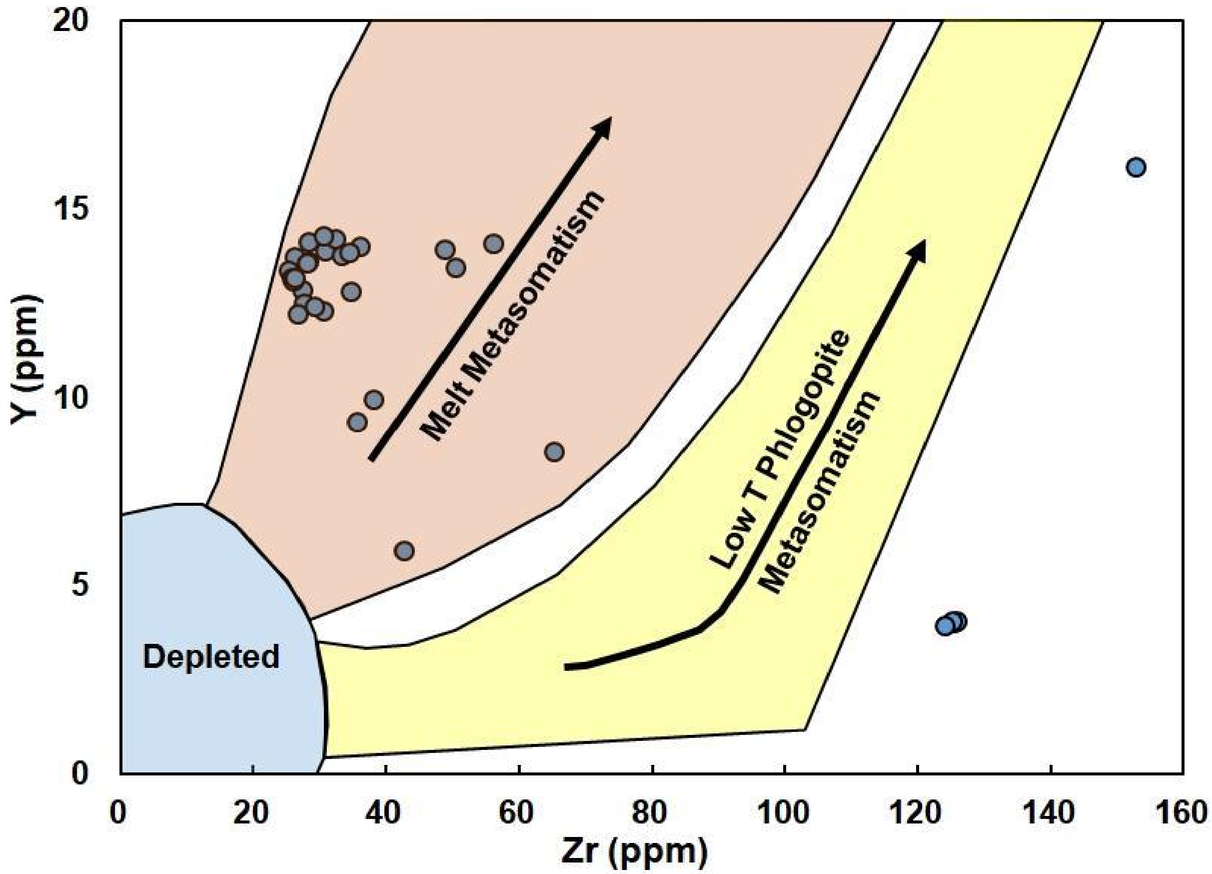

Figure 2.17 Y versus Zr (wt ppm) for peridotitic garnets from Darby. Diagram modified from Griffin and Ryan (1995), garnets found in the "depleted" field would be invariably re-enriched in LREE. More intense fluid metasomatism with enrichment in Zr (and negligible addition of Y and MREE–HREE) appears to be characteristic for the harzburgitic paragenesis. Lherzolitic garnets have concurrent addition of Zr and Y (and MREE–HREE).

metasomatic fields of Stachel and Harris (2008) were based on garnet inclusions in diamonds and while the Darby xenoliths follow these rough trends it remains unclear if their interpretations hold true for xenoliths.

Low-Cr garnet

Garnets from the 19 pyroxenitic xenoliths were analysed for trace elements to employ the "crust-mantle" classification of Hardman et al. (2018b, submitted). The median garnet analysis of major and trace elements was used for xenolith classification. Of the nineteen xenoliths, 14 (74 %) classify as mantle-derived. Seven (37 %) are classified as mantle due to positive Eu-anomalies ($2*Eu_N/(Sm_N+Gd_N)$) and/or high Sr-concentrations. This demonstrates the importance of trace element analysis in this data set to correctly classify garnet origin. All of the pyroxenites displaying lamproitic metasomatic mineral assemblages are classified as mantle. The REE_N patterns (Figure 2.18) are typical $LREE_N$ depleted patterns from eclogitic/pyroxenitic garnet with La < CI Chondrite and considerable Lu_N enrichment (~ 100 x CI Chondrite). Of the nineteen samples analyzed, thirteen samples have positive Eu anomalies (Eu/Eu* > 1.00), with all but one classifying as mantle. One highly metasomatized xenolith (M-2B) with the hottest Fe-Mg temperature has a $HREE_N$ depleted with a pattern that appears "sinusoidal," indicating the sample has undergone lamproitic metasomatism resulting in the mineral assemblage of freudenbergite, jeppeite, and priderite.

Olivine

Garnet peridotites with large (> 90 µm) olivine and mantle derived olivine concentrate (Mg# > 91 %) were selected for trace element analysis in hopes to apply the Al-in-olivine

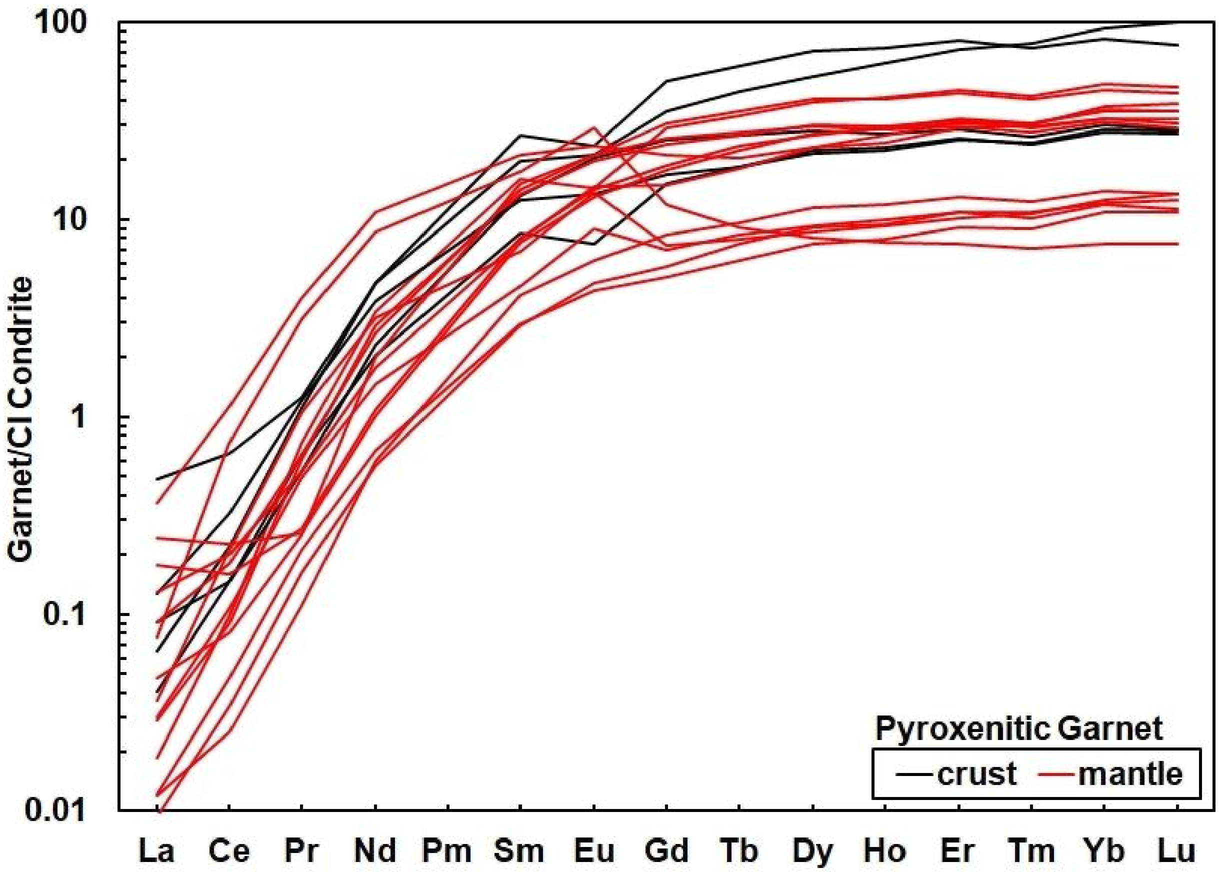

Figure 2.18 REE_N diagram of trace elements in low-Cr garnet xenoliths, CI Carbonaceous chondrite normalized (McDonough and Sun 1995).

thermometer of Bussweiler et al. (2017). Grains were highly fractured and some grains contained inclusions. A total of 43 % of the olivine had Al present below detection limit, resulting in 43 out of 176 analyses being suitable for filtering for garnet or spinel facies using the Al vs V filter (Figure 2.19) of Bussweiler et al (2017). Of the 43 grains filtered, 28 were identified as "garnet facies" and were used for the Al-in-olivine thermometer, with calculated temperatures ranging widely from 785 to 1390 °C.

Clinopyroxene

Of the twelve pyroxenite xenoliths with fresh pyroxene, eight samples had trace elements analyses completed on diopside. The REE_N patterns (Figure 2.20) are $LREE_N$ enriched patterns typical of eclogitic/pyroxenitic pyroxene with La < ~100 x CI Chondrite and Lu < CI Chondrite. Of these, pyroxenes in seven samples have positive Eu anomalies including the plagioclase pyroxenite.

Three clinopyroxenes, two peridotites and one macrocryst share similar REE_N patterns (Figure 2.21), with $LREE_N$ ~ 10 x CI chondrite. A positive anomaly in Eu and Dy is observed in two of these samples. Clinopyroxenes from concentrate were broken into four groups (Figure 2.22). The main group (66 %) of the grains has $LREE_N$ with ~ 10 to 100 x CI chondrite abundances, the second dominant group (29 %) has negative Eu anomalies, the third group (10 %) is $LREE_N$ enriched with flat to slightly elevated $HREE_N$ ~ 1 to 10 x CI chondrite with an increase in the $HREE_N$ elements (Yb and Lu). The last group consists of two grains that appear to be derived from metasomatic agents.

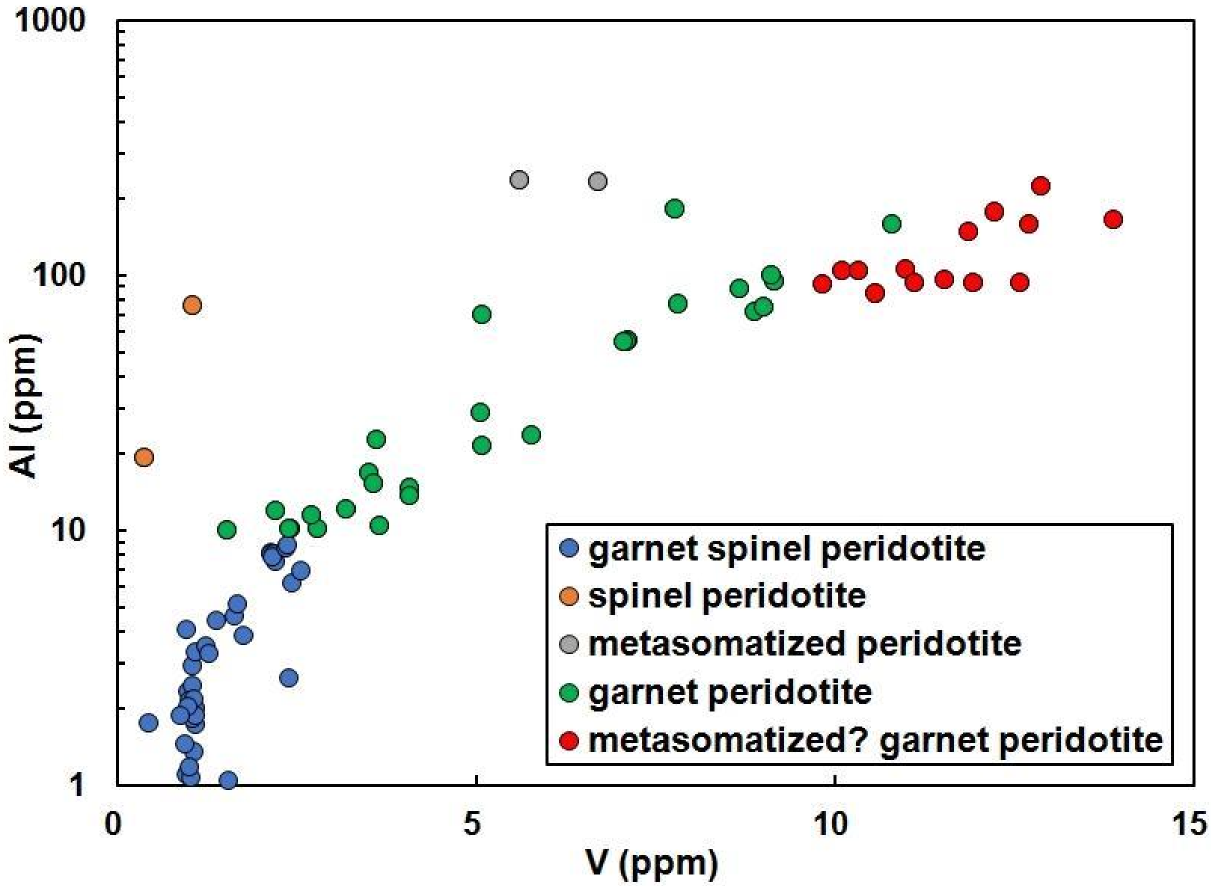

Figure 2.19 Trace element analyses for olivine xenoliths and concentrate with Mg# > 91. Discriminant of Al (ppm) vs. V (ppm) outlined by Bussweiler et al. (2017) used to identify garnet peridotites which were used for olivine thermometry.

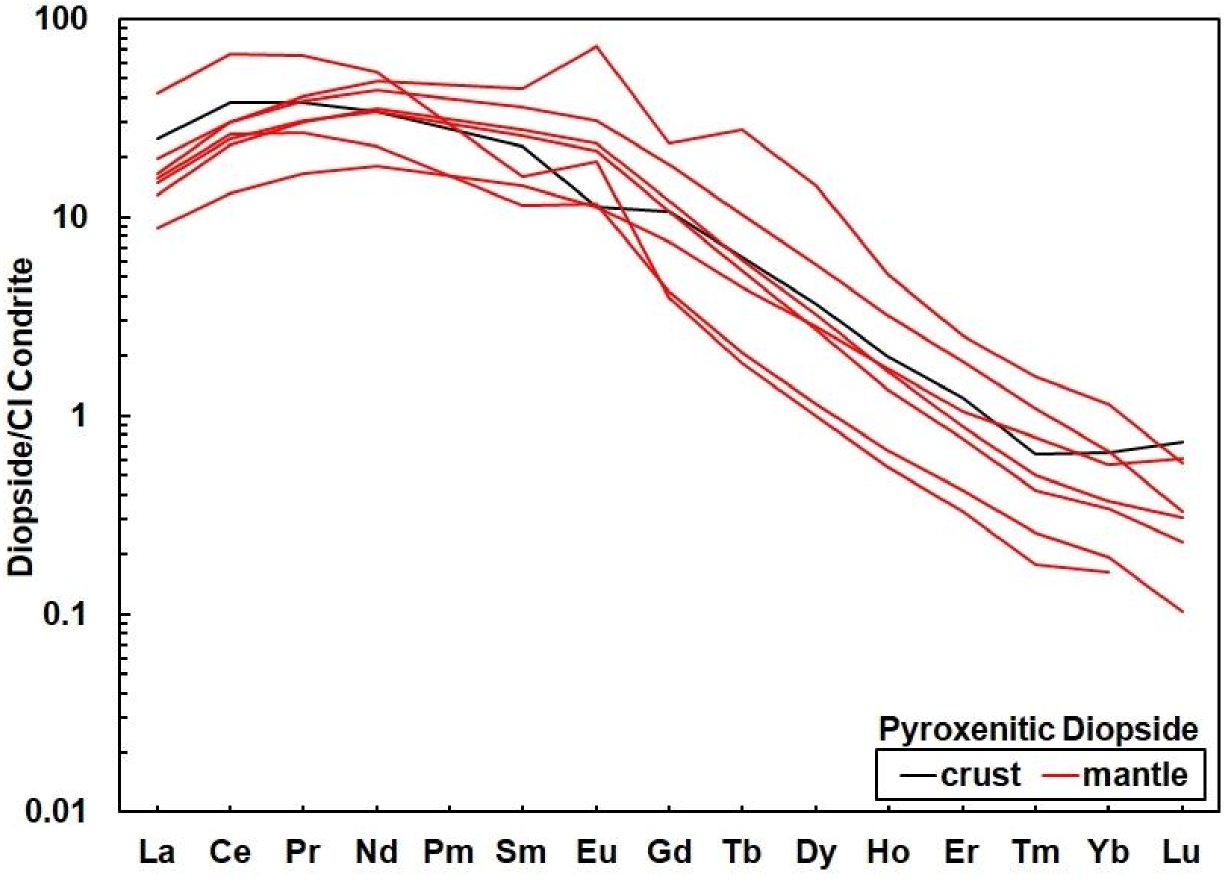

Figure 2.20 REE_N diagram of trace elements in clinopyroxene of pyroxenites, CI Carbonaceous chondrite normalized (McDonough and Sun 1995).

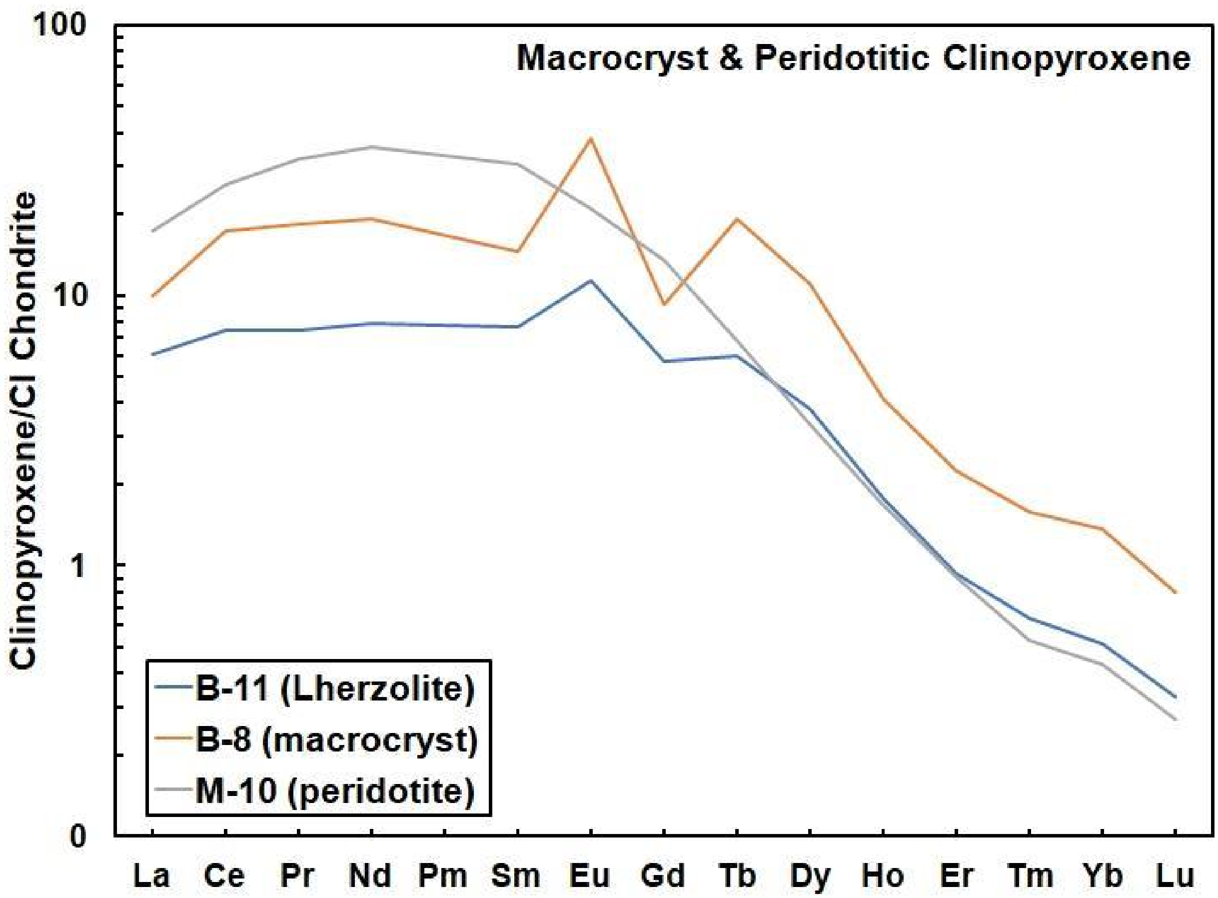

Figure 2.21 REE_N diagram of trace elements in clinopyroxenes from lherzolites and macrocryst, CI Carbonaceous chondrite normalized (McDonough and Sun 1995).

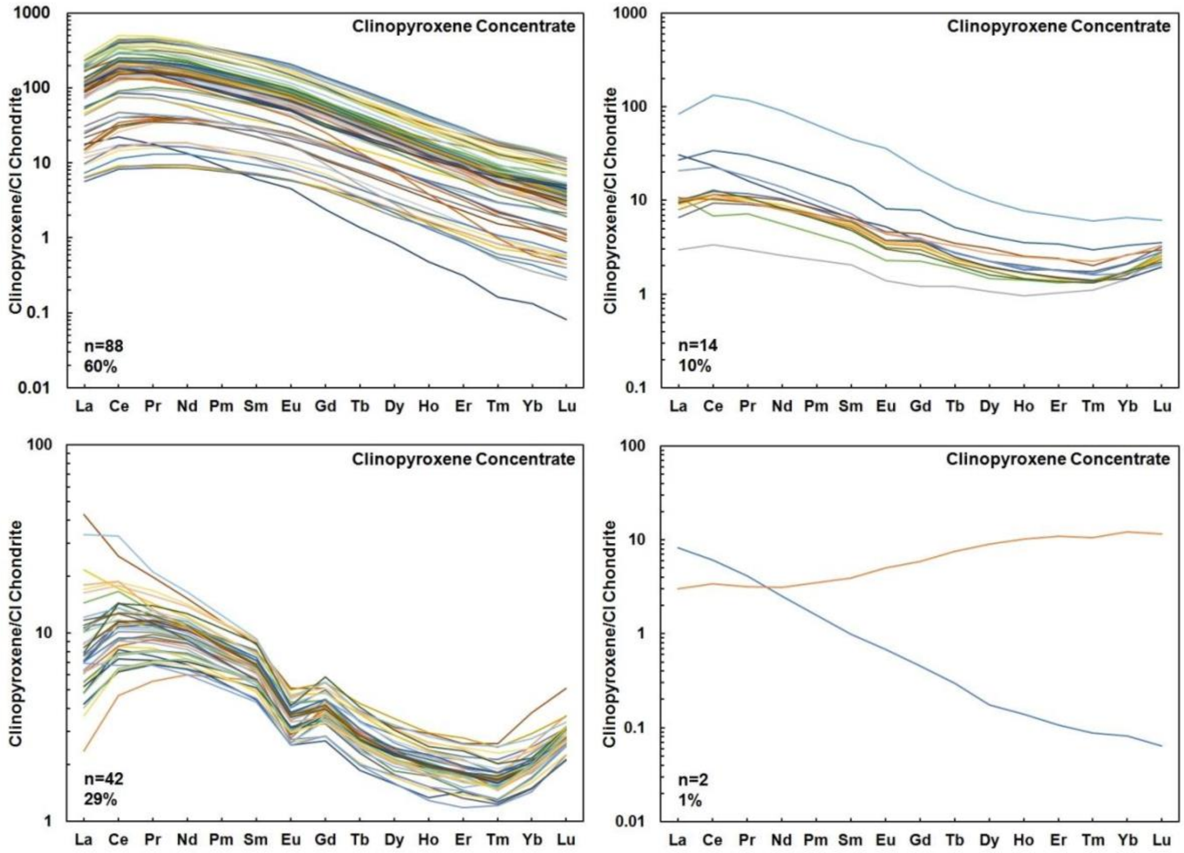

Figure 2.22 REE_N diagram of trace elements in clinopyroxene from concentrate sub-divided on the basis of the shape of their REE patterns, CI Carbonaceous chondrite normalized (McDonough and Sun 1995).

Rutile

Seven of eight rutile bearing pyroxenites had trace element analysis completed on them. The majority of the rutile analyzed has subchondritic Nb/Ta (< 19.9; Münker et al. 2003; Weyer et al. 2002), with three samples containing only subchondritic Nb/Ta while the remaining four samples contained some rutile with superchondritic Nb/Ta (> 19.9).

2.3.4 Whole-rock major elements

Peridotite whole-rock major element trends show the effects of some carbonation/host rock infiltration in trends of high CaO contents at low to moderate Al_2O_3 (Table 7; Appendix A). Therefore, we rely on bulk rock Al_2O_3 as the most robust indicator of whole rock major element depletion (Figure 2.23). The Darby peridotites are low in Al_2O_3 (median ~ 0.75 wt%), somewhat lower (more depleted) than the peridotite xenoliths from the eastern portion of the Rae Craton (Pelly Bay & Repulse Bay; Liu et al. 2016). These low Al_2O_3 contents are very comparable to typical cratonic mantle peridotite compositions (Figure 2.23).

2.4 Discussion

2.4.1 A geotherm for the west central Rae Craton and mantle sampling

Darby peridotite xenoliths are too altered to perform multiphase geothermobarometry. Instead, garnet-peridotite-derived clinopyroxenes, from kimberlite heavy mineral concentrate were used, (values used to construct the geotherm Table 8; Appendix A). A total of 148 clinopyroxenes from concentrate had the Grütter et al. (2009) and Ziberna et al. (2016) filters applied to them. Of these only ten passed the Grütter et al. (2009) and two passed the Ziberna et al. (2016) filter. Thus, the Grütter et al. (2009) filter was selected for employment, however three

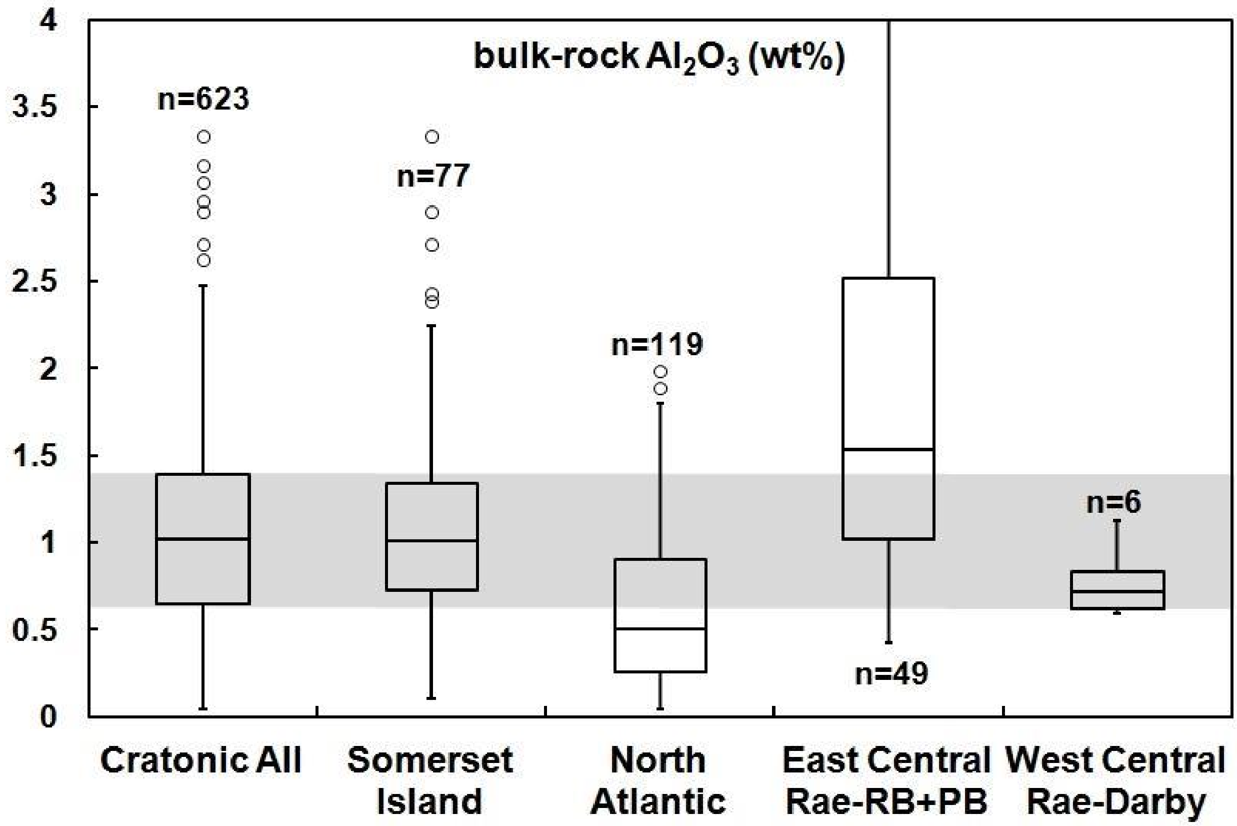

Figure 2.23 Box and whisker plots of bulk-rock Al_2O_3 of peridotites from a variety of localities. Number of samples (n) given for each category. Data from Pearson and Wittig (2014).

of the ten gave temperatures > 1400 °C and were not used for geothermobarometry. The remaining seven grains were used to construct the geotherm based on the T-P caluclations of Nimis and Taylor (2000). This yield a tightly-constrained geotherm for the west central Rae lithosphere (Figure 2.24) indicating a lithospheric thickness of ~ 200 km, and a diamond window ~ 75 km thick. This lithospheric thickness is consistent with the seismic estimate of lithospheric thickness beneath this area (Figure 2.25) and is within error of that constrained from the geotherm for the east central Rae (Liu et al. 2016), but significantly deeper than the lithosphere beneath Somerset Island, north Rae (~160 to 170 km; Mather et al. 2011). As such, the Rae lithosphere appears to be thicker beneath Darby, in the eastern Central Rae, based on both geophysical and petrological considerations, than at its northern edge. This may be a function of the lateral accretion of cratons, which geodynamic modelling predicts will result in thinner craton margins (Wang et al. in press).

Nickel-in-garnet temperatures (Table 3; Appendix A) were averaged (Shu et al. 2013) from the formulations of Griffin et al. (1989) and Canil (1999). The four garnet peridotite xenoliths and 49 peridotitic garnets from concentrate yield two distinct modes in mantle sampling depths when extrapolated to the Darby geotherm. A cluster of garnets from the higher Ca/Cr lherzolitic garnets equilibrated at 765 to 920 °C. In contrast, a group of peridotitic garnets (50 % of xenoliths and 28 % of concentrate) from the lower Ca/Cr lherzolitic garnets (94 %) have anomalously high Ti concentrations and very high Ni, yielding unreasonable T_{Ni} values of >> 1400 °C, i.e., super-adiabatic values, well outside the lithospheric "diamond window". All of the super-adiabatic xenoliths and 11 of 15 of the lherzolitic concentrate garnets classify as G11 or High-TiO_2. The one concentrate garnet narrowly classifies as G1 Low-Cr megacryst garnet (Grütter et al. 2004) is most likely they result of Ca-Fe-Ti metasomatism that drives garnet

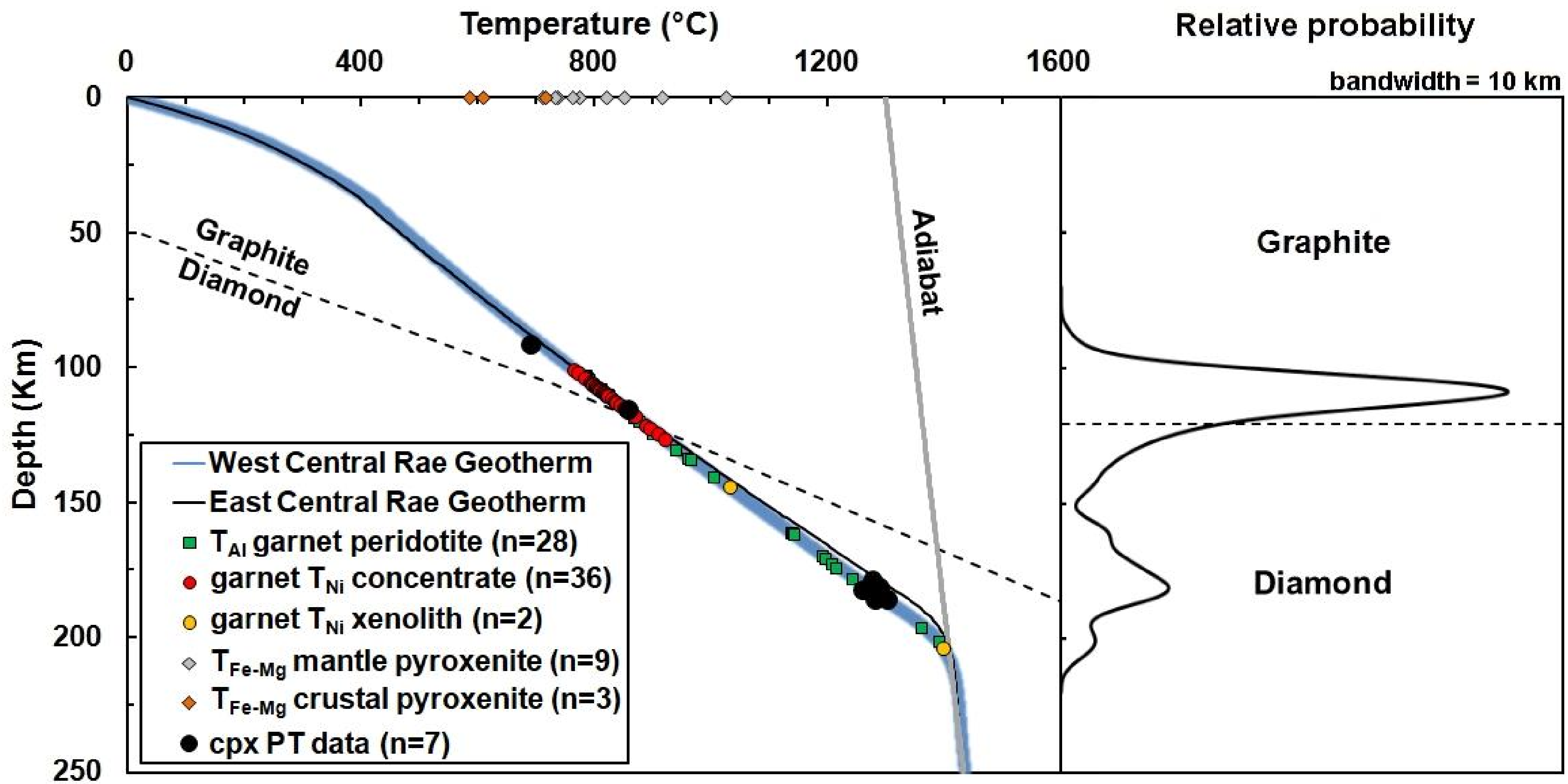

Figure 2.24 FITPLOT (Mather et al. 2011) geotherm modeled from Darby clinopyroxene concentrate (Gr tter 2009) – all locations composited using crustal thickness of 38.6 ± 0.3 km (Snyder et al. 2015). Ni-in-garnet and Al-in-olivine temperatures from peridotite xenoliths and concentrate are extrapolated to this geotherm while Fe-Mg temperatures are plotted at 0 km clarity. Right panel shows mantle depth sampling.

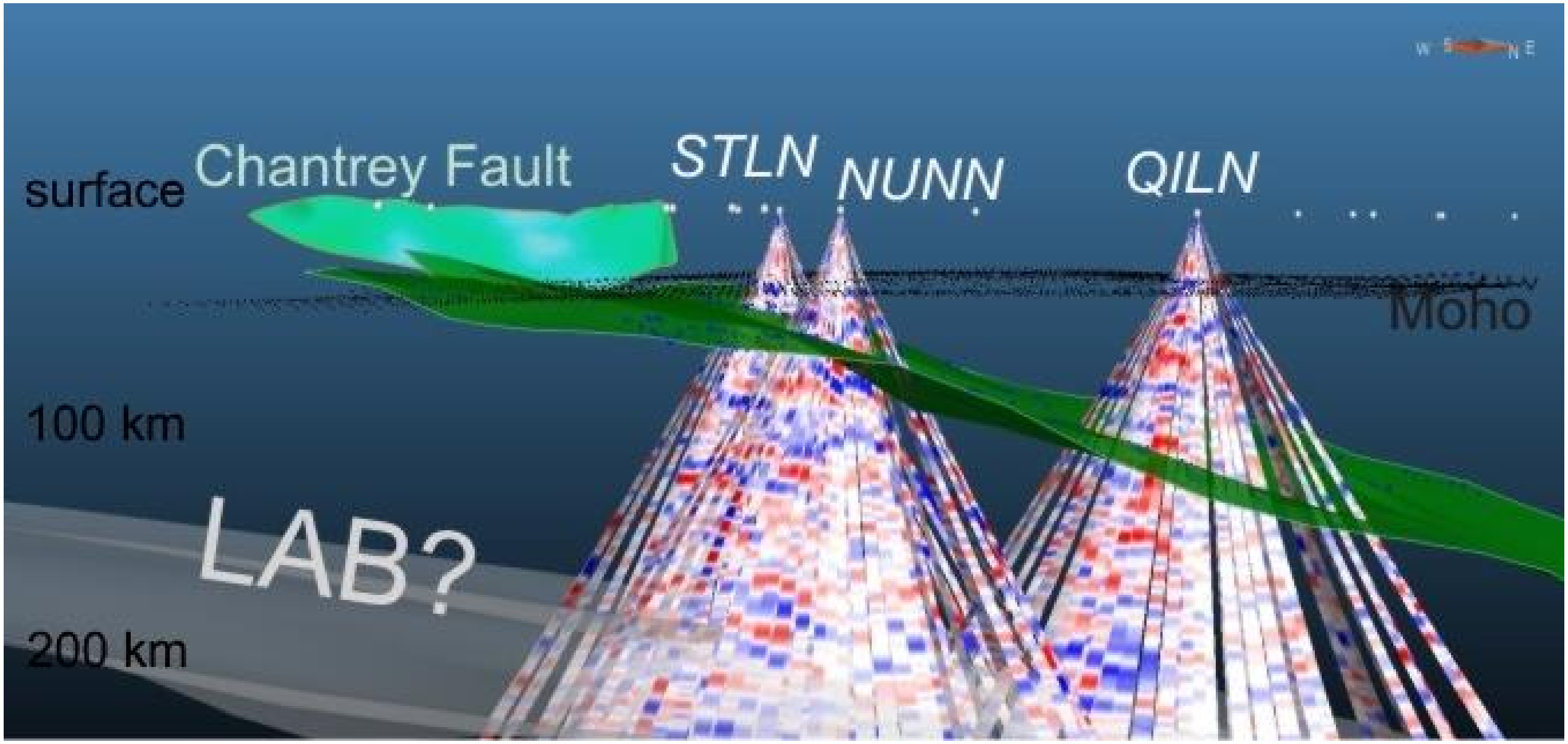

Figure 2.25 Snapshot of Geocad 3-D model of the Rae Craton telesiesmic study summarized in Snyder et al. (2017). From left to right the three receiver function cones 'point' to Darby, Nanuq, and Qilaluqak. The green surface is the Nanuq surface and strikes NNW/SSE and dips to the east. The smaller, near-vertical surface in the crust is the down-dip projection of the Chantrey fault using gravity 'worms'. LAB was identified based on distinct velocity changes. It's possible position is augmented by a white surface on the plot. Estimates of the projected depths of the Nanuq surface beneath a few seismic stations: 52 km @ Darby/STLN, 72 km @ Nanuq/NUNN, 99 km @ Amaruk/KUGN/Pelly Bay, 137 km @ QILN/Repulse Bay, 148 km @ Igloolik/ILON.

compositions in high-temperature mantle peridotites toward the megacrystic garnets (e.g. Burgess and Harte, 1999 and references therein). Therefore, this G1 garnet is most likely represents the overlap between megacrystic garnets and lower-Cr_2O_3 and high-TiO_2 peridotitic garnets whose primary composition belongs to the G11 suite (Grütter et al. 2004) as a result of the Ti metasomatism observed beneath Darby. However, the high Ni-Ti observed in the peridotitic garnets did not have a large affect on the olivine compositions (NiO < 0.42 wt%; Figure 2.8).

The experimentally calibrated aluminum-in-olivine thermometer of Bussweiler et al. (2017) was applied to olivine from concentrate and xenoliths (Table 4; Appendix A) after applying the Al – V "garnet facies" filter (Figure 2.19). Olivine thermometry indicates two distinct mantle sampling regimes (Figure 2.24), from 785 to 1005 °C, in broad agreement with the Ni-in-garnet sampling mode and a higher temperature region of mantle sampling, well into the diamond stability at 1140 to 1390 °C, with the higher temperatures exceeding the typical MORB-source asthenospheric isentrope of ~ 1315 °C (e.g., Mather et al. 2011; Mckenzie and Bickle 1988).

The presence of elevated Ti in ~ 30 % of peridotitic garnets (G11) derived from the lithosphere beneath Darby may be indicative of Ti melt-associated metasomatism in the base of the lithosphere where thermal disturbance of the lowermost lithosphere was transient and did not have sufficient time to equilibrate prior to sampling by kimberlite. All of the Ti metasomatised garnets have very high T_{Ni}, above the mantle adiabat and this heating event may have reduced the diamond tenor of the lithosphere. These high Ti and T_{Ni} garnets exclusively fall into the "on-craton" category (Figure 2.6; lower Ca/Cr), which make up the $LREE_N$ depleted patterns (Figure 2.16). The apparent difference in mantle sampling profiles between the non-disturbed garnet and olivine warrants further investigation with a larger sample set. The super-adiabatic garnet concentrate populations and the peculiar Ti metasomatism in the pyroxenites (discussed further in Chapter 4) indicates that the amount of high-T melt-related metasomatism at Darby is unusual compared with other cratonic locations where high-T metasomatised peridotites are found (Nixon and Boyd 1973).

2.4.2 Peridotite compositions

The highly depleted olivine Mg# of the Darby peridotites (92.5) is indistinguishable from the worldwide median value of 92.6 for cratonic peridotites world-wide (Pearson and Wittig 2014). While the mantle xenolith suite is relatively small, the Mg# mode in the mantle olivines extracted from concentrate and analysed as macrocrysts in sections is also high (92.2) and similar to the xenolith median value. This and the low bulk rock Al_2O_3 contents of these peridotites are consistent with the mantle lithosphere beneath Darby representing extremely melt-depleted (40 % or more) residual mantle. This conclusion is supported by the presence of a G10D harzburgitic garnet in one peridotite as well as their low Pt concentrations (low Pt/Ir), that also indicate extensive melt extraction (Aulbach et al. 2015). It is difficult to make a direct comparison of the level of depletion of the Darby mantle sample relative to that of the most eastern Rae Craton mantle samples analysed by Liu et al. (2016) because of the very altered nature of those rocks, but the lower median Al_2O_3 content of the Darby samples is an indication of a slightly more depleted mantle. The peridotite xenoliths from Somerset Island (north central Rae Craton; Irvine et al. 2003) are much fresher than those in the eastern Rae, making comparison with the Darby data more straightforward. The Darby mantle suite has higher median olivine Mg# and significantly lower and more tightly constrained bulk Al_2O_3 than the median Somerset Island compositions (Figures 2.2 and 2.17, respectively), making it perhaps the most depleted mantle lithosphere found beneath the Rae Craton.

A significant proportion of garnet REE_N patterns are "sinusoidal" (50 % of xenoliths and 63 % of concentrate). These signatures are often associated with rocks that have interacted with a diamond forming fluid (Stachel and Harris 2008). The harzburgitic G10D garnet has the strongest "sinusoidal" pattern, consistent with the common occurrence of this type of REE pattern in G10 garnets (Klein-BenDavid and Pearson 2009). The other group of G11 garnet REE_N patterns are $LREE_N$ depleted (50 % of xenoliths and 27 % of the concentrate), typical of lherzolitic garnets from cratonic peridotites (Stachel and Harris 2008). Stachel and Harris (2008), on the basis of diamond inclusion geochemistry, propose that more intense fluid metasomatism associated with enrichment in Zr (and negligible addition of Y and MREE-HREE) appears to be characteristic of the harzburgitic paragenesis. However, the Darby peridotitic garnet with the lowest Y and is enriched in Zr and has Cr-Ca systematics that are clearly lherzolitic (G9) in nature while a sample with moderate Y and enriched Zr has a harzburgitic Cr-Ca signature. Similar to diamond inclusions studied by Stachel and Harris (2008), the lherzolitic garnets studied at Darby have concurrent addition of Zr and Y (and MREE-HREE), likely related to silicate melt metasomatism.

2.4.3 Pyroxenite compositions

Whereas the Darby peridotites are typical of depleted cratonic mantle lithosphere, the high abundance of low-Cr G3 and G4 garnets in concentrate and the anomalously high relative abundance of pyroxenite xenoliths at Darby is unusual in a cratonic setting, especially as this is a feature of all the Darby intrusions. As shown above, applying the low-Cr garnet crust-mantle graphical discrimination plot of Hardman et al. (2018a), reveals that only 23 % of the concentrate low-Cr garnet grains and 47 % of the pyroxenitic xenoliths are of mantle origin, correctly classifying the plagioclase pyroxenites as crustal. Although the Hardman et al. (2018a) scheme is not infallible, the classification failure rate (crust vs mantle) is vastly improved over alternative methods (39 % Schulze 2003; 10 % Hardman et al. 2018a) and therefore the Hardman et al. (2018a) scheme is considered a more accurate representation for our data-set. However, since a large amount of the data fall near the decision boundary, its proximity to the decision boundary increases the likelihood that this data may be misclassified, and hence it is difficult to state, at a high level of certainty, the crust or mantle provenance of the pyroxenites that do not contain plagioclase. Nonetheless, the Hardman et al. (2018a) scheme gives the user an idea of the certainty of the data's classification, which is not present in the Schulze (2003) scheme. Although having a visual classification using the graphical approach of Hardman et al. (2018a) has its value, due to the higher probability of these samples being misclassified the LR approach was taken as the best representative of the "crust-mantle" classification. Utilizing trace elements into this classification greatly increases the proportion of mantle samples in the xenoliths (74 %), demonstrating the value of trace element analysis in eclogitic/pyroxenitic garnets. The mantle proportion of low-Cr concentrate (28 %) is likely underestimated due to the lack of trace element analyses.

Fe-Mg temperature estimates (calculated at 1 GPa for crustal, 4 GPa for mantle; Krogh 2000) for the pyroxenites range from 590 to 1030 °C (Table 2.2B; below), with the plagioclase pyroxenite giving a temperature of 610 °C. While the highest equilibration temperatures, in the mantle-derived samples, might reflect equilibrium along a geotherm, the high Fe-Mg temperatures of the crustal pyroxenites likely reflect the closing of Fe-Mg exchange during their crystallization in the lower crust, with the garnet-clinopyroxene temperatures retaining palaeo-equilibration temperatures due to rapid cooling (e.g., Harte et al. 1981). This is further implied by the presence of pigeonite. Putting aside the high-T samples that are altered by lamproitic metasomatism as well as the crustal samples, temperatures in the "normal" mantle pyroxenite suite range from 710 to 820 °C, which corresponds to a ~ 15 km (this value is assumes no error in thermometry; 50 °C error of gives range of ~ 1 to 30 km) thick region in the mantle along a cratonic geotherm.

The pyroxenitic garnets are $LREE_N$ depleted (Figure 2.18) which is typical of pyroxenites from orogenic massifs and cratonic eclogites (Jacob 2004). $HREE_N$ are variably enriched with one sample showing extreme enrichment (Lu_N = 100), similar to some Roberts Victor eclogites (Harte and Kirkley 1997) or Beni Bousera orogenic pyroxenites (Pearson et al., 1993). Twelve pyroxenites whose garnets have positive Eu-anomalies and nearly flat $HREE_N$ have been interpreted as evidence of a prograde metamorphic reaction forming garnet from a plagioclase-bearing assemblage, likely reflecting a parentage of these rocks from subducted oceanic crust (e.g., Jacob et al. 2003; Jagoutz et al. 1984) and hence these rocks are Na-poor. Diopsides in the pyroxenites show convex-upward REE_N patterns with enriched $LREE_N$ concentrations typical of mantle eclogites (Jacob 2004). The seven positive Eu-anomalies documented in diopside occur when coexisting garnets also show positive anomalies, supporting an origin perhaps from oceanic crust or crystallised melts of oceanic crust which inherit the positive Eu-anomalies of their source (e.g., Yaxley and Green 1998).

2.4.4 Mantle structure and tectonic implications

Even though many of the Darby G3/G4 concentrate garnets classify as crustal in origin using the Hardman et al. (2018a) discrimination, the overall amount of mantle eclogite/pyroxenite material significantly exceeds the estimate for cratonic lithospheric mantle of between one and five vol % made by Schulze (1989) and Dawson and Stephens (1975). This anomalous proportion of pyroxenite could indicate the introduction of basaltic material from a underthrust slab or a pyroxenite-rich zone that crystallised from magma infiltrating the Rae lithosphere during one of the later tectono-thermal events to affecting the craton. The restricted temperature range of the mantle pyroxenites indicates a ~ 15 km depth range of sampling for these xenoliths and may correspond to a thicker oceanic slab formed under a hotter Archean thermal regime or a zone of enhanced pyroxenite crystallisation.

To investigate these possibilities, we can interrogate further the seismic dataset for the Rae Craton recently summarized and presented by Snyder et al. (2015; 2017). A new 3-D image produced from this dataset (Figure 2.25) highlights surfaces - determined from seismic discontinuities in Ps receiver functions - that define three distinct layers beneath Darby at 36 km (Moho), 52 km ("Nanuq", projects to surface at the Chantrey fault zone although the strikes are slightly discordant), and at 200 km (lithosphere asthenosphere boundary = LAB). The layered structure of the Rae lithosphere has been interpreted by Snyder et al. (2017) to reflect an origin by lateral accretion and tectonic wedging. This together with the crustal deformation and thickening at 2.57 Ga documented by Regan et al. (2017) supports an origin for the structure of the Rae Craton lithosphere by compression, following dynamics similar to those outlined by Wang et al. (in press).

In the above scenario the "Nanuq" surface, the strongest surface evident in the three receiver cones in Figure 2.25, may document the anomalous abundance of basic material crystallised in both the Rae crust and mantle beneath Darby. The occurrence of an anomalously high abundance of pyroxenite at all the Darby kimberlites is consistent with the inferences drawn from seismological characteristics (Bostock 1998) of the Nanuq surface that suggests the presence of a layer rich in isotropic basic material overlain by a more anisotropic ultramafic layer in the shallowest upper mantle. This discontinuity could be a possible upper slab surface or simply a zone where basic melts have crystallised in the upper mantle. Further studies of the physical properties of mantle xenoliths from the Rae Craton will better constrain these possibilities.

2.5 Conclusions

A small suite of peridotite xenoliths collected, along with mineral concentrate grains from kimberlites of the Darby kimberlite field, Nunavut, documents the presence of highly-depleted (low bulk rock Al_2O_3, high olivine Mg#) cratonic mantle beneath this region. A xenolith with a diamond-facies harzburgitic (G10D) garnet clearly originated well within the diamond stability field, together with the melt-depleted nature of the peridotites and their Archean ages are all encouraging for diamond exploration. In particular, the extensive diamond window (~ 75 km) defined by the geotherm and the mantle sampling within the diamond stability field evident from olivine thermometry is encouraging evidence of diamond-facies peridotitic mantle being sampled.

The presence of very high T_{Ni} in some peridotitic garnets and Al-in-olivine temperatures approaching 1400 °C, along with the abundant lower Ca/Cr (G11) lherzolitic garnets are indicative of late thermal disturbance of the lowermost lithosphere, close to kimberlite eruption. This heating event may have reduced the diamond tenor of the lithosphere, resulting in the low diamond counts reported in the evaluation of the kimberlite bodies at Darby (Weir and Farmer 2008). Pyroxenites of mantle and crustal origin are anomalously abundant in our sample of indicator minerals and xenoliths at Darby, in contrast to the low observed abundance present in typical cratonic lithospheric mantle worldwide. The discontinuity shown as the "Nanuq surface" in the new seismic image produced from the data in Snyder et al. (2015; 2017) may represent a possible upper slab surface or simply a zone where basic melts have crystallised in the upper mantle that may correlate with this anomalous abundance of pyroxenite.

Chapter 3
Rb-Sr, U-Pb and Re-Os Geochronology

3.1 Introduction

Obtaining P/T information for Darby mantle samples and hence a geotherm allows a mantle “stratigraphy” to be created if age information on the different mantle components can be obtained. A key starting point in this is to determine the age of the host kimberlite, which is useful in an exploration context, because in certain cratons, such as the Slave Craton, kimberlites of a specific age have a higher likelihood of being diamondiferous. In addition, specific types of Os model age calculations reference the intrusion age. In order to determine when the Darby kimberlite cluster erupted, Rb-Sr analyses of phlogopite were completed by Bluestone Resources Inc. during exploration on the property. In addition, U-Pb age determinations on pyroxenitic rutile were completed to compare the results from this method with those of the more established Rb-Sr phlogopite method. Due to scarcity of perovskite in the Darby kimberlites, where it mostly occurs as reaction rims on rutile crystals and discrete grains in the kimberlites that were < 10 µm, U-Pb perovskite dating could not be attempted.

3.2 Methods

3.2.1 Rb–Sr of phlogopite

Rubidium–Sr analyses on phlogopite were completed at the Radiogenic Isotope Facility at the University of Alberta. For detailed methodology of this procedure see Creaser et al. (2004). Fresh, individual phlogopite grains were selected from drill-core, heavy mineral concentrate, and kimberlite float from Iceberg south and north, Stealth, Inferno, and float trend from Sky to Stealth for Rb-Sr isotope analysis. These grains were then cleaned of any chlorite rims or alteration zones. Samples typically weighed 3 to 15 mg and were leached in dilute (~ 0.7 N) hydrochloric acid (Brown et al. 1989) in an ultrasonic bath for ~ 30 min to remove trace carbonate minerals, before repeated rinses in ultrapure water. The leach-cleaned mica was spiked with a known amount of a mixed ^{84}Sr–^{87}Rb spike to enable isotope dilution analysis and dissolved in a 5:1 mix of 24 N HF:16 N HNO_3 in PFA Teflon containers. Strontium and Rb were separated by standard cation-exchange chromatographic methods (e.g., Holmden et al. 1996) and isotopic analysis of both elements was performed using Thermal Ionization Mass Spectrometry, a single Re filament, and the tantalum gel loading method. Strontium isotope analyses were performed using either a VG354 5-collector machine in multi-dynamic data collection mode, or a Micromass Sector 54 instrument in either multi-dynamic or static data collection mode. All analyses are corrected for variable mass fractionation using an exponential law and $^{86}Sr/^{88}Sr$ = 0.1194. Accuracy of the Sr isotopic composition was monitored using the NIST SRM987 Sr isotopic standard, and all isotopic ratios are reported relative to a value of 0.710245 for the NIST SRM987 Sr isotope standard.

3.2.2 U–Pb pyroxenitic *Rutile*

Rutile grains in all thick sections were first analyzed and imaged by EPMA to ensure grains were free of inclusions or any exsolution. For example, Figure 3.1A is a clean large grain which was then ablated by LA-ICP-MS for U–Pb isotopes while other grains were not selected for ablation due to zircon inclusions or ilmenite exsolution, Figure 3.1B and C respectively.

Uranium–Pb isotopes were analysed for rutile by sector-field laser ablation ICP mass spectrometry using an Element XR2 mass spectrometer and Resonetics LR50 193 nm laser ablation system. Due to low uranium counts for the Darby rutile, clean cones, optimally tuned nitrogen (7 mL/min) and helium (700 mL/min) were critical in achieving maximum signals in order to get precise ages from the relatively low signals of radiogenic Pb present. The laser operated at a frequency of 5 Hz, with 14 J/cm^2 laser energy (fluence), attenuator at 11.4 % with a spot size of 90 μm. All standards and laser set up were consistent with trace element analyses of rutile as shown above. To correct for the effects of the relatively high common Pb present in rutile, the Andersen (2002) method of common Pb correction was applied to each of the samples during data reduction in Iolite. Rutile R10 (Luvizotto et al. 2009) was used as a reference material for these analyses. Twenty analyses of this rutile gave a mean age of 1091.6 ± 3.8 Ma (2 σ, MSWD 2.1) during the course of this study (Figure 3.2), within uncertainty of the accepted ID-TIMS value (1095.2 ± 4.7 Ma; Luvizotto et al. 2009).

3.2.3 Whole-rock highly siderophile element abundance analysis

Highly siderophile element (HSE) concentrations and isotope analyses were conducted using an isotope dilution technique (after Pearson and Woodland 2000) coupled with High Pressure Asher aqua regia digestion at the University of Alberta. Osmium isotope ratios were measured as OsO^{3-} using multiple Faraday collectors and amplifiers equipped with 10^{12} resistors on a Thermo Scientific Triton Plus TIMS (see Liu and Pearson, 2014 for detailed performance and standard repeatability). Re-PGE column cuts were measured in Low Resolution mode on a Nu instruments Attom.

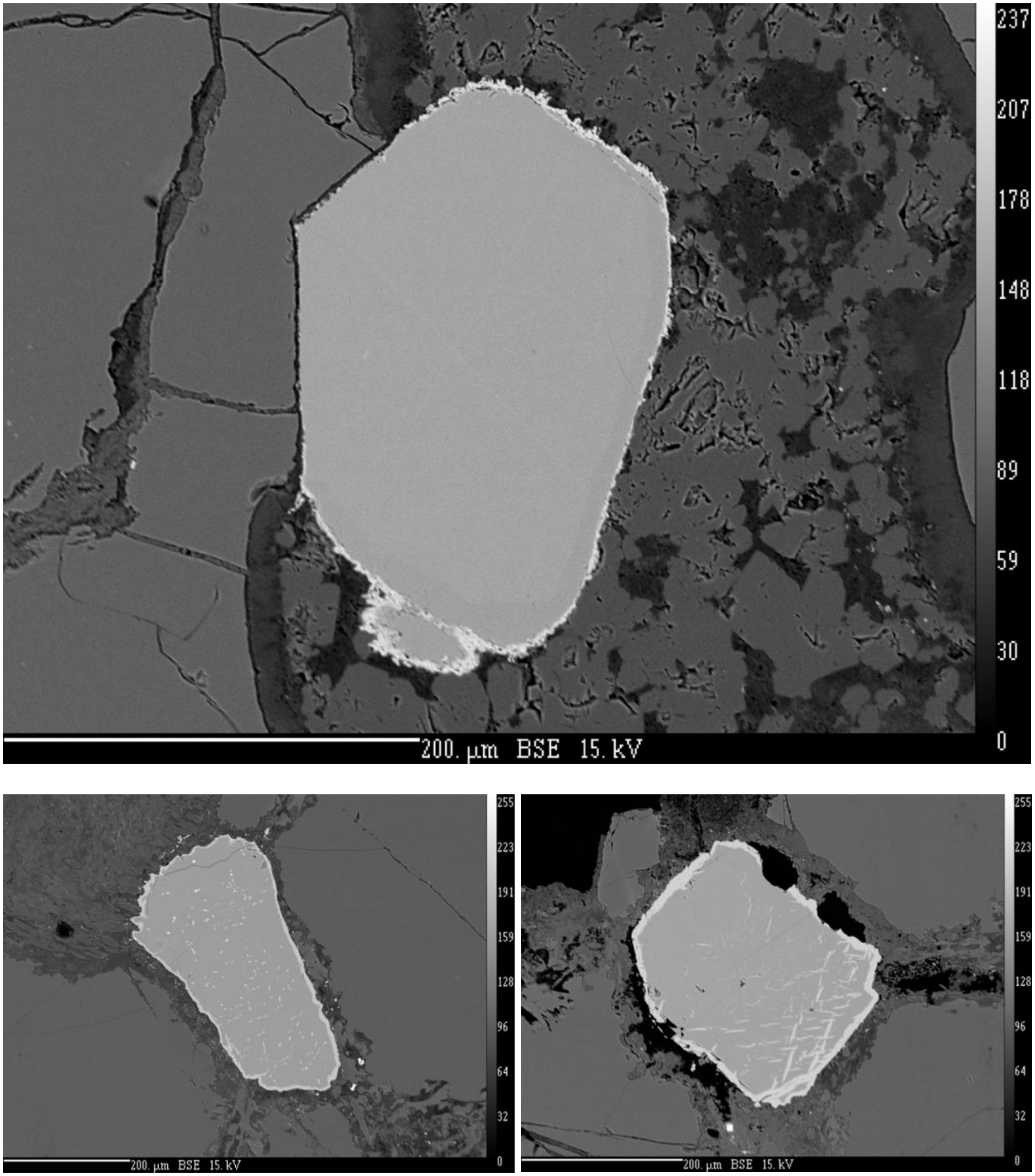

Figure 3.1 BSE images of rutile grains **A** clean grain used for U-Pb isotopes, **B** dirty grain with zircon inclusions not used for U-Pb isotopes, **C** dirty grain with ilmenite exsolution not used for U-Pb isotopes.

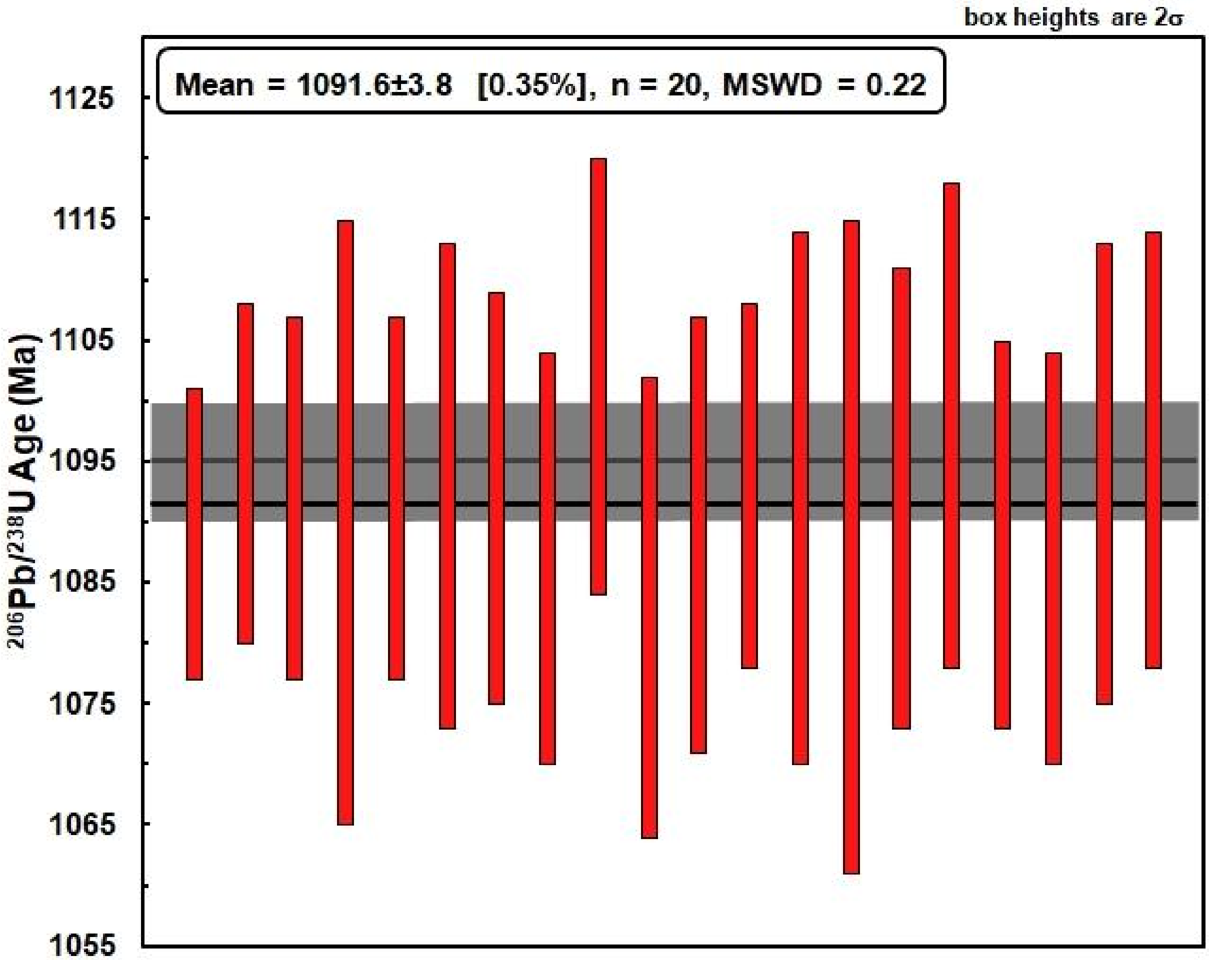

Figure 3.2 LA-ICP-MS analyses of secondary rutile standard R10 (red bars). Black line represents mean age, grey line represents accepted ID-TIMS age and error (Luvizotto et al. 2009).

Re-PGE concentrations were purified via cation exchange chromatography (Li et al. 2013) to reduce the concentration level of interfering elements such as Y, Cd, Rb, Zn, Cu, Ni and BPHA solvent extraction (Shinotsuka and Suzuki 2007; Ishikawa et al. 2014) for Zr, Mo, Hf, and W. The solution remaining after the Os extraction was evaporated to dryness, and the residues were dissolved in 5 ml of 6 mol L^{-1} HCl. Following this, 1 ml of 30 % H_2O_2 was slowly added to reduce Cr^{VI} to Cr^{III}, and the solution was dried down again. The residue was dissolved in 10 ml of 0.1 mol L^{-1} HCl and loaded onto the cation exchange columns (AG50W-X8, 200-400 mesh, 16 mm x 240 mm column with a 50 ml reservoir; Bio-Rad Laboratories, Inc., Berkeley, CA, USA). Before sample loading the columns were cleaned with 60 ml 6 mol L^{-1} HCl and conditioned with 80 ml of 0.1 mol L^{-1} HCl. Following the sample loading and additional 11 ml of 0.1 mol L^{-1} HCl was eluted and collected, the resulting ~ 21 ml solution was then dried down and 80 ml of 6 mol L^{-1} HCl was used to clean the columns. The residues were dissolved in 2 ml of 0.5 mol L^{-1} HCl and 300 μL of fresh 0.025 mol L^{-1} BPHA (Tokyo Chemical Industry: P0158-25G) in $CHCl_3$ was added to the solution and was vigorously shaken for 5 minutes then centrifuged. The solvent extraction was completed three times, after which the 2 ml of 0.5 mol L^{-1} HCl was pipetted off and analyzed for Re-PGEs in a single cut via ICP-MS.

Osmium isotope ratios were measured as OsO^{3-} using multiple Faraday collectors and amplifiers equipped with 10^{12} Ω resistors with a Thermo Scientific Triton Plus thermal ionization mass spectrometer (TIMS) at the University of Alberta (Liu and Pearson 2014). Typical Faraday intensities of mass 238 (mainly $^{190}Os^{16}O^{3-}$) were 0.1 to 0.4 V (10^{11} Ω amplifier equivalent signals; 0.001 V is equivalent to ~ 62500 cps), while SEM intensities were ~ 200,000 to 300,000 cps with 50 ratios taken at 8 seconds integration per ratio. Raw ratios were first corrected for gain and baseline, followed by oxygen correction using $^{17}O/^{16}O$ = 0.0003749 and $^{18}O/^{16}O$ =

0.0020439 (Nier 1950) and spike correction, and finally by instrumental mass fractionation correction using $^{192}Os/^{188}Os$ = 3.083 via the exponential law. Internal precision on $^{187}Os/^{188}Os$ ratios was typically better than 0.05 % (2σ). During the analytical campaign, repeated measurements of 0.5 to 2.5 ng loads of Os reference materials yielded a $^{187}Os/^{188}Os$ mean value of 0.160927 ± 0.000173 (2σ, n = 14) for the DrOsS Reference Material and 0.113796 ± 0.000022 (2σ, n = 10) for the University of Maryland Johnson Matthey Os Standard; these ratios are within 0.01 % of the accepted values (Luguet et al. 2008). Procedural blanks during the Hi-Os peridotite analyses yielded 0.972 ± 0.066 pg, while the Lo-Os pyroxenitic analyses yielded a procedural blank of 0.180 ± 0.063 pg.

All Re-PGE column cuts were measured via low resolution mode on a Nu instruments Attom at the University of Alberta. Given that the $^{175}Lu^+$ and $^{178}Hf^+$ signals were less than 10,000 and 1,000 counts per second (cps), respectively, in the sample solutions, the Lu and Hf oxide isobaric interference corrections for Ir and Pt were negligible. For the Pd analysis, the zirconium (^{90}Zr) standard solution was measured to determine the oxide production rate (ZrO^+/Zr^+), which was < 1 % during the analytical measurements. The isobaric interference correction of $^{90}ZrO^+$ on mass 106 was < 0.1 %, as Zr/Pd ratios were low in the sample solutions. Instrumental mass fractionation was corrected via periodic measurement of in-house standards (usually one per four sample analyses) using the standard bracketing method, resulting in normally less than 1 % correction.

3.3 Results

3.3.1 Kimberlite eruption age

3.3.1.1 Rb-Sr of phlogopite

Individual phlogopite grains were selected from drill-core from Iceberg south and north for Rb-Sr isotope analysis in hopes to constrain an eruption age. Of 17 phlogopite grains (Table 8; Appendix A), ten were selected that had $^{87}Rb/^{86}Sr > 10$ ($^{87}Rb/^{86}Sr$: 70 to 850) and consistent model ages for Rb-Sr isochron regression (Figure 3.3A). This yielded an age of 542.2 ± 2.6 Ma (2 σ; MSWD = 0.36) with an initial $^{87}Sr/^{86}Sr$ ratio of 0.7057 ± 0.0011. This initial ratio is within the range obtained by Sarkar et al. (in press) for other Rae Craton kimberlites and kimberlitic perovskites. This result is taken to be a precise estimate of the eruption age of the Iceberg bodies in the Darby field. Of the remaining seven grains, four analyses not used for isochron regression are plotted on the insert of Figure 3.3A. The remaining seven grains are unusable due to low $^{87}Rb/^{86}Sr$ ratio and do not pass the criteria outlined by Sarkar et al. (2015). These seven extraneous data points (insert on Figure 3.3A) most likely represent older xenocrystic micas such as those identified in Ar–Ar dating studies of mantle xenoliths (e.g., Pearson et al. 1997).

3.3.1.2 U–Pb of pyroxenitic rutile

Eight of the nineteen pyroxenite xenoliths contain rutile. Major element analysis of rutile attempted to use the Cr_2O_3 element discriminator of Malkovets et al. (2016) to identify mantle rutiles, which appears non-definitive for the Darby pyroxenites (Figure 3.4) in that they have lower Cr_2O_3 than rutiles of supposed mantle derivation. However, even for the crustal pyroxenites, the high Fe-Mg temperatures recorded by Gt-Cpx thermometry (Chapter 2) and the

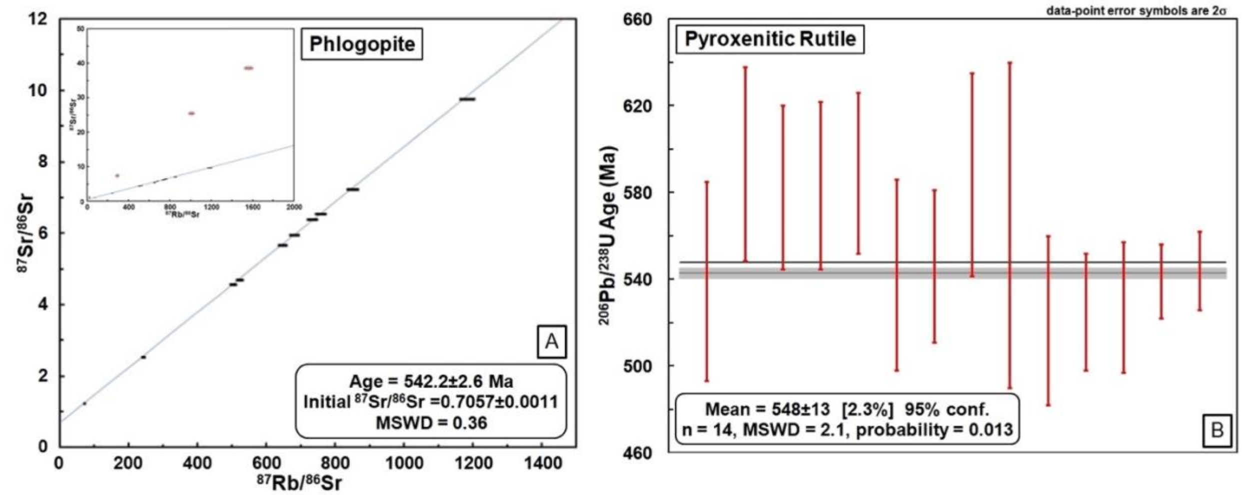

Figure 3.3A Rb-Sr isochron of individual phlogopite grains taken from drill core and kimberlite float. For increased visibility data points are 4σ on ^{87}Sr/^{86}Sr but remain 2σ on ^{87}Rb/^{86}Sr. Within insert plots all samples measured except three samples with low ^{87}Sr/^{86}Sr are not resolvable, with samples not used for regression in red circles. **B** Laser ablation ICPMS ^{206}Pb/^{238}U ages for rutiles from Darby pyroxenite xenoliths, corrected for ^{204}Pb using the Andersen (2002) method. Each red line is an individual rutile grain. Grains selected from two pyroxenite xenoliths. Black line represents weighted mean ^{206}Pb/^{238}U emplacement age, grey line is Rb/Sr phlogopite emplacement age. Widths of grey lines denote 2 σ uncertainty.

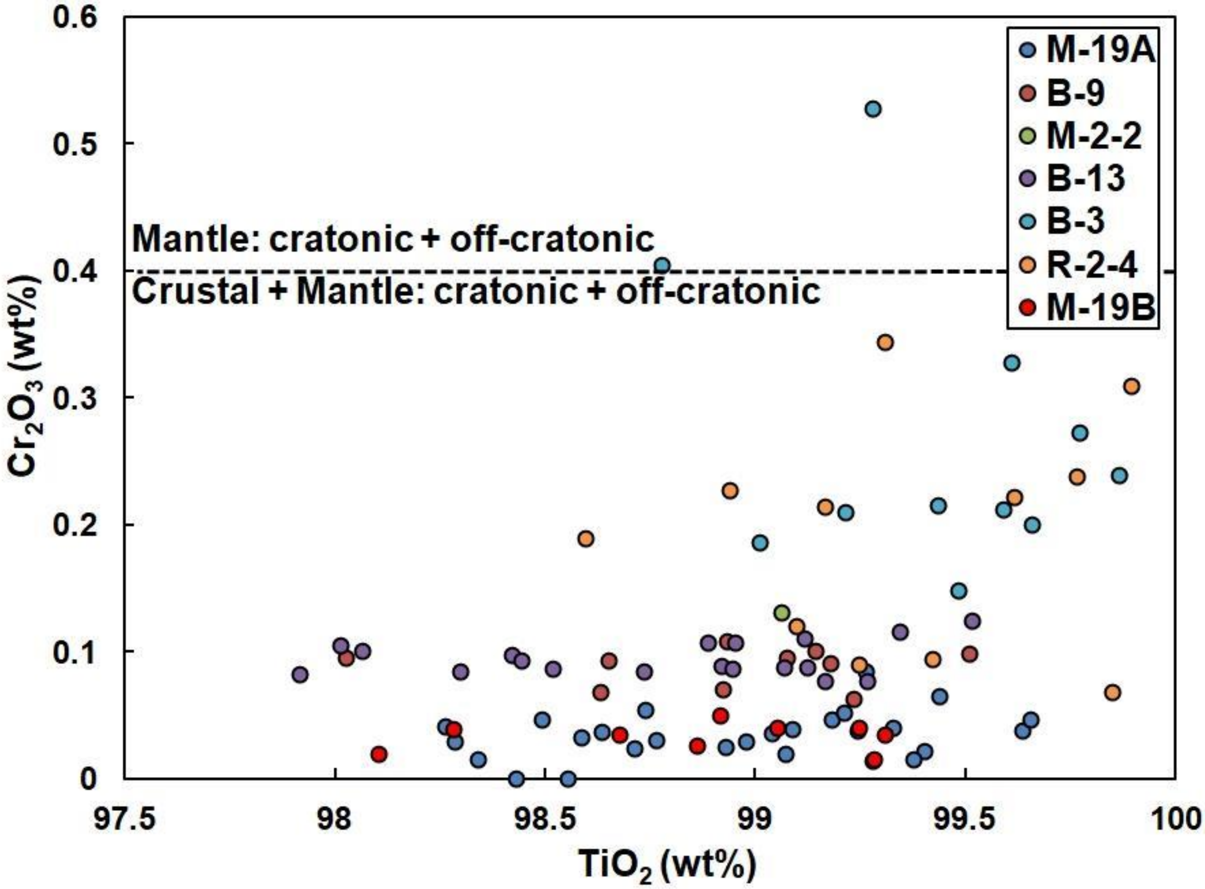

Figure 3.4 Cr_2O_3 vs. TiO_2 (wt%) for pyroxenitic rutile. Most plot below the mantle field of Malkovets et al. (2016).

low blocking temperature for the U–Pb system in rutile (600 to 640 °C; Cherniak 2000) means that the U–Pb system probably closed only at the time of kimberlite eruption. This is certainly the case for the rutiles analysed from the mantle-derived pyroxenites with high Fe-Mg temperatures (900 to 1000 °C).

Fourteen individual rutile grains analysed in two different samples (Figure 3.3B) give a weighted mean $^{238}U/^{206}Pb$ age of 548 ± 13 [2.3%] Ma (2 σ, MSWD = 2.1), which is identical, within error, to the Rb–Sr phlogopite isochron age, and hence clearly reflects closure of the U–Pb system at the time of kimberlite eruption. An exception is rutile in pyroxenite sample B-13, where ten out of twelve of the rutiles in that rocks gave a range of older $^{238}U/^{206}Pb$ ages from ~ 635 to 893 Ma which may reflect incomplete Pb-loss from older rutiles (Table 9; Appendix A). Since the Rb–Sr isochron derived from the Darby kimberlites is the more precise age determination compared with the rutile U–Pb age, we adopt it here as the eruption age for the Darby kimberlites. Nonetheless, the U–Pb results highlight the potential utility of U–Pb rutile dating in mantle xenoliths as a means to constrain kimberlite eruption ages.

3.3.2 Highly siderophile elements

HSE were measured on a total of five peridotites and six pyroxenites (Table 10; Appendix A). Duplicate measurements were performed on all samples due to poor spiking during the first round of analyses.

Initial Osmium isotopes and PGE elements were completed on eight peridotites and six pyroxenites, duplicate analyses were then completed due to inappropriate spiking and issues with a new PGE chemistry not removing enough interference isotopes resulting in low quality analyses.

Osmium isotopic compositions in the peridotites are unradiogenic, with γOs values, corrected for the time of kimberlite eruption of 542.2 Ma, clustering at the unradiogenic end of cratonic peridotite compositions (Figure 3.5). The mantle-normalised HSE patterns of these rocks (Figure 3.6) reveal that although Os concentrations in the peridotites vary widely, they have relatively un-fractionated iridium-group (I-PGE) patterns, with strong Pt depletions that mirror the Pt-IPGE fractionations observed in cratonic peridotites (Pearson et al. 2004; Aulbach et al. 2015). However, their Pd and Re values are significantly higher than "undisturbed" residual cratonic peridotites (Figure 3.6). Re and Pd, the most incompatible of the list of HSEs analysed, are enriched due to post-melting metasomatic effects that tend to re-enrich Pd and Re, creating extended PGE plots that have a "kick" in Pd and Re.

Pyroxenite Os isotope ratios are very radiogenic (Figure 3.5) with γOs values ranging from ~ 1,800 to 10,200. These values are as radiogenic as the highest $^{187}Os/^{188}Os$ ratios measured in any suite of cratonic eclogites. The HSE patterns of these rocks have the typical positive slopes showing enrichment of P-PGEs over IPGEs that are seen in other pyroxenites world-wide (Figure 3.7; Marchesi et al. 2014).

3.4 Discussion

3.4.1 Depletion age constraints

Whole-rock Re-depletion ages for five of the peridotites range from Mesoarchean to Paleoproterozoic. The model age histogram (Figure 3.8) demonstrates that the peridotitic mantle beneath Darby, based on our limited sampling, appears older than the east central Rae and older than the more substantive peridotite suites analysed from the east central Rae and also older then the lithospheric mantle beneath Somerset Island, northern Rae. The small dataset from Darby has

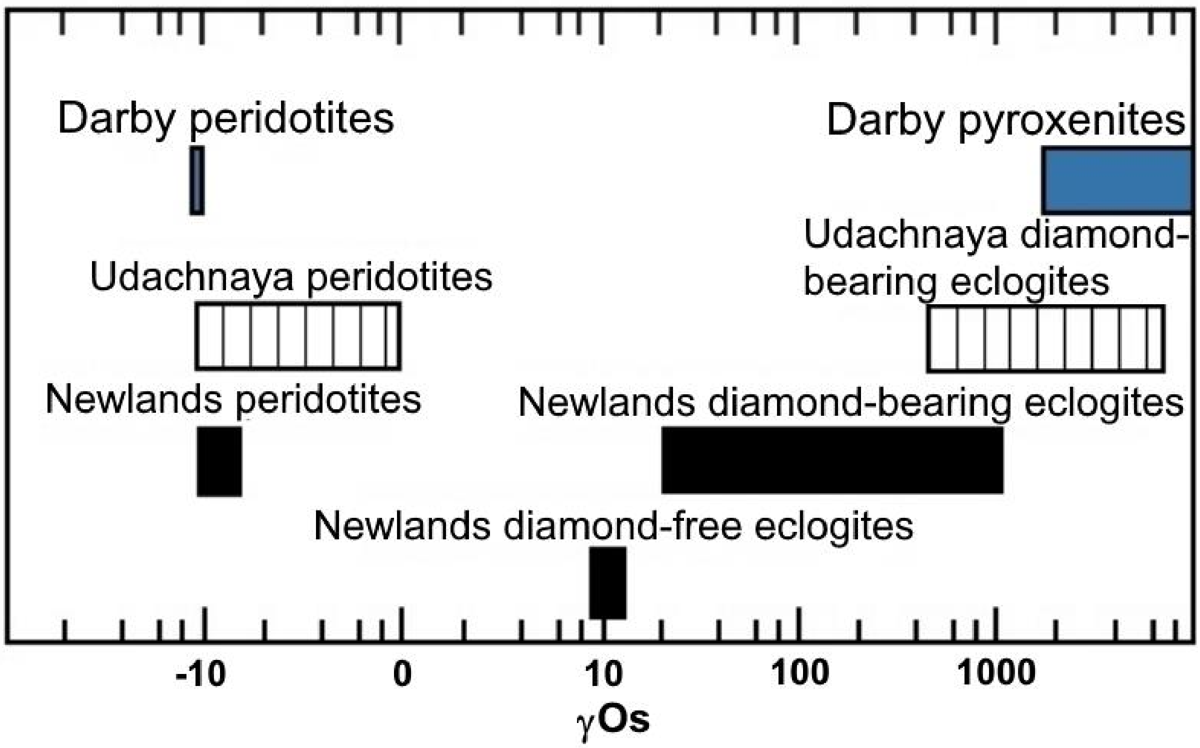

Figure 3.5 γOs plot displaying Darby unradiogenic peridotites and highly radiogenic pyroxenites compared to Udachnaya and Newlands (Menzies et al. 2003). γOs is the percent difference in $^{187}Os/^{188}Os$ between chondrite and the sample at the time of kimberlite eruption.

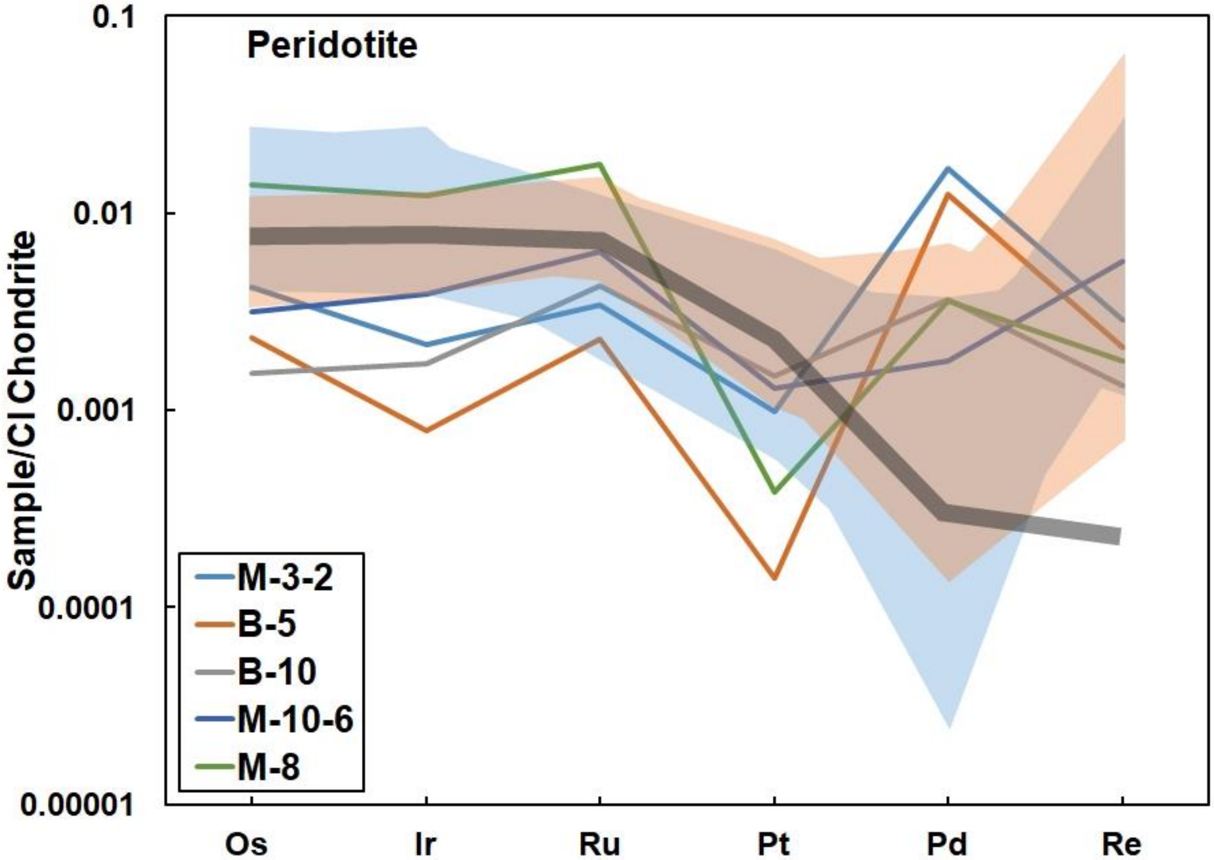

Figure 3.6 CI Chondrite-normalized (McDonough and Sun 1995) HSE patterns of peridotites. Thick grey line denotes pattern for highly melt depleted cratonic peridotite with minimal re-enrichment (Pearson et al. 2004). Two fields in background showing patterns from other peridotite suites: orange-Somerset Island (Irvine et al. 2003) and blue-Repulse Bay and Pelly Bay (Liu et al. 2016).

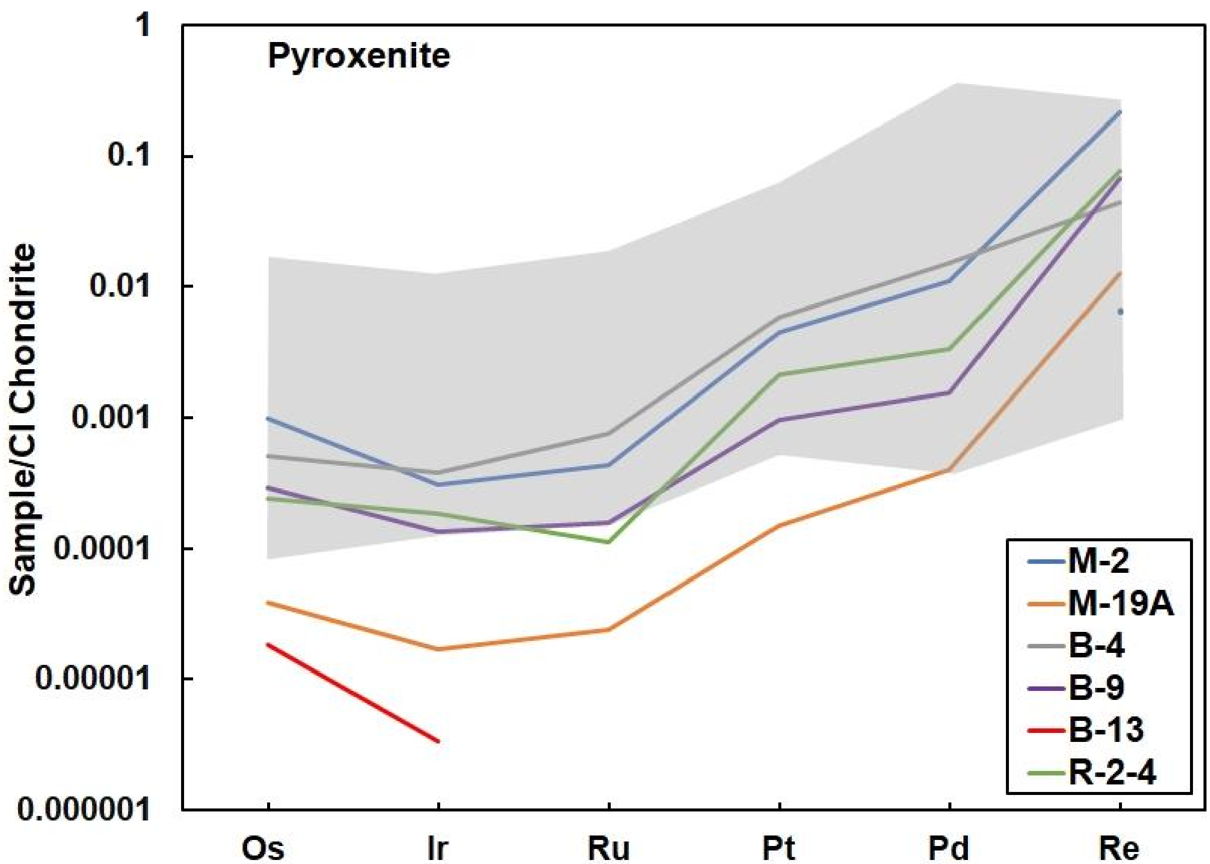

Figure 3.7 HSE patterns of pyroxenites, grey field represents global pyroxenites (Marchesi et al. 2014). CI Chondrite normalized from McDonough and Sun (1995).

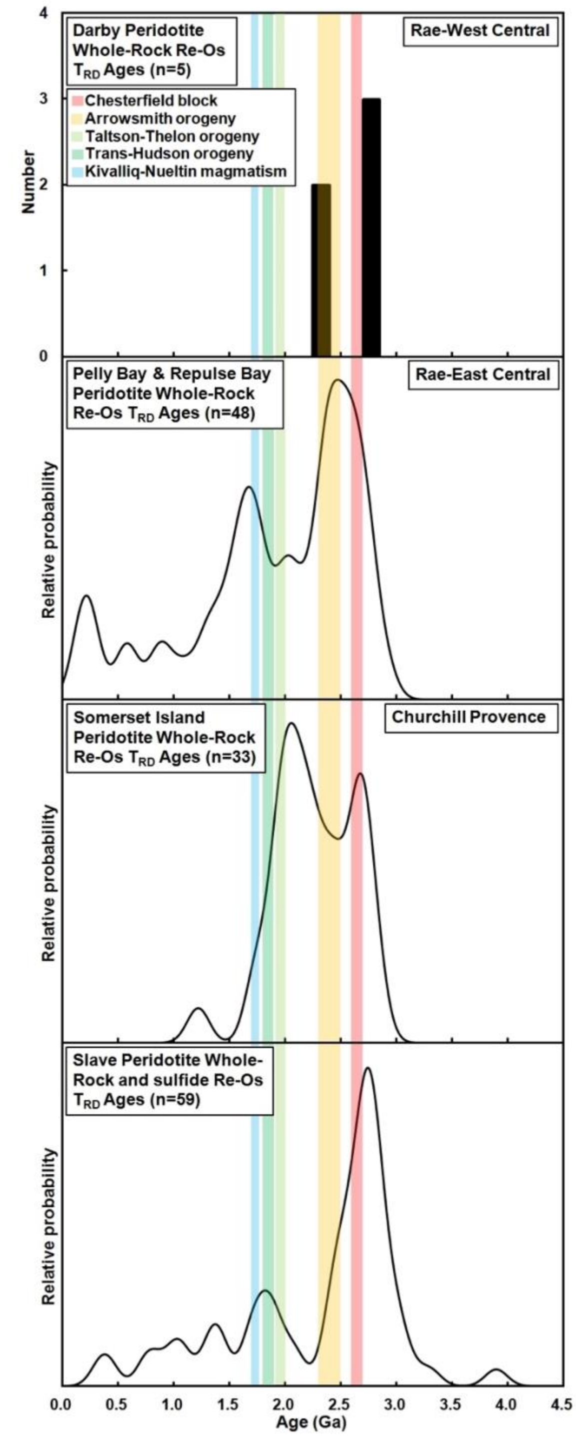

Figure 3.8 Histogram for Darby and probability density diagrams for Repulse Bay and Pelly Bay (Liu et al. 2016), Somerset Island (Irvine et al. 2003), and Slave (Pearson and Wittig 2014) of peridotite Re-Os T_{RD} ages. Coloured bands represent the age range of major regional tectono-thermal events expressed in crustal rocks of the Rae Craton summarized by Liu et al. (2016).

two age clusters, at 2.3 and 2.7 Ga, indicating lithospheric stabilization at least in the early Neoarchean. In contrast, the east central Rae lithospheric mantle has three peaks, one in the Phanerozoic, one at ~ 1.7 and the oldest at 2.5 Ga (Figure 3.8). Somerset Island has two main age peaks at 2.0 and 2.6 Ga (Figure 3.8). The slightly older mode in Archean ages at Darby (Figure 3.8) is consistent with the observation that the oldest crustal ages in the Rae Craton lie to the west, with Mesoarchean crust being found in the western Margin of the Rae (Hartlaub et al. 2005) and the Queen Maud block (Schultz et al. 2007). While the limited number of peridotites analysed establish the presence of Archean lithospheric mantle beneath this western-most part of the central Rae craton, the limited depth coverage and small sample set do not allow us to adequately test the stratigraphic relationship of the oldest archean lithosphere in the uppermost portion of the lithosphere with the lowermost portion consisting of younger Paleoproterozoic lithosphere suggested for the Rae lithospheric mantle by Liu et al. (2016). However, the small numbers of Darby peridotites amenable to dating means that these observations need to be tested if additional samples become available. A Neoarchean age for the eastern portion of the Rae Craton lithosphere is consistent with stabilization shortly after the abundant komatiitic and tholeiitic basalt magmatism that erupted throughout that part of the Rae (e.g., Schultz et al. 2007), which would have required melting beneath lithosphere no greater than ~ 80 km thick, followed by thickening and stabilization of a thick, ~ 200 km mantle root.

Overall, the additional peaks in Re depletion ages observed both at Darby and in the larger sample suites from elsewhere in the Rae can be broadly correlated with the numerous Proterozoic tectonothermal/igneous events that the Rae Craton has experienced since its stabilization in the Archean, as outlined by Liu et al. (2016). Hence, the indications from the Os isotope data across the Rae Craton are that depletion and the stabilization of the cratonic root

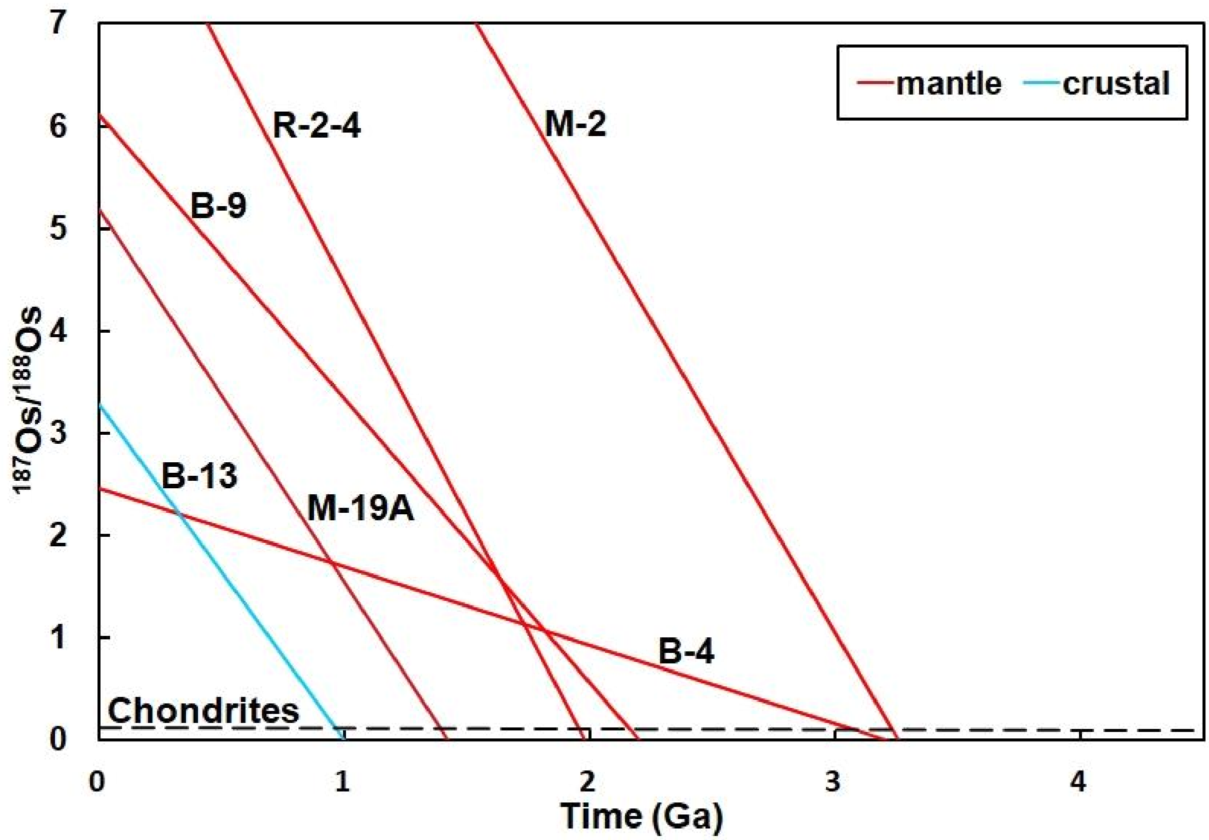

Figure 3.9 Osmium isotope evolution diagram for Darby pyroxenites. Dashed line = chondrite evolution. Solid lines denote the isotope evolution of a sample. Model age given by the intersection of the sample evolution line and chondrite line. All High Os samples classified as mantle using garnet chemistry.

occurred in the Neoarchean. Our observation of a few ~ 2.3 Ga model ages in the Darby dataset may be the first expression of the ~ 2.3 Ga Arrowsmith orogeny (Berman et al., 2013). However, the few Darby peridotites analysed and the imprecise nature of Os model ages - largely because of the uncertainty in the appropriate model reservoir - do not allow a firm conclusion to be reached with the currently available data. Neoarchean stabilization of the cratonic root is consistent with the observation of widespread 2.63 to 2.60 Ga arc-related plutonic rocks intruded through the Rae (Regan et al. 2017). The lithosphere may have either formed from or been thickened by this subduction event, followed by further evidence of intense lithospheric thickening at ~ 2.57 Ga (Regan et al. 2017).

3.4.2 Pyroxenite model ages

The Darby mantle-derived pyroxenites give T_{MA} ages of 1.3, 2.0 to 2.2 and 3.1 to 3.2 Ga (Figure 3.9). The T_{MA} ages reflect primary Re-Os fractionation during derivation of the parental melt from the mantle due to their high Re/Os ratios. The oldest ages would appear to document that the production of mafic material either recycled back into the mantle, or mafic/ultramafic magmas produced in the hot Mesoarchean mantle froze in nascent lithospheric mantle of oceanic or continental affinity. The older T_{MA} (3.1 to 3.2 Ga) ages are older than the T_{RD} ages from the peridotites and as old as some Nd model "mantle extraction ages" produced from the oldest crust of the western Rae (e.g., Hartlaub et al. 2005; Schultze et al. 2007). Hence, they might reflect the production of mafic magmas during the formation of the earliest Rae crust. If the source of this basic material is from an underthrust slab this would agree with the interpretation of Chacko et al. (2000) that the Slave and Rae were not separated at 2.00 Ga but were together in the earliest Paleoproterozoic or Archean.

The 2.0 to 2.2 Ga Darby pyroxenites may have been produced from melts freezing in thick continental lithosphere from a wide spectrum of magmatic events that occurred in the Rae between 1.8 to 2.3. The precision on the Re-Os model ages is not sufficient to resolve this further. The younger ~ 1.0 to 1.3 Ga Re-Os model ages, one of which is a plagioclase pyroxenite (B-13) of crustal origin, could reflect their formation from melts related to the Mackenzie Large Igneous event that were injected from the site of the proposed plume head to the WNW, which froze in the lower crust beneath Darby. This is consistent with their anomalously high Fe-Mg temperatures being the result of heat advected into the lower crust at this time. The young pyroxenite of mantle derivation (M-19A) may be a melt from Mackenzie magmatism crystallising at shallow mantle depths.

3.5 Conclusion

Our new Rb–Sr geochronology reveals that the Darby kimberlite field, west central Rae Craton, erupted at 542.2 ± 2.6 Ma. This age is within error of the U–Pb perovskite ages for the Aviat and Repulse Bay kimberlite fields (540 to 530 Ma) in the eastern central Rae Craton, indicating an intense phase of Cambrian kimberlite activity in the Rae Craton (Sarkar et al. in press).

Re–Os dating of the five largest peridotite xenoliths from Darby indicates that the main lithospheric stabilization event occurred in the Neoarchean, forming ~ 200 km thick cratonic mantle, as constrained by clinopyroxene thermobarometry. A Neoarchean stabilization of thick lithosphere beneath the Rae Craton is consistent with the complex and active Neoarchean magmatic history of the Rae (Regan et al. 2017) and indicates mantle thickening during Neoarchean tectonism to stabilise the bulk of the lithospheric mantle evident today.

While some of the high-T crustal pyroxenites likely represent magma crystallised in the lower crust due to Proterozoic magmatism, possibly during the Mackenzie LIP event -as indicated by their Re–Os model ages - the oldest of the pyroxenites may represent Mesoarchean high pressure cumulates from magma infiltrating early oceanic or continental mantle, prior to its thickening in the Neoarchean, or even recycled oceanic crust. The common presence of this basic material in the mantle of the western Rae craton could explain the prominent "surface" evident in receiver-function seismic studies of the Rae lithosphere (Figure 2.25).

Chapter 4
Ti-rich Mantle Metasomatism in the west central Rae Lithosphere

4.1 Introduction

Five pyroxenites erupted by the Darby kimberlite contain a variety of rare Ti-rich minerals, notably, jeppeite as discrete grains or reaction rims on rutile. One heavily-metasomatised pyroxenite xenolith contains rutile with a complex reaction rim (Figure 4.1) comprised of the minerals perovskite, freudenbergite, priderite, ilmenite and $Na_2Ti_6O_{13}$ - a mineral not previously observed in nature (See Table 11; Appendix A, for compositional data). This first natural occurrence of $Na_2Ti_6O_{13}$ is a Na-rich end member of the mineral jeppeite, usually observed in lamproites (Pryce et al. 1984; Grey et al. 1998; Jaques 2016). Previously, $Na_2Ti_6O_{13}$ was a synthetic material commonly used in batteries. Currently steps are being taken to have $Na_2Ti_6O_{13}$ officially named and recognized by the Commission on New Minerals and Mineral Names (CNMMN). In this chapter I review the pervious occurrences of Ti-rich mantle metasomatic minerals and attempt to fit those observed in the pyroxenites at Darby into a genetic framework.

4.2 Occurrences of Ti-rich metasomatic minerals in the mantle

Rutile is observed in a variety of mantle xenocrysts and xenoliths: eclogite, pyroxenites, MARID and zircon suite, metasomatized peridotite xenoliths, inclusions and intergrowths in diamond, as discrete grains in groundmass kimberlites, discrete xenoliths, and in olivine-rutile symplectic intergrowths (Haggerty 1991; Meinhold 2010). Of the above mantle lithologies rutile

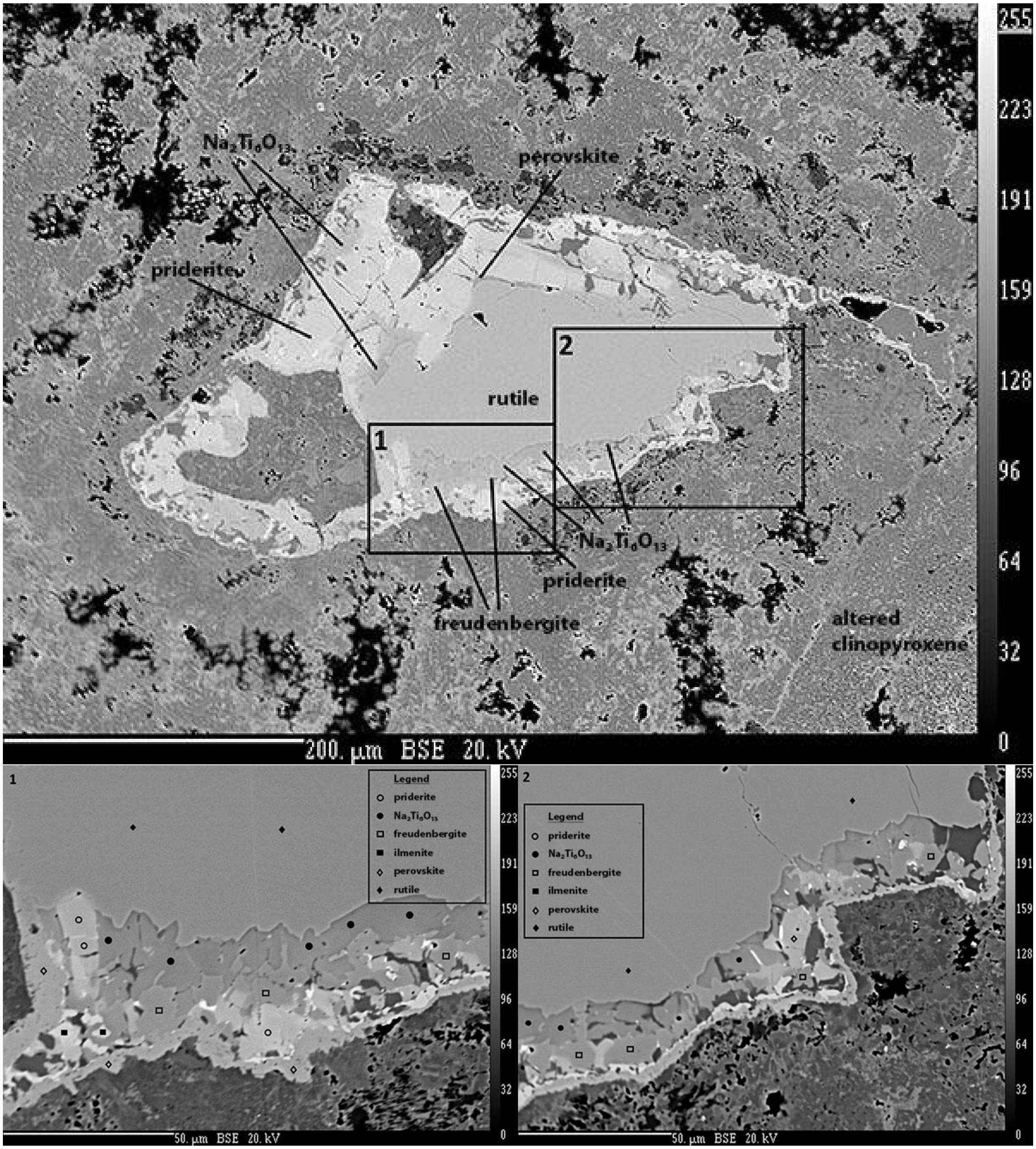

Figure 4.1 New mineral-$Na_2Ti_6O_{13}$ discovered within an pyroxenite xenolith. Mineral-Nixonite (currently unnamed) is a Na analogue of jeppeite-$K_2Ti_6O_{13}$ and was found in a complex reaction rim with priderite, freudenbergite, perovskite, and ilmenite. Other rutiles have a single reaction rim of jeppeite. Priderite and jeppeite are normally associated with lamproites.

is most commonly found in eclogitic (Sobolev et al. 1997; Sobolev et al. 2000; Carswell 1990; Smith and Dawson 1975) or mantle metasomatic assemblages (eg. MARID associations; Haggerty 1991; Dawson and Smith 1977). Minerals such as priderite, jeppeite, freudenbergite, lindsleyite–mathiasite, Cr–Ca–Zr–Nb-bearing armalcolite, baddeleyite, zirconolite, Nb–Cr-bearing rutile and those from the crichtonite and magnetoplumbite mineral groups, have all been documented in metasomatized mantle lithologies. These minerals have an affinity to take on elements that behave highly incompatibly during mantle melting such as the HFSE, LREE, P, Ti, alkalis, Sr, Ba, U, Th into their crystal structure and thus play a major role in the distribution of these elements in the upper mantle.

Priderite-$(K,Ba)(Ti,Fe^{3+})_8O_{16}$ and jeppeite-$(K,Ba)_2(Ti,Fe^{3+})_6O_{13}$ are both minerals observed in lamproites. Jeppeite was first described in a lamproite from Walgidee Hills, Western Australia as prismatic to acicular aggregates associated with and overgrown on priderite (Pryce et al. 1984; Jaques 2016). Since the initial discovery of jeppeite it has been also noted during the discovery of Haggertyite in the Prairie Creek (Arkansas) lamproite (Grey et al. 1998). Although very few occurrences of jeppeite have been reported it appears to be solely associated with lamproitic intrusions. Priderite is abundant in the groundmass of lamproites (first observed by Norrish 1951; Bagshaw et al. 1977) and has been documented in association with diopside and richterite in a nodule of the Prairie Creek (Arkansas) lamproite (Mitchell and Lewis 1983) and in a discrete marcocryst with armalcolite from the Argyle lamproite, Australia (Jaques et al. 1989). In addition, a priderite-related mineral was described in metasomatised and veined peridotites from Bultfontein (Jones et al. 1982). Priderite has also been reported in a metasomatized harzburgite xenolith sampled by one of the kimberlites of the Kimberley cluster, central Kaapvaal Craton (Konzett et al. 2013), and primary priderite macrocrysts have been reported in kimberlites from the Lac de Gras field (Chakhmouradian et al. 2001). Priderite, together with freudenbergite-$Na_2(Ti,Fe)_8O_{16}$ have been found along the grain boundaries of picroilmenites (Kamenetsky et al. 2014).

Freudenbergite was first described in apatite-rich syenites from the Katzenbuckel alkali complex, Germany (Frenzel 1961; Frenzel et al. 1971; McKie 1963; McKie and Long 1970). Furthermore, freudenbergite has been previously observed within granulites from kimberlites in Liberia, West Africa (Haggerty 1983); in metasomatic zircon-bearing xenoliths from Bultfontein (Haggerty and Gurney 1984); and a phlogopite garnet wehrlite (Soltys et al. 2016). However, this mineral is most often found in picroilmenite grains and in zircon reaction suites (Haggerty 1995; Patchen et al. 1997). Freudenbergite contains approximately 8 to 9 wt% Na_2O (Haggerty 1991) which exceeds that of all upper mantle minerals except some omphacites.

4.3 Methods

Initial discovery as well as follow up analyses of the Na-jeppeite reported here was all completed by EPMA at the University of Alberta. After the initial discovery, this analytical campaign included several runs specifically set up to analyze these rare metasomatic minerals. The elements analyzed included: Na_2O, MgO, Al_2O_3, SiO_2, K_2O, CaO, TiO_2, V_2O_3, Cr_2O_3, MnO, FeO, SrO, Nb_2O_5, and BaO. In addition, elemental maps were created on the grain of the host rutile for the new mineral discovery $Na_2Ti_6O_{13}$. The elemental maps created were for the following elements: Na, Ca, K, Ti, and Fe. These elemental maps outlined zones of interest for future analysis, for example, for sampling of the $Na_2Ti_6O_{13}$ for X-ray diffraction characterisation.

4.4 Results

4.4.1 Jeppeite, priderite, freudenbergite and $Na_2Ti_6O_{13}$

Jeppeite ($K_2Ti_6O_{13}$) was first observed in the Darby mantle xenolith suite within one of the first pyroxenite xenoliths studied by EPMA. With the discovery of the new mineral $Na_2Ti_6O_{13}$, oxides in each pyroxenites thick section were studied in extreme detail in hopes to find another occurrence of this mineral. New thin sections were cut for every pyroxenite and several were cut from the xenolith with the new mineral (M-2B). The small size of this xenolith (~ 1 cm x 1cm x 0.5cm) precluded the manufacture of three more thick sections. No other occurrences of Na-Jeppeite were found. As shown in Figure 4.1 the reaction rim of this rutile is extremely complex, being intergrown with multiple phases. No other reaction rims on rutile were observed to be this complex. Within the complex reaction rim on rutile illustrated in Fig. 4.1, minerals identified include: Na-jeppeite, priderite, freudenbergite, perovskite, and ilmenite and jeppeite. Jeppeite is also found as discrete grains in other thin sections from this pyroxenite. Furthermore, the rest of the xenolith had high levels of alteration and was heavily metasomatized.

As stated in Chapter 3, the host rutile observed in the Darby pyroxenites is very pure (TiO_2 > 98 wt%), low in Cr. The rutile observed in the jeppeite-free and jeppeite-bearing xenoliths has no observable difference in composition, likewise the rutile in the Na-jeppeite sample is not distinct from other rutile-bearing pyroxenites.

In the new mineral discovery xenolith, almost no primary clinopyroxene was found, the altered clinopyroxene that was observed had a diopside composition with high Al (> 7 wt%). In addition, a low abundance of garnet was found in this sample with approximately 30:70 garnet to pyroxene. The garnet had the highest Ca observed out of any xenoliths (8.6 – 9.3 wt%) with only four of 233 low-Cr grains from concentrate having Ca of this level, one falling in this range and three > 12 wt%. Although no more $Na_2Ti_6O_{13}$ was found, several discrete jeppeite grains and other jeppeite reaction rims on rutiles were found in this sample and in four other samples. All the jeppeite measured in the xenoliths had little to no Ba which has been documented to substitute for K – $(K, Ba)_2(Ti, Fe)_6O_{13}$. Instead various amounts of Na were found to substitute into jeppeite. However, Ba was observed in priderite (BaO < 2 wt%) – $(K, Ba)(Ti, Fe)_8O_{16}$. The $Na_2Ti_6O_{13}$ and freudenbergite reaction rim is clearly shown by the Na elemental abundance map, Figure 4.2A, with the red zone being the most concentrated portion of $Na_2Ti_6O_{13}$. Other elemental maps show K – priderite, jeppeite, $Na_2Ti_6O_{13}$ (Na-jeppeite), and freudenbergite, Figure 4.2B; Ti – rutile host and rare Ti minerals surrounding it, Figure 4.2C; Ca –perovskite and heavy alteration of surrounding rutile and rim, Figure 4.2D; Fe –ilmenite and heavy alteration of surrounding rutile and rim, Figure 4.2E. The variation in the minerals found in the Na-jeppeite are shown in the ternary plot in Figure 4.3. All major element results are found in Table 11; Appendix A.

4.5 Discussion

4.5.1 Ti-rich Mantle Metasomatism beneath Darby

Several minerals found in the metasomatic assemblage around Darby rutile grains have only been previously reported in lamproites. These minerals include jeppeite in five pyroxenites as well as priderite, freudenburgite, and a new mineral $Na_2Ti_6O_{13}$ (Na-end-member of jeppeite) in one of the heavily metasomatized pyroxenites. These K-Na and Ti-rich metasomatic phases are indicative of a particular style of metasomatic enrichment that is restricted to highly alkaline, Ti-rich melts. While the Darby kimberlites have been classified as archetypal kimberlites (Weir

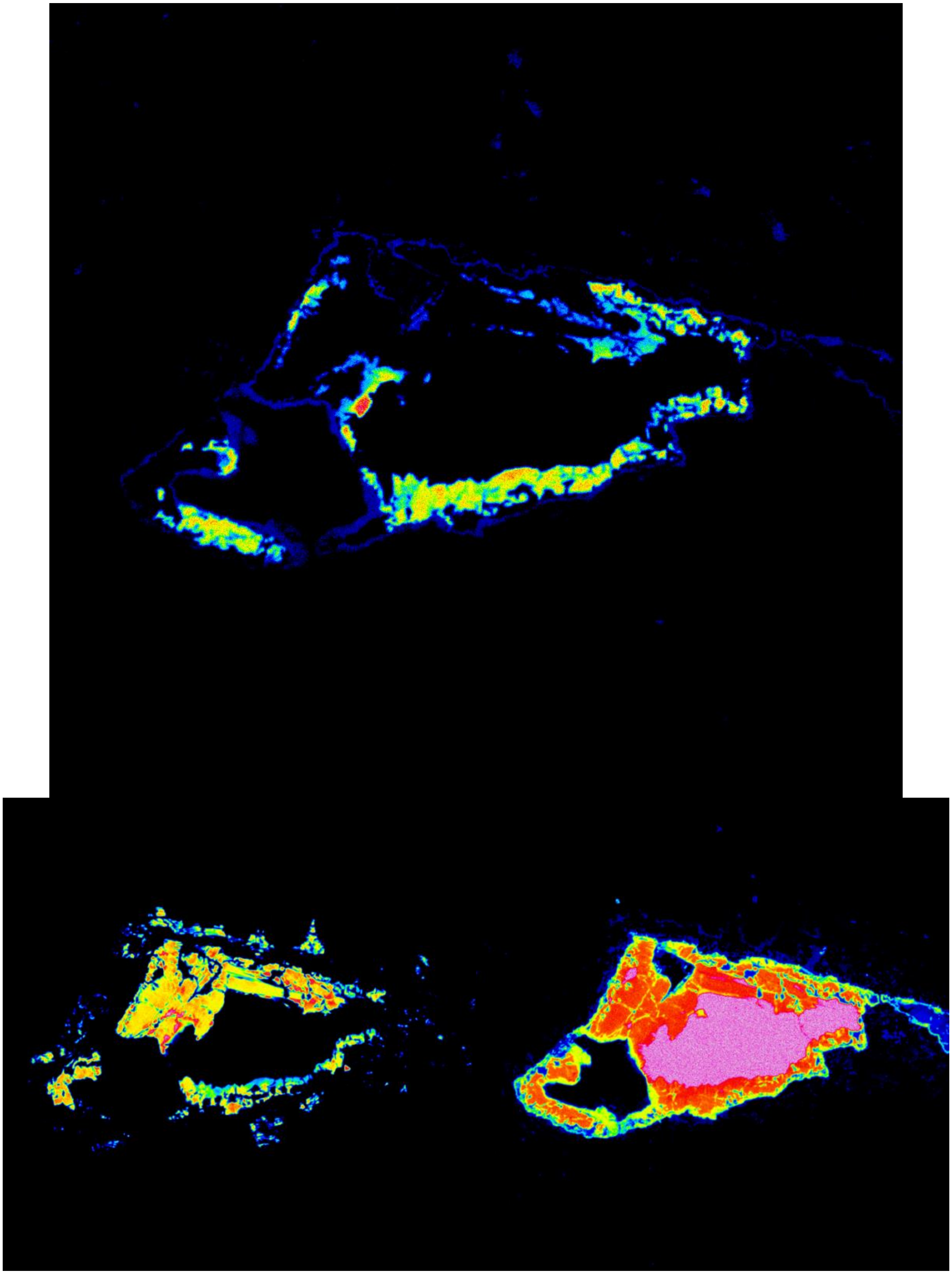

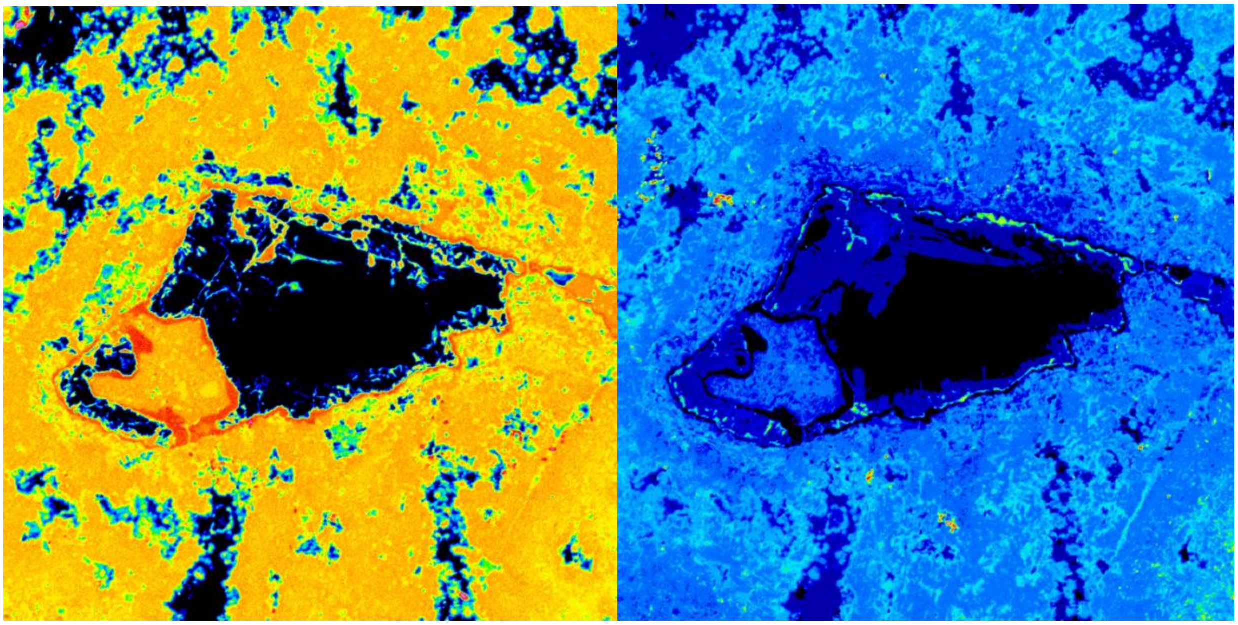

Figure 4.2A Na elemental map displaying $Na_2Ti_6O_{13}$ (Na-jeppeite) and freudenbergite reaction rim. Dark red shows zone where Na-Jeppeite is the most abundant. **B** K elemental map dominantly showing priderite, jeppeite, $Na_2Ti_6O_{13}$ (Na-jeppeite), and freudenbergite **C** Ti elemental map showing shows rutile host and rare Ti minerals surrounding it. **D** Ca elemental map shows perovskite and heavy alteration of surrounding material of rutile and rim **E** Fe elemental map shows ilmenite and heavy alteration of surrounding material of rutile and rim.

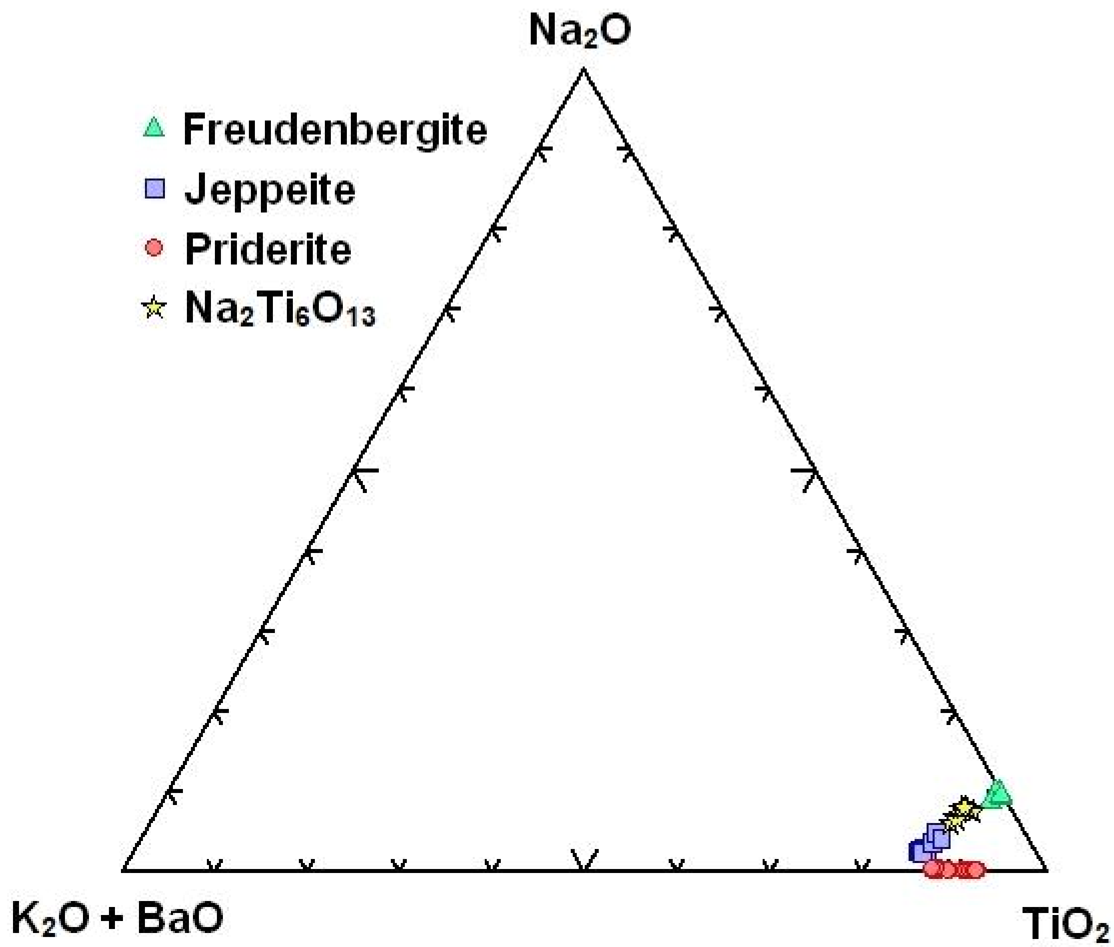

Figure 4.3 K_2O+BaO-Na_2O-TiO_2 ternary showing range in composition of priderite, jeppeite, Nixonite (currently unnamed; $Na_2Ti_6O_{13}$) and freudenbergite.

and Farmer 2009), at least one body is reported as being of lamprophyre affinity. Moreover Sarkar et al. (in press) have recently reported the occurrence of intrusive rocks at Aviat, to the east of the Darby field, that are akin to Group II kimberlites. This group of kimberlites has mineralogical similarities to lamproites and are known to have K-Ba-V titanates in their ground mass (Mitchell 1995). The occurrences of freudenburgite and the critchonite-magnetoplumbite series minerals in metasomatised peridotites at Kimberley is notable because the Ti-K, Na-rich MARID-like metasomatism there has been proposed to be the source of Group II kimberlites (Guiliani et al. 2015). Hence, these metasomatic assemblages recorded in the Darby mantle could be records of the metasomatic priming of the lithospheric mantle that took place prior to the generation of the Group II kimberlites observed in the eastern Central Rae craton, at Aviat.

The observation, at Darby, of three polymict breccias also may indicate a failed intrusion at depth as they have been interpreted as failed kimberlite intrusions produced by primitive or precursor kimberlite magmas that terminated at mantle depth (Lawless et al. 1979; Pokhilenko 2009). If lamproitic or Group II kimberlite melt was ascending through the sublithospheric mantle and it encountered a pyroxenite-rich horizon such as a subducted slab, it could have been temporarily stalled and unable to reach the surface (e.g., as proposed at Lac de Gras; Snyder and Lockhart 2009). Snyder and Lockhart (2009) propose that numerous wehrlite-pyroxenite stalled dyke stockworks were required to explain intense SKS anisotropy observed in the lithospheric mantle beneath the La de Gras kimberlite field. Darby (STLN on Fig. 2.20) does not show this 2-layered anisotropy signature that may be indicative of intense metasomatism, only a single 070 polarization. However, no Group II kimberlites have been recorded in the central Lac de Gras kimberlite field - a much more extensive kimberlite field of > 250 bodies - and hence the K-Na-Ti metasomatism required to generate Group II kimberlites may not be expressed by a seismic signature than the dense intrusions of the lithospheric mantle that must have taken place beneath the Lac de Gras region.

4.6 Conclusions

The first co-existing assemblage of freudenbergite, priderite, jeppeite and Na-jeppeite has been recorded within a pyroxenite xenolith from the Darby kimberlite field. This occurrence is also the first occurrence in nature of the as yet unnamed Na- endmember of jeppeite and also the first record of jeppeite except in the groundmass of lamproites. An unusual metasomatic melt must have percolated into the lithospheric mantle beneath the Darby field to produce this complex Na-K-Ti rich metasomatic mineral assemblage. Elsewhere in the Rae Craton lithosphere, to the east, this type of melt may have generated the enriched source regions required to form the Group II kimberlites recorded in the 540 to 530 Ma Aviat kimberlite field (Sarkar et al. in press). Isotopic work is required on these assemblages to try to define the timing of their formation in the Rae lithosphere.

Chapter 5
Conclusions

5.1 Key findings

- The eruption of the Darby kimberlite field is dated here at 542.2 ± 2.6 Ma by Rb-Sr and 548 ± 13 Ma by U-Pb rutile. These estimates are within uncertainty of the ages of the Cambrian kimberlite fields at Aviat and Repulse Bay (540 to 530 Ma; Sarkar et al. in press).
- The small suite of peridotite xenoliths recorded at Darby - the first to be analysed from the western central Rae Craton - have bulk rock and mineral compositions consistent with them representing cratonic mantle lithosphere. Based on the small sample set, these compositions appear to be the most melt-depleted peridotite compositions so far recorded from the Rae lithospheric mantle, being more depleted than those from Somerset Island to the north (e.g., Irvine et al. 2003) and Pelly Bay/Repulse Bay to the east (Liu et al. 2016).
- Garnets within the peridotites and those recovered from both kimberlite heavy mineral concentrate and till are dominantly G9 lherzolitic in composition, although one of the small xenoliths contains a G10D garnet.
- Diopsides separated from kimberlite heavy mineral concentrate and till define a mantle geotherm that indicates a lithospheric thickness beneath Darby of ~ 200 km at 542.2 ± 2.6 Ma.
- Nickel-in garnet and Al-in-olivine thermometry indicates the sampling of mantle material by the Darby intrusions throughout the lithosphere.

- A super-adiabatic population of garnets indicates a possible significant mantle thermal disturbance shortly before kimberlite eruption, with insufficient time for the thermally equilibrated geotherm defined by the diopsides to reflect this disturbance.
- Garnet pyroxenite was recovered as xenoliths in the field over every Darby intrusion sampled. The garnet xenocryst population also contains a significant population of pyroxenitic garnets that greatly exceed the volume of eclogitic/pyroxenitic material generally thought to be extant in cratonic lithospheric mantle. Some of these pyroxenites may originate from a foundered mantle slab or frozen mantle intrusions of melt while others appear to reflect crystallisation in the crust, perhaps from melts related to the Mackenzie LIP event.
- Rhenium-Os dating of the small suite of mantle peridotites indicate likely Neoarchean formation, as seen in other parts of the Rae lithosphere.
- The timing of residue formation indicated by the Neoarchean assembly of the Rae lithospheric mantle is consistent with the complex thermo-tectonic evolution of the crustal rocks throughout the Rae (Reagan et al. 2017) and indicates lithospheric formation by collisional processes at that time.
- A new seismic image shows a distinct layering in the western Rae lithosphere. This demonstrates the collisional forces required during lithosphere formation, furthermore this distinct layer may reflect a body of mafic nature resulting in the large proportion of pyroxenite/eclogite recovered at Darby.
- Implications for diamond tenor - Teck found the diamond grade was low - likely linked to the lithosphere heating event.

5.2 Future work

In order to obtain a more robust age constraint of the timing of lithospheric mantle formation, more peridotites should be analysed for Re-Os isotopes. Due to the fact the surface kimberlite is highly altered, the drill core currently owned by Teck would be an additional source of samples. This would perhaps allow definition of whether there is any spatial age difference in the lithospheric mantle beneath the Rae, as observed in the crust (e.g., Schultz et al. 2007). Obtaining fresh kimberlite host rock would allow petrographical and geochemical work on the kimberlites; something that has not been undertaken so far.

If larger pyroxenites were found in the drill core it would be interesting to see if the K-Na-Ti rich suite of metasomatic minerals are spread throughout the pyroxenite xenoliths. In addition, three of the pyroxenites may have sufficient material for Lu-Hf isotopes and this, plus isotopic analysis of some of the metasomatic minerals should be carried out to further refine the formation ages of the pyroxenite suite and its metasomatic history and possible link with Group II kimberlite magmatism in the east of the Rae craton. If more mantle xenoliths were available, a thorough search for the Na-K-Ti metasomatic assemblage within peridotites would reveal whether this metasomatism was restricted only to the pyroxenites, or affects the peridotites as found in the Kaapvaal Craton. The possible link between the super-adiatic heating event suggested by the peridotitic garnets and the poor diamond grades that led to the abandonment of the Darby project would be investigated by more indicator mineral and mantle xenolith P-T and chemistry work.

Lastly, sufficient material, in powder form, should be obtained from the Na-jeppeite to allow an X-ray diffraction pattern to be produced. This data would be sufficient to allow the mineral to be named and officially recognized by the Commission on New Minerals and Mineral Names (CNMMN).

References

Ansdell KM, Norman AR (1995) U–Pb geochronology and tectonic development of the southern bank of the Kisseynew domain, Trans-Hudson Orogen, Canada. Precambrian Research 72:147-167

Andersen T (2002) Correction of common lead in U–Pb analyses that do not report ^{204}Pb. Chemical Geology 192:59-79

Aspler LB, Chiarenzelli JR (1998) Two Neoarchean supercontinents? Evidence from the Paleoproterozoic. Sedimentary Geology 120:75-104

Aulbach S, O'Reilly SY, Griffin WL, Pearson NJ (2008) Subcontinental lithospheric mantle origin of high niobium/tantalum ratios in eclogites. Nature Geoscience 1(7):468-472

Aulbach S, Mungall JE, Pearson DG (2015) Distribution and Processing of Highly Siderophile Elements in Cratonic Mantle Lithosphere. Reviews in Mineralogy & Geochemistry 81:239-304

Bagshaw AN, Doran BH, White AH, Willis AC (1977) Crystal Structure of a Natural Potassium-Barium Hexatitanate Isostructural with $K_2Ti_6O_{13}$ 33:1995-2000

Berman RG, Sanborn-Barrie M, Stern RA, Carson CJ (2005) Tectonometamorphism at ca. 2.35 and 1.85 Ga in the Rae Domain, western Churchill Province, Nunavut, Canada: insights from structural, metamorphic and in situ geochronological analysis of the southwestern Committee Bay Belt. Can Mineral 43:409-442

Berman RG, Davis WJ, Pehrsson S (2007) Collisional Snowbird tectonic zone resurrected: growth of Laurentia during the 1.9 Ga accretionary phase of the Hudsonian orogeny. Geology 35:911-914.

Berman RG (2010) Metamorphic map of the western Churchill Province. Geological Survey of Canada. Open File 5279 (3 sheets, 49 p. report)

Berman RG, Pehrsson S, Davis WJ, Ryan JJ, Qui H, Ashton KE (2013) The Arrowsmith orogeny: Geochronological and thermobarometric constraints on its extent and tectonic setting in the Rae craton, with implications for pre-Nuna supercontinent reconstruction. Precambrian Research 232:44-69

Bethune KM, Scammel RJ (1997) Legend and descriptive notes, Koch Island area, District of Franklin, Northwest Territories, (Part of NTS 37C), Geological Survey of Canada, Open file 3391 Scale 1:50 000

Birck JL, Barman MR (1991) Re-Os Isotopic Measurements at the Femtomole Level in Natural Samples, 20

Bostock MG (1998) Mantle stratigraphy and evolution of the Slave province. Journal of Geophysical Research 103(B9):183-200

Boyd FR, Mertzman SA (1987) Composition and structure of the Kaapvaal lithosphere, South Africa. Magmatic Processes: Physicochemical Principles. The Geochemical Society, Special Publication No. I. 13-24

Brown RW, Allsopp HL, Bristow JW, Smith CB (1989) Improved precision of Rb–Sr dating of kimberlitic micas: an assessment of a leaching technique. Chemical Geology 79:125-136

Bussweiler Y, Brey GP, Pearson DG, Stachel T, Stern RA, Hardman MF, Kjarsgaard BA, Jackson SE (2017) The aluminum-in-olivine thermometer for mantle peridotites – Experimental versus empirical calibration and potential applications. Lithos 272-273:301-314

Canil D (1999) The Ni-in-garnet geothermometer: calibration at natural abundances. Contrib Mineral Petrol 136: 240-246

Carswell DA (1990) Eclogites and the eclogite facies: definitions and classification. In: Carswell DA (ed) Eclogite facies rocks. Blackie, Glasgow, London, pp 1-13

Chacko T, De SK, Creaser RA, Muehlenbachs K (2000) Tectonic setting of the Taltson magmatic zone at 1.9–2.0 Ga; a granitoid-based perspective. Canadian Journal of Earth Sciences 37:1597-1609

Chakhmouradian AR, Mitchell R (2001) Three compositional varieties of perovskite from kimberlites of the Lac de Gras field (Northwest Territories, Canada). Mineralogical Magazine 65(1):133-148

Cherniak DJ (2000) Pb diffusion in rutile. Contributions to Mineralogy and Petrology 139:198-207

Cohen AS, Waters FG (1996) CHIMICA Separation of osmium from geological materials by solvent extraction for analysis by thermal ionisation mass spectrometry *2670*(96)

Counts B (July 31, 2008) http://www.marketwired.com/press-release/indicator-minerals-darby-project-yields-more-kimberlite-partner-increases-budget-tsx-venture-ime-884912.htm. Accessed Nov 24, 2017

Creaser RA, Gru H, Carlson J, Crawford B (2004) Macrocrystal phlogopite Rb–Sr dates for the Ekati property kimberlites, Slave Province, Canada: evidence for multiple intrusive episodes in the Paleocene and Eocene. Lithos 76:399-414

Davis WJ, Hanmer S, Tella S, Sandeman HA, Ryan JJ (2006) U–Pb geochronology of the MacQuoid supracrustal belt and Cross Bay plutonic complex: key components of the northwestern Hearne subdomain, western Churchill Province, Nunavut, Canada. Precambrian Res. 145:53-80

Dawson JB, Stephens WE (1975) Statistical Classification of Garnets from kimberlite and Associated Xenoliths. The Journal of Geology 83(5):589-607

Dawson JB, Smith JV (1977) MARID (mica-amphibole-rutile-ilmenite-diopside) suite of xenoliths in kimberlite. Geochim Cosmochim Acta 41(2):309-323

Desmons J, Smulikowski W (2007) A systematic nomenclature for metamorphic rocks: 4. In: High P/T metamorphic rocks. Recommendations by the IUGS Subcommission on the Systematics of Metamorphic Rocks. SCMR website. www.bgs.ac.uk/SCMR

Foley SF, Prelevic D, Rehfeldt T, Jacob DE (2013) Minor and trace elements in olivines as probes into early igneous and mantle melting processes. Earth and Planetary Science Letters 363:181-191

Frenzel G (1961) Ein neues mineral: Freudenbergit ($Na_2Fe_2Ti_7O_{18}$) N. Jb. Mineral Mh 12-22

Frenzel G, Ottemann J, Nuber B (1971) Meue mikrosonden-untersuchun-gen an Freudenbergit. N. Jb. Mineral. Montash 547-551

Frisch T, (1982) Precambrian geology of the Prince Albert Hills, western Melville Peninsula, northwest territories. Geological Survey of Canada Bulletin 346

Grey IE, Velde D, Criddle AJ (1998) Haggertyite, a new magnetoplumbite-type titanate mineral from the Prairie Creek (Arkansas) lamproite. American Mineralogist 83(12):1323-1329

Griffin WL, Cousens DR, Ryan CG, Sie SH, Suter GF (1989) Ni in chrome pyrope garnets: a new geothermometer. Contributions to Mineralogy and Petrology 103(2):199-202

Griffin WL, Ryan CG (1995). Trace elements in indicator minerals: area selection and target evaluation in diamond exploration. Journal of Geochemical Exploration 53:311-337

Grütter HS, Gurney JJ, Menzies AH, Winter F (2004) An updated classification scheme for mantle-derived garnet, for use by diamond explorers. Lithos 77:841-857

Grütter HS, Latti D, and Menzies A, (2006) Cr-Saturation Arrays in Concentrate Garnet Compositions from Kimberlite and their Use in Mantle Barometry. Journal of Petrology 47(4):801-820

Grütter HS (2009). Pyroxene xenocryst geotherms: Techniques and application. Lithos 112S:1167-1178

Gurney JJ, Zweistra, P (1995) The interpretation of the major element compositions of mantle minerals in diamond exploration. Journal of Geochemical Exploration 53:293-309

Haggerty SE (1983) The mineral chemistry of new titanates from the jagersfontein kimberlite, South Africa: Implications for metasomatism in the upper mantle. Geochimica et Cosmochimica Acta 47(11):1833-1854

Haggerty SE, Gurney JJ (1984) Zircon-bearing nodules from the upper mantle. (Abs.) EOS Trans. Am. Geophys. Union 65:301

Haggerty SE (1991) Oxide Minerals: Petrological and Magnetic Significance. Reviews in Mineralogy 25:355-416

Haggerty SE (1995) Upper mantle mineralogy 20(4):331–364

Hanmer S, Bowring S, Vanbreemen O, Parrish R, (1992) Great Slave Lake shear zone, NW Canada – mylonitic record of Early Proterozoic continental convergence, collision and indentation. J Struct Geol 14:757-773

Hardman MF, Pearson DG, Stachel T, Sweeney RJ (2018a) Statistical approaches to the discrimination of crust- and mantle-derived low-Cr garnet -- major-element-based methods and their application in diamond exploration. Journal of Geochemical Exploration 186: 24-35

Hardman MF, Pearson DG, Stachel T, Sweeney RJ (2018b) Statistical approaches to the discrimination of mantle- and crust-derived Low-Cr garnets using major and trace element data. Mineralogy and Petrology, submitted

Harte B, Kirkley MB (1997) Partitioning of trace elements between clinopyroxene and garnet: data from mantle eclogites. Chem. Geol. 136:1–24

Harte, B, Jackson, PM, Macintyre, RM (1981) Age of mineral equilibria in granulite facies nodules from kimberlites. Nature 291:147-148

Hartlaub RP, Chacko T, Heaman LM, Creaser RA, Ashton KE, Simonetti A (2005) Anchient (Meso- to Paleoarchean) crust in the Rae Province, Canada: Evidence from Sm-Nd and U-Pb Constraints. Precambrian Research 141:137-153

Hartlaub RP, Heaman LM, Ashton KE and Chacko T (2001) The Murmac Bay Group, Rae Provience: record of a giant Archean rift? In 4th International Archean Symposium 2001, Extended Abstract, KF Cassidy, JM Dunphy, MJ Van Kranendok (eds.); Australian Geological Survey Organization-Geoscience Australia, Record 2001/37:317-318

Heaman LM, LeCheminant AN, Rainbird RH (1992) Nature and timing of Franklin igneous events, Canada: Implications for a Late Proterozoic mantle plume and the breakup of Laurentia. Earth and Planetary Science Letters, 109:117-131

Henderson JR, Boome J (1990) Geometry and kinematics of the Wager shear zone interpreted from structural fabrics and magnetic data. Canadian Journal of Earth Sciences 27:590-604

Heywood WW (1961) Geological Notes, Northern District of Keewatin, Parts of 56, 57,66 and 67; Geol Surv of Canada, Paper 61-18, 9 p

Heywood WW, Schau M (1978) A subdivision of the Northern Churchill Structural Province. Geol Surv of Canada, Paper 78-1A, 139-143 p

Hoffman PF (1987) Continental transform tectonics: Great Slave Lake shear zone (ca. 1.9 Ga), Northwest Canada. Geology 15:785-788

Hoffman PF (1988) United Plates of America, the birth of a craton – Early Proterozoic assembly and growth of Laurentia. Annu Rev Earth Planet Sci 16:543-603

Holmden CE, Creaser RA, Muehlenbachs K, Bergstrom SM, Leslie SA (1996) Isotopic and elemental systematics of Sr and Nd in 454 Ma biogenic apatites: implications for paleoseawater studies. Earth and Planetary Science Letters 142:425-437

Irvine GJ, Pearson DG, Kjarsgaard BA, Carlson RW, Kopylova MG, Dreibus G (2003) A Re – Os isotope and PGE study of kimberlite-derived peridotite xenoliths from Somerset Island and a comparison to the Slave and Kaapvaal cratons. Lithos 71:461-488

Ishikawa A, Senda R, Suzuki K, Dale CW, Meisel T (2014). Re-evaluating digestion methods for highly siderophile element and Os isotope analysis: Evidence from geological reference materials. Chemical Geology 384:27-46

Jackson GD (1966) Geology and mineral possibilities of the Mary River region, northern Baffin Island. Can Mineral 87:57-61

Jacob DE, Schmickler B, Schulze DJ (2003) Trace element geochemistry of coesite-bearing eclogites from the Roberts Victor kimberlite, Kaapvaal craton. Lithos 71:337-351

Jacob DE (2004) Nature and origin of eclogite xenoliths from kimberlites. Lithos 77(1–4):295-316

Jagoutz E, Dawson JB, Hoernes S, Spettel B, Wänke H (1984) Anorthositic oceanic crust in the Archean Earth. 15th Lunar Planet. Sci. Conf., 395-396 Abs.

Jaques AL, Kerr ID, Lucas H, Sun SS, Chappell BW (1989) Mineralogy and petrology of picritic monchiquites from Wandagee, Carnarvon Basin, Western Australia. Geological Society of Australia Special Publication 14:120-139

Jones AG, Snyder D, Hanmer S, Asudeh I, White D, Eaton D, Clarke G (2002) Magnetotelluric and teleseismic study across the Snowbird tectonic zone, Canadian Shield; a Neoarchean mantle suture? Geophysical Research Letters 29

Jones AP, Smith JV, Dawson JB (2016) Mantle Metasomatism in 14 Veined Peridotites from Bultfontein Mine, South Africa. The University of Chicago Press Stable 13, 90(4):435-453

Kamenetsky VS, Golovin AV, Maas R, Giuliani A, Kamenetsky MB, Weiss Y (2014) Towards a new model for kimberlite petrogenesis: Evidence from unaltered kimberlites and mantle minerals. Earth-Science Reviews 139:145-167

Kjarsgaard BA (2007) Kimberlite diamond deposits. W. Goodfellow (Ed.), Mineral Deposits of Canada, Geological Association of Canada Mineral Deposits Division Special Publication, vol. 5 (2007), pp. 245-272

Kjarsgaard BA, Peterson TD (1992) Kimberlite-derived ultramafic xenoliths from the diamond stability field: a new Cretaceous geotherm for Somerset Island, Northwest Territories. Current Research, Part B; Geological Survey of Canada, Paper 92-1B:1-6

Klein-BenDavid O, Graham Pearson D (2009) Origins of subcalcic garnets and their relation to diamond forming fluids-Case studies from Ekati (NWT-Canada) and Murowa (Zimbabwe). Geochimica et Cosmochimica Acta 73(3):837-855

Konzett J, Wirth R, Hauzenberger C, Whitehouse M (2013) Two episodes of fluid migration in the Kaapvaal Craton lithospheric mantle associated with Cretaceous kimberlite activity: Evidence from a harzburgite containing a unique assemblage of metasomatic zirconium-phases. Lithos 182-183:165-184

Krogh RE (2000) The garnet – clinopyroxene Fe^{2+} – Mg geothermometer: an updated calibration. Journal of Metamorphic Geology 18:211-219

LaFlamme C, McFarlane CRM, Corrigan D (2014) U–Pb, Lu–Hf and REE in zircon from 3.2 to 2.6 Ga Archean gneisses of the Repulse Bay block, Melville Peninsula, Nunavut. Precambrian Res 252:223-239

Lawless P J, Gurney JJ, Dawson JB (1979) Polymict peridotites from the Bultfontein and De Beers mines, Kimberley, South Africa. In: Boyd, F. R. & Meyer, H. O. A. (eds) The Mantle Sample. 2nd International Kimberlite Conference. American Geophysical Union, 145-155 p

LeCheminant AN, Roddick JC, Tessier AC, Bethune KM (1987) Geology U-Pb ages of early Proterozoic calc-alkaline plutons northwest of wager Bay, District of Keewatin. Geological Survey of Canada Current Research 87-1A, 773-782

LeCheminant AN, Heaman LM (1989) MacKenzie igneous events, Canada: Middle Proterozoic hotspot magmatism associated with ocean opening. Earth and Planetary Science Letters 96:38-48

LeCheminant AN, Roddick JC (1991) U-Pb zircon evidence for widespread 2.6 Ga felsic magmatism in the central District of Keewatin, N.W.T.: In Radiogenic Age and isotopic studies: report 4, Geological Survey of Canada, Paper 90-02, 91-99

Li J, Jiang X, Xu J, Wang X (2013) Determination of Platinum-Group Elements and Re-Os Isotopes using ID-ICP-MS and N-TIMS from a Single Digestion after Two-Stage Column Separation, 38:37-50

Little EC, Ferbey T, McMartin I, Ozyer C, Utting D (2002) Overview of Quaternary research for the Committee Bay Project, central Nunavut. Geological Survey of Canada Current Research 2002-C13

Liu J, Riches AJV, Pearson DG, Luo Y, Kienlen B, Kjarsgaard BA, Stachel T, Armstrong JP (2016) Age and evolution of the deep continental root beneath the central Rae craton, northern Canada. Precambrian Research 272:168-184

Liu J, Pearson DG (2014) Rapid, precise and accurate Os isotope ratio measurements of nanogram to sub-nanogram amounts using multiple Faraday collectors and amplifiers equipped with 10^{12} Ω resistors by N-TIMS. Chemical Geology 363:301-311

Luvizotto GL, Zack T, Meyer HP, Ludwig T, Triebold S, Kronz A, Münker C, Stockli DF, Prowatke S, Klemme S, Jacob DE, von Eynatten H (2009) Rutile crystals as potential trace element and isotope mineral standards for microanalysis. Chemical Geology 261(3-4):346-369

MacHattie T (Ph.D. thesis) (2008) Geochemistry and Geochronology of the Late Archean Prince Albert Group (PAG), Nunavut, Canada. University of Alberta, 61-63, 339p.

Malkovets VG, Rezvukhin DI, Belousova EA, Griffin WL, Sharygin IS, Tretiakova IG, Gibsher AA, O'Reilly SY, Kuzmin DV, Litasov KD, Logvinova AM, Pokilenko NP, Sobolev NV (2016) Cr-rich rutile: A powerful tool for diamond exploration. Lithos 265:304-311

Marchesi C, Dale CW, Garrido CJ, Pearson DG, Bosch D, Bodinier J, Gervilla F, Hidas K (2014) Fractionation of highly siderophile elements in refertilized mantle: Implications for the Os isotope composition of basalts. Earth and Planetary Science Letters 400:33-44

Martel E, Van Breemen O, Berman RG, Pehrsson S (2008) Geochronology and tectonometamorphic history of the Snowbird Lake area, Northwest Territories, Canada: new insights into the architecture and significance of the Snowbird tectonic zone. Precambrian Res 161:201-230

Maynes A, Doulos D (2007) Assessment report on the Darby Property 2006 diamond exploration program, ground and airborne geophysics, drilling, and heavy mineral sampling. Unpublished report prepared by Indicator Minerals Inc

Mather KA, Pearson DG, McKenzie D, Kjarsgaard B, Priestley K (2011) Constraining the depth and thermal history of cratonic lithosphere using peridotite xenolith and xenocryst thermobarometry and seismology. Lithos 125:729-742

McDonough WF, Sun S-s (1995) The composition of the Earth. Chemical Geology 120:223-253

Mckenzie D, Bickle MJ (1988) The Volume and Composition of Melt Generated by Extension of the Lithosphere. Journal of Petrology 29:625-679

McKie D (1963) The unit cell of freudenbergite. Z. Krist 119:157-160

McKie D, Long JVP (1970) The unit cell contents of freudenbergite. Z. Krist 132:157-160

McMartin I, Little EC, Ferbey T, Ozyer C, Utting D (2003) Ice flow history and drift prospecting in the Committee Bay belt, central Nunavut: results from the Targeted Geoscience Initiative. Geological Survey of Canada, Current Research 2003-C4

Menzies A (2003) Re–Os systematics of diamond-bearing eclogites from the Newlands kimberlite. Lithos 71(2–4):323-336

Meinhold G (2010) Rutile and its applications in earth sciences. Earth-Science Reviews 102:1-28

Mitchell RH, Lewis RD (1983) Priderite bearing xenoliths from the Prairie Creek Mica Pebidotite, Arkansas. Canadian Mineralogist 21:59-64

Mitchell RH (1987) Mantle-derived xenoliths in Canada. In: Nixon PH (Ed.), Mantle Xenoliths. Wiley, Chichester, pp. 33-40

Münker C, Pfänder JA, Weyer S, Büchl A, Kleine T, Mezger K (2003) Evolution of planetary cores and the Earth–Moon system from Nb/Ta systematics. Science 301:84-87

Nier AO (1950) A Redetermination of the Relative Abundances of the Isotopes of Carbon, Nitrogen, Oxygen, Argon, and Potassium. Physical Review 77:789-793

Nimis P, Taylor WR (2000) Single clinopyroxene thermobarometry for garnet peridotites. Part I. Calibration and testing of a Cr-in-Cpx barometer and an enstatite-in-Cpx thermometer. Contributions to Mineralogy and Petrology 139(50):541-554

Nixon PH, Boyd FR (1973) Petrogenesis of the granular and sheared ultrabasic nodule suite in kimberlite. In P.H. Nixon, Ed., Lesotho Kimberlites, Lesotho National Development Corp., Maseru, Lesotho, 48-56

Norrish K (1951) Priderite, a New Mineral from the Leucite-Lamproites of the West Kimberley Area, Western Australia. Mineralogical Magazine 29(212):496-501

Parrish RR (1989) U-Pb geochronology of the Cape Smith Belt and Sugluk Block, northern Quebec; Geoscience Canada, 16:126-130

Pearson DG, Wittig N (2014) 3.6 - The formation and evolution of the subcontinental mantle lithosphere - evidence from mantle xenoliths. In: Treatise of Geochemistry 2nd edition, Elsevier, Oxford, pp 255-292

Pearson DG, Wittig N (2008) Formation of Archaean continental lithosphere and its diamonds: the root of the problem. Journal of the Geological Society 165:895-914

Pearson DG, Irvine GJ, Ionov DA, Boyd FR, Dreibus GE (2004) Re – Os isotope systematics and platinum group element fractionation during mantle melt extraction: a study of massif and xenolith peridotite suites. Chemical Geology 208:29-59

Pearson DG, Woodland S J (2000) Solvent extraction/anion exchange separation and determination of PGEs (Os, Ir, Pt, Pd, Ru) and Re-Os isotopes in geological samples by isotope dilution ICP-MS. Chemical Geology 165(1–2):87-107

Pearson DG, Kelley SP, Pokhilenko NP, Boyd FR (1997) Laser $^{40}Ar/^{39}Ar$ analyses of phlogopites from southern African and Siberian kimberlites and their xenoliths: constraints on eruption ages, melt degassing and mantle volatile compositions. Russian Journal of Geology & Geophysics 38:106-117

Pearson DG, Nixon PH (1996) Diamonds in young orogenic belts: graphitisied diamonds from Beni Bousera, N. Morocco, a comparison with kimberlite-derived diamond occurrences and implications for diamond genesis and exploration. Africa Geoscience Reviews 3:295-31

Pearson, DG, Davies GR, Nixon PH (1993) Geochemical constraints on the petrogenesis of diamond facies pyroxenites from the Beni Bousera peridotite massif, North Morocco: Journal of Petrology, v. 34, p. 125-172.

Regan SP, Williams ML, Mahan KH, Dumond G, Jercinovic MJ, Orlandini OF (2017) Neoarchean arc magmatism and subsequent collisional orogenesis along the eastern Rae domain, western Churchill Province: Implications for the early growth of Laurentia. Precambrian Research 294:151-174

Prelević D, Foley SF, Romer R, Conticelli S (2008) Mediterranean Tertiary lamproites derived from multiple source components in postcollisional geodynamics. Geochimica et Cosmochimica Acta 72:2125-2156

Rudnick RL, Barth M, Horn I, McDonough WF (2000) Rutile-bearing refractory eclogites: Missing link between continents and depleted mantle. Science 287:278–281

Patchen AD, Taylor LA, Pokhilenko N (1997) Ferrous freudenbergite in ilmenite megacrysts: A unique paragenesis from the Dalnaya kimberlite, Yakutia. American Mineralogist 82(1964):991-1000

Pehrsson SJ, Berman RG, Davis WJ, (2013) Paleoproterozoic orogenesis during Nuna aggregation: a case study of reworking of the Rae craton, Woodburn Lake, Nunavut. Precambrian Res 232:167-188

Peterson TD, Van Breemen O, Sandeman H, Cousens B (2002) Proterozoic (1.85–1.75 Ga) igneous suites of the Western Churchill Province: granitold and ultrapotassic magmatism in a reworked Archean hinterland. Precambrian Res 119:73-100

Peterson TD, Pehrsson S, Skulski T, Sandeman H (2010) Compilation of Sm–Nd isotope analyses of igneous suites, western Churchill Province. Geology Survey of Canada Open File 6439, 18p

Peterson TD, Scott JMJ, LeCheminant AN, Jefferson CW, Pehrsson SJ (2015) The Kivalliq Igneous Suite: anorogenic bimodal magmatism at 1.75 Ga in the western Churchill Province, Canada. Precambrian Res 262:101-119

Petts DC, Davis WJ, Moser DE, Longstaffe FJ (2014) Age and evolution of the lower crust beneath the western Churchill Province: U–Pb zircon geochronology of kimberlite-hosted granulite xenoliths, Nunavut, Canada. Precambrian Res 241:129-145

Pokhilenko NP (2009) Polymict breccia xenoliths: Evidence for the complex character of kimberlite formation. Lithos 112S:934-941

Pryce MW, Hodge LC, Criddle AJ (1984) Jeppeite, a new K-Ba-Fe titanate from Walgidee Hills, Western Australia. Mineralogical Magazine 48:263-66

Sanborn-Barrie M, Davis WJ, Berman RG, Rayner N, Skulski T, Sandeman H (2014) Neoarchean continental crust formation and Paleoproterozoic deformation of the central Rae craton, Committee Bay belt, Nunavut. Can J Earth Sci 51:635-667

Sandeman HA, Brown J, Studnicki-Gizbert C, MacHattie T, Hyde D, Johnstone S, Griener E, Plaza D (2001a) Bedrock mapping in the Committee Bay Belt, Laughland lake area, central mainland Nunavut, Geological Survey of Canada, Current Research 2001-C12, 1-10

Sandeman HA, Brown J, Studnicki-Gizbert C, MacHattie T, Hyde D, Johnstone S, Griener E, Plaza D (2001b) Bedrock Geology of the Laughland Lake map sheet NTS 56K: Geological Survey of Canada, Open file 4190, scale 1:100 000

Sandeman HA, Schultz M, Rubingh K (2005) Results of bedrock mapping of the Darby Lake-Arrowsmith River north map areas, central Rae Domain, Nunavut, Geological Survey of Canada, Current Research 2005-C2, 1-11

Sarkar C, Kjarsgaard BA, Pearson DG, Heaman LM, Locock A, Armstrong JA (Miner Petrol, 2018) Geochronology, classification and mantle source characteristics of kimberlites and related rocks from the Rae Craton, Melville Peninsula, Nunavut, Canada

Sarkar, C, Heaman, LM, Pearson, DG (2015) Duration and periodicity of kimberlite volcanic activity in the Lac de Gras kimberlite field, Canada and some recommendations for kimberlite geochronology. Lithos, 218:155-166

Schau M (1982) Geology of the Prince Albert Group in parts of the Walker Lake and Laughland Lake map areas, District of Keewatin, Geological Survey of Canada, Bulletin 337:1-75

Schmidberger SS, Francis D (1999) Nature of the mantle roots beneath the North American craton: mantle xenolith evidence from Somerset Island kimberlites. Lithos 48:195-216

Schultz MEJ, Chacko T, Heaman LM, Sandeman HA, Simonetti A, Creaser RA (2007) Queen Maud block: A newly recognized Paleoproterozoic (2.4–2.5 Ga) terrane in northwest Laurentia. Geology 35(8):707-710

Schulze DJ (1989) Constraints on the abundance of eclogite in the upper mantle. Journal of Geophysical Research 94(B4):4205-4212

Shinotsuka K, Suzuki K (2007) Simultaneous determination of platinum group elements and rhenium in rock samples using isotope dilution inductively coupled plasma mass spectrometry after cation exchange separation followed by solvent extraction. 3:129-139

Shu Q, Brey GP, Gerdes A, Hoefer HE (2013) Geochronological and geochemical constraints on the formation and evolution of the mantle underneath the Kaapvaal craton: Lu-Hf and Sm-Nd systematics of subcalcic garnets from highly depleted peridotites. Geochimica et Cosmochimica Acta 113:1-20

Skulski T, Sandeman HA, Sandborn-Barrie M, MacHattie T, Hyde D, Johnstone S, Panagapko D, Byrne D (2002) Contrasting crustal domains in the Committee Bay belt, Walker Lake-Arrowsmith River area, central Nunavut, Geological Survey of Canada Current Research 2002-C12

Skulski T, Sandeman HA, Sandborn-Barrie M, MacHattie T, Young M, Carson C, Berman R, Brown J, Rayner N, Panagapko D, Byrne D, Deyell C (2003) Bedrock geology of the

Ellice Hills map area and new constraints on the regional geology of the Committee Bay area, Nunavut; Geological Survey of Canada, Current Research 2003-C22

Smith JV, Dawson JB (1975) Chemistry of Ti-poor spinels, ilmenites and rutiles from peridotite and eclogite xenoliths. J. Geophys. Res. 93:309-322

Snyder DB, Craven JA, Pilkington M, Hillier MJ (2015) The 3-dimensional construction of the Rae craton, central Canada. Geochem. Geophys. Geosyst. 16:3555-3574

Snyder DB, Humphreys E, Pearson DG (2017) Tectonophysics Construction and destruction of some North American cratons. Tectonophysics 694:464-485

Sobolev NV, Kaminsky FV, Griffin WL, Yefimova ES, Win TT, Ryan CG, Botkunov AI (1997) Mineral inclusions in diamonds from the Sputnik kimberlite pipe, Yakutia. Lithos 39:135-157

Sobolev NV, Yefimova ES (2000) Composition and petrogenesis of Ti-oxides associated with diamonds. International Geology Review 42:758-767

Soltys A, Giuliani A, Phillips D, Kamenetsky VS, Maas R, Woodhead J, Rodemann T (2016) In-situ assimilation of mantle minerals by kimberlitic magmas - Direct evidence from a garnet wehrlite xenolith entrained in the Bultfontein kimberlite (Kimberley, South Africa). Lithos 256-257:182-196

St-Onge MR, Jackson GD, Henderson I, (2006a) Geology, Baffin Island (south of 70◦N and east of 80◦W), Nunavut. Geol. Surv. Canada Open File 4931 (scale 1:500,000)

St-Onge MR, Searle MP, Wodicka N, (2006b) Trans-Hudson Orogen of North America and Himalaya-Karakoram-Tibetan Orogen of Asia: structural and thermal characteristics of the lower and upper plates. Tectonics 25

Stachel T, Harris JW (2008) The origin of cratonic diamonds - Constraints from mineral inclusions. Ore Geology Reviews 34(1-2): 5-32

Stern RA, Syme EC, Bailes AH, Lucas SB (1995) Paleoproterozoic (1.90–1.86 Ga) arc volcanism in the Flin-Flon Belt, Trans-Hudson Orogen, Canada. Contrib. Mineral Petrol 119:117-141

Taylor SR (1964) Chondritic Earth model. Nature 202:281-282

Thompson PH (1998) A new perspective on the regional geology of the southwestern part of the Committee Bay belt, District of Keewatin; unpublished report prepared by Peter H. Thompson Geological Consulting Ltd. For Committee Bay Joint Venture

Wang H, Van Hunen J, Pearson DG (2018) Making Archean cratonic roots by lateral compression: a two-stage thickening and stabilization model. Tectonophysics, in press

Weir JK, Farmer R (2008) Assessment Report on the Darby property 2007 Diamond exploration program: airborne and ground geophysics, diamond drilling and heavy mineral sampling. Nunavut Geoscience Assessment Report 085342.

Weyer S, Münker C, Rehkämper M, Mezger K (2002) Determination of ultra-low Nb, Ta, Zr and Hf concentrations and the chondritic Zr/Hf and Nb/Ta by isotope dilution analyses with multiple collector ICP-MS. Chem. Geol. 187:295-313

Wodicka N, Corrigan D, Nadeau L, Erdmann S (2011) New U–Pb geochronological results from Melville Peninsula: unravelling the Archean and Early Paleoproterozoic magmatic history of the north-central Rae craton. Geol Assn Canada, Mineral Assn Canada Abst 36

Wyatt BA, Baumgartner M, Anckar E, Grütter H (2004) Compositional classification of "'kimberlitic'" and "'non-kimberlitic'" ilmenite. Lithos 77:819-840

Yavuz F (2013) WinPyrox: A Windows program for pyroxene calculation classification and thermobarometry. American Mineralogist 98:1338-1359

Yaxley GM, Green DH (1998) Reactions between eclogite and peridotite: Mantle refertilisation by subduction of oceanic crust. Schweiz Mineral Pertrogr Mitt 78:243-255

Zaleski E, L'Heureaux R, Duke N, Wilkinson L, Davis WJ (1999) Komatiitic and felsic volcanic rocks overlain by quartzite, Woodburn Lake group, Meadowbank River area, western Churchill Provience, Northwest Territories (Nunavut), Geological Survey of Canada Current Research 1999-C

Ziberna L, Nimis P, Kuzmin D, Malkovets VG (2016) Error sources in single-clinopyroxene thermobarometry and a mantle geotherm for the Novinka kimberlite, Yakutia. American Mineralogist 101:2222–2232

Appendix A

1.EPMA

sample name	rock type	mineral from composition	SiO2	TiO2	Al2O3	V2O3	Cr2O3	MnO	FeO	NiO	MgO	CaO	Na2O	K2O	P2O5	Total	notes	Crust-Mantle
B-10-2	lherzolite	diopside	54.28	0.03	1.32	0.03	1.02	0.07	1.51	0.04	16.75	23.00	0.95	0.01	0.01	99.01		
B-10-2	lherzolite	diopside	54.02	0.01	1.38	0.04	1.23	0.07	1.49	0.04	16.69	22.96	0.96	0.01	0.02	98.91		
B-10-2	lherzolite	olivine	39.97	0.00	0.00	0.01	0.00	0.12	7.78	0.38	50.25	0.01	0.00	0.00	0.01	98.52		
B-10-2	lherzolite	olivine	40.20	0.00	0.01	0.01	0.01	0.12	7.96	0.34	50.14	0.01	0.00	0.00	0.00	98.80		
B-10-2	lherzolite	olivine	40.27	0.01	0.00	0.00	0.00	0.10	7.96	0.36	50.24	0.01	0.00	0.00	0.00	98.95		
B-10-2	lherzolite	olivine	40.10	0.02	0.00	0.00	0.01	0.12	7.82	0.38	50.14	0.01	0.00	0.00	0.01	98.61		
B-10-1	lherzolite	orthopyroxene	56.57	0.00	1.14	0.02	0.43	0.11	4.91	0.06	35.76	0.14	0.03	0.00	0.01	99.17		
B-10-1	lherzolite	orthopyroxene	56.54	0.03	1.09	0.02	0.35	0.12	4.90	0.07	35.96	0.27	0.03	0.00	0.00	99.39		
B-10-1	lherzolite	orthopyroxene	56.57	0.00	0.91	0.01	0.27	0.13	4.92	0.06	35.83	0.28	0.03	0.00	0.00	99.01		
B-10-1	lherzolite	orthopyroxene	56.53	0.02	1.12	0.00	0.27	0.12	4.86	0.07	35.38	0.44	0.02	0.00	0.00	98.83		
B-10-1	lherzolite	orthopyroxene	57.26	0.01	1.00	0.02	0.25	0.14	4.86	0.07	35.58	0.73	0.04	0.00	0.00	99.95		
B-10-1	lherzolite	orthopyroxene	56.59	0.00	1.06	0.01	0.38	0.14	4.96	0.08	35.94	0.16	0.02	0.00	0.00	99.34		
B-10-1	lherzolite	orthopyroxene	57.21	0.00	0.99	0.00	0.33	0.13	4.86	0.07	35.85	0.17	0.02	0.01	0.01	99.64		
B-10-1	lherzolite	orthopyroxene	56.63	0.00	0.99	0.00	0.27	0.12	4.77	0.07	35.77	0.26	0.02	0.00	0.01	98.92		
B-10-1	lherzolite	orthopyroxene	56.83	0.03	0.98	0.01	0.37	0.12	4.84	0.08	35.99	0.14	0.02	0.00	0.01	99.43		
B-10-2	lherzolite	orthopyroxene	56.79	0.00	0.56	0.01	0.32	0.14	5.20	0.06	35.62	0.16	0.02	0.03	0.00	98.91		
B-11A	lherzolite	diopside	52.29	0.54	4.64	0.05	1.09	0.06	1.82	0.02	14.96	21.55	1.81	0.00	0.02	98.86		
B-11A	lherzolite	diopside	52.42	0.47	5.11	0.06	1.08	0.07	1.85	0.03	14.61	21.03	1.97	0.00	0.00	98.70		
B-11A	lherzolite	diopside	52.63	0.49	4.57	0.05	1.07	0.06	1.74	0.05	14.93	21.37	1.90	0.00	0.03	98.88		
B-11A	lherzolite	diopside	52.04	0.47	4.92	0.05	1.10	0.07	1.83	0.04	14.84	21.23	1.96	0.00	0.02	98.57		
M-15A	garnet dunite	garnet	41.78	0.48	20.52	0.04	2.65	0.25	6.82	0.02	21.67	4.77	0.04	0.00	0.02	99.05		
M-15A	garnet dunite	olivine	39.47	0.02	0.04	0.00	0.05	0.11	9.07	0.38	49.56	0.10	0.02	0.00	0.00	98.82		
M-15A	garnet dunite	olivine	40.09	0.02	0.03	0.00	0.02	0.10	9.09	0.38	49.52	0.10	0.02	0.00	0.00	99.38		
M-15A	garnet dunite	olivine	39.39	0.02	0.03	0.00	0.07	0.11	9.06	0.37	49.61	0.09	0.03	0.00	0.00	98.78		
B-5-1	lherzolite	diopside	54.99	0.00	0.91	0.03	1.85	0.09	1.82	0.04	15.90	22.44	1.35	0.00	0.02	99.44		
B-5-1	lherzolite	diopside	54.50	0.03	0.75	0.01	1.54	0.08	1.95	0.03	16.37	22.06	1.29	0.00	0.01	98.62		
B-5-1	lherzolite	augite	53.78	0.62	1.03	0.04	1.81	0.16	3.48	0.02	17.61	18.82	1.18	0.00	0.01	98.55		
B-5-1	lherzolite	diopside	54.65	0.00	0.37	0.04	1.86	0.08	2.27	0.02	16.12	21.90	1.41	0.02	0.00	98.74		
B-5-1	lherzolite	diopside	54.64	0.01	0.70	0.03	1.42	0.08	1.96	0.03	16.36	22.02	1.30	0.00	0.01	98.56		
B-5-1	lherzolite	augite	53.77	0.50	1.91	0.04	1.80	0.11	3.49	0.05	17.05	18.95	1.31	0.02	0.00	99.02		
B-5-1	lherzolite	augite	53.53	0.46	2.64	0.05	1.57	0.11	2.86	0.05	17.00	19.03	1.37	0.01	0.01	98.70		
B-5-1	lherzolite	diopside	54.55	0.01	0.29	0.01	1.87	0.07	2.25	0.03	16.00	22.08	1.36	0.00	0.00	98.51		
B-5-1	lherzolite	diopside	54.52	0.00	0.28	0.02	2.04	0.08	2.29	0.02	15.94	22.01	1.39	0.01	0.00	98.61		
B-5-1	lherzolite	augite	54.46	0.27	1.33	0.04	1.84	0.12	2.76	0.04	17.75	19.42	1.14	0.01	0.02	99.20		
B-5-1	lherzolite	diopside	54.60	0.00	0.62	0.02	1.50	0.09	2.03	0.03	16.35	22.11	1.34	0.00	0.01	98.70		
B-5-1	lherzolite	diopside	54.80	0.02	0.87	0.01	1.71	0.08	1.80	0.04	16.28	21.88	1.38	0.00	0.00	98.86		
B-5-1	lherzolite	diopside	54.77	0.00	0.63	0.03	1.69	0.07	1.97	0.03	16.27	21.92	1.37	0.00	0.00	98.77		
B-5-1	lherzolite	diopside	54.56	0.01	0.41	0.04	2.01	0.08	2.15	0.02	16.05	21.91	1.34	0.01	0.01	98.60		
B-5-1	lherzolite	diopside	54.82	0.02	0.86	0.01	1.28	0.07	1.85	0.03	16.37	22.07	1.23	0.01	0.02	98.63		
B-5-2	lherzolite	diopside	54.43	0.00	0.50	0.03	1.73	0.07	2.10	0.03	16.30	22.03	1.32	0.01	0.01	98.55		
B-5-2	lherzolite	diopside	54.65	0.03	0.72	0.02	1.23	0.09	1.91	0.04	16.49	22.25	1.19	0.00	0.02	98.64		
B-5-2	lherzolite	diopside	54.75	0.01	0.77	0.04	1.11	0.08	1.91	0.02	16.55	22.29	1.12	0.00	0.02	98.66		
B-5-2	lherzolite	diopside	54.82	0.01	0.42	0.01	1.53	0.08	2.15	0.03	16.22	22.10	1.29	0.00	0.02	98.68		
B-5-2	lherzolite	diopside	55.02	0.02	0.52	0.01	1.34	0.08	1.98	0.02	16.38	22.09	1.20	0.00	0.01	98.66		
B-5-2	lherzolite	diopside	54.53	0.03	0.86	0.02	1.38	0.06	1.97	0.04	16.42	21.95	1.27	0.00	0.02	98.55		
B-5-2	lherzolite	diopside	54.83	0.01	0.91	0.03	1.23	0.08	1.66	0.03	16.45	22.35	1.14	0.00	0.01	98.75		
B-5-2	lherzolite	diopside	54.91	0.00	0.54	0.00	1.36	0.08	2.05	0.05	16.40	22.25	1.17	0.00	0.01	98.81		

sample name	rock type	mineral from composition	SiO2	TiO2	Al2O3	V2O3	Cr2O3	MnO	FeO	NiO	MgO	CaO	Na2O	K2O	P2O5	Total	notes	Crust-Mantle
B-5-2	lherzolite	augite	53.07	0.49	2.89	0.05	1.91	0.11	3.04	0.04	16.59	18.76	1.58	0.01	0.00	98.54		
B-5-2	lherzolite	augite	53.78	0.44	2.37	0.02	1.78	0.12	3.03	0.03	16.95	18.98	1.43	0.03	0.01	98.97		
B-5-2	lherzolite	augite	54.79	0.08	0.88	0.03	1.43	0.11	2.43	0.05	17.72	19.99	1.20	0.01	0.04	98.75		
B-5-2	lherzolite	augite	53.46	0.49	2.00	0.05	1.66	0.12	2.98	0.06	17.17	19.33	1.35	0.01	0.02	98.70		
B-5-2	lherzolite	augite	53.55	0.47	1.79	0.04	1.49	0.11	3.17	0.05	17.66	19.23	1.21	0.02	0.01	98.80		
B-5-2	lherzolite	augite	54.47	0.03	3.68	0.02	1.87	0.08	2.19	0.06	16.49	17.63	2.37	0.00	0.02	98.91		
B-5-2	lherzolite	augite	53.52	0.05	4.48	0.01	1.91	0.08	2.29	0.04	16.32	17.68	2.41	0.01	0.00	98.81		
B-5-2	lherzolite	augite	54.11	0.02	3.63	0.02	1.91	0.10	2.32	0.04	16.58	17.58	2.43	0.00	0.01	98.75		
B-5-3	lherzolite	augite	54.25	0.52	1.00	0.04	0.75	0.15	3.58	0.03	18.98	18.84	0.78	0.00	0.02	98.94		
B-5-3	lherzolite	augite	53.88	0.43	1.93	0.03	1.87	0.11	2.89	0.05	17.05	19.37	1.30	0.02	0.01	98.93		
B-5-3	lherzolite	augite	53.02	0.49	2.55	0.03	1.49	0.13	2.95	0.04	16.91	19.34	1.44	0.10	0.05	98.54		
B-5-3	lherzolite	augite	54.75	0.48	1.70	0.03	1.70	0.11	2.62	0.04	17.49	19.94	1.20	0.01	0.01	100.08		
B-5-3	lherzolite	augite	54.01	0.27	4.26	0.03	1.66	0.10	2.50	0.04	16.38	18.20	2.03	0.01	0.01	99.49		
B-5-3	lherzolite	augite	54.50	0.10	3.54	0.03	1.67	0.10	2.36	0.05	16.13	18.38	2.21	0.00	0.04	99.11		
B-5-1	lherzolite	olivine	40.39	0.00	0.00	0.00	0.00	0.13	7.75	0.34	49.96	0.01	0.01	0.00	0.01	98.60		
B-5-1	lherzolite	olivine	40.24	0.01	0.00	0.00	0.00	0.13	7.59	0.36	50.34	0.00	0.00	0.00	0.01	98.70		
B-5-1	lherzolite	olivine	40.25	0.01	0.00	0.00	0.00	0.14	7.66	0.36	50.30	0.01	0.00	0.00	0.02	98.74		
B-5-1	lherzolite	olivine	40.28	0.01	0.00	0.00	0.02	0.13	7.57	0.36	50.26	0.01	0.00	0.00	0.00	98.64		
B-5-1	lherzolite	olivine	40.36	0.00	0.00	0.00	0.03	0.13	7.67	0.36	50.15	0.01	0.00	0.00	0.00	98.71		
B-5-1	lherzolite	olivine	40.56	0.00	0.00	0.00	0.00	0.15	7.70	0.36	50.21	0.01	0.00	0.01	0.00	98.99		
B-5-1	lherzolite	olivine	40.33	0.02	0.00	0.00	0.00	0.14	7.82	0.36	50.10	0.01	0.00	0.00	0.01	98.79		
B-5-1	lherzolite	olivine	40.24	0.00	0.00	0.00	0.00	0.14	7.66	0.37	50.15	0.00	0.01	0.00	0.01	98.58		
B-5-1	lherzolite	olivine	40.16	0.00	0.00	0.00	0.00	0.13	7.61	0.35	50.30	0.01	0.00	0.00	0.01	98.56		
B-5-1	lherzolite	olivine	40.28	0.00	0.00	0.00	0.00	0.12	7.57	0.36	50.37	0.01	0.00	0.00	0.01	98.73		
B-5-1	lherzolite	olivine	40.28	0.00	0.00	0.01	0.00	0.14	7.59	0.36	50.20	0.01	0.00	0.00	0.01	98.59		
B-5-2	lherzolite	olivine	40.43	0.00	0.00	0.00	0.00	0.14	7.63	0.35	50.09	0.00	0.01	0.00	0.00	98.67		
B-5-2	lherzolite	olivine	40.03	0.01	0.00	0.00	0.02	0.13	7.77	0.36	50.32	0.00	0.00	0.00	0.02	98.66		
B-5-2	lherzolite	olivine	40.83	0.00	0.00	0.00	0.00	0.14	7.66	0.36	50.40	0.01	0.00	0.00	0.01	99.40		
B-5-2	lherzolite	olivine	40.23	0.01	0.00	0.00	0.02	0.13	7.69	0.35	50.30	0.00	0.01	0.01	0.01	98.77		
B-5-2	lherzolite	olivine	40.32	0.00	0.01	0.00	0.00	0.14	7.62	0.36	50.15	0.01	0.00	0.00	0.00	98.60		
B-5-2	lherzolite	olivine	40.20	0.00	0.00	0.01	0.00	0.14	7.73	0.35	50.31	0.01	0.01	0.00	0.02	98.78		
B-5-2	lherzolite	olivine	40.45	0.00	0.00	0.01	0.00	0.14	7.60	0.35	50.08	0.00	0.01	0.00	0.00	98.64		
B-5-3	lherzolite	olivine	40.39	0.00	0.00	0.01	0.01	0.14	7.61	0.38	49.97	0.01	0.00	0.00	0.00	98.51		
B-7A	garnet dunite	garnet	41.04	0.38	18.84	0.03	4.95	0.28	6.93	0.05	21.32	4.95	0.06	0.01	0.01	98.85		
B-7A	garnet dunite	garnet	40.88	0.39	18.93	0.04	4.96	0.28	6.93	0.04	21.05	4.97	0.05	0.00	0.04	98.56		
L-5A	garnet harzburgite	Harbugitic garnet	41.06	0.38	15.32	0.05	9.72	0.27	6.17	0.02	22.35	3.68	0.01	0.00	0.04	99.06		
M-10-4	lherzolite	olivine	41.67	0.00	0.00	0.01	0.00	0.09	5.75	0.36	52.96	0.00	0.00	0.00	0.00	100.85		
M-10-4	lherzolite	olivine	41.14	0.00	0.00	0.00	0.00	0.09	5.70	0.38	52.87	0.01	0.00	0.00	0.01	100.21		
M-10-4	lherzolite	olivine	41.82	0.00	0.00	0.00	0.00	0.10	5.62	0.36	52.96	0.00	0.00	0.01	0.02	100.89		
M-10-4	lherzolite	olivine	41.78	0.00	0.00	0.00	0.00	0.09	5.64	0.36	52.98	0.00	0.00	0.00	0.02	100.87		
M-10-4	lherzolite	olivine	41.55	0.00	0.00	0.01	0.02	0.10	5.81	0.38	52.87	0.00	0.00	0.00	0.01	100.75		
M-10-4	lherzolite	orthopyroxene	57.01	0.00	1.95	0.00	0.27	0.13	4.06	0.06	35.55	0.21	0.01	0.00	0.00	99.26		
M-10-6	wehrlite	diopside	54.54	0.01	0.29	0.06	1.69	0.06	2.07	0.05	16.87	22.06	1.19	0.03	0.02	98.94		
M-10-6	wehrlite	diopside	55.11	0.11	0.43	0.07	2.12	0.07	2.62	0.03	16.25	21.31	1.76	0.01	0.02	99.91		
M-10-6	wehrlite	diopside	54.72	0.04	0.45	0.05	1.27	0.06	2.19	0.05	16.59	22.30	1.31	0.08	0.04	99.16		

sample name	rock type	mineral from composition	SiO2	TiO2	Al2O3	V2O3	Cr2O3	MnO	FeO	NiO	MgO	CaO	Na2O	K2O	P2O5	Total	notes	Crust-Mantle
M-10-6	wehrlite	diopside	54.86	0.07	0.34	0.06	1.75	0.05	2.62	0.04	15.91	21.74	1.72	0.02	0.02	99.21		
M-10-6	wehrlite	diopside	54.95	0.03	0.22	0.04	0.11	0.07	2.83	0.03	17.00	23.08	0.98	0.01	0.01	99.38		
M-10-6	wehrlite	olivine	40.93	0.00	0.00	0.00	0.00	0.11	6.88	0.36	50.31	0.01	0.00	0.00	0.00	98.60		
M-10-6	wehrlite	olivine	40.88	0.02	0.00	0.00	0.00	0.11	6.91	0.37	50.33	0.00	0.00	0.00	0.01	98.64		
M-10-6	wehrlite	olivine	40.93	0.00	0.01	0.00	0.00	0.12	6.89	0.37	50.25	0.00	0.00	0.00	0.02	98.59		
M-10-6	wehrlite	olivine	40.95	0.00	0.00	0.00	0.01	0.10	6.77	0.36	50.31	0.00	0.00	0.00	0.00	98.51		
M-10-6	wehrlite	olivine	41.02	0.00	0.00	0.01	0.00	0.10	6.75	0.36	50.32	0.00	0.00	0.00	0.02	98.59		
M-21-3	wehrlite	diopside	52.97	0.86	1.00	0.01	1.84	0.12	2.85	0.04	16.84	21.11	0.91	0.03	0.09	98.69		
M-21-3	wehrlite	augite	53.70	0.68	1.03	0.04	1.97	0.15	3.23	0.04	18.39	18.29	1.17	0.01	0.04	98.75		
M-21-3	wehrlite	augite	52.83	1.06	1.53	0.03	1.82	0.12	3.48	0.02	17.42	19.04	1.13	0.01	0.04	98.52		
M-21-3	wehrlite	augite	53.68	0.65	0.95	0.01	1.81	0.15	3.55	0.04	18.24	18.46	1.18	0.01	0.05	98.80		
M-21-3	wehrlite	augite	54.17	0.51	0.43	0.02	1.41	0.14	2.96	0.04	18.15	19.94	0.97	0.01	0.04	98.79		
M-21-3	wehrlite	olivine	40.83	0.00	0.00	0.00	0.00	0.10	6.93	0.39	50.36	0.01	0.00	0.00	0.01	98.64		
M-21-3	wehrlite	olivine	40.89	0.00	0.00	0.00	0.00	0.10	6.87	0.38	50.27	0.02	0.00	0.01	0.01	98.55		
M-21-3	wehrlite	olivine	40.85	0.00	0.01	0.01	0.00	0.10	6.96	0.38	50.22	0.00	0.00	0.01	0.01	98.55		
M-21-3	wehrlite	olivine	40.84	0.00	0.00	0.00	0.02	0.12	6.91	0.38	50.26	0.01	0.00	0.00	0.02	98.57		
M-21-3	wehrlite	picotite = chromian spinel	0.02	0.16	10.45	0.26	56.87	0.41	19.55	0.05	10.86	0.00	0.04	0.00	0.00	98.65		
M-21-3	wehrlite	picotite = chromian spinel	0.01	0.17	11.09	0.24	56.19	0.41	19.32	0.08	11.11	0.01	0.03	0.00	0.01	98.65		
M-21-3	wehrlite	picotite = chromian spinel	0.00	0.19	11.44	0.24	56.38	0.42	17.21	0.08	12.57	0.01	0.02	0.01	0.00	98.56		
M-21-3	wehrlite	picotite = chromian spinel	0.00	0.18	11.59	0.25	56.50	0.38	17.19	0.07	12.75	0.01	0.04	0.01	0.00	99.00		
M-21-3	wehrlite	picotite = chromian spinel	0.01	0.15	11.43	0.22	56.41	0.41	16.99	0.08	12.88	0.03	0.01	0.00	0.01	98.62		
M-21-3	wehrlite	picotite = chromian spinel	0.00	0.16	11.49	0.23	56.04	0.43	17.14	0.11	12.72	0.23	0.02	0.00	0.01	98.58		
M-21-3	wehrlite	picotite = chromian spinel	0.07	0.40	44.29	0.09	21.63	0.37	13.70	0.16	18.30	0.06	0.00	0.00	0.01	99.05	Al rich?	
M-21-3	wehrlite	picotite = chromian spinel	0.10	0.29	44.46	0.08	20.91	0.58	15.99	0.03	16.16	0.05	0.00	0.00	0.00	98.66	Al rich?	
M-22A	lherzolite	diopside	54.46	0.04	0.06	0.04	0.97	0.08	2.46	0.04	16.81	23.36	0.96	0.00	0.03	99.30		
M-22A	lherzolite	diopside	54.41	0.00	0.07	0.03	0.97	0.06	2.47	0.05	16.79	23.33	0.93	0.00	0.04	99.15		
M-22A	lherzolite	diopside	54.44	0.03	0.09	0.01	0.98	0.06	2.44	0.03	16.79	23.46	0.94	0.00	0.00	99.27		
M-22A	lherzolite	diopside	54.36	0.01	0.08	0.02	0.96	0.08	2.45	0.03	16.64	23.32	0.90	0.00	0.00	98.85		
M-22A	lherzolite	diopside	54.09	0.02	0.08	0.02	1.19	0.07	2.46	0.03	16.65	23.28	1.02	0.00	0.01	98.92		
M-22A	lherzolite	diopside	54.52	0.02	0.09	0.03	1.30	0.09	2.62	0.04	16.48	22.93	1.09	0.00	0.03	99.25		
M-22A	lherzolite	diopside	54.29	0.02	0.08	0.01	0.93	0.08	2.46	0.04	16.84	23.36	0.91	0.00	0.02	99.03		
M-22B	lherzolite	olivine	38.95	0.01	0.00	0.00	0.00	0.21	10.60	0.36	48.86	0.02	0.00	0.00	0.00	99.01		
M-22B	lherzolite	olivine	39.29	0.01	0.00	0.00	0.01	0.23	10.63	0.32	48.87	0.01	0.00	0.00	0.00	99.37		
M-22B	lherzolite	olivine	39.50	0.00	0.01	0.00	0.00	0.21	10.57	0.35	48.64	0.01	0.00	0.00	0.00	99.29		
M-22B	lherzolite	olivine	39.49	0.00	0.00	0.01	0.02	0.21	10.70	0.34	48.72	0.02	0.00	0.01	0.00	99.51		
M-22B	lherzolite	olivine	39.25	0.00	0.00	0.02	0.01	0.21	10.66	0.33	48.53	0.02	0.00	0.01	0.02	99.04		
M-22B	lherzolite	olivine	39.27	0.01	0.00	0.00	0.00	0.21	10.61	0.32	48.53	0.01	0.00	0.00	0.00	98.96		
M-23-1	mantle polymict breccia	diopside	53.35	0.12	1.20	0.02	0.11	0.15	5.65	0.01	14.14	23.23	0.97	0.00	0.02	98.99		
M-23-1	mantle polymict breccia	diopside	54.00	0.03	0.75	0.02	0.10	0.17	5.22	0.01	14.41	23.90	0.64	0.01	0.03	99.28		
M-23-1	mantle polymict breccia	diopside	53.61	0.02	0.88	0.00	0.07	0.16	5.47	0.02	14.52	23.72	0.67	0.01	0.02	99.18		
M-23-1	mantle polymict breccia	diopside	53.44	0.06	0.84	0.04	0.12	0.16	5.14	0.01	14.45	23.94	0.65	0.00	0.04	98.89		
M-23-1	mantle polymict breccia	diopside	54.68	0.04	0.43	0.02	0.08	0.17	4.86	0.02	14.94	24.37	0.42	0.00	0.03	100.06		
M-23-1	mantle polymict breccia	diopside	53.98	0.02	0.64	0.00	0.15	0.17	4.99	0.02	14.71	24.06	0.63	0.00	0.03	99.38		
M-23-1	mantle polymict breccia	diopside	54.41	0.05	0.79	0.03	0.12	0.17	5.33	0.02	14.46	23.74	0.95	0.01	0.03	100.09		
M-23-1	mantle polymict breccia	diopside	54.35	0.08	0.75	0.00	0.06	0.17	5.16	0.01	14.53	24.09	0.63	0.00	0.01	99.83		
M-23-1	mantle polymict breccia	diopside	54.54	0.02	0.50	0.01	0.09	0.16	4.72	0.01	15.04	24.31	0.56	0.00	0.03	99.98		

sample name	rock type	mineral from composition	SiO2	TiO2	Al2O3	V2O3	Cr2O3	MnO	FeO	NiO	MgO	CaO	Na2O	K2O	P2O5	Total	notes	Crust-Mantle
M-23-1	mantle polymict breccia	diopside	54.20	0.05	0.72	0.00	0.04	0.16	5.21	0.01	14.56	23.94	0.64	0.00	0.04	99.56		
M-23-1	mantle polymict breccia	ilmenite	0.03	51.38	0.54	0.20	2.82	0.43	30.58	0.08	12.59	0.08	0.00	0.00	0.00	98.71		
M-23-1	mantle polymict breccia	ilmenite	0.04	52.02	0.58	0.26	2.03	0.39	31.13	0.11	12.35	0.07	0.00	0.00	0.00	98.98		
M-23-1	mantle polymict breccia	ilmenite	0.31	48.75	0.45	0.23	2.69	0.51	28.81	0.08	15.88	2.18	0.03	0.00	0.00	99.92		
M-23-1	mantle polymict breccia	olivine	40.04	0.03	0.01	0.02	0.02	0.15	11.46	0.21	47.26	0.05	0.01	0.01	0.02	99.28		
M-23-1	mantle polymict breccia	olivine	40.51	0.05	0.03	0.00	0.04	0.14	10.45	0.30	48.31	0.07	0.00	0.01	0.00	99.90		
M-23-1	mantle polymict breccia	olivine	40.52	0.05	0.02	0.00	0.06	0.13	10.79	0.28	47.54	0.06	0.00	0.01	0.01	99.46		
M-23-1	mantle polymict breccia	titanite	31.39	34.39	2.61	0.16	0.31	0.04	0.66	0.00	0.03	28.90	0.01	0.01	0.03	98.52		
M-24-1	garnet dunite	garnet	40.91	0.12	17.33	0.02	8.10	0.44	7.35	0.00	19.26	6.18	0.03	0.00	0.04	99.79	chrome rich	
M-24-1	garnet dunite	garnet	40.97	0.16	17.26	0.06	8.09	0.45	7.55	0.02	19.47	5.96	0.04	0.00	0.06	100.09	chrome rich	
M-24-1	garnet dunite	garnet	40.86	0.14	17.27	0.03	8.14	0.44	7.35	0.01	19.18	6.15	0.04	0.00	0.04	99.63	chrome rich	
M-24-1	garnet dunite	garnet	40.96	0.13	17.04	0.03	8.28	0.43	7.38	0.01	19.42	6.12	0.04	0.00	0.07	99.91	chrome rich	
M-24-1	garnet dunite	olivine	40.59	0.00	0.01	0.00	0.02	0.10	7.43	0.36	51.27	0.02	0.01	0.00	0.01	99.82		
M-24-1	garnet dunite	olivine	40.52	0.01	0.00	0.00	0.03	0.11	7.40	0.36	50.94	0.01	0.02	0.00	0.01	99.41		
M-3-2A	wehrlite	chromite	0.03	0.30	1.82	0.24	62.24	0.54	25.27	0.10	8.84	0.01	0.00	0.02	0.00	99.40		
M-3-2A	wehrlite	chromite	0.10	0.21	1.93	0.26	61.03	0.52	24.90	0.11	9.74	0.16	0.00	0.09	0.00	99.04		
M-3-2A	wehrlite	augite	53.81	0.33	0.41	0.05	1.35	0.12	3.08	0.05	17.39	20.99	1.09	0.03	0.04	98.73		
M-3-2A	wehrlite	augite	54.21	0.27	0.41	0.05	1.34	0.11	3.05	0.05	17.38	21.04	1.05	0.00	0.02	99.00		
M-3-2A	wehrlite	augite	54.07	0.30	0.33	0.05	0.86	0.14	3.51	0.04	17.17	21.32	0.90	0.00	0.03	98.71		
M-3-2A	wehrlite	augite	54.44	0.13	0.40	0.06	1.67	0.13	2.96	0.06	18.75	18.92	1.14	0.02	0.03	98.69		
M-3-2A	wehrlite	augite	55.24	0.21	0.79	0.03	1.15	0.10	2.73	0.06	17.74	20.28	1.28	0.03	0.04	99.69		
M-3-2A	wehrlite	olivine	40.28	0.00	0.00	0.01	0.01	0.14	7.23	0.36	51.48	0.00	0.00	0.00	0.00	99.50		
M-3-2A	wehrlite	olivine	40.41	0.00	0.00	0.01	0.00	0.13	7.27	0.36	51.54	0.00	0.00	0.00	0.01	99.72		
M-3-2A	wehrlite	olivine	40.81	0.00	0.00	0.00	0.01	0.14	7.32	0.35	51.42	0.01	0.00	0.00	0.01	100.07		
M-3-2A	wehrlite	olivine	40.49	0.02	0.00	0.02	0.01	0.13	7.18	0.36	51.41	0.00	0.00	0.00	0.00	99.61		
M-3-2A	wehrlite	olivine	41.04	0.01	0.00	0.01	0.01	0.13	7.11	0.37	51.05	0.00	0.00	0.00	0.01	99.74		
M-3-2A	wehrlite	olivine	41.58	0.02	0.00	0.01	0.00	0.13	7.18	0.37	51.07	0.01	0.00	0.00	0.00	100.35		
M-3-2A	wehrlite	olivine	40.76	0.00	0.00	0.00	0.00	0.15	7.24	0.37	51.30	0.01	0.00	0.01	0.00	99.84		
R-2-2	lherzolite	diopside	54.86	0.03	1.48	0.01	1.29	0.08	1.78	0.02	16.49	22.02	1.55	0.06	0.01	99.68		
R-2-2	lherzolite	diopside	54.98	0.02	1.46	0.02	1.27	0.07	1.68	0.03	16.62	22.11	1.36	0.02	0.02	99.65		
R-2-3	lherzolite	diopside	54.63	0.00	1.12	0.06	1.21	0.08	1.66	0.02	16.61	22.52	1.19	0.00	0.04	99.13		
R-2-3	lherzolite	diopside	54.60	0.01	1.09	0.03	1.24	0.06	1.64	0.03	16.69	22.50	1.19	0.00	0.03	99.13		
R-2-3	lherzolite	diopside	54.43	0.03	1.34	0.03	1.32	0.07	1.69	0.03	16.58	22.21	1.32	0.02	0.03	99.09		
R-2-3	lherzolite	diopside	54.65	0.01	1.29	0.01	1.33	0.07	1.67	0.04	16.64	22.29	1.30	0.03	0.02	99.35		
R-2-3	lherzolite	augite	54.17	0.01	1.47	0.03	1.92	0.12	2.18	0.03	17.19	20.59	1.30	0.01	0.04	99.06		
R-2-2	lherzolite	olivine	40.68	0.00	0.00	0.01	0.02	0.12	7.54	0.35	51.03	0.01	0.00	0.00	0.00	99.75		
R-2-2	lherzolite	olivine	40.65	0.02	0.00	0.00	0.01	0.12	7.53	0.34	50.81	0.01	0.00	0.00	0.00	99.48		
R-2-2	lherzolite	olivine	40.48	0.02	0.00	0.00	0.00	0.10	7.57	0.38	50.92	0.01	0.00	0.00	0.01	99.49		
R-2-2	lherzolite	olivine	40.48	0.00	0.00	0.01	0.02	0.11	7.53	0.36	51.05	0.00	0.00	0.00	0.02	99.58		
R-2-2	lherzolite	olivine	40.54	0.02	0.00	0.00	0.01	0.11	7.54	0.36	50.93	0.02	0.00	0.00	0.00	99.52		
R-2-2	lherzolite	olivine	40.51	0.02	0.00	0.00	0.01	0.11	7.53	0.36	50.87	0.00	0.01	0.00	0.00	99.41		
R-2-3	lherzolite	olivine	40.82	0.00	0.00	0.01	0.00	0.11	6.98	0.39	50.18	0.00	0.00	0.00	0.01	98.50		
R-2-3	lherzolite	olivine	40.89	0.01	0.01	0.00	0.00	0.11	7.03	0.35	50.23	0.01	0.00	0.00	0.00	98.64		
R-2-3	lherzolite	olivine	40.82	0.01	0.00	0.00	0.00	0.12	7.12	0.37	50.10	0.00	0.00	0.01	0.01	98.55		
R-2-2	lherzolite	orthopyroxene	57.74	0.02	0.56	0.01	0.26	0.14	4.81	0.07	38.25	0.15	0.03	0.00	0.00	102.03		
R-2-2	lherzolite	orthopyroxene	57.64	0.01	1.01	0.01	0.37	0.13	4.88	0.07	37.91	0.27	0.04	0.00	0.00	102.34		

sample name	rock type	mineral from composition	SiO2	TiO2	Al2O3	V2O3	Cr2O3	MnO	FeO	NiO	MgO	CaO	Na2O	K2O	P2O5	Total	notes	Crust-Mantle
R-2-2	lherzolite	orthopyroxene	57.19	0.00	1.12	0.01	0.43	0.15	4.84	0.07	37.73	0.29	0.03	0.00	0.00	101.86		
R-2-2	lherzolite	orthopyroxene	57.43	0.00	0.94	0.00	0.42	0.15	4.86	0.07	37.69	0.30	0.04	0.00	0.00	101.90		
R-2-2	lherzolite	orthopyroxene	57.44	0.01	0.91	0.01	0.42	0.13	4.90	0.06	38.01	0.16	0.04	0.00	0.01	102.11		
R-2-2	lherzolite	orthopyroxene	57.85	0.00	0.69	0.00	0.31	0.13	4.84	0.08	38.23	0.16	0.03	0.00	0.01	102.33		
R-2-3	lherzolite	orthopyroxene	57.55	0.00	0.40	0.01	0.14	0.15	4.67	0.07	35.72	0.15	0.00	0.00	0.00	98.84		
R-2-3	lherzolite	orthopyroxene	57.05	0.00	0.89	0.01	0.44	0.14	4.68	0.07	35.13	0.35	0.01	0.00	0.00	98.77		
R-2-3	lherzolite	orthopyroxene	57.87	0.00	0.28	0.00	0.11	0.13	4.67	0.07	35.75	0.14	0.00	0.01	0.01	99.04		
R-2-3	lherzolite	orthopyroxene	57.84	0.01	0.29	0.01	0.10	0.13	4.69	0.07	35.84	0.15	0.00	0.00	0.00	99.12		
R-2-3	lherzolite	orthopyroxene	57.35	0.01	0.83	0.01	0.39	0.14	4.71	0.07	35.49	0.14	0.00	0.00	0.01	99.15		
R-2-3	lherzolite	orthopyroxene	57.28	0.01	0.85	0.01	0.38	0.15	4.65	0.06	35.17	0.53	0.02	0.00	0.00	99.13		
R-2-3	lherzolite	orthopyroxene	57.04	0.01	1.08	0.01	0.47	0.14	4.65	0.08	35.02	0.59	0.03	0.00	0.01	99.13		
R-2-3	lherzolite	orthopyroxene	57.31	0.01	0.79	0.01	0.35	0.14	4.75	0.07	35.56	0.16	0.00	0.00	0.01	99.16		
R-2-3	lherzolite	orthopyroxene	57.20	0.01	0.97	0.01	0.39	0.15	4.77	0.07	35.37	0.16	0.00	0.00	0.00	99.10		
R-2-3	lherzolite	orthopyroxene	57.78	0.01	0.54	0.01	0.20	0.15	4.71	0.06	35.65	0.13	0.02	0.00	0.01	99.25		
R-2-3	lherzolite	orthopyroxene	57.27	0.00	0.80	0.00	0.38	0.13	4.68	0.08	35.31	0.34	0.01	0.01	0.01	99.01		
R-2-3	lherzolite	picotite = chromian spinel	0.00	0.13	11.80	0.22	51.06	0.47	24.94	0.10	10.02	0.00	0.01	0.00	0.00	98.76		
R-2-3	lherzolite	picotite = chromian spinel	0.02	0.15	12.44	0.25	50.08	0.46	25.31	0.10	10.09	0.00	0.02	0.00	0.00	98.93		
B-12A	eclogite/pyroxenite	garnet	38.77	0.11	21.97	0.00	0.15	0.42	19.70	0.00	10.57	7.20	0.02	0.00	0.06	98.96		
B-12A	eclogite/pyroxenite	garnet	39.00	0.14	22.20	0.01	0.11	0.43	20.00	0.01	10.45	6.95	0.02	0.00	0.05	99.37		
B-12A	eclogite/pyroxenite	garnet	39.03	0.08	22.17	0.04	0.14	0.41	19.84	0.01	10.69	6.95	0.02	0.00	0.06	99.43		
B-12A	eclogite/pyroxenite	garnet	38.84	0.16	22.03	0.02	0.15	0.40	19.85	0.00	10.40	6.94	0.03	0.00	0.07	98.89		
B-12A	eclogite/pyroxenite	garnet	39.05	0.09	22.09	0.02	0.13	0.41	19.83	0.01	10.50	6.86	0.03	0.00	0.06	99.07		
B-12A	eclogite/pyroxenite	garnet	39.02	0.11	22.14	0.01	0.11	0.42	19.79	0.01	10.51	6.94	0.03	0.00	0.08	99.17		
B-12A	eclogite/pyroxenite	garnet	39.08	0.11	22.19	0.03	0.13	0.41	19.69	0.00	10.61	6.98	0.04	0.00	0.03	99.30		
B-13-1	garnet plagioclase pyroxenite	augite	53.02	0.45	3.51	0.05	0.03	0.05	5.71	0.01	15.29	20.57	0.81	0.00	0.02	99.50		
B-13-1	garnet plagioclase pyroxenite	diopside	52.83	0.39	3.71	0.06	0.03	0.05	4.13	0.03	14.31	22.21	1.06	0.00	0.02	98.82		
B-13-1	garnet plagioclase pyroxenite	diopside	52.90	0.52	3.79	0.08	0.04	0.06	4.45	0.01	14.22	22.30	0.98	0.00	0.01	99.35		
B-13-1	garnet plagioclase pyroxenite	diopside	53.12	0.38	3.39	0.08	0.02	0.04	4.07	0.01	14.66	22.48	0.90	0.00	0.00	99.15		
B-13-1	garnet plagioclase pyroxenite	diopside	53.03	0.44	3.81	0.07	0.03	0.04	4.30	0.00	14.11	22.27	0.97	0.00	0.01	99.08		
B-13-1	garnet plagioclase pyroxenite	diopside	52.86	0.48	3.80	0.08	0.02	0.04	4.56	0.00	14.01	22.14	0.92	0.00	0.01	98.91		
B-13-1	garnet plagioclase pyroxenite	diopside	53.28	0.41	3.23	0.05	0.04	0.04	4.26	0.01	14.88	22.38	0.85	0.00	0.03	99.45		
B-13-1	garnet plagioclase pyroxenite	diopside	53.10	0.46	3.84	0.08	0.03	0.06	4.33	0.01	14.12	22.41	0.97	0.01	0.02	99.44		
B-13-1	garnet plagioclase pyroxenite	diopside	53.20	0.36	3.23	0.06	0.02	0.04	3.38	0.01	14.93	22.82	0.91	0.00	0.01	98.96		
B-13-1	garnet plagioclase pyroxenite	diopside	52.70	0.47	4.05	0.06	0.02	0.05	4.54	0.02	13.96	22.31	1.03	0.00	0.04	99.24		
B-13-1	garnet plagioclase pyroxenite	garnet	39.70	0.05	22.60	0.02	0.06	0.40	19.07	0.00	11.89	5.80	0.02	0.00	0.01	99.61		
B-13-1	garnet plagioclase pyroxenite	garnet	39.52	0.05	22.65	0.01	0.06	0.38	18.89	0.00	11.84	6.16	0.00	0.00	0.05	99.61		
B-13-1	garnet plagioclase pyroxenite	garnet	39.85	0.04	22.68	0.02	0.04	0.39	19.20	0.00	11.82	5.89	0.02	0.00	0.03	99.97		
B-13-1	garnet plagioclase pyroxenite	garnet	39.63	0.04	22.69	0.01	0.04	0.41	18.81	0.00	11.74	6.29	0.02	0.01	0.00	99.68		
B-13-1	garnet plagioclase pyroxenite	garnet	39.88	0.03	22.66	0.04	0.07	0.41	19.06	0.00	11.84	5.91	0.02	0.00	0.02	99.95		
B-13-1	garnet plagioclase pyroxenite	garnet	39.82	0.07	22.54	0.02	0.05	0.42	19.18	0.01	11.66	6.00	0.02	0.00	0.02	99.80		
B-13-1	garnet plagioclase pyroxenite	garnet	39.89	0.08	22.63	0.03	0.07	0.41	19.11	0.00	11.82	5.99	0.03	0.00	0.03	100.08		
B-13-1	garnet plagioclase pyroxenite	garnet	39.95	0.05	22.73	0.02	0.05	0.38	19.15	0.00	11.79	5.94	0.01	0.00	0.01	100.08		
B-13-1	garnet plagioclase pyroxenite	garnet	39.96	0.06	22.66	0.02	0.06	0.37	19.04	0.00	11.79	6.01	0.01	0.00	0.02	100.00		
B-13-1	garnet plagioclase pyroxenite	garnet	39.88	0.09	22.58	0.03	0.05	0.39	19.02	0.00	11.82	6.03	0.02	0.00	0.00	99.90		
B-13-1	garnet plagioclase pyroxenite	garnet	39.68	0.05	22.68	0.03	0.04	0.42	19.31	0.01	11.69	5.98	0.00	0.00	0.04	99.93		
B-13A	garnet plagioclase pyroxenite	garnet	39.36	0.06	22.43	0.01	0.08	0.39	19.09	0.00	12.00	5.95	0.01	0.01	0.01	99.40		
B-13A	garnet plagioclase pyroxenite	garnet	39.25	0.06	22.41	0.03	0.06	0.38	18.99	0.00	11.96	5.95	0.01	0.00	0.04	99.14		

sample name	rock type	mineral from composition	SiO2	TiO2	Al2O3	V2O3	Cr2O3	MnO	FeO	NiO	MgO	CaO	Na2O	K2O	P2O5	Total	notes	Crust-Mantle
B-13A	garnet plagioclase pyroxenite	garnet	39.25	0.04	22.41	0.00	0.07	0.39	18.87	0.01	12.04	6.05	0.00	0.00	0.03	99.16		
B-13A	garnet plagioclase pyroxenite	garnet	39.16	0.04	22.34	0.03	0.07	0.38	19.12	0.00	12.08	5.97	0.03	0.00	0.04	99.26		
B-13-1	garnet plagioclase pyroxenite	plagioclase	59.04	0.00	25.39	0.00	0.00	0.00	0.00	0.00	0.00	6.91	7.04	0.32	0.03	98.73		
B-13-1	garnet plagioclase pyroxenite	plagioclase	59.14	0.00	25.27	0.00	0.00	0.00	0.01	0.01	0.00	6.89	7.05	0.34	0.00	98.72		
B-3-1	garnet pyroxenite	augite	49.60	0.51	9.31	0.18	0.09	0.06	5.21	0.02	16.10	18.95	0.35	0.01	0.03	100.41		
B-3-1	garnet pyroxenite	pigeonite	51.83	0.13	6.64	0.20	0.17	0.11	9.76	0.02	26.58	3.35	0.03	0.04	0.01	98.86		
B-3-1	garnet pyroxenite	garnet	40.68	0.02	23.16	0.02	0.13	0.39	16.90	0.01	13.69	5.56	0.01	0.00	0.04	100.59		
B-3-1	garnet pyroxenite	garnet	40.57	0.04	23.07	0.01	0.12	0.40	16.86	0.01	13.54	5.57	0.01	0.00	0.05	100.27		
B-3-1	garnet pyroxenite	garnet	40.46	0.04	23.00	0.03	0.13	0.39	16.90	0.00	13.43	5.59	0.01	0.00	0.03	100.01		
B-3-1	garnet pyroxenite	garnet	40.47	0.03	22.94	0.04	0.10	0.38	16.90	0.01	13.44	5.64	0.02	0.00	0.06	100.03		
B-3-1	garnet pyroxenite	garnet	40.65	0.07	22.89	0.02	0.12	0.41	16.79	0.00	13.42	5.59	0.01	0.00	0.06	100.03		
B-3-1	garnet pyroxenite	garnet	40.52	0.04	22.90	0.03	0.13	0.37	17.01	0.00	13.53	5.50	0.00	0.00	0.06	100.11		
B-3-1	garnet pyroxenite	garnet	40.38	0.05	22.86	0.05	0.11	0.41	17.09	0.00	13.17	5.71	0.02	0.00	0.07	99.91		
B-3-1	garnet pyroxenite	garnet	40.39	0.02	23.00	0.02	0.11	0.40	17.00	0.00	13.35	5.66	0.02	0.00	0.04	100.01		
B-3-1	garnet pyroxenite	garnet	40.16	0.02	22.85	0.02	0.11	0.42	17.73	0.00	12.69	5.78	0.02	0.00	0.06	99.86		
B-3-1	garnet pyroxenite	garnet	40.52	0.04	22.93	0.04	0.13	0.39	17.08	0.00	13.33	5.61	0.00	0.00	0.05	100.11		
B-3-1	garnet pyroxenite	garnet	40.50	0.03	22.99	0.04	0.10	0.40	16.91	0.00	13.41	5.69	0.01	0.00	0.06	100.16		
B-3-1	garnet pyroxenite	garnet	40.40	0.06	22.99	0.01	0.12	0.38	16.78	0.01	13.40	5.64	0.01	0.00	0.05	99.85		
B-3-1	garnet pyroxenite	garnet	40.45	0.04	22.95	0.04	0.12	0.38	16.85	0.00	13.37	5.62	0.01	0.00	0.06	99.89		
B-3-1	garnet pyroxenite	garnet	40.43	0.04	22.98	0.02	0.10	0.41	17.11	0.00	13.23	5.63	0.01	0.01	0.06	100.02		
B-3-1	garnet pyroxenite	garnet	40.47	0.02	22.94	0.03	0.11	0.38	16.79	0.00	13.46	5.71	0.00	0.00	0.07	100.00		
B-3-1	garnet pyroxenite	garnet	40.44	0.01	23.08	0.02	0.11	0.41	16.94	0.01	13.45	5.58	0.01	0.00	0.07	100.13		
B-3-1	garnet pyroxenite	garnet	40.41	0.04	22.93	0.05	0.11	0.38	17.11	0.00	13.14	5.64	0.01	0.00	0.06	99.88		
B-3-1	garnet pyroxenite	garnet	40.25	0.03	22.83	0.04	0.13	0.41	17.56	0.00	12.99	5.61	0.01	0.01	0.05	99.92		
B-3-1	garnet pyroxenite	ilmenite	0.00	62.66	0.08	0.23	0.17	0.42	32.73	0.01	4.36	0.02	0.01	0.00	0.01	100.71		
B-3-1	garnet pyroxenite	ilmenite	0.01	58.91	0.08	0.29	0.20	0.48	35.69	0.00	4.79	0.05	0.03	0.00	0.00	100.53		
B-3-1	garnet pyroxenite	ilmenite	0.03	55.77	0.03	0.09	0.19	0.39	40.88	0.03	2.92	0.09	0.01	0.00	0.00	100.44		
B-3-1	garnet pyroxenite	ilmenite	0.40	53.65	0.42	0.31	0.60	0.75	37.71	0.04	5.76	0.10	0.03	0.00	0.00	99.76		
B-3-1	garnet pyroxenite	rutile	0.01	98.67	0.07	0.34	0.20	0.00	0.02	0.01	0.01	0.00	0.00	0.00	0.01	99.34		
B-3-1	garnet pyroxenite	rutile	0.00	98.48	0.02	0.16	0.19	0.00	0.07	0.01	0.01	0.01	0.00	0.00	0.00	98.95		
B-3-1	garnet pyroxenite	rutile	0.00	97.65	0.04	0.22	0.54	0.01	0.31	0.00	0.08	0.00	0.00	0.00	0.00	98.85		
B-3-1	garnet pyroxenite	rutile	0.01	98.11	0.03	0.21	0.55	0.00	0.04	0.00	0.01	0.00	0.00	0.00	0.00	98.96		
B-4-1	garnet pyroxenite	diopside	54.63	0.21	4.67	0.04	0.13	0.04	2.29	0.02	14.49	20.36	2.45	0.00	0.01	99.33		
B-4-1	garnet pyroxenite	diopside	54.64	0.24	4.62	0.06	0.10	0.05	2.35	0.01	14.49	20.39	2.45	0.00	0.00	99.39		
B-4-1	garnet pyroxenite	diopside	54.42	0.25	5.07	0.03	0.13	0.04	2.50	0.01	14.10	19.86	2.65	0.01	0.02	99.10		
B-4-1	garnet pyroxenite	diopside	54.52	0.24	4.86	0.04	0.11	0.03	2.42	0.01	14.17	20.15	2.63	0.00	0.01	99.19		
B-4-1	garnet pyroxenite	diopside	54.80	0.16	4.06	0.03	0.11	0.04	2.35	0.02	14.87	20.96	2.20	0.00	0.02	99.62		
B-4-1	garnet pyroxenite	diopside	54.70	0.11	4.11	0.02	0.12	0.04	2.28	0.01	14.97	20.95	2.22	0.00	0.00	99.53		
B-4-1	garnet pyroxenite	diopside	54.65	0.16	4.17	0.05	0.10	0.04	2.28	0.02	14.54	20.91	2.21	0.00	0.03	99.16		
B-4-1	garnet pyroxenite	diopside	54.55	0.30	5.11	0.05	0.11	0.05	2.54	0.03	14.16	19.73	2.72	0.00	0.03	99.39		
B-4-1	garnet pyroxenite	diopside	54.55	0.20	4.21	0.06	0.09	0.04	2.38	0.01	14.74	20.78	2.22	0.00	0.01	99.28		
B-4-1	garnet pyroxenite	diopside	54.65	0.15	4.13	0.04	0.10	0.05	2.43	0.01	14.64	20.99	2.22	0.01	0.00	99.41		
B-4-1	garnet pyroxenite	diopside	54.70	0.19	4.72	0.04	0.12	0.04	2.45	0.01	14.41	20.23	2.59	0.01	0.00	99.50		
B-4-1	garnet pyroxenite	diopside	54.65	0.14	4.39	0.05	0.11	0.05	2.34	0.02	14.57	20.64	2.34	0.00	0.02	99.32		
B-4A	garnet pyroxenite	diopside	53.99	0.20	4.70	0.06	0.19	0.06	2.49	0.03	14.32	20.24	2.46	0.01	0.00	98.76		
B-4A	garnet pyroxenite	diopside	54.00	0.21	5.29	0.04	0.18	0.05	2.53	0.03	13.90	19.90	2.63	0.01	0.01	98.77		
B-4A	garnet pyroxenite	diopside	54.21	0.22	4.61	0.05	0.20	0.05	2.49	0.04	14.37	20.28	2.40	0.00	0.02	98.93		

sample name	rock type	mineral from composition	SiO2	TiO2	Al2O3	V2O3	Cr2O3	MnO	FeO	NiO	MgO	CaO	Na2O	K2O	P2O5	Total	notes	Crust-Mantle
B-4A	garnet pyroxenite	diopside	54.17	0.14	4.68	0.06	0.16	0.04	2.48	0.04	14.67	20.27	2.39	0.00	0.00	99.10		
B-4-1	garnet pyroxenite	garnet	41.31	0.08	23.05	0.02	0.11	0.33	11.32	0.00	18.16	4.64	0.03	0.00	0.00	99.05		
B-4-1	garnet pyroxenite	garnet	41.13	0.09	22.79	0.01	0.11	0.37	12.64	0.01	17.47	4.38	0.05	0.00	0.01	99.06		
B-4-1	garnet pyroxenite	garnet	41.16	0.10	23.07	0.01	0.10	0.32	11.39	0.00	18.08	4.77	0.02	0.01	0.02	99.05		
B-4-1	garnet pyroxenite	garnet	41.35	0.07	22.95	0.00	0.13	0.33	11.45	0.01	18.03	4.81	0.03	0.00	0.02	99.18		
B-4-1	garnet pyroxenite	garnet	41.19	0.13	23.01	0.01	0.12	0.34	11.45	0.01	18.16	4.74	0.03	0.00	0.02	99.22		
B-4-1	garnet pyroxenite	garnet	41.21	0.09	23.03	0.00	0.13	0.38	13.05	0.00	17.51	4.25	0.02	0.00	0.02	99.69		
B-4-1	garnet pyroxenite	garnet	41.15	0.07	23.01	0.01	0.09	0.34	11.58	0.00	18.18	4.74	0.01	0.00	0.04	99.23		
B-4-1	garnet pyroxenite	garnet	41.20	0.09	23.04	0.00	0.12	0.37	12.18	0.00	17.94	4.40	0.02	0.00	0.02	99.37		
B-4-1	garnet pyroxenite	garnet	41.33	0.06	23.00	0.00	0.13	0.35	11.34	0.00	18.21	4.83	0.03	0.00	0.05	99.33		
B-4-1	garnet pyroxenite	garnet	41.32	0.11	23.02	0.00	0.11	0.36	11.93	0.02	18.14	4.50	0.02	0.00	0.04	99.56		
B-4-1	garnet pyroxenite	garnet	41.33	0.08	23.07	0.00	0.12	0.33	11.26	0.00	18.03	4.96	0.02	0.00	0.02	99.21		
B-4-1	garnet pyroxenite	garnet	41.01	0.07	22.89	0.00	0.12	0.43	13.71	0.00	16.93	4.27	0.03	0.00	0.02	99.48		
B-4-1	garnet pyroxenite	garnet	41.37	0.07	23.14	0.02	0.11	0.33	11.31	0.00	18.24	4.83	0.02	0.00	0.01	99.45		
B-4-1	garnet pyroxenite	garnet	41.21	0.08	23.11	0.02	0.12	0.35	12.22	0.00	17.89	4.43	0.03	0.00	0.02	99.48		
B-4A	garnet pyroxenite	garnet	40.86	0.08	23.15	0.00	0.20	0.35	10.93	0.01	19.00	4.52	0.00	0.00	0.02	99.12		
B-4A	garnet pyroxenite	garnet	40.98	0.13	23.14	0.01	0.22	0.35	11.15	0.00	18.80	4.54	0.02	0.00	0.02	99.36		
B-4A	garnet pyroxenite	garnet	41.10	0.07	23.16	0.02	0.22	0.35	11.06	0.00	18.96	4.36	0.02	0.00	0.02	99.33		
B-4A	garnet pyroxenite	garnet	40.99	0.08	23.02	0.01	0.19	0.32	10.92	0.01	18.75	4.56	0.02	0.00	0.01	98.88		
B-4A	garnet pyroxenite	garnet	40.86	0.08	23.08	0.02	0.23	0.33	11.07	0.00	18.77	4.43	0.01	0.00	0.01	98.90		
B-4A	garnet pyroxenite	garnet	40.77	0.10	22.93	0.01	0.21	0.36	11.77	0.00	18.32	4.30	0.03	0.00	0.01	98.82		
B-9-1	garnet pyroxenite	augite	52.86	0.48	4.11	0.09	0.04	0.07	5.92	0.00	16.50	18.92	0.75	0.00	0.01	99.74		
B-9-1	garnet pyroxenite	diopside	53.17	0.49	3.84	0.11	0.03	0.05	2.95	0.01	14.77	22.87	0.78	0.00	0.01	99.08		
B-9-1	garnet pyroxenite	diopside	52.56	0.60	4.13	0.08	0.04	0.04	3.50	0.01	14.57	22.46	0.86	0.00	0.02	98.85		
B-9-1	garnet pyroxenite	diopside	52.67	0.56	4.03	0.10	0.04	0.03	2.95	0.01	14.65	22.70	0.84	0.00	0.01	98.60		
B-9-1	garnet pyroxenite	diopside	52.87	0.42	3.73	0.12	0.04	0.01	2.90	0.00	15.02	22.97	0.79	0.00	0.01	98.87		
B-9-1	garnet pyroxenite	diopside	53.22	0.53	4.00	0.08	0.04	0.03	3.54	0.02	15.13	22.35	0.83	0.00	0.01	99.78		
B-9-1	garnet pyroxenite	diopside	52.18	0.61	4.28	0.07	0.01	0.04	3.54	0.01	14.38	22.52	0.88	0.00	0.02	98.55		
B-9-1	garnet pyroxenite	diopside	53.18	0.44	3.83	0.08	0.02	0.04	3.26	0.00	14.72	22.64	0.83	0.00	0.00	99.04		
B-9-1	garnet pyroxenite	diopside	52.96	0.52	4.11	0.09	0.08	0.04	3.12	0.00	14.81	22.73	0.85	0.00	0.02	99.33		
B-9-1	garnet pyroxenite	diopside	52.96	0.51	4.04	0.10	0.02	0.03	2.92	0.01	14.88	22.68	0.87	0.00	0.02	99.05		
B-9-1	garnet pyroxenite	garnet	40.04	0.02	22.74	0.04	0.04	0.34	16.06	0.01	13.50	5.89	0.00	0.00	0.00	98.67		
B-9-1	garnet pyroxenite	garnet	39.95	0.03	22.69	0.03	0.04	0.34	16.17	0.01	13.17	6.09	0.02	0.00	0.01	98.56		
B-9-1	garnet pyroxenite	garnet	39.87	0.09	22.76	0.03	0.03	0.34	16.19	0.00	13.32	5.93	0.01	0.00	0.01	98.57		
B-9-1	garnet pyroxenite	garnet	40.44	0.05	22.76	0.05	0.02	0.35	16.23	0.00	13.51	5.94	0.01	0.00	0.01	99.38		
B-9-1	garnet pyroxenite	garnet	40.17	0.08	22.70	0.02	0.02	0.32	16.11	0.00	13.31	6.11	0.03	0.00	0.03	98.88		
B-9-1	garnet pyroxenite	garnet	40.19	0.03	22.62	0.04	0.04	0.34	16.02	0.02	13.40	5.89	0.01	0.00	0.05	98.66		
B-9-1	garnet pyroxenite	garnet	40.06	0.05	22.90	0.03	0.04	0.34	15.94	0.00	13.51	5.89	0.02	0.01	0.02	98.80		
B-9-1	garnet pyroxenite	garnet	39.95	0.05	22.74	0.06	0.02	0.33	15.99	0.00	13.49	5.89	0.01	0.01	0.03	98.54		
B-9-1	garnet pyroxenite	garnet	39.96	0.04	22.66	0.04	0.02	0.34	16.13	0.00	13.44	5.96	0.01	0.00	0.00	98.59		
B-9-1	garnet pyroxenite	garnet	40.12	0.06	22.72	0.03	0.03	0.35	16.01	0.00	13.42	5.94	0.01	0.00	0.03	98.71		
B-9-1	garnet pyroxenite	garnet	40.36	0.06	22.71	0.04	0.02	0.34	16.02	0.00	13.22	5.93	0.01	0.00	0.04	98.73		
B-9-1	garnet pyroxenite	garnet	39.98	0.08	22.62	0.03	0.03	0.35	16.38	0.02	13.12	5.95	0.01	0.01	0.03	98.59		
B-9-1	garnet pyroxenite	garnet	40.37	0.06	22.60	0.02	0.03	0.34	15.98	0.01	13.25	5.91	0.01	0.00	0.02	98.60		
B-9-1	garnet pyroxenite	garnet	40.13	0.04	22.72	0.04	0.02	0.33	16.11	0.01	13.36	5.94	0.01	0.00	0.02	98.74		
B-9-1	garnet pyroxenite	garnet	40.36	0.07	22.69	0.04	0.04	0.34	16.19	0.00	13.29	5.93	0.01	0.00	0.03	98.98		
B-9-1	garnet pyroxenite	garnet	40.29	0.07	22.62	0.04	0.06	0.33	16.08	0.00	13.37	5.89	0.01	0.00	0.01	98.78		

sample name	rock type	mineral from composition	SiO2	TiO2	Al2O3	V2O3	Cr2O3	MnO	FeO	NiO	MgO	CaO	Na2O	K2O	P2O5	Total	notes	Crust-Mantle
M-10B	garnet pyroxenite	diopside	52.33	0.40	3.87	0.09	0.04	0.04	3.54	0.01	14.64	22.48	1.10	0.00	0.00	98.54		
M-10B	garnet pyroxenite	diopside	52.09	0.49	4.54	0.08	0.04	0.06	4.36	0.00	13.82	22.08	1.19	0.00	0.01	98.77		
M-10B	garnet pyroxenite	garnet	39.53	0.07	22.61	0.03	0.05	0.44	19.58	0.00	10.78	6.91	0.03	0.00	0.05	100.07		
M-10B	garnet pyroxenite	garnet	39.64	0.04	22.70	0.02	0.04	0.45	19.30	0.00	10.83	6.96	0.02	0.00	0.03	100.03		
M-10B	garnet pyroxenite	garnet	39.56	0.06	22.62	0.01	0.07	0.45	19.40	0.00	10.90	6.88	0.03	0.00	0.07	100.05		
M-12A	eclogite/pyroxenite	garnet	38.48	0.05	22.00	0.03	0.05	0.49	24.00	0.02	7.10	7.43	0.00	0.00	0.03	99.67		
M-12A	eclogite/pyroxenite	garnet	38.42	0.03	22.08	0.05	0.08	0.49	24.17	0.01	7.10	7.51	0.02	0.00	0.06	100.02		
M-12A	eclogite/pyroxenite	garnet	38.11	0.12	22.00	0.04	0.07	0.48	23.87	0.01	7.07	7.54	0.03	0.00	0.06	99.40		
M-12A	eclogite/pyroxenite	garnet	38.20	0.04	21.86	0.04	0.06	0.50	24.15	0.01	6.93	7.49	0.02	0.00	0.06	99.36		
M-12A	eclogite/pyroxenite	garnet	38.36	0.11	21.92	0.03	0.07	0.47	24.19	0.01	6.96	7.47	0.03	0.00	0.05	99.66		
M-16A	eclogite/pyroxenite	garnet	40.77	0.04	23.21	0.02	0.16	0.33	14.19	0.01	15.41	5.85	0.03	0.00	0.01	100.03		
M-16A	eclogite/pyroxenite	garnet	40.29	0.08	23.23	0.02	0.17	0.32	14.12	0.01	15.36	5.82	0.01	0.00	0.02	99.45		
M-16A	eclogite/pyroxenite	garnet	40.29	0.05	23.25	0.02	0.17	0.34	14.12	0.00	15.49	5.79	0.01	0.00	0.03	99.55		
M-16A	eclogite/pyroxenite	garnet	40.74	0.06	23.13	0.03	0.16	0.32	14.14	0.00	15.53	5.81	0.00	0.00	0.04	99.95		
M-16A	eclogite/pyroxenite	garnet	40.43	0.06	23.22	0.02	0.16	0.32	14.25	0.00	15.59	5.78	0.00	0.00	0.01	99.84		
M-18A	eclogite/pyroxenite	garnet	40.67	0.04	23.13	0.04	0.10	0.30	14.25	0.01	15.49	5.69	0.03	0.01	0.02	99.77		
M-18A	eclogite/pyroxenite	garnet	40.92	0.05	23.22	0.02	0.10	0.29	14.21	0.01	15.28	5.83	0.00	0.00	0.01	99.94		
M-18A	eclogite/pyroxenite	garnet	40.57	0.05	23.17	0.03	0.10	0.31	14.32	0.00	15.40	5.68	0.02	0.00	0.03	99.68		
M-18A	eclogite/pyroxenite	garnet	40.66	0.16	23.11	0.02	0.08	0.30	14.22	0.00	15.65	5.38	0.03	0.01	0.00	99.62		
M-18A	eclogite/pyroxenite	garnet	40.55	0.03	23.08	0.04	0.09	0.31	14.23	0.01	15.26	5.76	0.03	0.01	0.02	99.43		
M-19A-1	garnet pyroxenite	diopside	52.19	0.40	3.31	0.07	0.01	0.07	8.11	0.01	12.23	21.07	1.26	0.00	0.02	98.75		
M-19A-1	garnet pyroxenite	diopside	52.13	0.40	3.37	0.06	0.00	0.07	7.96	0.00	12.62	20.87	1.29	0.00	0.00	98.77		
M-19A-1	garnet pyroxenite	diopside	52.05	0.38	3.27	0.08	0.00	0.06	8.26	0.00	12.52	20.86	1.30	0.01	0.02	98.81		
M-19A-1	garnet pyroxenite	diopside	52.21	0.40	3.44	0.08	0.00	0.07	7.99	0.00	12.34	20.97	1.38	0.03	0.00	98.91		
M-19A-1	garnet pyroxenite	diopside	51.99	0.39	3.16	0.10	0.03	0.05	7.74	0.00	12.70	21.44	1.12	0.00	0.01	98.72		
M-19A-1	garnet pyroxenite	diopside	52.16	0.39	3.39	0.08	0.02	0.05	7.86	0.01	12.47	21.10	1.27	0.01	0.01	98.83		
M-19A-1	garnet pyroxenite	diopside	52.79	0.24	3.01	0.08	0.03	0.05	6.68	0.00	12.87	21.72	1.38	0.00	0.00	98.84		
M-19A-1	garnet pyroxenite	diopside	52.45	0.35	3.20	0.08	0.01	0.04	7.73	0.00	12.56	21.17	1.27	0.00	0.04	98.90		
M-19A-1	garnet pyroxenite	diopside	53.11	0.26	3.20	0.09	0.02	0.04	6.84	0.00	12.94	21.32	1.38	0.00	0.03	99.23		
M-19A-1	garnet pyroxenite	diopside	52.18	0.39	3.47	0.06	0.02	0.06	8.04	0.00	12.21	21.01	1.37	0.00	0.00	98.82		
M-19A	garnet pyroxenite	garnet	39.19	0.07	22.07	0.03	0.06	0.44	22.70	0.00	8.68	6.67	0.01	0.01	0.08	100.00		
M-19A	garnet pyroxenite	garnet	39.08	0.07	22.10	0.09	0.03	0.43	22.87	0.00	8.74	6.71	0.03	0.00	0.08	100.22		
M-19A	garnet pyroxenite	garnet	39.01	0.09	22.11	0.05	0.04	0.44	22.87	0.01	8.69	6.73	0.02	0.00	0.07	100.14		
M-19A	garnet pyroxenite	garnet	39.17	0.06	22.15	0.05	0.04	0.43	22.85	0.00	8.87	6.55	0.00	0.00	0.06	100.23		
M-19A-1	garnet pyroxenite	garnet	38.81	0.08	21.44	0.02	0.03	0.48	25.60	0.00	6.71	6.72	0.02	0.00	0.09	100.01		
M-19A-1	garnet pyroxenite	garnet	38.80	0.08	21.68	0.04	0.02	0.51	25.29	0.00	7.08	6.55	0.04	0.00	0.03	100.11		
M-19A-1	garnet pyroxenite	garnet	38.50	0.14	21.55	0.02	0.05	0.51	25.55	0.00	6.89	6.62	0.04	0.00	0.07	99.94		
M-19A-1	garnet pyroxenite	garnet	38.57	0.13	21.50	0.02	0.03	0.50	25.51	0.01	6.80	6.63	0.01	0.00	0.08	99.80		
M-19A-1	garnet pyroxenite	garnet	38.58	0.13	21.45	0.05	0.02	0.47	25.22	0.02	6.92	6.68	0.02	0.00	0.06	99.60		
M-19A-1	garnet pyroxenite	garnet	38.68	0.05	21.43	0.04	0.06	0.53	25.18	0.00	7.05	6.57	0.02	0.00	0.07	99.67		
M-19A-1	garnet pyroxenite	garnet	38.66	0.12	21.48	0.03	0.03	0.49	25.69	0.01	6.69	6.70	0.02	0.00	0.03	99.95		
M-19A-1	garnet pyroxenite	garnet	38.58	0.13	21.38	0.03	0.05	0.49	25.16	0.00	7.04	6.66	0.04	0.00	0.06	99.63		
M-19B	garnet pyroxenite	diopside	52.13	0.46	3.54	0.08	0.03	0.08	9.08	0.00	12.61	20.32	1.25	0.00	0.02	99.60		
M-19B	garnet pyroxenite	diopside	52.42	0.33	3.12	0.07	0.01	0.05	7.56	0.01	12.58	21.51	1.21	0.00	0.02	98.88		

sample name	rock type	mineral from composition	SiO2	TiO2	Al2O3	V2O3	Cr2O3	MnO	FeO	NiO	MgO	CaO	Na2O	K2O	P2O5	Total	notes	Crust-Mantle
M-19B	garnet pyroxenite	diopside	52.47	0.23	3.26	0.08	0.02	0.05	7.59	0.00	12.39	21.34	1.38	0.00	0.01	98.81		
M-19B	garnet pyroxenite	diopside	52.04	0.83	3.29	0.06	0.03	0.06	7.82	0.00	12.39	21.18	1.32	0.00	0.01	99.04		
M-19B	garnet pyroxenite	diopside	52.19	0.35	3.16	0.09	0.01	0.05	7.25	0.00	12.67	21.40	1.35	0.00	0.02	98.53		
M-19B	garnet pyroxenite	garnet	38.35	0.11	21.78	0.04	0.02	0.49	25.38	0.01	7.00	6.70	0.02	0.00	0.07	99.97		
M-19B	garnet pyroxenite	garnet	38.58	0.12	21.89	0.04	0.01	0.51	25.10	0.00	6.99	6.80	0.02	0.00	0.07	100.13		
M-19B	garnet pyroxenite	garnet	38.51	0.14	21.71	0.05	0.02	0.51	25.13	0.00	6.92	6.94	0.02	0.00	0.09	100.03		
M-19B-1	garnet pyroxenite	garnet	39.61	0.08	22.24	0.05	0.04	0.43	22.72	0.00	8.64	7.14	0.02	0.00	0.07	101.04		
M-19B-1	garnet pyroxenite	garnet	39.48	0.09	22.16	0.05	0.02	0.44	22.93	0.00	8.81	6.72	0.05	0.01	0.06	100.81		
M-19B-1	garnet pyroxenite	garnet	39.56	0.08	22.21	0.04	0.01	0.44	22.88	0.00	8.88	6.68	0.02	0.00	0.08	100.88		
M-19B-1	garnet pyroxenite	garnet	39.67	0.02	22.15	0.04	0.04	0.45	22.82	0.00	8.84	6.65	0.02	0.00	0.04	100.73		
M-19B-1	garnet pyroxenite	garnet	39.63	0.08	22.23	0.03	0.05	0.43	22.73	0.00	8.77	6.80	0.03	0.00	0.07	100.85		
M-19B-1	garnet pyroxenite	garnet	39.72	0.07	21.96	0.06	0.05	0.40	22.95	0.01	8.85	6.69	0.02	0.01	0.03	100.82		
M-19B-1	garnet pyroxenite	garnet	39.66	0.14	22.06	0.07	0.03	0.43	22.58	0.00	8.69	7.11	0.03	0.00	0.08	100.88		
M-19B-1	garnet pyroxenite	garnet	39.65	0.14	22.07	0.06	0.05	0.42	22.46	0.00	8.58	7.40	0.02	0.00	0.06	100.91		
M-19B-1	garnet pyroxenite	garnet	39.58	0.08	22.03	0.05	0.03	0.43	22.73	0.00	8.81	6.86	0.03	0.00	0.06	100.68		
M-19B-1	garnet pyroxenite	garnet	39.66	0.08	22.14	0.04	0.05	0.43	22.79	0.00	8.66	6.96	0.02	0.00	0.06	100.89		
M-19B-1	garnet pyroxenite	garnet	39.72	0.07	22.23	0.04	0.02	0.43	22.96	0.00	8.89	6.63	0.01	0.00	0.06	101.06		
M-1A	eclogite	garnet	39.21	0.09	22.40	0.03	0.04	0.41	21.56	0.03	9.41	6.72	0.02	0.00	0.04	99.95		
M-1A	eclogite	garnet	39.15	0.09	22.48	0.04	0.05	0.43	21.58	0.00	9.36	6.81	0.03	0.00	0.02	100.04		
M-1A	eclogite	garnet	38.86	0.52	22.40	0.03	0.02	0.44	21.43	0.00	9.42	6.62	0.01	0.01	0.03	99.79		
M-1A	eclogite	garnet	38.96	0.05	22.49	0.02	0.04	0.44	21.57	0.00	9.42	6.72	0.02	0.00	0.04	99.78		
M-1A	eclogite	garnet	38.88	0.05	23.29	0.03	0.05	0.43	21.38	0.02	9.46	6.63	0.02	0.00	0.05	100.28		
M-2-1	garnet pyroxenite	diopside	53.08	0.48	4.09	0.19	0.12	0.05	3.24	0.00	15.18	22.29	0.88	0.00	0.02	99.62		
M-2-1	garnet pyroxenite	diopside	52.89	0.53	4.33	0.20	0.08	0.03	3.19	0.00	14.98	22.33	0.90	0.00	0.02	99.47		
M-2-1	garnet pyroxenite	diopside	51.52	0.56	4.23	0.15	0.08	0.05	3.39	0.01	14.47	23.83	0.80	0.00	0.03	99.12		
M-2-1	garnet pyroxenite	diopside	52.72	0.49	4.10	0.14	0.09	0.03	3.16	0.00	14.76	22.77	0.87	0.00	0.03	99.15		
M-2-1	garnet pyroxenite	diopside	52.77	0.50	4.07	0.15	0.07	0.04	3.28	0.02	15.49	22.16	0.86	0.00	0.00	99.40		
M-2-1	garnet pyroxenite	diopside	53.49	0.26	3.29	0.11	0.06	0.01	1.80	0.00	15.75	23.66	0.76	0.01	0.01	99.21		
M-2-2	garnet pyroxenite	diopside	53.17	0.35	3.89	0.20	0.11	0.03	2.81	0.02	15.31	22.68	0.88	0.00	0.02	99.47		
M-2-2	garnet pyroxenite	diopside	53.15	0.29	3.69	0.18	0.10	0.03	2.41	0.01	15.36	22.89	0.87	0.00	0.01	98.99		
M-2-2	garnet pyroxenite	diopside	52.79	0.37	3.88	0.21	0.12	0.04	3.04	0.00	15.06	22.65	0.87	0.00	0.03	99.05		
M-2-2	garnet pyroxenite	diopside	53.25	0.29	3.79	0.20	0.10	0.02	2.36	0.01	15.24	23.09	0.89	0.00	0.02	99.27		
M-2-2	garnet pyroxenite	diopside	52.72	0.44	4.09	0.20	0.13	0.02	2.94	0.00	15.03	22.43	0.97	0.00	0.02	98.99		
M-2-2	garnet pyroxenite	diopside	52.41	0.56	4.52	0.22	0.11	0.04	3.07	0.01	14.51	22.59	0.96	0.00	0.01	99.00		
M-2-2	garnet pyroxenite	diopside	52.73	0.46	4.31	0.19	0.14	0.06	3.81	0.01	15.40	21.21	0.90	0.00	0.01	99.23		
M-2-2	garnet pyroxenite	diopside	54.35	0.21	0.07	0.03	0.00	0.08	2.51	0.01	16.58	24.76	0.37	0.00	0.00	98.97		
M-2-2	garnet pyroxenite	diopside	52.46	0.45	3.97	0.19	0.09	0.05	3.31	0.00	14.78	22.64	0.82	0.01	0.02	98.79		
M-2-1	garnet pyroxenite	garnet	40.87	0.05	23.08	0.06	0.12	0.26	15.92	0.00	14.21	5.81	0.00	0.00	0.02	100.39		
M-2-1	garnet pyroxenite	garnet	40.80	0.05	22.95	0.07	0.13	0.27	15.83	0.00	14.23	6.12	0.01	0.00	0.02	100.48		
M-2-1	garnet pyroxenite	garnet	40.70	0.04	23.05	0.07	0.12	0.27	15.78	0.00	14.29	5.90	0.01	0.00	0.01	100.25		
M-2-1	garnet pyroxenite	garnet	40.70	0.05	22.99	0.08	0.09	0.25	15.68	0.00	14.44	5.81	0.02	0.00	0.02	100.13		
M-2-1	garnet pyroxenite	garnet	40.49	0.04	23.03	0.05	0.10	0.26	15.57	0.00	14.38	5.81	0.01	0.00	0.02	99.76		
M-2-1	garnet pyroxenite	garnet	40.64	0.04	23.10	0.03	0.08	0.23	15.60	0.01	14.76	5.43	0.01	0.00	0.00	99.93		
M-2-1	garnet pyroxenite	garnet	40.67	0.07	22.97	0.05	0.11	0.28	15.65	0.00	14.36	5.87	0.00	0.00	0.01	100.04		
M-2-1	garnet pyroxenite	garnet	40.55	0.03	22.99	0.05	0.11	0.27	15.61	0.01	14.32	5.80	0.01	0.00	0.00	99.74		
M-2-1	garnet pyroxenite	garnet	40.35	0.03	23.12	0.04	0.07	0.26	15.57	0.01	14.28	5.99	0.00	0.01	0.02	99.76		
M-2-1	garnet pyroxenite	garnet	40.36	0.05	22.99	0.05	0.06	0.25	15.67	0.00	14.38	5.82	0.01	0.01	0.02	99.68		

sample name	rock type	mineral from composition	SiO2	TiO2	Al2O3	V2O3	Cr2O3	MnO	FeO	NiO	MgO	CaO	Na2O	K2O	P2O5	Total	notes	Crust-Mantle
M-2-1	garnet pyroxenite	garnet	40.23	0.05	22.99	0.05	0.10	0.28	15.76	0.00	14.27	5.90	0.01	0.00	0.03	99.66		
M-2-1	garnet pyroxenite	garnet	40.46	0.06	23.02	0.03	0.09	0.25	15.56	0.00	14.45	5.84	0.01	0.01	0.02	99.79		
M-2-1	garnet pyroxenite	garnet	40.33	0.05	22.95	0.04	0.10	0.26	15.50	0.01	14.35	6.02	0.00	0.00	0.03	99.65		
M-2-1	garnet pyroxenite	garnet	40.38	0.07	22.81	0.04	0.09	0.24	15.56	0.00	14.52	5.80	0.00	0.00	0.03	99.54		
M-2-2	garnet pyroxenite	garnet	40.24	0.05	22.74	0.06	0.12	0.26	15.51	0.00	14.33	5.86	0.00	0.00	0.03	99.20		
M-2-2	garnet pyroxenite	garnet	40.29	0.03	22.80	0.03	0.14	0.26	15.49	0.00	14.26	5.92	0.01	0.00	0.00	99.24		
M-2-2	garnet pyroxenite	garnet	40.47	0.02	22.74	0.04	0.12	0.25	15.48	0.01	14.33	5.86	0.01	0.00	0.04	99.36		
M-2-2	garnet pyroxenite	garnet	40.32	0.06	22.72	0.06	0.11	0.26	15.53	0.00	14.26	6.17	0.02	0.00	0.01	99.52		
M-2-2	garnet pyroxenite	garnet	40.48	0.02	22.74	0.05	0.13	0.25	15.53	0.00	14.54	5.83	0.00	0.00	0.00	99.57		
M-2-2	garnet pyroxenite	garnet	40.44	0.03	22.80	0.04	0.15	0.26	15.69	0.00	14.23	6.01	0.02	0.00	0.01	99.68		
M-2-2	garnet pyroxenite	garnet	40.35	0.04	22.68	0.07	0.13	0.26	15.56	0.00	14.36	5.91	0.01	0.00	0.03	99.40		
M-2-2	garnet pyroxenite	garnet	40.11	0.05	22.70	0.08	0.13	0.26	15.56	0.00	14.06	6.13	0.00	0.00	0.03	99.11		
M-2-2	garnet pyroxenite	garnet	40.40	0.06	22.63	0.09	0.16	0.25	15.72	0.00	14.28	5.95	0.00	0.00	0.01	99.54		
M-2-2	garnet pyroxenite	garnet	40.43	0.04	22.78	0.05	0.13	0.26	15.54	0.00	14.45	5.88	0.02	0.00	0.02	99.60		
M-2-2	garnet pyroxenite	garnet	40.45	0.04	22.79	0.06	0.15	0.26	15.52	0.01	14.38	5.99	0.01	0.01	0.02	99.69		
M-2-2	garnet pyroxenite	garnet	40.40	0.04	22.77	0.06	0.18	0.27	15.62	0.00	14.28	6.09	0.01	0.00	0.02	99.73		
M-2-2	garnet pyroxenite	garnet	40.52	0.05	22.78	0.05	0.15	0.27	15.63	0.00	14.24	5.91	0.00	0.00	0.01	99.61		
M-2-2	garnet pyroxenite	garnet	40.48	0.05	22.59	0.07	0.17	0.25	15.49	0.01	14.44	5.81	0.02	0.00	0.03	99.39		
M-2-2	garnet pyroxenite	garnet	40.35	0.06	22.67	0.05	0.11	0.24	15.35	0.00	14.09	6.13	0.01	0.01	0.01	99.08		
M-2-2	garnet pyroxenite	jeppeite	0.04	79.58	0.07	1.76	0.00	0.01	5.20	0.00	1.07	0.11	0.13	10.81	0.00	98.79		
M-2-2	garnet pyroxenite	jeppeite	0.02	80.58	0.04	0.23	0.00	0.01	6.49	0.01	0.72	0.13	0.18	10.88	0.00	99.30		
M-2B-3	garnet pyroxenite	diopside	48.65	1.41	7.26	0.08	0.02	0.04	8.06	0.01	11.23	22.46	1.07	0.00	0.03	100.32	High Al	
M-2B-3	garnet pyroxenite	diopside	48.56	1.47	7.37	0.08	0.02	0.04	8.22	0.02	11.16	22.46	1.12	0.00	0.03	100.55	High Al	
M-2B-3	garnet pyroxenite	diopside	48.42	1.46	7.26	0.09	0.02	0.04	8.27	0.02	11.09	22.48	1.10	0.00	0.03	100.28	High Al	
M-2B-3	garnet pyroxenite	garnet	39.14	0.24	21.63	0.04	0.02	0.39	22.00	0.00	7.94	8.67	0.02	0.00	0.04	100.13		
M-2B-3	garnet pyroxenite	garnet	38.98	0.20	21.78	0.04	0.02	0.40	21.97	0.01	7.89	8.62	0.00	0.00	0.03	99.93		
M-2B-3	garnet pyroxenite	garnet	39.00	0.27	21.80	0.04	0.02	0.40	22.18	0.01	7.98	8.60	0.02	0.00	0.05	100.37		
M-2B-3	garnet pyroxenite	garnet	39.02	0.25	21.75	0.06	0.02	0.40	21.78	0.00	7.85	8.92	0.03	0.00	0.04	100.11		
M-2B-3	garnet pyroxenite	garnet	39.17	0.21	21.77	0.02	0.00	0.37	21.70	0.00	7.76	9.07	0.01	0.00	0.04	100.12		
M-2B-3	garnet pyroxenite	garnet	39.07	0.23	21.71	0.02	0.01	0.39	21.79	0.00	7.82	8.94	0.02	0.00	0.03	100.04		
M-2B-3	garnet pyroxenite	garnet	39.10	0.24	21.73	0.04	0.03	0.38	21.75	0.00	7.83	8.91	0.00	0.00	0.04	100.06		
M-2B-3	garnet pyroxenite	garnet	39.13	0.20	21.65	0.04	0.01	0.38	21.91	0.00	7.77	8.90	0.01	0.00	0.06	100.07		
M-2B-3	garnet pyroxenite	garnet	39.14	0.22	21.60	0.04	0.01	0.41	21.86	0.01	7.70	9.07	0.01	0.00	0.03	100.09		
M-2B-3	garnet pyroxenite	garnet	39.05	0.19	21.79	0.03	0.04	0.37	21.78	0.00	7.69	9.07	0.02	0.00	0.06	100.10		
M-2B-3	garnet pyroxenite	garnet	38.92	0.24	21.74	0.06	0.02	0.40	21.89	0.00	7.60	9.07	0.01	0.00	0.02	99.97		
M-2B-3	garnet pyroxenite	garnet	38.79	0.23	21.57	0.04	0.04	0.39	22.59	0.00	7.30	8.78	0.01	0.00	0.05	99.80		
M-2B-3	garnet pyroxenite	garnet	38.85	0.24	21.53	0.04	0.02	0.40	22.57	0.00	7.35	8.69	0.00	0.00	0.03	99.73		
M-2B-3	garnet pyroxenite	garnet	39.07	0.22	21.68	0.05	0.00	0.38	22.45	0.00	7.44	8.86	0.01	0.00	0.03	100.20		
M-2B-3	garnet pyroxenite	garnet	38.99	0.20	21.58	0.02	0.04	0.40	22.39	0.00	7.46	8.87	0.01	0.00	0.04	100.01		
M-2B-3	garnet pyroxenite	garnet	38.97	0.21	21.67	0.03	0.00	0.42	22.62	0.00	7.25	8.78	0.01	0.00	0.03	99.98		
M-2B-3	garnet pyroxenite	garnet	39.07	0.18	21.73	0.03	0.01	0.40	22.41	0.00	7.11	9.08	0.02	0.00	0.03	100.08		
M-2B-3	garnet pyroxenite	garnet	38.96	0.22	21.67	0.03	0.03	0.41	22.69	0.00	7.28	8.87	0.01	0.00	0.04	100.19		
M-2B-3	garnet pyroxenite	garnet	38.80	0.20	21.62	0.03	0.04	0.40	22.45	0.00	7.17	8.98	0.00	0.00	0.05	99.74		
M-2B-3	garnet pyroxenite	garnet	39.01	0.14	21.70	0.04	0.00	0.39	22.21	0.00	7.08	9.33	0.00	0.00	0.04	99.93		
M-2B-3	garnet pyroxenite	garnet	39.13	0.19	21.71	0.03	0.01	0.41	21.74	0.00	7.64	9.00	0.01	0.00	0.04	99.92		
M-2B-3	garnet pyroxenite	garnet	39.17	0.25	21.80	0.04	0.02	0.39	21.96	0.01	7.91	8.70	0.01	0.00	0.05	100.32		
M-2B-3	garnet pyroxenite	priderite	0.00	83.50	0.07	0.40	0.08	0.01	6.55	0.00	0.65	0.17	0.07	7.11	0.00	98.61		
M-2B-3	garnet pyroxenite	priderite	0.00	83.34	0.15	0.55	0.10	0.01	7.00	0.00	0.55	0.18	0.07	6.92	0.00	98.88		

sample name	rock type	mineral from composition	SiO2	TiO2	Al2O3	V2O3	Cr2O3	MnO	FeO	NiO	MgO	CaO	Na2O	K2O	P2O5	Total	notes	Crust-Mantle
M-2B-3	garnet pyroxenite	rutile	0.00	99.86	0.00	0.00	0.08	0.00	0.03	0.00	0.02	0.01	0.01	0.01	0.00	100.03		
M-2B-3	garnet pyroxenite	rutile	0.00	99.71	0.01	0.00	0.07	0.00	0.04	0.00	0.00	0.03	0.01	0.01	0.01	99.90		
M-4A	eclogite/pyroxenite	garnet	39.89	0.07	22.70	0.00	0.41	0.34	17.09	0.00	13.46	5.48	0.04	0.00	0.05	99.52		
M-4A	eclogite/pyroxenite	garnet	39.92	0.05	22.80	0.01	0.38	0.35	16.99	0.01	13.68	5.48	0.01	0.00	0.06	99.74		
M-4A	eclogite/pyroxenite	garnet	40.52	0.02	22.81	0.04	0.36	0.34	16.96	0.00	13.94	5.23	0.02	0.00	0.08	100.32		
M-4A	eclogite/pyroxenite	garnet	40.26	0.04	22.80	0.01	0.40	0.34	17.18	0.00	13.64	5.45	0.02	0.01	0.07	100.22		
M-4A	eclogite/pyroxenite	garnet	39.69	0.18	22.63	0.02	0.43	0.34	17.54	0.00	13.40	5.45	0.02	0.00	0.06	99.77		
M-4A	eclogite/pyroxenite	garnet	39.69	0.16	22.61	0.01	0.44	0.35	17.55	0.01	13.40	5.43	0.02	0.00	0.04	99.72		
M-4A	eclogite/pyroxenite	garnet	39.63	0.14	22.56	0.02	0.41	0.34	17.61	0.00	13.26	5.46	0.03	0.00	0.05	99.51		
M-4A	eclogite/pyroxenite	garnet	40.32	0.04	22.75	0.01	0.39	0.32	16.97	0.00	13.68	5.44	0.01	0.00	0.04	99.97		
M-5A	garnet pyroxenite	diopside	53.23	0.25	3.27	0.08	0.05	0.05	3.74	0.00	14.98	22.78	0.97	0.00	0.01	99.42		
M-5A	garnet pyroxenite	garnet	39.49	0.09	22.60	0.03	0.06	0.45	19.38	0.00	10.87	6.90	0.02	0.00	0.04	99.92		
M-5A	garnet pyroxenite	garnet	39.50	0.11	22.66	0.03	0.06	0.43	19.36	0.00	10.88	6.86	0.02	0.00	0.06	99.98		
M-5A	garnet pyroxenite	garnet	39.63	0.07	22.66	0.03	0.03	0.46	19.53	0.00	10.76	6.86	0.03	0.00	0.05	100.10		
M-5A	garnet pyroxenite	garnet	39.60	0.08	22.62	0.02	0.06	0.45	19.50	0.00	10.82	6.92	0.02	0.00	0.07	100.16		
M-5A	garnet pyroxenite	garnet	39.55	0.02	22.67	0.01	0.07	0.46	19.77	0.01	10.83	6.71	0.01	0.00	0.06	100.17		
M-5A	garnet pyroxenite	garnet	39.11	0.07	22.58	0.03	0.04	0.46	19.60	0.00	10.79	6.75	0.01	0.00	0.04	99.47		
R-1A	eclogite/pyroxenite	garnet	39.11	0.03	22.44	0.03	0.14	0.47	18.77	0.01	12.57	5.38	0.03	0.00	0.03	99.01		
R-1A	eclogite/pyroxenite	garnet	39.42	0.01	22.51	0.01	0.16	0.47	18.39	0.00	12.92	5.36	0.02	0.00	0.03	99.31		
R-1A	eclogite/pyroxenite	garnet	39.28	0.01	22.53	0.01	0.17	0.50	18.67	0.00	12.78	5.36	0.01	0.01	0.05	99.39		
R-1A	eclogite/pyroxenite	garnet	39.26	0.02	22.46	0.02	0.15	0.50	18.70	0.00	12.78	5.30	0.00	0.00	0.05	99.24		
R-1A	eclogite/pyroxenite	garnet	39.45	0.01	22.57	0.00	0.16	0.48	18.43	0.00	12.81	5.31	0.00	0.00	0.02	99.24		
R-1A	eclogite/pyroxenite	garnet	39.38	0.03	22.40	0.02	0.13	0.47	18.66	0.00	12.66	5.36	0.02	0.00	0.06	99.21		
R-1A	eclogite/pyroxenite	garnet	39.47	0.01	22.58	0.02	0.15	0.49	18.28	0.00	13.02	5.29	0.03	0.00	0.04	99.38		
R-2-4	garnet pyroxenite	diopside	53.19	0.26	3.59	0.08	0.09	0.05	3.66	0.02	14.99	22.24	1.15	0.00	0.02	99.33		
R-2-4	garnet pyroxenite	diopside	53.10	0.29	3.91	0.05	0.08	0.05	3.55	0.01	14.80	22.46	1.18	0.00	0.04	99.53		
R-2-4	garnet pyroxenite	diopside	52.42	0.69	5.39	0.06	0.07	0.04	3.32	0.00	14.00	21.66	1.67	0.00	0.02	99.33		
R-2-4	garnet pyroxenite	diopside	51.78	0.82	6.00	0.08	0.04	0.05	3.82	0.00	13.41	21.28	1.80	0.00	0.03	99.11		
R-2-4	garnet pyroxenite	diopside	52.36	0.70	5.79	0.06	0.05	0.03	3.11	0.01	13.77	21.53	1.75	0.00	0.01	99.17		
R-2-4	garnet pyroxenite	diopside	51.96	0.88	6.00	0.05	0.05	0.04	3.65	0.00	13.45	21.33	1.80	0.00	0.02	99.24		
R-2-4	garnet pyroxenite	diopside	51.88	0.77	6.36	0.06	0.05	0.05	3.50	0.01	13.29	21.36	1.83	0.01	0.03	99.20		
R-2-4	garnet pyroxenite	diopside	51.77	0.99	6.00	0.08	0.03	0.03	3.27	0.02	13.75	21.36	1.72	0.01	0.02	99.05		
R-2-4	garnet pyroxenite	diopside	52.04	0.56	6.21	0.07	0.04	0.05	3.21	0.00	13.69	21.42	1.79	0.00	0.04	99.13		
R-2-4	garnet pyroxenite	diopside	52.01	0.87	6.09	0.08	0.05	0.04	3.22	0.02	13.73	21.53	1.75	0.00	0.03	99.42		
R-2-4	garnet pyroxenite	garnet	40.37	0.02	22.97	0.00	0.09	0.45	18.06	0.00	12.86	5.32	0.01	0.00	0.04	100.18		
R-2-4	garnet pyroxenite	garnet	40.23	0.00	22.86	0.00	0.08	0.45	17.80	0.00	12.93	5.35	0.02	0.00	0.06	99.78		
R-2-4	garnet pyroxenite	garnet	40.36	0.07	22.94	0.01	0.10	0.43	17.17	0.00	13.20	5.38	0.00	0.00	0.06	99.73		
R-2-4	garnet pyroxenite	garnet	40.53	0.01	22.98	0.03	0.08	0.43	17.03	0.00	13.55	5.35	0.00	0.00	0.05	100.04		
R-2-4	garnet pyroxenite	garnet	40.39	0.03	23.01	0.01	0.07	0.42	17.01	0.02	13.50	5.39	0.01	0.00	0.06	99.92		
R-2-4	garnet pyroxenite	garnet	40.40	0.33	23.02	0.03	0.08	0.43	17.18	0.00	13.31	5.34	0.00	0.00	0.05	100.17		
R-2-4	garnet pyroxenite	garnet	40.46	0.01	23.07	0.01	0.08	0.45	17.00	0.01	13.48	5.44	0.01	0.00	0.03	100.03		
R-2-4	garnet pyroxenite	garnet	40.35	0.01	23.00	0.00	0.08	0.42	17.22	0.00	13.35	5.37	0.00	0.00	0.05	99.86		
R-2-4	garnet pyroxenite	garnet	40.34	0.02	22.95	0.02	0.07	0.44	17.13	0.01	13.28	5.46	0.00	0.00	0.03	99.74		
R-2-4	garnet pyroxenite	garnet	40.50	0.00	22.93	0.03	0.06	0.42	16.77	0.00	13.48	5.47	0.00	0.00	0.03	99.70		
R-2-4	garnet pyroxenite	garnet	40.31	0.15	22.90	0.02	0.05	0.45	17.35	0.00	13.09	5.46	0.01	0.00	0.05	99.86		

sample name	rock type	mineral from composition	SiO2	TiO2	Al2O3	V2O3	Cr2O3	MnO	FeO	NiO	MgO	CaO	Na2O	K2O	P2O5	Total	notes	Crust-Mantle
R-2-4	garnet pyroxenite	garnet	40.26	0.01	22.99	0.01	0.03	0.42	17.30	0.00	13.36	5.40	0.00	0.00	0.04	99.83		
R-2-4	garnet pyroxenite	garnet	40.32	0.04	22.94	0.02	0.05	0.44	17.24	0.00	13.12	5.57	0.01	0.00	0.05	99.79		
R-2-4	garnet pyroxenite	garnet	40.28	0.03	22.94	0.01	0.03	0.40	16.85	0.01	13.17	5.81	0.01	0.00	0.06	99.60		
R-2-4	garnet pyroxenite	garnet	40.33	0.03	22.97	0.01	0.03	0.41	17.26	0.01	13.17	5.60	0.00	0.00	0.05	99.87		
R-2-4	garnet pyroxenite	garnet	40.26	0.02	22.88	0.00	0.02	0.46	17.70	0.00	12.81	5.56	0.00	0.00	0.05	99.78		
R-2-4	garnet pyroxenite	rutile	0.03	97.77	0.01	0.32	0.18	0.00	0.21	0.00	0.00	0.30	0.00	0.00	0.01	98.83		
R-2-4	garnet pyroxenite	rutile	0.00	97.93	0.07	0.23	0.16	0.00	0.13	0.00	0.00	0.18	0.00	0.00	0.00	98.72		
R-2-4	garnet pyroxenite	rutile	0.01	98.02	0.01	0.37	0.06	0.00	0.19	0.00	0.03	0.03	0.00	0.01	0.00	98.73		
R-2-4	garnet pyroxenite	rutile	0.00	97.86	0.06	0.29	0.07	0.00	0.19	0.01	0.01	0.17	0.00	0.00	0.01	98.67		
R-5A	garnet pyroxenite	diopside	51.85	0.87	5.94	0.08	0.06	0.04	3.50	0.02	13.35	21.26	1.88	0.01	0.00	98.85		
R-5A	garnet pyroxenite	garnet	39.56	0.10	22.46	0.02	0.07	0.42	19.35	0.00	11.69	6.06	0.02	0.00	0.07	99.82		
R-5A	garnet pyroxenite	garnet	39.66	0.08	22.35	0.01	0.08	0.42	19.19	0.00	11.70	6.15	0.02	0.00	0.06	99.71		
R-5A	garnet pyroxenite	garnet	39.51	0.08	22.49	0.01	0.04	0.41	19.23	0.00	11.67	6.17	0.03	0.00	0.08	99.72		
R-5A	garnet pyroxenite	garnet	39.39	0.10	22.35	0.02	0.07	0.42	19.25	0.00	11.81	6.19	0.04	0.00	0.08	99.71		
R-5A	garnet pyroxenite	garnet	39.61	0.08	22.32	0.03	0.07	0.45	19.46	0.01	11.63	6.08	0.03	0.00	0.07	99.83		
Concentrate		diopside	54.37	0.04	0.03	0.04	0.06	0.12	3.59	0.02	16.36	23.39	0.69	0.00	0.03	98.74		
Concentrate		diopside	54.30	0.05	0.03	0.03	0.05	0.10	3.53	0.02	16.26	23.46	0.64	0.01	0.03	98.51		
Concentrate		diopside	54.56	0.00	0.22	0.03	1.34	0.10	2.54	0.03	16.33	22.25	1.23	0.02	0.03	98.69		
Concentrate		diopside	54.51	0.02	0.17	0.02	1.32	0.09	2.72	0.02	16.29	22.38	1.19	0.01	0.04	98.79		
Concentrate		diopside	54.56	0.02	0.13	0.02	1.52	0.09	2.82	0.02	16.12	22.31	1.32	0.00	0.02	98.95		
Concentrate		diopside	53.35	0.03	0.59	0.01	0.03	0.20	6.50	0.02	13.95	23.57	0.62	0.00	0.04	98.91		
Concentrate		diopside	54.57	0.03	0.17	0.00	0.97	0.08	2.63	0.04	16.63	22.73	1.01	0.00	0.02	98.89		
Concentrate		diopside	53.24	0.01	0.56	0.02	0.00	0.21	6.79	0.02	13.79	23.32	0.72	0.00	0.03	98.71		
Concentrate		diopside	54.61	0.01	0.64	0.03	1.13	0.08	1.85	0.04	16.80	22.46	1.07	0.00	0.02	98.76		
Concentrate		diopside	54.38	0.01	0.26	0.01	1.64	0.09	2.46	0.03	16.46	21.91	1.27	0.01	0.05	98.57		
Concentrate		diopside	53.38	0.02	0.50	0.02	0.01	0.19	6.27	0.02	14.08	23.66	0.58	0.00	0.03	98.77		
Concentrate		diopside	53.21	0.03	0.68	0.01	0.00	0.20	6.69	0.02	13.79	23.47	0.70	0.00	0.03	98.83		
Concentrate		diopside	54.45	0.02	0.23	0.03	0.71	0.07	2.53	0.03	16.74	22.99	0.95	0.01	0.02	98.78		
Concentrate		diopside	54.47	0.03	0.22	0.02	1.55	0.09	2.81	0.02	16.16	22.19	1.37	0.00	0.02	98.95		
Concentrate		diopside	54.43	0.02	0.17	0.03	1.19	0.10	2.74	0.03	16.34	22.57	1.20	0.00	0.04	98.86		
Concentrate		diopside	54.47	0.02	0.22	0.04	1.20	0.10	2.68	0.04	16.31	22.52	1.19	0.00	0.03	98.83		
Concentrate		diopside	54.50	0.01	0.15	0.05	1.27	0.11	2.68	0.03	16.30	22.38	1.18	0.00	0.04	98.70		
Concentrate		augite	54.93	0.20	1.74	0.04	0.72	0.14	3.99	0.06	21.06	14.86	1.11	0.03	0.00	98.89		
Concentrate		diopside	53.13	0.03	0.49	0.03	0.00	0.21	6.37	0.01	14.06	23.52	0.63	0.00	0.03	98.52		
Concentrate		diopside	54.31	0.08	0.10	0.01	1.12	0.11	3.10	0.00	16.03	22.78	1.06	0.01	0.02	98.72		
Concentrate		diopside	54.42	0.03	0.16	0.00	1.80	0.09	2.75	0.03	15.99	22.01	1.38	0.00	0.01	98.69		
Concentrate		diopside	54.76	0.00	0.11	0.02	1.14	0.07	2.11	0.03	16.73	23.22	1.00	0.01	0.02	99.23		
Concentrate		diopside	54.40	0.05	0.02	0.02	0.03	0.10	3.46	0.02	16.41	23.69	0.68	0.00	0.03	98.92		
Concentrate		diopside	54.45	0.04	0.04	0.01	0.06	0.10	3.53	0.02	16.45	23.57	0.72	0.00	0.03	99.02		
Concentrate		diopside	54.36	0.00	0.56	0.02	1.71	0.08	1.99	0.03	16.37	22.00	1.40	0.01	0.02	98.56		
Concentrate		diopside	54.48	0.01	0.18	0.02	1.43	0.11	2.77	0.03	16.23	22.39	1.21	0.00	0.03	98.89		
Concentrate		augite	54.44	0.50	1.92	0.04	1.07	0.13	3.36	0.07	18.81	16.60	1.58	0.04	0.02	98.58		
Concentrate		diopside	54.49	0.01	0.19	0.02	1.40	0.07	2.07	0.04	16.59	22.66	1.16	0.00	0.03	98.74		
Concentrate		diopside	54.43	0.01	0.17	0.02	1.60	0.06	2.30	0.04	16.44	22.41	1.21	0.00	0.03	98.72		
Concentrate		diopside	53.92	0.06	2.48	0.03	1.51	0.06	2.46	0.05	15.31	20.98	1.91	0.02	0.03	98.81		
Concentrate		diopside	53.11	0.05	0.61	0.01	0.00	0.21	6.80	0.02	13.72	23.51	0.66	0.00	0.01	98.72		
Concentrate		diopside	54.37	0.01	0.15	0.02	1.23	0.10	2.68	0.02	16.47	22.35	1.12	0.00	0.04	98.56		

sample name	rock type	mineral from composition	SiO2	TiO2	Al2O3	V2O3	Cr2O3	MnO	FeO	NiO	MgO	CaO	Na2O	K2O	P2O5	Total	notes	Crust-Mantle
Concentrate		diopside	54.51	0.02	0.21	0.02	1.39	0.07	2.13	0.02	16.61	22.60	1.12	0.00	0.02	98.72		
Concentrate		diopside	53.40	0.02	0.56	0.02	0.02	0.18	6.37	0.01	13.97	23.55	0.66	0.00	0.02	98.77		
Concentrate		diopside	53.15	0.02	0.71	0.02	0.02	0.19	6.87	0.01	13.76	23.24	0.79	0.00	0.02	98.80		
Concentrate		diopside	53.07	0.03	0.57	0.03	0.03	0.18	6.60	0.01	13.91	23.63	0.57	0.00	0.02	98.66		
Concentrate		diopside	54.59	0.01	0.10	0.02	1.04	0.10	2.54	0.04	16.56	23.04	1.00	0.00	0.02	99.05		
Concentrate		diopside	54.64	0.00	0.62	0.04	1.36	0.07	1.99	0.04	16.63	22.15	1.27	0.00	0.03	98.85		
Concentrate		diopside	53.24	0.03	0.53	0.01	0.03	0.20	6.66	0.01	13.92	23.37	0.61	0.00	0.00	98.62		
Concentrate		diopside	53.38	0.01	0.50	0.02	0.01	0.20	6.49	0.02	14.06	23.50	0.58	0.01	0.03	98.81		
Concentrate		diopside	53.33	0.02	0.59	0.03	0.02	0.16	5.31	0.01	14.66	23.72	0.65	0.00	0.05	98.55		
Concentrate		diopside	54.44	0.00	0.19	0.03	1.53	0.09	2.50	0.03	16.46	22.09	1.18	0.01	0.01	98.56		
Concentrate		diopside	54.64	0.00	1.27	0.03	1.41	0.06	1.43	0.04	16.65	22.30	1.24	0.02	0.03	99.12		
Concentrate		diopside	54.58	0.03	0.27	0.03	1.34	0.09	2.36	0.02	16.54	22.24	1.22	0.01	0.02	98.72		
Concentrate		diopside	54.59	0.02	0.20	0.02	1.44	0.08	2.12	0.03	16.58	22.78	1.15	0.00	0.03	99.05		
Concentrate		diopside	54.46	0.02	0.18	0.02	1.24	0.09	2.67	0.03	16.25	22.52	1.20	0.00	0.05	98.74		
Concentrate		diopside	54.62	0.03	0.56	0.01	1.35	0.06	1.92	0.04	16.63	22.37	1.30	0.01	0.02	98.92		
Concentrate		diopside	54.08	0.08	0.17	0.02	0.01	0.11	4.38	0.00	15.88	23.13	0.83	0.00	0.01	98.70		
Concentrate		diopside	54.58	0.00	0.10	0.03	1.15	0.09	2.17	0.04	16.65	23.27	0.95	0.01	0.00	99.05		
Concentrate		diopside	54.72	0.00	0.76	0.02	1.31	0.06	2.17	0.03	16.41	21.90	1.45	0.03	0.03	98.88		
Concentrate		diopside	53.01	0.04	0.60	0.02	0.01	0.20	6.65	0.00	13.77	23.54	0.63	0.01	0.04	98.51		
Concentrate		diopside	54.50	0.02	0.19	0.02	1.52	0.10	2.77	0.02	16.13	22.11	1.32	0.00	0.03	98.73		
Concentrate		diopside	54.35	0.04	0.04	0.01	0.01	0.10	3.20	0.02	16.48	23.64	0.64	0.01	0.01	98.56		
Concentrate		diopside	53.47	0.02	0.79	0.01	0.04	0.16	5.42	0.01	14.47	23.59	0.77	0.00	0.03	98.79		
Concentrate		diopside	53.37	0.03	0.61	0.02	0.00	0.20	6.69	0.02	13.74	23.60	0.67	0.01	0.04	99.00		
Concentrate		diopside	53.31	0.01	0.67	0.00	0.02	0.17	6.41	0.01	13.88	23.44	0.63	0.00	0.03	98.58		
Concentrate		diopside	53.57	0.10	1.27	0.02	0.57	0.11	3.79	0.02	15.09	23.42	0.97	0.00	0.02	98.95		
Concentrate		diopside	53.12	0.03	0.60	0.03	0.02	0.20	6.49	0.00	13.81	23.54	0.71	0.00	0.03	98.56		
Concentrate		diopside	53.19	0.03	0.51	0.01	0.01	0.18	6.41	0.01	13.99	23.57	0.61	0.00	0.04	98.54		
Concentrate		diopside	53.24	0.03	0.51	0.02	0.01	0.19	6.47	0.01	13.90	23.49	0.65	0.00	0.04	98.56		
Concentrate		diopside	53.07	0.03	0.55	0.01	0.07	0.19	6.58	0.01	13.85	23.53	0.64	0.00	0.03	98.56		
Concentrate		diopside	53.20	0.04	0.56	0.01	0.05	0.19	6.56	0.02	13.87	23.47	0.65	0.00	0.02	98.63		
Concentrate		diopside	53.24	0.02	0.61	0.01	0.02	0.21	6.83	0.01	13.78	23.24	0.78	0.00	0.03	98.77		
Concentrate		diopside	53.20	0.02	0.59	0.04	0.00	0.21	6.77	0.02	13.78	23.14	0.71	0.00	0.01	98.50		
Concentrate		diopside	54.66	0.02	0.16	0.03	1.28	0.07	1.88	0.03	16.85	22.81	0.95	0.00	0.01	98.74		
Concentrate		diopside	53.04	0.03	0.56	0.01	0.01	0.19	6.64	0.02	13.80	23.51	0.66	0.00	0.02	98.51		
Concentrate		diopside	53.06	0.03	0.54	0.02	0.01	0.20	7.13	0.01	13.51	23.32	0.68	0.00	0.01	98.51		
Concentrate		diopside	53.05	0.04	0.75	0.03	0.00	0.21	6.86	0.01	13.71	23.39	0.68	0.01	0.02	98.76		
Concentrate		diopside	53.22	0.04	0.59	0.04	0.03	0.19	6.47	0.01	13.89	23.49	0.69	0.00	0.05	98.69		
Concentrate		diopside	54.46	0.02	0.16	0.01	1.25	0.11	2.77	0.02	16.31	22.56	1.23	0.00	0.04	98.92		
Concentrate		diopside	53.25	0.05	0.96	0.03	0.01	0.17	5.74	0.00	14.29	23.49	0.84	0.00	0.01	98.85		
Concentrate		diopside	54.73	0.03	0.49	0.06	1.33	0.08	1.93	0.03	16.68	22.40	1.25	0.01	0.01	99.04		
Concentrate		diopside	54.42	0.02	0.42	0.03	1.91	0.08	2.33	0.04	16.01	21.82	1.52	0.01	0.04	98.65		
Concentrate		augite	54.81	0.36	2.33	0.02	0.69	0.11	3.58	0.08	18.78	16.05	1.76	0.03	0.02	98.62		
Concentrate		diopside	53.41	0.04	0.50	0.00	0.02	0.20	6.56	0.02	13.89	23.36	0.62	0.00	0.02	98.63		
Concentrate		diopside	54.71	0.01	0.19	0.02	1.62	0.08	2.23	0.03	16.49	22.25	1.21	0.02	0.04	98.90		
Concentrate		diopside	54.53	0.01	1.43	0.01	1.25	0.07	1.37	0.03	16.66	22.57	1.05	0.00	0.01	99.00		
Concentrate		augite	54.99	0.19	1.75	0.01	0.58	0.13	3.71	0.07	21.08	15.16	1.11	0.04	0.02	98.84		
Concentrate		diopside	54.66	0.00	0.20	0.03	1.39	0.09	2.18	0.03	16.50	22.57	1.16	0.00	0.03	98.85		
Concentrate		diopside	54.61	0.06	0.55	0.03	1.98	0.08	2.05	0.03	16.24	21.61	1.60	0.00	0.03	98.88		
Concentrate		diopside	54.74	0.03	0.69	0.04	1.36	0.07	1.91	0.02	16.52	22.20	1.31	0.02	0.03	98.95		

sample name	rock type	mineral from composition	SiO2	TiO2	Al2O3	V2O3	Cr2O3	MnO	FeO	NiO	MgO	CaO	Na2O	K2O	P2O5	Total	notes	Crust-Mantle
Concentrate		diopside	53.16	0.04	0.64	0.03	0.02	0.20	6.54	0.02	13.84	23.55	0.67	0.01	0.01	98.71		
Concentrate		diopside	54.49	0.01	0.22	0.00	1.61	0.08	2.32	0.03	16.45	22.32	1.21	0.00	0.00	98.75		
Concentrate		diopside	54.47	0.01	0.16	0.03	1.20	0.09	2.70	0.03	16.36	22.57	1.15	0.00	0.01	98.80		
Concentrate		diopside	54.55	0.02	0.19	0.05	1.18	0.09	2.35	0.02	16.70	22.32	1.11	0.01	0.03	98.61		
Concentrate		diopside	54.73	0.00	0.21	0.03	1.44	0.07	1.96	0.04	16.60	22.53	1.13	0.00	0.02	98.76		
Concentrate		diopside	54.63	0.01	0.18	0.02	1.21	0.10	2.71	0.03	16.29	22.31	1.17	0.00	0.03	98.70		
Concentrate		diopside	54.54	0.04	1.20	0.04	1.58	0.09	1.96	0.03	16.24	21.71	1.45	0.00	0.02	98.89		
Concentrate		diopside	54.21	0.00	1.95	0.05	2.83	0.07	1.96	0.04	15.51	19.96	2.24	0.02	0.02	98.87		
Concentrate		diopside	54.77	0.01	0.29	0.01	1.64	0.08	1.96	0.02	16.59	22.16	1.27	0.00	0.03	98.84		
Concentrate		diopside	54.28	0.09	0.16	0.06	0.61	0.09	4.20	0.02	15.52	21.88	1.55	0.01	0.02	98.50		
Concentrate		diopside	54.70	0.01	0.40	0.01	0.97	0.09	2.00	0.05	16.90	22.63	1.02	0.00	0.02	98.81		
Concentrate		diopside	54.21	0.09	0.49	0.06	1.86	0.09	3.22	0.03	15.58	21.53	1.52	0.00	0.01	98.68		
Concentrate		augite	55.09	0.19	1.75	0.04	0.83	0.13	3.51	0.08	20.65	15.67	1.21	0.04	0.01	99.18		
Concentrate		diopside	54.52	0.01	0.12	0.01	1.15	0.11	2.68	0.03	16.27	22.60	1.09	0.00	0.04	98.62		
Concentrate		augite	54.57	0.43	1.65	0.03	1.40	0.11	2.94	0.06	18.90	17.00	1.57	0.02	0.02	98.72		
Concentrate		clinopyroxene	54.67	0.02	0.09	0.03	1.14	0.09	2.53	0.03	16.47	22.78	1.04	0.00	0.02	98.92		
Concentrate		clinopyroxene	54.63	0.02	0.42	0.03	1.76	0.09	2.29	0.02	16.00	21.82	1.43	0.00	0.02	98.54		
Concentrate		augite	54.62	0.43	1.75	0.04	1.22	0.11	2.89	0.06	18.47	17.32	1.55	0.04	0.00	98.51		
Concentrate		diopside	53.07	0.19	5.13	0.04	0.74	0.07	1.48	0.03	14.84	21.48	1.70	0.00	0.04	98.80		
Concentrate		diopside	54.46	0.01	0.18	0.04	1.55	0.09	2.67	0.02	16.20	22.08	1.31	0.00	0.03	98.63		
Concentrate		diopside	54.78	0.00	0.42	0.03	1.34	0.07	1.82	0.03	16.67	22.18	1.14	0.00	0.03	98.50		
Concentrate		diopside	53.27	0.04	0.56	0.03	0.00	0.17	6.43	0.02	13.98	23.48	0.58	0.00	0.02	98.58		
Concentrate		diopside	53.67	0.01	0.40	0.01	0.00	0.19	6.23	0.00	14.24	23.74	0.48	0.00	0.04	99.00		
Concentrate		diopside	54.88	0.01	0.18	0.01	0.71	0.06	2.10	0.02	17.04	23.09	0.84	0.00	0.02	98.95		
Concentrate		diopside	54.62	0.00	0.57	0.02	1.46	0.07	1.83	0.03	16.56	22.11	1.24	0.00	0.03	98.53		
Concentrate		diopside	54.65	0.04	0.72	0.04	1.36	0.07	1.92	0.03	16.64	21.96	1.41	0.04	0.03	98.89		
Concentrate		diopside	53.12	0.04	0.63	0.02	0.03	0.19	6.78	0.00	13.72	23.27	0.70	0.00	0.02	98.51		
Concentrate		diopside	54.46	0.01	0.12	0.01	1.25	0.10	2.65	0.01	16.25	22.51	1.15	0.01	0.02	98.55		
Concentrate		diopside	54.65	0.00	0.17	0.02	1.48	0.09	2.38	0.03	16.46	22.41	1.17	0.00	0.02	98.89		
Concentrate		diopside	54.71	0.02	0.13	0.01	1.28	0.09	2.71	0.02	16.32	22.49	1.23	0.00	0.03	99.05		
Concentrate	Low-Cr (< 1 wt%)	garnet	38.64	0.10	21.59	0.05	0.04	0.52	24.09	0.01	7.28	6.75	0.02	0.00	0.08	99.17	eclogitic	crust
Concentrate	Low-Cr (< 1 wt%)	garnet	39.96	0.07	22.69	0.03	0.04	0.38	17.77	0.00	12.11	6.30	0.02	0.00	0.01	99.38	eclogitic	crust
Concentrate	Low-Cr (< 1 wt%)	garnet	38.39	0.11	21.62	0.05	0.04	0.51	24.28	0.01	7.17	6.73	0.01	0.00	0.07	98.99	eclogitic	crust
Concentrate	Low-Cr (< 1 wt%)	garnet	38.24	0.13	21.47	0.03	0.01	0.52	25.15	0.00	6.53	6.79	0.01	0.00	0.06	98.95	eclogitic	crust
Concentrate	Low-Cr (< 1 wt%)	garnet	39.44	0.04	22.34	0.03	0.11	0.41	19.48	0.00	11.02	6.07	0.02	0.00	0.04	99.00	eclogitic	crust
Concentrate	Low-Cr (< 1 wt%)	garnet	38.83	0.07	21.85	0.08	0.07	0.48	22.36	0.01	8.09	7.24	0.02	0.00	0.07	99.17	eclogitic	crust
Concentrate	Low-Cr (< 1 wt%)	garnet	38.66	0.10	21.67	0.03	0.02	0.51	24.04	0.00	7.23	6.66	0.01	0.00	0.02	98.96	eclogitic	crust
Concentrate	Low-Cr (< 1 wt%)	garnet	38.67	0.07	21.69	0.05	0.02	0.50	24.18	0.01	7.07	6.60	0.01	0.00	0.06	98.92	eclogitic	crust
Concentrate	Low-Cr (< 1 wt%)	garnet	39.70	0.07	22.34	0.03	0.10	0.44	19.58	0.00	11.04	5.99	0.01	0.01	0.03	99.34	eclogitic	crust
Concentrate	Low-Cr (< 1 wt%)	garnet	38.54	0.10	21.66	0.06	0.02	0.50	24.16	0.00	7.15	6.83	0.03	0.00	0.06	99.10	eclogitic	crust
Concentrate	Low-Cr (< 1 wt%)	garnet	40.43	0.05	22.90	0.02	0.10	0.34	16.23	0.00	13.49	5.87	0.01	0.00	0.02	99.48	eclogitic	crust
Concentrate	Low-Cr (< 1 wt%)	garnet	37.78	0.01	21.57	0.01	0.02	0.86	31.50	0.01	5.61	1.16	0.04	0.00	0.08	98.64	eclogitic	crust
Concentrate	Low-Cr (< 1 wt%)	garnet	38.29	0.01	21.81	0.01	0.01	0.38	29.61	0.00	7.22	1.32	0.01	0.00	0.04	98.71	eclogitic	crust
Concentrate	Low-Cr (< 1 wt%)	garnet	39.73	0.06	22.45	0.04	0.16	0.42	18.97	0.00	11.31	6.07	0.03	0.00	0.05	99.29	eclogitic	mantle
Concentrate	Low-Cr (< 1 wt%)	garnet	39.70	0.07	22.34	0.05	0.12	0.39	19.67	0.00	11.15	6.06	0.02	0.00	0.04	99.62	eclogitic	crust
Concentrate	Low-Cr (< 1 wt%)	garnet	40.38	0.06	22.79	0.02	0.08	0.37	16.48	0.00	13.22	5.92	0.00	0.01	0.03	99.36	eclogitic	crust
Concentrate	Low-Cr (< 1 wt%)	garnet	39.85	0.07	22.35	0.05	0.15	0.43	19.06	0.00	11.24	5.94	0.01	0.01	0.04	99.20	eclogitic	crust
Concentrate	Low-Cr (< 1 wt%)	garnet	39.36	0.11	22.23	0.02	0.03	0.46	19.53	0.00	9.87	7.30	0.03	0.01	0.04	98.99	eclogitic	crust
Concentrate	Low-Cr (< 1 wt%)	garnet	38.66	0.09	21.69	0.03	0.02	0.51	23.95	0.00	7.19	6.69	0.02	0.00	0.06	98.90	eclogitic	crust

sample name	rock type	mineral from composition	SiO2	TiO2	Al2O3	V2O3	Cr2O3	MnO	FeO	NiO	MgO	CaO	Na2O	K2O	P2O5	Total	notes	Crust-Mantle
Concentrate	Low-Cr (< 1 wt%)	garnet	40.30	0.03	22.84	0.02	0.12	0.34	16.12	0.00	13.53	5.82	0.01	0.00	0.05	99.20	eclogitic	mantle
Concentrate	Low-Cr (< 1 wt%)	garnet	38.55	0.10	21.59	0.01	0.02	0.50	24.20	0.00	6.92	6.85	0.02	0.00	0.07	98.83	eclogitic	crust
Concentrate	Low-Cr (< 1 wt%)	garnet	38.58	0.14	21.64	0.05	0.03	0.52	24.04	0.00	7.22	6.88	0.01	0.00	0.06	99.16	eclogitic	crust
Concentrate	Low-Cr (< 1 wt%)	garnet	39.97	0.07	22.48	0.00	0.20	0.40	18.59	0.00	11.56	6.03	0.00	0.01	0.04	99.36	eclogitic	crust
Concentrate	Low-Cr (< 1 wt%)	garnet	38.59	0.12	21.61	0.05	0.02	0.53	24.13	0.00	7.10	6.67	0.02	0.00	0.06	98.91	eclogitic	crust
Concentrate	Low-Cr (< 1 wt%)	garnet	38.71	0.09	21.67	0.04	0.01	0.51	24.12	0.00	7.29	6.70	0.03	0.00	0.08	99.24	eclogitic	crust
Concentrate	Low-Cr (< 1 wt%)	garnet	38.66	0.08	21.62	0.06	0.03	0.67	20.60	0.00	4.89	12.57	0.03	0.00	0.04	99.26	eclogitic	crust
Concentrate	Low-Cr (< 1 wt%)	garnet	38.53	0.06	21.51	0.05	0.02	0.51	24.76	0.00	6.79	6.68	0.02	0.00	0.03	98.96	eclogitic	crust
Concentrate	Low-Cr (< 1 wt%)	garnet	37.52	0.01	21.46	0.00	0.02	0.50	33.06	0.01	5.08	0.96	0.00	0.00	0.02	98.65	eclogitic	crust
Concentrate	Low-Cr (< 1 wt%)	garnet	40.43	0.05	22.86	0.03	0.10	0.38	16.24	0.01	13.51	5.93	0.01	0.00	0.02	99.57	eclogitic	crust
Concentrate	Low-Cr (< 1 wt%)	garnet	41.31	0.05	23.36	0.03	0.09	0.28	12.23	0.00	16.50	5.75	0.01	0.00	0.04	99.64	eclogitic	mantle
Concentrate	Low-Cr (< 1 wt%)	garnet	38.37	0.14	21.64	0.03	0.02	0.49	24.36	0.00	7.00	6.77	0.03	0.00	0.06	98.92	eclogitic	crust
Concentrate	Low-Cr (< 1 wt%)	garnet	40.89	0.04	23.21	0.05	0.08	0.28	12.92	0.01	16.02	5.80	0.00	0.00	0.00	99.30	eclogitic	crust
Concentrate	Low-Cr (< 1 wt%)	garnet	38.52	0.05	21.62	0.04	0.01	0.50	24.03	0.01	7.29	6.56	0.04	0.00	0.09	98.77	eclogitic	crust
Concentrate	Low-Cr (< 1 wt%)	garnet	38.59	0.06	21.67	0.04	0.04	0.55	23.90	0.00	7.32	6.62	0.00	0.01	0.08	98.87	eclogitic	mantle
Concentrate	Low-Cr (< 1 wt%)	garnet	40.17	0.06	22.81	0.03	0.08	0.35	16.30	0.00	13.50	5.87	0.01	0.00	0.01	99.19	eclogitic	mantle
Concentrate	Low-Cr (< 1 wt%)	garnet	38.49	0.05	21.58	0.03	0.03	0.52	24.26	0.01	6.98	6.71	0.00	0.00	0.08	98.76	eclogitic	crust
Concentrate	Low-Cr (< 1 wt%)	garnet	38.37	0.11	21.47	0.05	0.04	0.56	24.64	0.01	6.76	6.66	0.01	0.01	0.08	98.77	eclogitic	crust
Concentrate	Low-Cr (< 1 wt%)	garnet	38.54	0.04	21.75	0.05	0.03	0.52	24.23	0.01	6.99	6.75	0.02	0.00	0.07	98.99	eclogitic	crust
Concentrate	Low-Cr (< 1 wt%)	garnet	37.30	0.00	21.30	0.00	0.00	1.66	32.61	0.01	4.16	1.48	0.00	0.01	0.00	98.54	eclogitic	crust
Concentrate	Low-Cr (< 1 wt%)	garnet	38.57	0.09	21.76	0.05	0.01	0.52	24.16	0.00	7.09	6.69	0.03	0.00	0.05	99.02	eclogitic	crust
Concentrate	Low-Cr (< 1 wt%)	garnet	38.65	0.08	21.65	0.05	0.03	0.53	24.01	0.01	7.28	6.67	0.02	0.01	0.06	99.04	eclogitic	crust
Concentrate	Low-Cr (< 1 wt%)	garnet	39.96	0.07	22.65	0.01	0.03	0.40	17.82	0.00	11.91	6.30	0.01	0.00	0.04	99.20	eclogitic	crust
Concentrate	Low-Cr (< 1 wt%)	garnet	40.80	0.03	23.06	0.03	0.16	0.33	13.60	0.00	15.30	5.87	0.01	0.00	0.02	99.21	eclogitic	mantle
Concentrate	Low-Cr (< 1 wt%)	garnet	40.67	0.05	23.20	0.02	0.10	0.26	12.85	0.00	15.90	5.86	0.00	0.00	0.02	98.94	eclogitic	mantle
Concentrate	Low-Cr (< 1 wt%)	garnet	39.51	0.10	22.19	0.04	0.19	0.39	18.64	0.00	11.47	6.06	0.00	0.00	0.05	98.65	eclogitic	crust
Concentrate	Low-Cr (< 1 wt%)	garnet	41.66	0.06	23.18	0.01	0.80	0.42	8.28	0.00	19.70	5.17	0.00	0.00	0.03	99.31	eclogitic	mantle
Concentrate	Low-Cr (< 1 wt%)	garnet	38.39	0.06	21.49	0.03	0.02	0.53	24.17	0.00	7.14	6.59	0.03	0.00	0.07	98.54	eclogitic	crust
Concentrate	Low-Cr (< 1 wt%)	garnet	41.40	0.11	22.85	0.02	0.96	0.36	9.85	0.01	18.53	5.11	0.01	0.01	0.02	99.25	eclogitic	mantle
Concentrate	Low-Cr (< 1 wt%)	garnet	39.24	0.07	22.31	0.02	0.05	0.47	19.51	0.01	10.02	7.19	0.03	0.00	0.07	98.99	eclogitic	crust
Concentrate	Low-Cr (< 1 wt%)	garnet	39.47	0.07	22.41	0.02	0.14	0.39	18.95	0.00	11.48	6.04	0.03	0.00	0.06	99.06	eclogitic	mantle
Concentrate	Low-Cr (< 1 wt%)	garnet	39.70	0.09	22.32	0.04	0.17	0.42	19.06	0.00	11.17	6.10	0.02	0.01	0.05	99.16	eclogitic	mantle
Concentrate	Low-Cr (< 1 wt%)	garnet	40.47	0.04	22.97	0.03	0.13	0.37	14.74	0.00	14.36	6.15	0.01	0.00	0.02	99.30	eclogitic	mantle
Concentrate	Low-Cr (< 1 wt%)	garnet	38.60	0.04	21.47	0.04	0.02	0.51	24.41	0.01	6.95	6.69	0.02	0.00	0.05	98.79	eclogitic	crust
Concentrate	Low-Cr (< 1 wt%)	garnet	41.63	0.07	23.12	0.02	0.82	0.40	8.11	0.00	19.61	5.20	0.01	0.00	0.02	99.01	eclogitic	mantle
Concentrate	Low-Cr (< 1 wt%)	garnet	40.77	0.05	23.12	0.03	0.11	0.28	13.17	0.01	15.73	5.85	0.00	0.00	0.03	99.16	eclogitic	crust
Concentrate	Low-Cr (< 1 wt%)	garnet	41.12	0.08	23.18	0.02	0.12	0.29	12.31	0.00	16.48	5.71	0.00	0.00	0.03	99.33	eclogitic	mantle
Concentrate	Low-Cr (< 1 wt%)	garnet	40.27	0.11	22.77	0.03	0.11	0.35	15.94	0.02	13.62	5.78	0.01	0.00	0.06	99.07	eclogitic	mantle
Concentrate	Low-Cr (< 1 wt%)	garnet	38.60	0.08	21.55	0.04	0.04	0.51	24.03	0.01	7.21	6.65	0.01	0.00	0.09	98.80	eclogitic	crust
Concentrate	Low-Cr (< 1 wt%)	garnet	38.66	0.12	21.47	0.06	0.03	0.52	23.84	0.00	7.23	6.75	0.02	0.00	0.04	98.73	eclogitic	crust
Concentrate	Low-Cr (< 1 wt%)	garnet	38.58	0.10	21.57	0.04	0.04	0.54	24.11	0.00	7.08	6.64	0.02	0.01	0.06	98.78	eclogitic	crust
Concentrate	Low-Cr (< 1 wt%)	garnet	38.33	0.06	21.57	0.02	0.05	0.75	21.11	0.00	4.54	12.41	0.03	0.00	0.05	98.92	eclogitic	crust
Concentrate	Low-Cr (< 1 wt%)	garnet	38.42	0.14	21.52	0.01	0.03	0.49	24.36	0.00	6.82	6.79	0.01	0.00	0.07	98.67	eclogitic	crust
Concentrate	Low-Cr (< 1 wt%)	garnet	38.53	0.08	21.65	0.03	0.04	0.52	24.01	0.00	7.25	6.67	0.02	0.00	0.08	98.88	eclogitic	crust
Concentrate	Low-Cr (< 1 wt%)	garnet	41.64	0.19	23.29	0.03	0.65	0.41	9.10	0.00	19.15	5.07	0.01	0.01	0.03	99.58	eclogitic	mantle
Concentrate	Low-Cr (< 1 wt%)	garnet	38.50	0.25	21.60	0.03	0.03	0.52	24.05	0.00	7.03	6.68	0.01	0.00	0.07	98.76	eclogitic	crust
Concentrate	Low-Cr (< 1 wt%)	garnet	38.56	0.05	21.62	0.05	0.03	0.53	24.28	0.00	6.99	6.67	0.05	0.00	0.07	98.90	eclogitic	crust
Concentrate	Low-Cr (< 1 wt%)	garnet	41.23	0.06	23.34	0.04	0.11	0.28	11.84	0.01	16.73	5.66	0.02	0.00	0.03	99.34	eclogitic	mantle
Concentrate	Low-Cr (< 1 wt%)	garnet	41.07	0.06	23.26	0.03	0.09	0.27	12.93	0.00	16.02	5.74	0.00	0.00	0.01	99.49	eclogitic	crust

sample name	rock type	mineral from composition	SiO2	TiO2	Al2O3	V2O3	Cr2O3	MnO	FeO	NiO	MgO	CaO	Na2O	K2O	P2O5	Total	notes	Crust-Mantle
Concentrate	Low-Cr (< 1 wt%)	garnet	40.53	0.05	23.04	0.03	0.13	0.36	14.64	0.00	14.35	6.05	0.02	0.00	0.05	99.25	eclogitic	mantle
Concentrate	Low-Cr (< 1 wt%)	garnet	38.62	0.09	21.55	0.03	0.01	0.51	23.86	0.01	7.23	6.57	0.02	0.01	0.05	98.56	eclogitic	crust
Concentrate	Low-Cr (< 1 wt%)	garnet	41.07	0.04	23.28	0.04	0.08	0.28	12.68	0.00	15.99	5.78	0.02	0.00	0.02	99.31	eclogitic	mantle
Concentrate	Low-Cr (< 1 wt%)	garnet	38.91	0.09	21.80	0.05	0.04	0.47	22.17	0.00	8.02	7.03	0.02	0.01	0.07	98.69	eclogitic	crust
Concentrate	Low-Cr (< 1 wt%)	garnet	39.75	0.08	22.37	0.03	0.14	0.40	19.17	0.00	11.29	5.98	0.05	0.00	0.06	99.34	eclogitic	mantle
Concentrate	Low-Cr (< 1 wt%)	garnet	42.09	0.08	23.38	0.01	0.81	0.37	7.71	0.00	20.20	5.27	0.02	0.00	0.00	99.94	eclogitic	mantle
Concentrate	Low-Cr (< 1 wt%)	garnet	42.04	0.09	23.39	0.02	0.83	0.41	7.69	0.01	20.07	5.23	0.00	0.00	0.00	99.79	eclogitic	mantle
Concentrate	Low-Cr (< 1 wt%)	garnet	39.86	0.06	22.54	0.02	0.08	0.35	18.38	0.01	11.59	6.46	0.01	0.00	0.07	99.44	eclogitic	crust
Concentrate	Low-Cr (< 1 wt%)	garnet	41.21	0.06	23.38	0.02	0.10	0.27	12.93	0.01	16.13	5.83	0.00	0.00	0.01	99.95	eclogitic	crust
Concentrate	Low-Cr (< 1 wt%)	garnet	40.40	0.02	22.84	0.01	0.19	0.35	16.25	0.01	13.57	5.87	0.00	0.00	0.04	99.55	eclogitic	mantle
Concentrate	Low-Cr (< 1 wt%)	garnet	42.19	0.05	23.40	0.02	0.80	0.38	8.07	0.00	19.95	5.19	0.00	0.00	0.00	100.05	eclogitic	mantle
Concentrate	Low-Cr (< 1 wt%)	garnet	39.54	0.05	22.36	0.01	0.04	0.45	19.47	0.00	9.89	7.28	0.01	0.00	0.06	99.15	eclogitic	crust
Concentrate	Low-Cr (< 1 wt%)	garnet	38.58	0.12	21.66	0.02	0.02	0.51	24.14	0.00	6.88	6.81	0.02	0.00	0.04	98.80	eclogitic	crust
Concentrate	Low-Cr (< 1 wt%)	garnet	41.50	0.11	23.06	0.01	0.85	0.37	10.39	0.01	18.22	5.09	0.02	0.00	0.03	99.67	eclogitic	mantle
Concentrate	Low-Cr (< 1 wt%)	garnet	39.80	0.07	22.34	0.03	0.13	0.38	19.15	0.00	11.11	5.98	0.02	0.00	0.04	99.03	eclogitic	crust
Concentrate	Low-Cr (< 1 wt%)	garnet	38.72	0.08	21.75	0.05	0.05	0.52	24.06	0.01	7.19	6.65	0.02	0.00	0.06	99.14	eclogitic	crust
Concentrate	Low-Cr (< 1 wt%)	garnet	40.56	0.02	23.06	0.03	0.06	0.35	15.26	0.01	14.22	6.07	0.02	0.01	0.03	99.71	eclogitic	mantle
Concentrate	Low-Cr (< 1 wt%)	garnet	41.09	0.04	23.21	0.03	0.08	0.26	12.88	0.00	15.90	5.73	0.02	0.00	0.03	99.27	eclogitic	mantle
Concentrate	Low-Cr (< 1 wt%)	garnet	36.96	0.02	21.03	0.00	0.01	5.57	31.26	0.00	2.10	1.73	0.00	0.01	0.02	98.72	eclogitic	crust
Concentrate	Low-Cr (< 1 wt%)	garnet	39.52	0.06	22.22	0.03	0.04	0.45	19.56	0.00	9.86	7.24	0.02	0.00	0.08	99.07	eclogitic	crust
Concentrate	Low-Cr (< 1 wt%)	garnet	39.41	0.08	22.29	0.02	0.06	0.45	19.57	0.00	9.86	7.20	0.00	0.00	0.05	98.99	eclogitic	crust
Concentrate	Low-Cr (< 1 wt%)	garnet	40.21	0.04	22.79	0.03	0.06	0.37	16.91	0.00	12.51	6.39	0.00	0.00	0.06	99.38	eclogitic	crust
Concentrate	Low-Cr (< 1 wt%)	garnet	41.13	0.03	23.36	0.01	0.09	0.27	12.87	0.00	15.99	5.81	0.00	0.00	0.03	99.59	eclogitic	mantle
Concentrate	Low-Cr (< 1 wt%)	garnet	38.83	0.12	21.71	0.04	0.03	0.51	23.72	0.00	7.28	6.78	0.02	0.01	0.06	99.11	eclogitic	crust
Concentrate	Low-Cr (< 1 wt%)	garnet	39.71	0.10	22.26	0.03	0.16	0.41	18.98	0.00	11.27	6.02	0.03	0.00	0.06	99.02	eclogitic	mantle
Concentrate	Low-Cr (< 1 wt%)	garnet	38.75	0.08	21.73	0.04	0.02	0.51	23.78	0.01	7.27	6.67	0.02	0.00	0.05	98.93	eclogitic	crust
Concentrate	Low-Cr (< 1 wt%)	garnet	38.53	0.10	21.62	0.04	0.00	0.48	23.97	0.00	6.80	7.13	0.00	0.00	0.01	98.68	eclogitic	mantle
Concentrate	Low-Cr (< 1 wt%)	garnet	38.53	0.10	21.63	0.04	0.03	0.52	24.30	0.00	6.87	6.86	0.00	0.00	0.07	98.95	eclogitic	crust
Concentrate	Low-Cr (< 1 wt%)	garnet	39.41	0.10	22.23	0.04	0.04	0.44	19.64	0.00	9.86	7.26	0.02	0.00	0.07	99.12	eclogitic	crust
Concentrate	Low-Cr (< 1 wt%)	garnet	39.66	0.08	22.28	0.02	0.06	0.41	18.61	0.01	10.81	6.85	0.01	0.00	0.02	98.80	eclogitic	crust
Concentrate	Low-Cr (< 1 wt%)	garnet	39.63	0.09	22.27	0.03	0.13	0.41	19.22	0.01	11.18	6.05	0.02	0.00	0.03	99.06	eclogitic	crust
Concentrate	Low-Cr (< 1 wt%)	garnet	38.53	0.09	21.62	0.04	0.03	0.52	24.28	0.00	6.90	6.61	0.02	0.00	0.08	98.70	eclogitic	crust
Concentrate	Low-Cr (< 1 wt%)	garnet	40.09	0.04	22.72	0.02	0.07	0.39	16.99	0.01	12.40	6.30	0.01	0.00	0.07	99.12	eclogitic	crust
Concentrate	Low-Cr (< 1 wt%)	garnet	38.69	0.04	21.63	0.03	0.01	0.52	23.79	0.00	7.19	6.62	0.00	0.01	0.05	98.57	eclogitic	mantle
Concentrate	Low-Cr (< 1 wt%)	garnet	39.52	0.05	22.28	0.03	0.04	0.46	19.66	0.01	9.90	7.24	0.02	0.00	0.02	99.22	eclogitic	crust
Concentrate	Low-Cr (< 1 wt%)	garnet	38.61	0.09	21.61	0.04	0.02	0.52	23.80	0.01	7.18	6.73	0.04	0.00	0.05	98.71	eclogitic	crust
Concentrate	Low-Cr (< 1 wt%)	garnet	39.72	0.07	22.40	0.05	0.21	0.40	18.61	0.00	11.31	6.09	0.00	0.00	0.07	98.93	eclogitic	crust
Concentrate	Low-Cr (< 1 wt%)	garnet	38.64	0.10	21.67	0.04	0.02	0.51	23.84	0.00	7.29	6.66	0.02	0.00	0.06	98.85	eclogitic	crust
Concentrate	Low-Cr (< 1 wt%)	garnet	40.30	0.02	22.78	0.03	0.16	0.35	16.22	0.01	13.50	5.80	0.02	0.00	0.07	99.26	eclogitic	mantle
Concentrate	Low-Cr (< 1 wt%)	garnet	40.99	0.05	23.16	0.03	0.11	0.26	12.97	0.00	15.90	5.78	0.00	0.00	0.03	99.27	eclogitic	mantle
Concentrate	Low-Cr (< 1 wt%)	garnet	41.99	0.07	23.33	0.02	0.81	0.38	7.65	0.00	20.09	5.27	0.01	0.01	0.00	99.63	eclogitic	mantle
Concentrate	Low-Cr (< 1 wt%)	garnet	38.52	0.09	21.60	0.03	0.04	0.52	24.07	0.00	7.08	6.82	0.03	0.00	0.08	98.88	eclogitic	crust
Concentrate	Low-Cr (< 1 wt%)	garnet	38.54	0.09	21.52	0.04	0.03	0.54	24.12	0.00	7.25	6.63	0.04	0.00	0.07	98.86	eclogitic	crust
Concentrate	Low-Cr (< 1 wt%)	garnet	39.48	0.09	22.37	0.02	0.03	0.44	19.33	0.00	9.91	7.34	0.02	0.00	0.05	99.08	eclogitic	crust
Concentrate	Low-Cr (< 1 wt%)	garnet	38.55	0.10	21.57	0.02	0.04	0.50	23.80	0.00	7.24	6.75	0.01	0.00	0.07	98.66	eclogitic	crust
Concentrate	Low-Cr (< 1 wt%)	garnet	40.35	0.04	22.70	0.01	0.16	0.35	16.13	0.00	13.40	5.80	0.02	0.00	0.04	98.99	eclogitic	mantle
Concentrate	Low-Cr (< 1 wt%)	garnet	40.29	0.02	22.82	0.00	0.17	0.36	16.15	0.00	13.45	5.76	0.02	0.00	0.05	99.09	eclogitic	mantle
Concentrate	Low-Cr (< 1 wt%)	garnet	40.78	0.05	23.06	0.04	0.07	0.29	13.94	0.00	15.03	5.84	0.00	0.00	0.01	99.11	eclogitic	mantle
Concentrate	Low-Cr (< 1 wt%)	garnet	40.62	0.05	22.96	0.03	0.13	0.36	14.33	0.00	14.64	6.09	0.00	0.01	0.00	99.22	eclogitic	crust

sample name	rock type	mineral from composition	SiO2	TiO2	Al2O3	V2O3	Cr2O3	MnO	FeO	NiO	MgO	CaO	Na2O	K2O	P2O5	Total	notes	Crust-Mantle
Concentrate	Low-Cr (< 1 wt%)	garnet	38.53	0.08	21.63	0.05	0.01	0.52	23.84	0.00	7.24	6.62	0.03	0.00	0.08	98.63	eclogitic	crust
Concentrate	Low-Cr (< 1 wt%)	garnet	38.65	0.07	21.72	0.02	0.04	0.52	23.87	0.00	7.21	6.69	0.02	0.01	0.05	98.86	eclogitic	crust
Concentrate	Low-Cr (< 1 wt%)	garnet	40.12	0.00	22.66	0.01	0.07	0.45	17.28	0.00	12.83	5.50	0.01	0.00	0.06	98.99	eclogitic	mantle
Concentrate	Low-Cr (< 1 wt%)	garnet	38.56	0.02	21.68	0.05	0.02	0.51	23.90	0.01	7.30	6.62	0.02	0.00	0.08	98.76	eclogitic	crust
Concentrate	Low-Cr (< 1 wt%)	garnet	40.31	0.03	22.78	0.03	0.15	0.36	16.15	0.00	13.48	5.83	0.02	0.00	0.04	99.18	eclogitic	mantle
Concentrate	Low-Cr (< 1 wt%)	garnet	38.55	0.11	21.62	0.03	0.04	0.48	24.14	0.00	6.91	6.87	0.02	0.00	0.05	98.81	eclogitic	crust
Concentrate	Low-Cr (< 1 wt%)	garnet	38.65	0.08	21.73	0.06	0.03	0.52	24.05	0.00	7.11	6.64	0.03	0.01	0.04	98.96	eclogitic	crust
Concentrate	Low-Cr (< 1 wt%)	garnet	40.39	0.03	22.84	0.03	0.15	0.36	16.06	0.00	13.44	5.85	0.00	0.00	0.06	99.22	eclogitic	mantle
Concentrate	Low-Cr (< 1 wt%)	garnet	38.72	0.03	21.58	0.03	0.03	0.52	23.88	0.00	7.08	6.61	0.03	0.00	0.04	98.55	eclogitic	crust
Concentrate	Low-Cr (< 1 wt%)	garnet	40.73	0.06	23.11	0.03	0.09	0.26	12.87	0.01	15.78	5.85	0.02	0.00	0.02	98.82	eclogitic	mantle
Concentrate	Low-Cr (< 1 wt%)	garnet	38.71	0.09	21.62	0.04	0.01	0.52	23.82	0.00	7.21	6.66	0.02	0.00	0.06	98.77	eclogitic	crust
Concentrate	Low-Cr (< 1 wt%)	garnet	40.87	0.04	23.25	0.02	0.08	0.26	12.92	0.00	15.74	5.75	0.00	0.00	0.01	98.94	eclogitic	mantle
Concentrate	Low-Cr (< 1 wt%)	garnet	37.31	0.00	21.18	0.01	0.03	3.55	32.42	0.00	2.95	1.15	0.00	0.00	0.01	98.63	eclogitic	crust
Concentrate	Low-Cr (< 1 wt%)	garnet	38.67	0.09	21.72	0.03	0.01	0.52	24.13	0.01	7.08	6.65	0.03	0.00	0.06	99.01	eclogitic	crust
Concentrate	Low-Cr (< 1 wt%)	garnet	38.93	0.10	21.87	0.06	0.07	0.49	22.19	0.00	8.06	7.15	0.05	0.00	0.05	99.01	eclogitic	crust
Concentrate	Low-Cr (< 1 wt%)	garnet	38.71	0.13	21.63	0.03	0.02	0.52	24.05	0.00	7.17	6.70	0.02	0.01	0.06	99.05	eclogitic	crust
Concentrate	Low-Cr (< 1 wt%)	garnet	38.67	0.08	21.70	0.01	0.01	0.52	23.83	0.00	7.25	6.66	0.02	0.01	0.07	98.82	eclogitic	crust
Concentrate	Low-Cr (< 1 wt%)	garnet	38.65	0.10	21.68	0.04	0.02	0.51	24.15	0.00	7.16	6.72	0.02	0.00	0.09	99.14	eclogitic	crust
Concentrate	Low-Cr (< 1 wt%)	garnet	38.76	0.12	21.70	0.06	0.01	0.51	23.94	0.01	7.23	6.74	0.03	0.01	0.04	99.16	eclogitic	crust
Concentrate	Low-Cr (< 1 wt%)	garnet	39.62	0.05	22.37	0.02	0.17	0.39	18.98	0.00	11.15	6.09	0.02	0.00	0.02	98.87	eclogitic	crust
Concentrate	Low-Cr (< 1 wt%)	garnet	38.53	0.08	21.67	0.02	0.00	0.49	24.61	0.00	6.48	7.11	0.03	0.00	0.02	99.05	eclogitic	crust
Concentrate	Low-Cr (< 1 wt%)	garnet	38.58	0.09	21.64	0.04	0.02	0.49	24.21	0.00	6.81	7.09	0.03	0.00	0.05	99.04	eclogitic	crust
Concentrate	Low-Cr (< 1 wt%)	garnet	38.55	0.10	21.61	0.02	0.04	0.51	23.91	0.00	7.26	6.71	0.02	0.01	0.07	98.81	eclogitic	crust
Concentrate	Low-Cr (< 1 wt%)	garnet	38.90	0.17	21.81	0.03	0.04	0.62	19.42	0.01	5.63	12.65	0.06	0.00	0.05	99.40	eclogitic	mantle
Concentrate	Low-Cr (< 1 wt%)	garnet	38.59	0.09	21.75	0.02	0.01	0.48	24.16	0.00	6.84	6.88	0.02	0.00	0.05	98.90	eclogitic	crust
Concentrate	Low-Cr (< 1 wt%)	garnet	38.50	0.12	21.58	0.05	0.02	0.47	24.43	0.00	6.59	6.94	0.04	0.00	0.02	98.75	eclogitic	crust
Concentrate	Low-Cr (< 1 wt%)	garnet	40.00	0.05	22.57	0.02	0.19	0.41	18.45	0.00	11.52	5.95	0.00	0.01	0.05	99.22	eclogitic	mantle
Concentrate	Low-Cr (< 1 wt%)	garnet	37.94	1.81	21.50	0.05	0.03	0.52	23.63	0.00	6.75	6.84	0.02	0.00	0.06	99.16	eclogitic	crust
Concentrate	Low-Cr (< 1 wt%)	garnet	39.71	0.08	22.45	0.03	0.15	0.40	18.85	0.00	11.25	6.00	0.01	0.00	0.04	98.97	eclogitic	crust
Concentrate	Low-Cr (< 1 wt%)	garnet	38.63	0.08	21.65	0.00	0.01	0.53	23.90	0.01	7.16	6.67	0.04	0.00	0.08	98.76	eclogitic	crust
Concentrate	Low-Cr (< 1 wt%)	garnet	38.61	0.09	21.69	0.04	0.01	0.53	24.15	0.00	7.01	6.68	0.03	0.00	0.08	98.92	eclogitic	crust
Concentrate	Low-Cr (< 1 wt%)	garnet	38.64	0.02	21.76	0.03	0.02	0.51	24.05	0.00	7.22	6.53	0.03	0.00	0.08	98.90	eclogitic	crust
Concentrate	Low-Cr (< 1 wt%)	garnet	38.56	0.07	21.70	0.02	0.03	0.52	24.29	0.00	6.90	6.69	0.01	0.00	0.06	98.86	eclogitic	crust
Concentrate	Low-Cr (< 1 wt%)	garnet	38.62	0.10	21.62	0.06	0.03	0.50	23.97	0.01	7.17	6.77	0.02	0.00	0.05	98.92	eclogitic	crust
Concentrate	Low-Cr (< 1 wt%)	garnet	39.57	0.09	22.37	0.02	0.04	0.44	19.50	0.00	9.99	7.37	0.00	0.00	0.06	99.45	eclogitic	crust
Concentrate	Low-Cr (< 1 wt%)	garnet	38.49	0.15	21.51	0.03	0.03	0.49	24.41	0.00	6.81	6.80	0.02	0.00	0.07	98.81	eclogitic	crust
Concentrate	Low-Cr (< 1 wt%)	garnet	37.64	0.06	20.80	0.10	0.01	1.35	27.78	0.00	2.43	8.81	0.01	0.00	0.01	99.00	eclogitic	crust
Concentrate	Low-Cr (< 1 wt%)	garnet	38.54	0.06	21.67	0.04	0.01	0.52	24.18	0.00	6.89	6.93	0.03	0.00	0.06	98.92	eclogitic	crust
Concentrate	Low-Cr (< 1 wt%)	garnet	38.63	0.05	21.68	0.01	0.00	0.51	24.30	0.00	6.98	6.66	0.00	0.00	0.02	98.84	eclogitic	mantle
Concentrate	Low-Cr (< 1 wt%)	garnet	38.69	0.10	21.69	0.02	0.02	0.51	23.92	0.00	7.30	6.61	0.01	0.00	0.08	98.97	eclogitic	crust
Concentrate	Low-Cr (< 1 wt%)	garnet	38.57	0.02	21.81	0.01	0.02	0.51	24.05	0.00	7.08	6.60	0.02	0.00	0.08	98.78	eclogitic	crust
Concentrate	Low-Cr (< 1 wt%)	garnet	37.10	0.01	21.12	0.00	0.01	4.84	30.92	0.01	2.85	1.64	0.02	0.00	0.01	98.55	eclogitic	crust
Concentrate	Low-Cr (< 1 wt%)	garnet	41.26	0.04	23.36	0.03	0.12	0.28	11.99	0.00	16.57	5.80	0.01	0.00	0.02	99.46	eclogitic	mantle
Concentrate	Low-Cr (< 1 wt%)	garnet	39.89	0.07	22.45	0.01	0.18	0.39	18.69	0.00	11.63	6.10	0.01	0.00	0.03	99.46	eclogitic	crust
Concentrate	Low-Cr (< 1 wt%)	garnet	40.39	0.02	22.84	0.03	0.07	0.38	16.66	0.00	13.07	5.96	0.00	0.00	0.02	99.45	eclogitic	mantle
Concentrate	Low-Cr (< 1 wt%)	garnet	39.85	0.07	22.50	0.03	0.05	0.40	18.58	0.00	11.02	6.71	0.00	0.00	0.02	99.23	eclogitic	crust
Concentrate	Low-Cr (< 1 wt%)	garnet	40.54	0.03	22.95	0.02	0.14	0.37	16.00	0.00	13.63	5.86	0.00	0.00	0.04	99.57	eclogitic	crust
Concentrate	Low-Cr (< 1 wt%)	garnet	41.04	0.07	23.26	0.03	0.10	0.25	13.04	0.01	15.87	5.88	0.00	0.00	0.02	99.56	eclogitic	mantle
Concentrate	Low-Cr (< 1 wt%)	garnet	40.36	0.01	23.00	0.03	0.11	0.37	16.14	0.00	13.70	5.61	0.02	0.00	0.07	99.43	eclogitic	crust

sample name	rock type	mineral from composition	SiO2	TiO2	Al2O3	V2O3	Cr2O3	MnO	FeO	NiO	MgO	CaO	Na2O	K2O	P2O5	Total	notes	Crust-Mantle
Concentrate	Low-Cr (< 1 wt%)	garnet	39.56	0.08	22.34	0.03	0.03	0.45	19.31	0.00	10.03	7.32	0.01	0.00	0.06	99.24	eclogitic	crust
Concentrate	Low-Cr (< 1 wt%)	garnet	41.06	0.05	23.28	0.02	0.10	0.27	12.95	0.00	15.91	5.77	0.00	0.00	0.02	99.42	eclogitic	crust
Concentrate	Low-Cr (< 1 wt%)	garnet	37.22	0.01	21.14	0.02	0.03	1.98	33.55	0.00	3.26	1.32	0.01	0.00	0.02	98.56	eclogitic	crust
Concentrate	Low-Cr (< 1 wt%)	garnet	38.62	0.05	21.77	0.01	0.02	0.52	23.82	0.00	7.07	6.82	0.02	0.00	0.07	98.79	eclogitic	crust
Concentrate	Low-Cr (< 1 wt%)	garnet	38.56	0.14	21.58	0.04	0.04	0.47	24.18	0.00	6.90	6.72	0.03	0.00	0.09	98.75	eclogitic	crust
Concentrate	Low-Cr (< 1 wt%)	garnet	39.65	0.03	22.31	0.02	0.11	0.40	19.59	0.00	10.72	5.97	0.02	0.00	0.04	98.87	eclogitic	crust
Concentrate	Low-Cr (< 1 wt%)	garnet	38.57	0.02	21.69	0.03	0.02	0.50	24.00	0.00	7.01	6.62	0.02	0.01	0.09	98.58	eclogitic	crust
Concentrate	Low-Cr (< 1 wt%)	garnet	39.75	0.13	22.29	0.05	0.14	0.42	19.40	0.01	11.02	5.97	0.02	0.01	0.02	99.21	eclogitic	mantle
Concentrate	Low-Cr (< 1 wt%)	garnet	38.64	0.06	21.67	0.03	0.02	0.50	24.12	0.00	7.04	6.51	0.02	0.01	0.05	98.68	eclogitic	crust
Concentrate	Low-Cr (< 1 wt%)	garnet	39.46	0.06	22.35	0.02	0.04	0.44	19.63	0.00	9.82	7.28	0.02	0.01	0.08	99.20	eclogitic	crust
Concentrate	Low-Cr (< 1 wt%)	garnet	38.45	0.15	21.52	0.03	0.02	0.49	24.71	0.00	6.70	6.61	0.02	0.00	0.04	98.74	eclogitic	crust
Concentrate	Low-Cr (< 1 wt%)	garnet	37.58	0.00	21.37	0.00	0.03	0.97	32.71	0.01	4.59	1.22	0.00	0.00	0.06	98.53	eclogitic	crust
Concentrate	Low-Cr (< 1 wt%)	garnet	38.69	0.07	21.77	0.03	0.03	0.52	24.17	0.00	6.95	6.80	0.02	0.00	0.04	99.09	eclogitic	crust
Concentrate	Low-Cr (< 1 wt%)	garnet	38.67	0.13	21.60	0.04	0.04	0.51	24.35	0.00	6.93	6.67	0.02	0.00	0.07	99.03	eclogitic	crust
Concentrate	Low-Cr (< 1 wt%)	garnet	38.65	0.11	21.73	0.02	0.00	0.50	23.68	0.01	7.21	6.84	0.00	0.00	0.03	98.78	eclogitic	mantle
Concentrate	Low-Cr (< 1 wt%)	garnet	38.70	0.12	21.63	0.03	0.01	0.51	23.84	0.00	7.26	6.69	0.00	0.00	0.08	98.88	eclogitic	crust
Concentrate	Low-Cr (< 1 wt%)	garnet	38.71	0.10	21.63	0.03	0.03	0.52	23.81	0.01	7.23	6.56	0.02	0.00	0.08	98.73	eclogitic	crust
Concentrate	Low-Cr (< 1 wt%)	garnet	38.72	0.09	21.62	0.03	0.02	0.51	23.99	0.01	7.19	6.65	0.02	0.00	0.07	98.92	eclogitic	crust
Concentrate	Low-Cr (< 1 wt%)	garnet	40.97	0.03	23.30	0.02	0.09	0.28	13.03	0.00	15.66	5.65	0.01	0.00	0.03	99.05	eclogitic	mantle
Concentrate	Low-Cr (< 1 wt%)	garnet	41.08	0.05	23.21	0.02	0.09	0.27	12.76	0.00	15.85	5.65	0.00	0.01	0.02	99.00	eclogitic	crust
Concentrate	Low-Cr (< 1 wt%)	garnet	40.32	0.05	22.87	0.02	0.15	0.37	16.04	0.00	13.49	5.71	0.02	0.00	0.07	99.12	eclogitic	mantle
Concentrate	Low-Cr (< 1 wt%)	garnet	40.07	0.07	22.58	0.01	0.04	0.38	17.74	0.01	11.92	6.21	0.00	0.00	0.01	99.03	eclogitic	crust
Concentrate	Low-Cr (< 1 wt%)	garnet	40.46	0.05	22.81	0.03	0.19	0.34	15.50	0.01	13.89	5.70	0.00	0.00	0.01	98.99	eclogitic	mantle
Concentrate	Low-Cr (< 1 wt%)	garnet	39.80	0.08	22.41	0.03	0.03	0.39	18.34	0.00	10.99	6.84	0.00	0.00	0.01	98.92	eclogitic	crust
Concentrate	Low-Cr (< 1 wt%)	garnet	39.84	0.05	22.51	0.02	0.07	0.43	18.58	0.00	11.24	6.08	0.01	0.00	0.07	98.89	eclogitic	crust
Concentrate	Low-Cr (< 1 wt%)	garnet	40.54	0.05	22.91	0.01	0.10	0.36	16.12	0.00	13.47	5.83	0.01	0.00	0.02	99.43	eclogitic	mantle
Concentrate	Low-Cr (< 1 wt%)	garnet	39.87	0.06	22.37	0.03	0.15	0.41	19.10	0.00	11.20	5.91	0.01	0.01	0.02	99.12	eclogitic	crust
Concentrate	Low-Cr (< 1 wt%)	garnet	39.85	0.06	22.40	0.05	0.17	0.41	19.03	0.00	11.34	5.94	0.00	0.01	0.05	99.30	eclogitic	crust
Concentrate	Low-Cr (< 1 wt%)	garnet	39.66	0.07	22.35	0.04	0.14	0.40	19.12	0.00	11.24	5.93	0.02	0.00	0.04	99.01	eclogitic	mantle
Concentrate	Low-Cr (< 1 wt%)	garnet	39.82	0.06	22.40	0.03	0.14	0.40	19.12	0.00	11.22	5.93	0.01	0.00	0.03	99.15	eclogitic	crust
Concentrate	Low-Cr (< 1 wt%)	garnet	39.71	0.08	22.37	0.04	0.15	0.42	19.15	0.00	11.06	5.99	0.02	0.00	0.06	99.05	eclogitic	mantle
Concentrate	Low-Cr (< 1 wt%)	garnet	39.67	0.09	22.30	0.03	0.16	0.40	18.87	0.00	11.26	5.94	0.03	0.00	0.05	98.80	eclogitic	mantle
Concentrate	Low-Cr (< 1 wt%)	garnet	39.60	0.05	22.30	0.02	0.15	0.41	19.17	0.00	11.02	5.83	0.03	0.00	0.03	98.62	eclogitic	mantle
Concentrate	Low-Cr (< 1 wt%)	garnet	40.33	0.03	22.75	0.02	0.15	0.37	16.04	0.00	13.38	5.73	0.01	0.00	0.06	98.88	eclogitic	mantle
Concentrate	Low-Cr (< 1 wt%)	garnet	39.74	0.08	22.37	0.02	0.05	0.38	18.60	0.01	10.90	6.76	0.01	0.00	0.02	98.94	eclogitic	crust
Concentrate	Low-Cr (< 1 wt%)	garnet	41.19	0.05	23.18	0.01	0.14	0.25	11.97	0.00	16.52	5.71	0.02	0.01	0.01	99.07	eclogitic	mantle
Concentrate	Low-Cr (< 1 wt%)	garnet	39.83	0.05	22.36	0.03	0.18	0.39	18.41	0.00	11.52	5.94	0.03	0.00	0.03	98.78	eclogitic	mantle
Concentrate	Low-Cr (< 1 wt%)	garnet	39.48	0.11	22.28	0.03	0.04	0.45	19.48	0.00	9.73	7.23	0.03	0.01	0.06	98.92	eclogitic	crust
Concentrate	Low-Cr (< 1 wt%)	garnet	39.88	0.06	22.42	0.03	0.19	0.38	18.66	0.00	11.47	5.99	0.01	0.00	0.06	99.16	eclogitic	crust
Concentrate	Low-Cr (< 1 wt%)	garnet	38.58	0.12	21.59	0.04	0.01	0.51	23.91	0.00	7.19	6.66	0.03	0.00	0.09	98.74	eclogitic	crust
Concentrate	Low-Cr (< 1 wt%)	garnet	41.63	0.13	22.87	0.03	0.98	0.35	9.73	0.01	18.54	5.10	0.02	0.00	0.00	99.39	eclogitic	mantle
Concentrate	Low-Cr (< 1 wt%)	garnet	38.68	0.09	21.63	0.03	0.01	0.49	23.91	0.01	7.31	6.60	0.03	0.01	0.07	98.87	eclogitic	crust
Concentrate	Low-Cr (< 1 wt%)	garnet	38.67	0.12	21.25	0.02	0.08	0.63	23.90	0.00	7.53	6.29	0.02	0.00	0.03	98.52	eclogitic	crust
Concentrate	Low-Cr (< 1 wt%)	garnet	38.67	0.09	21.63	0.01	0.03	0.51	23.85	0.00	7.23	6.62	0.03	0.00	0.07	98.75	eclogitic	crust
Concentrate	Low-Cr (< 1 wt%)	garnet	38.62	0.13	21.61	0.04	0.05	0.52	23.62	0.01	7.14	6.75	0.02	0.00	0.07	98.55	eclogitic	crust
Concentrate	Low-Cr (< 1 wt%)	garnet	38.79	0.12	21.61	0.03	0.04	0.51	23.81	0.00	7.10	6.64	0.01	0.00	0.06	98.74	eclogitic	crust
Concentrate	Low-Cr (< 1 wt%)	garnet	38.65	0.03	21.61	0.04	0.03	0.52	24.02	0.00	6.91	6.74	0.04	0.00	0.08	98.67	eclogitic	crust
Concentrate	Low-Cr (< 1 wt%)	garnet	38.54	0.11	21.68	0.04	0.02	0.52	24.73	0.00	6.66	6.67	0.04	0.00	0.04	99.06	eclogitic	crust
Concentrate	Low-Cr (< 1 wt%)	garnet	38.65	0.06	21.80	0.03	0.03	0.51	23.98	0.00	7.14	6.76	0.05	0.01	0.07	99.08	eclogitic	crust

sample name	rock type	mineral from composition	SiO2	TiO2	Al2O3	V2O3	Cr2O3	MnO	FeO	NiO	MgO	CaO	Na2O	K2O	P2O5	Total	notes	Crust-Mantle
Concentrate	Low-Cr (< 1 wt%)	garnet	38.77	0.09	21.59	0.03	0.03	0.52	23.91	0.00	7.31	6.60	0.03	0.00	0.06	98.95	eclogitic	crust
Concentrate	Low-Cr (< 1 wt%)	garnet	38.63	0.09	21.67	0.03	0.00	0.53	24.34	0.00	6.86	6.67	0.02	0.00	0.08	98.91	eclogitic	crust
Concentrate	Low-Cr (< 1 wt%)	garnet	38.59	0.14	21.53	0.04	0.02	0.51	24.91	0.00	6.50	6.74	0.03	0.00	0.10	99.10	eclogitic	crust
Concentrate	Low-Cr (< 1 wt%)	garnet	38.58	0.10	21.62	0.04	0.01	0.51	24.26	0.00	6.85	6.77	0.01	0.00	0.06	98.80	eclogitic	crust
Concentrate	Low-Cr (< 1 wt%)	garnet	38.51	0.07	21.59	0.04	0.03	0.53	24.12	0.00	6.93	6.73	0.04	0.00	0.07	98.66	eclogitic	crust
Concentrate	Low-Cr (< 1 wt%)	garnet	38.52	0.11	21.52	0.04	0.03	0.56	24.56	0.01	6.60	6.81	0.01	0.01	0.05	98.82	eclogitic	crust
Concentrate	Low-Cr (< 1 wt%)	garnet	38.76	0.20	21.64	0.03	0.04	0.54	24.15	0.00	7.04	6.65	0.04	0.00	0.08	99.17	eclogitic	crust
Concentrate	Low-Cr (< 1 wt%)	garnet	40.95	0.06	23.23	0.06	0.10	0.25	12.80	0.00	15.92	5.80	0.01	0.01	0.03	99.22	eclogitic	mantle
Concentrate	Low-Cr (< 1 wt%)	garnet	40.02	0.04	22.53	0.02	0.17	0.39	18.56	0.01	11.65	5.86	0.02	0.01	0.05	99.34	eclogitic	mantle
Concentrate	Low-Cr (< 1 wt%)	garnet	38.96	0.10	21.91	0.05	0.05	0.49	22.11	0.00	8.14	6.93	0.03	0.00	0.05	98.82	eclogitic	crust
Concentrate	Low-Cr (< 1 wt%)	garnet	39.83	0.05	22.38	0.02	0.14	0.41	18.95	0.00	11.30	5.87	0.01	0.01	0.05	99.01	eclogitic	crust
Concentrate	Low-Cr (< 1 wt%)	garnet	39.71	0.08	22.35	0.03	0.14	0.41	18.92	0.00	11.16	5.90	0.00	0.00	0.07	98.77	eclogitic	mantle
Concentrate	Low-Cr (< 1 wt%)	garnet	37.28	0.00	21.09	0.00	0.02	1.41	31.79	0.00	2.61	4.41	0.02	0.01	0.02	98.65	eclogitic	crust
Concentrate	Low-Cr (< 1 wt%)	garnet	39.77	0.04	22.45	0.03	0.16	0.41	18.77	0.00	11.34	5.96	0.01	0.01	0.09	99.03	eclogitic	crust
Concentrate	Low-Cr (< 1 wt%)	garnet	38.83	0.05	21.80	0.01	0.03	0.51	23.86	0.00	7.27	6.65	0.03	0.00	0.05	99.10	eclogitic	crust
Concentrate	Low-Cr (< 1 wt%)	garnet	40.18	0.04	22.73	0.03	0.07	0.37	16.91	0.00	12.26	6.44	0.01	0.00	0.03	99.07	eclogitic	crust
Concentrate	Low-Cr (< 1 wt%)	garnet	39.50	0.08	22.40	0.04	0.04	0.45	19.43	0.00	9.94	7.25	0.03	0.00	0.05	99.20	eclogitic	crust
Concentrate	Low-Cr (< 1 wt%)	garnet	39.91	0.06	22.41	0.03	0.16	0.39	18.83	0.00	11.26	6.00	0.01	0.00	0.05	99.11	eclogitic	crust
Concentrate	peridotitic (≥ 1 wt%)	garnet	41.31	0.02	20.40	0.03	4.48	0.47	7.62	0.01	19.09	6.16	0.01	0.00	0.02	99.60	peridotitic	
Concentrate	peridotitic (≥ 1 wt%)	garnet	41.32	0.02	20.63	0.02	4.05	0.50	8.06	0.00	18.89	5.98	0.01	0.00	0.03	99.53	peridotitic	
Concentrate	peridotitic (≥ 1 wt%)	garnet	41.11	0.00	20.33	0.03	4.58	0.60	8.56	0.01	18.08	6.35	0.01	0.00	0.03	99.69	peridotitic	
Concentrate	peridotitic (≥ 1 wt%)	garnet	41.07	0.00	20.22	0.03	4.32	0.66	8.50	0.00	18.03	6.36	0.00	0.01	0.00	99.19	peridotitic	
Concentrate	peridotitic (≥ 1 wt%)	garnet	40.98	0.00	20.18	0.03	4.54	0.62	8.53	0.00	18.07	6.49	0.00	0.00	0.00	99.43	peridotitic	
Concentrate	peridotitic (≥ 1 wt%)	garnet	41.27	0.03	20.79	0.03	4.04	0.49	7.38	0.00	19.26	6.02	0.00	0.01	0.01	99.32	peridotitic	
Concentrate	peridotitic (≥ 1 wt%)	garnet	42.07	0.83	18.93	0.02	3.95	0.25	7.18	0.02	21.27	5.00	0.06	0.00	0.03	99.63	peridotitic	
Concentrate	peridotitic (≥ 1 wt%)	garnet	42.28	0.71	20.11	0.04	2.97	0.25	6.82	0.01	21.74	4.90	0.04	0.00	0.02	99.90	peridotitic	
Concentrate	peridotitic (≥ 1 wt%)	garnet	42.45	0.23	20.77	0.05	2.59	0.24	6.57	0.01	21.82	4.66	0.03	0.01	0.04	99.47	peridotitic	
Concentrate	peridotitic (≥ 1 wt%)	garnet	41.38	0.03	20.55	0.03	4.36	0.44	7.12	0.00	19.42	6.24	0.03	0.00	0.01	99.61	peridotitic	
Concentrate	peridotitic (≥ 1 wt%)	garnet	41.64	0.02	20.96	0.02	3.94	0.43	6.92	0.00	19.73	5.97	0.00	0.00	0.00	99.64	peridotitic	
Concentrate	peridotitic (≥ 1 wt%)	garnet	41.35	0.03	20.19	0.03	4.66	0.52	7.62	0.01	18.71	6.36	0.01	0.00	0.01	99.49	peridotitic	
Concentrate	peridotitic (≥ 1 wt%)	garnet	41.81	0.00	21.43	0.02	3.27	0.43	7.06	0.00	19.81	5.99	0.02	0.01	0.01	99.85	peridotitic	
Concentrate	peridotitic (≥ 1 wt%)	garnet	42.37	0.56	20.71	0.05	2.59	0.26	6.44	0.01	21.75	4.84	0.03	0.00	0.02	99.63	peridotitic	
Concentrate	peridotitic (≥ 1 wt%)	garnet	41.69	0.03	20.88	0.05	4.14	0.44	6.90	0.01	19.68	6.09	0.00	0.01	0.00	99.94	peridotitic	
Concentrate	peridotitic (≥ 1 wt%)	garnet	42.44	0.34	20.03	0.05	3.62	0.25	6.48	0.02	21.69	4.96	0.04	0.00	0.02	99.97	peridotitic	
Concentrate	peridotitic (≥ 1 wt%)	garnet	41.50	0.03	20.37	0.03	4.75	0.47	7.19	0.00	19.08	6.37	0.01	0.00	0.00	99.80	peridotitic	
Concentrate	peridotitic (≥ 1 wt%)	garnet	42.21	0.20	18.26	0.05	6.16	0.24	5.68	0.02	21.43	5.52	0.02	0.00	0.03	99.83	peridotitic	
Concentrate	peridotitic (≥ 1 wt%)	garnet	41.11	0.03	19.80	0.02	5.15	0.71	8.17	0.01	18.08	6.50	0.00	0.00	0.02	99.59	peridotitic	
Concentrate	peridotitic (≥ 1 wt%)	garnet	41.45	0.03	20.45	0.05	4.59	0.50	7.30	0.01	19.20	6.32	0.01	0.01	0.02	99.93	peridotitic	
Concentrate	peridotitic (≥ 1 wt%)	garnet	41.51	0.00	20.25	0.05	4.66	0.49	7.67	0.00	18.64	6.39	0.00	0.00	0.00	99.66	peridotitic	
Concentrate	peridotitic (≥ 1 wt%)	garnet	41.38	0.01	20.13	0.03	4.87	0.65	8.15	0.00	18.43	6.03	0.01	0.00	0.02	99.71	peridotitic	
Concentrate	peridotitic (≥ 1 wt%)	garnet	41.38	0.02	20.39	0.02	4.55	0.71	8.21	0.00	18.99	5.38	0.01	0.00	0.01	99.68	peridotitic	
Concentrate	peridotitic (≥ 1 wt%)	garnet	42.25	0.37	19.98	0.05	3.67	0.26	6.48	0.02	21.81	5.00	0.04	0.00	0.04	99.96	peridotitic	
Concentrate	peridotitic (≥ 1 wt%)	garnet	41.26	0.02	20.48	0.00	4.24	0.61	8.11	0.01	18.60	6.08	0.00	0.00	0.02	99.42	peridotitic	
Concentrate	peridotitic (≥ 1 wt%)	garnet	41.15	0.02	19.84	0.01	4.97	0.70	8.20	0.00	18.30	6.32	0.02	0.00	0.03	99.55	peridotitic	
Concentrate	peridotitic (≥ 1 wt%)	garnet	41.23	0.00	20.68	0.02	4.01	0.50	7.88	0.00	18.63	6.21	0.01	0.00	0.02	99.19	peridotitic	
Concentrate	peridotitic (≥ 1 wt%)	garnet	41.04	0.02	19.97	0.03	4.89	0.61	8.05	0.01	18.25	6.29	0.02	0.00	0.00	99.17	peridotitic	
Concentrate	peridotitic (≥ 1 wt%)	garnet	41.42	0.01	20.46	0.01	4.26	0.66	8.10	0.00	18.37	6.10	0.00	0.00	0.02	99.41	peridotitic	
Concentrate	peridotitic (≥ 1 wt%)	garnet	42.29	0.40	19.26	0.02	4.72	0.24	5.48	0.01	21.87	5.12	0.05	0.00	0.01	99.44	peridotitic	
Concentrate	peridotitic (≥ 1 wt%)	garnet	41.41	0.01	20.68	0.03	4.02	0.48	7.62	0.00	18.85	6.25	0.00	0.00	0.00	99.36	peridotitic	

sample name	rock type	mineral from composition	SiO2	TiO2	Al2O3	V2O3	Cr2O3	MnO	FeO	NiO	MgO	CaO	Na2O	K2O	P2O5	Total	notes	Crust-Mantle
Concentrate	peridotitic (≥ 1 wt%)	garnet	41.50	0.01	20.89	0.00	3.74	0.45	7.25	0.00	19.33	6.10	0.00	0.01	0.02	99.30	peridotitic	
Concentrate	peridotitic (≥ 1 wt%)	garnet	41.01	0.01	20.37	0.02	4.16	0.75	8.61	0.00	17.60	6.63	0.00	0.00	0.02	99.19	peridotitic	
Concentrate	peridotitic (≥ 1 wt%)	garnet	41.28	0.01	20.44	0.02	4.29	0.71	8.32	0.01	19.12	5.09	0.02	0.00	0.01	99.32	peridotitic	
Concentrate	peridotitic (≥ 1 wt%)	garnet	41.54	0.03	20.24	0.03	4.82	0.42	6.78	0.00	19.45	6.41	0.02	0.00	0.02	99.75	peridotitic	
Concentrate	peridotitic (≥ 1 wt%)	garnet	41.56	0.00	20.60	0.03	4.35	0.43	7.03	0.00	19.09	6.44	0.01	0.00	0.03	99.57	peridotitic	
Concentrate	peridotitic (≥ 1 wt%)	garnet	41.72	0.00	21.78	0.02	2.86	0.44	7.03	0.00	19.67	5.78	0.00	0.00	0.01	99.31	peridotitic	
Concentrate	peridotitic (≥ 1 wt%)	garnet	41.57	0.00	21.30	0.03	3.34	0.43	7.07	0.00	19.61	5.91	0.00	0.00	0.02	99.29	peridotitic	
Concentrate	peridotitic (≥ 1 wt%)	garnet	41.22	0.02	20.11	0.04	4.78	0.47	7.38	0.00	18.64	6.36	0.01	0.00	0.02	99.05	peridotitic	
Concentrate	peridotitic (≥ 1 wt%)	garnet	41.20	0.03	20.14	0.03	4.78	0.65	7.98	0.01	18.28	6.29	0.02	0.00	0.01	99.41	peridotitic	
Concentrate	peridotitic (≥ 1 wt%)	garnet	42.37	0.38	19.20	0.04	4.70	0.24	5.47	0.02	21.81	5.15	0.03	0.02	0.03	99.46	peridotitic	
Concentrate	peridotitic (≥ 1 wt%)	garnet	42.37	0.04	19.40	0.07	4.59	0.26	6.26	0.03	21.03	5.50	0.00	0.00	0.03	99.58	peridotitic	
Concentrate	peridotitic (≥ 1 wt%)	garnet	41.36	0.01	20.01	0.02	4.88	0.69	8.19	0.00	18.31	6.28	0.02	0.00	0.00	99.79	peridotitic	
Concentrate	peridotitic (≥ 1 wt%)	garnet	41.20	0.00	20.55	0.01	4.13	0.72	8.51	0.00	18.03	6.24	0.01	0.01	0.01	99.41	peridotitic	
Concentrate	peridotitic (≥ 1 wt%)	garnet	41.37	0.02	20.25	0.03	4.50	0.54	7.95	0.01	18.37	6.19	0.00	0.00	0.02	99.26	peridotitic	
Concentrate	peridotitic (≥ 1 wt%)	garnet	41.54	0.03	20.81	0.04	4.00	0.46	7.27	0.00	19.35	6.02	0.00	0.00	0.02	99.53	peridotitic	
Concentrate	peridotitic (≥ 1 wt%)	garnet	42.43	0.40	20.33	0.05	3.19	0.25	6.18	0.01	22.06	4.87	0.03	0.01	0.05	99.85	peridotitic	
Concentrate	peridotitic (≥ 1 wt%)	garnet	42.18	0.38	19.37	0.05	4.24	0.25	6.41	0.03	21.56	5.13	0.02	0.00	0.02	99.63	peridotitic	
Concentrate	peridotitic (≥ 1 wt%)	garnet	42.15	0.74	19.70	0.05	3.41	0.26	6.61	0.03	21.48	5.01	0.03	0.00	0.03	99.50	peridotitic	
Concentrate	peridotitic (≥ 1 wt%)	garnet	42.35	0.36	19.73	0.04	3.72	0.25	6.45	0.01	21.62	5.01	0.02	0.00	0.04	99.59	peridotitic	
Concentrate	peridotitic (≥ 1 wt%)	garnet	42.36	0.36	20.82	0.04	2.53	0.23	6.47	0.02	21.63	4.72	0.04	0.00	0.02	99.24	peridotitic	
Concentrate		ilmenite	0.04	52.80	0.18	0.15	0.26	0.30	32.91	0.06	11.94	0.02	0.01	0.00	0.00	98.68	mg-ilmenite	
Concentrate		ilmenite	0.03	50.94	0.40	0.15	1.07	0.43	34.52	0.09	10.97	0.01	0.00	0.00	0.01	98.61	mg-ilmenite	
Concentrate		ilmenite	0.05	54.86	0.45	0.16	1.43	0.68	24.12	0.11	16.90	0.03	0.04	0.00	0.00	98.83	mg-ilmenite	
Concentrate		ilmenite	0.00	50.35	0.37	0.17	2.74	0.78	21.46	0.07	22.58	0.00	0.11	0.00	0.00	98.65	mg-ilmenite	
Concentrate		ilmenite	0.03	51.72	1.18	0.32	0.48	0.48	30.33	0.16	13.97	0.03	0.01	0.00	0.00	98.71	mg-ilmenite	
Concentrate		ilmenite	0.04	48.57	1.02	0.36	2.37	0.49	33.16	0.11	12.68	0.06	0.23	0.00	0.00	99.07	mg-ilmenite	
Concentrate		ilmenite	0.03	48.26	0.72	0.36	6.15	0.64	27.67	0.14	14.92	0.03	0.02	0.00	0.01	98.95	mg-ilmenite	
Concentrate		ilmenite	0.03	51.41	0.51	0.18	4.88	0.97	22.24	0.05	18.23	0.07	0.04	0.00	0.00	98.62	mg-ilmenite	
Concentrate		ilmenite	0.07	51.53	0.96	0.18	5.34	0.69	25.65	0.11	17.14	0.05	0.03	0.00	0.00	101.76		
Concentrate		ilmenite	0.08	17.73	3.80	0.15	3.78	0.95	57.16	0.12	14.74	0.52	0.03	0.00	0.01	99.06	fe rich	
Concentrate		ilmenite	0.05	52.96	0.60	0.22	0.56	0.29	33.90	0.12	12.13	0.02	0.01	0.00	0.00	100.86		
Concentrate		ilmenite	0.02	53.01	0.63	0.15	0.55	0.28	33.59	0.12	12.22	0.02	0.02	0.00	0.00	100.62		
Concentrate		ilmenite	0.05	53.13	0.63	0.16	0.55	0.31	32.85	0.11	12.80	0.02	0.02	0.00	0.03	100.65		
Concentrate		olivine	40.67	0.00	0.00	0.02	0.00	0.12	7.12	0.37	50.29	0.00	0.00	0.00	0.00	98.60		
Concentrate		olivine	40.75	0.00	0.00	0.00	0.01	0.12	7.24	0.35	50.11	0.00	0.00	0.00	0.00	98.59		
Concentrate		olivine	40.85	0.00	0.00	0.00	0.02	0.09	6.00	0.39	51.32	0.00	0.00	0.00	0.00	98.68		
Concentrate		olivine	40.98	0.00	0.00	0.00	0.00	0.09	6.70	0.37	50.82	0.00	0.00	0.00	0.00	98.97		
Concentrate		olivine	40.56	0.00	0.00	0.01	0.00	0.15	8.18	0.36	49.26	0.00	0.00	0.00	0.00	98.51		
Concentrate		olivine	41.01	0.00	0.00	0.00	0.00	0.10	6.03	0.37	51.32	0.00	0.00	0.01	0.00	98.84		
Concentrate		olivine	40.69	0.00	0.00	0.00	0.00	0.10	7.08	0.38	50.38	0.00	0.00	0.01	0.00	98.64		
Concentrate		olivine	40.74	0.00	0.00	0.01	0.00	0.13	7.10	0.37	50.37	0.00	0.00	0.00	0.00	98.71		
Concentrate		olivine	40.73	0.00	0.00	0.00	0.00	0.16	7.31	0.36	50.02	0.00	0.00	0.01	0.00	98.58		
Concentrate		olivine	40.58	0.01	0.00	0.00	0.02	0.14	7.90	0.31	49.72	0.00	0.00	0.00	0.00	98.68		
Concentrate		olivine	40.66	0.00	0.00	0.00	0.02	0.14	7.07	0.35	50.33	0.00	0.00	0.00	0.00	98.57		
Concentrate		olivine	40.63	0.00	0.00	0.01	0.00	0.13	7.47	0.38	49.99	0.00	0.00	0.00	0.01	98.62		
Concentrate		olivine	40.42	0.00	0.00	0.00	0.00	0.20	8.77	0.35	48.93	0.01	0.00	0.00	0.00	98.68		
Concentrate		olivine	40.64	0.00	0.00	0.00	0.00	0.14	7.02	0.38	50.34	0.00	0.00	0.01	0.01	98.53		
Concentrate		olivine	40.73	0.00	0.00	0.00	0.01	0.14	7.12	0.34	50.33	0.01	0.00	0.01	0.00	98.69		
Concentrate		olivine	40.81	0.00	0.00	0.00	0.00	0.11	7.11	0.35	50.24	0.00	0.00	0.00	0.01	98.65		

sample name	rock type	mineral from composition	SiO2	TiO2	Al2O3	V2O3	Cr2O3	MnO	FeO	NiO	MgO	CaO	Na2O	K2O	P2O5	Total	notes	Crust-Mantle
Concentrate		olivine	40.83	0.00	0.00	0.00	0.01	0.12	7.07	0.36	50.34	0.00	0.00	0.00	0.00	98.74		
Concentrate		olivine	40.77	0.00	0.00	0.00	0.00	0.11	7.07	0.36	50.41	0.00	0.00	0.01	0.00	98.74		
Concentrate		olivine	40.71	0.00	0.00	0.00	0.02	0.13	7.77	0.34	49.65	0.01	0.00	0.01	0.00	98.63		
Concentrate		olivine	40.86	0.02	0.02	0.00	0.05	0.12	9.15	0.38	48.04	0.09	0.00	0.00	0.01	98.73		
Concentrate		olivine	40.00	0.05	0.00	0.00	0.01	0.14	13.67	0.21	44.68	0.06	0.00	0.00	0.01	98.84	fe rich	
Concentrate		olivine	41.15	0.00	0.00	0.00	0.00	0.12	7.81	0.38	50.12	0.01	0.00	0.00	0.01	99.59		
Concentrate		olivine	40.62	0.01	0.00	0.01	0.00	0.20	10.34	0.35	47.63	0.02	0.00	0.00	0.01	99.20	fe rich	
Concentrate		olivine	39.73	0.05	0.02	0.00	0.03	0.16	15.47	0.07	44.01	0.04	0.00	0.00	0.01	99.59	fe rich	
Concentrate		olivine	40.45	0.05	0.02	0.00	0.06	0.15	11.81	0.25	46.42	0.08	0.00	0.01	0.01	99.31	fe rich	
Concentrate		olivine	40.28	0.04	0.02	0.01	0.03	0.15	12.40	0.31	45.78	0.07	0.00	0.00	0.02	99.11	fe rich	
Concentrate		olivine	41.23	0.01	0.01	0.00	0.00	0.15	7.85	0.37	49.43	0.01	0.00	0.00	0.01	99.07		
Concentrate		olivine	41.04	0.06	0.03	0.01	0.03	0.10	7.94	0.35	49.73	0.05	0.00	0.01	0.00	99.35		
Concentrate		olivine	41.14	0.00	0.00	0.01	0.00	0.18	8.16	0.36	49.56	0.01	0.00	0.00	0.01	99.43		
Concentrate		olivine	40.23	0.03	0.03	0.00	0.05	0.14	12.74	0.29	45.67	0.07	0.00	0.00	0.00	99.25	fe rich	
Concentrate		olivine	40.93	0.04	0.03	0.00	0.03	0.12	8.73	0.38	48.64	0.06	0.00	0.00	0.02	98.99		
Concentrate		olivine	40.33	0.06	0.01	0.00	0.03	0.16	12.21	0.30	46.01	0.08	0.00	0.00	0.00	99.17	fe rich	
Concentrate		olivine	40.06	0.05	0.03	0.00	0.03	0.15	13.10	0.22	45.06	0.07	0.00	0.00	0.02	98.79	fe rich	
Concentrate		olivine	41.15	0.00	0.00	0.02	0.00	0.13	7.35	0.35	49.85	0.00	0.00	0.00	0.00	98.85		
Concentrate		olivine	41.15	0.00	0.00	0.00	0.00	0.09	7.49	0.38	49.75	0.00	0.00	0.00	0.01	98.88		
Concentrate		olivine	40.61	0.01	0.01	0.01	0.04	0.13	9.54	0.36	48.21	0.08	0.00	0.00	0.01	99.00		
Concentrate		olivine	41.08	0.01	0.00	0.00	0.01	0.12	7.50	0.38	49.77	0.01	0.00	0.00	0.00	98.88		
Concentrate		olivine	41.07	0.01	0.02	0.00	0.03	0.10	7.73	0.37	49.63	0.01	0.00	0.00	0.01	98.97		
Concentrate		olivine	40.59	0.02	0.04	0.01	0.07	0.12	10.28	0.35	47.62	0.11	0.00	0.00	0.00	99.20		
Concentrate		olivine	41.35	0.01	0.01	0.00	0.00	0.12	7.20	0.41	50.30	0.00	0.00	0.00	0.00	99.40	fe rich	
Concentrate		olivine	40.63	0.03	0.03	0.01	0.06	0.12	10.39	0.33	47.45	0.09	0.00	0.00	0.01	99.15		
Concentrate		olivine	40.92	0.02	0.03	0.01	0.03	0.12	9.32	0.37	48.92	0.09	0.00	0.00	0.00	99.84	fe rich	
Concentrate		olivine	40.94	0.05	0.02	0.00	0.05	0.11	8.21	0.40	49.11	0.05	0.00	0.00	0.00	98.93		
Concentrate		olivine	40.99	0.03	0.06	0.00	0.13	0.11	8.64	0.37	49.04	0.09	0.00	0.00	0.00	99.47		
Concentrate		olivine	40.90	0.05	0.04	0.00	0.04	0.11	8.70	0.36	49.13	0.05	0.00	0.00	0.00	99.38		
Concentrate		olivine	39.96	0.03	0.01	0.01	0.02	0.15	14.30	0.15	44.54	0.04	0.00	0.00	0.02	99.22		
Concentrate		olivine	40.40	0.02	0.02	0.01	0.04	0.14	11.87	0.33	46.62	0.07	0.00	0.00	0.02	99.53	fe rich	
Concentrate		olivine	40.32	0.06	0.02	0.00	0.04	0.13	12.11	0.28	46.41	0.07	0.00	0.00	0.01	99.45	fe rich	
Concentrate		olivine	40.60	0.03	0.03	0.01	0.04	0.13	10.34	0.33	47.66	0.08	0.00	0.00	0.00	99.26	fe rich	
Concentrate		olivine	40.71	0.02	0.02	0.00	0.05	0.11	9.51	0.34	48.25	0.09	0.00	0.00	0.01	99.11		
Concentrate		olivine	40.89	0.04	0.03	0.00	0.03	0.10	8.64	0.40	49.08	0.05	0.00	0.00	0.01	99.27		
Concentrate		olivine	40.85	0.04	0.04	0.01	0.05	0.13	9.42	0.39	48.45	0.08	0.00	0.00	0.01	99.46		
Concentrate		olivine	40.09	0.04	0.01	0.00	0.00	0.15	13.07	0.21	46.00	0.04	0.00	0.00	0.01	99.62	fe rich	
Concentrate		olivine	40.76	0.00	0.00	0.00	0.00	0.16	9.27	0.38	48.80	0.00	0.00	0.00	0.00	99.37		
Concentrate		olivine	41.04	0.00	0.02	0.00	0.00	0.16	7.73	0.36	49.99	0.01	0.00	0.00	0.02	99.33		
Concentrate		olivine	40.61	0.02	0.05	0.00	0.07	0.12	9.81	0.36	48.30	0.10	0.00	0.00	0.00	99.44		
Concentrate		olivine	41.10	0.00	0.00	0.00	0.00	0.15	7.48	0.37	50.20	0.01	0.00	0.00	0.00	99.31		
Concentrate		olivine	40.76	0.01	0.03	0.00	0.07	0.12	9.86	0.35	48.33	0.10	0.00	0.00	0.01	99.64		
Concentrate		olivine	39.99	0.00	0.01	0.01	0.04	0.31	13.26	0.33	45.65	0.03	0.00	0.00	0.00	99.63	fe rich	
Concentrate		olivine	41.21	0.00	0.01	0.00	0.00	0.13	7.05	0.33	50.55	0.01	0.00	0.00	0.00	99.29		
Concentrate		olivine	41.07	0.00	0.02	0.00	0.03	0.12	7.32	0.40	50.64	0.01	0.00	0.00	0.00	99.62		
Concentrate		olivine	40.95	0.04	0.01	0.00	0.03	0.12	7.78	0.35	50.07	0.01	0.00	0.00	0.01	99.35		
Concentrate		olivine	41.13	0.00	0.01	0.00	0.01	0.11	6.66	0.35	50.94	0.01	0.00	0.00	0.00	99.22		
Concentrate		olivine	41.05	0.00	0.01	0.02	0.05	0.11	7.36	0.41	50.48	0.03	0.00	0.00	0.01	99.53		
Concentrate		olivine	40.68	0.01	0.07	0.00	0.06	0.12	9.59	0.36	48.69	0.08	0.00	0.00	0.00	99.66		

sample name	rock type	mineral from composition	SiO2	TiO2	Al2O3	V2O3	Cr2O3	MnO	FeO	NiO	MgO	CaO	Na2O	K2O	P2O5	Total	notes	Crust-Mantle
Concentrate		olivine	40.72	0.04	0.04	0.00	0.06	0.12	9.30	0.37	48.47	0.10	0.00	0.01	0.00	99.23		
Concentrate		olivine	40.51	0.02	0.03	0.00	0.04	0.13	11.14	0.33	47.16	0.08	0.00	0.00	0.01	99.46	fe rich	
Concentrate		olivine	40.82	0.01	0.05	0.02	0.06	0.12	9.32	0.35	48.77	0.10	0.00	0.00	0.01	99.62		
Concentrate		olivine	41.07	0.00	0.00	0.00	0.00	0.15	8.30	0.35	49.94	0.01	0.00	0.00	0.00	99.82		
Concentrate		olivine	40.55	0.03	0.03	0.00	0.03	0.14	10.87	0.33	47.77	0.08	0.00	0.00	0.02	99.85	fe rich	
Concentrate		olivine	40.50	0.02	0.09	0.01	0.08	0.12	10.35	0.36	47.84	0.11	0.00	0.00	0.01	99.49	fe rich	
Concentrate		olivine	40.55	0.01	0.04	0.01	0.05	0.13	10.59	0.33	48.06	0.09	0.00	0.00	0.02	99.87	fe rich	
Concentrate		olivine	40.32	0.06	0.03	0.01	0.06	0.13	11.48	0.34	47.41	0.08	0.00	0.00	0.00	99.92	fe rich	
Concentrate		olivine	40.71	0.01	0.02	0.01	0.05	0.13	9.80	0.33	48.47	0.09	0.00	0.00	0.01	99.63		
Concentrate		olivine	41.22	0.01	0.02	0.01	0.00	0.10	6.99	0.37	50.93	0.00	0.00	0.00	0.00	99.66		
Concentrate		olivine	40.36	0.03	0.03	0.00	0.04	0.14	11.72	0.32	46.81	0.08	0.00	0.00	0.02	99.55	fe rich	
Concentrate		olivine	40.98	0.02	0.05	0.00	0.04	0.11	8.44	0.40	49.27	0.06	0.00	0.00	0.01	99.38		
Concentrate		olivine	41.15	0.01	0.00	0.00	0.02	0.14	7.60	0.36	50.53	0.00	0.00	0.00	0.00	99.83		
Concentrate		olivine	40.79	0.03	0.01	0.00	0.00	0.15	8.63	0.35	49.47	0.00	0.00	0.00	0.01	99.44		
Concentrate		olivine	40.67	0.05	0.03	0.00	0.02	0.10	9.31	0.40	48.87	0.05	0.00	0.00	0.00	99.51		
Concentrate		olivine	40.81	0.03	0.05	0.02	0.13	0.12	8.85	0.37	49.05	0.10	0.00	0.00	0.00	99.52		
Concentrate		olivine	40.72	0.03	0.05	0.00	0.05	0.13	9.77	0.33	48.59	0.09	0.00	0.00	0.00	99.76		
Concentrate		olivine	40.97	0.02	0.01	0.00	0.03	0.12	7.69	0.40	50.44	0.02	0.00	0.00	0.00	99.70		
Concentrate		olivine	40.84	0.04	0.07	0.01	0.04	0.11	8.84	0.39	48.95	0.08	0.00	0.00	0.01	99.38		
Concentrate		olivine	40.75	0.03	0.05	0.01	0.05	0.11	8.91	0.40	49.07	0.07	0.00	0.00	0.00	99.46		
Concentrate		olivine	41.03	0.01	0.02	0.01	0.01	0.10	7.08	0.36	50.72	0.01	0.00	0.00	0.00	99.35		
Concentrate		olivine	41.00	0.01	0.00	0.02	0.00	0.10	7.52	0.37	50.53	0.00	0.00	0.01	0.00	99.57		
Concentrate		olivine	40.02	0.05	0.00	0.00	0.02	0.15	13.96	0.11	45.55	0.02	0.00	0.00	0.00	99.89	fe rich	
Concentrate		olivine	40.76	0.01	0.03	0.01	0.05	0.12	9.14	0.39	49.05	0.09	0.00	0.00	0.00	99.66		
Concentrate		olivine	39.83	0.04	0.02	0.01	0.01	0.15	15.00	0.07	44.48	0.03	0.00	0.00	0.02	99.66	fe rich	
Concentrate		olivine	41.10	0.01	0.01	0.00	0.04	0.09	7.34	0.36	50.59	0.01	0.00	0.00	0.00	99.54		
Concentrate		olivine	40.39	0.03	0.04	0.00	0.03	0.13	11.05	0.32	47.57	0.08	0.00	0.00	0.02	99.68	fe rich	
Concentrate		olivine	40.03	0.06	0.02	0.00	0.02	0.13	12.91	0.29	46.05	0.05	0.00	0.00	0.01	99.58	fe rich	
Concentrate		olivine	41.07	0.02	0.01	0.00	0.01	0.12	7.80	0.37	50.33	0.01	0.00	0.01	0.01	99.75		
Concentrate		olivine	39.79	0.04	0.02	0.00	0.02	0.17	13.85	0.20	45.25	0.05	0.00	0.00	0.01	99.39	fe rich	
Concentrate		olivine	40.47	0.00	0.02	0.00	0.02	0.28	10.66	0.35	47.80	0.01	0.00	0.00	0.01	99.63	fe rich	
Concentrate		olivine	40.17	0.04	0.03	0.00	0.02	0.13	12.89	0.28	46.07	0.06	0.00	0.00	0.00	99.70	fe rich	
Concentrate		olivine	40.85	0.01	0.02	0.00	0.04	0.11	9.34	0.38	48.77	0.09	0.00	0.00	0.00	99.62		
Concentrate		olivine	40.85	0.02	0.00	0.00	0.01	0.11	7.82	0.39	50.13	0.01	0.00	0.00	0.01	99.37	fe rich	
Concentrate		olivine	40.52	0.03	0.03	0.00	0.05	0.12	10.31	0.33	48.15	0.08	0.00	0.00	0.01	99.64	fe rich	
Concentrate		olivine	40.31	0.05	0.04	0.00	0.06	0.13	11.78	0.28	46.49	0.07	0.00	0.00	0.00	99.20		
Concentrate		olivine	41.03	0.00	0.01	0.00	0.02	0.12	7.78	0.36	50.13	0.01	0.00	0.00	0.01	99.47		
Concentrate		olivine	41.11	0.02	0.00	0.00	0.00	0.11	6.49	0.35	51.45	0.00	0.00	0.00	0.00	99.53		
Concentrate		olivine	40.68	0.03	0.05	0.00	0.06	0.11	9.04	0.38	49.52	0.09	0.00	0.00	0.02	99.99		
Concentrate		olivine	40.55	0.02	0.03	0.00	0.08	0.13	10.43	0.36	48.01	0.11	0.00	0.00	0.00	99.71	fe rich	
Concentrate		olivine	40.28	0.03	0.01	0.00	0.07	0.15	11.83	0.30	47.20	0.07	0.00	0.00	0.02	99.97	fe rich	
Concentrate		olivine	41.03	0.01	0.00	0.00	0.01	0.13	8.16	0.35	50.08	0.01	0.00	0.00	0.00	99.77		
Concentrate		olivine	41.21	0.01	0.00	0.00	0.00	0.12	7.12	0.40	50.72	0.01	0.00	0.00	0.01	99.60		
Concentrate		olivine	40.14	0.05	0.03	0.00	0.03	0.15	12.67	0.29	46.82	0.06	0.00	0.00	0.01	100.25	fe rich	
Concentrate		olivine	41.06	0.01	0.00	0.00	0.00	0.14	7.84	0.33	50.40	0.01	0.00	0.00	0.01	99.80		
Concentrate		olivine	40.76	0.02	0.06	0.02	0.07	0.11	8.90	0.39	49.36	0.09	0.00	0.00	0.00	99.79		
Concentrate		olivine	40.53	0.00	0.02	0.01	0.03	0.13	10.67	0.33	47.74	0.09	0.00	0.00	0.01	99.55	fe rich	
Concentrate		olivine	40.27	0.05	0.00	0.00	0.07	0.13	11.73	0.30	47.09	0.08	0.00	0.00	0.00	99.72	fe rich	
Concentrate		olivine	40.65	0.02	0.05	0.00	0.05	0.12	9.17	0.39	49.06	0.09	0.00	0.00	0.01	99.61		

sample name	rock type	mineral from composition	SiO2	TiO2	Al2O3	V2O3	Cr2O3	MnO	FeO	NiO	MgO	CaO	Na2O	K2O	P2O5	Total	notes	Crust-Mantle
Concentrate		olivine	41.12	0.02	0.00	0.00	0.00	0.13	7.51	0.36	50.38	0.00	0.00	0.00	0.01	99.53		
Concentrate		olivine	38.81	0.01	0.00	0.00	0.00	0.26	20.38	0.10	40.23	0.02	0.00	0.00	0.03	99.84	fe rich**	
Concentrate		olivine	41.18	0.02	0.00	0.00	0.00	0.11	7.35	0.35	51.09	0.01	0.00	0.00	0.01	100.10		
Concentrate		olivine	40.34	0.04	0.04	0.02	0.05	0.12	11.69	0.31	47.30	0.07	0.00	0.00	0.02	100.01		
Concentrate		olivine	40.77	0.00	0.00	0.00	0.00	0.13	8.45	0.32	49.94	0.01	0.00	0.00	0.01	99.65		
Concentrate		olivine	39.70	0.03	0.03	0.01	0.00	0.17	15.44	0.19	44.10	0.06	0.00	0.00	0.04	99.76	fe rich	
Concentrate		olivine	40.74	0.04	0.02	0.01	0.03	0.11	8.96	0.40	49.57	0.05	0.00	0.00	0.01	99.92		
Concentrate		olivine	41.03	0.00	0.02	0.00	0.02	0.11	7.29	0.40	50.99	0.00	0.00	0.00	0.00	99.86		
Concentrate		olivine	40.03	0.05	0.01	0.02	0.04	0.15	13.15	0.25	45.81	0.08	0.00	0.00	0.01	99.58	fe rich	
Concentrate		olivine	40.76	0.06	0.04	0.00	0.03	0.12	9.62	0.38	48.91	0.05	0.00	0.00	0.00	99.97		
Concentrate		olivine	40.94	0.04	0.02	0.00	0.05	0.11	8.00	0.34	50.01	0.04	0.00	0.00	0.00	99.55		
Concentrate		olivine	40.48	0.01	0.09	0.00	0.09	0.12	10.36	0.34	48.01	0.10	0.00	0.00	0.00	99.60	fe rich	
Concentrate		olivine	40.39	0.04	0.01	0.00	0.05	0.11	10.72	0.33	48.10	0.02	0.00	0.00	0.02	99.79	fe rich	
Concentrate		olivine	40.00	0.03	0.03	0.00	0.06	0.16	11.94	0.29	46.77	0.06	0.00	0.00	0.01	99.37	fe rich	
Concentrate		olivine	40.76	0.00	0.01	0.01	0.00	0.19	9.30	0.37	49.08	0.01	0.00	0.00	0.00	99.75		
Concentrate		olivine	40.56	0.00	0.01	0.00	0.00	0.24	10.09	0.37	48.39	0.02	0.00	0.00	0.00	99.69	fe rich	
Concentrate		olivine	41.50	0.00	0.03	0.01	0.00	0.10	6.03	0.35	52.03	0.00	0.00	0.00	0.02	100.07		
Concentrate		olivine	40.66	0.04	0.04	0.00	0.05	0.13	9.65	0.37	48.67	0.08	0.00	0.00	0.02	99.70		
Concentrate		olivine	40.39	0.04	0.02	0.01	0.05	0.13	10.53	0.31	47.90	0.09	0.00	0.00	0.00	99.46	fe rich	
Concentrate		olivine	40.82	0.00	0.01	0.01	0.01	0.15	8.44	0.35	49.82	0.01	0.00	0.00	0.01	99.63		
Concentrate		olivine	40.82	0.04	0.01	0.00	0.06	0.11	8.73	0.39	49.37	0.05	0.00	0.01	0.00	99.57		
Concentrate		olivine	40.18	0.06	0.03	0.01	0.03	0.15	12.75	0.23	46.06	0.07	0.00	0.00	0.00	99.56	fe rich	
Concentrate		olivine	40.49	0.02	0.03	0.00	0.07	0.12	10.48	0.34	48.39	0.11	0.00	0.00	0.00	100.05	fe rich	
Concentrate		olivine	40.55	0.03	0.04	0.00	0.04	0.12	10.51	0.33	48.10	0.09	0.00	0.00	0.00	99.80	fe rich	
Concentrate		olivine	41.04	0.00	0.00	0.02	0.00	0.12	7.21	0.37	50.74	0.01	0.00	0.00	0.00	99.51		
Concentrate		olivine	41.24	0.00	0.00	0.00	0.00	0.10	6.83	0.36	51.36	0.01	0.00	0.00	0.00	99.92		
Concentrate		olivine	40.89	0.00	0.00	0.00	0.00	0.14	8.40	0.35	49.72	0.02	0.00	0.00	0.01	99.53		
Concentrate		olivine	41.11	0.01	0.01	0.00	0.01	0.10	7.13	0.38	51.07	0.01	0.00	0.00	0.00	99.82		
Concentrate		olivine	40.94	0.01	0.02	0.00	0.00	0.13	7.94	0.36	50.60	0.01	0.00	0.00	0.00	99.99	fe rich	
Concentrate		olivine	40.65	0.03	0.03	0.01	0.04	0.13	10.22	0.33	48.29	0.09	0.00	0.00	0.01	99.82	fe rich	
Concentrate		olivine	40.51	0.03	0.05	0.01	0.03	0.13	10.25	0.32	48.33	0.09	0.00	0.00	0.00	99.75		
Concentrate		olivine	40.96	0.02	0.01	0.02	0.00	0.14	8.26	0.34	50.06	0.01	0.00	0.00	0.00	99.82	fe rich	
Concentrate		olivine	40.28	0.03	0.03	0.00	0.06	0.14	11.73	0.32	46.64	0.07	0.00	0.00	0.00	99.31	fe rich	
Concentrate		olivine	40.56	0.03	0.04	0.02	0.04	0.12	10.39	0.32	48.32	0.09	0.00	0.00	0.01	99.96	fe rich	
Concentrate		olivine	40.65	0.03	0.03	0.01	0.04	0.11	10.37	0.32	48.36	0.08	0.00	0.00	0.02	100.03	fe rich	
Concentrate		olivine	40.78	0.02	0.04	0.01	0.06	0.13	9.47	0.37	49.28	0.09	0.00	0.00	0.01	100.25		
Concentrate		olivine	39.94	0.04	0.02	0.00	0.02	0.17	13.79	0.22	45.83	0.06	0.00	0.00	0.04	100.13	fe rich	
Concentrate		olivine	41.17	0.00	0.00	0.00	0.01	0.11	7.67	0.36	50.63	0.00	0.00	0.00	0.02	99.97		
Concentrate		olivine	40.34	0.03	0.02	0.00	0.03	0.13	11.28	0.32	47.46	0.08	0.00	0.00	0.00	99.70	fe rich	
Concentrate		olivine	40.64	0.03	0.05	0.00	0.04	0.13	10.60	0.33	48.06	0.08	0.00	0.00	0.01	99.97	fe rich	
Concentrate		olivine	40.51	0.01	0.07	0.01	0.05	0.11	9.81	0.35	48.71	0.09	0.00	0.00	0.00	99.73		
Concentrate		olivine	40.14	0.04	0.03	0.00	0.00	0.14	12.86	0.21	46.16	0.02	0.00	0.00	0.02	99.62	fe rich	
Concentrate		olivine	40.25	0.01	0.00	0.00	0.01	0.23	10.82	0.33	47.86	0.01	0.00	0.00	0.01	99.53	fe rich	
Concentrate		olivine	40.75	0.05	0.02	0.00	0.05	0.11	8.70	0.40	49.59	0.05	0.00	0.00	0.00	99.72		
Concentrate		olivine	40.68	0.02	0.02	0.00	0.06	0.12	9.92	0.35	48.10	0.09	0.00	0.00	0.00	99.38		
Concentrate		olivine	41.26	0.00	0.02	0.01	0.07	0.11	7.37	0.40	50.41	0.03	0.00	0.00	0.00	99.68		
Concentrate		olivine	40.82	0.04	0.03	0.00	0.03	0.11	8.20	0.39	49.85	0.05	0.00	0.00	0.02	99.53		
Concentrate		olivine	40.93	0.02	0.04	0.00	0.06	0.11	7.93	0.36	49.98	0.05	0.00	0.00	0.01	99.47		
Concentrate		olivine	40.31	0.03	0.02	0.00	0.04	0.16	11.83	0.32	46.86	0.07	0.00	0.00	0.01	99.66	fe rich	

sample name	rock type	mineral from composition	SiO2	TiO2	Al2O3	V2O3	Cr2O3	MnO	FeO	NiO	MgO	CaO	Na2O	K2O	P2O5	Total	notes	Crust-Mantle
Concentrate		olivine	40.98	0.02	0.04	0.00	0.05	0.10	8.62	0.37	49.36	0.07	0.00	0.00	0.00	99.63		
Concentrate		olivine	40.46	0.00	0.01	0.01	0.04	0.14	10.24	0.32	48.09	0.10	0.00	0.00	0.00	99.41	fe rich	
Concentrate		olivine	40.94	0.02	0.00	0.00	0.02	0.11	7.62	0.36	50.55	0.01	0.00	0.00	0.01	99.64		
Concentrate		olivine	40.75	0.00	0.00	0.01	0.00	0.18	8.14	0.36	50.44	0.01	0.00	0.00	0.02	99.91		
Concentrate		olivine	40.80	0.01	0.01	0.00	0.00	0.16	8.46	0.31	50.05	0.00	0.00	0.00	0.00	99.80	fe rich	
Concentrate		olivine	40.22	0.03	0.02	0.00	0.07	0.14	11.92	0.33	46.81	0.07	0.00	0.00	0.03	99.63	fe rich	
Concentrate		olivine	40.48	0.05	0.03	0.00	0.03	0.12	10.09	0.36	48.21	0.06	0.00	0.00	0.01	99.44		
Concentrate		olivine	40.62	0.00	0.01	0.01	0.00	0.18	8.95	0.35	49.37	0.01	0.00	0.00	0.00	99.49		
Concentrate		olivine	41.02	0.01	0.03	0.02	0.06	0.11	7.63	0.37	50.90	0.05	0.00	0.00	0.00	100.21		
Concentrate		olivine	40.72	0.01	0.03	0.00	0.02	0.10	9.17	0.38	49.15	0.09	0.00	0.00	0.00	99.69		
Concentrate		olivine	40.50	0.02	0.09	0.00	0.04	0.12	9.56	0.34	48.72	0.08	0.00	0.00	0.00	99.47		
Concentrate		olivine	40.20	0.03	0.03	0.00	0.04	0.15	11.92	0.29	46.91	0.06	0.00	0.00	0.03	99.66	fe rich	
Concentrate		olivine	41.49	0.00	0.02	0.00	0.00	0.08	5.64	0.36	52.29	0.00	0.00	0.00	0.00	99.90		
Concentrate		olivine	40.04	0.03	0.02	0.00	0.00	0.15	13.25	0.13	45.82	0.03	0.00	0.00	0.00	99.46	fe rich	
Concentrate		olivine	40.67	0.01	0.01	0.00	0.00	0.17	9.43	0.37	49.17	0.02	0.00	0.00	0.01	99.86		
Concentrate		olivine	40.92	0.00	0.00	0.00	0.00	0.15	8.22	0.35	50.27	0.01	0.00	0.00	0.00	99.91		
Concentrate		olivine	40.60	0.00	0.01	0.00	0.01	0.25	10.29	0.33	48.42	0.01	0.00	0.00	0.00	99.92	fe rich	
Concentrate		olivine	41.08	0.00	0.01	0.00	0.00	0.13	7.67	0.35	50.25	0.01	0.00	0.00	0.00	99.50		
Concentrate		olivine	40.52	0.00	0.04	0.00	0.06	0.12	10.42	0.38	48.30	0.10	0.00	0.00	0.02	99.97	fe rich	
Concentrate		olivine	40.94	0.01	0.00	0.00	0.03	0.14	8.06	0.36	50.01	0.02	0.00	0.01	0.01	99.58		
Concentrate		olivine	40.65	0.05	0.03	0.00	0.06	0.12	9.43	0.39	48.70	0.09	0.00	0.00	0.03	99.55		
Concentrate		olivine	40.90	0.04	0.02	0.01	0.05	0.10	8.55	0.36	50.14	0.06	0.00	0.00	0.00	100.23		
Concentrate		olivine	40.21	0.07	0.03	0.01	0.02	0.13	12.29	0.28	46.77	0.07	0.00	0.00	0.01	99.89	fe rich	
Concentrate		olivine	40.99	0.00	0.02	0.00	0.00	0.13	8.02	0.35	50.61	0.01	0.00	0.00	0.01	100.14		
Concentrate		olivine	40.00	0.05	0.02	0.00	0.00	0.14	12.93	0.22	46.23	0.03	0.00	0.00	0.02	99.63	fe rich	
Concentrate		olivine	39.77	0.04	0.02	0.01	0.01	0.17	14.58	0.08	44.91	0.03	0.00	0.00	0.01	99.62	fe rich	
Concentrate		olivine	40.53	0.02	0.03	0.01	0.07	0.13	10.21	0.36	48.43	0.10	0.00	0.00	0.03	99.93	fe rich	
Concentrate		olivine	40.68	0.00	0.01	0.00	0.01	0.16	8.66	0.35	49.48	0.01	0.00	0.00	0.00	99.35		
Concentrate		olivine	41.08	0.00	0.02	0.00	0.01	0.13	7.87	0.33	50.44	0.00	0.00	0.00	0.01	99.89		
Concentrate		olivine	39.84	0.05	0.02	0.01	0.01	0.14	14.33	0.13	45.40	0.03	0.00	0.00	0.01	99.99	fe rich	
Concentrate		olivine	40.98	0.00	0.00	0.00	0.02	0.15	7.98	0.34	50.33	0.01	0.00	0.00	0.00	99.81		
Concentrate		olivine	39.95	0.04	0.01	0.00	0.01	0.15	13.84	0.13	45.52	0.03	0.00	0.00	0.01	99.69	fe rich	
Concentrate		olivine	41.00	0.00	0.02	0.01	0.02	0.11	7.42	0.36	50.63	0.01	0.00	0.00	0.01	99.60		
Concentrate		olivine	40.74	0.04	0.02	0.00	0.04	0.11	8.97	0.35	49.32	0.05	0.00	0.00	0.00	99.64		
Concentrate		olivine	40.22	0.03	0.03	0.00	0.06	0.13	12.12	0.30	46.54	0.06	0.00	0.00	0.02	99.51	fe rich	
Concentrate		olivine	40.75	0.05	0.00	0.00	0.04	0.13	9.74	0.33	49.14	0.04	0.00	0.01	0.01	100.23		
Concentrate		olivine	41.11	0.00	0.00	0.00	0.01	0.12	7.86	0.35	50.30	0.00	0.00	0.01	0.01	99.77		
Concentrate		olivine	41.16	0.00	0.00	0.01	0.00	0.10	7.22	0.37	50.98	0.01	0.00	0.00	0.00	99.86		
Concentrate		olivine	40.51	0.03	0.03	0.00	0.08	0.12	10.51	0.36	47.88	0.11	0.00	0.00	0.01	99.65	fe rich	
Concentrate		olivine	39.94	0.04	0.02	0.00	0.03	0.17	13.87	0.26	45.66	0.06	0.00	0.00	0.02	100.08	fe rich	
Concentrate		olivine	41.08	0.00	0.03	0.00	0.11	0.09	7.30	0.40	50.61	0.03	0.00	0.00	0.00	99.66		
Concentrate		olivine	39.72	0.06	0.01	0.00	0.01	0.14	14.96	0.08	44.86	0.03	0.00	0.00	0.01	99.88	fe rich	
Concentrate		olivine	40.54	0.01	0.00	0.01	0.00	0.28	10.81	0.33	47.70	0.01	0.00	0.00	0.01	99.70	fe rich	
Concentrate		olivine	40.77	0.03	0.03	0.00	0.06	0.12	9.35	0.38	48.88	0.09	0.00	0.00	0.01	99.70		
Concentrate		olivine	41.00	0.00	0.02	0.00	0.00	0.11	7.77	0.38	50.22	0.00	0.00	0.00	0.01	99.51		
Concentrate		olivine	40.53	0.02	0.05	0.00	0.03	0.13	10.59	0.33	47.97	0.08	0.00	0.00	0.00	99.73	fe rich	
Concentrate		olivine	40.49	0.02	0.04	0.00	0.06	0.11	10.55	0.32	48.00	0.08	0.00	0.00	0.00	99.67	fe rich	
Concentrate		olivine	39.91	0.06	0.01	0.01	0.00	0.16	14.22	0.16	45.06	0.03	0.00	0.00	0.02	99.64	fe rich	
Concentrate		olivine	41.19	0.00	0.00	0.00	0.02	0.11	7.65	0.37	50.66	0.01	0.00	0.00	0.00	100.01		

sample name	rock type	mineral from composition	SiO2	TiO2	Al2O3	V2O3	Cr2O3	MnO	FeO	NiO	MgO	CaO	Na2O	K2O	P2O5	Total	notes	Crust-Mantle
Concentrate		olivine	40.18	0.00	0.01	0.00	0.01	0.13	11.85	0.32	47.60	0.02	0.00	0.00	0.00	100.13	fe rich	
Concentrate		olivine	40.76	0.03	0.03	0.00	0.06	0.13	8.91	0.37	49.59	0.09	0.00	0.00	0.00	99.99		
Concentrate		olivine	41.06	0.00	0.00	0.00	0.00	0.10	7.48	0.35	51.16	0.00	0.00	0.00	0.01	100.18		
Concentrate		olivine	40.03	0.04	0.04	0.00	0.01	0.14	13.70	0.18	46.12	0.05	0.00	0.00	0.00	100.31	fe rich	
Concentrate		olivine	40.58	0.02	0.04	0.01	0.02	0.13	10.35	0.33	48.57	0.09	0.00	0.00	0.01	100.14	fe rich	
Concentrate		olivine	41.04	0.01	0.01	0.00	0.00	0.09	7.58	0.35	50.65	0.00	0.00	0.00	0.01	99.73		
Concentrate		olivine	40.97	0.01	0.02	0.00	0.05	0.10	8.28	0.38	49.98	0.05	0.00	0.00	0.01	99.85		
Concentrate		olivine	40.79	0.01	0.05	0.01	0.06	0.11	9.17	0.37	49.33	0.11	0.00	0.00	0.00	100.01		
Concentrate		olivine	40.41	0.00	0.00	0.00	0.01	0.23	11.46	0.31	47.39	0.02	0.00	0.00	0.02	99.83	fe rich	
Concentrate		olivine	40.17	0.04	0.03	0.01	0.06	0.13	12.16	0.29	46.71	0.08	0.00	0.00	0.03	99.70	fe rich	
Concentrate		olivine	41.08	0.00	0.00	0.00	0.00	0.11	7.48	0.35	50.93	0.00	0.00	0.00	0.00	99.96		
Concentrate		olivine	39.90	0.04	0.02	0.01	0.02	0.17	13.71	0.23	45.77	0.07	0.00	0.00	0.02	99.95	fe rich	
Concentrate		olivine	39.59	0.03	0.01	0.00	0.01	0.17	15.72	0.06	43.93	0.03	0.00	0.00	0.01	99.56	fe rich	
Concentrate		olivine	41.15	0.00	0.00	0.00	0.01	0.10	7.23	0.37	50.89	0.00	0.00	0.00	0.01	99.76		
Concentrate		olivine	41.10	0.01	0.00	0.02	0.00	0.11	7.43	0.37	51.01	0.01	0.00	0.00	0.00	100.04		
Concentrate		olivine	41.03	0.06	0.03	0.00	0.05	0.12	8.84	0.39	49.49	0.05	0.00	0.00	0.00	100.05		
Concentrate		olivine	40.99	0.05	0.02	0.00	0.07	0.11	7.49	0.40	50.74	0.04	0.00	0.00	0.00	99.90		
Concentrate		olivine	41.17	0.01	0.02	0.00	0.02	0.11	6.98	0.35	51.16	0.00	0.00	0.00	0.01	99.83		
Concentrate		olivine	41.17	0.01	0.00	0.00	0.01	0.10	7.19	0.38	51.35	0.00	0.00	0.00	0.00	100.21		
Concentrate		olivine	40.40	0.00	0.01	0.01	0.00	0.12	10.94	0.37	48.09	0.02	0.00	0.00	0.01	99.98	fe rich	
Concentrate		olivine	40.67	0.02	0.05	0.00	0.04	0.13	9.86	0.34	48.34	0.09	0.00	0.00	0.00	99.54		
Concentrate		olivine	40.30	0.05	0.04	0.00	0.02	0.12	12.85	0.27	46.39	0.06	0.00	0.00	0.02	100.13	fe rich	
Concentrate		olivine	40.57	0.03	0.00	0.00	0.01	0.16	9.80	0.35	48.43	0.01	0.00	0.01	0.00	99.37		
Concentrate		olivine	41.05	0.00	0.01	0.00	0.00	0.12	7.95	0.36	50.31	0.00	0.00	0.00	0.00	99.81		
Concentrate		olivine	40.48	0.01	0.06	0.00	0.03	0.12	10.54	0.33	48.08	0.09	0.00	0.01	0.00	99.75	fe rich	
Concentrate		olivine	40.42	0.02	0.03	0.00	0.04	0.14	12.10	0.17	46.65	0.08	0.00	0.00	0.01	99.67	fe rich	
Concentrate		olivine	41.39	0.00	0.01	0.00	0.01	0.12	6.64	0.36	51.33	0.00	0.00	0.00	0.00	99.87		
Concentrate		olivine	40.34	0.04	0.03	0.00	0.05	0.14	11.86	0.31	46.87	0.06	0.00	0.00	0.00	99.70		
Concentrate		olivine	39.95	0.03	0.03	0.00	0.01	0.15	13.64	0.16	45.54	0.04	0.00	0.00	0.02	99.56	fe rich	
Concentrate		olivine	40.95	0.01	0.04	0.00	0.07	0.11	8.44	0.38	49.52	0.07	0.00	0.00	0.01	99.62		
Concentrate		olivine	41.21	0.00	0.00	0.00	0.00	0.12	7.59	0.37	50.82	0.00	0.00	0.01	0.00	100.11		
Concentrate		olivine	41.28	0.00	0.00	0.00	0.00	0.11	7.36	0.34	50.73	0.01	0.00	0.00	0.00	99.83		
Concentrate		olivine	40.21	0.05	0.01	0.01	0.04	0.15	12.87	0.27	46.42	0.07	0.00	0.00	0.02	100.13	fe rich	
Concentrate		olivine	41.21	0.02	0.00	0.00	0.01	0.11	7.70	0.36	50.85	0.00	0.00	0.00	0.00	100.26		
Concentrate		olivine	41.22	0.01	0.00	0.01	0.00	0.09	7.56	0.37	50.90	0.01	0.00	0.00	0.01	100.20		
Concentrate		olivine	40.91	0.05	0.02	0.00	0.03	0.11	9.39	0.39	49.34	0.05	0.00	0.01	0.00	100.30		
Concentrate		olivine	39.97	0.05	0.02	0.01	0.05	0.16	13.53	0.25	45.92	0.06	0.00	0.00	0.03	100.07	fe rich	
Concentrate		olivine	40.18	0.01	0.00	0.00	0.00	0.25	13.15	0.29	46.11	0.01	0.00	0.00	0.02	100.03	fe rich	
Concentrate		olivine	40.08	0.04	0.02	0.00	0.05	0.17	13.27	0.23	46.05	0.07	0.00	0.01	0.03	100.01	fe rich	
Concentrate		olivine	41.22	0.00	0.01	0.02	0.00	0.11	7.48	0.36	50.91	0.00	0.00	0.00	0.00	100.12		
Concentrate		olivine	40.21	0.05	0.02	0.00	0.00	0.14	13.90	0.12	45.75	0.02	0.00	0.00	0.03	100.23	fe rich	
Concentrate		olivine	40.66	0.01	0.07	0.01	0.07	0.13	10.42	0.35	48.16	0.09	0.00	0.00	0.00	99.96	fe rich	
Concentrate		olivine	41.03	0.06	0.03	0.00	0.07	0.10	8.04	0.40	50.30	0.05	0.00	0.00	0.00	100.08		
Concentrate		olivine	41.18	0.00	0.01	0.03	0.00	0.11	7.07	0.36	51.15	0.01	0.00	0.00	0.01	99.92		
Concentrate		olivine	41.14	0.01	0.02	0.00	0.02	0.10	7.04	0.37	51.28	0.00	0.00	0.00	0.01	99.98		
Concentrate		olivine	40.81	0.02	0.01	0.00	0.03	0.10	9.41	0.37	49.09	0.01	0.00	0.00	0.02	99.88		
Concentrate		olivine	40.17	0.06	0.02	0.01	0.03	0.13	13.01	0.24	45.96	0.07	0.00	0.00	0.01	99.71	fe rich	
Concentrate		olivine	40.75	0.02	0.06	0.01	0.06	0.13	9.98	0.35	48.83	0.10	0.00	0.00	0.00	100.28		
Concentrate		olivine	40.41	0.04	0.04	0.00	0.05	0.12	11.15	0.32	47.52	0.07	0.00	0.00	0.02	99.74	fe rich	

sample name	rock type	mineral from composition	SiO2	TiO2	Al2O3	V2O3	Cr2O3	MnO	FeO	NiO	MgO	CaO	Na2O	K2O	P2O5	Total	notes	Crust-Mantle
Concentrate		olivine	40.84	0.01	0.01	0.01	0.00	0.14	8.09	0.36	50.08	0.00	0.00	0.00	0.02	99.56		
Concentrate		olivine	40.43	0.03	0.04	0.01	0.08	0.12	10.36	0.36	48.04	0.10	0.00	0.01	0.01	99.59	fe rich	
Concentrate		olivine	41.11	0.00	0.01	0.02	0.03	0.10	7.76	0.39	50.23	0.01	0.00	0.00	0.00	99.66		
Concentrate		olivine	41.18	0.00	0.01	0.00	0.02	0.09	7.03	0.35	50.99	0.01	0.00	0.00	0.01	99.68		
Concentrate		olivine	40.83	0.03	0.05	0.00	0.07	0.12	9.57	0.36	48.48	0.10	0.00	0.00	0.00	99.61		
Concentrate		olivine	40.62	0.00	0.01	0.01	0.00	0.21	10.78	0.33	47.79	0.01	0.00	0.00	0.00	99.76	fe rich	
Concentrate		olivine	41.08	0.00	0.02	0.00	0.01	0.12	7.90	0.31	50.07	0.00	0.00	0.00	0.01	99.53		
Concentrate		olivine	41.06	0.00	0.00	0.00	0.00	0.17	8.31	0.37	49.73	0.00	0.00	0.00	0.00	99.64		
Concentrate		olivine	40.60	0.04	0.02	0.00	0.05	0.12	10.37	0.36	47.90	0.07	0.00	0.00	0.02	99.55	fe rich	
Concentrate		olivine	40.91	0.00	0.01	0.00	0.01	0.21	8.97	0.37	49.31	0.01	0.00	0.00	0.01	99.81		
Concentrate		olivine	40.48	0.03	0.03	0.00	0.03	0.12	10.95	0.32	47.85	0.07	0.00	0.00	0.01	99.88	fe rich	
Concentrate		olivine	41.29	0.00	0.01	0.00	0.01	0.09	6.79	0.37	51.06	0.00	0.00	0.00	0.00	99.62		
Concentrate		olivine	41.11	0.00	0.01	0.00	0.01	0.12	7.60	0.36	50.52	0.01	0.00	0.00	0.00	99.74		
Concentrate		olivine	41.08	0.00	0.00	0.00	0.00	0.11	7.77	0.36	50.32	0.01	0.00	0.00	0.01	99.65		
Concentrate		olivine	40.31	0.03	0.02	0.02	0.04	0.14	11.43	0.32	47.27	0.07	0.00	0.00	0.02	99.67	fe rich	
Concentrate		olivine	41.32	0.00	0.00	0.00	0.01	0.10	7.42	0.37	50.78	0.00	0.00	0.01	0.01	100.02		
Concentrate		olivine	41.15	0.00	0.02	0.00	0.02	0.10	7.39	0.38	50.60	0.01	0.00	0.00	0.00	99.68		
Concentrate		olivine	41.23	0.02	0.02	0.01	0.05	0.09	6.92	0.36	51.10	0.05	0.00	0.00	0.00	99.86		
Concentrate		olivine	41.25	0.01	0.00	0.00	0.00	0.11	7.24	0.38	51.13	0.00	0.00	0.00	0.01	100.14		
Concentrate		olivine	41.29	0.01	0.00	0.01	0.00	0.09	6.75	0.36	51.26	0.00	0.00	0.00	0.00	99.78		
Concentrate		olivine	40.48	0.04	0.00	0.00	0.08	0.13	11.16	0.33	47.31	0.08	0.00	0.00	0.01	99.64	fe rich	
Concentrate		olivine	40.29	0.05	0.02	0.00	0.05	0.14	12.07	0.25	47.07	0.06	0.00	0.00	0.02	100.03	fe rich	
Concentrate		olivine	39.96	0.06	0.00	0.00	0.03	0.16	13.63	0.22	45.27	0.07	0.00	0.00	0.07	99.47	fe rich	
Concentrate		olivine	40.88	0.01	0.05	0.01	0.10	0.11	9.68	0.35	48.85	0.10	0.00	0.00	0.01	100.17		
Concentrate		olivine	41.22	0.00	0.04	0.01	0.13	0.11	7.28	0.40	50.74	0.03	0.00	0.00	0.00	99.96		
Concentrate		olivine	40.03	0.07	0.00	0.00	0.03	0.13	12.81	0.27	46.25	0.06	0.00	0.00	0.01	99.65	fe rich	
Concentrate		olivine	40.71	0.02	0.04	0.01	0.05	0.12	10.26	0.36	47.80	0.11	0.00	0.00	0.01	99.48	fe rich	
Concentrate		olivine	41.03	0.01	0.04	0.01	0.09	0.11	8.08	0.38	49.87	0.09	0.00	0.00	0.00	99.71		
Concentrate		olivine	40.26	0.03	0.03	0.00	0.05	0.15	12.32	0.31	46.45	0.07	0.00	0.00	0.02	99.68	fe rich	
Concentrate		olivine	41.08	0.00	0.02	0.00	0.01	0.10	7.80	0.34	50.07	0.01	0.00	0.00	0.02	99.45		
Concentrate		olivine	41.19	0.00	0.00	0.00	0.00	0.13	7.58	0.33	50.04	0.00	0.00	0.00	0.00	99.28		
Concentrate		olivine	40.76	0.03	0.04	0.03	0.03	0.12	9.16	0.37	49.13	0.09	0.00	0.00	0.01	99.77		
Concentrate		olivine	40.69	0.04	0.01	0.00	0.04	0.12	10.38	0.34	47.86	0.07	0.00	0.00	0.00	99.57	fe rich	
Concentrate		olivine	41.21	0.00	0.00	0.00	0.00	0.13	7.69	0.33	50.42	0.00	0.00	0.00	0.00	99.79		
Concentrate		olivine	40.17	0.05	0.02	0.01	0.02	0.16	12.22	0.29	46.49	0.07	0.00	0.00	0.01	99.49	fe rich	
Concentrate		olivine	40.62	0.02	0.03	0.01	0.06	0.13	10.45	0.34	47.92	0.08	0.00	0.00	0.02	99.67	fe rich	
Concentrate		olivine	41.15	0.02	0.00	0.00	0.00	0.12	7.53	0.35	50.35	0.00	0.00	0.00	0.00	99.53		
Concentrate		olivine	41.11	0.01	0.05	0.01	0.07	0.10	8.02	0.37	49.48	0.10	0.00	0.00	0.02	99.33		
Concentrate		olivine	41.01	0.04	0.03	0.00	0.06	0.11	7.92	0.42	49.96	0.05	0.00	0.01	0.00	99.62		
Concentrate		olivine	40.67	0.03	0.03	0.00	0.03	0.14	10.28	0.34	48.39	0.09	0.00	0.00	0.00	100.00	fe rich	
Concentrate		olivine	40.40	0.05	0.01	0.00	0.05	0.13	11.31	0.32	47.36	0.07	0.00	0.00	0.03	99.73	fe rich	
Concentrate		olivine	41.30	0.00	0.00	0.00	0.11	0.10	7.25	0.41	50.70	0.04	0.00	0.00	0.00	99.92		
Concentrate		olivine	39.89	0.04	0.02	0.00	0.00	0.15	14.34	0.07	45.08	0.03	0.00	0.00	0.01	99.66	fe rich	
Concentrate		olivine	40.10	0.05	0.01	0.00	0.00	0.14	13.06	0.22	45.98	0.04	0.00	0.00	0.03	99.62	fe rich	
Concentrate		olivine	39.46	0.02	0.00	0.00	0.00	0.18	16.49	0.05	43.46	0.02	0.00	0.00	0.00	99.68	fe rich	
Concentrate		olivine	41.14	0.01	0.00	0.00	0.00	0.11	7.62	0.35	50.58	0.00	0.00	0.00	0.00	99.81		
Concentrate		olivine	40.90	0.00	0.00	0.00	0.00	0.17	8.39	0.38	50.03	0.01	0.00	0.00	0.01	99.90		
Concentrate		olivine	40.96	0.00	0.01	0.00	0.12	0.10	7.40	0.41	50.78	0.03	0.00	0.00	0.00	99.81		
Concentrate		olivine	41.02	0.00	0.00	0.00	0.01	0.12	7.43	0.36	50.68	0.00	0.00	0.00	0.00	99.62		

sample name	rock type	mineral from composition	SiO2	TiO2	Al2O3	V2O3	Cr2O3	MnO	FeO	NiO	MgO	CaO	Na2O	K2O	P2O5	Total	notes	Crust-Mantle
Concentrate		olivine	40.49	0.02	0.03	0.01	0.04	0.11	10.29	0.32	48.55	0.08	0.00	0.00	0.00	99.96	fe rich	
Concentrate		olivine	40.75	0.03	0.02	0.00	0.12	0.12	8.33	0.39	49.88	0.10	0.00	0.00	0.00	99.73		
Concentrate		olivine	39.97	0.06	0.03	0.00	0.02	0.14	12.97	0.22	46.15	0.05	0.00	0.00	0.00	99.60	fe rich	
Concentrate		olivine	40.18	0.02	0.01	0.02	0.00	0.21	11.77	0.32	46.93	0.02	0.00	0.00	0.02	99.50	fe rich	
Concentrate		orthopyroxene	57.02	0.17	0.59	0.01	0.01	0.17	8.34	0.04	32.63	0.81	0.11	0.00	0.00	99.88		
Concentrate		orthopyroxene	57.16	0.14	0.57	0.01	0.04	0.16	7.92	0.03	32.73	0.63	0.09	0.00	0.01	99.49		
Concentrate		orthopyroxene	56.95	0.13	0.63	0.02	0.03	0.17	8.23	0.02	32.61	0.75	0.11	0.00	0.01	99.66		
Concentrate		perovskite	0.06	50.62	0.33	0.00	0.30	0.00	2.23	0.01	0.00	36.22	0.58	0.02	0.00	90.36		
Concentrate		perovskite	0.04	52.40	0.24	0.00	0.38	0.02	1.81	0.00	0.00	36.94	0.59	0.01	0.00	92.42		
Concentrate		Picotite = chromian spinel	0.00	0.29	20.42	0.19	48.66	0.43	18.39	0.04	10.98	0.01	0.01	0.00	0.01	99.43		
Concentrate		Picotite = chromian spinel	0.00	0.02	30.66	0.16	38.59	0.30	15.40	0.06	14.21	0.00	0.01	0.00	0.00	99.41		
Concentrate		Picotite = chromian spinel	0.01	0.07	28.24	0.14	41.45	0.33	15.90	0.05	13.37	0.00	0.01	0.00	0.00	99.58		
Concentrate		Picotite = chromian spinel	0.00	0.17	15.85	0.21	50.29	0.74	22.25	0.05	9.08	0.00	0.02	0.01	0.00	98.67		
Concentrate		Picotite = chromian spinel	0.06	6.59	6.80	0.30	41.55	0.68	29.07	0.15	12.76	0.06	0.01	0.00	0.02	98.04		
Concentrate		titanomagnitite	0.01	34.53	0.50	0.30	2.16	0.17	53.05	0.08	6.42	0.01	0.00	0.00	0.00	97.23		
Concentrate		titanomagnitite	0.01	32.20	0.06	0.40	1.38	0.49	55.42	0.06	6.46	0.02	0.05	0.00	0.00	96.55		
Macrocrysts		chromite	0.10	0.21	0.30	0.27	59.78	0.46	30.01	0.08	7.21	0.03	0.04	0.05	0.00	98.54	mg rich	
Macrocrysts		chromite	0.14	8.01	6.12	0.29	41.54	0.24	32.18	0.22	11.69	0.00	0.00	0.00	0.00	100.44	Cr rich	
Macrocrysts		chromite	0.13	7.85	6.29	0.26	41.70	0.29	32.10	0.23	11.81	0.02	0.01	0.00	0.00	100.68	Cr rich	
Macrocrysts		augite	54.11	0.23	1.76	0.05	0.09	0.14	4.65	0.02	17.70	18.92	1.43	0.02	0.01	99.12		
Macrocrysts		augite	53.91	0.20	1.74	0.05	0.08	0.13	4.59	0.02	17.61	19.08	1.38	0.02	0.02	98.82		
Macrocrysts		augite	54.03	0.43	1.08	0.02	0.06	0.12	5.04	0.01	16.41	21.46	1.02	0.00	0.01	99.69		
Macrocrysts		augite	47.19	0.15	1.35	0.01	0.05	0.12	10.71	0.01	15.14	23.87	1.29	0.00	0.02	99.90		
Macrocrysts		diopside	54.37	0.33	0.28	0.00	0.37	0.05	1.84	0.04	17.30	23.87	0.70	0.00	0.02	99.16		
Macrocrysts		diopside	53.95	0.03	0.63	0.01	0.52	0.04	1.32	0.04	17.94	23.99	0.35	0.24	0.02	99.07		
Macrocrysts		diopside	54.77	0.16	0.28	0.01	0.27	0.04	1.82	0.05	17.33	24.01	0.64	0.01	0.03	99.42		
Macrocrysts		diopside	55.07	0.05	0.13	0.03	0.32	0.01	1.15	0.06	17.70	24.48	0.48	0.02	0.02	99.52		
Macrocrysts		ilmenite	0.02	49.68	0.38	0.23	6.21	0.97	21.02	0.04	20.21	0.07	0.04	0.00	0.00	98.87		
Macrocrysts		ilmenite	0.06	52.40	0.00	0.20	0.00	2.88	44.19	0.11	0.22	0.03	0.02	0.00	0.00	100.10	Mn rich	
Macrocrysts		ilmenite	0.08	51.66	0.01	0.14	0.00	3.56	43.14	0.06	0.19	0.60	0.05	0.00	0.01	99.49	Mn rich	
Macrocrysts		ilmenite	0.04	52.02	0.01	0.03	0.00	4.04	43.25	0.04	0.12	0.06	0.10	0.01	0.00	99.71	Mn rich	
Macrocrysts		ilmenite	0.04	47.97	0.03	0.18	0.84	0.29	41.85	0.04	7.88	0.04	0.42	0.01	0.01	99.58		
Macrocrysts		ilmenite	0.15	51.53	0.00	0.02	0.00	3.52	43.27	0.03	0.08	0.30	0.00	0.01	0.01	98.92		
Macrocrysts		ilmenite	0.06	52.84	0.60	0.24	2.04	0.48	28.55	0.13	15.59	0.14	0.07	0.01	0.00	100.74	Cr rich	
Macrocrysts		ilmenite	0.07	48.45	0.65	0.16	7.95	0.94	22.35	0.03	20.23	0.26	0.02	0.01	0.00	101.12	Cr rich	
Macrocrysts		ilmenite	0.03	47.08	0.71	0.22	8.85	0.90	22.37	0.03	20.21	0.09	0.04	0.00	0.00	100.54	Cr rich	
Macrocrysts		ilmenite	0.03	47.89	0.18	0.22	1.29	0.40	36.92	0.07	11.58	0.05	0.44	0.00	0.00	99.07	Cr rich	
Macrocrysts		ilmenite	0.05	49.13	0.16	0.23	0.99	0.22	41.35	0.04	7.16	0.11	0.38	0.00	0.00	99.80		
Macrocrysts		ilmenite	0.06	51.56	0.06	0.23	0.22	0.49	38.55	0.12	9.06	0.04	0.20	0.01	0.00	100.59		
Macrocrysts		ilmenite	0.05	52.35	0.03	0.26	0.25	0.47	36.67	0.08	10.14	0.07	0.05	0.00	0.01	100.43		
Macrocrysts		ilmenite	0.06	52.62	0.08	0.29	0.27	0.44	35.80	0.10	11.20	0.06	0.06	0.00	0.00	100.97		
Macrocrysts		ilmenite	0.05	52.67	0.05	0.22	0.25	0.43	35.48	0.07	11.11	0.11	0.04	0.00	0.00	100.48		
Macrocrysts		ilmenite	0.06	52.40	0.08	0.27	0.28	0.44	35.86	0.07	11.04	0.08	0.07	0.00	0.00	100.66		
Macrocrysts		ilmenite	0.06	52.53	0.18	0.30	0.30	0.38	34.54	0.06	12.04	0.09	0.06	0.00	0.00	100.54		
Macrocrysts		ilmenite	0.05	52.73	0.09	0.24	0.21	0.43	34.55	0.08	11.87	0.27	0.07	0.01	0.00	100.58		
Macrocrysts		ilmenite	0.05	52.14	0.04	0.25	0.00	0.47	35.60	0.08	11.42	0.16	0.00	0.00	0.00	100.19		
Macrocrysts		ilmenite	0.07	52.17	0.02	0.27	0.06	0.46	35.53	0.08	11.33	0.19	0.05	0.00	0.01	100.25		
Macrocrysts		ilmenite	0.05	50.18	0.47	0.34	0.00	0.22	37.64	0.08	11.18	0.06	0.10	0.00	0.00	100.31		
Macrocrysts		ilmenite	0.04	41.23	1.59	0.40	0.21	0.26	45.32	0.10	10.89	0.07	0.18	0.00	0.00	100.29		

sample name	rock type	mineral from composition	SiO2	TiO2	Al2O3	V2O3	Cr2O3	MnO	FeO	NiO	MgO	CaO	Na2O	K2O	P2O5	Total	notes	Crust-Mantle
Macrocrysts		ilmenite	0.05	44.76	1.53	0.40	0.17	0.38	39.31	0.12	13.63	0.05	0.18	0.00	0.00	100.57		
Macrocrysts		ilmenite	0.06	50.68	0.74	0.37	0.00	0.35	33.61	0.10	14.27	0.06	0.24	0.01	0.00	100.49		
Macrocrysts		ilmenite	0.02	51.46	0.11	0.12	0.58	0.42	35.09	0.06	11.17	0.06	0.34	0.00	0.01	99.42		
Macrocrysts		ilmenite	0.09	54.22	0.11	0.10	0.37	0.40	31.58	0.06	13.19	0.07	0.40	0.01	0.00	100.59		
Macrocrysts		ilmenite	0.15	20.57	0.38	0.42	0.69	0.48	67.65	0.22	7.19	1.29	0.08	0.01	0.00	99.13	fe rich	
Macrocrysts		magnetite	0.06	19.08	0.38	0.45	0.91	0.49	69.74	0.19	7.30	0.25	0.09	0.00	0.01	98.93		
Macrocrysts		olivine	40.83	0.05	0.01	0.00	0.01	0.11	7.84	0.37	49.81	0.04	0.01	0.00	0.01	99.09		
Macrocrysts		olivine	40.79	0.04	0.02	0.00	0.03	0.11	7.73	0.37	49.56	0.05	0.01	0.00	0.00	98.71		
Macrocrysts		olivine	41.13	0.06	0.02	0.00	0.02	0.11	7.81	0.36	49.91	0.05	0.01	0.00	0.01	99.50		
Macrocrysts		olivine	40.87	0.03	0.02	0.00	0.02	0.11	7.78	0.36	49.68	0.05	0.03	0.00	0.00	98.96		
Macrocrysts		olivine	39.99	0.04	0.01	0.01	0.00	0.16	14.32	0.10	44.52	0.04	0.01	0.00	0.00	99.19		
Macrocrysts		olivine	39.85	0.02	0.02	0.00	0.00	0.17	14.33	0.11	44.69	0.04	0.02	0.00	0.01	99.25		
Macrocrysts		olivine	39.93	0.04	0.01	0.00	0.00	0.14	14.22	0.09	44.74	0.03	0.02	0.00	0.01	99.23		
Macrocrysts		olivine	39.94	0.03	0.02	0.01	0.01	0.16	14.29	0.09	44.81	0.04	0.01	0.00	0.03	99.44		
Macrocrysts		olivine	39.95	0.04	0.00	0.00	0.00	0.15	13.59	0.11	45.08	0.05	0.01	0.00	0.01	98.99		
Macrocrysts		olivine	39.74	0.05	0.01	0.00	0.00	0.14	13.64	0.11	45.00	0.04	0.02	0.00	0.01	98.75		
Macrocrysts		olivine	39.78	0.03	0.00	0.01	0.00	0.14	13.60	0.12	44.94	0.04	0.01	0.00	0.02	98.69		
Macrocrysts		olivine	39.86	0.05	0.00	0.00	0.00	0.12	13.68	0.12	44.96	0.04	0.01	0.00	0.03	98.87		
Macrocrysts		olivine	41.19	0.03	0.02	0.00	0.03	0.12	7.81	0.37	49.85	0.06	0.03	0.00	0.00	99.50		
Macrocrysts		olivine	41.02	0.04	0.03	0.01	0.05	0.12	8.04	0.37	49.62	0.05	0.01	0.00	0.01	99.37		
Macrocrysts		olivine	40.95	0.03	0.02	0.00	0.05	0.11	7.90	0.36	49.71	0.05	0.01	0.00	0.00	99.19		
Macrocrysts		olivine	40.41	0.04	0.01	0.00	0.07	0.15	11.17	0.33	46.90	0.07	0.03	0.00	0.01	99.18		
Macrocrysts		olivine	40.10	0.03	0.01	0.01	0.07	0.15	12.44	0.27	46.05	0.07	0.00	0.00	0.00	99.21		
Macrocrysts		olivine	41.34	0.00	0.00	0.00	0.00	0.14	7.49	0.37	50.00	0.01	0.00	0.00	0.01	99.35		
Macrocrysts		olivine	41.15	0.00	0.00	0.00	0.02	0.14	7.47	0.36	49.91	0.01	0.00	0.00	0.00	99.05		
Macrocrysts		olivine	41.45	0.00	0.00	0.00	0.00	0.14	7.55	0.37	50.13	0.00	0.00	0.00	0.00	99.63		
Macrocrysts		olivine	40.15	0.02	0.02	0.00	0.00	0.18	14.70	0.10	44.22	0.02	0.00	0.00	0.01	99.42		
Macrocrysts		olivine	40.01	0.03	0.01	0.02	0.00	0.18	14.62	0.09	44.55	0.04	0.02	0.00	0.00	99.56		
Macrocrysts		olivine	40.01	0.03	0.00	0.00	0.00	0.17	14.55	0.10	44.63	0.02	0.00	0.00	0.02	99.53		
Macrocrysts		olivine	40.18	0.02	0.00	0.00	0.00	0.18	14.51	0.09	44.49	0.03	0.02	0.00	0.00	99.52		
Macrocrysts		olivine	40.11	0.02	0.01	0.01	0.00	0.18	14.52	0.08	44.73	0.03	0.00	0.00	0.00	99.68		
Macrocrysts		olivine	41.52	0.06	0.02	0.01	0.06	0.10	6.92	0.36	50.16	0.05	0.03	0.00	0.00	99.30		
Macrocrysts		olivine	41.38	0.06	0.02	0.00	0.06	0.11	6.95	0.37	50.50	0.05	0.02	0.00	0.00	99.52		
Macrocrysts		olivine	41.09	0.07	0.02	0.01	0.08	0.11	6.93	0.36	50.43	0.05	0.02	0.00	0.00	99.16		
Macrocrysts		olivine	41.17	0.04	0.00	0.00	0.06	0.10	6.96	0.37	50.51	0.06	0.03	0.00	0.01	99.29		
Macrocrysts		olivine	40.49	0.02	0.01	0.02	0.02	0.13	11.65	0.28	47.06	0.06	0.01	0.01	0.02	99.78		
Macrocrysts		olivine	40.47	0.05	0.01	0.00	0.03	0.14	11.51	0.28	47.29	0.06	0.02	0.00	0.01	99.86		
Macrocrysts		olivine	40.43	0.04	0.01	0.01	0.03	0.12	11.55	0.27	47.22	0.06	0.01	0.00	0.01	99.76		
Macrocrysts		olivine	39.44	0.02	0.01	0.00	0.00	0.19	15.52	0.06	43.55	0.03	0.00	0.00	0.00	98.84		
Macrocrysts		olivine	39.20	0.04	0.00	0.00	0.00	0.15	13.02	0.11	45.97	0.05	0.00	0.00	0.01	98.54		
Macrocrysts		olivine	39.76	0.04	0.00	0.00	0.01	0.15	13.02	0.10	46.00	0.03	0.00	0.00	0.02	99.11		
Macrocrysts		olivine	40.22	0.04	0.01	0.01	0.05	0.13	10.67	0.32	48.04	0.09	0.00	0.00	0.00	99.59		
Macrocrysts		olivine	39.92	0.03	0.04	0.00	0.06	0.13	9.67	0.34	49.16	0.08	0.01	0.00	0.00	99.43		
Macrocrysts		olivine	40.69	0.01	0.00	0.00	0.01	0.08	6.33	0.37	51.80	0.00	0.00	0.00	0.00	99.29		
Macrocrysts		olivine	40.60	0.00	0.00	0.00	0.01	0.10	6.33	0.38	51.81	0.00	0.00	0.00	0.01	99.23		
Macrocrysts		olivine	40.62	0.00	0.00	0.01	0.00	0.10	6.28	0.38	51.84	0.00	0.01	0.00	0.01	99.24		
Macrocrysts		olivine	40.54	0.00	0.00	0.00	0.00	0.08	6.19	0.37	51.81	0.01	0.00	0.00	0.00	99.01		
Macrocrysts		olivine	40.35	0.00	0.00	0.00	0.01	0.09	6.34	0.38	51.67	0.00	0.06	0.02	0.00	98.90		
Macrocrysts		olivine	40.24	0.02	0.05	0.01	0.03	0.12	9.75	0.36	49.09	0.10	0.03	0.00	0.01	99.81		

sample name	rock type	mineral from composition	SiO2	TiO2	Al2O3	V2O3	Cr2O3	MnO	FeO	NiO	MgO	CaO	Na2O	K2O	P2O5	Total	notes	Crust-Mantle
Macrocrysts		olivine	39.64	0.03	0.01	0.00	0.03	0.13	11.76	0.30	47.21	0.06	0.00	0.01	0.00	99.18		
Macrocrysts		olivine	39.43	0.04	0.02	0.00	0.02	0.16	13.56	0.14	46.19	0.06	0.01	0.00	0.01	99.63		
Macrocrysts		olivine	39.26	0.05	0.02	0.00	0.02	0.17	14.15	0.07	45.97	0.05	0.01	0.00	0.00	99.77		
Macrocrysts		olivine	38.51	0.01	0.00	0.00	0.00	0.29	18.82	0.09	42.25	0.03	0.00	0.01	0.03	100.04		
Macrocrysts		olivine	39.88	0.04	0.03	0.00	0.05	0.13	9.68	0.35	48.79	0.09	0.02	0.00	0.00	99.04		
Macrocrysts		olivine	39.95	0.02	0.04	0.00	0.03	0.12	9.70	0.33	48.88	0.09	0.02	0.00	0.01	99.18		
Macrocrysts		olivine	39.86	0.01	0.04	0.00	0.06	0.12	9.63	0.35	48.68	0.09	0.01	0.00	0.00	98.85		
Macrocrysts		olivine	40.24	0.01	0.01	0.01	0.02	0.10	7.31	0.38	50.84	0.02	0.00	0.00	0.00	98.94		
Macrocrysts		olivine	40.41	0.00	0.00	0.01	0.01	0.10	7.28	0.37	50.86	0.01	0.01	0.00	0.00	99.07		
Macrocrysts		olivine	38.35	0.00	0.00	0.01	0.00	0.32	19.81	0.05	41.39	0.02	0.00	0.00	0.00	99.95		
Macrocrysts		olivine	38.19	0.00	0.00	0.00	0.01	0.33	19.81	0.04	41.25	0.03	0.01	0.00	0.00	99.67		
Macrocrysts		olivine	40.14	0.06	0.02	0.00	0.02	0.10	8.25	0.35	49.96	0.05	0.02	0.00	0.00	98.97		
Macrocrysts		olivine	40.32	0.05	0.01	0.00	0.03	0.11	8.21	0.36	50.03	0.05	0.01	0.00	0.01	99.18		
Macrocrysts		olivine	40.38	0.07	0.01	0.00	0.02	0.10	8.29	0.37	50.11	0.05	0.00	0.00	0.00	99.40		
Macrocrysts		olivine	40.26	0.00	0.00	0.00	0.01	0.10	9.63	0.36	49.43	0.01	0.01	0.00	0.01	99.83		
Macrocrysts		olivine	40.31	0.03	0.01	0.00	0.02	0.10	9.63	0.34	49.57	0.01	0.00	0.00	0.01	100.03		
Macrocrysts		olivine	40.28	0.00	0.00	0.00	0.01	0.11	9.66	0.35	49.21	0.01	0.00	0.00	0.01	99.64		
Macrocrysts		olivine	39.58	0.02	0.01	0.00	0.00	0.16	14.65	0.14	45.48	0.03	0.00	0.00	0.04	100.12		
Macrocrysts		olivine	40.33	0.02	0.00	0.00	0.06	0.12	9.16	0.37	49.54	0.10	0.01	0.00	0.00	99.71		
Macrocrysts		olivine	40.11	0.04	0.03	0.01	0.04	0.13	10.50	0.34	48.45	0.09	0.02	0.00	0.01	99.76		
Macrocrysts		olivine	39.71	0.05	0.02	0.00	0.00	0.14	13.09	0.18	46.69	0.06	0.01	0.00	0.02	99.96		
Macrocrysts		olivine	39.67	0.02	0.02	0.01	0.01	0.15	14.17	0.18	46.01	0.05	0.00	0.01	0.00	100.30		
Macrocrysts		olivine	39.48	0.03	0.00	0.01	0.01	0.16	15.49	0.07	45.23	0.00	0.03	0.00	0.00	100.51		
Macrocrysts		olivine	38.91	0.02	0.00	0.01	0.00	0.28	19.41	0.08	42.24	0.03	0.01	0.00	0.07	101.05		
Macrocrysts		olivine	38.93	0.00	0.00	0.01	0.00	0.28	19.35	0.07	42.30	0.03	0.00	0.00	0.00	100.97		
Macrocrysts		olivine	38.87	0.02	0.00	0.00	0.01	0.28	19.28	0.07	42.49	0.04	0.01	0.00	0.04	101.11		
Macrocrysts		olivine	39.10	0.01	0.00	0.00	0.01	0.29	19.63	0.08	42.31	0.03	0.00	0.01	0.07	101.54		
Macrocrysts		olivine	38.95	0.05	0.01	0.00	0.00	0.15	13.54	0.12	46.30	0.03	0.02	0.00	0.00	99.17		
Macrocrysts		olivine	38.96	0.05	0.00	0.00	0.00	0.16	13.45	0.11	46.20	0.03	0.00	0.00	0.03	98.97		
Macrocrysts		olivine	39.23	0.04	0.02	0.00	0.00	0.14	13.56	0.12	46.49	0.03	0.01	0.00	0.02	99.65		
Macrocrysts		olivine	39.42	0.04	0.00	0.00	0.01	0.16	13.65	0.11	46.29	0.04	0.00	0.00	0.04	99.75		
Macrocrysts		olivine	39.53	0.04	0.00	0.01	0.00	0.15	13.67	0.12	46.48	0.03	0.01	0.00	0.00	100.04		
Macrocrysts		olivine	38.79	0.01	0.00	0.00	0.01	0.28	18.36	0.11	42.56	0.03	0.01	0.00	0.02	100.18		
Macrocrysts		olivine	38.82	0.00	0.00	0.02	0.00	0.27	18.36	0.11	42.47	0.03	0.01	0.00	0.02	100.10		
Macrocrysts		olivine	39.49	0.03	0.01	0.01	0.01	0.16	14.92	0.06	45.29	0.03	0.01	0.00	0.02	100.04		
Macrocrysts		olivine	39.62	0.03	0.00	0.01	0.00	0.16	14.94	0.07	45.44	0.04	0.02	0.00	0.03	100.35		
Macrocrysts		olivine	39.49	0.03	0.00	0.01	0.00	0.17	13.21	0.32	46.33	0.02	0.01	0.00	0.02	99.62		
Macrocrysts		olivine	39.60	0.04	0.00	0.00	0.01	0.19	13.58	0.35	46.45	0.02	0.00	0.00	0.00	100.23		
Macrocrysts		olivine	39.61	0.05	0.02	0.00	0.02	0.15	13.45	0.14	46.17	0.05	0.00	0.00	0.00	99.66		
Macrocrysts		olivine	40.66	0.00	0.00	0.00	0.01	0.12	6.55	0.41	51.34	0.01	0.00	0.00	0.00	99.10		
Macrocrysts		olivine	40.79	0.00	0.00	0.00	0.00	0.21	8.43	0.36	49.54	0.01	0.00	0.00	0.00	99.34		
Macrocrysts		olivine	40.92	0.00	0.00	0.00	0.00	0.20	8.35	0.38	49.37	0.01	0.00	0.00	0.02	99.25		
Macrocrysts		olivine	40.95	0.00	0.01	0.00	0.00	0.21	8.41	0.38	49.50	0.01	0.00	0.00	0.00	99.47		
Macrocrysts		olivine	40.83	0.00	0.00	0.00	0.01	0.20	8.48	0.37	49.20	0.01	0.00	0.00	0.01	99.12		
Macrocrysts		olivine	40.66	0.03	0.01	0.01	0.07	0.15	9.74	0.42	48.36	0.09	0.01	0.00	0.02	99.56		
Macrocrysts		olivine	41.28	0.00	0.01	0.00	0.04	0.10	7.55	0.39	50.14	0.02	0.01	0.00	0.01	99.55		
Macrocrysts		olivine	41.14	0.00	0.01	0.01	0.03	0.09	7.54	0.40	50.33	0.01	0.01	0.00	0.00	99.58		
Macrocrysts		olivine	41.20	0.00	0.01	0.00	0.02	0.11	7.59	0.36	50.04	0.02	0.00	0.00	0.01	99.34		
Macrocrysts		olivine	41.12	0.01	0.09	0.00	0.05	0.12	8.72	0.37	48.84	0.09	0.05	0.00	0.00	99.46		

sample name	rock type	mineral from composition	SiO2	TiO2	Al2O3	V2O3	Cr2O3	MnO	FeO	NiO	MgO	CaO	Na2O	K2O	P2O5	Total	notes	Crust-Mantle
Macrocrysts		olivine	40.61	0.04	0.01	0.02	0.04	0.12	10.79	0.34	47.53	0.05	0.00	0.00	0.00	99.55		
Macrocrysts		olivine	40.74	0.03	0.00	0.01	0.04	0.14	10.06	0.37	47.91	0.08	0.01	0.00	0.01	99.40		
Macrocrysts		olivine	40.89	0.02	0.02	0.00	0.06	0.13	9.32	0.40	48.73	0.08	0.00	0.00	0.00	99.65		
Macrocrysts		olivine	41.46	0.00	0.00	0.01	0.01	0.13	6.97	0.35	50.71	0.00	0.01	0.00	0.00	99.65		
Macrocrysts		olivine	41.33	0.01	0.00	0.00	0.01	0.13	6.88	0.37	50.55	0.00	0.00	0.00	0.00	99.28		
Macrocrysts		olivine	41.29	0.00	0.00	0.00	0.00	0.13	6.90	0.33	50.67	0.00	0.00	0.00	0.01	99.32		
Macrocrysts		olivine	41.05	0.01	0.00	0.02	0.00	0.13	6.83	0.35	50.65	0.00	0.00	0.00	0.01	99.06		
Macrocrysts		olivine	41.15	0.01	0.00	0.01	0.00	0.12	6.85	0.34	50.63	0.00	0.00	0.00	0.02	99.13		
Macrocrysts		olivine	41.35	0.00	0.00	0.00	0.02	0.11	6.81	0.35	50.50	0.01	0.01	0.00	0.01	99.16		
Macrocrysts		olivine	41.28	0.02	0.01	0.00	0.00	0.12	6.93	0.42	50.50	0.01	0.01	0.00	0.00	99.29		
Macrocrysts		olivine	41.09	0.00	0.00	0.00	0.01	0.13	6.98	0.39	50.61	0.02	0.01	0.00	0.00	99.23		
Macrocrysts		olivine	40.52	0.04	0.01	0.00	0.16	0.25	10.88	0.18	47.08	0.37	0.02	0.00	0.06	99.56		
Macrocrysts		olivine	41.23	0.02	0.00	0.01	0.00	0.12	6.89	0.34	50.61	0.00	0.00	0.00	0.00	99.22		
Macrocrysts		olivine	41.38	0.00	0.00	0.00	0.00	0.12	6.87	0.33	50.69	0.00	0.00	0.00	0.01	99.41		
Macrocrysts		olivine	41.29	0.00	0.00	0.01	0.00	0.11	6.98	0.36	50.61	0.01	0.00	0.00	0.00	99.37		
Macrocrysts		olivine	40.44	0.03	0.01	0.03	0.01	0.19	11.82	0.15	46.78	0.12	0.00	0.00	0.02	99.60		
Macrocrysts		olivine	40.80	0.02	0.03	0.00	0.08	0.14	9.89	0.35	48.20	0.07	0.03	0.00	0.01	99.61		
Macrocrysts		olivine	41.21	0.01	0.01	0.00	0.01	0.08	6.67	0.35	50.59	0.02	0.01	0.00	0.00	98.96		
Macrocrysts		olivine	40.82	0.03	0.01	0.00	0.03	0.11	9.20	0.34	48.68	0.05	0.02	0.00	0.01	99.29		
Macrocrysts		olivine	40.51	0.04	0.03	0.02	0.01	0.14	10.23	0.37	47.55	0.06	0.01	0.00	0.01	98.97		
Macrocrysts		olivine	40.44	0.03	0.01	0.00	0.06	0.13	10.35	0.33	47.54	0.05	0.02	0.00	0.00	98.97		
Macrocrysts		olivine	40.45	0.03	0.02	0.00	0.08	0.15	10.53	0.34	47.12	0.09	0.01	0.00	0.04	98.86		
Macrocrysts		olivine	40.08	0.04	0.01	0.04	0.03	0.15	11.37	0.30	46.52	0.07	0.00	0.00	0.01	98.61		
Macrocrysts		olivine	40.43	0.03	0.02	0.00	0.06	0.14	10.84	0.31	46.99	0.07	0.01	0.00	0.01	98.92		
Macrocrysts		olivine	40.66	0.04	0.03	0.00	0.04	0.14	10.39	0.31	47.38	0.07	0.02	0.01	0.01	99.09		
Macrocrysts		olivine	40.07	0.03	0.01	0.00	0.00	0.15	13.17	0.11	45.50	0.03	0.01	0.00	0.02	99.09		
Macrocrysts		olivine	40.12	0.05	0.01	0.01	0.00	0.16	13.22	0.09	45.37	0.03	0.00	0.00	0.01	99.07		
Macrocrysts		olivine	39.90	0.04	0.02	0.00	0.01	0.16	13.21	0.11	45.52	0.03	0.01	0.00	0.02	99.04		
Macrocrysts		olivine	40.08	0.04	0.01	0.00	0.00	0.15	13.14	0.11	45.45	0.03	0.02	0.00	0.00	99.04		
Macrocrysts		olivine	40.06	0.05	0.00	0.01	0.02	0.16	13.10	0.11	45.56	0.03	0.02	0.00	0.01	99.13		
Macrocrysts		olivine	40.18	0.04	0.02	0.01	0.02	0.15	13.18	0.10	45.28	0.04	0.01	0.00	0.01	99.04		
Macrocrysts		olivine	39.87	0.03	0.02	0.01	0.01	0.15	13.10	0.12	45.78	0.02	0.01	0.00	0.02	99.15		
Macrocrysts		olivine	40.16	0.04	0.01	0.01	0.01	0.16	12.96	0.24	45.69	0.06	0.02	0.00	0.02	99.37		
Macrocrysts		olivine	39.97	0.04	0.00	0.00	0.03	0.15	13.42	0.10	45.77	0.03	0.01	0.00	0.02	99.53		
Macrocrysts		olivine	40.33	0.05	0.01	0.00	0.07	0.13	10.95	0.32	47.16	0.06	0.03	0.00	0.02	99.12		
Macrocrysts		olivine	40.79	0.01	0.03	0.01	0.07	0.14	10.05	0.35	47.87	0.07	0.03	0.00	0.02	99.44		
Macrocrysts		olivine	40.78	0.04	0.03	0.01	0.03	0.14	10.07	0.35	47.84	0.08	0.02	0.00	0.02	99.40		
Macrocrysts		olivine	41.59	0.02	0.00	0.00	0.02	0.12	7.10	0.36	51.50	0.01	0.00	0.00	0.01	100.72		
Macrocrysts		olivine	41.72	0.01	0.00	0.00	0.00	0.12	7.09	0.37	51.41	0.01	0.00	0.00	0.00	100.74		
Macrocrysts		olivine	40.66	0.04	0.03	0.00	0.07	0.12	10.31	0.32	47.79	0.08	0.04	0.00	0.01	99.46		
Macrocrysts		olivine	40.56	0.03	0.03	0.02	0.07	0.12	9.97	0.34	48.03	0.09	0.03	0.00	0.03	99.33		
Macrocrysts		olivine	40.47	0.04	0.02	0.00	0.02	0.15	11.78	0.24	46.64	0.06	0.01	0.00	0.02	99.46		
Macrocrysts		olivine	39.14	0.00	0.00	0.00	0.01	0.30	18.68	0.10	41.55	0.02	0.00	0.00	0.01	99.81		
Macrocrysts		olivine	40.65	0.02	0.04	0.00	0.08	0.13	9.80	0.39	48.09	0.10	0.02	0.00	0.00	99.31		
Macrocrysts		olivine	40.97	0.00	0.00	0.00	0.00	0.17	9.65	0.26	48.36	0.01	0.00	0.00	0.00	99.42		
Macrocrysts		olivine	40.86	0.01	0.01	0.00	0.00	0.19	9.68	0.24	48.26	0.01	0.00	0.00	0.00	99.27		
Macrocrysts		olivine	40.77	0.02	0.00	0.00	0.01	0.19	9.69	0.24	48.32	0.00	0.01	0.00	0.00	99.25		
Macrocrysts		olivine	40.77	0.00	0.00	0.00	0.00	0.20	9.61	0.26	48.40	0.01	0.01	0.01	0.02	99.28		
Macrocrysts		olivine	40.85	0.01	0.00	0.02	0.00	0.19	9.67	0.29	48.55	0.01	0.01	0.00	0.00	99.59		

sample name	rock type	mineral from composition	SiO2	TiO2	Al2O3	V2O3	Cr2O3	MnO	FeO	NiO	MgO	CaO	Na2O	K2O	P2O5	Total	notes	Crust-Mantle
Macrocrysts		olivine	40.97	0.00	0.00	0.00	0.01	0.18	8.25	0.39	49.78	0.01	0.00	0.00	0.00	99.59		
Macrocrysts		olivine	41.03	0.04	0.03	0.01	0.03	0.10	7.20	0.41	50.14	0.06	0.01	0.00	0.00	99.06		
Macrocrysts		olivine	40.95	0.04	0.02	0.00	0.02	0.11	7.18	0.41	50.32	0.06	0.01	0.00	0.00	99.13		
Macrocrysts		olivine	40.67	0.04	0.01	0.00	0.05	0.14	11.38	0.29	46.93	0.08	0.01	0.00	0.00	99.60		
Macrocrysts		olivine	40.90	0.00	0.00	0.00	0.00	0.23	10.01	0.36	48.24	0.01	0.00	0.00	0.01	99.76		
Macrocrysts		olivine	40.81	0.00	0.01	0.00	0.01	0.20	9.42	0.37	48.54	0.01	0.00	0.00	0.00	99.37		
Macrocrysts		olivine	40.72	0.00	0.00	0.00	0.00	0.26	10.76	0.34	47.56	0.02	0.01	0.00	0.01	99.67		
Macrocrysts		olivine	41.27	0.00	0.00	0.00	0.00	0.19	8.14	0.40	49.87	0.01	0.00	0.00	0.00	99.88		
Macrocrysts		olivine	40.15	0.04	0.02	0.00	0.00	0.16	13.35	0.19	45.34	0.11	0.00	0.00	0.01	99.37		
Macrocrysts		olivine	39.90	0.05	0.00	0.00	0.02	0.25	14.59	0.05	44.63	0.02	0.00	0.00	0.01	99.52		
Macrocrysts		olivine	39.58	0.05	0.00	0.01	0.00	0.21	15.51	0.07	44.04	0.04	0.00	0.00	0.03	99.55		
Macrocrysts		olivine	39.36	0.04	0.01	0.00	0.01	0.18	16.82	0.04	44.30	0.03	0.00	0.00	0.00	100.80		
Macrocrysts		olivine	39.29	0.04	0.01	0.00	0.00	0.18	16.82	0.05	44.50	0.03	0.01	0.00	0.00	100.92		
Macrocrysts		olivine	39.15	0.03	0.01	0.01	0.00	0.18	16.87	0.04	44.59	0.03	0.00	0.00	0.00	100.91		
Macrocrysts		olivine	39.36	0.02	0.01	0.00	0.00	0.18	16.79	0.04	44.31	0.03	0.01	0.00	0.00	100.75		
Macrocrysts		olivine	39.14	0.03	0.00	0.00	0.00	0.19	16.86	0.05	44.24	0.03	0.00	0.00	0.02	100.56		
Macrocrysts		olivine	40.48	0.01	0.00	0.00	0.05	0.09	7.46	0.35	50.75	0.01	0.01	0.00	0.02	99.25		
Macrocrysts		olivine	40.42	0.02	0.01	0.00	0.05	0.10	7.42	0.36	50.97	0.02	0.01	0.00	0.01	99.39		
Macrocrysts		olivine	40.48	0.01	0.02	0.00	0.03	0.10	7.49	0.35	50.69	0.02	0.00	0.00	0.02	99.21		
Macrocrysts		olivine	40.19	0.05	0.01	0.00	0.03	0.11	9.86	0.36	49.11	0.05	0.02	0.00	0.01	99.79		
Macrocrysts		olivine	40.37	0.04	0.01	0.01	0.05	0.13	9.69	0.36	49.28	0.05	0.01	0.00	0.00	99.99		
Macrocrysts		olivine	40.05	0.04	0.02	0.00	0.02	0.12	9.61	0.34	48.79	0.05	0.01	0.01	0.00	99.05		
Macrocrysts		olivine	39.95	0.05	0.02	0.01	0.00	0.12	9.69	0.35	49.18	0.04	0.02	0.00	0.01	99.43		
Macrocrysts		olivine	39.33	0.02	0.04	0.00	0.06	0.12	10.27	0.35	48.38	0.11	0.02	0.00	0.00	98.69		
Macrocrysts		olivine	39.42	0.01	0.05	0.01	0.08	0.12	10.26	0.34	48.60	0.11	0.03	0.00	0.01	99.04		
Macrocrysts		olivine	39.77	0.04	0.08	0.00	0.07	0.14	10.31	0.35	48.47	0.10	0.03	0.00	0.00	99.36		
Macrocrysts		olivine	40.12	0.02	0.07	0.01	0.07	0.13	10.29	0.35	48.67	0.11	0.03	0.00	0.00	99.87		
Macrocrysts		olivine	39.51	0.01	0.04	0.01	0.07	0.12	10.18	0.35	48.77	0.12	0.05	0.01	0.00	99.23		
Macrocrysts		olivine	40.42	0.01	0.00	0.00	0.00	0.14	8.03	0.36	50.84	0.01	0.01	0.00	0.01	99.84		
Macrocrysts		olivine	39.86	0.01	0.00	0.00	0.00	0.12	7.95	0.35	50.85	0.01	0.00	0.00	0.00	99.14		
Macrocrysts		olivine	39.90	0.04	0.03	0.00	0.04	0.11	10.70	0.33	48.44	0.08	0.02	0.00	0.00	99.70		
Macrocrysts		olivine	39.97	0.02	0.01	0.00	0.08	0.10	8.85	0.35	49.91	0.10	0.01	0.00	0.01	99.40		
Macrocrysts		olivine	40.27	0.02	0.02	0.00	0.08	0.12	8.85	0.34	49.83	0.10	0.02	0.00	0.00	99.64		
Macrocrysts		olivine	40.19	0.02	0.04	0.01	0.11	0.13	8.78	0.34	49.63	0.10	0.02	0.00	0.00	99.37		
Macrocrysts		olivine	39.13	0.04	0.00	0.00	0.01	0.17	14.31	0.10	45.95	0.04	0.01	0.00	0.02	99.77		
Macrocrysts		olivine	39.27	0.03	0.02	0.00	0.02	0.17	14.29	0.11	45.88	0.03	0.00	0.00	0.01	99.82		
Macrocrysts		olivine	39.04	0.03	0.00	0.00	0.01	0.14	14.26	0.09	46.08	0.03	0.01	0.00	0.01	99.71		
Macrocrysts		olivine	39.55	0.05	0.01	0.00	0.03	0.14	12.67	0.26	47.11	0.07	0.00	0.00	0.00	99.89		
Macrocrysts		olivine	39.09	0.02	0.00	0.00	0.01	0.22	18.58	0.09	41.23	0.04	0.02	0.00	0.00	99.31		
Macrocrysts		olivine	40.04	0.04	0.03	0.00	0.03	0.15	10.89	0.31	46.98	0.08	0.01	0.00	0.00	98.55		
Macrocrysts		olivine	40.22	0.03	0.01	0.01	0.06	0.15	11.77	0.23	46.69	0.07	0.02	0.00	0.01	99.27		
Macrocrysts		olivine	39.56	0.02	0.01	0.00	0.01	0.20	16.84	0.07	42.49	0.03	0.01	0.00	0.01	99.25		
Macrocrysts		olivine	40.55	0.05	0.01	0.00	0.04	0.12	11.17	0.27	47.11	0.08	0.00	0.00	0.02	99.42		
Macrocrysts		olivine	40.51	0.04	0.02	0.02	0.04	0.15	10.86	0.28	47.30	0.08	0.02	0.00	0.00	99.31		
Macrocrysts		olivine	41.17	0.01	0.00	0.00	0.01	0.15	7.59	0.38	50.00	0.01	0.00	0.00	0.00	99.32		
Macrocrysts		olivine	40.93	0.00	0.00	0.01	0.00	0.14	7.62	0.37	49.90	0.01	0.00	0.00	0.01	98.99		
Macrocrysts		olivine	39.70	0.00	0.01	0.00	0.00	0.23	16.12	0.16	43.29	0.03	0.00	0.00	0.00	99.54		
Macrocrysts		olivine	40.94	0.00	0.01	0.00	0.00	0.16	7.92	0.39	49.78	0.01	0.01	0.00	0.00	99.22		
Macrocrysts		olivine	40.82	0.00	0.00	0.00	0.00	0.19	8.55	0.39	49.22	0.01	0.00	0.00	0.00	99.18		

sample name	rock type	mineral from composition	SiO2	TiO2	Al2O3	V2O3	Cr2O3	MnO	FeO	NiO	MgO	CaO	Na2O	K2O	P2O5	Total	notes	Crust-Mantle
Macrocrysts		olivine	41.10	0.01	0.00	0.01	0.02	0.15	7.75	0.38	49.90	0.01	0.00	0.00	0.00	99.32		
Macrocrysts		olivine	39.62	0.00	0.00	0.00	0.00	0.25	16.70	0.13	42.96	0.03	0.00	0.00	0.01	99.70		
Macrocrysts		olivine	39.67	0.01	0.00	0.00	0.02	0.24	16.48	0.13	43.02	0.02	0.00	0.00	0.02	99.60		
Macrocrysts		olivine	39.79	0.02	0.00	0.00	0.00	0.22	14.40	0.21	44.73	0.02	0.00	0.00	0.00	99.38		
Macrocrysts		olivine	40.98	0.06	0.02	0.00	0.05	0.11	8.43	0.37	49.16	0.05	0.02	0.00	0.00	99.26		
Macrocrysts		olivine	40.86	0.04	0.02	0.00	0.06	0.13	8.48	0.38	49.00	0.06	0.02	0.00	0.00	99.05		
Macrocrysts		olivine	40.95	0.04	0.01	0.01	0.03	0.10	8.48	0.36	49.28	0.05	0.02	0.00	0.00	99.33		
Macrocrysts		olivine	40.88	0.06	0.01	0.00	0.06	0.11	8.52	0.38	49.00	0.05	0.03	0.00	0.00	99.10		
Macrocrysts		olivine	40.34	0.06	0.04	0.00	0.03	0.12	10.31	0.30	47.56	0.06	0.04	0.00	0.00	98.85		
Macrocrysts		olivine	40.61	0.04	0.01	0.00	0.02	0.13	10.35	0.30	47.82	0.06	0.03	0.00	0.00	99.36		
Macrocrysts		olivine	40.58	0.04	0.01	0.01	0.00	0.13	10.33	0.30	47.42	0.06	0.02	0.00	0.00	98.91		
Macrocrysts		orthopyroxene	56.09	0.13	0.54	0.00	0.03	0.16	8.13	0.03	35.28	0.68	0.14	0.00	0.01	101.21		
Macrocrysts		orthopyroxene	56.44	0.13	0.55	0.00	0.04	0.17	8.20	0.03	35.51	0.72	0.12	0.00	0.00	101.91		
Macrocrysts		orthopyroxene	56.21	0.13	0.54	0.01	0.01	0.16	8.16	0.03	35.69	0.69	0.13	0.00	0.01	101.76		
Macrocrysts		Picotite = chromian spinel	0.40	0.88	11.77	0.20	43.03	0.21	29.34	0.23	12.65	0.00	0.00	0.00	0.00	98.70		
Macrocrysts		Picotite = chromian spinel	0.40	0.85	11.69	0.21	43.06	0.20	29.52	0.24	12.48	0.00	0.00	0.01	0.00	98.66		
Macrocrysts		Picotite = chromian spinel	0.40	0.87	11.72	0.20	43.07	0.19	29.82	0.24	12.50	0.00	0.00	0.00	0.00	99.02		
Macrocrysts		Picotite = chromian spinel	0.15	13.38	3.71	0.24	2.01	0.74	64.78	0.14	13.49	0.05	0.12	0.02	0.01	98.83	fe rich	
Macrocrysts		Picotite = chromian spinel	0.07	20.40	1.95	0.90	6.42	0.19	63.73	0.08	5.47	0.05	0.33	0.00	0.01	99.59	fe rich	
Macrocrysts		Picotite = chromian spinel	0.06	22.89	1.27	0.61	4.69	0.40	60.41	0.09	9.06	0.06	0.32	0.00	0.00	99.86	fe rich	
Macrocrysts		Picotite = chromian spinel	0.12	6.05	12.98	0.25	36.85	0.59	27.04	0.08	16.11	0.01	0.03	0.01	0.00	100.12		
Macrocrysts		Picotite = chromian spinel	0.06	29.74	2.41	0.62	1.42	0.31	52.01	0.24	11.62	0.05	0.18	0.00	0.00	98.67		
Macrocrysts		Picotite = chromian spinel	0.05	20.36	0.73	0.64	1.32	0.47	68.24	0.23	6.88	0.49	0.06	0.00	0.01	99.49	fe rich	
Macrocrysts		Picotite = chromian spinel	0.06	19.89	0.90	0.54	0.48	0.49	68.15	0.23	7.87	0.20	0.10	0.02	0.00	98.92	fe rich	
Macrocrysts		Picotite = chromian spinel	0.09	20.96	4.52	0.13	1.55	1.14	52.37	0.08	17.71	0.31	0.05	0.00	0.00	98.90	fe rich	
Macrocrysts		Picotite = chromian spinel	0.04	21.52	1.17	0.30	6.05	0.41	58.87	0.14	10.32	0.01	0.29	0.00	0.01	99.12	fe rich	
Macrocrysts		Picotite = chromian spinel	0.05	38.95	0.61	0.28	3.48	0.51	40.76	0.11	15.90	0.05	0.31	0.00	0.01	101.02		
Macrocrysts		spinel	0.12	13.66	5.91	0.15	2.87	0.66	57.40	0.19	17.68	0.06	0.03	0.01	0.00	98.73	mg rich	

Sample	Rock Type	Mineral	Nb2O5	SiO2	ZrO2	TiO2	Al2O3	V2O3	Cr2O3	Fe2O3	MnO	MgO	CaO	TOTAL
M-19A	pyroxenite	rutile	0.06	0.00	0.15	98.34	0.00	0.23	0.02	0.00	0.00	0.00	0.00	98.79
M-19A	pyroxenite	rutile	0.01	0.00	0.14	99.28	0.01	0.00	0.01	0.03	0.00	0.03	0.03	99.54
M-19A	pyroxenite	rutile	0.04	0.00	0.16	99.07	0.00	0.00	0.02	0.03	0.00	0.00	0.03	99.35
M-19A	pyroxenite	rutile	0.05	0.00	0.14	98.26	0.01	0.07	0.04	0.03	0.00	0.04	0.01	98.65
M-19A	pyroxenite	rutile	0.01	0.00	0.08	98.98	0.00	0.00	0.03	0.01	0.00	0.03	0.00	99.14
M-19A	pyroxenite	rutile	0.00	0.00	0.08	99.25	0.00	0.00	0.04	0.00	0.00	0.04	0.00	99.40
M-19A	pyroxenite	rutile	0.05	0.00	0.13	98.49	0.00	0.00	0.05	0.03	0.00	0.00	0.01	98.75
M-19A	pyroxenite	rutile	0.08	0.00	0.12	98.29	0.00	0.00	0.03	0.02	0.00	0.00	0.05	98.59
M-19A	pyroxenite	rutile	0.01	0.00	0.14	98.93	0.02	0.33	0.02	0.02	0.00	0.02	0.01	99.51
M-19A	pyroxenite	rutile	0.00	0.00	0.14	99.18	0.04	0.10	0.05	0.03	0.00	0.00	0.01	99.54
M-19A	pyroxenite	rutile	0.00	0.00	0.15	98.43	0.00	0.20	0.00	0.04	0.00	0.00	0.01	98.82
M-19A	pyroxenite	rutile	0.04	0.00	0.15	99.64	0.00	0.12	0.04	0.07	0.00	0.00	0.03	100.07
M-19A	pyroxenite	rutile	0.01	0.00	0.16	98.74	0.00	0.07	0.05	0.08	0.00	0.00	0.03	99.16
M-19A	pyroxenite	rutile	0.00	0.03	0.14	98.72	0.02	0.00	0.02	0.08	0.00	0.04	0.12	99.16
M-19A	pyroxenite	rutile	0.03	0.00	0.13	99.33	0.03	0.00	0.04	0.02	0.00	0.00	0.01	99.59
M-19A	pyroxenite	rutile	0.00	0.00	0.21	98.59	0.00	0.10	0.03	0.06	0.00	0.04	0.07	99.10
M-19A	pyroxenite	rutile	0.02	0.01	0.16	99.44	0.00	0.00	0.06	0.00	0.00	0.05	0.01	99.76
M-19A	pyroxenite	rutile	0.02	0.00	0.21	98.64	0.00	0.05	0.04	0.05	0.00	0.03	0.01	99.05
M-19A	pyroxenite	rutile	0.01	0.01	0.16	99.21	0.01	0.00	0.05	0.03	0.00	0.02	0.02	99.53
M-19A	pyroxenite	rutile	0.02	0.00	0.16	99.40	0.00	0.00	0.02	0.02	0.00	0.00	0.02	99.64
M-19A	pyroxenite	rutile	0.00	0.01	0.17	99.38	0.00	0.00	0.01	0.04	0.00	0.02	0.03	99.67
M-19A	pyroxenite	rutile	0.00	0.00	0.13	99.65	0.00	0.00	0.05	0.03	0.00	0.00	0.01	99.87
M-19A	pyroxenite	rutile	0.04	0.01	0.21	98.77	0.00	0.11	0.03	0.13	0.00	0.02	0.06	99.37
M-19A	pyroxenite	rutile	0.00	0.00	0.12	99.04	0.00	0.14	0.04	0.04	0.00	0.00	0.02	99.39
M-19A	pyroxenite	rutile	0.05	0.00	0.15	99.26	0.00	0.00	0.08	0.03	0.00	0.02	0.01	99.62
M-19A	pyroxenite	rutile	0.08	0.00	0.28	98.56	0.02	0.13	0.00	0.04	0.00	0.03	0.00	99.13
M-19A	pyroxenite	rutile	0.00	0.00	0.13	99.09	0.03	0.08	0.04	0.06	0.00	0.00	0.02	99.44
B-9	eclogite	rutile	0.07	0.01	0.21	99.18	0.01	0.00	0.09	0.12	0.00	0.02	0.06	99.76
B-9	eclogite	rutile	0.05	0.00	0.19	99.51	0.00	0.00	0.10	0.06	0.00	0.00	0.05	99.96
B-9	eclogite	rutile	0.42	0.03	0.28	98.03	0.03	0.00	0.09	0.18	0.00	0.00	0.21	99.27
B-9	eclogite	rutile	0.15	0.00	0.21	98.63	0.00	0.01	0.07	0.19	0.01	0.03	0.15	99.44
B-9	eclogite	rutile	0.00	0.02	0.19	98.92	0.00	0.00	0.07	0.15	0.00	0.00	0.27	99.62

Sample	Rock Type	Mineral	Nb2O5	SiO2	ZrO2	TiO2	Al2O3	V2O3	Cr2O3	Fe2O3	MnO	MgO	CaO	TOTAL
B-9	eclogite	rutile	0.09	0.00	0.22	99.08	0.00	0.00	0.10	0.06	0.00	0.06	0.08	99.69
B-9	eclogite	rutile	0.11	0.00	0.18	99.24	0.00	0.00	0.06	0.17	0.00	0.00	0.23	99.99
B-9	eclogite	rutile	0.09	0.01	0.20	99.15	0.00	0.00	0.10	0.16	0.01	0.04	0.08	99.85
B-9	eclogite	rutile	0.09	0.00	0.20	98.94	0.00	0.00	0.11	0.13	0.01	0.00	0.08	99.56
B-9	eclogite	rutile	0.06	0.00	0.20	98.65	0.00	0.01	0.09	0.09	0.01	0.00	0.08	99.20
M-2-2	pyroxenite	rutile	0.01	0.00	0.20	99.06	0.01	0.01	0.13	0.00	0.00	0.00	0.03	99.47
B-13	pyroxenite	rutile	0.00	0.00	0.33	99.13	0.14	0.00	0.09	0.32	0.00	0.00	0.08	100.08
B-13	pyroxenite	rutile	0.00	0.01	0.36	99.52	0.02	0.00	0.12	0.09	0.00	0.00	0.07	100.20
B-13	pyroxenite	rutile	0.00	0.00	0.36	99.17	0.10	0.00	0.08	0.53	0.00	0.07	0.01	100.32
B-13	pyroxenite	rutile	0.01	0.00	0.33	98.74	0.20	0.00	0.08	0.30	0.00	0.06	0.03	99.75
B-13	pyroxenite	rutile	0.00	0.00	0.32	99.12	0.10	0.00	0.11	0.34	0.00	0.05	0.06	100.09
B-13	pyroxenite	rutile	0.00	0.00	0.34	98.89	0.01	0.00	0.11	0.26	0.00	0.00	0.04	99.64
B-13	pyroxenite	rutile	0.00	0.00	0.33	98.42	0.06	0.00	0.10	0.39	0.01	0.02	0.01	99.34
B-13	pyroxenite	rutile	0.00	0.00	0.30	98.95	0.15	0.00	0.11	0.30	0.00	0.00	0.01	99.81
B-13	pyroxenite	rutile	0.00	0.00	0.30	99.07	0.14	0.00	0.09	0.28	0.00	0.03	0.03	99.93
B-13	pyroxenite	rutile	0.00	0.00	0.36	99.34	0.01	0.00	0.12	0.28	0.00	0.08	0.02	100.20
B-13	pyroxenite	rutile	0.00	0.07	0.36	98.01	0.11	0.33	0.10	0.45	0.00	0.04	0.03	99.50
B-13	pyroxenite	rutile	0.00	0.04	0.34	97.92	0.10	0.21	0.08	0.22	0.01	0.00	0.05	98.97
B-13	pyroxenite	rutile	0.03	0.04	0.29	98.52	0.22	0.10	0.09	0.32	0.00	0.02	0.00	99.63
B-13	pyroxenite	rutile	0.00	0.05	0.00	99.27	0.15	0.11	0.08	0.32	0.00	0.04	0.02	100.03
B-13	pyroxenite	rutile	0.02	0.04	0.33	98.92	0.13	0.14	0.09	0.24	0.00	0.04	0.00	99.94
B-13	pyroxenite	rutile	0.00	0.03	0.37	98.06	0.04	0.29	0.10	0.29	0.00	0.00	0.01	99.19
B-13	pyroxenite	rutile	0.01	0.03	0.36	98.45	0.03	0.13	0.09	0.36	0.00	0.05	0.03	99.53
B-13	pyroxenite	rutile	0.00	0.04	0.35	98.30	0.13	0.17	0.08	0.28	0.00	0.00	0.01	99.36
B-13	pyroxenite	rutile	0.02	0.01	0.34	98.95	0.01	0.10	0.09	0.28	0.00	0.03	0.02	99.84
B-3	pyroxenite	rutile	0.13	0.00	0.49	99.01	0.00	0.00	0.19	0.14	0.00	0.05	0.00	100.02
B-3	pyroxenite	rutile	0.22	0.01	0.15	99.66	0.03	0.00	0.20	0.06	0.00	0.08	0.00	100.42
B-3	pyroxenite	rutile	0.02	0.03	0.41	99.61	0.00	0.00	0.33	0.10	0.00	0.02	0.08	100.60
B-3	pyroxenite	rutile	0.06	0.00	0.22	99.49	0.10	0.00	0.15	0.30	0.00	0.01	0.07	100.40
B-3	pyroxenite	rutile	0.19	0.01	0.01	99.22	0.07	0.00	0.21	0.20	0.00	0.01	0.04	99.96
B-3	pyroxenite	rutile	0.02	0.02	0.45	99.59	0.05	0.00	0.21	0.20	0.00	0.03	0.03	100.60
B-3	pyroxenite	rutile	0.09	0.00	0.01	99.87	0.05	0.00	0.24	0.08	0.00	0.00	0.00	100.34

Sample	Rock Type	Mineral	Nb2O5	SiO2	ZrO2	TiO2	Al2O3	V2O3	Cr2O3	Fe2O3	MnO	MgO	CaO	TOTAL
B-3	pyroxenite	rutile	0.08	0.02	0.26	99.28	0.03	0.00	0.53	0.05	0.00	0.02	0.01	100.27
B-3	pyroxenite	rutile	0.05	0.00	0.10	99.77	0.02	0.00	0.27	0.25	0.00	0.02	0.01	100.49
B-3	pyroxenite	rutile	0.11	0.01	0.13	99.44	0.00	0.00	0.21	0.05	0.00	0.00	0.00	99.96
B-3	pyroxenite	rutile	0.06	0.00	0.22	98.78	0.00	0.00	0.40	0.18	0.00	0.03	0.10	99.77
R-2-4	pyroxenite	rutile	0.00	0.00	0.18	99.62	0.00	0.14	0.33	0.06	0.00	0.00	0.01	100.34
R-2-4	pyroxenite	rutile	0.00	0.01	0.23	99.77	0.03	0.20	0.12	0.05	0.00	0.04	0.05	100.49
R-2-4	pyroxenite	rutile	0.00	0.00	0.11	99.90	0.01	0.25	0.16	0.09	0.01	0.01	0.02	100.55
R-2-4	pyroxenite	rutile	0.00	0.00	0.23	98.94	0.06	0.04	0.22	0.15	0.00	0.01	0.31	99.97
R-2-4	pyroxenite	rutile	0.00	0.00	0.22	99.17	0.01	0.00	0.24	0.37	0.00	0.04	0.01	100.05
R-2-4	pyroxenite	rutile	0.00	0.00	0.22	99.31	0.00	0.00	0.31	0.17	0.00	0.00	0.15	100.16
R-2-4	pyroxenite	rutile	0.00	0.00	0.23	100.15	0.00	0.00	0.23	0.18	0.00	0.00	0.11	100.90
R-2-4	pyroxenite	rutile	0.00	0.00	0.21	99.85	0.07	0.00	0.21	0.13	0.00	0.00	0.07	100.54
R-2-4	pyroxenite	rutile	0.00	0.00	0.23	99.25	0.00	0.00	0.34	0.05	0.00	0.02	0.00	99.89
R-2-4	pyroxenite	rutile	0.00	0.01	0.20	99.10	0.03	0.00	0.09	0.36	0.00	0.02	0.09	99.89
R-2-4	pyroxenite	rutile	0.00	0.01	0.18	99.42	0.03	0.00	0.07	0.30	0.00	0.00	0.12	100.13
R-2-4	pyroxenite	rutile	0.00	0.00	0.21	98.60	0.02	0.00	0.09	0.41	0.00	0.02	0.05	99.39
R-2-4	pyroxenite	rutile	0.00	0.00	0.24	99.31	0.01	0.00	0.12	0.12	0.00	0.00	0.11	99.92
R-2-4	pyroxenite	rutile	0.00	0.00	0.00	98.99	0.00	0.02	0.09	0.10	0.00	0.00	0.02	99.23
R-2-4	pyroxenite	rutile	0.00	0.00	0.15	99.14	0.01	0.00	0.19	0.19	0.00	0.06	0.10	99.83
M-19B	pyroxenite	rutile	0.09	0.00	0.64	98.11	0.00	0.00	0.02	0.09	0.00	0.00	0.03	98.97
M-19B	pyroxenite	rutile	0.05	0.00	0.66	98.28	0.00	0.07	0.04	0.04	0.00	0.01	0.00	99.15
M-19B	pyroxenite	rutile	0.11	0.05	0.14	99.05	0.00	0.04	0.04	0.02	0.00	0.04	0.07	99.57
M-19B	pyroxenite	rutile	0.10	0.00	0.77	98.92	0.05	0.00	0.05	0.01	0.00	0.00	0.04	99.93
M-19B	pyroxenite	rutile	0.08	0.01	0.56	98.68	0.00	0.13	0.03	0.08	0.00	0.02	0.13	99.73
M-19B	pyroxenite	rutile	0.08	0.00	0.82	99.25	0.02	0.00	0.04	0.05	0.00	0.03	0.06	100.35
M-19B	pyroxenite	rutile	0.06	0.00	0.60	98.86	0.00	0.10	0.03	0.10	0.00	0.00	0.19	99.95
M-19B	pyroxenite	rutile	0.08	0.00	0.67	99.31	0.01	0.06	0.03	0.03	0.00	0.04	0.01	100.25
M-19B	pyroxenite	rutile	0.08	0.00	0.58	99.28	0.00	0.00	0.01	0.24	0.00	0.00	0.57	100.75
B-13	pyroxenite	Srilankite	0.00	2.58	39.29	54.25	0.56	0.09	0.00	0.46	0.02	1.20	0.06	98.52
B-13	pyroxenite	Srilankite	0.00	0.07	42.68	55.30	0.10	0.17	0.00	0.33	0.00	0.13	0.02	98.82
B-13	pyroxenite	Srilankite	0.00	1.39	41.10	54.82	0.36	0.12	0.00	0.40	0.00	0.64	0.05	98.87

Sample	Rock Type	Mineral	Nb2O5	SiO2	ZrO2	TiO2	Al2O3	V2O3	Cr2O3	Fe2O3	MnO	MgO	CaO	TOTAL
B-13	pyroxenite	Srilankite	0.00	1.43	41.98	54.70	0.16	0.11	0.00	0.37	0.01	0.31	0.76	99.84
B-13	pyroxenite	Srilankite	0.00	0.35	42.26	55.48	0.07	0.14	0.00	0.27	0.00	0.20	0.56	99.32
B-13	pyroxenite	Srilankite	0.00	1.62	42.05	54.39	0.20	0.11	0.00	0.30	0.00	0.73	0.90	100.30
B-13	pyroxenite	Srilankite	0.00	0.40	42.25	56.35	0.05	0.10	0.00	0.19	0.00	0.17	0.24	99.75
B-13	pyroxenite	Srilankite	0.00	0.42	42.26	56.51	0.06	0.00	0.00	0.20	0.00	0.30	0.24	99.99
B-13	pyroxenite	Srilankite	0.00	0.83	41.57	55.64	0.14	0.00	0.00	0.32	0.00	0.52	0.04	99.06
B-13	pyroxenite	Srilankite	0.00	0.64	42.15	55.62	0.19	0.00	0.00	0.36	0.00	0.34	0.04	99.33
B-13	pyroxenite	Srilankite	0.00	0.06	42.78	55.69	0.06	0.00	0.00	0.32	0.00	0.05	0.03	98.98

rock type	sample	Si 29 (ppm)	Ti 47 (ppm)	Ti 49 (ppm)	Ni 60 (ppm)	Sr 88 (ppm)	Y 89 (ppm)	Zr 90 (ppm)	Nb 93 (ppm)	Ba 137 (ppm)	La 139 (ppm)	Ce 140 (ppm)	Pr 141 (ppm)	Nd 146 (ppm)	Sm 147 (ppm)	Eu 153 (ppm)	Gd 157 (ppm)	Tb 159 (ppm)	Dy 163 (ppm)	Ho 164 (ppm)	Er 166 (ppm)	Tm 169 (ppm)	Yb 172 (ppm)	Lu 175 (ppm)	Hf 178 (ppm)	Temp TNi (Griffen et al. 1989)	Temp (Canil 1999)	Average Temp (Griffin/Canil)	Major elements mantle vs crust (Hardman et al. 2018a)	Trace elements mantle vs crust (Hardman et al. 2018b)
harzburgite	L-5	203875	2725	2756	121	0.96	4.0	125	0.978	0.05	0.141	1.08	0.38	3.73	2.38	0.84	2.34	0.28	1.20	0.16	0.33	0.04	0.31	0.06	3.09	1492	1305	1399		
lherzolite	M-24-1_core	234000	979	1006	213	3.88	16.1	153	0.506	3.61	0.396	1.97	0.64	6.06	3.81	1.58	4.95	0.72	4.03	0.66	1.65	0.20	1.27	0.20	2.55	1900	1483	1692		
lherzolite	M-24-1_rim	214400	880	905	39	0.84	7.2	54	0.337	0.10	0.209	2.11	0.60	4.26	1.77	0.64	1.83	0.28	1.51	0.26	0.70	0.10	0.73	0.12	0.71	1006	1037	1022		
lherzolite	B-7	230413	2834	2895	128	0.72	13.6	29	0.414	0.30	0.073	0.62	0.17	1.39	0.86	0.40	1.65	0.33	2.38	0.50	1.53	0.22	1.69	0.27	0.59	1528	1322	1425		
lherzolite	M-15	205090	3708	3752	161	0.67	12.3	38	0.325	0.37	0.087	0.59	0.17	1.47	0.88	0.38	1.46	0.27	2.07	0.47	1.49	0.22	1.67	0.26	0.97	1677	1390	1533		
pyroxenite	B-12	204150	980	994	1.4	0.24	60.0	27	0.002	0.15	0.004	0.06	0.07	1.55	2.36	0.81	5.79	1.21	9.69	2.24	7.18	1.05	7.85	1.16	0.37				mantle	mantle
plagioclase pyroxenite	B-13	221433	568	582	0.9	0.02	34.3	17	0.001	0.00	0.010	0.09	0.06	0.94	1.26	0.42	3.03	0.67	5.48	1.27	4.09	0.60	4.49	0.67	0.29				crust	crust
pyroxenite	B-3	237000	N/A	479	1.3	0.05	90.6	25	0.004	BDL	0.015	0.13	0.10	2.16	2.95	1.19	7.02	1.61	13.11	3.41	11.73	1.93	14.89	2.44	0.36				crust	crust
pyroxenite	B-4	214525	733	742	7.5	0.07	17.4	9	0.110	0.04	0.003	0.02	0.01	0.28	0.61	0.35	1.65	0.35	2.81	0.65	2.09	0.30	2.24	0.33	0.17				mantle	mantle
pyroxenite	B-9	236489	N/A	588	0.5	0.01	13.8	11	0.019	0.03	0.007	0.07	0.05	0.67	0.68	0.50	1.38	0.30	2.28	0.55	1.73	0.27	1.96	0.31	0.26				crust	mantle (>Eu*)
pyroxenite	M-10-5	214633	873	897	0.5	0.08	40.5	14	0.003	0.10	0.022	0.09	0.05	1.05	1.94	1.16	5.01	0.96	6.92	1.49	4.58	0.65	4.85	0.70	0.21				crust	crust
pyroxenite	M-12	203950	776	795	1.7	0.16	109.8	14	0.001	0.13	0.115	0.40	0.12	2.19	3.92	1.34	9.99	2.16	17.47	4.04	12.83	1.82	13.28	1.89	0.20				crust	crust
pyroxenite	M-16	219300	420	430	1.0	0.03	11.9	11	0.010	0.10	0.003	0.03	0.02	0.31	0.44	0.25	1.02	0.22	1.86	0.43	1.47	0.22	1.75	0.27	0.19				mantle	mantle
pyroxenite	M-18	226633	473	482	1.3	0.08	14.1	9	0.005	0.07	0.002	0.02	0.01	0.26	0.43	0.27	1.15	0.27	2.23	0.52	1.73	0.25	1.91	0.28	0.16				mantle	mantle
pyroxenite	M-19A	198433	950	970	1.7	0.18	36.4	49	0.001	0.18	0.087	0.69	0.37	4.93	3.13	1.34	4.23	0.74	5.73	1.33	4.67	0.74	5.95	0.96	0.82				crust	mantle (>Sr)
pyroxenite	M-19B	191167	1028	1055	0.6	0.37	42.3	7	0.002	0.22	0.007	0.05	0.06	1.33	2.00	1.12	4.81	0.97	7.38	1.63	5.11	0.71	5.24	0.76	0.16				crust	mantle (>Sr)
pyroxenite	M-1	207550	719	725	0.7	0.08	32.0	12	0.001	0.11	0.030	0.20	0.11	1.76	1.86	0.75	3.34	0.67	5.31	1.23	4.02	0.60	4.61	0.70	0.18				crust	crust
pyroxenite	M-2	241275	N/A	355	0.4	0.03	13.0	18	0.002	0.03	0.009	0.13	0.10	1.44	1.01	0.77	1.47	0.29	2.12	0.50	1.64	0.26	2.01	0.33	0.37				mantle	mantle
pyroxenite	M-2B	229700	N/A	1738	5.0	0.05	10.3	21	0.006	0.03	0.018	0.45	0.29	3.93	2.58	1.65	2.38	0.33	1.99	0.42	1.19	0.17	1.21	0.18	0.25				crust	mantle (>Eu*)
pyroxenite	M-4	213180	922	945	4.7	0.13	38.5	21	0.008	0.03	0.030	0.12	0.05	0.80	1.17	0.83	2.97	0.65	5.66	1.45	5.01	0.76	5.77	0.87	0.38				mantle	mantle
pyroxenite	M-5	210175	1253	1285	0.6	0.17	42.9	17	0.012	0.21	0.021	0.11	0.06	1.22	2.10	1.19	5.14	1.00	7.29	1.56	4.72	0.68	5.00	0.72	0.27				crust	mantle (>Sr)
pyroxenite	R-1	214629	658	676	2.3	0.20	42.9	9	0.003	0.02	0.057	0.14	0.02	0.47	1.13	0.73	3.55	0.81	6.65	1.59	5.14	0.75	5.71	0.87	0.11				crust	mantle (>Sr)
pyroxenite	R-2-4	237538	N/A	728	1.8	0.15	39.5	10	0.002	0.04	0.042	0.10	0.02	0.50	1.20	0.80	3.74	0.85	6.54	1.59	4.89	0.73	5.23	0.81	0.15				crust	mantle (>Sr)
pyroxenite	R-5	200800	671	683	0.9	0.14	61.2	18	0.002	0.08	0.011	0.05	0.02	0.92	2.25	1.20	6.12	1.27	10.01	2.24	7.04	1.00	7.29	1.07	0.27				mantle	mantle
lherzolite	Concentrate	231650	197	200	14	0.14	2.8	8	0.073	0.02	0.048	0.68	0.20	1.36	0.44	0.14	0.37	0.06	0.42	0.10	0.41	0.08	0.82	0.18	0.16	754	864	809		
lherzolite	Concentrate	244400	200	202	15	0.10	2.5	8	0.083	0.02	0.028	0.56	0.18	1.26	0.43	0.13	0.37	0.06	0.43	0.09	0.40	0.07	0.84	0.17	0.18	766	873	820		
lherzolite	Concentrate	237600	128	130	14	0.08	2.5	12	0.072	BDL	0.017	0.28	0.10	0.86	0.42	0.16	0.55	0.07	0.46	0.08	0.24	0.04	0.47	0.11	0.27	748	860	804		
lherzolite	Concentrate	241050	17	17	13	0.10	3.7	3	0.076	BDL	0.025	0.36	0.14	1.30	0.53	0.19	0.50	0.07	0.50	0.10	0.37	0.08	0.88	0.18	0.02	734	850	792		
lherzolite	Concentrate	218000	29	28	11	0.09	1.8	1	0.092	0.06	0.023	0.25	0.13	1.22	0.31	0.13	0.40	0.05	0.27	0.05	0.21	0.05	0.62	0.15	BDL	710	831	771		
lherzolite	Concentrate	211200	30	32	11	0.87	1.4	1	0.546	1.20	0.326	1.30	0.28	1.79	0.44	0.22	0.34	0.04	0.20	0.04	0.18	0.05	0.54	0.13	0.01	704	827	765		
lherzolite	Concentrate	233650	241	241	16	0.11	2.9	9	0.086	0.01	0.064	0.68	0.20	1.49	0.47	0.15	0.43	0.07	0.49	0.11	0.43	0.08	0.87	0.18	0.16	777	881	829		
lherzolite	Concentrate	234000	27	29	13	0.18	0.9	3	0.087	BDL	0.063	0.65	0.19	1.45	0.50	0.16	0.36	0.03	0.13	0.03	0.14	0.04	0.42	0.09	0.02	746	858	802		
lherzolite	Concentrate	230650	97	99	13	0.17	4.5	7	0.131	0.03	0.035	0.48	0.19	1.50	0.66	0.24	0.63	0.11	0.74	0.15	0.49	0.09	0.92	0.18	0.13	740	854	797		
lherzolite	Concentrate	223850	55	55	14	3.20	9.1	6	0.462	1.47	0.744	1.58	0.24	1.73	0.84	0.37	0.96	0.19	1.35	0.26	0.91	0.15	1.45	0.25	0.12	754	864	809		
lherzolite	Concentrate	223000	2702	2687	162	0.63	13.2	33	0.460	0.08	0.093	0.66	0.19	1.71	0.93	0.34	1.42	0.27	2.17	0.51	1.59	0.23	1.74	0.27	0.92	1684	1393	1539		
lherzolite	Concentrate	236200	234	242	22	0.33	3.3	9	0.125	0.80	0.390	1.15	0.29	1.73	0.53	0.16	0.49	0.08	0.54	0.11	0.38	0.07	0.78	0.15	0.14	856	937	896		
lherzolite	Concentrate	232750	2674	2674	169	1.13	12.5	30	0.619	0.48	0.441	1.09	0.25	1.73	0.86	0.36	1.34	0.26	1.97	0.46	1.51	0.23	1.64	0.26	0.81	1715	1407	1561		
lherzolite	Concentrate	233400	255	260	16	0.18	3.1	9	0.090	BDL	0.156	1.39	0.31	1.82	0.49	0.16	0.44	0.07	0.49	0.12	0.46	0.08	0.86	0.19	0.16	787	888	838		
lherzolite	Concentrate	241850	2731	2704	179	0.70	6.0	15	0.740	0.01	0.117	1.01	0.25	1.74	0.76	0.27	0.96	0.15	0.98	0.20	0.63	0.10	0.79	0.13	0.31	1755	1424	1589		
lherzolite	Concentrate	288250	73	74	17	0.27	19.6	7	0.226	0.03	0.054	0.47	0.19	1.98	1.32	0.63	1.81	0.39	2.82	0.58	1.85	0.32	2.87	0.50	0.11	795	894	844		
lherzolite	Concentrate	237000	137	139	15	0.11	2.6	11	0.093	0.07	0.028	0.32	0.12	0.84	0.43	0.18	0.49	0.09	0.47	0.09	0.26	0.05	0.52	0.12	0.27	763	871	817		
lherzolite	Concentrate	222200	117	120	16	10.89	4.4	8	1.048	7.16	2.120	4.05	0.54	2.88	0.78	0.27	0.77	0.12	0.75	0.16	0.44	0.08	0.88	0.17	0.14	783	886	835		
lherzolite	Concentrate	198100	67	67	14	4.71	9.6	5	0.472	3.64	0.759	1.52	0.32	1.94	0.83	0.36	1.07	0.21	1.40	0.31	0.94	0.16	1.36	0.25	0.13	760	868	814		
lherzolite	Concentrate	237000	231	235	16	0.17	5.6	30	0.096	0.02	0.085	0.67	0.16	1.17	0.66	0.27	1.02	0.17	1.14	0.22	0.66	0.10	0.80	0.15	0.64	786	888	837		
lherzolite	Concentrate	238100	27	29	24	0.18	0.7	1	0.086	BDL	0.071	0.67	0.19	1.42	0.40	0.09	0.10	0.01	0.06	0.02	0.13	0.03	0.47	0.10	BDL	871	948	910		
lherzolite	Concentrate	236900	27	27	15	0.16	0.7	1	0.072	0.05	0.046	0.46	0.15	1.06	0.36	0.12	0.18	0.02	0.10	0.03	0.12	0.04	0.44	0.10	0.01	764	872	818		
lherzolite	Concentrate	229300	24	24	13	0.15	0.8	2	0.059	0.02	0.052	0.49	0.16	1.13	0.44	0.13	0.25	0.03	0.08	0.03	0.11	0.03	0.37	0.09	0.01	746	858	802		
lherzolite	Concentrate	240200	229	228	14	0.15	2.5	9	0.109	0.02	0.053	0.69	0.21	1.59	0.48	0.17	0.41	0.06	0.44	0.10	0.35	0.07	0.74	0.18	0.17	752	863	807		
lherzolite	Concentrate	242000	150	152	15	0.10	3.7	7	0.095	0.03	0.030	0.32	0.15	1.04	0.54	0.20	0.46	0.09	0.56	0.13	0.41	0.08	0.81	0.16	0.12	764	871	818		
lherzolite	Concentrate	238100	3017	2955	168	0.74	10.9	31	0.521	0.02	0.090	0.75	0.23	1.90	0.98	0.40	1.56	0.29	1.97	0.41	1.24	0.17	1.35	0.21	0.79	1711	1405	1558		
lherzolite	Concentrate	230800	23	24	13	0.23	1.0	2	0.073	0.16	0.054	0.52	0.16	1.25	0.44	0.14	0.26	0.02	0.12	0.03	0.14	0.04	0.46	0.10	0.02	740	853	797		
lherzolite	Concentrate	204200	129	131	26	20.39	5.1	10	1.788	15.61	3.359	4.34	0.77	3.82	0.87	0.29	0.78	0.13	0.85	0.17	0.57	0.10	0.92	0.19	0.19	897	965	931		
lherzolite	Concentrate	246250	98	100	14	0.11	4.2	8	0.152	0.03	0.034	0.36	0.16	1.42	0.61	0.21	0.59	0.10	0.69	0.14	0.49	0.09	0.96	0.20	0.15	754	864	809		
lherzolite	Concentrate	237000	2970	2966	166	0.68	10.7	29	0.493	BDL	0.077	0.76	0.22	1.87	0.92	0.40	1.44	0.26	1.90	0.41	1.25	0.18	1.39	0.22	0.77	1699	1400	1549		
lherzolite	Concentrate	232700	28	30	13	0.17	0.9	2	0.066	0.07	0.048	0.55	0.17	1.32	0.47	0.14	0.29	0.03	0.12	0.03	0.14	0.04	0.43	0.10	0.01	738	852	795		
lherzolite	Concentrate	224600	24	24	18	0.18	0.7	1	0.063	0.08	0.073	0.53	0.15	1.18	0.42	0.10	0.10	0.01	0.05	0.02	0.14	0.03	0.37	0.08	0.00	802	899	851		
lherzolite	Concentrate	223100	6	6	12	0.15	29.9	4	0.161	0.06	0.055	0.24	0.09	1.12	1.07	0.53	1.94	0.47	3.79	0.86	2.95	0.54	5.21	0.95	0.02	725	843	784		
lherzolite	Concentrate	254000	308	314	180	0.53	3.3	9	0.825	0.29	0.159	1.12	0.32	1.48	0.45	0.18	0.30	0.06	0.42	0.13	0.50	0.10	0.83	0.15	0.21	1761	1426	1593		
lherzolite	Concentrate	238900	181	179	15	0.52	2.7	7	0.142	0.34	0.076	0.44	0.17	1.31	0.48	0.17	0.44	0.07	0.41	0.09	0.29	0.06	0.67	0.14	0.15	769	876	822		
lherzolite	Concentrate	236900	31	33	14	0.30	1.1	3	0.122	0.19	0.045	0.54	0.17	1.28	0.51	0.17	0.36	0.05	0.18	0.04	0.14	0.04	0.42	0.10	0.04	761	869	815		
lherzolite	Concentrate	225800	937	942	3	0.09	96.3	50	0.050	0.08	0.029	0.32	0.33	7.49	11.31	4.39	19.13	3.03	18.35	3.30	8.84	1.14	7.94	1.08	0.70	528	684	606		
lherzolite	Concentrate	237100	164	169	14	0.11	2.2	12	0.093	0.03	0.029	0.48	0.14	1.01	0.51	0.21	0.56	0.08	0.45	0.08	0.23	0.03	0.49	0.10	0.25	759	868	813		
lherzolite	Concentrate	240900	2897	2867	173	0.57	11.7	28	0.464	0.06	0.068	0.66	0.21	1.50	0.84	0.36	1.25	0.26	1.89	0.44	1.44	0.21	1.69	0.26	0.75	1731	1413	1572		
lherzolite	Concentrate	233300	2914	2875	166	0.78	13.4	33	0.542	0.02	0.109	0.75	0.22	1.74	0.96	0.39	1.49	0.31	2.15	0.49	1.68	0.25	1.69	0.27	0.89	1701	1401	1551		
lherzolite	Concentrate	234700	5660	5584	178	0.85	15.6	53	0.381	0.56	0.076	0.63	0.19	1.67	1.16	0.53	1.98	0.35	2.72	0.62	1.78	0.26	1.86	0.30	1.32	1753	1423	1588		
lherzolite	Concentrate	241200	2776	2735	172	0.69	12.7	31	0.484	0.02	0.077	0.71	0.21	1.63	0.80	0.36	1.29	0.26	2.06	0.47	1.53	0.23	1.73	0.27	0.90	1725	1411	1568		
lherzolite	Concentrate	238550	6799	6746	207	0.96	25.1	63	0.360	BDL	0.082	0.70	0.21	1.92	1.41	0.67	2.67	0.55	4.25	0.95	2.95	0.40	3.04	0.44	1.77	1877	1474	1676		
lherzolite	Concentrate	243600	3393	3349	174	0.52	12.2	13	0.460	0.03	0.068	0.53	0.15	0.91	0.48	0.26	1.02	0.24	1.83	0.45	1.51	0.22	1.73	0.27	0.26	1735	1416	1575		
lherzolite	Concentrate	237800	5627	5570	175	0.72	15.9	42	0.343	0.02	0.070	0.57	0.18	1.56	1.08	0.47	1.79	0.36	2.70	0.60	1.89	0.25	1.91	0.29	1.13	1740	1418	1579		
lherzolite	Concentrate	239250	2234	2208	173	0.26	11.8	8	0.734	0.01	0.071	0.48	0.11	0.60	0.33	0.17	0.82	0.20	1.73	0.43	1.47	0.23	1.79	0.28	0.20	1730	1413	1572		
lherzolite	Concentrate	232200	220	224	15	0.58	2.9	8	0.131	0.25	0.183	1.03	0.24	1.44	0.48	0.16	0.40	0.07	0.45	0.12	0.44	0.09	0.94	0.19	0.17	768	874	821		
lherzolite	Concentrate	234800	219	224	19	0.25	3.3	9	0.107	0.13	0.075	0.64	0.20	1.34	0.47	0.15	0.47	0.08	0.53	0.13	0.49	0.09	0.89	0.21	0.18	824	915	869		
lherzolite	Concentrate	247500	199	202	14	0.12	2.8	8	0.091	0.02	0.038	0.50	0.18	1.41	0.49	0.16	0.38	0.07	0.45	0.11	0.38	0.08	0.79	0.18	0.15	760	869	815		
lherzolite	Concentrate	242700	23	24	22	0.16	0.7	1	0.067	0.01	0.052	0.49	0.15	1.20	0.35	0.09	0.14	0.01	0.07	0.02	0.11	0.03	0.38	0.08	0.01	848	932	890		
lherzolite	Concentrate	239450	4548	4500	183	0.66	13.6	45	0.323	0.01	0.059	0.51	0.16	1.47	0.95	0.45	1.70	0.32	2.38	0.53	1.59	0.23	1.78	0.28	1.19	1773	1431	1602		

		Li 6	Li 7	Na 23	Mg 25	Al 27	Si 29	P 31	K 39	Ca 43	Ca 44	Sc 45	Ti 47	V 51	Cr 53	Mn 55	Fe 57	Co 59	Ni 60	Cu 63	Zn 66	Ga 69	Ga 71	Sr 88	Y 89	Zr 90	Nb 93	Ce 140	Nd 145
Sample	**Clasification**	(ppm)	(ppm)	(ppm)	(ppm)	(ppm)	(ppm)	(ppm)	(ppm)	(ppm)	(ppm)	(ppm)	(ppm)	(ppm)	(ppm)	(ppm)	(ppm)	(ppm)	(ppm)	(ppm)	(ppm)	(ppm)	(ppm)	(ppm)	(ppm)	(ppm)	(ppm)	(ppm)	(ppm)
M-10-4 - 5	**Spinel peridotite**	0.95	1.00	BDL	BDL	19.4	192700	1	BDL	20	527	4.48	0.7	0.37	2.7	942	59360	134	3101	0.01	32.9	0.069	0.047	0.058	0.013	0.032	0.006	0.030	0.011
D-6-215	**Spinel peridotite**	1.45	1.31	BDL	1139000	76.7	187200	11	BDL	27	354	3.13	7.9	1.03	96.0	924	61800	132	3076	0.11	26.5	0.037	0.011	0.009	BDL	0.028	0.014	0.003	BDL
M-24-1 - 1	**Metasomatized peridotite**	1.45	1.44	60	1300000	237.0	186900	20	1.78	156	439	1.80	85.1	5.59	287.0	863	64100	129	2787	1.76	59.3	0.116	0.103	0.018	0.007	0.836	0.959	0.015	0.007
M-24-1 - 5	**Metasomatized peridotite**	1.47	1.34	58	BDL	234.0	188500	58	0.46	175	445	1.90	81.5	6.69	319.0	919	67600	133	3132	2.67	61.1	0.291	0.239	0.173	0.017	0.947	0.884	0.064	0.010
M-24-1 - 2	**garnet peridotite**	1.43	1.43	61	2732000	70.6	185900	35	BDL	84	364	1.70	83.7	5.08	187.6	853	63660	130	2797	2.10	58.8	0.124	0.099	BDL	0.004	0.764	0.968	0.001	BDL
M-24-1 - 3	**garnet peridotite**	1.52	1.55	62	BDL	29.1	187000	30	BDL	80	350	1.68	80.8	5.05	185.7	860	64420	133	2848	1.39	59.3	0.066	0.040	BDL	0.001	0.715	0.920	0.001	0.002
M-24-1 - 4	**garnet peridotite**	1.30	1.47	71	BDL	184.0	189300	58	BDL	155	433	1.98	88.3	7.75	314.0	883	66290	135	2896	3.14	59.4	0.164	0.167	BDL	0.014	0.816	0.962	0.005	0.004
D-6-21	**garnet peridotite**	1.57	1.59	37	1196000	14.8	187900	67	BDL	56	532	2.33	9.5	4.06	112.2	1065	72700	153	3152	1.34	59.2	0.054	0.022	BDL	BDL	0.230	0.575	BDL	BDL
D-6-45	**garnet peridotite**	2.79	2.63	76	2627000	17.0	186200	43	BDL	62	536	3.32	108.4	3.49	208.5	1119	69680	142	2926	BDL	64.0	0.058	0.033	BDL	0.007	1.006	1.034	BDL	BDL
D-6-47	**garnet peridotite**	1.28	1.23	73	2731000	56.3	187000	15	BDL	132	593	2.78	12.8	7.12	630.8	1022	65500	148	3305	3.30	55.4	0.061	0.030	0.003	0.001	0.166	0.151	BDL	BDL
D-6-60	**garnet peridotite**	1.85	1.73	163	2855000	89.3	188500	26	BDL	321	785	2.79	106.3	8.66	275.5	1067	77600	162	3400	8.04	72.2	0.172	0.145	0.010	0.015	0.125	0.013	0.003	BDL
D-6-69	**garnet peridotite**	1.52	1.41	27	4385000	12.1	186800	79	BDL	54	452	3.42	17.4	2.19	98.8	959	61360	134	2909	0.38	49.6	0.037	0.009	0.003	0.007	0.367	1.733	0.001	0.000
D-6-74	**garnet peridotite**	1.88	1.91	52	8200000	21.5	189400	11	BDL	68	496	2.21	38.4	5.07	194.2	964	65770	144	2998	1.42	58.0	0.063	0.031	BDL	0.001	0.682	1.101	0.001	BDL
D-6-82	**garnet peridotite**	1.58	1.60	21	BDL	13.8	187700	30	BDL	52	471	2.27	145.9	4.06	99.5	1017	70210	146	3058	0.75	59.5	0.058	0.029	BDL	0.002	0.516	1.161	0.002	BDL
D-6-85	**garnet peridotite**	1.33	1.34	9	BDL	22.9	189500	1	BDL	54	445	1.98	1.6	3.59	223.0	1019	68020	142	2893	1.35	50.9	0.043	0.016	BDL	0.001	0.113	0.429	0.001	BDL
D-6-125	**garnet peridotite**	1.21	1.26	27	1270600	12.3	187500	19	BDL	50	402	2.05	8.0	3.17	96.6	880	61540	131	2828	0.30	45.4	0.033	0.009	BDL	0.003	0.329	1.728	0.000	BDL
D-6-143	**garnet peridotite**	1.09	1.20	72	1767000	55.8	188700	13	BDL	132	499	2.36	12.8	7.09	617.0	961	65700	144	3212	3.17	51.9	0.063	0.029	0.004	0.002	0.154	0.154	0.000	BDL
D-6-144	**garnet peridotite**	1.69	1.67	142	1855000	95.5	184800	19	BDL	270	609	2.54	221.1	9.14	250.1	968	71200	145	3022	6.84	60.8	0.154	0.124	0.004	0.007	0.165	0.066	BDL	BDL
D-6-145	**garnet peridotite**	1.44	1.58	173	2005000	100.4	186900	19	BDL	268	616	2.58	128.4	9.11	420.2	926	69500	139	2854	5.94	58.7	0.151	0.117	0.003	0.006	0.189	0.049	0.000	BDL
D-6-149	**garnet peridotite**	1.61	1.61	30	2351000	10.3	185500	80	BDL	48	414	2.82	32.5	2.78	91.8	1057	69200	143	2949	0.44	54.9	0.041	0.013	BDL	0.008	0.392	2.514	0.001	BDL
D-6-155	**garnet peridotite**	1.36	1.41	151	3883000	78.5	186300	16	BDL	220	567	2.28	36.2	7.80	438.2	973	67500	140	2933	4.47	55.9	0.089	0.062	0.004	0.007	0.256	0.066	0.001	BDL
D-6-185	**garnet peridotite**	1.27	1.39	15	3900000	10.5	187700	13	BDL	52	404	1.59	7.9	3.64	104.4	934	66300	149	3262	0.83	56.4	0.037	0.015	BDL	BDL	0.221	0.680	0.002	0.001
D-6-188	**garnet peridotite**	1.15	1.18	68	3562000	55.6	187500	13	BDL	130	452	2.15	12.9	7.05	603.4	939	63800	143	3192	3.12	50.5	0.059	0.029	BDL	0.001	0.147	0.143	BDL	BDL
D-6-213	**garnet peridotite**	1.35	1.48	163	1336000	72.6	185200	5	BDL	263	565	2.52	260.7	8.88	509.8	933	64150	137	3108	6.77	54.3	0.189	0.166	0.004	0.013	0.280	0.061	BDL	BDL
D-6-225	**garnet peridotite**	1.90	1.90	207	887600	161.5	185600	25	BDL	386	698	2.78	108.2	10.79	443.6	991	72940	141	2883	7.05	61.5	0.232	0.213	0.009	0.017	0.215	0.018	0.001	BDL
D-6-239	**garnet peridotite**	1.37	1.23	23	962600	10.2	186500	27	BDL	47	379	2.87	13.9	2.40	98.8	975	64300	143	3131	0.63	53.2	0.035	0.008	BDL	0.007	0.296	1.518	0.000	BDL
D-6-240	**garnet peridotite**	1.20	1.21	22	991000	10.3	187500	29	BDL	52	369	2.85	13.6	2.37	96.0	948	63190	138	3019	0.61	51.2	0.037	0.009	BDL	0.006	0.301	1.545	0.000	BDL
D-6-247	**garnet peridotite**	1.48	1.45	58	1050400	23.8	187800	14	BDL	94	386	1.52	19.5	5.76	200.2	887	67700	149	3293	2.46	59.3	0.060	0.040	0.002	0.001	0.105	0.575	0.001	BDL
D-6-248	**garnet peridotite**	1.49	1.36	18	1091600	11.5	188700	26	BDL	53	352	1.63	10.9	2.69	106.9	894	62990	138	2940	1.09	53.7	0.036	0.013	BDL	0.001	0.186	1.625	0.001	BDL
D-6-261	**garnet peridotite**	1.48	1.52	145	1259000	76.1	188800	15	BDL	191	541	2.10	87.1	9.00	457.0	934	66700	146	3304	5.20	70.2	0.144	0.114	0.003	0.005	0.276	0.064	0.002	BDL
D-6-274	**garnet peridotite**	1.42	1.43	36	1284600	15.4	187000	30	BDL	56	345	1.74	33.5	3.56	124.4	973	68540	138	2856	1.07	62.6	0.054	0.030	BDL	0.002	0.325	0.583	0.000	BDL
D-5-2-7	**garnet peridotite**	0.90	0.95	BDL	1196200	10.2	188200	7	BDL	13	337	3.26	8.5	1.53	155.0	867	58840	137	3314	BDL	36.4	0.030	0.004	0.068	0.005	0.052	0.163	0.062	0.015
D-5-12-7	**metasomatized ? Garnet peridotite**	1.66	1.60	211	987800	166.4	185800	11	BDL	443	732	3.11	97.0	13.87	674.0	1100	79070	160	3387	6.25	72.5	0.235	0.205	0.013	0.013	0.102	0.011	0.003	0.001
D-5-14-2	**metasomatized ? Garnet peridotite**	1.91	1.92	171	914700	97.3	184600	50	BDL	325	609	2.39	214.2	11.53	274.0	989	75600	150	3181	8.14	69.9	0.198	0.180	0.021	0.015	0.184	0.023	0.013	0.002
D-6-269	**metasomatized ? Garnet peridotite**	2.40	2.38	190	1188000	102.1	188500	38	BDL	286	586	2.70	263.7	15.94	158.2	1284	118600	198	2483	8.94	111.6	0.323	0.302	0.003	0.012	0.200	0.032	0.001	BDL
D-6-272	**metasomatized ? Garnet peridotite**	2.09	2.01	194	1294000	178.6	188200	24	1.05	438	714	2.40	52.1	12.22	484.6	979	70630	141	3036	8.20	63.4	0.264	0.240	0.056	0.008	0.079	0.018	0.023	0.004
D-6-238	**metasomatized ? Garnet peridotite**	2.06	2.06	180	910000	85.8	187600	12	BDL	231	577	2.43	242.5	10.55	374.2	1007	75300	161	3452	9.87	72.4	0.175	0.148	0.003	0.007	0.228	0.043	0.001	BDL
D-6-203	**metasomatized ? Garnet peridotite**	2.09	2.18	185	1913000	92.5	186500	27	BDL	249	584	2.50	114.7	9.81	415.3	1013	77500	156	3280	7.70	74.1	0.187	0.163	BDL	0.008	0.196	0.048	0.001	0.000
D-6-9	**metasomatized ? Garnet peridotite**	1.66	1.67	155	779400	94.1	188500	8	BDL	255	711	3.26	291.2	11.92	315.8	1052	73600	141	2818	7.81	57.9	0.256	0.219	0.003	0.012	0.233	0.048	0.000	BDL
D-6-26	**metasomatized ? Garnet peridotite**	1.94	1.91	179	1427000	105.6	184400	25	BDL	253	688	3.18	280.7	10.10	277.3	1032	74000	150	3174	8.96	61.4	0.181	0.145	0.005	0.012	0.241	0.039	0.001	BDL
D-6-27	**metasomatized ? Garnet peridotite**	1.85	1.82	258	1567000	226.7	186100	1	BDL	486	909	3.87	105.7	12.87	768.0	1141	77500	148	3043	8.92	61.9	0.263	0.233	0.014	0.020	0.116	0.010	0.003	0.002
D-6-34	**metasomatized ? Garnet peridotite**	1.80	1.73	158	1719000	106.3	182600	25	BDL	263	676	2.96	270.9	10.98	211.1	1003	74900	146	3079	8.49	62.7	0.216	0.170	0.006	0.011	0.194	0.039	0.004	BDL
D-6-108	**metasomatized ? Garnet peridotite**	1.87	1.82	141	BDL	94.1	188100	10	BDL	276	639	2.90	302.8	12.58	298.0	1015	69500	136	2708	7.98	60.6	0.240	0.225	0.005	0.011	0.262	0.054	0.002	BDL
D-6-141	**metasomatized ? Garnet peridotite**	2.22	2.20	199	1604000	105.4	186600	35	BDL	264	620	2.88	296.5	10.32	340.5	997	76300	149	3198	8.53	68.0	0.192	0.171	0.004	0.011	0.305	0.043	BDL	0.002
D-6-147	**metasomatized ? Garnet peridotite**	2.06	2.13	221	2155000	149.7	184400	27	BDL	361	741	2.83	98.6	11.85	498.0	1082	78190	152	3131	8.10	69.2	0.264	0.234	0.009	0.014	0.119	0.012	0.001	BDL
D-6-168	**metasomatized ? Garnet peridotite**	1.67	1.84	173	5199000	94.0	183200	21	BDL	263	597	2.73	196.1	11.10	384.3	1071	77000	150	2988	5.63	70.1	0.202	0.181	0.004	0.007	0.182	0.035	0.001	0.001
D-5-3-1	**metasomatized ? Garnet peridotite**	1.89	1.81	184	1107900	160.9	183300	26	BDL	371	662	2.55	120.4	12.69	276.4	1012	77000	153	3083	6.88	72.7	0.248	0.222	0.006	0.013	0.116	0.013	0.000	BDL
B-10-1 - 1	**garnet spinel peridotite**	1.76	1.72	90	352600	4.1	184800	8	BDL	27	499	3.01	2.7	0.96	22.0	1154	81200	151	3211	0.12	51.2	0.050	0.027	0.017	0.002	0.012	1.294	0.023	0.007
B-10-1 - 2	**garnet spinel peridotite**	1.73	1.74	21	361700	2.4	183500	9	1.38	29	493	3.00	2.6	0.98	25.8	1137	84300	156	3257	0.10	52.9	0.063	0.026	0.059	0.002	0.016	1.317	0.025	0.005
B-10-1 - 5	**garnet spinel peridotite**	1.91	1.83	15	426500	2.5	184100	10	BDL	25	490	3.01	2.8	1.03	32.2	1106	83000	148	3018	0.10	54.2	0.041	0.016	0.006	0.001	0.015	1.284	0.007	0.003
B-5-1 - 1	**garnet spinel peridotite**	2.01	1.99	10	817900	2.2	184900	12	BDL	31	508	3.21	12.5	0.99	24.3	1314	71630	148	2981	0.17	67.2	0.036	0.011	0.012	0.011	0.106	7.300	0.046	0.004
B-5-1 - 2	**garnet spinel peridotite**	2.02	1.98	9	1494000	1.1	186000	13	BDL	27	487	3.23	12.6	0.96	22.5	1312	71000	148	3001	0.10	67.0	0.034	0.009	0.005	0.009	0.078	7.520	0.015	0.005
B-5-1 - 3	**garnet spinel peridotite**	1.99	1.98	BDL	6080000	1.1	185700	8	BDL	26	518	3.61	13.2	1.02	23.9	1245	68910	143	2902	0.10	68.4	0.041	0.009	0.003	0.009	0.077	8.129	0.010	0.002
B-5-1 - 4	**garnet spinel peridotite**	2.29	2.19	11	BDL	1.4	186300	22	BDL	25	516	3.57	13.6	1.06	24.0	1297	69680	145	2987	0.11	70.7	0.036	0.010	0.004	0.009	0.090	8.608	0.006	0.002
B-5-1 - 5	**garnet spinel peridotite**	1.99	1.94	5	BDL	3.0	184900	10	BDL	31	502	3.41	14.0	1.04	24.2	1230	67720	138	2753	0.23	65.4	0.037	0.012	0.016	0.012	0.105	8.360	0.033	0.003
R-2-3 - 1	**garnet spinel peridotite**	1.62	1.68	2	798500	1.7	185800	9	BDL	22	426	3.08	15.2	1.07	20.4	1125	70600	149	3146	0.06	54.5	0.030	0.007	BDL	0.002	0.033	1.982	0.001	BDL
R-2-3 - 2	**garnet spinel peridotite**	1.50	1.53	BDL	854900	2.0	184900	9	BDL	23	394	3.17	21.2	1.08	19.6	1037	66140	135	2821	0.07	49.7	0.031	0.006	0.005	0.003	0.043	2.376	0.004	BDL
R-2-3 - 3	**garnet spinel peridotite**	1.61	1.62	BDL	886900	2.2	185100	7	BDL	24	416	2.81	13.1	1.05	20.4	1112	68500	144	3076	0.06	52.7	0.032	0.008	0.003	0.002	0.030	1.725	0.005	BDL
R-2-3 - 4	**garnet spinel peridotite**	1.62	1.58	BDL	952300	1.8	186100	6	BDL	20	408	2.70	12.0	1.03	19.9	1081	67080	141	2949	0.06	50.3	0.030	0.006	BDL	0.002	0.029	1.634	0.003	BDL
R-2-3 - 5	**garnet spinel peridotite**	1.74	1.63	BDL	1010900	1.9	185200	11	BDL	25	412	2.82	13.1	1.09	20.3	1107	68400	145	3044	0.07	53.7	0.034	0.008	0.005	0.002	0.031	2.003	0.008	BDL
M-21-3 - 1	**garnet spinel peridotite**	1.49	1.55	16	BDL	7.6	187300	59	BDL	35	491	2.46	22.1	2.20	51.8	1005	70200	143	3094	0.51	54.2	0.036	0.014	0.014	BDL	0.195	1.240	0.012	0.002
M-21-3 - 2	**garnet spinel peridotite**	1.40	1.45	20.7	BDL	8.2	185400	46	BDL	38	476	2.42	24.1	2.14	50.2	964	68250	137	2895	0.48	50.6	0.036	0.014	0.032	0.005	0.235	1.707	0.043	0.014
M-21-3 - 3	**garnet spinel peridotite**	1.55	1.55	16.3	BDL	8.1	185900	65	BDL	32	463	2.43	23.3	2.13	49.3	953	68200	137	2881	0.48	51.3	0.037	0.013	0.018	0.002	0.201	1.711	0.020	0.005
M-21-3 - 4	**garnet spinel peridotite**	1.53	1.50	17.75	BDL	8.1	187400	52	BDL	47	488	2.45	23.9	2.18	51.3	965	68940	138	2980	0.62	52.9	0.040	0.018	0.068	0.007	0.266	1.710	0.083	0.026
M-21-3 - 5	**garnet spinel peridotite**	1.43	1.44	8.38	BDL	8.0	186200	46	BDL	37	476	2.45	23.8	2.15	50.9	965	67870	137	2939	0.59	51.7	0.035	0.016	0.059	0.002	0.217	1.856	0.061	0.016
D-6-17	**garnet spinel peridotite**	1.64	1.57	BDL	995900	4.6	187500	16	BDL	26	518	2.32	3.9	1.62	33.2	998	71500	155	3337	0.17	56.5	0.036	0.010	BDL	0.002	0.072	1.992	0.002	BDL
D-6-19	**garnet spinel peridotite**	1.41	1.42	2.01	1057000	3.4	186000	9	1.43	34	513	2.63	5.9	1.07	26.8	1150	70600	151	3274	0.15	51.4	0.042	0.008	0.099	0.005	0.072	1.403	0.034	0.011
D-6-44	**garnet spinel peridotite**	1.49	1.35	BDL	2589000	1.8	186200	6	BDL	13	507	4.18	1.9	0.43	5.1	1081	67610	149	3440	0.01	27.3	0.031	BDL	BDL	0.001	0.010	0.003	0.002	0.002
D-6-66	**garnet spinel peridotite**	1.34	1.34	29.94	3697000	8.6	186600	59	BDL	51	454	3.34	62.9	2.35	91.8	1029	65930	140	3039	0.27	53.6	0.043	0.014	BDL	0.009	0.385	3.241	0.000	BDL
D-6-70	**garnet spinel peridotite**	1.63	1.56	BDL	5491000	5.2	187600	13	BDL	37	453	2.08	4.1	1.66	33.2	944	67200	147	3113	0.17	56.5	0.039	0.007	0.004	0.002	0.077	2.251	0.005	BDL
D-6-135	**garnet spinel peridotite**	1.51	1.61	BDL	1517000	2.1	186700	15	BDL	25	407	2.30	2.5	0.97	17.8	1081	68550	139	2808	0.04	54.1	0.030	0.005	0.003	0.004	0.066	3.685	0.004	BDL
D-6-175	**garnet spinel peridotite**	1.54	1.58	BDL	5961000	1.9	187200	11	BDL	31	347	3.20	5.7	0.88	24.1	1148	68560	134	2698	0.08	46.8	0.029	0.004	0.004	0.006	0.045	2.612	0.006	0.002
D-6-180	**garnet spinel peridotite**	2.37	2.61	53.4	5643000	6.2	188400	70	BDL	49	388	2.41	17.4	2.42	139.1	1067	66500	144	3052	0.17	57.4	0.030	0.006	BDL	0.008	0.459	0.912	BDL	BDL
D-6-192	**garnet spinel peridotite**	2.31	2.26	BDL	3086000	0.1	187000	5	BDL	36	342	1.88	0.5	0.80	17.1	1053	66400	133	2908	0.07	47.5	0.028	BDL	0.091	0.024	0.018	0.245	0.024	0.009
D-6-196	**garnet spinel peridotite**	1.79	1.75	BDL	2726000	1.5	188100	8	BDL	30	377	2.32	2.5	0.94	25.4	1120	69560	143	3045	0.08	50.1	0.031	0.004	0.004	0.006	0.027	2.250	0.005	BDL
D-6-199	**garnet spinel peridotite**	1.79	1.88	38.7	2392000	7.0	186700	43	BDL	57	397	1.90	17.2	2.56	111.2	1057	69100	147	3095	0.35	58.7	0.031	0.019	BDL	0.006	0.345	1.054	0.001	BDL
D-6-207	**garnet spinel peridotite**	1.43	1.39	BDL	1774000	3.6	187600	6	BDL	35	373	1.44	1.6	1.22	20.2	924	65480	141	2984	0.09	47.9	0.027	0.005	0.007	0.002	0.027	0.919	0.007	0.001
D-6-211	**garnet spinel peridotite**	1.42	1.41	BDL	1462000	4.5	185300	6	BDL	35	341	1.78	9.5	1.38	20.2	923	64360	139	2924	0.08	47.0	0.026	0.004	0.007	0.004	0.032	1.931	0.009	0.002

Sample	Clasification	(ppm)	(ppm)	(ppm)	(ppm)	(ppm)	(ppm)	(ppm)	(ppm)	(ppm)	(ppm)	(ppm)	(ppm)	(ppm)	(ppm)	(ppm)	(ppm)	(ppm)	(ppm)	(ppm)	(ppm)	(ppm)	(ppm)	(ppm)	(ppm)	(ppm)	(ppm)	(ppm)	(ppm)
D-6-235	**garnet spinel peridotite**	1.71	1.65	BDL	898000	3.3	189300	9	BDL	37	393	2.17	6.4	1.28	32.8	1133	72600	158	3471	0.15	59.2	0.032	0.008	0.005	0.005	0.065	2.031	0.002	BDL
D-6-257	**garnet spinel peridotite**	1.93	1.97	BDL	1210000	1.2	188800	19	BDL	28	357	2.35	4.0	1.00	26.0	1134	70800	147	3110	0.08	54.8	0.026	0.005	0.010	0.006	0.033	3.370	0.020	0.006
D-6-260	**garnet spinel peridotite**	1.68	1.74	BDL	1247000	3.9	189800	14	BDL	33	366	1.52	3.5	1.75	36.3	949	70800	157	3490	0.19	66.2	0.029	0.008	BDL	0.002	0.074	1.964	0.004	BDL
D-5-1-5	**garnet spinel peridotite**	1.72	1.78	BDL	1257000	1.1	186600	25	BDL	32	349	1.67	32.1	1.54	24.1	1014	69320	145	3040	0.29	52.5	0.025	0.007	0.005	0.002	0.020	1.601	0.007	0.002
D-5-2-3	**garnet spinel peridotite**	1.28	1.17	25.15	1218000	8.9	186600	7	1.90	50	369	2.48	10.0	2.35	97.5	988	64000	137	3120	0.63	52.2	0.068	0.038	0.088	0.006	0.239	1.304	0.002	BDL
D-5-2-4	**garnet spinel peridotite**	2.49	2.34	7.1	1175000	0.3	183800	8	0.20	69	412	1.84	8.2	1.10	22.9	1493	80100	148	3120	0.16	70.1	0.058	0.027	0.512	0.011	0.129	1.351	0.072	BDL
D-5-5-7	**garnet spinel peridotite**	2.49	2.56	BDL	1074000	1.0	187300	9	BDL	53	361	1.75	0.4	0.90	20.2	1195	71690	145	3239	0.07	61.3	0.027	BDL	0.230	0.046	0.031	0.241	0.084	0.063
D-5-14-7	**garnet spinel peridotite**	1.88	1.72	BDL	916900	0.3	184200	14	BDL	22	308	2.65	3.7	0.37	4.3	992	64800	137	2990	0.06	39.5	0.024	BDL	0.012	0.016	0.013	0.622	0.011	0.004
D-5-18-6	**garnet spinel peridotite**	2.19	2.20	23.95	845900	2.7	185700	31	BDL	60	374	1.62	9.1	2.38	82.0	1150	71700	134	2930	0.35	71.7	0.056	0.035	0.008	0.005	0.323	1.038	0.001	BDL

Sample	Rock Type	Si 29 (ppm)	Ti 49 (ppm)	Cr 52 (ppm)	Cr 53 (ppm)	Ni 60 (ppm)	Sr 88 (ppm)	Y 89 (ppm)	Zr 90 (ppm)	Nb 93 (ppm)	Ba 137 (ppm)	La 139 (ppm)	Ce 140 (ppm)	Pr 141 (ppm)	Nd 146 (ppm)	Sm 147 (ppm)	Eu 153 (ppm)	Gd 157 (ppm)	Tb 159 (ppm)	Dy 163 (ppm)	Ho 164 (ppm)	Er 166 (ppm)	Tm 169 (ppm)	Yb 172 (ppm)	Lu 175 (ppm)	Hf 178 (ppm)	Pb 204 (ppm)	Pb 208 (ppm)	Th 232 (ppm)	ThO16 232 (ppm)	Notes
	Concentrate	271900	242	N/A	N/A	140	579	21.14	48	0.13	0.1	27.1	137.5	20.9	91.8	18.9	5.52	13.09	1.63	7.48	1.05	2.07	0.20	1.01	0.10	3.17	BDL	BDL	0.06	0.03	
	Concentrate	270000	239	N/A	N/A	137	566	20.02	47	0.15	0.9	24.8	129.5	19.7	87.1	18.0	5.29	12.47	1.57	7.11	1.01	1.98	0.20	0.95	0.10	3.09	BDL	BDL	0.06	0.03	
	Concentrate	275400	240	N/A	N/A	146	590	17.09	31	0.12	0.1	23.4	124.2	18.4	80.1	16.1	4.68	11.03	1.36	6.04	0.85	1.67	0.16	0.77	0.09	1.92	BDL	BDL	0.05	0.02	
	Concentrate	275000	42	N/A	N/A	292	219	9.33	23	0.89	13.4	11.0	47.2	6.6	26.7	5.4	1.70	4.00	0.55	2.77	0.43	0.96	0.11	0.62	0.07	0.66	BDL	BDL	0.35	0.39	
	Concentrate	271000	96	N/A	N/A	268	990	17.03	45	0.43	5.4	29.0	140.4	19.1	79.4	14.9	4.31	10.02	1.20	5.40	0.78	1.54	0.16	0.74	0.08	1.75	BDL	BDL	0.10	0.04	
	Concentrate	273500	136	N/A	N/A	262	921	18.29	61	1.35	17.6	32.5	148.4	20.5	84.4	15.7	4.56	10.58	1.27	5.62	0.81	1.66	0.17	0.83	0.10	2.39	BDL	BDL	0.22	0.15	
	Concentrate	224300	308	N/A	N/A	96	48	3.30	8	0.10	9.5	2.6	7.2	1.1	5.0	1.2	0.23	1.00	0.12	0.71	0.13	0.35	0.05	0.40	0.08	0.59	BDL	BDL	0.91	0.77	
	Concentrate	189900	87	N/A	N/A	193	987	15.14	34	0.40	22.4	21.9	89.8	14.8	67.3	13.4	3.81	9.09	1.07	4.97	0.70	1.39	0.14	0.67	0.08	1.29	BDL	BDL	0.07	0.03	
	Concentrate	231600	207	N/A	N/A	106	32	2.77	3	0.05	0.2	0.6	2.9	0.5	2.8	0.8	0.17	0.78	0.11	0.61	0.12	0.31	0.04	0.35	0.08	0.31	BDL	BDL	0.04	BDL	
	Concentrate	248300	61	N/A	N/A	223	1596	13.66	15	0.44	4.2	39.8	152.0	19.4	74.6	11.9	3.32	7.57	0.87	3.85	0.59	1.23	0.13	0.76	0.10	0.56	BDL	BDL	0.07	0.03	
	Concentrate	239900	141	N/A	N/A	280	880	16.47	41	1.66	13.7	22.4	99.0	15.7	69.6	14.0	4.08	9.78	1.19	5.35	0.78	1.55	0.15	0.76	0.09	1.65	BDL	BDL	0.23	0.12	
	Concentrate	242400	372	N/A	N/A	37	188	5.96	54	0.31	3.2	3.5	18.0	3.4	17.3	4.4	1.35	3.55	0.46	2.06	0.29	0.56	0.06	0.27	0.03	3.33	BDL	BDL	0.02	BDL	
	Concentrate	236300	236	N/A	N/A	99	58	2.46	7	0.04	21.3	1.7	6.7	1.0	4.4	0.9	0.20	0.81	0.11	0.56	0.11	0.28	0.04	0.31	0.07	0.53	BDL	BDL	0.33	0.43	
	Concentrate	238900	225	N/A	N/A	132	149	2.48	11	0.01	26.0	2.4	7.6	1.1	4.8	0.9	0.21	0.74	0.10	0.55	0.10	0.29	0.04	0.34	0.07	0.72	BDL	BDL	0.95	0.68	
	Concentrate	239500	260	N/A	N/A	106	184	3.01	8	0.88	27.3	5.2	10.6	1.3	5.6	1.1	0.26	0.96	0.13	0.71	0.13	0.34	0.04	0.37	0.08	0.49	BDL	BDL	0.38	0.27	
	Concentrate	274300	18	N/A	N/A	262	1802	52.06	36	0.75	0.6	48.3	268.9	41.4	184.6	38.7	11.58	27.63	3.43	15.70	2.30	4.60	0.47	2.33	0.26	1.54	BDL	BDL	0.10	0.07	
	Concentrate	275200	254	N/A	N/A	143	58	2.97	8	0.04	14.2	2.5	8.8	1.2	5.3	1.1	0.24	0.88	0.12	0.64	0.12	0.34	0.05	0.37	0.08	0.63	BDL	BDL	1.62	1.74	
	Concentrate	281100	281	N/A	N/A	131	89	2.71	10	0.05	41.0	3.4	10.2	1.2	5.1	1.1	0.24	0.87	0.11	0.57	0.11	0.29	0.04	0.32	0.07	0.54	BDL	BDL	0.97	1.03	
	Concentrate	266100	103	N/A	N/A	310	1013	17.28	43	0.56	4.3	24.7	124.8	18.2	78.7	15.3	4.37	10.34	1.21	5.43	0.78	1.54	0.15	0.79	0.09	1.59	BDL	BDL	0.12	0.15	
	Concentrate	241300	164	N/A	N/A	237	950	18.35	51	0.70	9.3	28.7	118.3	17.8	78.3	15.1	4.28	10.47	1.26	5.74	0.84	1.69	0.16	0.82	0.10	1.94	BDL	BDL	0.13	0.09	
	Concentrate	274300	35	N/A	N/A	263	1806	50.03	42	1.89	6.4	49.7	255.2	40.1	182.4	37.6	10.81	26.48	3.25	14.90	2.20	4.50	0.45	2.29	0.27	1.76	BDL	BDL	0.17	0.17	
	Concentrate	261500	103	N/A	N/A	261	1021	20.10	47	0.39	0.5	31.6	145.4	20.7	89.4	17.1	4.90	11.78	1.41	6.34	0.91	1.81	0.18	0.89	0.10	1.84	BDL	BDL	0.09	0.05	
	Concentrate	268500	124	N/A	N/A	271	1019	19.57	53	0.57	2.7	32.0	147.2	20.5	87.8	16.6	4.74	11.41	1.37	6.20	0.90	1.80	0.18	0.86	0.10	2.02	BDL	BDL	0.14	0.11	
	Concentrate	255500	107	N/A	N/A	253	1002	20.65	46	0.43	1.5	31.0	144.1	20.5	86.9	16.9	4.87	11.52	1.39	6.29	0.93	1.88	0.19	0.93	0.11	1.73	BDL	BDL	0.10	0.03	
	Concentrate	241000	41	N/A	N/A	224	1556	49.40	31	1.64	1.0	56.3	276.1	42.6	182.9	36.1	10.43	24.10	3.00	14.11	2.14	4.48	0.48	2.52	0.29	0.99	BDL	BDL	0.16	0.14	
	Concentrate	266300	1255	N/A	N/A	637	91	2.14	3	0.11	0.4	1.3	5.1	0.8	3.9	1.0	0.32	0.89	0.12	0.58	0.09	0.19	0.02	0.11	0.01	0.16	BDL	BDL	0.01	BDL	
	Concentrate	244200	141	N/A	N/A	96	29	1.87	4	0.00	4.4	1.1	5.0	0.7	3.1	0.7	0.14	0.53	0.07	0.39	0.07	0.23	0.03	0.24	0.05	0.27	BDL	BDL	0.16	0.22	
	Concentrate	262100	326	N/A	N/A	162	236	5.19	81	0.36	3.2	4.1	21.3	3.6	18.0	4.4	1.32	3.37	0.41	1.85	0.27	0.51	0.05	0.21	0.02	4.70	BDL	BDL	0.02	BDL	
	Concentrate	245500	99	N/A	N/A	224	1010	18.28	49	0.50	2.1	29.9	134.7	19.7	83.8	16.0	4.60	10.96	1.31	5.88	0.86	1.67	0.17	0.79	0.09	1.88	BDL	BDL	0.11	0.16	
	Concentrate	238200	609	N/A	N/A	354	623	16.29	29	6.26	676.0	25.8	81.5	12.6	50.9	9.6	2.79	6.21	0.82	4.01	0.62	1.44	0.17	1.00	0.13	1.56	BDL	BDL	6.20	4.36	
	Concentrate	247100	278	N/A	N/A	112	656	18.41	40	0.11	0.3	25.4	118.9	19.2	84.2	17.1	4.90	11.54	1.40	6.31	0.88	1.68	0.17	0.79	0.09	2.57	BDL	BDL	0.05	0.02	
	Concentrate	247700	253	N/A	N/A	123	595	22.29	48	0.12	0.1	27.0	129.1	20.7	90.5	18.6	5.45	12.99	1.60	7.39	1.04	2.05	0.20	0.99	0.11	3.11	BDL	BDL	0.06	0.03	
	Concentrate	241400	16	N/A	N/A	227	1796	46.11	38	0.74	32.0	46.1	241.8	38.3	171.2	35.1	10.25	23.86	2.95	13.50	2.02	4.12	0.42	2.11	0.24	1.50	BDL	BDL	0.13	0.06	
	Concentrate	242300	70	N/A	N/A	261	949	13.96	35	0.46	18.0	20.6	90.7	14.2	61.7	12.2	3.57	8.32	0.99	4.46	0.64	1.29	0.13	0.62	0.07	1.37	BDL	BDL	0.12	0.07	
	Concentrate	240400	3097	N/A	N/A	474	146	3.03	13	1.02	18.9	3.2	10.7	1.7	8.3	2.0	0.63	1.70	0.21	0.90	0.13	0.25	0.03	0.12	0.01	0.91	BDL	BDL	0.10	BDL	
	Concentrate	249700	259	N/A	N/A	105	306	3.80	133	0.48	109.3	10.2	15.8	1.9	7.0	1.3	0.29	1.02	0.14	0.78	0.16	0.42	0.06	0.61	0.13	3.30	BDL	BDL	1.64	1.55	
	Concentrate	257000	2986	N/A	N/A	573	132	2.56	9	0.19	1.9	2.2	9.0	1.5	7.5	1.9	0.56	1.40	0.17	0.72	0.11	0.21	0.02	0.12	0.01	0.71	BDL	BDL	0.02	BDL	
	Concentrate	222700	97	N/A	N/A	239	925	18.58	39	1.11	10.4	26.1	110.0	17.8	80.9	16.3	4.63	10.94	1.30	5.92	0.85	1.71	0.17	0.82	0.10	1.62	BDL	BDL	0.25	0.20	
	Concentrate	264200	77	N/A	N/A	300	992	14.98	37	1.66	27.4	22.5	107.6	16.3	69.7	13.4	3.92	9.11	1.08	4.82	0.69	1.34	0.13	0.66	0.08	1.46	BDL	BDL	0.24	0.08	
	Concentrate	258200	424	N/A	N/A	287	119	0.60	7	0.32	0.2	4.2	13.7	1.7	6.1	0.9	0.26	0.48	0.05	0.21	0.03	0.05	0.00	0.02	0.00	0.19	BDL	BDL	0.19	0.08	
	Concentrate	262500	1446	N/A	N/A	280	184	4.10	88	0.18	0.1	5.9	24.9	3.8	17.1	3.3	0.93	2.15	0.27	1.22	0.18	0.37	0.04	0.21	0.02	3.05	BDL	BDL	0.04	0.02	
	Concentrate	272400	214	N/A	N/A	124	52	2.38	7	0.03	14.6	1.9	6.5	0.9	3.8	0.8	0.19	0.65	0.08	0.49	0.09	0.25	0.04	0.28	0.06	0.49	BDL	BDL	0.59	0.32	
	Concentrate	256300	262	N/A	N/A	116	49	2.49	9	0.03	19.7	1.7	7.1	1.0	4.4	1.0	0.20	0.78	0.10	0.52	0.10	0.28	0.04	0.30	0.06	0.68	BDL	BDL	0.42	0.38	
	Concentrate	219700	262	N/A	N/A	104	52	2.62	6	0.08	8.5	1.5	5.6	0.9	4.2	0.9	0.21	0.79	0.10	0.56	0.11	0.29	0.04	0.30	0.07	0.48	BDL	BDL	0.44	0.36	
	Concentrate	280200	910	N/A	N/A	387	880	20.62	49	2.41	85.2	27.7	116.5	17.8	77.4	15.4	4.53	10.87	1.32	6.18	0.90	1.85	0.19	0.95	0.11	1.85	BDL	BDL	1.39	1.45	
	Concentrate	218700	104	N/A	N/A	224	1324	41.26	17	1.63	22.7	39.5	182.1	29.7	133.0	26.7	7.68	18.81	2.31	11.14	1.74	3.77	0.42	2.31	0.29	0.80	BDL	BDL	0.11	0.01	
	Concentrate	255700	95	N/A	N/A	284	881	19.85	38	0.98	11.7	28.5	141.2	21.0	91.6	18.3	5.28	12.33	1.46	6.47	0.91	1.79	0.18	0.85	0.09	1.75	BDL	BDL	0.24	0.20	
	Concentrate	239900	277	N/A	N/A	127	45	2.89	6	0.06	12.8	1.8	7.0	1.1	5.0	1.1	0.22	0.88	0.11	0.58	0.12	0.31	0.05	0.33	0.07	0.51	BDL	BDL	1.16	1.12	
	Concentrate	267300	247	N/A	N/A	114	126	2.65	13	0.02	35.7	2.4	8.9	1.2	4.9	1.0	0.20	0.83	0.10	0.60	0.10	0.29	0.04	0.35	0.07	0.91	BDL	BDL	0.39	0.37	
	Concentrate	230800	231	N/A	N/A	87	61	1.88	6	0.02	24.3	1.0	3.9	0.6	2.9	0.7	0.15	0.56	0.07	0.39	0.07	0.19	0.03	0.23	0.06	0.49	BDL	BDL	0.45	0.28	
	Concentrate	256400	104	N/A	N/A	244	653	15.09	51	0.55	5.0	18.0	88.6	13.9	61.3	13.1	3.84	9.25	1.12	5.11	0.72	1.38	0.13	0.62	0.07	2.55	BDL	BDL	0.06	BDL	
	Concentrate	283400	36	N/A	N/A	308	2075	52.15	33	4.44	4.3	45.8	242.8	38.1	172.6	36.9	10.88	26.24	3.27	15.13	2.23	4.52	0.47	2.40	0.28	1.25	BDL	BDL	0.17	0.10	
	Concentrate	256800	197	N/A	N/A	110	49	2.60	66	0.01	14.3	1.5	5.8	0.9	3.9	0.9	0.17	0.75	0.09	0.52	0.11	0.28	0.04	0.41	0.09	2.48	BDL	BDL	0.68	0.69	
	Concentrate	266700	245	N/A	N/A	119	70	2.77	10	0.06	25.4	2.5	8.4	1.1	5.0	1.0	0.21	0.85	0.11	0.59	0.12	0.31	0.04	0.33	0.07	0.74	BDL	BDL	0.46	0.74	
	Concentrate	242800	153	N/A	N/A	97	27	2.03	4	0.01	2.6	1.2	5.2	0.8	3.3	0.7	0.15	0.56	0.07	0.42	0.08	0.22	0.03	0.26	0.06	0.31	BDL	BDL	0.20	0.13	
	Concentrate	257000	239	N/A	N/A	101	19	1.44	8	0.05	36.8	0.7	2.1	0.3	1.2	0.3	0.08	0.24	0.04	0.26	0.05	0.17	0.03	0.23	0.06	0.41	BDL	BDL	0.03	BDL	
	Concentrate	242900	79	N/A	N/A	258	949	15.58	38	1.31	29.9	22.9	105.2	16.0	68.7	13.6	3.93	9.23	1.11	5.03	0.71	1.40	0.14	0.71	0.08	1.46	BDL	BDL	0.22	0.19	
	Concentrate	246600	296	N/A	N/A	101	99	2.61	11	0.07	51.3	2.9	8.3	1.1	4.6	1.0	0.19	0.80	0.11	0.58	0.10	0.28	0.04	0.31	0.07	0.81	BDL	BDL	0.70	0.84	
	Concentrate	252700	18	N/A	N/A	271	583	19.50	10	2.53	5.0	18.7	89.2	14.0	60.3	12.7	3.90	8.55	1.10	5.20	0.80	1.69	0.19	1.04	0.13	0.17	BDL	BDL	0.15	0.12	
	Concentrate	248800	105	N/A	N/A	262	1832	38.45	39	1.89	26.3	63.0	306.6	45.9	192.6	34.6	9.50	21.83	2.52	11.27	1.61	3.31	0.34	1.77	0.21	1.34	BDL	BDL	0.76	0.80	
	Concentrate	257300	86	N/A	N/A	282	1026	21.52	39	1.60	14.1	32.0	152.4	22.6	98.0	19.1	5.45	12.67	1.52	6.86	0.97	1.91	0.18	0.93	0.10	1.65	BDL	BDL	0.44	0.25	
	Concentrate	251700	101	N/A	N/A	234	1023	18.15	49	0.35	0.3	28.9	130.0	19.0	80.8	15.4	4.49	10.56	1.26	5.71	0.81	1.62	0.16	0.79	0.09	1.86	BDL	BDL	0.09	0.09	
	Concentrate	289000	246	N/A	N/A	303	640	16.40	17	2.16	36.4	25.5	122.2	15.1	56.6	10.0	2.90	6.59	0.82	4.12	0.65	1.45	0.17	0.96	0.12	1.11	BDL	BDL	0.40	0.58	
	Concentrate	252400	393	N/A	N/A	37	194	6.17	56	0.15	0.0	3.6	19.3	3.5	17.8	4.5	1.39	3.53	0.45	2.08	0.29	0.57	0.05	0.27	0.03	3.45	BDL	BDL	0.02	BDL	
	Concentrate	258000	34	N/A	N/A	255	185	4.38	17	0.35	9.3	7.3	28.6	4.1	17.2	3.3	0.95	2.22	0.28	1.35	0.21	0.43	0.05	0.24	0.03	0.49	BDL	BDL	0.06	BDL	
	Concentrate	263100	14	N/A	N/A	299	562	29.05	12	5.22	4.6	24.4	117.3	16.7	67.3	13.9	4.27	9.87	1.38	7.03	1.14	2.66	0.31	1.80	0.23	0.11	BDL	BDL	0.06	BDL	
	Concentrate	244900	265	N/A	N/A	103	106	2.25	9	0.04	37.5	2.2	6.9	1.0	4.1	0.8	0.20	0.69	0.08	0.47	0.09	0.23	0.03	0.27	0.06	0.64	BDL	BDL	0.80	0.91	
	Concentrate	244300	129	N/A	N/A	229	1031	20.35	57	0.58	1.8	32.8	137.6	20.4	88.1	16.8	4.81	11.41	1.35	6.20	0.91	1.84	0.18	0.93	0.10	2.11	BDL	BDL	0.15	0.03	
	Concentrate	255400	425	N/A	N/A	354	711	11.23	15	18.48	95.0	20.0	80.9	11.0	41.3	6.7	2.02	4.20	0.49	2.43	0.42	1.09	0.15	1.06	0.15	0.72	BDL	BDL	0.09	0.03	
	Concentrate	230700	65	N/A	N/A	227	1653	20.29	43	0.52	7.2	45.1	178.2	25.8	105.3	17.8	4.85	11.25	1.28	5.81	0.87	1.77	0.18	0.97	0.12	1.33	BDL	BDL	0.10	0.04	
	Concentrate	237700	274	N/A	N/A	104	662	13.27	32	0.14	4.2	18.5	84.0	13.8	60.6	12.4	3.53	8.36	1.00	4.50	0.63	1.20	0.12	0.55	0.06	1.84	BDL	BDL	0.04	BDL	
	Concentrate	232000	314	N/A	N/A	93	44	2.00	10	0.10	31.2	2.5	4.2	0.7	2.6	0.5	0.13	0.45	0.07	0.36	0.08	0.21	0.03	0.28	0.07	0.45	BDL	BDL	0.32	0.24	
	Concentrate	227200	196	N/A	N/A	97	29	2.52	5	0.01	0.4	1.1	4.7	0.7	3.6	0.8	0.18	0.69	0.09	0.53	0.10	0.26	0.04	0.31	0.07	0.46	BDL	BDL	0.29	0.22	
	Concentrate	158000	320	N/A	N/A	60	1306	2.44	7	0.34	1603.0	7.2	14.4	1.5	5.4	1.0	0.29	0.73	0.09	0.48	0.09	0.24	0.03	0.24	0.05	0.35	BDL	BDL	0.46	0.40	

Sample	Rock Type	(ppm)	(ppm)	(ppm)	(ppm)	(ppm)	(ppm)	(ppm)	(ppm)	(ppm)	(ppm)	(ppm)	(ppm)	(ppm)	(ppm)	(ppm)	(ppm)	(ppm)	(ppm)	(ppm)	(ppm)	(ppm)	(ppm)	(ppm)	(ppm)	(ppm)	(ppm)	(ppm)	(ppm)	(ppm)	Notes
	Concentrate	229300	632	N/A	N/A	83	91	3.71	22	0.07	9.0	2.2	7.2	1.0	4.6	1.0	0.26	0.88	0.13	0.76	0.14	0.39	0.05	0.42	0.07	0.73	BDL	BDL	0.57	0.14	
	Concentrate	247000	288	N/A	N/A	115	62	2.76	7	0.05	27.7	1.6	5.7	0.8	3.8	0.9	0.21	0.72	0.10	0.55	0.11	0.28	0.04	0.34	0.08	0.51	BDL	BDL	0.58	0.59	
	Concentrate	228500	308	N/A	N/A	97	43	2.92	7	0.06	5.0	1.7	6.6	1.0	4.7	1.1	0.21	0.89	0.11	0.60	0.12	0.32	0.05	0.34	0.07	0.60	BDL	BDL	0.75	0.64	
	Concentrate	215100	185	N/A	N/A	80	45	2.66	6	0.01	7.6	1.5	5.3	0.9	4.0	0.9	0.16	0.82	0.10	0.58	0.11	0.30	0.04	0.31	0.07	0.59	BDL	BDL	0.76	0.60	
	Concentrate	221700	365	N/A	N/A	31	181	6.11	53	0.14	0.0	3.3	15.9	3.1	16.7	4.4	1.33	3.53	0.43	2.05	0.29	0.57	0.06	0.27	0.03	3.19	BDL	BDL	0.01	BDL	
	Concentrate	223500	198	N/A	N/A	80	47	2.65	6	0.01	12.2	1.8	6.3	0.9	4.3	1.0	0.17	0.89	0.11	0.58	0.11	0.29	0.04	0.31	0.07	0.63	BDL	BDL	0.39	0.41	
	Concentrate	223600	600	N/A	N/A	99	80	4.29	6	0.32	15.6	2.1	6.8	1.1	4.9	1.2	0.28	1.09	0.15	0.87	0.16	0.44	0.06	0.47	0.09	0.50	BDL	BDL	0.28	0.11	
	Concentrate	198700	190	N/A	N/A	94	73	2.47	8	0.02	18.9	1.7	5.8	0.9	4.0	0.8	0.18	0.70	0.09	0.51	0.10	0.26	0.04	0.31	0.07	0.59	BDL	BDL	0.55	0.58	
	Concentrate	228300	209	N/A	N/A	98	149	2.05	6	0.08	33.5	2.5	6.2	0.9	3.7	0.8	0.18	0.60	0.08	0.44	0.08	0.22	0.03	0.26	0.06	0.52	BDL	BDL	1.28	1.34	
	Concentrate	207100	190	N/A	N/A	77	86	2.20	6	0.01	36.7	1.3	4.8	0.8	3.6	0.8	0.15	0.72	0.09	0.46	0.09	0.23	0.03	0.28	0.06	0.56	BDL	BDL	0.54	0.57	
	Concentrate	209000	204	N/A	N/A	84	30	2.30	7	0.01	6.9	1.5	5.6	0.8	3.7	0.8	0.15	0.68	0.09	0.48	0.10	0.24	0.04	0.29	0.06	0.52	BDL	BDL	0.23	0.30	
	Concentrate	222300	443	N/A	N/A	97	48	3.56	16	0.18	8.8	3.9	11.0	1.5	6.3	1.3	0.25	1.09	0.14	0.77	0.14	0.39	0.05	0.38	0.08	0.91	BDL	BDL	0.55	0.48	
	Concentrate	212500	352	N/A	N/A	103	44	3.19	14	0.10	4.1	2.1	7.8	1.2	5.4	1.2	0.24	0.97	0.12	0.66	0.13	0.34	0.05	0.35	0.08	0.86	BDL	BDL	0.30	0.23	
	Concentrate	185000	1322	N/A	N/A	85	353	3.55	29	0.92	398.0	4.1	11.5	1.6	6.5	1.4	0.27	1.01	0.14	0.76	0.14	0.40	0.06	0.39	0.07	1.08	BDL	BDL	0.58	0.77	
	Concentrate	222200	185	N/A	N/A	99	39	2.46	6	0.01	14.9	2.1	6.5	1.0	4.3	0.9	0.19	0.70	0.09	0.50	0.10	0.26	0.04	0.30	0.07	0.56	BDL	BDL	0.54	0.71	
	Concentrate	242300	307	N/A	N/A	128	67	2.65	8	0.11	23.3	2.4	7.3	1.0	4.3	1.0	0.21	0.77	0.10	0.55	0.11	0.29	0.04	0.32	0.07	0.49	BDL	BDL	0.63	0.67	
	Concentrate	226600	181	N/A	N/A	88	51	2.62	5	0.03	16.0	1.2	4.5	0.7	3.2	0.8	0.16	0.73	0.10	0.55	0.11	0.29	0.04	0.32	0.08	0.46	BDL	BDL	0.37	0.25	
	Concentrate	221100	1390	N/A	N/A	123	160	5.00	10	1.32	62.6	6.4	20.9	2.8	11.2	2.1	0.46	1.55	0.19	1.02	0.20	0.55	0.07	0.53	0.09	0.60	BDL	BDL	2.04	1.73	
	Concentrate	228500	84	N/A	N/A	236	1102	18.92	32	0.36	1.3	30.1	130.0	19.4	82.6	15.9	4.43	10.69	1.24	5.58	0.83	1.65	0.17	0.83	0.09	1.27	BDL	BDL	0.08	0.10	
	Concentrate	203300	275	N/A	N/A	86	80	2.74	7	0.08	28.7	2.0	7.1	1.1	4.7	1.0	0.20	0.78	0.10	0.57	0.11	0.29	0.04	0.32	0.07	0.52	BDL	BDL	0.63	0.60	
	Concentrate	267100	207	N/A	N/A	133	52	2.08	6	0.03	49.3	2.8	7.8	1.1	4.2	0.8	0.18	0.66	0.08	0.44	0.08	0.21	0.03	0.24	0.05	0.44	BDL	BDL	0.65	1.03	
	Concentrate	240900	204	N/A	N/A	114	127	1.93	7	0.26	42.6	2.3	7.9	1.0	3.8	0.7	0.17	0.54	0.07	0.39	0.08	0.22	0.03	0.28	0.05	0.43	BDL	BDL	0.24	0.26	
	Concentrate	228600	503	N/A	N/A	109	110	2.80	10	0.36	15.7	4.9	14.0	1.7	6.3	1.1	0.25	0.78	0.10	0.55	0.10	0.29	0.04	0.27	0.05	0.51	BDL	BDL	2.19	2.21	
	Concentrate	253900	281	N/A	N/A	122	50	2.57	9	0.03	22.5	2.6	7.9	1.1	5.0	1.0	0.21	0.83	0.10	0.56	0.11	0.29	0.04	0.32	0.07	0.75	BDL	BDL	0.88	0.75	
	Concentrate	266000	111	N/A	N/A	260	921	16.65	44	0.75	4.3	27.0	131.5	18.5	75.9	14.6	4.06	9.81	1.15	5.15	0.76	1.49	0.15	0.72	0.08	1.69	BDL	BDL	0.14	0.09	
	Concentrate	264800	760	N/A	N/A	134	25	3.31	12	1.83	66.8	2.3	7.2	0.9	3.6	0.9	0.25	0.76	0.12	0.67	0.14	0.38	0.06	0.42	0.08	0.55	BDL	BDL	0.26	0.08	
	Concentrate	263000	224	N/A	N/A	283	625	18.33	16	1.87	52.7	26.9	121.9	16.2	60.3	11.2	3.20	7.47	0.93	4.56	0.71	1.64	0.19	1.07	0.13	0.83	BDL	BDL	0.57	0.40	
	Concentrate	199200	140	N/A	N/A	181	429	17.22	60	0.89	10.7	18.3	75.7	13.5	62.3	13.8	3.93	10.11	1.15	5.52	0.80	1.58	0.16	0.78	0.08	3.17	BDL	BDL	0.17	BDL	
	Concentrate	208300	190	N/A	N/A	67	50	2.77	6	0.02	8.5	1.0	3.8	0.6	3.0	0.8	0.18	0.73	0.10	0.56	0.11	0.29	0.04	0.33	0.08	0.52	BDL	BDL	0.36	0.39	
	Concentrate	283200	2080	N/A	N/A	642	120	2.86	10	0.22	1.7	2.3	10.4	1.6	7.4	1.7	0.50	1.29	0.16	0.75	0.12	0.25	0.03	0.14	0.02	0.59	BDL	BDL	0.02	0.01	
	Concentrate	271800	406	N/A	N/A	118	46	3.30	12	0.15	13.0	1.9	8.8	1.3	5.8	1.3	0.23	1.16	0.15	0.75	0.14	0.38	0.05	0.35	0.08	0.88	BDL	BDL	0.18	0.11	
	Concentrate	195000	160	N/A	N/A	81	113	2.20	4	0.02	27.2	1.6	4.2	0.6	2.7	0.6	0.14	0.57	0.07	0.43	0.08	0.23	0.03	0.27	0.06	0.40	BDL	BDL	0.30	0.13	
	Concentrate	255500	193	N/A	N/A	115	56	2.43	6	0.01	22.9	4.3	11.6	1.2	4.9	0.9	0.19	0.72	0.09	0.51	0.10	0.27	0.04	0.30	0.07	0.53	BDL	BDL	0.68	0.41	
	Concentrate	200400	253	N/A	N/A	271	1212	12.71	34	1.36	265.3	19.1	80.4	12.0	51.0	10.5	3.00	7.49	0.84	3.84	0.56	1.14	0.11	0.52	0.06	1.33	BDL	BDL	2.72	2.50	
	Concentrate	257500	32	N/A	N/A	311	663	1.94	4	1.46	5.7	10.2	46.4	6.8	25.6	3.9	0.99	1.92	0.18	0.70	0.08	0.14	0.01	0.06	0.01	0.05	BDL	BDL	0.13	0.05	
	Concentrate	279800	1170	N/A	N/A	762	90	2.08	3	0.13	7.8	1.5	5.6	0.8	4.0	1.1	0.33	0.92	0.11	0.54	0.09	0.17	0.02	0.10	0.01	0.15	BDL	BDL	0.01	BDL	
	Concentrate	228500	87	N/A	N/A	257	954	18.44	38	0.34	0.4	25.7	116.2	18.6	80.7	16.3	4.45	11.06	1.28	5.69	0.83	1.69	0.16	0.80	0.09	1.52	BDL	BDL	0.09	0.08	
	Concentrate	239000	299	N/A	N/A	231	1534	24.76	41	1.18	58.9	44.3	182.0	25.0	100.0	18.7	5.16	12.27	1.43	6.57	1.01	2.18	0.23	1.28	0.17	1.82	BDL	BDL	0.14	0.36	
	Concentrate	227900	270	N/A	N/A	251	622	17.06	18	5.22	48.3	25.9	100.9	14.4	55.0	10.4	2.92	6.66	0.83	4.10	0.65	1.51	0.17	0.95	0.12	1.14	BDL	BDL	0.32	0.30	
	Concentrate	210400	204	N/A	N/A	88	69	2.53	6	0.01	22.8	1.5	4.7	0.8	3.5	0.8	0.17	0.67	0.09	0.50	0.10	0.26	0.04	0.32	0.07	0.59	BDL	BDL	0.64	0.52	
	Concentrate	220700	58	N/A	N/A	236	946	15.46	30	0.34	0.2	22.2	99.3	15.4	65.3	13.1	3.69	8.89	1.04	4.67	0.68	1.36	0.13	0.66	0.08	1.20	BDL	BDL	0.09	0.04	
	Concentrate	188100	429	N/A	N/A	194	204	7.57	29	6.38	13.0	5.1	19.4	3.3	15.4	3.9	1.21	3.15	0.40	2.00	0.32	0.70	0.07	0.41	0.05	1.07	BDL	BDL	0.09	BDL	
	Concentrate	219400	96	N/A	N/A	208	963	18.90	44	0.40	1.0	28.4	122.0	18.2	78.0	15.4	4.33	10.39	1.22	5.66	0.82	1.65	0.17	0.80	0.09	1.68	BDL	BDL	0.09	0.08	
	Concentrate	228800	110	N/A	N/A	258	1664	37.78	34	2.15	16.6	54.6	245.4	38.6	164.8	31.3	8.44	20.20	2.33	10.53	1.52	3.17	0.33	1.67	0.20	1.22	BDL	BDL	1.10	0.86	
	Concentrate	222400	52	N/A	N/A	227	1329	23.07	34	1.25	20.1	32.6	154.3	23.1	99.5	19.0	5.49	12.65	1.47	6.71	1.00	2.01	0.21	1.06	0.13	1.32	BDL	BDL	0.52	0.70	
	Concentrate	216800	97	N/A	N/A	194	908	18.13	46	0.47	0.6	27.3	115.5	17.5	75.7	14.6	4.19	10.09	1.19	5.50	0.81	1.64	0.16	0.80	0.08	1.73	BDL	BDL	0.12	0.08	
	Concentrate	211500	98	N/A	N/A	196	939	19.38	45	0.35	0.2	28.5	120.8	18.4	79.9	15.5	4.47	10.59	1.26	5.84	0.85	1.70	0.17	0.84	0.09	1.68	BDL	BDL	0.09	0.06	
	Concentrate	207900	215	N/A	N/A	203	619	11.47	23	0.20	0.1	12.7	52.6	8.9	40.2	8.6	2.50	6.02	0.73	3.39	0.50	1.04	0.11	0.58	0.07	1.09	BDL	BDL	0.14	0.08	
	Concentrate	210700	42	N/A	N/A	267	27	0.18	1	0.09	1.0	2.0	3.7	0.4	1.2	0.1	0.04	0.09	0.01	0.04	0.01	0.02	0.00	0.01	0.00	0.05	BDL	BDL	0.09	BDL	
	Concentrate	210400	61	N/A	N/A	195	1687	35.64	31	0.52	5.8	49.9	209.5	32.5	141.1	27.7	7.88	18.77	2.24	10.41	1.52	3.06	0.31	1.62	0.19	1.09	BDL	BDL	0.10	0.04	
	Concentrate	213000	646	N/A	N/A	148	194	6.43	63	1.94	31.7	6.3	24.8	4.1	19.0	4.3	1.33	3.25	0.42	2.03	0.30	0.64	0.07	0.40	0.05	3.46	BDL	BDL	0.25	0.03	
	Concentrate	235000	60	N/A	N/A	223	1172	22.60	23	0.39	15.0	41.7	206.0	28.3	112.7	20.7	5.96	13.37	1.55	6.83	1.03	2.04	0.22	1.07	0.14	1.05	BDL	BDL	0.12	0.14	
	Concentrate	220500	508	N/A	N/A	231	332	6.31	48	0.23	1.9	13.2	52.3	7.6	31.0	6.0	1.68	3.88	0.47	2.02	0.29	0.56	0.06	0.27	0.03	1.57	BDL	BDL	0.06	0.02	
	Concentrate	215300	530	N/A	N/A	221	734	4.63	29	1.09	2.6	24.9	84.1	11.7	47.8	8.6	2.35	5.03	0.50	1.88	0.21	0.32	0.02	0.09	0.01	1.11	BDL	BDL	0.65	0.76	
	Concentrate	234300	1187	N/A	N/A	569	95	1.76	3	0.12	0.4	1.5	5.4	0.9	4.3	1.1	0.33	0.86	0.11	0.48	0.08	0.15	0.02	0.08	0.01	0.19	BDL	BDL	0.01	BDL	
	Concentrate	203900	94	N/A	N/A	184	841	19.45	49	0.35	0.3	24.7	96.4	16.2	72.9	14.8	4.26	10.58	1.28	5.95	0.87	1.75	0.17	0.85	0.09	1.93	BDL	BDL	0.08	0.06	
	Concentrate	219500	2380	N/A	N/A	436	136	1.74	7	0.17	0.3	1.8	7.0	1.2	6.0	1.4	0.43	1.07	0.12	0.53	0.07	0.14	0.01	0.07	0.01	0.56	BDL	BDL	0.02	BDL	
	Concentrate	217100	82	N/A	N/A	202	549	10.43	36	0.28	0.2	12.4	56.0	9.5	42.6	9.1	2.74	6.48	0.77	3.47	0.49	0.95	0.09	0.46	0.05	1.85	BDL	BDL	0.04	0.02	
	Concentrate	216600	120	N/A	N/A	204	435	16.56	53	0.66	2.2	17.6	86.1	13.9	60.9	13.2	3.97	9.15	1.12	5.22	0.75	1.54	0.15	0.78	0.09	2.64	BDL	BDL	0.12	0.11	
	Concentrate	213800	2461	N/A	N/A	403	147	2.21	9	0.80	20.2	2.8	9.9	1.7	8.5	1.7	0.44	1.08	0.13	0.60	0.09	0.19	0.02	0.11	0.01	0.46	BDL	BDL	0.08	BDL	
	Concentrate	222500	1099	N/A	N/A	197	32	14.72	7	0.12	8.8	0.7	2.1	0.3	1.4	0.6	0.28	1.18	0.27	2.22	0.55	1.74	0.26	1.94	0.28	0.22	BDL	BDL	0.01	BDL	
	Concentrate	254600	76	N/A	N/A	270	638	13.17	37	1.36	12.6	16.9	88.3	13.1	55.3	11.3	3.42	7.80	0.95	4.31	0.61	1.19	0.12	0.56	0.06	1.66	BDL	BDL	0.22	0.31	
	Concentrate	202800	19	N/A	N/A	185	1757	42.89	30	0.36	1.0	54.1	226.0	36.2	158.9	31.8	9.01	21.72	2.60	12.19	1.80	3.74	0.38	1.96	0.23	1.15	BDL	BDL	0.10	0.05	
	Concentrate	228500	139	N/A	N/A	89	40	2.60	4	0.04	6.3	0.9	3.9	0.6	3.1	0.7	0.17	0.67	0.09	0.52	0.10	0.27	0.04	0.31	0.07	0.38	BDL	BDL	0.25	0.22	
	Concentrate	265200	452	N/A	N/A	129	77	3.54	17	0.24	26.4	7.9	20.2	2.0	7.6	1.4	0.26	1.10	0.14	0.80	0.15	0.41	0.06	0.45	0.08	0.88	BDL	BDL	1.92	2.04	
	Concentrate	235100	78	N/A	N/A	257	1251	27.57	35	0.32	0.2	42.4	185.0	28.0	121.3	23.2	6.50	15.65	1.87	8.41	1.23	2.40	0.24	1.14	0.13	1.55	BDL	BDL	0.09	BDL	
	Concentrate	229100	44	N/A	N/A	243	2034	31.92	25	0.44	1.4	50.1	217.7	33.4	144.6	27.0	7.51	18.43	2.18	9.49	1.40	2.81	0.29	1.48	0.16	1.02	BDL	BDL	0.12	BDL	
	Concentrate	251200	271	N/A	N/A	282	607	15.23	17	5.96	17.0	25.3	110.0	14.3	53.8	9.5	2.76	6.06	0.78	3.75	0.61	1.36	0.16	0.90	0.12	1.12	BDL	BDL	0.14	BDL	
	Concentrate	214300	179	N/A	N/A	107	34	2.47	4	0.00	3.2	1.0	4.0	0.7	3.3	0.8	0.17	0.74	0.10	0.53	0.10	0.28	0.04	0.33	0.08	0.42	BDL	BDL	0.08	BDL	
	Concentrate	245400	104	N/A	N/A	245	741	15.00	47	0.64	14.3	20.6	93.7	14.6	63.8	13.0	3.76	9.05	1.08	4.87	0.69	1.35	0.13	0.63	0.07	2.29	BDL	BDL	0.12	0.06	
	Concentrate	277400	77	N/A	N/A	292	835	15.58	37	0.83	5.2	21.2	110.6	15.8	66.5	13.1	3.87	9.16	1.07	4.90	0.70	1.40	0.14	0.68	0.08	1.55	BDL	BDL	0.14	0.23	
	Concentrate	243200	92	N/A	N/A	234	967	18.36	47	0.32	0.2	29.0	134.7	19.7	81.4	15.4	4.43	10.32	1.26	5.64	0.82	1.60	0.17	0.78	0.09	1.80	BDL	BDL	0.09	0.02	
				N/A	N/A																										
M-10	peridotite	206900	1698	N/A	N/A	29	163	2.52	31	0.65	165.0	5.3	19.7	3.6	19.3	5.3	1.39	3.13	0.28	0.97	0.12	0.19	0.02	0.09	0.01	1.20	BDL	BDL	0.08	BDL	
M-10	peridotite	160200	786	N/A	N/A	16	410	1.51	20	0.25	71.7	2.9	11.8	2.3	13.0	3.8	0.96	2.26	0.21	0.66	0.07	0.11	0.01	0.05	0.00	0.86	BDL	BDL	0.01	BDL	

Sample	Rock Type	(ppm)	(ppm)	(ppm)	(ppm)	(ppm)	(ppm)	(ppm)	(ppm)	(ppm)	(ppm)	(ppm)	(ppm)	(ppm)	(ppm)	(ppm)	(ppm)	(ppm)	(ppm)	(ppm)	(ppm)	(ppm)	(ppm)	(ppm)	(ppm)	(ppm)	(ppm)	(ppm)	(ppm)	(ppm)	Notes
B-8	cpx macrocryst	276000	1265	N/A	N/A	145	129	4.28	BDL	0.74	6.1	2.6	11.6	1.8	9.0	2.1	2.43	1.80	0.77	2.94	0.22	0.36	0.04	0.23	0.02	BDL	BDL	BDL	0.09	BDL	
B-8	cpx macrocryst	250600	1272	N/A	N/A	136	127	4.16	251	0.40	3.1	2.1	9.7	1.7	8.6	2.2	1.86	1.86	0.62	2.49	0.23	0.36	0.04	0.21	0.02	BDL	BDL	BDL	0.04	BDL	
B-11	lherzolite	248000	2867	N/A	N/A	249	99	2.13	71	0.41	25.5	1.8	5.1	0.7	3.7	1.1	0.88	1.19	0.30	1.28	0.10	0.14	0.02	0.08	0.01	4.01	BDL	BDL	0.09	BDL	
B-11	lherzolite	232400	2696	N/A	N/A	230	71	2.22	39	0.17	2.4	1.1	4.1	0.6	3.3	1.1	0.71	1.09	0.23	1.00	0.10	0.15	0.02	0.09	0.01	1.76	BDL	BDL	0.04	0.02	
B-11	lherzolite	224100	2853	N/A	N/A	210	70	1.83	30	0.09	1.2	1.1	3.7	0.6	3.3	1.1	0.57	1.08	0.19	0.82	0.09	0.12	0.01	0.06	0.01	1.25	BDL	BDL	0.02	BDL	
B-11	lherzolite	229100	2519	N/A	N/A	253	79	2.37	22	1.56	11.4	1.7	5.2	0.8	4.0	1.2	0.56	1.17	0.20	0.86	0.10	0.19	0.02	0.11	0.01	0.87	BDL	BDL	0.09	BDL	
B-11	lherzolite	227900	2760	N/A	N/A	221	83	2.06	19	0.16	14.2	1.4	4.6	0.7	3.7	1.1	0.45	1.12	0.15	0.72	0.09	0.15	0.02	0.08	0.01	0.72	BDL	BDL	0.05	BDL	
R-5	**pyroxenite**	196700	5099	N/A	N/A	34	309	5.89	354	0.004	102.7	4.7	18.7	3.8	22.1	6.6	4.12	4.69	1.00	3.52	0.28	0.40	0.039	0.19	0.014	19.85	BDL	BDL	0.058	0.02	
B-4	**pyroxenite**	217700	2000	N/A	N/A	200	190	2.12	BDL	0.970	5.6	2.2	8.2	1.6	8.6	2.1	2.71	1.40	0.57	1.81	0.11	0.15	0.019	0.10	0.007	BDL	BDL	BDL	0.109	0.02	
B-4	**pyroxenite**	213500	2340	N/A	N/A	196	190	2.20	BDL	1.250	3.5	2.3	8.4	1.6	8.6	2.1	3.29	1.43	0.72	2.15	0.11	0.17	0.019	0.11	0.008	BDL	BDL	BDL	0.098	0.13	
B-4	**pyroxenite**	225300	2030	N/A	N/A	177	199	2.00	BDL	0.344	1.6	2.1	8.5	1.5	8.3	2.1	3.18	1.34	0.68	1.92	0.11	0.15	0.016	0.10	0.008	BDL	BDL	BDL	0.067	0.05	
B-4	**pyroxenite**	218900	1570	N/A	N/A	187	194	2.09	BDL	0.270	2.6	2.2	8.7	1.6	8.6	2.1	2.88	1.43	0.63	1.93	0.10	0.17	0.017	0.09	0.008	BDL	BDL	BDL	0.082	0.02	
B-4	**pyroxenite**	265000	1820	822	804	110	212	2.14	15	2.260	1.5	2.0	8.1	1.5	7.9	2.0	0.60	1.41	0.15	0.64	0.08	0.17	0.017	0.12	BDL	0.72	BDL	BDL	0.040	0.30	
B-4	**pyroxenite**	245100	1348	776	772	104	206	1.97	16	0.055	0.2	2.3	8.9	1.7	8.7	2.2	0.65	1.51	0.16	0.65	0.10	0.14	0.018	0.06	0.011	0.71	BDL	BDL	0.058	BDL	
B-4	**pyroxenite**	262000	2250	796	780	110	202	2.23	16	0.224	0.6	2.3	8.2	1.6	9.1	2.2	0.72	1.56	0.15	0.77	0.11	0.18	0.019	0.09	0.013	0.68	BDL	BDL	0.050	0.80	
B-4	**pyroxenite**	239000	1073	779	766	97	207	2.13	15	0.039	0.1	2.1	7.8	1.5	8.1	2.1	0.60	1.49	0.17	0.67	0.09	0.17	0.027	0.09	0.042	0.76	BDL	BDL	0.041	BDL	
B-4	**pyroxenite**	253000	876	825	793	97	230	2.13	14	0.310	1.0	1.8	7.5	1.4	7.6	2.0	0.61	1.45	0.16	0.70	0.09	0.16	0.016	0.10	0.015	0.69	BDL	BDL	0.043	0.20	
B-4	**pyroxenite**	256700	2120	808	790	108	203	2.20	15	1.070	1.2	2.1	8.2	1.5	8.6	2.3	0.66	1.55	0.18	0.71	0.09	0.18	0.019	0.10	0.009	0.71	BDL	BDL	0.049	BDL	
B-13	**pyroxenite**	238700	2983	254	258	59	15	2.51	49	BDL	0.9	6.0	22.9	3.6	15.8	3.3	0.65	2.20	0.24	0.89	0.11	0.18	0.015	0.16	0.031	2.26	BDL	BDL	0.300	0.44	
B-13	**pyroxenite**	241100	2808	250	252	61	14	2.62	46	BDL	BDL	5.4	22.4	3.5	15.5	3.3	0.60	2.26	0.23	0.95	0.11	0.20	0.020	0.11	0.025	2.04	BDL	BDL	0.280	0.34	
B-13	**pyroxenite**	240700	2576	278	281	57	13	2.31	45	BDL	BDL	5.7	22.1	3.4	14.9	3.3	0.62	2.05	0.21	0.86	0.10	0.19	0.015	0.08	BDL	2.12	BDL	BDL	0.204	0.20	
B-13	**pyroxenite**	248600	2543	305	311	62	14	2.31	44	BDL	0.4	5.5	22.9	3.4	15.3	3.2	0.63	1.93	0.22	0.86	0.09	0.20	0.012	0.08	0.025	2.05	BDL	BDL	0.153	0.27	
B-13	**pyroxenite**	246700	3092	260	259	60	13	2.90	50	BDL	BDL	7.2	26.0	3.8	16.7	3.6	0.66	2.33	0.24	1.00	0.13	0.21	0.020	0.11	0.028	2.19	BDL	BDL	0.900	0.99	
B-13	**pyroxenite**	244000	2765	259	259	58	14	2.48	46	0.005	0.9	5.8	23.3	3.6	16.0	3.3	0.65	2.09	0.22	0.88	0.11	0.20	0.013	0.09	BDL	2.02	BDL	BDL	0.195	0.37	
B-9	**pyroxenite**	253000	3950	207	207	27	20	1.02	26	0.005	0.1	4.1	18.2	2.7	10.5	1.8	0.68	0.94	0.09	0.30	0.04	0.09	0.007	0.06	0.005	1.26	BDL	BDL	0.375	3.30	
B-9	**pyroxenite**	248200	3221	211	210	25	19	0.88	24	0.003	0.1	3.8	16.3	2.5	10.4	1.8	0.64	0.79	0.08	0.31	0.04	0.07	0.008	0.03	0.005	1.28	BDL	BDL	0.265	BDL	
B-9	**pyroxenite**	253500	3434	200	194	24	18	0.79	25	BDL	BDL	3.6	16.6	2.6	10.8	1.7	0.69	0.79	0.06	0.28	0.03	0.06	0.006	0.03	BDL	1.23	BDL	BDL	0.143	BDL	
B-9	**pyroxenite**	246400	3540	204	203	26	22	0.92	24	0.017	0.1	3.9	15.8	2.3	9.8	1.6	0.62	0.83	0.08	0.30	0.04	0.08	0.007	0.03	BDL	1.17	BDL	BDL	0.389	1.70	
B-9	**pyroxenite**	244000	3186	173	172	22	20	0.80	25	0.008	0.0	3.6	14.9	2.4	9.9	1.7	0.62	0.90	0.07	0.25	0.04	0.07	0.005	0.05	0.005	1.35	BDL	BDL	0.319	BDL	
B-9	**pyroxenite**	239700	3002	195	193	21	17	0.71	25	0.001	0.1	3.4	15.5	2.5	10.6	1.7	0.67	0.79	0.07	0.26	0.03	0.05	0.006	BDL	BDL	1.31	BDL	BDL	0.108	0.09	
M-19A	**pyroxenite**	236700	2540	146	142	31	33	2.26	28	0.006	0.2	3.3	14.1	2.8	15.6	4.1	1.43	2.50	0.24	0.89	0.10	0.14	0.013	0.05	0.008	1.60	BDL	BDL	0.002	BDL	
M-19A	**pyroxenite**	238200	2617	136	131	33	39	2.33	27	0.348	4.1	3.6	16.2	3.1	17.2	4.3	1.26	2.57	0.22	0.85	0.10	0.17	0.014	0.09	0.010	1.52	BDL	BDL	0.009	BDL	Ba (inclusion?)
M-19A	**pyroxenite**	235900	2198	124	120	29	34	1.65	24	0.101	1.1	2.4	13.0	2.8	16.4	4.1	1.33	2.21	0.19	0.64	0.07	0.11	0.009	0.06	0.005	1.45	BDL	BDL	0.003	BDL	
M-19A	**pyroxenite**	245400	2464	114	111	34	36	2.30	26	0.003	1.7	3.6	15.7	3.0	16.2	4.1	1.25	2.53	0.22	0.86	0.10	0.17	0.015	0.07	0.010	1.39	BDL	BDL	0.005	BDL	
M-19B	**pyroxenite**	210700	2566	N/A	N/A	27	29	2.20	25	0.003	0.0	3.0	15.1	2.9	15.9	4.0	1.24	2.32	0.22	0.82	0.09	0.17	0.014	0.08	0.008	1.29	BDL	BDL	0.006	BDL	
M-19B	**pyroxenite**	228900	1700	N/A	N/A	29	31	1.73	22	0.013	1.1	3.4	15.2	2.9	15.9	3.8	1.21	2.20	0.20	0.68	0.08	0.12	0.010	0.06	0.005	1.24	BDL	BDL	0.200	0.10	
M-19B	**pyroxenite**	213900	2075	N/A	N/A	27	29	1.29	21	BDL	7.3	3.2	13.7	2.6	14.9	3.7	1.21	1.91	0.16	0.54	0.05	0.08	0.007	0.03	0.003	1.13	BDL	BDL	0.013	BDL	Ba (inclusion?)
M-19B	**pyroxenite**	226300	2288	N/A	N/A	30	31	1.68	23	0.002	0.1	4.6	16.9	2.9	15.6	3.8	1.20	2.10	0.19	0.65	0.07	0.12	0.011	0.05	0.006	1.38	BDL	BDL	0.011	BDL	
M-2	**pyroxenite**	254900	2464	898	905	27	41	0.68	41	0.008	4.2	9.9	41.2	6.1	24.8	2.4	1.07	0.78	0.07	0.24	0.03	0.05	0.004	0.03	BDL	2.35	BDL	BDL	0.384	BDL	Ba (inclusion?)
M-2	**pyroxenite**	250300	2589	996	974	25	46	0.90	44	1.050	15.4	10.3	43.8	6.5	26.0	2.6	1.09	0.90	0.07	0.28	0.03	0.06	0.008	BDL	BDL	2.37	BDL	BDL	0.224	BDL	Ba (inclusion?)
R-2-4	**pyroxenite**	246600	6990	230	224	52	163	3.36	45	0.027	1.8	3.5	18.7	3.8	21.2	5.7	1.86	3.87	0.37	1.30	0.15	0.22	0.019	0.07	BDL	1.77	BDL	BDL	0.009	BDL	
R-2-4	**pyroxenite**	256300	3446	206	203	58	165	2.65	41	0.007	0.8	3.3	17.2	3.3	18.5	5.0	1.57	3.33	0.31	1.08	0.11	0.17	0.014	0.04	BDL	1.70	BDL	BDL	0.005	BDL	
R-2-4	**pyroxenite**	247900	6830	227	222	59	154	4.19	45	BDL	0.1	4.3	19.6	3.7	20.5	5.6	1.85	3.94	0.40	1.57	0.18	0.31	0.025	0.12	0.010	1.60	BDL	BDL	0.009	0.02	
R-2-4	**pyroxenite**	256300	6400	378	370	71	173	4.85	41	0.004	0.9	4.8	19.6	3.7	20.4	5.5	1.82	3.85	0.41	1.64	0.21	0.39	0.038	0.14	0.014	1.51	BDL	BDL	0.010	0.66	
R-2-4	**pyroxenite**	264300	6710	455	446	85	178	5.09	39	0.019	0.3	4.2	18.6	3.5	19.0	5.1	1.67	3.67	0.39	1.67	0.22	0.43	0.037	0.18	0.019	1.34	BDL	BDL	0.011	BDL	

Sample	Si 29 (ppm)	Ti 49 (ppm)	V 51 (ppm)	Cr 52 (ppm)	Cr 53 (ppm)	Ni 60 (ppm)	Rb 85 (ppm)	Sr 88 (ppm)	Y 89 (ppm)	Zr 90 (ppm)	Nb 93 (ppm)	Ba 137 (ppm)	La 139 (ppm)	Ce 140 (ppm)	Pr 141 (ppm)	Nd 146 (ppm)	Sm 147 (ppm)	Eu 153 (ppm)	Gd 157 (ppm)	Tb 159 (ppm)	Dy 163 (ppm)	Ho 164 (ppm)	Er 166 (ppm)	Tm 169 (ppm)	Yb 172 (ppm)	Lu 175 (ppm)	Hf 178 (ppm)	Ta 181 (ppm)	Pb 204 (ppm)	Pb 208 (ppm)	Th 232 (ppm)	U 238 (ppm)	ThO16 232 (ppm)	Nb/Ta
R-2-4	BDL	606300	1606	1480	1646	1.65	BDL	14.7	0.213	1761	0.987	1.08	0.78	2.89	0.576	3.21	0.63	0.198	0.259	0.034	0.091	BDL	0.013	BDL	BDL	BDL	43.2	0.919	BDL	0.038	BDL	0.681	BDL	1.1
R-2-4	BDL	598000	2109	2147	2351	BDL	BDL	0.426	0.066	1981	62.12	BDL	BDL	BDL	BDL	BDL	BDL	BDL	BDL	BDL	BDL	BDL	BDL	BDL	BDL	BDL	49.31	5.5	BDL	BDL	BDL	0.669	BDL	11.3
R-2-4	BDL	599100	1974	2168	2309	BDL	BDL	0.449	0.052	1974	60.75	BDL	BDL	BDL	BDL	BDL	BDL	BDL	BDL	BDL	BDL	BDL	BDL	BDL	BDL	BDL	49.55	5.47	0.73	0.45	BDL	0.664	BDL	11.1
R-2-4	BDL	598800	1604	738	779	16.9	3.5	47	4.9	1615	100.9	5	3.07	8.1	1.42	7.4	2.05	0.63	1.56	0.174	0.95	0.168	0.57	0.061	0.45	BDL	31.69	11.09	BDL	0.48	0.024	0.282	BDL	9.1
R-2-4	221000	598800	3170	880	891	60	20.4	450	6.9	2059	43	31.5	77	209	26.8	119	17.4	5.4	9.4	0.63	2.52	0.32	0.42	0.044	0.127	BDL	63.4	6.18	2.2	0.87	1.24	0.81	24	7.0
R-2-4	BDL	597000	2551	640.9	646	13.7	19.6	430	1.97	1740	24.03	24.1	33.6	85	10	40	4.5	1.33	2.49	0.157	0.5	0.051	0.139	0.0105	BDL	BDL	45.7	4.58	1.11	0.57	0.113	0.545	4	5.2
R-2-4	BDL	605900	2750	1115.6	1124	9.9	BDL	62	0.576	1223	7.88	10.9	4.21	7.14	1.16	5.93	1.43	1.19	0.86	0.07	0.246	0.0143	BDL	BDL	BDL	BDL	43.2	0.859	0.47	0.186	0.012	0.397	1.7	9.2
M-2	BDL	596400	834	841.1	833	BDL	BDL	0.403	BDL	1754	141.6	BDL	BDL	BDL	BDL	BDL	BDL	BDL	BDL	BDL	BDL	0.0003	BDL	0.0005	BDL	BDL	65.9	19.9	1.19	BDL	BDL	33.16	BDL	7.1
M-2	BDL	597200	1001	843.9	835	BDL	BDL	0.429	0.037	2207	195.1	BDL	BDL	BDL	BDL	BDL	BDL	BDL	BDL	BDL	BDL	BDL	BDL	BDL	0.061	BDL	84.8	25.4	0.95	BDL	BDL	40.18	BDL	7.7
M-2	BDL	597200	1141	861	827	BDL	BDL	0.414	0.057	2298	173.7	BDL	BDL	0.034	BDL	BDL	BDL	BDL	BDL	BDL	BDL	BDL	BDL	BDL	BDL	BDL	86.4	26.06	BDL	BDL	BDL	39.69	BDL	6.7
M-2	BDL	602800	957	782	759	BDL	BDL	0.414	0.033	2171	192.2	BDL	BDL	BDL	BDL	BDL	BDL	BDL	BDL	BDL	BDL	BDL	BDL	BDL	BDL	0.019	85.5	25.24	0.64	BDL	BDL	39.82	BDL	7.6
M-2	BDL	592600	1230	779	738	BDL	6.3	51	BDL	1216	89.2	27.9	0.42	0.41	0.03	BDL	BDL	0.0078	BDL	BDL	BDL	BDL	BDL	BDL	BDL	BDL	45.9	13.5	BDL	0.042	BDL	19.75	BDL	6.6
M-19B	BDL	593000	1440	258	252	28.9	22.8	109	0.92	4841	611.2	610	7.1	10.7	1.12	3.9	0.54	0.21	0.63	0.04	0.16	0.021	0.038	0.0128	BDL	BDL	129.4	33.62	2.06	2.28	0.046	7.3	BDL	18.2
M-19B	BDL	592600	1080	235.8	220.8	3.1	1.1	162	0.86	5496	628	185	7.2	9.6	0.95	3.5	0.52	0.181	0.43	0.045	0.24	0.019	0.023	0.0078	BDL	BDL	144.9	37.42	3.1	3.12	BDL	8.94	BDL	16.8
M-19B	BDL	591900	698	238.6	233.1	BDL	BDL	0.448	0.048	5415	630.6	BDL	0.019	BDL	BDL	BDL	BDL	BDL	BDL	BDL	BDL	BDL	BDL	0.0011	BDL	BDL	142.9	36.12	0.59	BDL	BDL	9.38	2.2	17.5
M-19B	BDL	591800	607	237	227.1	BDL	BDL	0.457	0.055	5345	635	BDL	BDL	BDL	BDL	BDL	BDL	0.0027	BDL	BDL	BDL	BDL	BDL	BDL	BDL	BDL	143.6	35.64	BDL	BDL	BDL	9.55	BDL	17.8
M-19A	BDL	597100	202.8	96	93.1	BDL	BDL	0.495	BDL	1258	422.2	BDL	0.021	0.029	BDL	BDL	BDL	BDL	BDL	0.0102	BDL	BDL	BDL	BDL	0.104	BDL	38.5	13.18	BDL	BDL	BDL	0.236	BDL	32.0
M-19A	BDL	595600	788	160	143.5	BDL	BDL	0.459	BDL	902	475.4	BDL	BDL	BDL	BDL	BDL	BDL	BDL	BDL	BDL	BDL	BDL	BDL	BDL	BDL	BDL	29.57	39.45	BDL	BDL	BDL	0.39	BDL	12.1
M-19A	BDL	588300	663	310.1	278.2	BDL	BDL	0.453	BDL	1170	384.5	BDL	BDL	BDL	BDL	BDL	BDL	BDL	BDL	BDL	BDL	BDL	BDL	BDL	BDL	BDL	39.89	27.78	BDL	BDL	BDL	0.365	BDL	13.8
M-19A	BDL	594000	522	197.1	173.9	BDL	0.17	4.1	BDL	690.2	334.5	4.3	BDL	BDL	BDL	BDL	BDL	BDL	BDL	BDL	BDL	BDL	BDL	BDL	BDL	BDL	16.33	8.09	0.66	0.096	BDL	0.194	BDL	41.3
M-19A	BDL	596400	444.5	198.2	178.9	BDL	BDL	0.455	0.041	1098	442.4	BDL	BDL	BDL	BDL	BDL	BDL	BDL	BDL	BDL	BDL	BDL	BDL	BDL	BDL	BDL	29.38	12.34	BDL	BDL	BDL	0.098	BDL	35.9
M-19A	BDL	581700	503.1	125.5	107.5	BDL	BDL	0.439	BDL	400.2	29.52	BDL	BDL	BDL	BDL	BDL	BDL	BDL	BDL	BDL	BDL	BDL	BDL	BDL	BDL	BDL	9.57	0.178	0.58	BDL	BDL	0.327	3.1	165.8
M-19A	BDL	598100	427.9	260.4	232	BDL	0.17	28.3	0.04	1116	398.4	29	0.164	0.255	0.0211	0.117	BDL	0.0034	0.122	BDL	BDL	BDL	BDL	BDL	BDL	BDL	37.8	27.92	BDL	BDL	BDL	0.444	BDL	14.3
M-19A	BDL	590300	342	276	243.3	BDL	BDL	11.5	BDL	1060	404	6	0.093	0.07	BDL	BDL	BDL	BDL	BDL	BDL	BDL	BDL	BDL	BDL	BDL	BDL	35.39	24.7	BDL	BDL	BDL	0.39	BDL	16.4
B-9	BDL	587000	1954	453.2	434	BDL	BDL	0.434	0.036	1598	454.5	BDL	BDL	0.027	BDL	BDL	BDL	BDL	BDL	BDL	BDL	BDL	BDL	BDL	BDL	BDL	53.2	14.89	BDL	BDL	BDL	20.41	BDL	30.5
B-9	BDL	595700	1963	561.7	527.8	BDL	10.2	375	0.055	1614	689.7	127	2.29	1.95	0.082	0.171	BDL	0.236	BDL	BDL	BDL	BDL	BDL	BDL	BDL	BDL	52.3	53.25	0.47	0.149	BDL	19.54	1.1	13.0
B-9	620000	590100	2560	377	380	46	6.6	540	4.9	1557	1008	376	29.6	28.2	1.78	5	0.67	1.67	0.73	0.101	0.78	0.162	0.56	0.061	0.44	0.067	50.5	60.4	2.1	2.01	0.5	19.36	BDL	16.7
B-9	BDL	583000	2150	586	560	BDL	BDL	0.497	0.045	1599	773	BDL	BDL	BDL	BDL	BDL	BDL	BDL	BDL	BDL	BDL	BDL	BDL	BDL	BDL	BDL	51.9	61.71	BDL	BDL	BDL	21.93	BDL	12.5
B-9	BDL	590800	2085	526.1	484.4	1.13	2.23	12.7	0.062	1600	659.5	8.2	0.155	0.093	0.015	BDL	BDL	0.026	BDL	BDL	BDL	BDL	BDL	BDL	BDL	BDL	50.83	47.97	0.96	1.23	BDL	20.65	BDL	13.7
B-3	BDL	598800	2492	1320	1352	BDL	BDL	0.485	BDL	1735	1418	BDL	BDL	BDL	BDL	BDL	BDL	BDL	BDL	BDL	BDL	BDL	BDL	BDL	BDL	BDL	55.8	113.6	BDL	BDL	BDL	1.44	BDL	12.5
B-3	140000	598200	1708	2810	2940	60	56.1	4590	99	2913	339.8	13400	7.7	29.3	5.14	28.4	6.8	1.36	8.8	1.65	14.9	3.78	14.4	2.32	18	3.13	101.9	8.67	8.2	7.8	1.41	0.417	BDL	39.2
B-3	BDL	592700	2019	4092	4243	2.2	BDL	0.464	BDL	2282	716.9	BDL	BDL	0.088	0.009	0.049	BDL	BDL	BDL	BDL	BDL	BDL	BDL	BDL	BDL	BDL	72.9	48.73	BDL	BDL	BDL	2.042	0.5	14.7
B-3	BDL	590300	2052	3956	4201	BDL	BDL	0.462	BDL	2215	722	BDL	BDL	0.035	BDL	0.056	BDL	BDL	BDL	BDL	BDL	BDL	BDL	0.0006	BDL	BDL	70.4	47.55	BDL	BDL	BDL	1.99	4.4	15.2
B-3	BDL	592400	2088	3829	4055	BDL	BDL	0.526	0.074	2415	721.5	BDL	BDL	0.027	BDL	BDL	BDL	BDL	BDL	BDL	BDL	BDL	BDL	BDL	BDL	BDL	76.2	49.37	0.33	BDL	BDL	2.061	3.6	14.6
B-3	BDL	601900	1258	1978	2164	6.2	3.5	2.91	14.1	711	381	3.3	1.87	4	0.4	1.6	0.41	0.048	1.21	0.25	2.2	0.58	2.08	0.3	2.8	0.53	27.89	5.5	0.77	0.98	0.24	1.262	0.4	69.3
B-13	BDL	600000	1116	484	464.1	BDL	BDL	0.434	0.041	2653	88	0.043	0.135	0.236	0.021	BDL	BDL	BDL	BDL	BDL	BDL	BDL	BDL	BDL	BDL	BDL	74.2	5.95	BDL	BDL	0.089	9.15	3.3	14.8
B-13	BDL	597500	1733	736.1	734	BDL	BDL	0.445	0.05	2856	73.7	BDL	BDL	BDL	BDL	BDL	BDL	BDL	BDL	BDL	BDL	BDL	BDL	BDL	BDL	BDL	89.6	7.04	BDL	BDL	BDL	10.67	0.7	10.5
B-13	BDL	593900	1281	558.9	531.5	BDL	BDL	0.54	BDL	2474	85.7	BDL	0.055	0.087	BDL	BDL	BDL	BDL	BDL	BDL	BDL	BDL	BDL	BDL	BDL	BDL	66.3	2.53	0.53	BDL	BDL	10.16	BDL	33.9
B-13	BDL	610000	1417	732	680	BDL	BDL	0.471	BDL	2812	89.3	BDL	BDL	BDL	BDL	BDL	BDL	BDL	BDL	BDL	BDL	BDL	BDL	BDL	BDL	BDL	78.7	5.57	0.7	BDL	BDL	10.79	BDL	16.0
B-13	BDL	597700	1375	713	679	BDL	BDL	0.493	0.044	2786	86	BDL	BDL	BDL	BDL	BDL	BDL	BDL	BDL	BDL	BDL	BDL	BDL	BDL	BDL	BDL	73.3	4.62	BDL	BDL	BDL	10.33	3.1	18.6

7.Whole-rock

Sample	rock type	Crust vs. Mantle Hardman et al. (2018)	SiO2 %	TiO2 %	Al2O3 %	Fe2O3,total %	FeO* All Fe as FeO	MnO %	MgO %	CaO %	Na2O %	K2O %	P2O5 %	SUM	Factor
Xenoliths															
B-9	pyroxenite	mantle	46.72	0.15	17.97	8.14	7.32	0.22	10.49	14.09	0.75	1.14	0.05	98.90	1.01
M-19A	pyroxenite	mantle	35.36	1.48	8.13	16.28	14.65	0.19	10.18	27.70	0.45	0.03	0.14	98.31	1.02
B-4	pyroxenite	mantle	45.13	0.22	10.68	7.85	7.06	0.19	18.07	16.26	1.15	0.07	0.02	98.86	1.01
R-2-4	pyroxenite	mantle	42.16	0.58	12.87	13.38	12.04	0.26	16.79	13.10	0.56	0.05	0.04	98.45	1.02
M-2	pyroxenite	mantle	34.55	0.22	10.24	13.78	12.40	0.14	15.66	24.79	0.21	0.03	0.11	98.33	1.02
B-13	plagioclase pyroxenite	crustal	48.09	0.40	16.47	9.69	8.72	0.18	12.22	9.85	1.81	0.86	0.02	98.61	1.01
M-3-2	peridotite		42.76	0.24	0.58	9.23	8.31	0.15	43.58	1.68	0.13	0.43	0.07	97.93	1.02
M-21-3	peridotite		39.10	0.34	0.63	9.16	8.24	0.13	44.25	4.54	0.09	0.34	0.22	97.89	1.02
B-5	lherzolite		41.98	0.14	1.10	8.24	7.41	0.15	45.30	1.18	0.09	0.62	0.06	98.03	1.02
B-10	peridotite		42.43	0.02	0.78	8.57	7.71	0.12	45.87	0.94	0.12	0.08	0.03	98.10	1.02
M-22	melt?		40.50	0.40	0.32	12.55	11.29	0.20	43.74	1.22	0.06	0.11	0.10	97.94	1.02
M-22-1	Mantle polymict breccia		44.13	0.64	6.35	9.57	8.61	0.17	19.30	16.38	0.71	2.01	0.13	98.43	1.02
M-10-6	peridotite		42.97	0.02	0.83	7.63	6.87	0.15	45.36	1.68	0.17	0.33	0.04	98.42	1.02
M-8	peridotite		42.72	0.01	0.60	6.83	6.15	0.13	47.40	0.29	0.01	0.03	0.01	97.35	1.03

Sample	rock type	Crust vs. Mantle Hardman et al. (2018)	SiO2 anhydrous	TiO2 anhydrous	Al2O3 anhydrous	FeO* anhydrous	MnO anhydrous	MgO anhydrous	CaO anhydrous	Na2O anhydrous	K2O anhydrous	P2O5 anhydrous	SUM anhydrous	Mg no	Volat %	Sum,maj. %
Xenoliths																
B-9	pyroxenite	mantle	47.24	0.15	18.17	7.41	0.22	10.61	14.25	0.75	1.15	0.05	100.00	0.72	12.28	99.06
M-19A	pyroxenite	mantle	35.97	1.51	8.27	14.90	0.20	10.36	28.18	0.45	0.03	0.15	100.00	0.55	3.11	98.80
B-4	pyroxenite	mantle	45.65	0.22	10.80	7.14	0.20	18.28	16.45	1.16	0.07	0.02	100.00	0.82	11.82	98.96
R-2-4	pyroxenite	mantle	42.82	0.59	13.07	12.23	0.26	17.05	13.31	0.57	0.05	0.04	100.00	0.71	10.84	98.64
M-2	pyroxenite	mantle	35.14	0.22	10.41	12.61	0.14	15.93	25.21	0.21	0.03	0.11	100.00	0.69	12.05	98.50
B-13	plagioclase pyroxenite	crustal	48.77	0.41	16.70	8.84	0.18	12.39	9.99	1.83	0.87	0.02	100.00	0.71	13.41	98.68
M-3-2	peridotite		43.66	0.25	0.59	8.48	0.15	44.50	1.72	0.14	0.44	0.07	100.00	0.90	8.68	98.88
M-21-3	peridotite		39.94	0.35	0.64	8.42	0.14	45.21	4.64	0.09	0.35	0.22	100.00	0.91	15.94	98.58
B-5	lherzolite		42.82	0.14	1.12	7.56	0.16	46.21	1.20	0.09	0.63	0.06	100.00	0.92	9.33	98.47
B-10	peridotite		43.25	0.02	0.80	7.86	0.13	46.76	0.96	0.12	0.08	0.03	100.00	0.91	11.90	98.54
M-22	melt?		41.35	0.41	0.33	11.53	0.20	44.66	1.25	0.06	0.11	0.10	100.00	0.87	11.99	98.78
M-22-1	Mantle polymict breccia		44.83	0.65	6.45	8.75	0.18	19.61	16.64	0.72	2.04	0.13	100.00	0.80	11.41	99.03
M-10-6	peridotite		43.66	0.02	0.84	6.98	0.15	46.09	1.71	0.17	0.34	0.04	100.00	0.92	10.52	99.36
M-8	peridotite		43.88	0.01	0.62	6.31	0.13	48.69	0.30	0.01	0.03	0.01	100.00	0.93	10.52	99.36

Sample	rock type	Crust vs. Mantle Hardman et al. (2018)	Rb	Sr	Y	Zr	V	Ni	Cr	Nb	Ga	Cu	Zn	Co	Ba	La	Ce	U	Th	Sc	Pb
Xenoliths																					
B-9	pyroxenite	mantle	17	576	5	23	156	73	103	5	12	136	79	28	2134	13	25	<0.5	<0.5	26	10
M-19A	pyroxenite	mantle	1	1413	21	47	346	29	91	7	7	37	98	7	1160	11	14	<0.5	<0.5	58	<1
B-4	pyroxenite	mantle	4	171	16	17	237	740	1182	1	8	298	29	47	310	8	12	<0.5	<0.5	38	<1
R-2-4	pyroxenite	mantle	5	113	36	23	328	243	355	<0.5	9	138	127	49	35	8	13	<0.5	<0.5	51	<1
M-2	pyroxenite	mantle	1	1070	8	34	320	319	292	4	6	452	136	97	600	14	25	<0.5	<0.5	39	<1
B-13	plagioclase pyroxenite	crustal	17	295	23	23	168	75	190	<0.5	15	33	74	43	765	10	13	<0.5	<0.5	31	<1
M-3-2	peridotite		25	87	5	15	54	2509	2332	29	3	10	64	110	237	<1	4	<0.5	<0.5	3	<1
M-21-3	peridotite		26	248	11	75	48	2605	2149	35	2	11	35	95	481	<1	7	<0.5	<0.5	7	<1
B-5	lherzolite		35	65	2	5	53	2665	2440	18	2	1	54	100	450	<1	2	<0.5	<0.5	4	<1
B-10	peridotite		6	45	3	5	42	2855	2880	4	1	1	40	96	87	<1	3	<0.5	<0.5	3	<1
M-22	melt?			111		17	152	2317	2038					118							
M-22-1	Mantle polymict breccia			402		40	156	316	1159					35							
M-10-6	peridotite			82		7	82	2225	1494					102							
M-8	peridotite			19		8	74	2828	7865					116							

GeothermT	GeothermP	-errorT	-errorP	+errorT	+errorP	isentropeT	isentropeP	XenoT	XenoP (depth)	XenoP (kbar)		T Ni-in-garnet (Xenolith)	Depth (km)	T Ni-in-garnet (concentrate)	Depth (km)	40mW/m^2 T Olivine	P (kbar)	Depth (km)	41mW/m^2 T Olivine	P (kbar)	Depth (km)	38mW/m^2 T Olivine	P (kbar)	Depth (km)	39mW/m^2 T Olivine	P (kbar)	Depth (km)
0.0	0.0	1.5	-1.0	16.2	0.0	1300.0	0.0	1277.6	-179.0	57.3		1399	-204	765	-101	761	28	-88	1157	48	-149	785	33	-103	771	30	-94
17.8	-1.0	18.8	-2.0	34.0	-1.0	1300.5	-1.0	1287.5	-181.5	58.1	core	1692		771	-102	762	28	-88	972	38	-119	785	33	-103	771	30	-94
35.1	-2.0	35.7	-3.0	51.3	-2.0	1301.0	-2.0	689.8	-91.4	29.3	rim	1032	-144	784	-104	763	28	-88	1357	58	-182	787	33	-103	773	30	-94
51.9	-3.0	52.1	-4.0	68.2	-3.0	1301.5	-3.0	1302.8	-186.0	59.5		1424	-224	792	-105	764	28	-89	831	30	-95	788	33	-103	774	30	-94
68.3	-4.0	68.1	-5.0	84.6	-4.0	1302.1	-4.0	857.4	-115.7	37.0		1531		795	-106	768	29	-89	860	32	-100	791	33	-104	777	30	-95
84.3	-5.0	83.6	-6.0	100.5	-5.0	1302.6	-5.0	1282.4	-185.9	59.5				796	-106	788	30	-93	1110	45	-141	812	34	-108	798	32	-99
99.8	-6.0	98.7	-7.0	116.0	-6.0	1303.1	-6.0	1261.4	-182.6	58.4				797	-106	798	30	-94	1206	50	-157	823	35	-110	809	32	-101
114.9	-7.0	113.3	-8.0	131.1	-7.0	1303.6	-7.0							802	-107	801	30	-95	789	28	-88	826	35	-110	811	32	-101
129.5	-8.0	127.4	-9.0	145.7	-8.0	1304.1	-8.0							802	-107	826	32	-99	909	35	-108	852	37	-115	837	34	-106
143.7	-9.0	141.2	-10.0	159.9	-9.0	1304.6	-9.0							804	-107	841	33	-102	816	30	-93	868	38	-118	852	35	-108
157.4	-10.0	154.4	-11.0	173.6	-10.0	1305.2	-10.0							807	-108	849	33	-103	922	35	-110	876	38	-120	860	35	-110
170.7	-11.0	167.3	-12.0	186.9	-11.0	1305.7	-11.0							808	-108	871	34	-107	792	28	-89	899	40	-124	882	36	-114
183.5	-12.0	179.7	-13.0	199.7	-12.0	1306.2	-12.0							809	-108	921	37	-115	1108	45	-141	940	42	-131	933	39	-123
195.9	-13.0	191.6	-14.0	212.1	-13.0	1306.7	-13.0							809	-108	934	38	-118	1220	51	-159	960	43	-133	946	40	-125
207.8	-14.0	203.1	-15.0	224.0	-14.0	1307.2	-14.0							813	-109	942	38	-119	1231	52	-161	965	43	-134	954	41	-127
219.3	-15.0	214.1	-16.0	235.5	-15.0	1307.7	-15.0							814	-109	985	41	-127	754	26	-83	1005	45	-142	998	43	-135
230.3	-16.0	224.7	-17.0	246.6	-16.0	1308.3	-16.0							814	-109	1123	48	-151	1179	49	-153	1164	56	-176	1138	51	-160
240.9	-17.0	234.8	-18.0	257.2	-17.0	1308.8	-17.0							815	-109	1124	48	-151	759	27	-83	1164	56	-176	1139	51	-160
251.1	-18.0	244.5	-19.0	267.3	-18.0	1309.3	-18.0							817	-110	1126	48	-151	1107	45	-141	1166	56	-177	1141	51	-161
260.8	-19.0	254.1	-20.0	277.0	-19.0	1309.8	-19.0							818	-110	1174	51	-160	1163	48	-150	1217	60	-187	1190	54	-170
270.3	-20.0	263.4	-21.0	286.5	-20.0	1310.3	-20.0							818	-110	1180	51	-161	1330	57	-177	1224	60	-188	1197	55	-171
279.6	-21.0	272.6	-22.0	295.9	-21.0	1310.8	-21.0							820	-110	1190	52	-162	753	26	-82	1234	61	-190	1207	55	-173
288.8	-22.0	281.6	-23.0	305.0	-22.0	1311.4	-22.0							821	-110	1197	52	-164	755	27	-83	1241	61	-191	1214	56	-174
297.8	-23.0	290.5	-24.0	314.1	-23.0	1311.9	-23.0							822	-111	1224	54	-168	930	36	-112	1270	63	-197	1242	57	-179
306.7	-24.0	299.2	-25.0	322.9	-24.0	1312.4	-24.0							829	-112	1239	55	-171	779	28	-87	1286	64	-200	1256	58	-182
315.4	-25.0	307.7	-26.0	331.6	-25.0	1312.9	-25.0							835	-113	1249	55	-173	1173	49	-152	1297	65	-203	1267	59	-184
323.9	-26.0	316.1	-27.0	340.2	-26.0	1313.4	-26.0							837	-113	1360	63	-196	838	31	-97	1405	72	-224	1371	65	-203
332.3	-27.0	324.3	-28.0	348.6	-27.0	1313.9	-27.0							838	-113	1390	65	-202	752	26	-82	1435	74	-230	1400	67	-209
340.5	-28.0	332.4	-29.0	356.8	-28.0	1314.5	-28.0							844	-114												
348.6	-29.0	340.3	-30.0	364.8	-29.0	1315.0	-29.0							850	-115												
356.5	-30.0	348.0	-31.0	372.7	-30.0	1315.5	-30.0							869	-118												
364.3	-31.0	355.6	-32.0	380.5	-31.0	1316.0	-31.0							889	-121												
371.8	-32.0	363.0	-33.0	388.1	-32.0	1316.5	-32.0							896	-123												
379.3	-33.0	370.3	-34.0	395.5	-33.0	1317.1	-33.0							910	-125												
386.5	-34.0	377.4	-35.0	402.8	-34.0	1317.6	-34.0							921	-127												
393.6	-35.0	384.3	-36.0	409.9	-35.0	1318.1	-35.0							1539													
400.6	-36.0	391.1	-37.0	416.8	-36.0	1318.6	-36.0							1549													
407.4	-37.0	397.7	-38.0	423.6	-37.0	1319.1	-37.0							1551													
414.0	-38.0	404.0	-39.0	430.2	-38.0	1319.7	-38.0							1558													
420.2	-39.0	409.1	-40.0	436.5	-39.0	1320.2	-39.0							1561													
425.4	-40.0	414.3	-41.0	441.6	-40.0	1320.7	-40.0							1568													
430.5	-41.0	419.4	-42.0	446.7	-41.0	1321.2	-41.0							1572													
435.7	-42.0	424.6	-43.0	451.9	-42.0	1321.8	-42.0							1572													
440.9	-43.0	429.8	-44.0	457.1	-43.0	1322.3	-43.0							1575													
446.0	-44.0	435.0	-45.0	462.3	-44.0	1322.8	-44.0							1579													
451.3	-45.0	440.3	-46.0	467.5	-45.0	1323.3	-45.0							1588													
456.5	-46.0	445.5	-47.0	472.7	-46.0	1323.8	-46.0							1589													
461.7	-47.0	450.8	-48.0	478.0	-47.0	1324.4	-47.0							1593													
467.0	-48.0	456.0	-49.0	483.2	-48.0	1324.9	-48.0							1602													
472.3	-49.0	461.3	-50.0	488.5	-49.0	1325.4	-49.0																				
477.6	-50.0	466.6	-51.0	493.8	-50.0	1325.9	-50.0																				
482.9	-51.0	472.0	-52.0	499.1	-51.0	1326.5	-51.0																				
488.2	-52.0	477.3	-53.0	504.4	-52.0	1327.0	-52.0																				
493.5	-53.0	482.7	-54.0	509.8	-53.0	1327.5	-53.0																				
498.9	-54.0	488.0	-55.0	515.1	-54.0	1328.0	-54.0																				
504.2	-55.0	493.4	-56.0	520.5	-55.0	1328.5	-55.0																				
509.6	-56.0	498.8	-57.0	525.9	-56.0	1329.1	-56.0																				
515.0	-57.0	504.2	-58.0	531.3	-57.0	1329.6	-57.0																				
520.4	-58.0	509.6	-59.0	536.7	-58.0	1330.1	-58.0																				
525.9	-59.0	515.1	-60.0	542.1	-59.0	1330.6	-59.0																				
531.3	-60.0	520.5	-61.0	547.5	-60.0	1331.2	-60.0																				
536.8	-61.0	526.0	-62.0	553.0	-61.0	1331.7	-61.0																				
542.2	-62.0	531.5	-63.0	558.5	-62.0	1332.2	-62.0																				
547.7	-63.0	537.0	-64.0	563.9	-63.0	1332.7	-63.0																				
553.2	-64.0	542.5	-65.0	569.4	-64.0	1333.3	-64.0																				
558.7	-65.0	548.0	-66.0	575.0	-65.0	1333.8	-65.0																				
564.3	-66.0	553.6	-67.0	580.5	-66.0	1334.3	-66.0																				
569.8	-67.0	559.1	-68.0	586.0	-67.0	1334.8	-67.0																				
575.3	-68.0	564.7	-69.0	591.6	-68.0	1335.4	-68.0																				
580.9	-69.0	570.3	-70.0	597.1	-69.0	1335.9	-69.0																				
586.5	-70.0	575.9	-71.0	602.7	-70.0	1336.4	-70.0																				
592.1	-71.0	581.5	-72.0	608.3	-71.0	1336.9	-71.0																				
597.7	-72.0	587.1	-73.0	613.9	-72.0	1337.5	-72.0																				
603.3	-73.0	592.7	-74.0	619.5	-73.0	1338.0	-73.0																				
608.9	-74.0	598.4	-75.0	625.2	-74.0	1338.5	-74.0																				
614.6	-75.0	604.0	-76.0	630.8	-75.0	1339.1	-75.0																				
620.3	-76.0	609.7	-77.0	636.5	-76.0	1339.6	-76.0																				
625.9	-77.0	615.4	-78.0	642.2	-77.0	1340.1	-77.0																				
631.6	-78.0	621.1	-79.0	647.8	-78.0	1340.6	-78.0																				
637.3	-79.0	626.8	-80.0	653.5	-79.0	1341.2	-79.0																				

GeothermT	GeothermP	-errorT	-errorP	+errorT	+errorP	isentropeT	isentropeP
643.0	-80.0	632.5	-81.0	659.2	-80.0	1341.7	-80.0
648.7	-81.0	638.2	-82.0	665.0	-81.0	1342.2	-81.0
654.5	-82.0	644.0	-83.0	670.7	-82.0	1342.7	-82.0
660.2	-83.0	649.7	-84.0	676.4	-83.0	1343.3	-83.0
666.0	-84.0	655.5	-85.0	682.2	-84.0	1343.8	-84.0
671.7	-85.0	661.3	-86.0	688.0	-85.0	1344.3	-85.0
677.5	-86.0	667.1	-87.0	693.7	-86.0	1344.9	-86.0
683.3	-87.0	672.9	-88.0	699.5	-87.0	1345.4	-87.0
689.1	-88.0	678.7	-89.0	705.3	-88.0	1345.9	-88.0
694.9	-89.0	684.5	-90.0	711.1	-89.0	1346.5	-89.0
700.7	-90.0	690.3	-91.0	717.0	-90.0	1347.0	-90.0
706.6	-91.0	696.2	-92.0	722.8	-91.0	1347.5	-91.0
712.4	-92.0	702.1	-93.0	728.7	-92.0	1348.0	-92.0
718.3	-93.0	707.9	-94.0	734.5	-93.0	1348.6	-93.0
724.1	-94.0	713.8	-95.0	740.4	-94.0	1349.1	-94.0
730.0	-95.0	719.7	-96.0	746.3	-95.0	1349.6	-95.0
735.9	-96.0	725.6	-97.0	752.1	-96.0	1350.2	-96.0
741.8	-97.0	731.5	-98.0	758.0	-97.0	1350.7	-97.0
747.7	-98.0	737.4	-99.0	764.0	-98.0	1351.2	-98.0
753.6	-99.0	743.4	-100.0	769.9	-99.0	1351.8	-99.0
759.6	-100.0	749.3	-101.0	775.8	-100.0	1352.3	-100.0
765.5	-101.0	755.2	-102.0	781.7	-101.0	1352.8	-101.0
771.5	-102.0	761.2	-103.0	787.7	-102.0	1353.4	-102.0
777.4	-103.0	767.2	-104.0	793.7	-103.0	1353.9	-103.0
783.4	-104.0	773.2	-105.0	799.6	-104.0	1354.4	-104.0
789.4	-105.0	779.1	-106.0	805.6	-105.0	1354.9	-105.0
795.4	-106.0	785.1	-107.0	811.6	-106.0	1355.5	-106.0
801.4	-107.0	791.2	-108.0	817.6	-107.0	1356.0	-107.0
807.4	-108.0	797.2	-109.0	823.6	-108.0	1356.5	-108.0
813.4	-109.0	803.2	-110.0	829.6	-109.0	1357.1	-109.0
819.4	-110.0	809.2	-111.0	835.7	-110.0	1357.6	-110.0
825.5	-111.0	815.3	-112.0	841.7	-111.0	1358.1	-111.0
831.5	-112.0	821.3	-113.0	847.7	-112.0	1358.7	-112.0
837.6	-113.0	827.4	-114.0	853.8	-113.0	1359.2	-113.0
843.6	-114.0	833.5	-115.0	859.9	-114.0	1359.7	-114.0
849.7	-115.0	839.5	-116.0	865.9	-115.0	1360.3	-115.0
855.8	-116.0	845.6	-117.0	872.0	-116.0	1360.8	-116.0
861.9	-117.0	851.7	-118.0	878.1	-117.0	1361.3	-117.0
868.0	-118.0	857.8	-119.0	884.2	-118.0	1361.9	-118.0
874.1	-119.0	864.0	-120.0	890.3	-119.0	1362.4	-119.0
880.2	-120.0	870.1	-121.0	896.4	-120.0	1363.0	-120.0
886.3	-121.0	876.2	-122.0	902.5	-121.0	1363.5	-121.0
892.4	-122.0	882.3	-123.0	908.7	-122.0	1364.0	-122.0
898.6	-123.0	888.5	-124.0	914.8	-123.0	1364.6	-123.0
904.7	-124.0	894.6	-125.0	920.9	-124.0	1365.1	-124.0
910.9	-125.0	900.8	-126.0	927.1	-125.0	1365.6	-125.0
917.0	-126.0	907.0	-127.0	933.3	-126.0	1366.2	-126.0
923.2	-127.0	913.1	-128.0	939.4	-127.0	1366.7	-127.0
929.4	-128.0	919.3	-129.0	945.6	-128.0	1367.2	-128.0
935.6	-129.0	925.5	-130.0	951.8	-129.0	1367.8	-129.0
941.7	-130.0	931.7	-131.0	958.0	-130.0	1368.3	-130.0
947.9	-131.0	937.9	-132.0	964.2	-131.0	1368.8	-131.0
954.1	-132.0	944.1	-133.0	970.4	-132.0	1369.4	-132.0
960.4	-133.0	950.3	-134.0	976.6	-133.0	1369.9	-133.0
966.6	-134.0	956.6	-135.0	982.8	-134.0	1370.5	-134.0
972.8	-135.0	962.8	-136.0	989.0	-135.0	1371.0	-135.0
979.0	-136.0	969.0	-137.0	995.3	-136.0	1371.5	-136.0
985.3	-137.0	975.3	-138.0	1001.5	-137.0	1372.1	-137.0
991.5	-138.0	981.5	-139.0	1007.7	-138.0	1372.6	-138.0
997.8	-139.0	987.8	-140.0	1014.0	-139.0	1373.1	-139.0
1004.0	-140.0	994.1	-141.0	1020.3	-140.0	1373.7	-140.0
1010.3	-141.0	1000.3	-142.0	1026.5	-141.0	1374.2	-141.0
1016.6	-142.0	1006.6	-143.0	1032.8	-142.0	1374.8	-142.0
1022.8	-143.0	1012.9	-144.0	1039.1	-143.0	1375.3	-143.0
1029.1	-144.0	1019.2	-145.0	1045.3	-144.0	1375.8	-144.0
1035.4	-145.0	1025.5	-146.0	1051.6	-145.0	1376.4	-145.0
1041.7	-146.0	1031.8	-147.0	1057.9	-146.0	1376.9	-146.0
1048.0	-147.0	1038.1	-148.0	1064.2	-147.0	1377.5	-147.0
1054.3	-148.0	1044.4	-149.0	1070.5	-148.0	1378.0	-148.0
1060.6	-149.0	1050.7	-150.0	1076.8	-149.0	1378.5	-149.0
1066.9	-150.0	1057.0	-151.0	1083.2	-150.0	1379.1	-150.0
1073.3	-151.0	1063.4	-152.0	1089.5	-151.0	1379.6	-151.0
1079.6	-152.0	1069.7	-153.0	1095.8	-152.0	1380.2	-152.0
1085.9	-153.0	1076.0	-154.0	1102.1	-153.0	1380.7	-153.0
1092.3	-154.0	1082.4	-155.0	1108.5	-154.0	1381.2	-154.0
1098.6	-155.0	1088.7	-156.0	1114.8	-155.0	1381.8	-155.0
1104.9	-156.0	1095.1	-157.0	1121.2	-156.0	1382.3	-156.0
1111.3	-157.0	1101.4	-158.0	1127.5	-157.0	1382.9	-157.0
1117.7	-158.0	1107.8	-159.0	1133.9	-158.0	1383.4	-158.0
1124.0	-159.0	1114.2	-160.0	1140.3	-159.0	1383.9	-159.0

XenoT	XenoP (depth)	XenoP (kbar)	T Ni-in-garnet (Xenolith)	Depth (km)	T Ni-in-garnet (concentrate)	Depth (km)	40mW/m² T Olivine	P (kbar)	Depth (km)	41mW/m² T Olivine	P (kbar)	Depth (km)	38mW/m² T Olivine	P (kbar)	Depth (km)	39mW/m² T Olivine	P (kbar)	Depth (km)

GeothermT	GeothermP	-errorT	-errorP	+errorT	+errorP	isentropeT	isentropeP	XenoT	XenoP (depth)	XenoP (kbar)	T Ni-in-garnet (Xenolith)	Depth (km)	T Ni-in-garnet (concentrate)	Depth (km)	$40mW/m^2$ T Olivine	P (kbar)	Depth (km)	$41mW/m^2$ T Olivine	P (kbar)	Depth (km)	$38mW/m^2$ T Olivine	P (kbar)	Depth (km)	$39mW/m^2$ T Olivine	P (kbar)	Depth (km)
1130.4	-160.0	1120.5	-161.0	1146.6	-160.0	1384.5	-160.0																			
1136.8	-161.0	1126.9	-162.0	1153.0	-161.0	1385.0	-161.0																			
1143.1	-162.0	1133.3	-163.0	1159.4	-162.0	1385.6	-162.0																			
1149.5	-163.0	1139.7	-164.0	1165.8	-163.0	1386.1	-163.0																			
1155.9	-164.0	1146.1	-165.0	1172.1	-164.0	1386.7	-164.0																			
1162.3	-165.0	1152.5	-166.0	1178.5	-165.0	1387.2	-165.0																			
1168.7	-166.0	1158.9	-167.0	1184.9	-166.0	1387.7	-166.0																			
1175.1	-167.0	1165.3	-168.0	1191.3	-167.0	1388.3	-167.0																			
1181.5	-168.0	1171.7	-169.0	1197.7	-168.0	1388.8	-168.0																			
1187.9	-169.0	1178.1	-170.0	1204.1	-169.0	1389.4	-169.0																			
1194.3	-170.0	1184.5	-171.0	1210.5	-170.0	1389.9	-170.0																			
1200.7	-171.0	1190.9	-172.0	1217.0	-171.0	1390.5	-171.0																			
1207.1	-172.0	1197.3	-173.0	1223.4	-172.0	1391.0	-172.0																			
1213.6	-173.0	1203.8	-174.0	1229.8	-173.0	1391.6	-173.0																			
1220.0	-174.0	1210.2	-175.0	1236.2	-174.0	1392.1	-174.0																			
1226.4	-175.0	1216.6	-176.0	1242.7	-175.0	1392.6	-175.0																			
1232.9	-176.0	1223.1	-177.0	1249.1	-176.0	1393.2	-176.0																			
1239.3	-177.0	1229.5	-178.0	1255.5	-177.0	1393.7	-177.0																			
1245.7	-178.0	1236.0	-179.0	1262.0	-178.0	1394.3	-178.0																			
1252.2	-179.0	1242.4	-180.0	1268.4	-179.0	1394.8	-179.0																			
1258.6	-180.0	1248.8	-181.0	1274.9	-180.0	1395.4	-180.0																			
1265.1	-181.0	1255.3	-182.0	1281.3	-181.0	1395.9	-181.0																			
1271.5	-182.0	1260.3	-182.8	1287.8	-182.0	1396.5	-182.0																			
1276.5	-182.8	1260.4	-182.8	1292.8	-182.8	1396.9	-182.8																			
1276.6	-182.8	1267.0	-183.8	1292.8	-182.8	1396.9	-182.8																			
1283.3	-183.8	1273.7	-184.8	1299.5	-183.8	1397.4	-183.8																			
1290.0	-184.8	1280.5	-185.8	1306.2	-184.8	1398.0	-184.8																			
1296.7	-185.8	1287.4	-186.8	1313.0	-185.8	1398.5	-185.8																			
1303.6	-186.8	1294.3	-187.8	1319.8	-186.8	1399.1	-186.8																			
1310.5	-187.8	1301.2	-188.8	1326.7	-187.8	1399.6	-187.8																			
1317.4	-188.8	1308.1	-189.8	1333.7	-188.8	1400.2	-188.8																			
1324.3	-189.8	1314.9	-190.8	1340.6	-189.8	1400.7	-189.8																			
1331.2	-190.8	1321.6	-191.8	1347.4	-190.8	1401.3	-190.8																			
1337.9	-191.8	1328.2	-192.8	1354.1	-191.8	1401.8	-191.8																			
1344.4	-192.8	1334.5	-193.8	1360.6	-192.8	1402.3	-192.8																			
1350.7	-193.8	1340.5	-194.8	1366.9	-193.8	1402.9	-193.8																			
1356.7	-194.8	1346.3	-195.8	1373.0	-194.8	1403.4	-194.8																			
1362.5	-195.8	1351.7	-196.8	1378.7	-195.8	1404.0	-195.8																			
1368.0	-196.8	1356.9	-197.8	1384.2	-196.8	1404.5	-196.8																			
1373.1	-197.8	1361.7	-198.8	1389.3	-197.8	1405.1	-197.8																			
1377.9	-198.8	1366.2	-199.8	1394.2	-198.8	1405.6	-198.8																			
1382.4	-199.8	1370.4	-200.8	1398.7	-199.8	1406.2	-199.8																			
1386.6	-200.8	1374.2	-201.8	1402.8	-200.8	1406.7	-200.8																			
1390.5	-201.8	1377.8	-202.8	1406.7	-201.8	1407.3	-201.8																			
1394.0	-202.8	1381.0	-203.8	1410.2	-202.8	1407.8	-202.8																			
1397.3	-203.8	1384.0	-204.8	1413.5	-203.8	1408.4	-203.8																			
1400.2	-204.8	1386.7	-205.8	1416.4	-204.8	1408.9	-204.8																			
1402.9	-205.8	1389.1	-206.8	1419.1	-205.8	1409.5	-205.8																			
1405.4	-206.8	1391.4	-207.8	1421.6	-206.8	1410.0	-206.8																			
1407.6	-207.8	1393.4	-208.8	1423.8	-207.8	1410.6	-207.8																			
1409.6	-208.8	1395.2	-209.8	1425.8	-208.8	1411.1	-208.8																			
1411.4	-209.8	1396.8	-210.8	1427.6	-209.8	1411.7	-209.8																			
1413.0	-210.8	1398.2	-211.8	1429.2	-210.8	1412.2	-210.8																			
1414.5	-211.8	1399.5	-212.8	1430.7	-211.8	1412.8	-211.8																			
1415.8	-212.8	1400.7	-213.8	1432.0	-212.8	1413.3	-212.8																			
1416.9	-213.8	1401.8	-214.8	1433.2	-213.8	1413.9	-213.8																			
1418.0	-214.8	1402.7	-215.8	1434.2	-214.8	1414.4	-214.8																			
1419.0	-215.8	1403.6	-216.8	1435.2	-215.8	1415.0	-215.8																			
1419.8	-216.8	1404.4	-217.8	1436.0	-216.8	1415.5	-216.8																			
1420.6	-217.8	1405.1	-218.8	1436.8	-217.8	1416.1	-217.8																			
1421.3	-218.8	1405.7	-219.8	1437.5	-218.8	1416.7	-218.8																			
1421.9	-219.8	1406.3	-220.8	1438.1	-219.8	1417.2	-219.8																			
1422.5	-220.8	1406.8	-221.8	1438.7	-220.8	1417.8	-220.8																			
1423.0	-221.8	1407.3	-222.8	1439.3	-221.8	1418.3	-221.8																			
1423.6	-222.8	1407.8	-223.8	1439.8	-222.8	1418.9	-222.8																			
1424.0	-223.8	1408.2	-224.8	1440.3	-223.8	1419.4	-223.8																			
1424.5	-224.8	1408.7	-225.8	1440.7	-224.8	1420.0	-224.8																			
1424.9	-225.8	1409.1	-226.8	1441.1	-225.8	1420.5	-225.8																			
1425.3	-226.8	1409.5	-227.8	1441.5	-226.8	1421.1	-226.8																			
1425.7	-227.8	1409.9	-228.8	1441.9	-227.8	1421.6	-227.8																			
1426.1	-228.8	1410.2	-229.8	1442.3	-228.8	1422.2	-228.8																			
1426.5	-229.8	1410.6	-230.8	1442.7	-229.8	1422.7	-229.8																			
1426.8	-230.8	1411.0	-231.8	1443.1	-230.8	1423.3	-230.8																			
1427.2	-231.8	1411.4	-232.8	1443.4	-231.8	1423.9	-231.8																			
1427.6	-232.8	1411.7	-233.8	1443.8	-232.8	1424.4	-232.8																			
1428.0	-233.8	1412.1	-234.8	1444.2	-233.8	1425.0	-233.8																			
1428.4	-234.8	1412.5	-235.8	1444.6	-234.8	1425.5	-234.8																			
1428.7	-235.8	1412.9	-236.8	1445.0	-235.8	1426.1	-235.8																			
1429.1	-236.8	1413.3	-237.8	1445.4	-236.8	1426.6	-236.8																			
1429.5	-237.8	1413.7	-238.8	1445.8	-237.8	1427.2	-237.8																			

GeothermT	GeothermP	-errorT	-errorP	+errorT	+errorP	isentropeT	isentropeP	XenoT	XenoP (depth)	XenoP (kbar)	T Ni-in-garnet (Xenolith)	Depth (km)	T Ni-in-garnet (concentrate)	Depth (km)	$40 mW/m^2$			$41 mW/m^2$			$38 mW/m^2$			$39 mW/m^2$		
															T Olivine	P (kbar)	Depth (km)	T Olivine	P (kbar)	Depth (km)	T Olivine	P (kbar)	Depth (km)	T Olivine	P (kbar)	Depth (km)
1429.9	-238.8	1414.1	-239.8	1446.2	-238.8	1427.7	-238.8																			
1430.3	-239.8	1414.5	-240.8	1446.6	-239.8	1428.3	-239.8																			
1430.8	-240.8	1415.0	-241.8	1447.0	-240.8	1428.9	-240.8																			
1431.2	-241.8	1415.4	-242.8	1447.4	-241.8	1429.4	-241.8																			
1431.6	-242.8	1415.8	-243.8	1447.8	-242.8	1430.0	-242.8																			
1432.1	-243.8	1416.3	-244.8	1448.3	-243.8	1430.5	-243.8																			
1432.5	-244.8	1416.7	-245.8	1448.7	-244.8	1431.1	-244.8																			
1433.0	-245.8	1417.2	-246.8	1449.2	-245.8	1431.6	-245.8																			
1433.4	-246.8	1417.6	-247.8	1449.6	-246.8	1432.2	-246.8																			
1433.9	-247.8	1418.1	-248.8	1450.1	-247.8	1432.8	-247.8																			
1434.3	-248.8	1418.6	-249.8	1450.6	-248.8	1433.3	-248.8																			
1434.8	-249.8			1451.1	-249.8	1433.9	-249.8																			

Kimberlite	Facies	Sample	Sample position	Report Age	Assumed_Ro	Reference	Rb ppm	Sr ppm	87Rb/86Sr	87Rb/86Sr error 2s	87Sr/86Sr	87Sr/86Sr error2s	Model age 0.705 intial ratio	Analyt error (Ma, 2s abs)	Worst error, Ma	Analyt uncert +	Analyt uncert -	Ro +	Ro -
Stealth	MK	PC-1	Drill hole DR-06-07 heavy mineral concentrate		0.705	GeospecFeb07	320.1	79.36	11.89	0.1783	0.89398	0.00003	1110.7	11.1	25.7	1121.9	1099.6	1136.6	1085.2
Inferno	MK	PD-1	Drill hole DR-06-06 heavy mineral concentrate		0.705	GeospecFeb07	313.4	52.98	17.62	0.2643	1.00640	0.00004	1194.5	11.9	21.8	1206.5	1182.6	1216.4	1172.9
Iceberg North	MK	PE-1	Drill hole DR-06-01 heavy mineral concentrate		0.705	GeospecFeb07	638.5	5.49	1561	23.41	38.7741	0.00225	1697.3	16.8	16.9	1714.2	1680.6	1714.3	1680.5
Iceberg South	MK	PF-1	Drill hole DR-06-02 heavy mineral concentrate		0.705	GeospecFeb07	494.9	8.26	289.2	4.337	7.57986	0.00014	1654.8	16.3	16.9	1671.2	1638.5	1671.8	1638.0
Iceberg North	MK	PH-1	Drill hole DR-06-01 @ 141.25m		0.705	GeospecFeb07	725.7	6.94	1005	15.08	25.5858	0.00169	1722.0	17.0	17.2	1739.1	1705.0	1739.3	1704.9
Darby	HK (altered)	PA-1	esker float	1876.0	0.705	CreaserNov05	6.57	11.44	1.69	0.0253	0.75059	0.00004	1876.8	20.1	121.6	1896.9	1856.8	1999.4	1756.2
Darby	HK (altered)	PA-2	esker float	547.7	0.705	CreaserNov05	49.20	15.44	9.29	0.1394	0.77756	0.00002	547.7	5.6	24.4	553.3	542.1	572.3	523.5
Iceberg South	MK	PG-1	Drill hole DR-06-02 @ 201.4m		0.705	GeospecFeb07	619.9	3.41	848.8	12.73	7.25313	0.00023	541.2	5.4	5.6	546.6	535.8	546.8	535.6
Iceberg South	MK	PG-2	Drill hole DR-06-02 @ 201.4m		0.705	GeospecFeb07	751.0	10.66	240.7	3.610	2.56263	0.00005	541.5	5.4	6.1	546.9	536.1	547.6	535.4
Iceberg South	MK	PG-3	Drill hole DR-06-02 @ 201.4m		0.705	GeospecFeb07	720.0	5.55	520.9	7.814	4.72516	0.00018	541.4	5.4	5.7	546.8	536.0	547.1	535.7
Iceberg South	MK	PG-4	Drill hole DR-06-02 @ 201.4m		0.705	GeospecFeb07	650.5	4.17	678.6	10.18	5.95866	0.00057	543.1	5.4	5.7	548.6	537.7	548.8	537.4
Iceberg South	MK	PG-5	Drill hole DR-06-02 @ 201.4m		0.705	GeospecFeb07	690.8	4.59	645.4	9.681	5.69815	0.00020	542.7	5.4	5.7	548.2	537.4	548.4	537.1
Iceberg South	MK	PI-1	Drill hole DR-06-08 @ 121.50m		0.705	GeospecFeb07	558.2	4.43	501.2	7.518	4.60393	0.00029	545.7	5.4	5.8	551.2	540.3	551.6	540.0
Iceberg South	MK	PI-2	Drill hole DR-06-08 @ 121.50m		0.705	GeospecFeb07	461.2	2.74	757.8	11.37	6.56122	0.00036	542.2	5.4	5.6	547.6	536.8	547.8	536.5
Iceberg South	MK	PI-3	Drill hole DR-06-08 @ 121.50m		0.705	GeospecFeb07	420.7	2.55	732.0	10.98	6.40648	0.00022	546.4	5.4	5.7	551.8	541.0	552.1	540.7
Darby	MK	PJ-1	float 484550/7479408 NAD83 UTM15N		0.705	GeospecFeb07	475.5	2.14	1183	17.75	9.79524	0.00094	539.0	5.4	5.5	544.5	533.7	544.6	533.5
Darby	MK	PJ-2	float 484550/7479408 NAD83 UTM15N		0.705	GeospecFeb07	278.6	11.94	71.12	1.067	1.25201	0.00008	539.6	5.4	7.9	545.0	534.2	547.5	531.7

	207Pb/235U		206Pb/238U		207Pb/206Pb		207Pb/206Pb		207Pb/235U		206Pb/238U	
Sample	**Ratio**	**Prop2SE**	**Ratio**	**Prop2SE**	**Ratio**	**Prop2SE**	**Age**	**Prop2SE**	**Age**	**Prop2SE**	**Age**	**Prop2SE**
M-19A	0.861	0.087	0.0968	0.0077	0.0635	0.00380	662	93	612	43	593	45
M-19A	0.752	0.060	0.0947	0.0065	0.0579	0.00130	514	51	568	36	582	38
M-19A	0.780	0.065	0.0950	0.0067	0.0586	0.00096	553	38	575	37	583	39
M-19A	0.807	0.065	0.0961	0.0063	0.0596	0.00110	581	40	589	35	589	37
M-19A	0.799	0.090	0.0882	0.0074	0.0694	0.00780	710	130	577	43	542	44
M-19A	0.722	0.053	0.0886	0.0060	0.0574	0.00097	500	38	545	31	546	35
M-19A	0.792	0.085	0.0959	0.0081	0.0585	0.00140	537	52	578	46	588	47
M-19A	0.770	0.130	0.0920	0.0130	0.0589	0.00190	555	68	561	72	565	75
M-19A	0.652	0.053	0.0845	0.0066	0.0565	0.00110	467	43	510	35	521	39
M-19A	0.687	0.045	0.0850	0.0045	0.0580	0.00082	531	29	525	27	525	27
M-19A	0.689	0.050	0.0853	0.0051	0.0580	0.00074	527	28	525	30	527	30
M-19A	0.890	0.220	0.0870	0.0100	0.0830	0.01300	960	210	612	71	532	59
M-19A	0.690	0.067	0.0875	0.0078	0.0575	0.00110	512	46	531	43	539	46
M-19A	0.760	0.420	0.0950	0.0110	0.0730	0.01000	800	160	609	61	556	80
M-19A	1.350	0.800	0.0900	0.0120	0.0970	0.01800	1090	240	660	78	575	90
M-19A	0.730	0.480	0.0860	0.0120	0.0890	0.01800	960	220	624	79	528	67
B-13	0.998	0.029	0.1165	0.0038	0.0624	0.00083	684	28	704	16	710	22
B-13	0.989	0.046	0.1151	0.0048	0.0620	0.00064	675	23	697	25	702	27
B-13	0.717	0.038	0.0874	0.0042	0.0593	0.00043	577	16	546	22	539	25
B-13	0.723	0.068	0.0881	0.0045	0.0593	0.00049	576	18	550	39	544	27
B-13	1.394	0.068	0.1486	0.0062	0.0680	0.00086	869	25	883	29	893	35
B-13	1.408	0.084	0.1490	0.0066	0.0685	0.00094	881	26	888	35	895	37
B-13	0.836	0.044	0.1035	0.0044	0.0593	0.00068	581	28	616	24	635	25
B-13	0.839	0.027	0.1030	0.0041	0.0598	0.00063	594	23	618	15	632	24
B-13	1.157	0.056	0.1323	0.0053	0.0641	0.00073	742	25	779	26	801	30
B-13	1.163	0.037	0.1309	0.0053	0.0647	0.00058	763	19	782	18	792	30
B-13	1.045	0.055	0.1189	0.0051	0.0637	0.00055	731	18	724	28	724	29
B-13	1.025	0.037	0.1171	0.0048	0.0637	0.00042	730	14	717	18	714	28

Sample	Os (ppb)	Ir (ppb)	Ru (ppb)	Pt (ppb)	Pd (ppb)	Re (ppb)	187Re/188Os	187Os/188Os	$187Os/188Os_i$	γOs	TRD erruption (Ga)	Abs. 2σ	TMA (Ga)	Abs. 2σ	Pd/Ir	Pt/Ir	Os/Ir	Ru/Ir	Crust vs. Mantle Hardman et al. (2018)
Peridotites																			
M-3-2	2.040	0.984	2.410	0.999	9.241	0.114	0.269	0.11065	0.10821	-13.6	2.77	0.20			9.39	0.41	2.07	2.45	
B-5	1.144	0.361	1.632	0.143	6.859	0.083	0.350	0.11468	0.11151	-10.5	2.32	0.18			19.02	0.09	3.17	4.53	
B-10	0.751	0.784	3.008	1.500	1.995	0.053	0.338	0.11506	0.11198	-10.2	2.26	0.18			2.54	0.50	0.96	3.83	
M-10-6	1.541	1.769	4.535	1.299	0.983	0.227	0.710	0.11501	0.10857	-10.2	2.72	0.20			0.56	0.29	0.87	2.56	
M-8	6.822	5.515	12.543	0.385	1.956	0.072	0.050	0.10892	0.10846	-15.0	2.74	0.20			0.35	0.03	1.24	2.27	
Pyroxenites																			
M-2	0.477	0.139	0.308	4.526	6.051	8.691	238	13.3	11.1	10252			3.23	0.15	43.63	14.71	3.44	2.22	mantle
M-19A	0.019	0.008	0.017	0.153	0.218	0.509	217	5.2	3.2	3957			1.39	0.08	28.44	9.02	2.45	2.21	mantle
B-4	0.247	0.173	0.538	5.879	8.306	1.763	45	2.5	2.1	1822			3.07	0.15	47.96	10.92	1.42	3.11	mantle
B-9	0.142	0.061	0.113	0.973	0.856	2.705	163	6.1	4.6	4668			2.16	0.07	13.98	8.63	2.32	1.84	mantle
B-13	0.009	0.002	<LOD	<LOD	<LOD	0.258	196	3.3	1.5	2465			0.96	0.91			5.80		crust
R-2-4	0.119	0.085	0.080	2.132	1.853	3.083	269	9.0	6.6	6940			1.96	0.08	21.89	26.77	1.41	0.94	mantle

SAMPLE	Nb2O5	SiO2	TiO2	Al2O3	V2O3	Cr2O3	FeO	MnO	MgO	CaO	SrO	BaO	Na2O	K2O	TOTAL	Mineral	notes
M-2B-3A_ilm_8	0.00	0.02	74.22	0.03	0.65	0.04	8.38	0.06	0.65	0.56	0.11	5.75	2.79	0.94	94.21	low total	
M-2B-3A_ilm_8a	0.00	0.04	73.56	0.08	0.68	0.03	8.67	0.06	0.66	0.55	0.18	5.99	2.07	0.80	93.39	low total	
M-2B-3A_ilm-22	0.07	0.05	53.53	0.06	0.09	0.03	27.93	13.27	0.25	2.41	0.28	0.00	0.25	0.21	98.43	ilmenite	
M-2B-3A_ilm-23	0.00	0.26	70.94	0.17	0.10	0.05	6.43	0.10	0.03	4.14	0.08	9.17	0.74	1.44	93.66	low total	
M-2B-3A_ilm-24	0.08	0.08	57.53	0.04	0.10	0.04	25.12	11.72	0.36	3.11	0.16	0.00	1.05	0.12	99.51	ilmenite	
M-2B-3C(A)_40	1.11	1.06	39.05	0.33	0.03	0.00	1.99	0.00	0.46	28.71	0.30	0.00	0.23	0.01	73.28	low total	
M-2B-3C(B)_ilm-75	0.00	0.68	68.05	0.11	0.06	0.00	8.58	0.42	0.09	2.02	1.04	11.70	0.14	1.57	94.46	low total	
M-2B-3C(B)_ilm-76	0.00	0.89	67.64	0.15	0.02	0.02	8.52	0.29	0.10	3.95	0.18	6.11	0.08	4.02	91.96	low total	
M-2B-3C(B)_ilm-77	0.00	0.72	72.39	0.21	0.05	0.04	9.88	0.04	0.07	1.78	0.09	0.67	0.20	6.60	92.74	low total	
M-2B-3C(B)_ilm-78	0.00	2.97	65.17	1.01	0.10	0.07	9.14	0.04	0.14	5.88	0.09	1.39	0.15	6.76	92.92	low total	
M-2B-3C(B)_ilm-79	0.00	0.47	72.65	0.16	0.13	0.07	10.04	0.03	0.28	1.18	0.00	1.02	0.18	7.25	93.46	low total	
M-2B-3C(B)_ilm-80	0.00	0.56	70.60	0.30	0.05	0.06	5.87	0.21	0.02	7.54	1.02	3.24	0.78	3.37	93.62	low total	
M-2B-3A_nix_1	0.00	0.00	85.29	0.00	0.31	0.00	0.20	0.00	0.00	0.40	0.05	0.00	7.56	5.15	98.97	NaTi6O13	
M-2B-3A_nix_2	0.00	0.00	85.30	0.01	0.32	0.04	0.24	0.01	0.01	0.49	0.07	0.00	6.60	6.47	99.57	NaTi6O13	
M-2B-3A_nix_3	0.00	0.00	84.73	0.01	0.33	0.00	0.15	0.00	0.00	0.32	0.09	0.00	5.93	7.33	98.88	NaTi6O13	
M-2B-3A_nix_4	0.00	0.00	84.08	0.00	0.39	0.05	0.33	0.02	0.00	1.26	0.11	0.00	7.16	4.11	97.51	NaTi6O13	
M-2B-3A_nix_5	0.00	0.00	85.34	0.00	0.37	0.05	0.19	0.00	0.00	0.30	0.04	0.00	7.60	4.56	98.45	NaTi6O13	
M-2B-3A_prid_6	0.00	0.00	81.53	0.02	1.57	0.10	7.38	0.04	0.28	0.26	0.05	0.00	0.10	6.95	98.27	priderite	
M-2B-3A_prid_7	0.00	0.13	80.95	0.07	0.74	0.04	7.95	0.04	0.40	0.62	0.08	0.00	0.20	7.07	98.29	priderite	
M-2B-3A_freud_9	0.00	0.03	78.60	0.02	1.00	0.00	8.91	0.05	0.77	0.60	0.00	0.00	8.28	0.25	98.52	freudenburgite	
M-2B-3A_freud_10	0.00	0.21	78.58	0.11	0.83	0.03	7.78	0.12	1.25	0.90	0.05	0.00	7.64	1.54	99.03	freudenburgite	
M-2B-3A_freud_11	0.00	0.11	55.58	0.05	0.47	0.03	32.43	1.10	6.69	1.11	0.00	0.00	0.10	0.64	98.32	ilmenite	
M-2B-3A_freud_12	0.08	0.04	58.75	0.02	0.57	0.02	30.89	0.98	6.62	0.76	0.00	0.00	2.46	0.11	101.28	high total	
M-2B-3A_freud_13	0.00	0.05	61.90	0.04	0.41	0.03	24.89	0.90	6.44	0.85	0.00	0.00	2.56	0.72	98.79	??	
M-2B-3A_freud_14	0.00	0.00	78.38	0.01	0.40	0.03	7.93	0.02	0.72	0.50	0.05	0.48	0.27	8.79	97.57	Priderite	
M-2B-3A_freud_15	0.00	0.69	55.78	0.19	0.42	0.00	1.09	0.00	0.08	37.26	0.89	0.00	0.99	0.07	97.45	perovskite	
M-2B-3A_freud-16	0.00	5.12	64.59	1.51	0.70	0.05	5.47	0.07	0.80	10.54	0.15	0.19	0.15	5.17	94.50	low total	
M-2B-3A_freud-17	0.00	0.12	77.32	0.04	0.93	0.06	7.47	0.08	1.15	1.85	0.04	0.00	1.87	5.86	96.78	low total	
M-2B-3A_freud-18	0.00	14.13	38.82	2.85	0.54	0.00	7.17	0.22	0.53	23.19	0.07	0.00	1.35	0.22	89.09	low total	
M-2B-3A_freud-19	0.00	0.00	80.41	0.00	0.90	0.03	7.33	0.02	1.45	0.46	0.00	0.00	8.25	0.28	99.11	freudenburgite	
M-2B-3A_freud-20	0.00	0.82	53.83	0.27	0.46	0.04	30.26	0.66	5.99	9.43	0.24	0.00	0.36	0.09	102.45	high total	
M-2B-3A_perov-21	0.00	0.17	57.03	0.07	0.37	0.02	0.65	0.04	0.06	36.77	0.67	0.00	1.15	0.14	97.15	perovskite	
M-2B-3A_prid-25	0.00	0.00	83.29	0.02	0.90	0.04	6.88	0.03	0.37	0.31	0.00	0.00	0.07	6.55	98.45	priderite	
M-2B-3A_prid-26	0.00	0.00	82.75	0.06	0.93	0.04	6.63	0.00	0.72	0.15	0.04	0.00	0.06	7.13	98.54	priderite	
M-2B-3A_prid-27	0.00	0.00	80.68	0.05	0.74	0.04	6.64	0.02	1.21	0.48	0.10	0.00	0.11	8.15	98.23	priderite	
M-2B-3A_prid-28	0.00	0.05	55.10	0.04	0.19	0.04	30.19	0.61	8.76	4.99	0.03	0.00	0.19	0.04	100.24	???	has Ca & Mg
M-2B-3A_prid-29	0.00	0.00	80.36	0.11	0.38	0.04	7.90	0.02	1.11	0.42	0.00	0.00	0.09	7.67	98.09	priderite	
M-2B-3A_prid-30	0.00	0.22	57.73	0.13	0.23	0.00	30.21	0.80	7.80	0.92	0.00	0.00	0.20	1.59	99.83	??	
M-2B-3A_nix-31	0.00	0.02	99.21	0.00	0.20	0.04	0.19	0.00	0.00	0.36	0.00	0.00	0.00	0.18	100.20	Rutile	
M-2B-3A_nix-32	0.00	0.01	85.18	0.01	0.15	0.07	0.31	0.00	0.00	0.65	0.05	0.00	6.35	6.40	99.17	NaTi6O13	
M-2B-3A_prid-33	0.00	0.00	81.62	0.17	1.02	0.05	7.53	0.03	0.47	0.22	0.07	0.00	0.08	7.23	98.48	priderite	
M-2B-3A_rut-34	0.00	0.01	99.49	0.02	0.27	0.07	0.04	0.00	0.00	0.02	0.00	0.00	0.00	0.01	99.94	rutile	

SAMPLE	Nb2O5	SiO2	TiO2	Al2O3	V2O3	Cr2O3	FeO	MnO	MgO	CaO	SrO	BaO	Na2O	K2O	TOTAL	Mineral	notes
M-2B-3A_rut-35	0.00	0.01	99.31	0.00	0.32	0.08	0.05	0.00	0.00	0.02	0.00	0.00	0.00	0.01	99.79	rutile	
M-2B-3C(A)_36	3.75	0.14	48.55	0.68	0.00	0.00	3.22	0.00	0.17	36.59	0.39	0.00	0.35	0.00	93.85	perovskite	
M-2B-3C(A)_37	3.35	0.21	49.34	0.64	0.00	0.00	2.84	0.00	0.37	36.54	0.38	0.00	0.30	0.01	93.97	perovskite	
M-2B-3C(A)_39	1.37	9.69	35.12	1.42	0.03	0.00	7.14	0.06	0.74	35.91	0.30	0.00	0.20	0.00	91.98	perovskite	
M-2B-3C(A)_38	4.42	0.32	47.57	0.75	0.00	0.00	3.33	0.00	0.27	36.21	0.40	0.00	0.32	0.02	93.60	perovskite	
M-2B-3C(A)_41	3.97	0.79	46.91	0.86	0.00	0.00	3.16	0.00	0.36	36.28	0.41	0.00	0.33	0.01	93.07	perovskite	
M-2B-3C(A)_42	2.74	7.20	37.98	1.44	0.00	0.00	6.49	0.02	0.23	35.86	0.31	0.00	0.20	0.01	92.47	perovskite	
M-2B-3C(A)_43	0.17	0.00	55.68	0.16	0.08	0.00	1.48	0.02	0.14	37.89	0.52	0.00	0.50	0.02	96.65	perovskite	
M-2B-3C(A)_44	0.44	0.21	54.84	0.23	0.00	0.00	1.53	0.00	0.06	38.06	0.39	0.00	0.36	0.00	96.13	perovskite	
M-2B-3C(A)_45	2.62	2.05	46.50	0.67	0.03	0.00	3.77	0.00	0.21	36.12	0.38	0.00	0.29	0.01	92.65	perovskite	
M-2B-3C(A)_46	2.88	0.78	49.82	0.28	0.07	0.00	2.77	0.00	0.10	36.38	0.50	0.00	0.60	0.02	94.21	perovskite	
M-2B-3C(A)_47	3.28	0.81	48.56	0.66	0.00	0.00	3.15	0.00	0.22	36.43	0.42	0.00	0.40	0.02	93.93	perovskite	
M-2B-3C(A)_48	0.60	0.36	53.92	0.30	0.00	0.00	1.90	0.00	0.07	37.66	0.39	0.00	0.31	0.00	95.50	perovskite	
M-2B-3C(B)_prid-49	0.00	0.00	78.57	0.05	1.19	0.12	8.87	0.04	0.06	0.48	0.03	0.58	0.17	8.67	98.84	Priderite	
M-2B-3C(B)_prid-50	0.00	0.00	76.55	0.03	0.00	0.07	10.40	0.04	0.11	0.73	0.04	1.50	0.19	9.29	98.94	Priderite	
M-2B-3C(B)_prid-51	0.00	0.00	78.15	0.03	0.00	0.07	9.96	0.04	0.11	0.41	0.04	1.04	0.14	9.16	99.15	Priderite	
M-2B-3C(B)_prid-52	0.00	0.28	76.05	0.02	0.00	0.05	10.63	0.04	0.07	1.08	0.00	1.16	0.18	9.12	98.68	Priderite	
M-2B-3C(B)_nix-53	0.00	0.00	83.75	0.01	0.00	0.07	0.49	0.00	0.00	0.76	0.09	0.00	2.43	12.48	100.09	Jeppeite	
M-2B-3C(B)_nix-54	0.00	0.00	83.16	0.03	0.00	0.05	0.65	0.02	0.00	0.69	0.18	0.00	2.67	11.74	99.17	Jeppeite	
M-2B-3C(B)_nix-55	0.00	0.00	81.88	0.02	0.00	0.05	1.07	0.30	0.00	1.39	0.21	0.24	2.32	11.56	99.04	Jeppeite	
M-2B-3C(B)_nix-56	0.00	0.00	83.98	0.01	0.00	0.06	0.53	0.00	0.00	0.50	0.21	0.00	2.50	12.38	100.17	Jeppeite	
M-2B-3C(B)_nix-57	0.00	0.00	83.53	0.02	0.00	0.05	0.50	0.01	0.00	0.71	0.21	0.00	2.50	12.02	99.55	Jeppeite	
M-2B-3C(B)_nix-58	0.00	0.93	79.68	0.37	0.00	0.08	0.67	0.05	0.03	4.19	0.19	0.00	2.28	11.14	99.61	Jeppeite	
M-2B-3C(B)_nix-59	0.00	1.22	79.71	0.48	0.00	0.05	0.80	0.06	0.03	3.42	0.11	0.00	2.43	11.22	99.52	Jeppeite	
M-2B-3C(B)_nix-60	0.00	0.00	83.02	0.02	0.00	0.06	0.90	0.05	0.00	1.09	0.23	0.00	2.74	11.59	99.70	Jeppeite	
M-2B-3C(B)_nix-61	0.00	0.00	83.64	0.02	0.00	0.08	0.64	0.00	0.00	0.86	0.15	0.00	2.57	12.24	100.19	Jeppeite	
M-2B-3C(B)_nix-62	0.00	0.00	82.41	0.03	0.00	0.04	2.08	0.05	0.02	0.90	0.29	0.00	2.45	11.62	99.89	Jeppeite	
M-2B-3C(B)_nix-63	0.00	0.07	82.77	0.03	0.00	0.06	0.74	0.00	0.00	0.94	0.29	0.00	2.67	11.95	99.52	Jeppeite	
M-2B-3C(B)_nix-64	0.00	0.90	80.00	0.31	0.00	0.06	0.85	0.16	0.02	3.70	0.15	0.00	2.48	10.87	99.48	Jeppeite	
M-2B-3C(B)_prid-65	0.00	0.00	76.70	0.03	0.09	0.05	10.30	0.04	0.17	0.85	0.05	1.40	0.19	9.03	98.89	Priderite	
M-2B-3C(B)_prid-66	0.00	0.00	77.59	0.03	0.00	0.07	10.37	0.03	0.14	0.69	0.03	1.24	0.20	8.86	99.25	Priderite	
M-2B-3C(B)_prid-67	0.00	0.11	77.67	0.05	0.00	0.07	10.53	0.06	0.17	0.98	0.05	0.96	0.18	8.11	98.94	Priderite	
M-2B-3C(B)_prid-68	0.00	0.00	77.23	0.03	0.00	0.07	10.65	0.03	0.10	0.36	0.08	1.29	0.16	8.69	98.69	Priderite	
M-2B-3C(B)_prid-69	0.00	0.00	73.46	0.02	0.00	0.06	8.95	0.04	0.18	8.19	0.14	0.90	0.15	6.09	98.18	Ca-Jeppeite or contamination?	
M-2B-3C(B)_prid-70	0.00	0.03	76.80	0.05	0.00	0.07	10.65	0.04	0.08	0.85	0.08	1.42	0.20	8.47	98.73	Priderite	
M-2B-3C(B)_prid-71	0.00	0.13	75.76	0.04	0.23	0.07	10.51	0.03	0.14	1.15	0.08	1.27	0.21	8.58	98.20	Priderite	
M-2B-3C(B)_prid-72	0.00	1.53	78.10	0.72	0.12	0.03	0.90	0.02	0.00	3.10	0.16	0.00	2.10	11.34	98.13	Jeppeite	
M-2B-3C(B)_prid-73	0.00	1.21	79.65	0.57	0.06	0.06	0.64	0.00	0.00	2.62	0.15	0.00	2.20	11.53	98.69	Jeppeite	
M-2B-3C(B)_prid-74	0.00	0.00	77.37	0.03	0.00	0.05	10.51	0.04	0.14	0.79	0.05	1.36	0.18	7.82	98.35	priderite	
M-2B-3C(B)_nix-81	0.00	0.09	83.43	0.05	0.05	0.03	0.50	0.03	0.00	1.85	0.11	0.00	4.04	9.63	99.81	Jeppeite	
M-2B-3C(B)_prid-81	0.00	1.03	62.00	0.26	0.05	0.02	2.66	0.56	0.16	23.28	0.13	0.00	0.90	2.14	93.21	low total	
M-2B-3C(B)_prid-83	0.00	1.00	54.92	0.11	0.08	0.00	0.97	0.04	0.05	36.81	1.97	0.00	0.13	0.27	96.36	low total	

SAMPLE	Nb2O5	SiO2	TiO2	Al2O3	V2O3	Cr2O3	FeO	MnO	MgO	CaO	SrO	BaO	Na2O	K2O	TOTAL	Mineral	notes
M-2B-3C(B)_nix-84	0.00	0.30	82.38	0.12	0.03	0.05	0.99	0.02	0.02	1.71	0.14	0.00	3.35	10.12	99.20	Jeppeite	
M-2B-3C(B)_freud-85	0.00	0.00	77.67	0.02	0.13	0.06	9.15	0.06	0.20	0.97	0.09	0.93	0.24	9.51	99.01	Priderite	
M-2B-3C(B)_freud-86	0.07	0.61	56.08	0.08	0.15	0.03	0.79	0.03	0.07	36.04	2.58	0.00	1.08	0.20	97.81	perovskite	
M-2B-3C(B)_prid-87	0.00	0.40	93.77	0.07	0.03	0.05	2.11	0.05	0.04	2.28	0.00	0.00	1.32	0.17	100.28	impure rutile?	
M-2B-3C(B)_prid-88	0.00	6.97	60.15	1.43	0.00	0.09	2.96	0.18	0.05	13.87	0.12	0.00	4.76	4.60	95.18	low total	
M-2B-3C(B)_prid-89	0.00	3.98	56.06	0.75	0.00	0.03	3.24	0.16	0.10	22.93	0.17	0.00	0.31	0.87	88.58	low total	
M-2B-3C(B)_prid-90	0.00	0.82	78.99	0.25	0.15	0.05	8.53	0.05	0.23	2.02	0.07	0.00	0.13	7.13	98.43	priderite	
M-2B-3C(B)_nix-91	0.00	9.77	49.43	1.64	0.02	0.08	5.32	0.51	0.07	18.86	0.13	0.18	1.33	4.61	91.97	low total	
M-2B-3C(B)_prid-92	0.00	0.13	75.79	0.07	0.22	0.04	8.69	0.07	0.39	2.27	0.08	1.98	0.23	8.55	98.50	Priderite	has Ca?
M-2B-3C(B)_nix-93	0.00	2.11	76.00	0.63	0.08	0.05	1.23	0.07	0.02	4.91	0.18	0.49	4.23	8.05	98.05	Jeppeite	
M-2B-3C(B)_nix-94	0.00	0.56	79.00	0.22	0.19	0.07	0.95	0.11	0.03	4.98	0.15	0.00	3.63	8.60	98.49	Jeppeite	

Appendix B

Harris GA, Pearson DG, Liu J, Hardman MF, Snyder DB, Kelsch D (2018) Mantle Composition, Age and Geotherm beneath the Darby Kimberlite field, West Central Rae Craton. Miner Petrol.

Mineralogy and Petrology
https://doi.org/10.1007/s00710-018-0609-4

ORIGINAL PAPER

Mantle composition, age and geotherm beneath the Darby kimberlite field, west central Rae Craton

Garrett A. Harris[1] · D. Graham Pearson[1] · Jingao Liu[1,2] · Matthew F. Hardman[1] · David B. Snyder[3] · Dave Kelsch[4]

Received: 6 December 2017 / Accepted: 13 June 2018

Abstract
The Rae Craton, northern Canada, contains several diamondiferous kimberlite fields that have been a focus of episodic diamond exploration. Relatively little is known about the deep mantle lithosphere underpinning the architecturally complex crust. We present bulk and mineral element and isotopic compositional data for peridotite and pyroxenite/eclogite xenoliths from the Darby kimberlites representing fragments of the west central Rae lithosphere, as well as the first kimberlite eruption age of 542.2 ±2.6 Ma (2 σ; phlogopite Rb-Sr isochron). Darby peridotites have low bulk Al_2O_3 contents with highly-depleted olivine (median Mg# = 92.5) characteristic of cratonic lithosphere globally, but more depleted than peridotites from other Rae Craton localities. One peridotite xenolith contains a harzburgitic G10D garnet. Re-Os T_{RD} model ages appear to be the oldest measured to date from peridotites of the Rae lithosphere, having a mode in the early Neoarchean and ranging to the Paleoproterozoic (~2.3 Ga). Concentrate clinopyroxene defines a well constrained mantle geotherm indicating the existence of a ~200 km thick lithosphere at the time of kimberlite eruption, greater than the lithospheric thickness beneath Somerset Island and in good agreement with modern seismic constraints. Nickel-in-garnet thermometry in grains that record temperatures below the mantle adiabat, indicates mantle sampling dominantly in the graphite stability field whereas Al-in-olivine thermometry shows a distinct mantle sampling mode in the diamond stability field. Abundant pyroxenite and eclogite xenoliths are recovered across the Darby property and low-Cr garnet ($Cr_2O_3 < 1$ wt%) is the most abundant garnet type recovered in kimberlite concentrate. Based on thermometry, these rocks range in likely depths of equilibration, from the lower crust into the shallow lithospheric mantle. They give variable Os model ages, with the oldest ages in the Mesoarchean. The abundance of this mafic material reflects derivation from a large mafic body possibly evident in the layered structure of the Rae Craton mantle root defined by new seismic studies.

Keywords Northern Canada · Peridotite · Pyroxenite · Xenolith · Kimberlite eruption · Lithosphere

Introduction

The Rae Craton of northern Canada is an extensive but complex crustal block that is as large as the Superior Craton and hosts numerous kimberlite fields (e.g., Kjarsgaard 2007; Sarkar et al. 2018). However, relatively little is known about the deep mantle lithosphere that underpins the architecturally complex crust of this craton. Recent studies of the mantle cargo of these kimberlites from the eastern portion of the craton (Liu et al. 2016) as well as seismic studies (e.g., Snyder et al. 2015, 2017), have indicated the presence of a thick Archean cratonic root. However, to date, no data on the mantle lithosphere and its diamond potential have been published for the western part of the central Rae Craton. Here we provide the first compositional and geochronological information on mantle xenoliths and kimberlite-derived mineral concentrate from the Darby kimberlite field. We use the data to determine

Editorial handling: R. Rudnick

Electronic supplementary material The online version of this article (https://doi.org/10.1007/s00710-018-0609-4) contains supplementary material, which is available to authorized users.

✉ Garrett A. Harris
gaharris@ualberta.ca

1 University of Alberta, 1-26 Earth Sciences Building, Edmonton, AB T6G 2E3, Canada

2 China University of Geosciences, 29 Xue Yuan Road, Haidian District, Beijing 100083, People's Republic of China

3 Willet Green Miller Centre, Laurentian University, 935 Ramsey Lake Road, Sudbury, ON P3E 2C6, Canada

4 Bluestone Resources Inc., Suite 1020 – 800 West Pender Street, Vancouver, BC V6C 2V6, Canada

the lithosphere depletion, age and thickness, and to examine the variation of these parameters across the Rae Craton. Constraints on the diamond potential of this part of the Rae Craton are discussed and using a new seismic image of the Rae lithosphere, we speculate on the larger-scale structure and evolution of the geologically complex Rae Craton and its mantle root.

Geological setting of the Darby kimberlite field and samples

The Rae Craton is dominantly comprised of Meso- to Neoarchean amphibolite- to granulite-grade granitoid gneisses and komatiite-bearing greenstone belts (e.g., Jackson 1966; Hartlaub et al. 2005; Schultz et al. 2007; Sanborn-Barrie et al. 2014). The western central Rae Craton, that hosts the Darby kimberlite field, is comprised predominantly of Archean granitic gneiss and mafic/felsic volcanics and sediments of the Archean Prince Albert Group (Berman et al. 2013) that are cut by numerous dyke swarms. The oldest supracrustal unit in the Committee Bay region in the northern Churchill Structural Province is the Prince Albert Group (~2.7 Ga, MacHattie 2008; Schau 1982) with well-defined detrital zircons predicting the presence of unrecognized and/or proposed ancient crustal components of ~2.7–3.7 Ga (MacHattie 2008). The Prince Albert Group has undergone multiple deformation and granitic intrusion events during the Late Archean and to a lesser extent Early to Middle Proterozoic (Maynes and Doulos 2007).

The Darby Kimberlite field within the Rae Craton is located ~200 km southwest of the community of Kugaaruk, Nunavut (Fig. 1) and was discovered via magnetic anomalies in 2004. Kimberlite was intersected by drilling in 2006, with eight kimberlite bodies proven so far (Counts 2008). Mantle xenoliths were collected from kimberlite float samples directly above proven (drilled) kimberlite targets on the Darby property (Fig. S1; Electronic Supplementary Material 1). The Darby kimberlites occur in a broad north to south trend, most likely unrelated to major SW-NE fault systems in the region. Most of the surface kimberlite is highly altered and the peridotite xenoliths they contain are generally serpentinized or deeply-weathered. Kimberlite sampled from the northern bodies (e.g., Inferno) is massive coherent hypabyssal kimberlite dominated by olivine and ilmenite macrocrysts plus modal phlogopite. Kimberlite float sampled from the southern bodies - Level and Chopin pipes - also consists of massive coherent kimberlite with rare olivine macrocrysts and large abundant ilmenite macrocrysts with no macro-crystalline phlogopite. From the suite collected, a total of 33 mantle xenoliths (14 peridotites and 19 pyroxenites/eclogites) were selected for mineral chemistry and bulk analysis, with rocks identified in the field as "eclogite" at every sampling location. For detailed methodology regarding sample preparation of grain mounts, thick (100 μm) sections and rock powders see Electronic Supplementary Material 1.

Analytical methods

Rubidium-Sr dating of phlogopite (detailed procedures in Creaser et al. 2004) were performed in association with Bluestone Resources Inc. in 2006. Major element analyses of mineral grains were performed by electron probe microanalysis (EPMA) on a CAMECA SX100 and JEOL8900R. Trace elements in garnet and olivine and U-Pb isotopes in rutile were analysed by laser ablation inductively-coupled plasma mass spectrometry (LA-ICP-MS) at the Arctic Resources Laboratory (ARL). Accuracy and precision for Ni-in-garnet at the ARL, over the period encompassing this study is documented in detail by Hardman et al. (2018b). Whole-rock major and trace compositions were determined via X-ray fluorescence on fused glass discs of rock powders following procedures outlined by Boyd and Mertzman (1987). Whole-rock highly siderophile element (HSE including Os, Ir, Pt, Pd and Re) concentrations were conducted using an isotope dilution technique following Pearson and Woodland (2000) coupled with high pressure asher aqua regia digestion. For detailed methodology, procedures, instrument setup, and secondary standards for all methodology utilized in this study see Electronic Supplementary Material 1.

Results

Kimberlite eruption age

Rb-Sr phlogopite

Of 17 phlogopite megacryst grains analysed from drill core, ten with $^{87}Rb/^{86}Sr > 10$ and consistent model ages were used for Rb-Sr isochron regression (Fig. 2a) yielding an age of 542.2±2.6 Ma (2 σ; mean square weighted deviation, MSWD = 0.36) with an initial $^{87}Sr/^{86}Sr$ ratio of 0.7057 ±0.0011. Of the remaining seven grains, three analyses not used for isochron regression are plotted on the insert of Fig. 2a. The remaining analyses are useable due to low $^{87}Rb/^{86}Sr$ ratios and do not pass the criteria outlined by Sarkar et al. (2015). We believe that the seven extraneous data points (insert on Fig. 2a) represent older xenocrystic micas such as those identified in Ar-Ar dating studies of mantle xenoliths (e.g., Pearson et al. 1997).

Fig. 1 Geological setting of the western Churchill Provence (Hearne and Rae cratons), showing interpreted extent and metamorphic zones of the Arrowsmith orogen on the western flank of the Rae Craton (simplified after Berman et al. 2013). Selected kimberlite fields shown are Darby (yellow star), Amaruk-Pelly Bay (blue star), Repulse Bay (green star), and Somerset Island (red star)

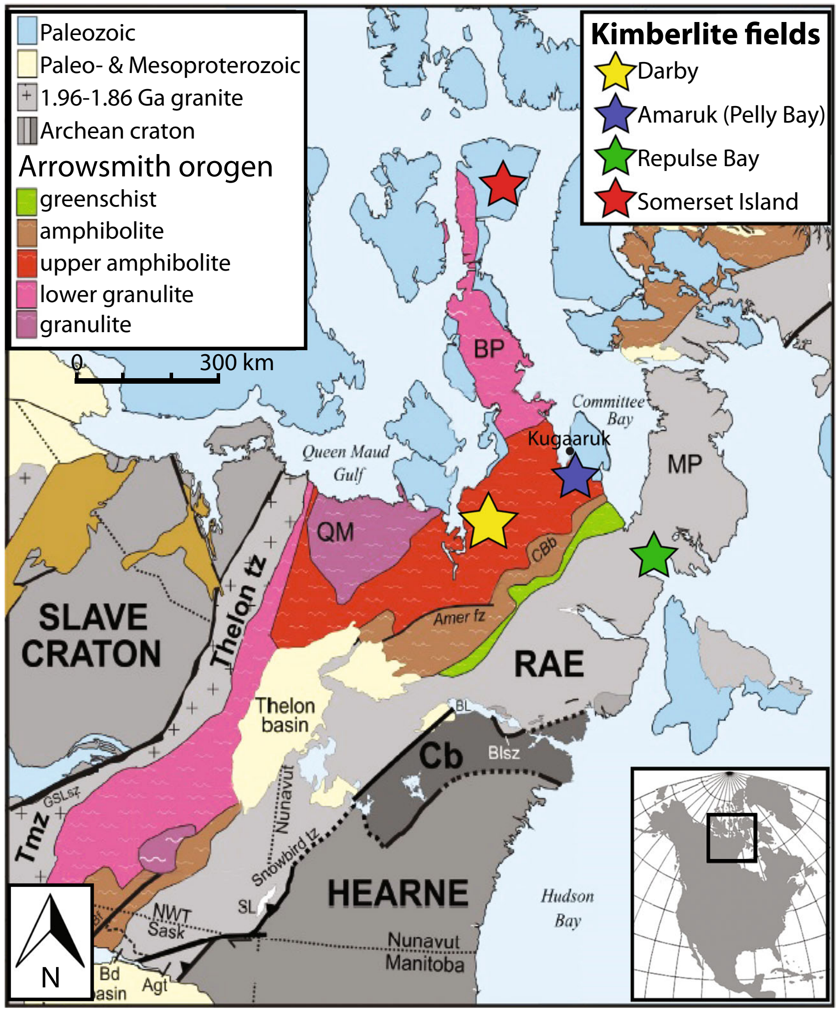

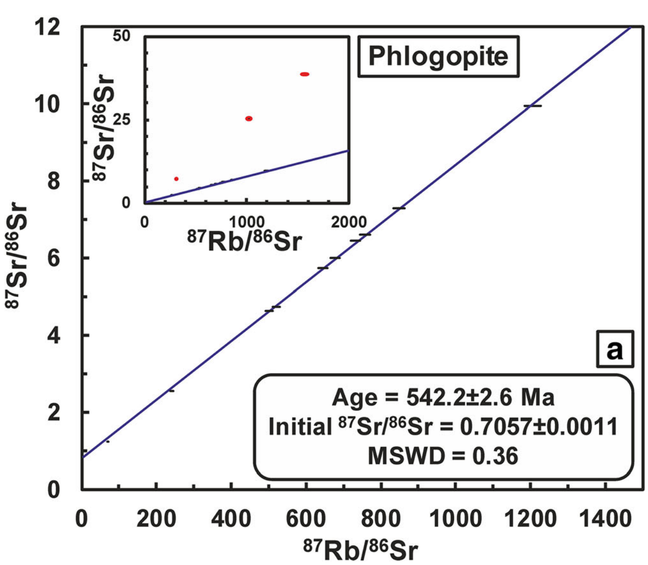

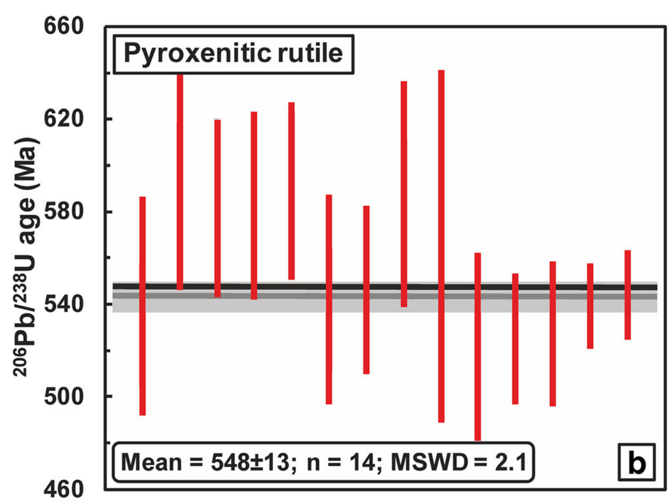

Fig. 2 **a** Rb-Sr isochron of individual phlogopite grains taken from drill core and kimberlite float. For increased visibility data points are 4σ on ^{87}Sr/^{86}Sr but remain 2σ on ^{87}Rb/^{86}Sr. Insert plots all samples measured except four samples with low ^{87}Sr/^{86}Sr are not resolvable, with samples not used for regression in red circles. **b** Laser ablation ICPMS ^{206}Pb/^{238}U ages for rutiles from Darby pyroxenite xenoliths, corrected for ^{204}Pb using the Andersen (2002) method. Each red line is an individual rutile grain. Grains selected from two pyroxenite xenoliths. Black line represents weighted mean ^{206}Pb/^{238}U emplacement age, grey line is Rb/Sr phlogopite emplacement age. Width of grey lines denote 2 σ uncertainty

U-Pb rutile in pyroxenite

Seven of the nineteen pyroxenite/eclogite xenoliths contain rutile. Major element analysis of rutile attempted to use the Cr_2O_3 element discriminator of Malkovets et al. (2016) to identify mantle rutiles, which appears non-definitive for the Darby pyroxenites (Fig. S2; Electronic Supplementary Material 1) in that they have lower Cr_2O_3 than rutiles of supposed mantle derivation. The low blocking temperature for the U-Pb system in rutile (600–640 °C; Cherniak 2000) means that the U-Pb system in any mantle-derived rutile has closed at the time of kimberlite eruption (e.g., Malkovets et al. 2016). Fourteen individual rutile grains analysed in two different samples (Fig. 2b), corrected for common Pb using the "Andersen method" (Andersen 2002) give a weighted mean $^{238}U/^{206}Pb$ age of 548±13 [2.3%] Ma (2 σ, MSWD = 2.1), which is identical, within error, of the Rb/Sr phlogopite isochron age, and hence clearly reflects closure of the U-Pb system at the time of kimberlite eruption. The exception is rutile in pyroxenite sample B-13, where ten out of twelve of the rutiles in that rock gave a range of older $^{238}U/^{206}Pb$ ages from ~635–893 Ma which may reflect incomplete Pb-loss from older rutiles. Since the Rb-Sr isochron derived from the Darby kimberlites is the more precise age determination compared with the rutile U-Pb age, we adopt it here as the eruption age for the Darby kimberlites.

Petrography

Representative photographs of the peridotites and eclogites in hand sample and thick section are shown in Fig. S3 (Electronic Supplementary Material 1). Table S2 (Electronic Supplementary Material 1), displays mineralogical, petrographic and other information on xenoliths studied.

Peridotites are generally highly altered, masking their primary mantle textures. The majority of peridotites are dominantly comprised of serpentine with some fresh residual areas of olivine and pyroxene (commonly <1 mm). Garnets in the peridotites range from 0.1–1.0 mm, with minor rare kelyphite rims. Some peridotites show variable levels of infiltration by the host kimberlite.

Eclogites and pyroxenites classified based on IUGS definition (Desmons and Smulikowski 2007) of their clinopyroxene chemistry (below) show equant granular textures. One of these rocks also contains primary plagioclase indicating a crustal origin. Rutile in these rocks is interstitial, forming grains up to 1 mm. Some rutiles have complex reaction rims consisting of perovskite, ilmenite, priderite (KTi_8O_{16}), freudenbergite ($Na_2Ti_8O_{16}$), plus jeppeite ($K_2Ti_6O_{13}$) that are most likely the product of an unusual metasomatic melt, of possible lamproitic affinity, producing a complex Na-K-Ti rich metasomatic mineral assemblage.

Mineral major element chemistry

Following petrographic characterization samples were analysed via EPMA for mineral major element chemistry in individual grains from the xenoliths, mantle xenocrysts and heavy mineral kimberlite concentrate (Table S1 and S2; Electronic Supplementary Material 2).

Peridotites

Fresh olivine within the peridotite xenoliths is scarce due to serpentinization and varying levels of carbonation. Olivine compositions were measured from eleven peridotite xenoliths, giving a median molar Mg# (100 × Mg/(Mg + Fe)) of 92.5, very similar to the median for cratonic peridotites worldwide (Pearson and Wittig 2014) and slightly more depleted than peridotites from Somerset Island (north central Rae Craton), and the North Atlantic and Slave Cratons (Fig. 3a). In addition to the xenoliths, 532 olivine grains from heavy mineral concentrate were analysed, with those of mantle origin distinguished based on their high Ni-Mg# relationship (Fig. S4; Electronic Supplementary Material 1). The cluster of high Ni-Mg# (0.3–0.42 wt% Ni; >91 Mg#) concentrate olivines give a median Mg# of 92.2, overlapping the olivines from the peridotite xenoliths. Most of the xenoliths are similar to the pristine mantle samples of Foley et al. (2013), although some samples have increased Ti with one sample enriched in Ca and another enriched in both Ti and Ca (Fig. 3b). The large scatter observed in Fig. 3b suggests that the "kimberlitic field" may be larger than suggested by Foley et al. 2013. Although kimberlite Ti-metasomatism appears to be a common feature of the phases sampled (i.e., garnets with high Ni and Ti) by the Darby kimberlites, in a number of samples, the metasomatic agent was lamproite based on other observations, such as the occurrence of jeppeite and priderite - phases only ever observed in lamproites. A small proportion of olivines overlap with the compositions of those from lamproites using the Foley et al. (2013) classification (Fig. 3b) but the Mediterranean lamproites analysed to create this field are regarded as chemically distinct from the lamproites intruding cratons (Prelević et al. 2008).

Four of the fourteen peridotites contained garnet, one sample containing harzburgitic (G10D) garnet that gives a minimum Cr-saturation pressure of 4.7 GPa using the P_{38} geobarometer (Grütter et al. 2004, 2006). The remaining three samples contain lherzolitic (G11) garnets. Of the garnets picked from the kimberlite concentrate, 51 grains (18%) are peridotitic. Of these, 98% are lherzolitic, in two distinct groups (31% G11, "on-craton" with lower Ca/Cr and 67% G9, "off-craton" with higher Ca/Cr; Fig. 4). One garnet classifies as wehrlite (G12).

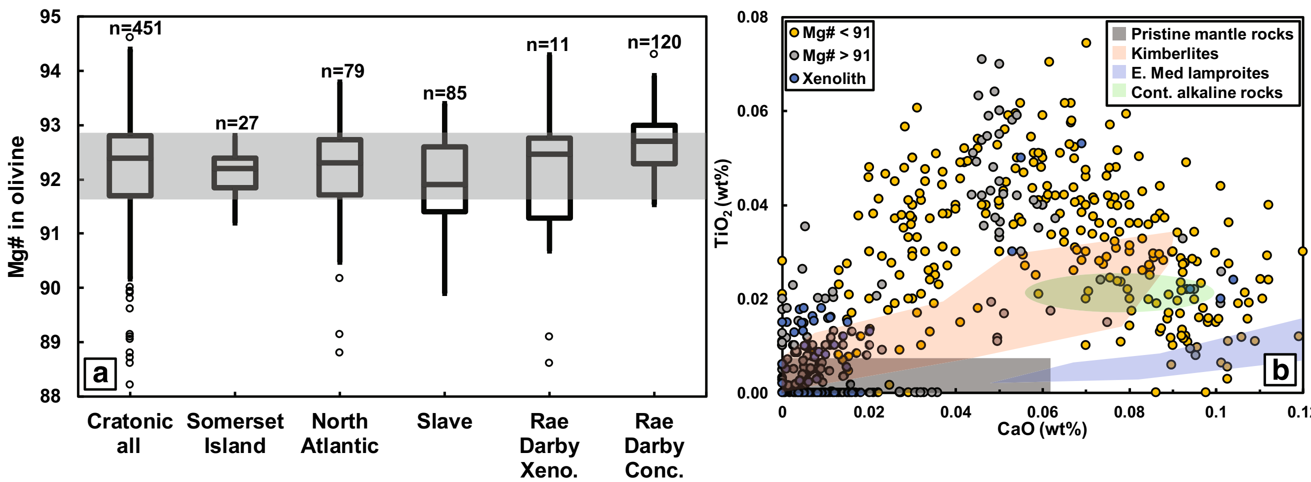

Fig. 3 **a** Box and whisker plot of Mg# for mantle olivines. Number of samples (n) given for each category. Data from Pearson and Wittig (2008). **b** Ti-Ca plot for all olivine measured. Fields of various rock types taken from of Foley et al. (2013)

Clinopyroxenes from the peridotite xenoliths are diopsides but did not pass the compositional filters of Grütter (2009) for use in thermobarometry. Likewise, seven clinopyroxene grains derived from mineral concentrate were classified as garnet peridotite-derived. These compositions were used for thermobarometry (below).

Pyroxenites and eclogites

Twelve of the nineteen "eclogites" are classified as pyroxenite sensu stricto on the basis of their CaTs versus jadeite contents (calculated via WinPyrox; Yavuz 2013) in clinopyroxene (Fig. S5; Electronic Supplementary Material 1), with all samples having low CaTs at <19% jadeite (classified as diopside-bearing pyroxenites). Three samples contain augite composition (B-13, B-9 and B-3) and one sample contains pigeonite (B-3). Garnets in these lithologies are pyrope-almandine in composition (28–65 mol% pyrope), with less than 30 mol% grossular component that is slightly more elevated at the more almandine rich end of the array (Fig. S6; Electronic Supplementary Material 1). Of these low-Cr xenolith-derived garnets, 53% of the garnets are G4 (low-CaO pyroxenite/eclogite; <6 wt% CaO), with the remainder being G3 (high-CaO eclogite; Fig. S7A; Electronic Supplementary Material 1).

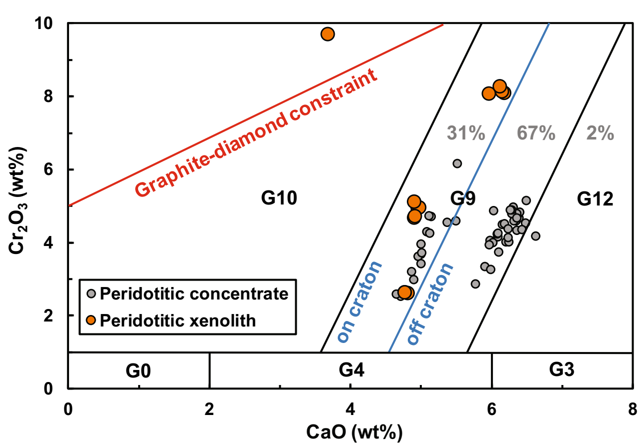

Fig. 4 Cr-Ca garnet classification plot (Grütter et al. 2004) of all analyses of Darby xenolith and concentrate garnets with $Cr_2O_3 \geq 1$ wt%. Xenolith analyses (orange circles, $n = 12$) and concentrate analyses (grey circles, $n = 51$)

Of the concentrate-derived garnets ($n = 233$) 82% classify as low-Cr, with $Cr_2O_3 < 1$ wt%. These garnets show a slightly higher ratio of G3 garnets (63% of concentrate versus 47% of xenoliths; Fig. S7B; Electronic Supplementary Material 1) but nonetheless confirm the high proportion of pyroxenites in the mantle and crust sampled by Darby kimberlites. TiO_2 and Na_2O contents of garnets from the xenoliths and concentrate are uniformly low (<0.20 and < 0.05 wt% respectively; Fig. S8; Electronic Supplementary Material 1).

Using the logistic regression "crust-mantle" major element discrimination method of Hardman et al. (2018a) on the Darby G3/G4 concentrate garnets, only 28% of the 233 grains classify as mantle in origin (Table S1, Electronic Supplementary Material 2), indicating that many may have been derived from plagioclase pyroxenite or lower-crustal garnet-bearing lithologies. This interpretation is consistent with the presence of plagioclase in one of the pyroxenites, which is correctly classified as crustal. However, using an enhanced major and trace element discrimination scheme, Hardman et al. (2018b) have shown that Eu-anomalies and Sr-concentrations are valuable in classifying mantle garnets and increase classification success rates of low-Cr crust and mantle garnets. The method of Hardman et al. (2018b) is utilized to classify "crust-mantle" garnets from xenoliths (below).

Mineral trace element chemistry

Trace element analyses of garnet, diopside and olivine are shown in Table S3, S4 and S5 (Electronic Supplementary

Material 2), respectively. Reported ppm elemental abundances for minerals within xenoliths analysed for rare earth elements (REE) are averaged values for multiple analyses on the same xenolith. Two of the garnet-bearing peridotites display "sinusoidal" garnet CI-normalized REE patterns (REE_N) and of the sample set, the harzburgitic (G10) garnet has the most-pronounced "sinusoidal" pattern (Fig. 5a). The other two garnet peridotites have garnets that are light rare earth element (LREE) depleted with La < CI Chondrite and are heavy rare earth element enriched (HREE) (~10 x CI Chondrite). Of the G9 concentrate garnets 70% ($n = 33$) show weakly "sinusoidal" patterns. These garnets are dominated by garnets that plot within the "off-craton" portion of the lherzolite (G9) field. The remaining 30% ($n = 14$) of the REE_N patterns show a $LREE_N$ depleted, $HREE_N$ enriched patterns. These garnets classify dominantly as high-Ti "on-craton" lherzolites (G11; Grütter et al. 2004).

Of the nineteen xenoliths, fourteen (74%) classify as mantle-derived (Hardman et al. 2018b). Seven of the total nineteen samples (37%) are classified as mantle due to positive Eu-anomalies ($2 \times Eu_N/(Sm_N + Gd_N)$) and/or high Sr-concentrations. This demonstrates the importance of trace element analysis in this data set to correctly classify garnet origin. All of the pyroxenites displaying lamproitic metasomatic mineral assemblages are classified as mantle suggesting that lamproitic metasomatism may have not reached the crust beneath Darby. The REE_N patterns (Fig. 5b) are typical $LREE_N$ depleted patterns from eclogitic/pyroxenitic garnet with La < CI Chondrite and considerable Lu_N enrichment (~100 x CI Chondrite). Of the nineteen samples analyzed, thirteen samples have positive Eu anomalies ($Eu/Eu^* > 1.00$), with all but one classifying as mantle. One highly metasomatized xenolith (M-2B) with the hottest Fe-Mg temperature has a $HREE_N$ depleted with a pattern that appears "sinusoidal," indicating the sample has undergone lamproitic metasomatism resulting in the mineral assemblage of freudenbergite, jeppeite, and priderite.

Of the twelve pyroxenite xenoliths with fresh pyroxene eight samples had trace elements analyses completed on diopside. The REE_N patterns (Fig. 5c) are $LREE_N$ enriched patterns typical of eclogitic/pyroxenitic pyroxene with La < 100 x CI Chondrite and Lu < CI Chondrite. Of these, pyroxenes in seven samples have positive Eu anomalies including the plagioclase pyroxenite.

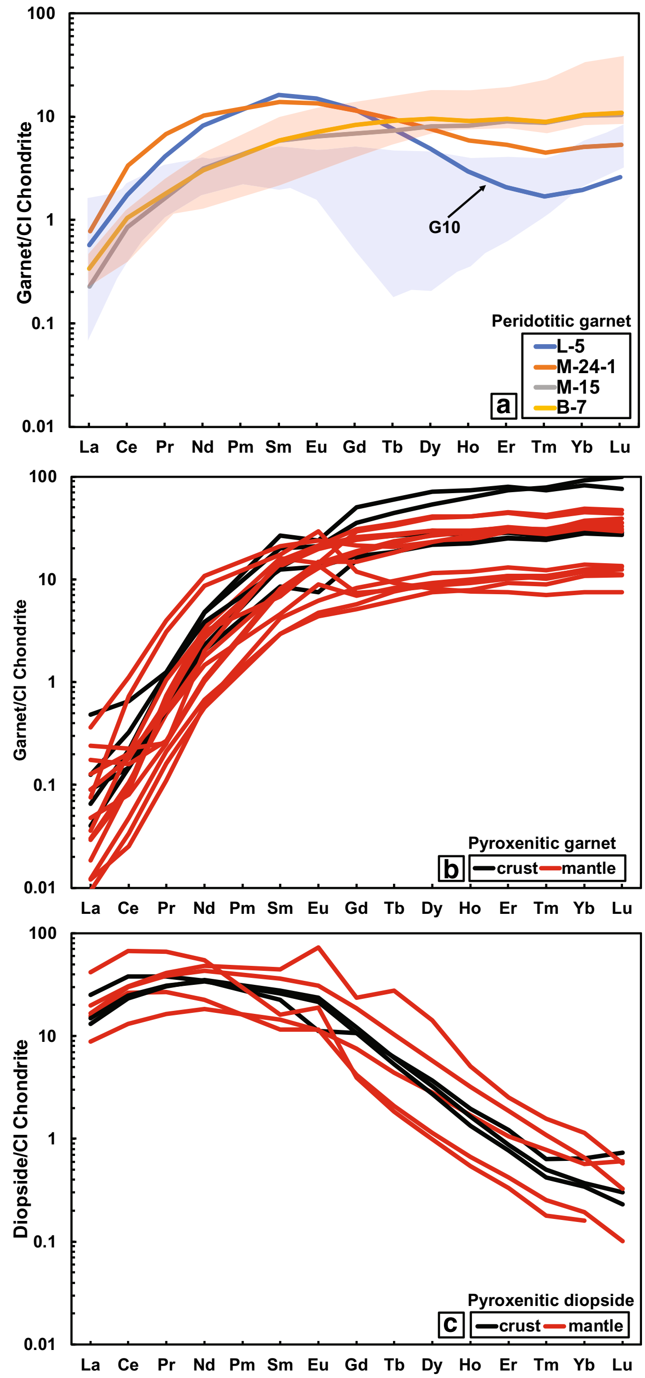

Fig. 5 REE_N garnet mineral plots of **a** Peridotitic $Cr_2O_3 \geq 1$ wt%, where lines are for xenoliths and two fields showing patterns observed in concentrate, **b** Low-Cr ($Cr_2O_3 < 1$ wt%) garnet in pyroxenites, and **c** diopside in pyroxenites. REEs are CI Carbonaceous Chondrite normalized (McDonough and Sun 1995)

Whole-rock major elements

Peridotite whole-rock major element trends show the effects of some carbonation/host rock infiltration in trends of high CaO contents at low to moderate Al_2O_3 (Table S6; Electronic Supplementary Material 2). Therefore, we rely on bulk rock Al_2O_3 as the most robust indicator of whole rock major element depletion (Fig. 6). The Darby peridotites are low in Al_2O_3 (median ~0.75 wt%), somewhat lower (more depleted) than the peridotite xenoliths from the more eastern portion of the Rae Craton (Pelly Bay and Repulse Bay; Liu et al. 2016). These low Al_2O_3 contents

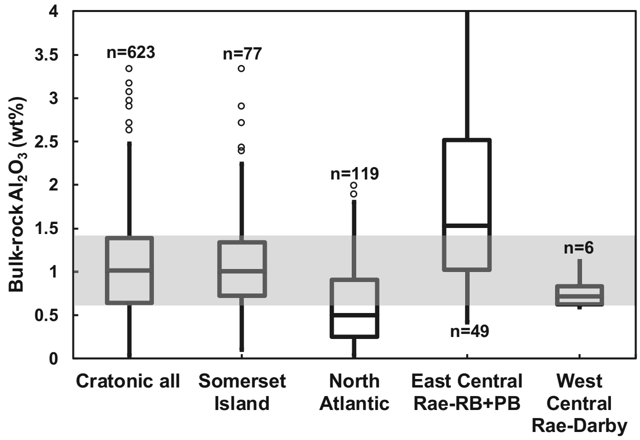

Fig. 6 Box and whisker plot of bulk-rock Al_2O_3 of peridotites from a variety of localities. Number of samples (n) given for each category. Data from Pearson and Wittig (2014)

are very comparable to typical cratonic mantle peridotite compositions (Fig. 6).

Highly siderophile elements

Highly siderophile element (HSE) determinations were measured on a total of five peridotites and six pyroxenites (Table S7; Electronic Supplementary Material 2). Duplicate measurements were performed on all pyroxenites.

Osmium isotopic compositions in the peridotites are unradiogenic, with γOs values, corrected for the time of kimberlite eruption of ca 542 Ma, clustering at the unradiogenic end of cratonic peridotite compositions (Fig. 7a). The mantle-normalised HSE patterns of these rocks (Fig. 8a) reveal that although Os concentrations in the peridotites vary widely, they have relatively unfractionated iridium-group (I-PGE) patterns, with strong Pt depletions that mirror the Pt-IPGE fractionations observed in cratonic peridotites (Pearson et al. 2004; Aulbach et al. 2015). However, their Pd and Re values are significantly higher than "undisturbed" residual cratonic peridotites (Fig. 8a). Rhenium and Pd, the most incompatible of the HSEs analysed, are enriched due to post-melting metasomatic effects that tend to re-enrich Pd and Re, creating extended PGE plots that have a "kick" in Pd and Re.

Pyroxenite Os isotope ratios are very radiogenic (Fig. 7a) with γOs values ranging from ~1,8000–10,200, as radiogenic as the highest $^{187}Os/^{188}Os$ ratios measured in any suite of cratonic eclogites. The HSE patterns of these rocks have the typical positive slopes showing enrichment of P-PGEs over IPGEs that are seen in other pyroxenites world-wide (Fig. 8b; Marchesi et al. 2014).

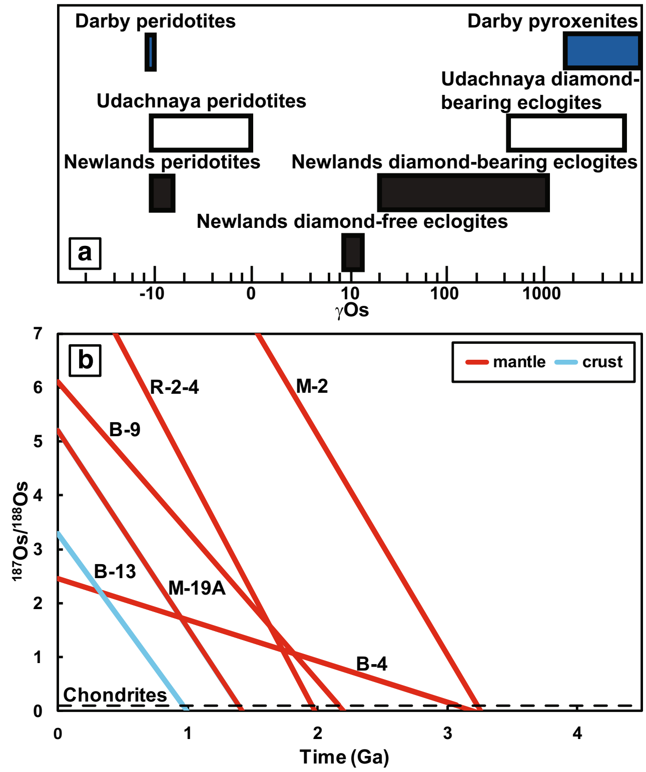

Fig. 7 **a** γOs plot displaying Darby unradiogenic peridotites and highly radiogenic eclogites compared to Udachnaya and Newlands (Menzies 2003). γOs is the percent difference in $^{187}Os/^{188}Os$ between chondrite and the sample at the time of kimberlite eruption. **b** Osmium isotope evolution diagram for Darby pyroxenites. Dashed line = chondrite evolution. Solid lines denote the isotope evolution of a sample. Model age given by the intersection of the sample evolution line and chondrite line

Discussion

A geotherm for the west central Rae Craton and mantle sampling

Darby peridotite xenoliths are too altered to perform multiphase geothermobarometry. Instead, garnet-peridotite-derived clinopyroxenes, from kimberlite heavy mineral concentrate, yield a tightly-constrained geotherm for the west central Rae lithosphere (Fig. 9) and indicated a lithospheric thickness of ~200 km, with a diamond window ~75 km thick. This lithospheric thickness is consistent with the seismic estimate of lithospheric thickness beneath this area (Fig. 10) and is within error of that constrained from the geotherm for the east central Rae (Liu et al. 2016), but significantly deeper than the lithosphere beneath Somerset Island, north Rae (~160–170 km; Mather et al. 2011). As such, the Rae lithosphere appears to be thicker beneath Darby, in the western central Rae, based on both geophysical and petrological considerations, than at its northern edge. This may be a

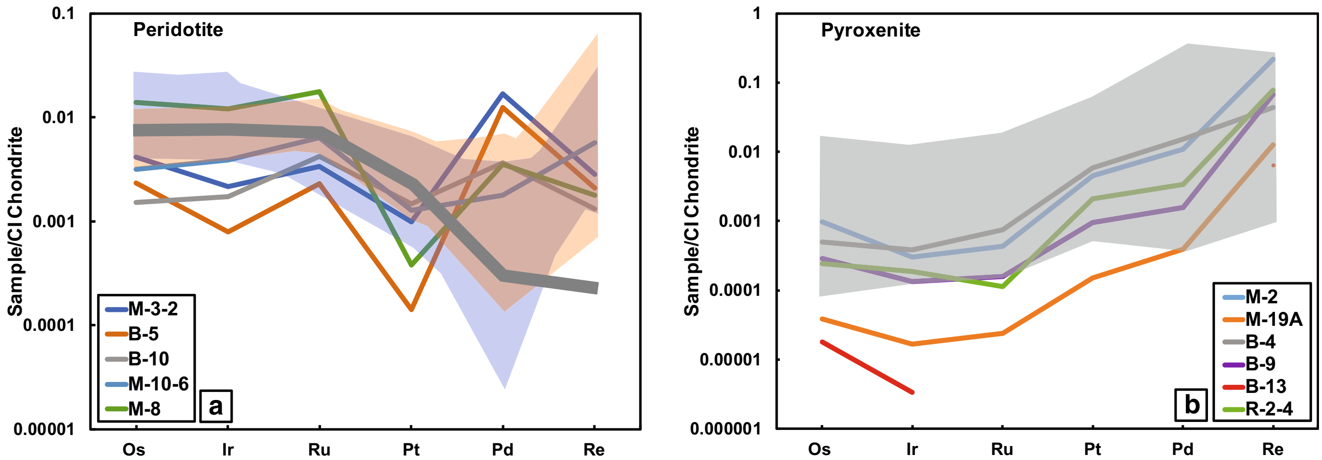

Fig. 8 **a** HSE patterns of peridotites. Thick grey line is "ideal" melt depleted cratonic peridotite HSE pattern (Pearson et al. 2004). Two fields in background showing patterns from other peridotite suites: orange-Somerset Island (Irvine et al. 2003) and blue-Repulse Bay and Pelly Bay (Liu et al. 2016) **b** HSE patterns of pyroxenites, grey field represents global pyroxenites (Marchesi et al. 2014). All patterns CI Chondrite-normalized (McDonough and Sun 1995)

function of the lateral accretion of cratons, which geodynamic modelling predicts will result in thinner craton margins (Wang et al. in press).

Nickel-in-garnet temperatures (Table S3; Electronic Supplementary Material 2) were averaged (Shu et al. 2013) from the formulations of Griffin et al. (1989) and Canil (1999). The four garnet peridotites and 49 peridotitic garnets from concentrate yield two distinct modes in mantle sampling depths when extrapolated to the Darby geotherm. A cluster of garnets from the higher Ca/Cr lherzolitic garnets equilibrated at 765–920 °C and a group of peridotitic garnets (50% of xenoliths and 28% of concentrate) from the lower Ca/Cr lherzolitic garnets (94%) have anomalously high Ti concentrations and very high Ni, yielding unreasonable T_{Ni} values of >> 1400 °C, i.e., super-adiabatic values, well outside the lithospheric "diamond window."

The experimentally calibrated Al-in-olivine thermometer of Bussweiler et al. (2017) was applied to olivine from concentrate and xenoliths (Table S5; Electronic Supplementary Material 2) after applying the Al - V "garnet facies" filter (Fig. S9; Electronic Supplementary Material 1). Olivine thermometry indicates two distinct mantle sampling regimes,

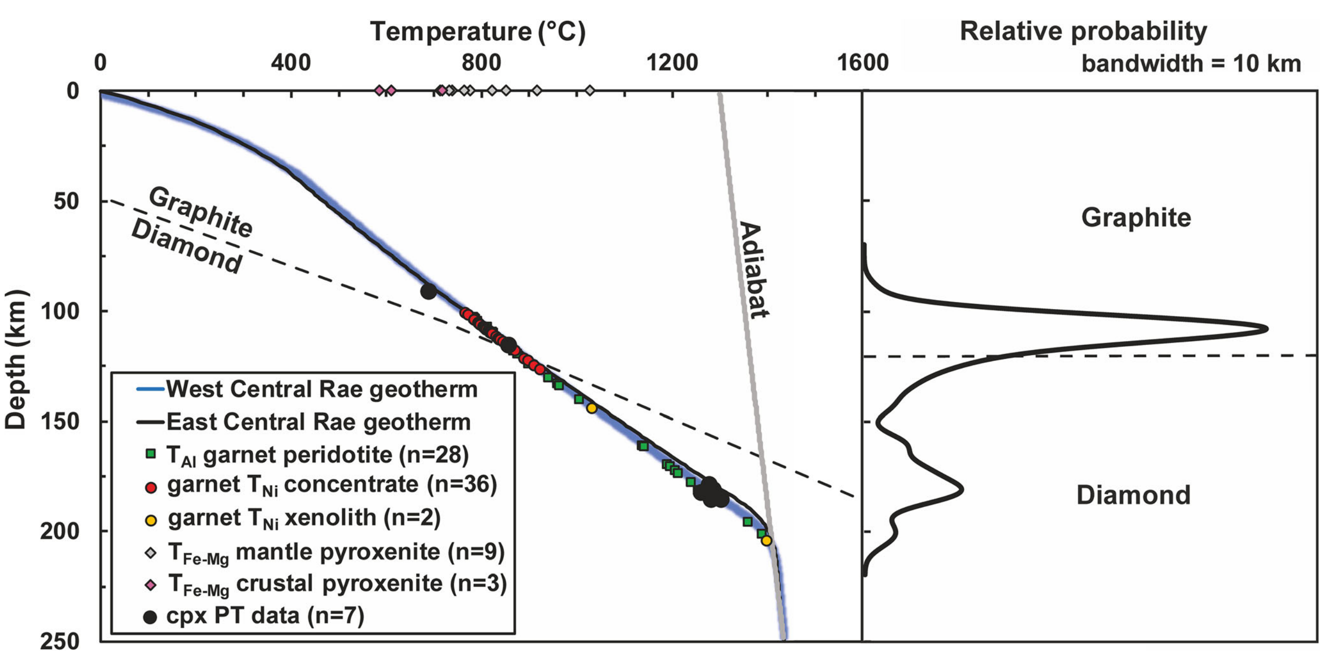

Fig. 9 FITPLOT (Mather et al. 2011) geotherm modeled from Darby clinopyroxene concentrate (Grütter 2009) - all locations composited using crustal thickness of 38.6±0.3 km (Snyder et al. 2015). Ni-in-garnet and Al-in-olivine temperatures from peridotite xenoliths and concentrate are extrapolated to this geotherm while Fe-Mg temperatures are plotted at 0 km for clarity. Right panel shows mantle depth sampling expressed as a probability density plot

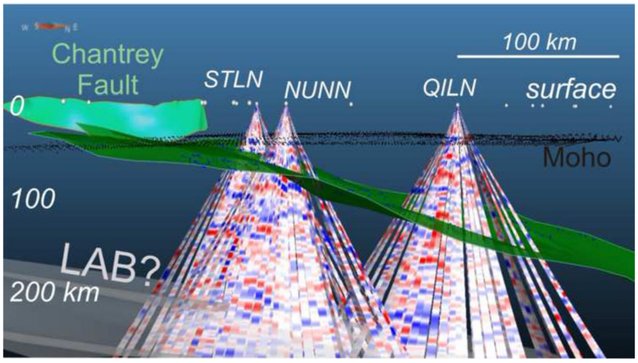

Fig. 10 Snapshot of Geocad 3-D model of the Rae Craton telesiesmic study (view from northwest) summarized in Snyder et al. (2017). From left to right the three receiver function cones 'point' to Darby, Nanuq, and Qilaluqak. The green surface is the Nanuq surface and strikes NNW/SSE and dips to the east. The smaller, near-vertical surface in the crust is the down-dip projection of the Chantrey fault using gravity 'worms'. LAB was identified based on distinct velocity changes. Its possible position is augmented by a white surface on the plot. Estimates of the projected depths of the Nanuq surface beneath a few seismic stations: 52 km @ Darby/STLN, 72 km @ Nanuq/NUNN, 99 km @ Amaruk/KUGN/Pelly Bay, 137 km @ QILN/Repulse Bay, 148 km @ Igloolik/ILON

from 785–1005 °C, in broad agreement with the Ni-in-garnet sampling mode and a higher temperature region of mantle sampling, well into the diamond stability at 1140–1390 °C.

The presence of elevated Ti in ~30% of peridotitic garnets derived from the lithosphere beneath Darby is indicative of Ti melt-associated metasomatism in the base of the lithosphere where thermal disturbance of the lowermost lithosphere was transient and did not have sufficient time to equilibrate prior to sampling by kimberlite. All of the Ti metasomatised garnets have very high T_{Ni}, above the mantle adiabat and this heating event may have reduced the diamond tenor of the lithosphere. These high Ti and T_{Ni} garnets exclusively fall into the "on-craton" category (Fig. 4; lower Ca/Cr), which make up the $LREE_N$ depleted patterns (Fig. 5a). The apparent difference in mantle sampling profiles between the non-disturbed garnet and olivine warrants further investigation with a larger sample set. The super-adiabatic garnet concentrate populations and the peculiar Ti metasomatism in the pyroxenites indicates that the amount of high-T melt-related metasomatism at Darby exceeded that normally seen in other cratonic locations where high-T metasomatised peridotites are found.

Mantle composition and age beneath the west central Rae Craton

Peridotite compositions

The highly depleted olivine Mg# of the Darby peridotites (92.5) is indistinguishable from the worldwide median value of 92.6 for cratonic peridotites world-wide (Pearson and Wittig 2014). While the mantle xenolith suite is relatively small, the Mg# mode in the mantle olivines extracted from concentrate is also high (92.2) and similar to the xenolith median value. This and the low bulk rock Al_2O_3 contents of these peridotites are consistent with the mantle lithosphere beneath Darby representing extremely melt-depleted (40% or more) residual mantle. This conclusion is supported by the presence of a G10D harzburgitic garnet in one peridotite as well as their low Pt concentrations (low Pt/Ir), that also indicate extensive melt extraction (Aulbach et al. 2015). It is difficult to make a direct comparison in the level of depletion of the Darby mantle sample relative to that of the most eastern Rae Craton mantle samples analysed by Liu et al. (2016) because of the very altered nature of those rocks, but the lower median Al_2O_3 content of the Darby samples is an indication of a slightly more depleted mantle. The peridotite xenoliths from Somerset Island (north central Rae Craton; Irvine et al. 2003) are much fresher than those in the eastern Rae, making comparison with the Darby data more straightforward. The Darby mantle suite has higher median olivine Mg# and significantly lower and more tightly constrained bulk Al_2O_3 (Figs. 3b and 5, respectively), making it perhaps the most depleted mantle lithosphere found beneath the Rae Craton. While the limited number of peridotites analysed here clearly establish the presence of Archean lithospheric mantle beneath this westernmost part of the central Rae Craton, the limited depth coverage and small sample set do not allow us to adequately test the stratigraphic relationship suggested for the Rae lithospheric mantle by Liu et al. (2016).

The garnet REE_N patterns are dominantly "sinusoidal" (50% of xenoliths and 70% of concentrate). These signatures are often associated with rocks that have interacted with a diamond forming fluid (Stachel and Harris 2008). The harzburgitic G10D garnet has the strongest "sinusoidal" pattern, consistent with the common occurrence of this type of REE pattern in G10 garnets (Klein-BenDavid and Pearson 2009). The other group of garnet REE_N patterns are $LREE_N$ depleted (50% of xenoliths and 30% of the concentrate), typical of lherzolitic garnets from cratonic peridotites (Stachel and Harris 2008). Stachel and Harris (2008), on the basis of diamond inclusion geochemistry, propose that more intense fluid metasomatism associated with enrichment in Zr (and negligible addition of Y and MREE-HREE) appears to be characteristic of the harzburgitic paragenesis. However, the Darby peridotitic garnet with the lowest Y is enriched in Zr and has Cr-Ca systematics that are clearly lherzolitic in nature while a sample with moderate Y and enriched Zr has a harzburgitic Cr-Ca signature (Fig. S10; Supplementary Material 1). Thus, it is unclear if these observations from diamond inclusions remain true for xenoliths. Similar to diamond inclusions studied by Stachel and Harris (2008), the lherzolitic garnets studied at Darby have concurrent addition of Zr and Y (and MREE-HREE), likely related to silicate melt metasomatism.

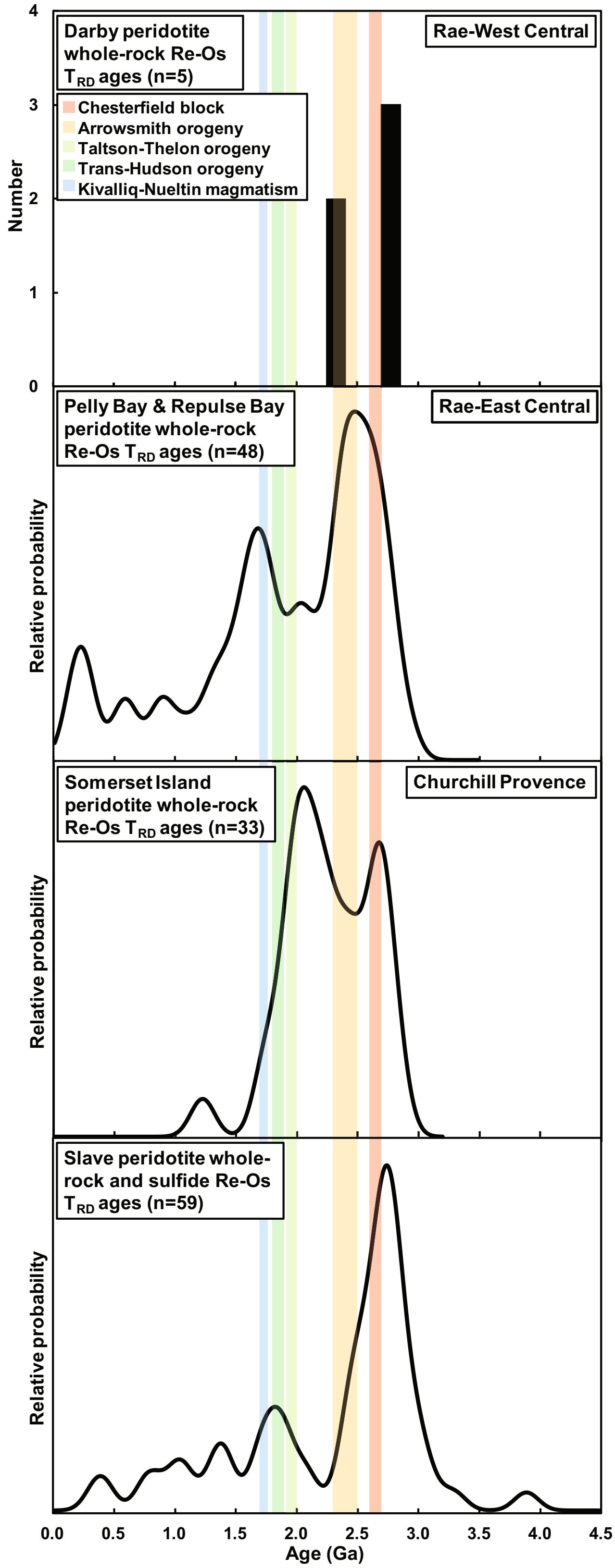

Fig. 11 Histogram for Darby and probability density diagrams for Repulse Bay and Pelly Bay (Liu et al. 2016), Somerset Island (Irvine et al. 2003), and Slave (Pearson and Wittig 2014) of peridotite Re-Os T_{RD} ages. Coloured bands represent the age range of major regional tectonothermal events expressed in crustal rocks of the Rae Craton summarized by Liu et al. (2016)

Depletion age constraints

Whole-rock Re-depletion ages for five of the peridotites range from early Neoarchean to Paleoproterozoic. The model age histogram for Darby (Fig. 11) demonstrates that the peridotitic mantle beneath Darby, based on our limited sampling, appears older than the more substantive peridotite suites analysed from the east central Rae and also older than the lithospheric mantle beneath Somerset Island, northern Rae. The small dataset from Darby has two age clusters, at ~2.3 and ~2.7 Ga, indicating lithospheric stabilization at least in the early Neoarchean. In contrast, the east central Rae lithospheric mantle has three peaks, one in the Phanerozoic, one at ~1.7 and the oldest at 2.5 Ga (Fig. 11). Somerset Island has two main age peaks at 2.0 and 2.6 Ga (Fig. 11). The slightly older mode in Archean ages at Darby (Fig. 11) is consistent with the observation that the oldest crustal ages in the Rae Craton lie to the west, with Mesoarchean crust being found in the western Margin of the Churchill Province of the Rae (Hartlaub et al. 2005) and the Queen Maud block (Schultz et al. 2007). However, the small numbers of Darby peridotites amenable to dating means that this observation needs to be tested if additional samples become available. A Neoarchean age for the eastern portion of the Rae Craton lithosphere is consistent with stabilization shortly after the abundant komatiitic and tholeiitic basalt magmatism that erupted throughout that part of the Rae (e.g., Schultz et al. 2007), which would have required melting beneath lithosphere no greater than ~80 km thick, followed by thickening and stabilization of a thick, ~200 km mantle root.

Overall, the additional peaks in Re depletion ages observed both at Darby and in the larger sample suites from elsewhere in the Rae can be broadly correlated with the numerous Proterozoic tectonothermal/igneous events that the Rae Craton has experienced since its stabilization in the Archean, as outlined by Liu et al. (2016). Hence, the indications from the Os isotope data across the Rae Craton are that depletion and the stabilization of the cratonic root occurred in the Neoarchean. Our observation of a few 2.3 Ga model ages in the Darby dataset may be the first expression of the ~2.3 Ga Arrowsmith orogeny (Berman et al. 2013). However, the few Darby peridotites analysed and the imprecise nature of Os model ages because of the uncertainty in the model reservoir do not allow a firm conclusion to be reached with the currently available data. Neoarchean stabilization of the cratonic root is consistent with the observation of wide-spread 2.63–2.60 Ga arc-related plutonic rocks intruded through the Rae (Regan et al. 2017). The lithosphere may have either formed from or been thickened by this subduction event, followed by further evidence of intense lithospheric thickening at ~2.57 Ga (Regan et al. 2017).

Pyroxenites, lithospheric mantle structure and tectonic implications

Whereas the Darby peridotites are typical of depleted cratonic mantle lithosphere, the high abundance of low-Cr G3 and G4 garnets in concentrate and the anomalous high relative abundance of pyroxenite xenoliths at Darby is unusual in a cratonic setting, especially as this is a feature of all the Darby intrusions. Applying the low-Cr garnet "crust-mantle" logistic regression classification of Hardman et al. (2018a) reveals that only 28% (underestimated due to lack of trace element analyses) of the concentrate low-Cr garnet grains and 74% (trace element classification available) of the pyroxenitic xenoliths are of mantle origin. Fe-Mg temperature estimates for the pyroxenites (calculated at 1 GPa for crustal, 4 GPa for mantle; Krogh 2000) range from 590–1030 °C (Fig. 9), with the plagioclase pyroxenite giving a temperature of 610 °C. While the highest equilibration temperatures, in the mantle-derived samples, might reflect equilibrium along a geotherm, the high Fe-Mg temperatures of the crustal pyroxenites likely reflect the closing of Fe-Mg exchange during their crystallization in the lower crust, with the garnet-clinopyroxene temperatures retaining palaeo-equilibration temperatures due to rapid cooling (e.g., Harte et al. 1981). This is further implied by the presence of pigeonite. Putting aside the high-T samples, that are altered by lamproitic metasomatism as well as crustal samples, temperatures in the "normal" mantle pyroxenite suite range from 710–820 °C, which corresponds to a ~15 km thick region in the mantle along the cratonic geotherm (assuming no error in thermometry).

The pyroxenitic garnets are $LREE_N$ depleted (Fig. 5b) which is typical of pyroxenites from orogenic massifs and cratonic eclogites (Jacob 2004). $HREE_N$ are variably enriched with one sample showing extreme enrichment ($Lu_N = 100$), similar to some Roberts Victor eclogites (Harte and Kirkley 1997) or Beni Bousera orogenic pyroxenites (Pearson et al. 1993). Twelve pyroxenites whose garnets have positive Eu-anomalies and nearly flat $HREE_N$ have been interpreted as evidence of a prograde metamorphic reaction forming garnet from a plagioclase-bearing assemblage, likely reflecting a parentage of these rocks from subducted oceanic crust (e.g., Jacob et al. 2003; Jagoutz et al. 1984) and consequently these rocks are Na-poor. Diopsides in the pyroxenites show convex-upward REE_N patterns with enriched $LREE_N$ concentrations typical of mantle eclogites (Jacob 2004). The seven positive Eu-anomalies documented in diopside occur when coexisting garnets also show positive anomalies, supporting an origin perhaps from oceanic crust or crystallised melts of oceanic crust which inherit the positive Eu-anomalies of their source (e.g., Yaxley and Green 1998).

The Darby mantle-derived pyroxenites give T_{MA} ages of 2.0–2.2 and 3.1–3.2 Ga (Fig. 7b). The T_{MA} ages reflect primary Re-Os fractionation during derivation of the parental melt from the mantle due to their high Re/Os ratios. The oldest ages appear to document that the production of mafic material either recycled back into the mantle, or mafic/ultramafic magmas produced in the hot Mesoarchean mantle froze in nascent lithospheric mantle. The older T_{MA} (3.1–3.2 Ga) ages are older than the T_{RD} ages from the peridotites and as old as some Nd model "mantle extraction ages" produced from the oldest crust of the western Rae (e.g., Hartlaub et al. 2005; Schultz et al. 2007). Hence, they might reflect the production of mafic magmas during the formation of the earliest Rae crust.

The 2.0–2.2 Ga pyroxenites may have been produced from melts freezing in thick continental lithosphere from a wide spectrum of magmatic events that occurred in the Rae between 2.3 and 1.8 Ga. The precision on the Re-Os model ages is not sufficient to resolve this further. The younger ~1.0–1.3 Ga Re-Os model ages, one of which is a plagioclase pyroxenite (B-13) of crustal origin could reflect its formation from melts related to the Mackenzie Large Igneous event that were injected from the site of the proposed plume head to the WNW, which froze in the lower crust beneath Darby. The young pyroxenite of mantle derivation (M-19A) may be a melt from Mackenzie magmatism crystallising at shallow mantle depths. This is consistent with their anomalously high Fe-Mg temperatures being the result of heat advected into the lower crust at this time.

Even though many of the Darby G3/G4 concentrate garnets classify as crustal in origin using the Hardman et al. (2018a) discrimination while garnets from xenoliths are dominantly mantle using Hardman et al. (2018b), the overall amount of mantle eclogite/pyroxenite material exceeds the estimate for cratonic lithospheric mantle of between one and five vol% made by Schulze (1989) and Dawson and Stephens (1975). This anomalous proportion of pyroxenite/eclogite could indicate the introduction of basic material from an underthrust slab or a pyroxenite-rich zone that crystallised from magma infiltrating the Rae lithosphere during one of the later tectono-thermal events to affecting the craton. The restricted temperature range of the mantle pyroxenites indicates a ~15 km depth range of sampling for these xenoliths and may correspond to a thicker oceanic slab formed under a hotter Archean thermal regime or a zone of enhanced pyroxenite crystallisation.

To investigate these possibilities, we can interrogate further the seismic dataset for the Rae Craton recently summarized and presented by Snyder et al. (2015, 2017). A new 3-D image produced from this dataset (Fig. 10) highlights surfaces - determined from seismic discontinuities in Ps receiver functions

- that define three distinct layers beneath Darby at 36 km (Moho), 52 km ("Nanuq", projects to surface at the Chantrey fault zone although the strikes are slightly discordant), and at 200 km (lithosphere asthenosphere boundary = LAB). The layered structure of the Rae lithosphere has been interpreted by Snyder et al. (2017) to reflect an origin by lateral accretion and tectonic wedging. This together with the crustal deformation and thickening at 2.57 Ga documented by Regan et al. (2017) supports an origin for the structure of the Rae Craton lithosphere by compression, following dynamics similar to those outlined by Wang et al. (in press).

In the above scenario the "Nanuq" surface, the strongest surface in the three receiver cones in Fig. 10, may document the anomalous abundance of basic material crystallised in both the Rae crust and mantle beneath Darby. The occurrence of an anomalously high abundance of pyroxenite at all the Darby kimberlites is consistent with the inferences drawn from seismological characteristics (Bostock 1998) of the Nanuq surface that suggests the presence of a layer rich in isotropic basic material overlain by a more anisotropic ultramafic layer in the shallowest upper mantle. This discontinuity could be a possible upper slab surface or simply a zone where basic melts have crystallised in the upper mantle. Further studies of the physical properties of mantle xenoliths from the Rae Craton will better constrain these possibilities.

Conclusions

Our new Rb-Sr geochronology reveals that the Darby kimberlite field, west-central Rae Craton, erupted at 542.2±2.6 Ma, overlapping in age other Cambrian/Neoproterozoic kimberlites intruding the Rae Craton (Sarkar et al. 2018). A small suite of peridotite xenoliths along with mineral concentrate grains document the presence of highly-depleted (low bulk rock Al_2O_3, high olivine Mg#) cratonic mantle beneath this region. Rhenium-Os dating of the five largest peridotite xenoliths indicates that the main lithospheric stabilization event occurred in the Neoarchean, forming ~200 km thick cratonic mantle, as constrained by clinopyroxene thermobarometry. A Neoarchean stabilization of thick lithosphere beneath the Rae Craton is consistent with the complex and active Neoarchean magmatic history of the Rae (Regan et al. 2017) and indicates mantle thickening during Neoarchean tectonism.

Pyroxenites and eclogites of mantle and crustal origin are anomalously abundant in our sample of indicator minerals and xenoliths at Darby, in contrast to the low observed abundance present in typical cratonic lithospheric mantle worldwide. While some of the high-T crustal pyroxenites likely represent magma crystallised in the lower crust due to Proterozoic magmatism (as indicated by their Re-Os model ages), the oldest of these samples may represent Mesoarchean high pressure cumulates from magma infiltrating early oceanic or continental mantle, prior to its thickening in the Neoarchean or even recycled oceanic crust. The common presence of this basic material in the mantle of the western Rae Craton could explain the prominent "surface" evident in receiver-function seismic studies of the Rae lithosphere (Fig. 10).

A xenolith with diamond-facies harzburgitic (G10D) garnet-bearing clearly originated well within the diamond stability field. This, coupled with the melt-depleted nature of the peridotites and their Archean age are all encouraging for diamond exploration. In particular, the extensive diamond window (~75 km) defined by our geotherm and the mantle sampling within the diamond stability field evident from olivine thermometry is encouraging evidence of diamond-facies peridotitic mantle being sampled.

Acknowledgements This research formed part of G.H.'s MSc. thesis funded by a Canada Excellence Research Chair (CERC) grant to D.G.P. and the Diamond Exploration and Research Training School (DERTS). We acknowledge Teck Resources Limited for granting access to the Darby property and support with field costs. Mike Merante provided invaluable assistance in the field. Unpublished data were provided by Bluestone Resources Inc. We thank Drs. Sarah Woodland, Andrew Locock, and Yan Luo for analytical assistance. We thank Grant Lockhart, Janina Czas, and Pedro Waterton for useful discussions. We are indebted to Véronique Le Roux, Richard Carlson and handling editor Roberta Rudnick for constructive comments that helped to improve the manuscript.

References

Andersen T (2002) Correction of common lead in U–Pb analyses that do not report ^{204}Pb. Chem Geol 192:59–79

Aulbach S, Mungall JE, Pearson DG (2015) Distribution and processing of highly siderophile elements in cratonic mantle lithosphere. Rev Mineral Geochem 81:239–304

Berman RG, Pehrsson S, Davis WJ, Ryan JJ, Qui H, Ashton KE (2013) The Arrowsmith orogeny: geochronological and thermobarometric constraints on its extent and tectonic setting in the Rae Craton, with implications for pre-Nuna supercontinent reconstruction. Precambrian Res 232:44–69

Bostock MG (1998) Mantle stratigraphy and evolution of the Slave Province. J Geophys Res 103(B9):183–200

Boyd FR, Mertzman SA (1987) Composition and structure of the Kaapvaal lithosphere, South Africa. Magmatic Processes: Physicochemical Principles. Geo Soc S P No. I. 13–24

Bussweiler Y, Brey GP, Pearson DG, Stachel T, Stern RA, Hardman MF, Kjarsgaard BA, Jackson SE (2017) The aluminum-in-olivine thermometer for mantle peridotites — experimental versus empirical calibration and potential applications. Lithos 272-273:301–314

Canil D (1999) The Ni-in-garnet geothermometer: calibration at natural abundances. Contrib Mineral Petrol 136:240–246

Cherniak DJ (2000) Pb diffusion in rutile. Contrib Mineral Petrol 139: 198–207

Counts B (2008) http://www.marketwired.com/press-release/indicator-minerals-darby-project-yields-more-kimberlite-partner-increases-budget-tsx-venture-ime-884912.htm. Accessed 12 May 2018

Creaser RA, Gru H, Carlson J, Crawford B (2004) Macrocrystal phlogopite Rb–Sr dates for the Ekati property kimberlites, Slave Province, Canada: evidence for multiple intrusive episodes in the Paleocene and Eocene. Lithos 76:399–414

Dawson JB, Stephens WE (1975) Statistical classification of garnets from kimberlite and associated xenoliths. J Geol 83(5):589–607

Desmons J, Smulikowski W (2007) A systematic nomenclature for Metamorphic rocks: 4. In: High P/T metamorphic rocks. Recommendations by the IUGS Subcommission on the Systematics of Metamorphic Rocks. SCMR website. www.bgs.ac.uk/SCMR

Foley SF, Prelevic D, Rehfeldt T, Jacob DE (2013) Minor and trace elements in olivines as probes into early igneous and mantle melting processes. Earth Planet Sci Lett 363:181–191

Griffin WL, Cousens DR, Ryan CG, Sie SH, Suter GF (1989) Ni in chrome pyrope garnets: a new geothermometer. Contrib Mineral Petrol 103(2):199–202

Grütter HS (2009) Pyroxene xenocryst geotherms: techniques and application. Lithos 112S:1167–1178

Grütter HS, Gurney JJ, Menzies AH, Winter F (2004) An updated classification scheme for mantle-derived garnet, for use by diamond explorers. Lithos 77:841–857

Grütter HS, Latti D, Menzies A (2006) Cr-saturation arrays in concentrate garnet compositions from kimberlite and their use in mantle barometry. J Petrol 47(4):801–820

Hardman MF, Pearson DG, Stachel T, Sweeney RJ (2018) Statistical approaches to the discrimination of crust- and mantle-derived low-Cr garnet – major-element-based methods and their application in diamond exploration. J Geochem Explor 186:24–35

Hardman MF, Pearson DG, Stachel T, Sweeney RJ (2018) Statistical approaches to the discrimination of mantle- and crust-derived low-Cr garnets using major and trace element data. Miner Petrol, this volume

Harte B, Kirkley MB (1997) Partitioning of trace elements between clinopyroxene and garnet: data from mantle eclogites. Chem Geol 136:1–24

Harte B, Jackson PM, Macintyre RM (1981) Age of mineral equilibria in granulite facies nodules from kimberlites. Nature 291:147–148

Hartlaub RP, Chacko T, Heaman LM, Creaser RA, Ashton KE, Simonetti A (2005) Anchient (Meso- to Paleoarchean) crust in the Rae Province, Canada: evidence from Sm-Nd and U-Pb constraints. Precambrian Res 141:137–153

Irvine GJ, Pearson DG, Kjarsgaard BA, Carlson RW, Kopylova MG, Dreibus G (2003) A Re – Os isotope and PGE study of kimberlite-derived peridotite xenoliths from Somerset Island and a comparison to the Slave and Kaapvaal cratons. Lithos 71:461–488

Jackson GD (1966) Geology and mineral possibilities of the Mary River region, northern Baffin Island. Can Miner 87:57–61

Jacob DE (2004) Nature and origin of eclogite xenoliths from kimberlites. Lithos 77(1–4):295–316

Jacob DE, Schmickler B, Schulze DJ (2003) Trace element geochemistry of coesite-bearing eclogites from the Roberts Victor kimberlite, Kaapvaal Craton. Lithos 71:337–351

Jagoutz E, Dawson JB, Hoernes S, Spettel B, Wänke H (1984) Anorthositic oceanic crust in the Archean Earth. 15th Lunar Planet Sci Conf, Abs 395–396

Kjarsgaard BA (2007) Kimberlite diamond deposits. In: W. Goodfellow (eds) Mineral deposits of Canada. Geological Association of Canada Mineral Deposits Division Special Publication, vol 5, pp 245–272

Klein-BenDavid O, Pearson DG (2009) Origins of subcalcic garnets and their relation to diamond forming fluids-case studies from Ekati (NWT-Canada) and Murowa (Zimbabwe). Geochim Cosmochim Acta 73(3):837–855

Krogh RE (2000) The garnet – clinopyroxene Fe^{2+} – Mg geothermometer: an updated calibration. J Metamorph Geol 18: 211–219

Liu J, Riches AJV, Pearson DG, Luo Y, Kienlen B, Kjarsgaard BA, Stachel T, Armstrong JP (2016) Age and evolution of the deep continental root beneath the central Rae Craton, northern Canada. Precambrian Res 272:168–184

MacHattie T (2008) Geochemistry and Geochronology of the Late Archean Prince Albert Group (PAG), Nunavut, Canada. Ph.D. thesis, University of Alberta, pp 61–63

Malkovets VG, Rezvukhin DI, Belousova EA, Griffin WL, Sharygin IS, Tretiakova IG, Gibsher AA, O'Reilly SY, Kuzmin DV, Litasov KD, Logvinova AM, Pokilenko NP, Sobolev NV (2016) Cr-rich rutile: a powerful tool for diamond exploration. Lithos 265:304–311

Marchesi C, Dale CW, Garrido CJ, Pearson DG, Bosch D, Bodinier J, Gervilla F, Hidas K (2014) Fractionation of highly siderophile elements in refertilized mantle: implications for the Os isotope composition of basalts. Earth Planet Sci Lett 400:33–44

Mather KA, Pearson DG, McKenzie D, Kjarsgaard B, Priestley K (2011) Constraining the depth and thermal history of cratonic lithosphere using peridotite xenolith and xenocryst thermobarometry and seismology. Lithos 125:729–742

Maynes A, Doulos D (2007) Assessment report on the Darby Property 2006 diamond exploration program, ground and airborne geophysics, drilling, and heavy mineral sampling. Unpublished report prepared by Indicator minerals Inc

McDonough WF, Sun S-S (1995) The composition of the Earth. Chem Geol 120:223–253

Menzies A (2003) Re–Os systematics of diamond-bearing eclogites from the Newlands kimberlite. Lithos 71(2–4):323–336

Pearson DG, Wittig N (2008) Formation of Archaean continental lithosphere and its diamonds: the root of the problem. J Geol Soc Lond 165:895–914

Pearson DG, Wittig N (2014) 3.6 - the formation and evolution of the subcontinental mantle lithosphere - evidence from mantle xenoliths. In: Treatise of geochemistry, 2nd edn. Elsevier, Oxford, pp 255–292

Pearson DG, Woodland SJ (2000) Solvent extraction/anion exchange separation and determination of PGEs (Os, Ir, Pt, Pd, Ru) and Re-Os isotopes in geological samples by isotope dilution ICP-MS. Chem Geol 165(1–2):87–107

Pearson DG, Davies GR, Nixon PH (1993) Geochemical constraints on the petrogenesis of diamond facies pyroxenites from the Beni Bousera peridotite massif, North Morocco. J Petrol 34:125–172

Pearson DG, Kelley SP, Pokhilenko NP, Boyd FR (1997) Laser $^{40}Ar/^{39}Ar$ analyses of phlogopites from southern African and Siberian kimberlites and their xenoliths: constraints on eruption ages, melt degassing and mantle volatile compositions. Russ Geol Geophys 38:106–117

Pearson DG, Irvine GJ, Ionov DA, Boyd FR, Dreibus GE (2004) Re – Os isotope systematics and platinum group element fractionation during mantle melt extraction: a study of massif and xenolith peridotite suites. Chem Geol 208:29–59

Prelević D, Foley SF, Romer R, Conticelli S (2008) Mediterranean Tertiary lamproites derived from multiple source components in postcollisional geodynamics. Geochim. Cosmochim. Acta 72: 2125–2156

Regan SP, Williams ML, Mahan KH, Dumond G, Jercinovic MJ, Orlandini OF (2017) Neoarchean arc magmatism and subsequent collisional orogenesis along the eastern Rae domain, western Churchill Province: implications for the early growth of Laurentia. Precambrian Res 294:151–174

Sanborn-Barrie M, Davis WJ, Berman RG, Rayner N, Skulski T, Sandeman H (2014) Neoarchean continental crust formation and Paleoproterozoic deformation of the central Rae craton, Committee Bay belt, Nunavut. Can J Earth Sci 51:635–667

Sarkar C, Heaman LM, Pearson DG (2015) Duration and periodicity of kimberlite volcanic activity in the Lac de Gras kimberlite field, Canada and some recommendations for kimberlite geochronology. Lithos 218:155–166

Sarkar C, Kjarsgaard BA, Pearson DG, Heaman LM, Locock A, Armstrong JA (2018) Geochronology, classification and mantle source characteristics of kimberlites and related rocks from the

Rae Craton, Melville Peninsula, Nunavut, Canada. Miner Petrol, this volume

Schau M (1982) Geology of the Prince Albert Group in parts of the Walker Lake and Laughland Lake map areas, district of Keewatin. Geol Surv Canada, Bull 337:1–75

Schultz MEJ, Chacko T, Heaman LM, Sandeman HA, Simonetti A, Creaser RA (2007) Queen Maud block: a newly recognized Paleoproterozoic (2.4–2.5 Ga) terrane in northwest Laurentia. Geology 35(8):707–710

Schulze DJ (1989) Constraints on the abundance of eclogite in the upper mantle. J Geophys Res 94(B4):4205–4212

Shu Q, Brey GP, Gerdes A, Hoefer HE (2013) Geochronological and geochemical constraints on the formation and evolution of the mantle underneath the Kaapvaal craton: Lu-Hf and Sm-Nd systematics of subcalcic garnets from highly depleted peridotites. Geochim Cosmochim Acta 113:1–20

Snyder DB, Craven JA, Pilkington M, Hillier MJ (2015) The 3-dimensional construction of the Rae Craton, central Canada. Geochem Geophys Geosyst 16:3555–3574

Snyder DB, Humphreys E, Pearson DG (2017) Tectonophysics construction and destruction of some North American cratons. Tectonophysics 694:464–485

Stachel T, Harris JW (2008) The origin of cratonic diamonds – constraints from mineral inclusions. Ore Geol Rev 34(1–2):5–32

Wang H, Van Hunen J, Pearson DG (in press) Making Archean cratonic roots by lateral compression: a two-stage thickening and stabilization model. Tectonophysics, in press

Yavuz F (2013) WinPyrox: a Windows program for pyroxene calculation classification and thermobarometry. Am Mineral 98: 1338–1359

Yaxley GM, Green DH (1998) Reactions between eclogite and peridotite: mantle refertilisation by subduction of oceanic crust. Schweiz Miner Pertrog 78:243–255